

Fall 2013

Design, Synthesis, And Evaluation Of Molecular Inhibitors For Biologically Relevant Enzymes

Sarah Emma St. John
Purdue University

Follow this and additional works at: https://docs.lib.purdue.edu/open_access_dissertations



Part of the [Biochemistry Commons](#), and the [Chemistry Commons](#)

Recommended Citation

St. John, Sarah Emma, "Design, Synthesis, And Evaluation Of Molecular Inhibitors For Biologically Relevant Enzymes" (2013). *Open Access Dissertations*. 62.
https://docs.lib.purdue.edu/open_access_dissertations/62

This document has been made available through Purdue e-Pubs, a service of the Purdue University Libraries. Please contact epubs@purdue.edu for additional information.

PURDUE UNIVERSITY
GRADUATE SCHOOL
Thesis/Dissertation Acceptance

This is to certify that the thesis/dissertation prepared

By Sarah Emma St. John

Entitled DESIGN, SYNTHESIS, AND EVALUATION OF MOLECULAR INHIBITORS FOR
BIOLOGICALLY RELEVANT ENZYMES

For the degree of Doctor of Philosophy

Is approved by the final examining committee:

Mark A. Lipton

Chair

Jean A. Chmielewski

Alexander Wei

Jonathan Wilker

To the best of my knowledge and as understood by the student in the *Research Integrity and Copyright Disclaimer (Graduate School Form 20)*, this thesis/dissertation adheres to the provisions of Purdue University's "Policy on Integrity in Research" and the use of copyrighted material.

Approved by Major Professor(s): Mark A. Lipton

Approved by: R. E. Wild

Head of the Graduate Program

September 19, 2013

Date

DESIGN, SYNTHESIS, AND EVALUATION OF MOLECULAR INHIBITORS FOR
BIOLOGICALLY RELEVANT ENZYMES

A Dissertation

Submitted to the Faculty

of

Purdue University

by

Sarah Emma St. John

In Partial Fulfillment of the

Requirements for the Degree

of

Doctor of Philosophy

December 2013

Purdue University

West Lafayette, Indiana

This work is dedicated to my father Ronald St. John, my mother Kathleen St. John, my partner Christopher Clark, and my beautiful dogs Marin and Melvin St. John-Clark for their continuous love, encouragement, and support.

ACKNOWLEDGMENTS

First and foremost, I must thank my advisor and mentor, Professor Mark A. Lipton. He has taught me an incredible amount of stuff (not just chemistry, although certainly quite a bit of that) throughout my years at Purdue University. I have been extremely fortunate under his kind supervision and it has been through his mentorship that I have grown into the scientist that I am today. I am lucky to have had such a great experience working for such a great scientist and man. Thank you for all of the opportunities you've given to me, the freedom you've allowed me to pursue my interests, and the words of support and direction you've offered over the years.

I would also like to thank all of my committee advisors, Professors Jean A. Chmielewski, Jonathan Wilker, and Alexander Wei. You have all taught me valuable lessons during my time at Purdue.

My graduate career would have been far less interesting if it weren't for the various past and present Lipton research group members. Specifically, I would like to thank Nawaporn Sanguantrakun and Benjamin Barth for being awesome older group members that were usually willing help me with just about anything. Ning was always patient and Ben was always impatient, so it worked out nicely as I had my choice of guidance style on any given day. On the down-side, I blame them for my bipolar mentoring approach. Sorry Matt and Bin, you're just victims of circumstance.

I would be remiss if I did not also mention the one-and-only Master Ruth Campbell. Ruth joined the Lipton lab when I was in my fourth year of graduate school and going through a time of pretty constant failure in my research. Her endless supply of alcoholic beverages, disgusting commentary, radical liberalism, excessive clumsiness, bad music (i.e. “Phat-Beats Hour”), and half-baked plans for weekend activities got me through that period of despair – and in the mean time, I made one of the best friends I have ever had. I should note that she is actually quite bright despite the aforementioned qualities, is now in medical school, and has been practicing not dropping and spilling things daily.

My family unquestionably deserves recognition. My mom and dad have been continuously supportive of me through this time, and without their encouragement and support this work would not have been possible. I am especially thankful that they fostered my scientific inclination from the time I was young and allowed me to follow whatever path I desired. I am also thankful that they have, for the most part, understood why I have been largely absent for the past five years. They have always praised me for learning, thinking, and being strong and independent.

Lastly, I would like to thank Christopher Clark, who has been with me through my entire tenure at Purdue. He has celebrated my accomplishments with me and loved and supported me through my low points. He is always confident in me, even when I am not confident in myself. Thank you for your love and support.

TABLE OF CONTENTS

	Page
LIST OF TABLES	viii
LIST OF FIGURES	ix
LIST OF SCHEMES.....	xxviii
LIST OF EQUATIONS	xx
LIST OF ABBREVIATIONS.....	xxi
ABSTRACT.....	xxv
CHAPTER ONE: RESVERATROL & QUINONE REDUCTASE 2	1
1.1. Introduction.....	1
1.2. Resveratrol	2
1.2.1. Dietary Sources of Resveratrol	2
1.2.2. Resveratrol and Carcinogenesis.....	3
1.2.3. Resveratrol and Cardiovascular Disease.....	4
1.2.4. Resveratrol and Longevity	5
1.2.5. Biological Availability of Resveratrol	7
1.2.6. Targets of Resveratrol.....	8
1.3. Quinone Reductase 2 (QR2)	10
1.3.1. QR1 vs. QR2 Comparison	10
1.3.2. QR2 Catalytic Mechanism.....	11
1.3.3. Resveratrol and QR2.....	13
1.4. Interest in Resveratrol and its Targets	15
1.5. References.....	16

CHAPTER TWO: QSAR DETERMINATION FOR COX1, COX2, NF- κ B AND QR2 RESVERATROL ANALOGUE MODELS	24
2.1. Previous Work	24
2.2. Structure-Activity Relationships (SARs).....	29
2.3. Quantitative Structure-Activity Relationships (QSARs).....	32
2.3.1. Molecular Descriptors.....	32
2.3.2. Stepwise Regression	35
2.3.3. COX1 QSAR	36
2.3.4. COX2 QSAR	36
2.3.5. NF- κ B QSAR.....	38
2.3.6. QR2 QSAR	39
2.4. 3D-QSAR.....	40
2.5. Conclusions.....	44
2.6. References.....	45
CHAPTER THREE: DESIGN, SYNTHESIS, AND EVALUATION OF SUBSTITUTED RESVERATROL ANALOGUES FOR THE INHIBITION OF QUINONE REDUCTASE 2 (QR2) AS CHEMOPREVENTATIVE AGENTS	46
3.1. Design of QR2 Inhibitors.....	46
3.1.1. First Generation Influences.....	47
3.1.2. Design of Second Generation Resveratrol Analogue Library	48
3.2. Construction of Second Generation Library	49
3.2.1. Construction of Olefin-Substituted Resveratrol Analogue Set.....	49
3.2.2. Construction of Benzanilide Resveratrol Analogue Set	54
3.3. Results of Second Generation Resveratrol Analogues Library	56
3.3.1. Biological Evaluation.....	56
3.3.2. Structural Evaluation of Second Generation Resveratrol Analogue Inhibitors	62
3.4. Conclusions.....	69
3.5. References.....	70
CHAPTER FOUR: DE NOVO DESIGN, SYNTHESIS, AND EVALUATION OF SUBSTITUTED PHENOTHIAZINES AS INHIBITORS OF THE CLASS-II HMG-COENZYME A REDUCTASE ENZYME FOR THE DEVELOPMENT OF NOVEL ANTIBACTERIALS	72
4.1. Introduction: Antibiotic-Resistant Bacteria	72
4.1.1. Current Demand for New Antibacterials	73
4.1.2. Methicillin-Resistant <i>Staphylococcus Aureus</i> (MRSA).....	76
4.1.3. Vancomycin-Resistant <i>Enterococcus</i> (VRE).....	77

	Page
4.2. Targeting MRSA and VRE.....	79
4.2.1. 3-Hydroxy-3-Methylglutaryl Coenzyme A Reductase (HMGR)	80
4.3. Previous Work	84
4.4. De Novo Design of II-HMGR Inhibitors.....	88
4.4.1. Tandem Design Approach: e-LEA3D and AutoDock Vina (ADV).....	88
4.4.2. Validation of ADV Results.....	92
4.5. Construction of Substituted Phenothiazine Library	94
4.5.1. Attempted Synthesis of Phenothiazine Cores.....	95
4.5.1.1. Smiles Rearrangement	95
4.5.1.2. CuI-Catalyzed Cascade C-S and C-N Bond Formation.....	98
4.5.2. The Cadogan Reaction: Synthesis of First Phenothiazine Set	100
4.5.3. Biological Evaluation of First Phenothiazine Set	109
4.5.4. Synthesis of Second Phenothiazine Set	112
4.5.5. Biological Evaluation of Second Phenothiazine Set.....	116
4.6. Conclusions.....	118
4.7. Future Directions	119
4.8. References.....	120
 APPENDICES	
Appendix A: Experimental Procedures	123
Appendix B: NMR, ESI-MS, and IR Spectra.....	176
VITA.....	332
PUBLICATION.....	333

LIST OF TABLES

Table	Page
1.1. Dietary sources of resveratrol	3
1.2. Activity of resveratrol on various enzymes	9
2.1. Inhibition of COX1, COX2, NF-kB, and QR2 by first generation resveratrol analogue library	26
2.2. Molecular descriptors used for the construction of QSAR models	34
3.1. Inhibition of QR2 by olefin-substituted and benzanilide resveratrol analogues.....	57
4.1. Inhibition of <i>E. faecalis</i> II-HMGR by first phenothiazine set	110
4.2. Inhibition of <i>E. faecalis</i> II-HMGR by second phenothiazine set.....	116

LIST OF FIGURES

Figure	Page
1.1. <i>Trans</i> - and <i>Cis</i> - resveratrol.	2
1.2. Metabolites of resveratrol	8
1.3. Mechanism of quinone reduction by QR2	12
1.4. Resveratrol-QR2 complex.	14
2.1. Determination of Hammett parameter	33
2.2. Determination of Taft steric parameter	33
2.3. Seven possible positions of substitution for each resveratrol analogue.....	35
2.4. Pictorial representation of COX2 QSAR.....	37
2.5. Pictorial representation of NF-kB QSAR	38
2.6. Pictorial representation of QR2 QSAR.....	40
2.7. 3-D QSAR for QR2	43
3.1. First generation resveratrol analogues with trifluoromethyl alkene substituents	48
3.2. Design of second generation resveratrol analogue library.....	49
3.3. Complete second generation resveratrol analogue library.....	55
3.4. Correlation of increased steric bulk with increased IC ₅₀ as shown by 3.4a - 3.4d	59
3.5. Effect of conformation on inhibition of QR2	60
3.6. X-ray crystal structures of (A) 3.4d , (B) 3.4f , (C) 3.4k , (D) 3.4r , (E) 3.8a , and (F) 3.8d in complex with QR2	63

Figure	Page
3.7. (A) Crystal structure of inhibitor 3.4k bound in the QR2 active site	68
4.1. Innovation gap in antibacterial drug discovery pipeline.....	75
4.2. Structures of penicillin and methicillin.....	77
4.3. Mevalonate pathway	81
4.4. Proposed reaction mechanism for <i>P. mevalonii</i> HMG-CoA reductase	82
4.5. Structure of lead compound <i>N</i> -bsha.....	85
4.6. (A) X-ray crystal structure of <i>N</i> -bsha bound in <i>E. faecalis</i> II-HMGR	87
4.7. (Left) Pictorial representation of tandem e-LEA3D/ADV design approach.....	91
4.8. (A) Validation of ADV exercise, predicted and actual binding conformation of <i>N</i> -bsha in <i>E. faecalis</i> II-HMGR, where the blue <i>N</i> -bsha molecule is the actual binding conformation determined by X-ray crystal structure and the white <i>N</i> -bsha molecule is the predicted binding conformation produced by ADV. (B) Designed phenothiazine compound 4.40 . (C) Overlay of predicted fourth binding mode of 4.40 superimposed on X-ray crystal structure of <i>N</i> -bsha	93
4.9. Predicted binding conformation of 4.24 produced by ADV	111

Appendix Figure	Page
B.1. 400 MHz ^1H NMR of compound 3.2a in CDCl_3	177
B.2. 100 MHz ^{13}C NMR of compound 3.2a in CDCl_3	178
B.3. 300 MHz ^1H NMR of compound 3.3d in CDCl_3	179
B.4. 75 MHz ^{13}C NMR of compound 3.3d in CDCl_3	180
B.5. 300 MHz ^1H NMR of compound 3.4a in CDCl_3	181
B.6. 300 MHz ^1H NMR of compound 3.4b in CDCl_3	182
B.7. 75 MHz ^{13}C NMR of compound 3.4b in CDCl_3	183
B.8. 300 MHz ^1H NMR of compound 3.4c in CDCl_3	184
B.9. 300 MHz nOe ^1H NMR of compound 3.4c in CDCl_3	185
B.10. 75 MHz ^{13}C NMR of compound 3.4c in CDCl_3	186
B.11. 400 MHz ^1H NMR of compound 3.4d in CD_3OD	187
B.12. 100 MHz ^{13}C NMR of compound 3.4d in CD_3OD	188
B.13. 400 MHz ^1H NMR of compound 3.4e in CD_3OD	189
B.14. 400 MHz nOe ^1H NMR of compound 3.4e in CD_3OD	190
B.15. 400 MHz nOe ^1H NMR of compound 3.4e in CD_3OD	191
B.16. 400 MHz ^1H NMR of compound 3.4f in CD_3OD	192
B.17. 400 MHz nOe ^1H NMR of compound 3.4f in CD_3OD	193
B.18. 100 MHz ^{13}C NMR of compound 3.4f in CD_3OD	194
B.19. 400 MHz ^1H NMR of compound 3.4g in CDCl_3	195
B.20. 100 MHz ^{13}C NMR of compound 3.4g in CDCl_3	196
B.21. 300 MHz ^1H NMR of compound 3.4h in CDCl_3	197
B.22. 300 MHz nOe ^1H NMR of compound 3.4h in CDCl_3	198
B.23. 75 MHz ^{13}C NMR of compound 3.4h in CDCl_3	199

Appendix Figure	Page
B.24. 300 MHz ^1H NMR of compound 3.4i in CDCl_3	200
B.25. 300 MHz nOe ^1H NMR of compound 3.4i in CDCl_3	201
B.26. 100 MHz ^{13}C NMR of compound 3.4i in CDCl_3	202
B.27. 400 MHz ^1H NMR of compound 3.4j in CDCl_3	203
B.28. 100 MHz ^{13}C NMR of compound 3.4j in CDCl_3	204
B.29. 300 MHz ^1H NMR of compound 3.4k in CDCl_3	205
B.30. 300 MHz nOe ^1H NMR of compound 3.4k in CDCl_3	206
B.31. 75 MHz ^{13}C NMR of compound 3.4k in CDCl_3	207
B.32. 300 MHz ^1H NMR of compound 3.4l in CDCl_3	208
B.33. 300 MHz nOe ^1H NMR of compound 3.4l in CDCl_3	209
B.34. 300 MHz ^1H NMR of compound 3.4m in CDCl_3	210
B.35. 300 MHz nOe ^1H NMR of compound 3.4m in CDCl_3	211
B.36. 300 MHz nOe ^1H NMR of compound 3.4m in CDCl_3	212
B.37. 400 MHz ^1H NMR of compound 3.4n in CDCl_3	213
B.38. 300 MHz nOe ^1H NMR of compound 3.4n in CDCl_3	214
B.39. 100 MHz ^{13}C NMR of compound 3.4n in CDCl_3	215
B.40. 400 MHz ^1H NMR of compound 3.4o in CDCl_3	216
B.41. 300 MHz nOe ^1H NMR of compound 3.4o in CDCl_3	217
B.42. 100 MHz ^{13}C NMR of compound 3.4o in CDCl_3	218
B.43. 400 MHz ^1H NMR of compound 3.4p in CD_3OD	219
B.44. 300 MHz ^1H NMR of compound 3.4q in CDCl_3	220
B.45. 100 MHz ^{13}C NMR of compound 3.4q in CDCl_3	221
B.46. 400 MHz ^1H NMR of compound 3.4r in CD_3OD	222

Appendix Figure	Page
B.47. 100 MHz ^{13}C NMR of compound 3.4r in CD_3OD	223
B.48. 400 MHz ^1H NMR of compound 3.4s in CDCl_3	224
B.49. 100 MHz ^{13}C NMR of compound 3.4s in CDCl_3	225
B.50. 400 MHz ^1H NMR of compound 3.4t in CDCl_3	226
B.51. 100 MHz ^{13}C NMR of compound 3.4t in CDCl_3	227
B.52. 400 MHz ^1H NMR of compound 3.4u in CDCl_3	228
B.53. 100 MHz ^{13}C NMR of compound 3.4u in CDCl_3	229
B.54. 800 MHz ^1H NMR of compound 4.1 in d^6 -DMSO.....	230
B.55. 75 MHz ^{13}C NMR of compound 4.1 in d^6 -DMSO: CD_3OD	231
B.56. 800 MHz COSY NMR of compound 4.1 in d^6 -DMSO: CD_3OD	232
B.57. FTIR of compound 4.1	233
B.58. 400 MHz ^1H NMR of compound 4.2 in CD_3OD	234
B.59. 800 MHz ^1H NMR of crude compound 4.3 in d^6 -DMSO.....	235
B.60. 300 MHz ^1H NMR of compound 4.4 in CDCl_3	236
B.61. 300 MHz ^{13}C NMR of compound 4.4 in CDCl_3	237
B.62. 300 MHz ^1H NMR of compound 4.5 in CDCl_3	238
B.63. 400 MHz ^1H NMR of compound 4.6 in CDCl_3	239
B.64. 100 MHz ^{13}C NMR of compound 4.6 in CDCl_3	240
B.65. FTIR of compound 4.6	241
B.66. 300 MHz ^1H NMR of compound 4.7 in CDCl_3	242
B.67. 75 MHz ^{13}C NMR of compound 4.7 in CDCl_3	243
B.68. FTIR compound 4.7	244
B.69. 300 MHz ^1H NMR of compound 4.8 in CDCl_3	245

Appendix Figure	Page
B.70. FTIR of compound 4.8	246
B.71. 300 MHz ^1H NMR of compound 4.9 in CDCl_3	247
B.72. 75 MHz ^{13}C NMR of compound 4.9 in CDCl_3	248
B.73. FTIR of compound 4.9	249
B.74. 300 MHz ^1H NMR of compound 4.10 in CDCl_3	250
B.75. 75 MHz ^{13}C NMR of compound 4.10 in CDCl_3	251
B.76. FTIR of compound 4.10	252
B.77. 300 MHz ^1H NMR of compound 4.11 in CDCl_3	253
B.78. 300 MHz ^1H NMR of compound 4.12 in CDCl_3	254
B.79. 75 MHz ^{13}C NMR of compound 4.12 in CDCl_3	255
B.80. FTIR of compound 4.12	256
B.81. 300 MHz ^1H NMR of compound 4.13 in CDCl_3	257
B.82. 75 MHz ^{13}C NMR of compound 4.13 in CDCl_3	258
B.83. FTIR of compound 4.13	259
B.84. 300 MHz ^1H NMR of compound 4.14 in CDCl_3	260
B.85. 75 MHz ^{13}C NMR of compound 4.14 in CDCl_3	261
B.86. FTIR of compound 4.14	262
B.87. 300 MHz ^1H NMR of compound 4.15 in CDCl_3	263
B.88. 75 MHz ^{13}C NMR of compound 4.15 in CDCl_3	264
B.89. FTIR of compound 4.15	265
B.90. 300 MHz ^1H NMR of compound 4.16 in CDCl_3	266
B.91. 75 MHz ^{13}C NMR of compound 4.16 in CDCl_3	267
B.92. FTIR of compound 4.16	268

Appendix Figure	Page
B.93. 300 MHz ^1H NMR of compound 4.17 in CDCl_3	269
B.94. 75 MHz ^{13}C NMR of compound 4.17 in CDCl_3	270
B.95. FTIR of compound 4.17	271
B.96. 300 MHz ^1H NMR of compound 4.18 in CD_3OD	272
B.97. 100 MHz ^{13}C NMR of compound 4.18 in CDCl_3	273
B.98. FTIR of compound 4.18	274
B.99. 300 MHz ^1H NMR of crude compound 4.19 in CDCl_3	275
B.100. 800 MHz ^1H NMR of compound 4.20 in d^6 -DMSO	276
B.101. 200 MHz ^1H NMR of compound 4.20 in d^6 -DMSO	277
B.102. FTIR of compound 4.20	278
B.103. 400 MHz ^1H NMR of compound 4.21 in CDCl_3	279
B.104. 100 MHz ^{13}C NMR of compound 4.21 in CDCl_3	280
B.105. FTIR of compound 4.21	281
B.106. 400 MHz ^1H NMR of compound 4.22 in CDCl_3	282
B.107. 100 MHz ^{13}C NMR of compound 4.22 in CDCl_3	283
B.108. FTIR of compound 4.22	284
B.109. 400 MHz ^1H NMR of compound 4.23 in CDCl_3	285
B.110. 100 MHz ^{13}C NMR of compound 4.23 in CDCl_3	286
B.111. 800 MHz ^1H NMR of compound 4.24 in CDCl_3	287
B.112. 200 MHz ^{13}C NMR of compound 4.24 in CDCl_3	288
B.113. FTIR of compound 4.24	289
B.114. 800 MHz ^1H NMR of compound 4.25 in CDCl_3	290
B.115. 400 MHz ^1H NMR of compound 4.26 in CDCl_3	291

Appendix Figure	Page
B.116. 100 MHz ^{13}C NMR of compound 4.26 in CDCl_3	292
B.117. FTIR of compound 4.26	293
B.118. 400 MHz ^1H NMR of compound 4.27 in CDCl_3	294
B.119. 100 MHz ^{13}C NMR of compound 4.27 in CDCl_3	295
B.120. FTIR of compound 4.27	296
B.121. 800 MHz ^1H NMR of compound 4.28 in CDCl_3	297
B.122. 200 MHz ^{13}C NMR of compound 4.28 in CDCl_3	298
B.123. FTIR of compound 4.28	299
B.124. 800 MHz ^1H NMR of compound 4.29 in d^6 -DMSO	300
B.125. 200 MHz ^{13}C NMR of compound 4.29 in d^6 -DMSO	301
B.126. FTIR of compound 4.29	302
B.127. 400 MHz ^1H NMR of compound 4.30 in CDCl_3	303
B.128. 100 MHz ^{13}C NMR of compound 4.30 in CDCl_3	304
B.129. FTIR of compound 4.30	305
B.130. 800 MHz ^1H NMR of compound 4.31 in d^6 -DMSO	306
B.131. 200 MHz ^{13}C NMR of compound 4.31 in d^6 -DMSO	307
B.132. FTIR of compound 4.31	308
B.133. 400 MHz ^1H NMR of compound 4.32 in CDCl_3	309
B.134. 100 MHz ^{13}C NMR of compound 4.32 in CDCl_3	310
B.135. FTIR of compound 4.32	311
B.136. 800 MHz ^1H NMR of compound 4.33 in d^6 -DMSO	312
B.137. 200 MHz ^{13}C NMR of compound 4.33 in d^6 -DMSO	313
B.138. FTIR of compound 4.33	314

Appendix Figure	Page
B.139. 800 MHz ^1H NMR of compound 4.34 in d^6 -DMSO.....	315
B.140. 200 MHz ^{13}C NMR of compound 4.33 in d^6 -DMSO.....	316
B.141. 300 MHz ^1H NMR of compound 4.35 in CDCl_3	317
B.142. 75 MHz ^{13}C NMR of compound 4.35 in CDCl_3	318
B.143. 400 MHz ^1H NMR of compound 4.36 in CDCl_3	319
B.144. 100 MHz ^{13}C NMR of compound 4.36 in CDCl_3	320
B.145. FTIR of compound 4.36	321
B.146. 400 MHz ^1H NMR of crude compound 4.37 in CDCl_3	322
B.147. 300 MHz ^1H -NMR of compound 4.38 in CDCl_3	323
B.148. 75 MHz ^{13}C -NMR of compound 4.38 in CDCl_3	324
B.149. 800 MHz ^1H NMR of crude compound 4.39 in d^6 -DMSO.....	325
B.150. 800 MHz ^1H NMR of compound 4.40 in d^6 -DMSO.....	326
B.151. 800 MHz ^{13}C NMR of compound 4.40 in d^6 -DMSO.....	327
B.152. FTIR of 4.40	328
B.153. 800 MHz ^1H NMR of compound 4.41 in d^6 -DMSO.....	329
B.154. 200 MHz ^{13}C NMR of compound 4.41 in d^6 -DMSO.....	330
B.155. FTIR of compound 4.41	331

LIST OF SCHEMES

Scheme	Page
3.1. Construction of starting materials 3.2a , 3.3c , and 3.3d and condensation reaction forming key nitrile analogues 3.4a-3.4c	50
3.2. Synthesis of analogues 3.4d-3.4f	51
3.3. Synthesis of analogues 3.4g-3.4m	52
3.4. Synthesis of analogues 3.4n-3.4p	53
3.5. Synthesis of analogues 4q-4s	54
4.1. Retrosynthetic route toward phenothiazine library.....	94
4.2. (<i>Top</i>) Mechanism of Smiles rearrangement. (<i>Bottom</i>) Synthesis of reactants and first attempt at production of phenothiazine core via Smiles rearrangement.....	96
4.3. Modified Smiles rearrangement resulting in compounds 4.7-4.10	97
4.4. Attempts at ligand-free CuI-catalyzed cascade C-S and C-N bond formation.....	99
4.5. CuI-catalyzed coupling using L-proline as a ligand.....	100
4.6. Intended formation of phenothiazine via reactive nitrene intermediate.....	101
4.7. Mechanism of Cadogan reaction.....	102
4.8. Formation of 4.17 via generation of a reactive nitrene.....	103

Scheme	Page
4.9. Two successful routes toward the same “one-armed” phenothiazine 4.20	105
4.10. Synthesis of “one-armed” phenothiazine 4.24	106
4.11. (<i>Top</i>) Synthesis of phenothiazines 4.2 , 4.26-4.28 . (<i>Bottom</i>) Synthesis of phenothiazines 4.29 and 4.30	108
4.12. Synthesis of 4.24 variants, 4.32-4.34	113
4.13. (<i>Top</i>) Synthetic route toward phenothiazine core 4.3 . (<i>Bottom</i>) Synthesis of phenothiazines 4.40 and 4.41	115

LIST OF EQUATIONS

Equation	Page
2.1. COX2 QSAR	37
2.2. NF-kB QSAR.....	38
2.3. QR2 QSAR	39
4.1. Reverse reaction of II-HMGR (non-physiological direction).....	84

LIST OF ABBREVIATIONS

Ac	acetyl
BAIB	[bis(acetoxy)-iodo]benzene
Bn	benzyl
Boc	<i>tert</i> -butyloxycarbonyl
Cbz	carbobenzyloxy (benzyloxycarbonyl)
d	doublet
DBU	1,8-diazobicyclo[5.4.0]undec-7-ene
DCC	<i>N,N'</i> -dicyclohexylcarbodiimide
DCM	dichloromethane
DDQ	2,3-dichloro-5,6-dicyano-1,4-benzoquinone
DEAD	diethyl azodicarboxylate
DIEA	<i>N,N</i> -diisopropylethylamine
DMAP	4-(dimethylamino)pyridine
DMF	<i>N,N</i> -dimethylformamide
DMSO	dimethylsulfoxide
DPPA	diphenylphosphoryl azide

EDCI	1-ethyl-3-(3-dimethylaminopropyl)carbodiimide
EDDA	ethylenediaminediacetic acid
EDTA	ethylenediaminetetraacetic acid
eq	equivalent
ESI	electrospray ionization
Et	ethyl
Fmoc	9-fluorenylmethyl carbamate
g	gram(s)
h	hour(s)
Hz	Hertz
IC ₅₀	50% inhibition concentration
<i>i</i> Pr	isopropyl
J	coupling constant
K _{<i>i</i>}	dissociation constant
LC ₅₀	50% lethal concentration
m	multiplet
M	molar
<i>m</i> CPBA	<i>m</i> -chloroperoxybenzoic acid
Me	methyl
Mhnb	mercaptohydroxynitrobenzene

min	minute(s)
mL	milliliter(s)
mMhnb	(methoxy)mercaptohydroxynitrobenzene
mmol	millimoles
Ms	methanesulfonyl
MTT	(3-(4,5-dimethylthiazol-2-yl)-2,5-diphenyltetrazolium bromide
NCL	native chemical ligation
nm	nanometer
NMR	nuclear magnetic resonance
nOe	nuclear overhauser effect
Ph	phenyl
PMB	<i>p</i> -methoxybenzyl
ppm	parts per million
PTSA	<i>p</i> -toluenesulfonic acid
Py	pyridine
q	quartet
QSAR	quantitative structure activity relationship
RT	room temperature (25 °C)
s	singlet
SAR	structure activity relationship

SPPS	solid phase peptide synthesis
t	triplet
TBAF	tetra- <i>n</i> -butylammonium fluoride
TBS	<i>tert</i> -butyldimethylsilyl
<i>t</i> -Bu	<i>tert</i> -butyl
TEMPO	(2,2,6,6-Tetramethylpiperidin-1-yl)oxyl, or (2,2,6,6-tetramethylpiperidin-1-yl)oxidanyl
TES	triethylsilane
TFA	trifluoroacetic acid
THF	tetrahydrofuran
TLC	thin layer chromatography
Trt (Tr)	trityl or triphenylmethyl
Ts	tosyl or <i>p</i> -toluenesulfonyl
UV	ultraviolet
δ	chemical shift in parts per million downfield of Me ₄ Si
μ	micro
°C	degrees Celsius

ABSTRACT

St. John, Sarah Emma. Ph.D., Purdue University, December 2013. Design, Synthesis, and Evaluation of Molecular Inhibitors for Biologically Relevant Enzymes. Major Professor: Mark A. Lipton.

The work in this thesis details the design, synthesis, and biological evaluation of molecular inhibitors for the inhibition of biologically relevant enzymes. The first three chapters of this thesis concern the polyphenol resveratrol and its inhibition of the quinone reductase 2 (QR2) enzyme. The work on this subject resulted in the complete design, synthesis, biological and structural evaluation of a second generation library of resveratrol analogues. From this work we identified a novel resveratrol analogue that inhibits QR2 in a previously unknown binding orientation. The fourth chapter of this thesis details the de novo design of molecules for the inhibition of the Class II HMGR enzyme. The work on this subject involved the de novo design and in silico screening of a set of phenothiazine molecules for the inhibition of II-HMGR. These molecules were synthesized and assayed against II-HMGR, resulting in the identification of a substituted phenothiazine compound found to inhibit II-HMGR with an IC_{50} of 130 μ M. This work resulted in a successful strategy for the identification of II-HMGR inhibitors.

CHAPTER ONE:
RESVERATROL & QUINONE REDUCTASE 2 (QR2)

1.1. Introduction

Many epidemiological studies have implicated the positive correlation between heightened consumption of total fat, saturated fat, cholesterol, and total caloric intake with mortality from heart disease. This trend has been found in most developed nations, with the exception of France; where mortality rates from coronary heart disease (CHD) are a third lower than comparable nations, including the United States and the United Kingdom, that have similar dietary fat intakes.¹ This finding, coined the “French paradox,” has been partially attributed to the increased consumption of red wine by the French. Red wine contains higher concentrations of polyphenols than white wine and other alcoholic beverages.² Polyphenols such as resveratrol, quercetin, catechin, and proanthocyanidins are abundant in the seeds and skins of grapes and have the ability to function as antioxidants, protecting low-density lipoproteins (LDL) from oxidation and inhibiting platelet aggregation.³ Understanding of the French paradox has stimulated further investigations questioning whether the polyphenolic compounds found in red wine have the ability to affect chemoprevention.

1.2. Resveratrol

Resveratrol (3,5,4'-trihydroxystilbene) is a naturally occurring polyphenol that was discovered in 1940 when it was isolated from the roots of white hellebore (*Veratrum grandiflorum* O. Loes) by Takaoka and coworkers (Figure 1.1).⁴ Initially there was little interest in the molecule as it was characterized as a phytoalexin.^{5, 6} However, in 1992 Siemann and coworkers proposed that resveratrol was behind the cardioprotective effects of red wine and the French paradox; since that time, interest in resveratrol has skyrocketed.⁷ Subsequently, numerous reports have indicated that resveratrol can prevent or retard the progression various disease states, including cancer, cardiovascular disease, ischemic injuries, and diabetes.⁸⁻¹² Resveratrol has even been shown to extend the lifespans of multiple life forms, from yeast to vertebrates.^{13, 14}

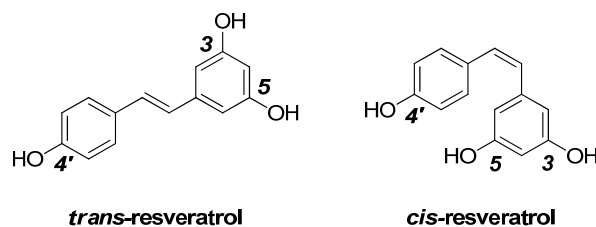


Figure 1.1. *Trans*- and *Cis*- resveratrol

1.2.1. Dietary Sources of Resveratrol

Since the time of its discovery, resveratrol has been isolated from over 70 different plant species including blueberries, peanuts, pistachios, rhubarb, hops, and most importantly, grapes (Table 1.1).¹⁵ A survey of just a few of resveratrol's dietary sources proves that the highest concentration of dietary resveratrol is found in red wine, and the

concentration of resveratrol found in red wine is significantly higher than that in white wine. Because resveratrol is found in the skins and seeds of grapes, and not the flesh, this finding can be largely attributed to the wine making techniques. White wine is pressed lightly and spends less time in contact with the skins of the grapes. In contrast, red wine is often fermented on the skins of the grapes, allowing more time to extract resveratrol.⁷ The geographical growing region of the grapes also has an effect on the concentration of resveratrol found in red wines. As a phytoalexin, higher concentrations of resveratrol are produced by plants growing under stressful conditions.

Table 1.1. Dietary sources of resveratrol.

Dietary Source of Resveratrol	<i>Trans</i> -Resveratrol Concentration
Red wines	0.1 to 14.3 mg/L ¹⁶⁻¹⁸
White wines	<0.1 to 2.1 mg/L ^{16, 19}
Grapes	0.16 to 3.54 µg/g ^{20, 21}
Raw cranberry juice	0.2 mg/L ²²
Blueberries	32 ng/g ²³
Peanuts	0.02 to 1.92 µg/g ²⁴
Peanut Butter	0.3 to 0.65 µg/g ²⁵
Pistachios	0.09 to 1.67 µg/g ²⁶
Hops	0.5 to 1.0 µg/g ²⁷

1.2.2. Resveratrol and Carcinogenesis

In 1997, a ground-breaking study was published by Jang and coworkers that indicated resveratrol could prevent the three major stages of carcinogenesis, inhibiting cellular events related to tumor initiation, promotion, and progression.⁸ Resveratrol has been found to relieve events that are associated with tumor initiation by functioning as an

antioxidant. For example, resveratrol was found to inhibit free radical formation upon treating human promyelocytic leukemia cells (HL-60) with 12-*O*-tetradecanoylphorbol-13-acetate (TPA) with an ED₅₀ of 27 μM.²⁸ Additionally, Prochaska and colleagues found that resveratrol was able to induce quinone reductase-1 (QR1) activity with cultured mouse hepatoma cells (Hepa 1c1c7), where a concentration of 21 μM was required to double QR1 activity.²⁹ This finding is relevant as QR1 is a phase II enzyme that is able to metabolically deactivate carcinogens, functioning in chemoprevention. Resveratrol's inhibition of tumor promotion stems from its ability to inhibit cyclooxygenase-1 (COX1), an enzyme that catalyzes the conversion of arachidonic acid to prostaglandins, which are compounds capable of stimulating tumor cell growth. COX1 has also been shown to activate various carcinogens, resulting in reactive forms that have the ability to damage DNA. Resveratrol was found to inhibit tumor promotion by Jang and colleagues. In an 18-week study of mice where 7,12-dimethylbenzanthracene (DMBA) was used as a tumor initiator and TPA was used as a tumor promoter, the topical application of 1, 5, 10, or 25 μmol of resveratrol together with TPA twice a week reduced the number of skin tumors per mouse by 68, 81, 76, or 98%, respectively.⁸

1.2.3. Resveratrol and Cardiovascular Disease

Systemic administration of resveratrol to rabbits fed a hypercholesterolaemic diet was found to inhibit the induced increase of platelet aggregation by Wang and coworkers.³⁰ Zini and coworkers found that resveratrol was capable of reducing the atherosclerotic area and the size of the blood clot produced by laser-induced damage of

the endothelium in mice that were genetically hypercholesterolaemic.³¹ The mechanism by which resveratrol exerts these helpful effects is not known; however, it may involve the preferential inhibition of COX1 over COX2 by resveratrol. The constitutive form of the enzyme, COX1, synthesizes thromboxane A₂ (TxA₂) in platelets, and is a powerful inducer of platelet aggregation and also a vasoconstrictor.³² The inducible form of the enzyme, COX2, synthesizes prostacyclin in vascular endothelial cells, and is an antiplatelet aggregator and also a vasodilator.³³ Thus, selective inhibition of COX1 by resveratrol may promote blood flow and decrease thrombus formation.

1.2.4. Resveratrol and Longevity

Perhaps the most intriguing effect of resveratrol is its ability to affect lifespan extension in a variety of organisms, resulting in it being termed the “molecular fountain of youth.” Many reports have implicated that resveratrol functions similarly to caloric restriction as it pertains to lifespan extension. Caloric restriction has been extensively studied in the past 70 years and is largely held as the most robust and reproducible method for the retardation of aging and age-related diseases.³⁴ Resveratrol has been postulated to function as a caloric restriction mimetic because an array of evidence exists that links resveratrol to the activation of sirtuin proteins.

The sirtuins are a family of conserved NAD⁺-dependent deacetylases that have been named after the *Saccharomyces cerevisiae* silent information regulator 2 (Sir2) protein, which is the founding member of the family.³⁵ There exist seven mammalian sirtuins SIRT1-7, where SIRT1 is the closest homolog of Sir2. In 2000, Lin and coworkers published a seminal report detailing that the increased longevity resulting from

caloric restriction is dependent on the activation of Sir2 by NAD.³⁶ Extra copies of the genes that encode for the sirtuin proteins in yeast, worms, and flies have also been associated with lifespan extension.³⁷⁻³⁹ In 2003, Howitz and colleagues showed that resveratrol was capable of activating Sir2 in *Saccharomyces cerevisiae* and linked it to extending the lifespan of the yeast by 70%.¹³ Since then, a host of studies have been performed investigating the link between SIRT1 and various diseases. Overexpression of SIRT1 in mice has been shown to protect mice from aging-related phenotypes comparable to type 2 diabetes,⁴⁰ cancer,⁴¹ and Alzheimer's disease;⁴² however, overexpression of SIRT1 has not been found to extend the lifespan of mice. Long term administration of resveratrol to mice induced gene expression that mimicked the effects of caloric restriction and retarded aging-related diseases.⁴³

Whether or not resveratrol is exerting these anti-aging effects by activation of the sirtuins is still unclear. The original findings of Howitz have been called into question as at least two reports have shown that the activation of Sir2 and SIRT1 by resveratrol is substrate specific. *In vitro* resveratrol was found to enhance the binding and deacetylation of peptide substrates that contained the non-physiological fluorescent moiety, Fluor de Lys, which was used by Howitz and colleagues in their original study. Resveratrol was found to have no activation effect on the binding and deacetylation of peptides lacking Fluor de Lys.⁴⁴ Borra and coworkers investigated the activation of Sir2, SIRT1, and SIRT2 by resveratrol and found only SIRT1 was significantly activated by resveratrol using a commercially available Fluor de Lys kit. Moreover, two other fluorophores were examined: 7-amino-4-methylcoumarin and rhodamine 110. It was found that peptides containing a fluorophore had a decreased ability to bind SIRT1 and

that the presence of resveratrol increased the ability of fluorophore-containing peptides to bind SIRT1, indicating that interaction of resveratrol with SIRT1 induces a conformational change that better accommodates the fluorophore.⁴⁵

Recently, a new mechanism for the activation of SIRT1 by resveratrol has been proposed by Park and colleagues.⁴⁶ Resveratrol was found to competitively inhibit cAMP-degrading phosphodiesterases, resulting in an increase in cAMP concentrations. Increased concentrations of cAMP subsequently activate Epac1, a cAMP-regulated guanine nucleotide exchange factor, which results in an increase in intracellular Ca^{2+} concentrations. Increase in Ca^{2+} levels activates the $\text{CamKK}\beta$ -AMPK pathway through phospholipase C and the ryanodine receptor Ca^{2+} -release channel. Overall, resveratrol increases the concentration of NAD^+ and the activity of SIRT1. Therefore, resveratrol may not directly increase the activity of SIRT1, but solid evidence exists that it does so indirectly through the cascade mechanism detailed above. In further support of this mechanism of indirect activation of SIRT1 by resveratrol, inhibition of the phosphodiesterase PDE4 with rolipram was found to mimic all of the effects of resveratrol including prevention of obesity despite a high-fat diet, increased mitochondrial function, increased physical stamina, and glucose tolerance in a mouse model.

1.2.5. Biological Availability of Resveratrol

One of the main issues complicating the use of resveratrol as a therapeutic lead is its low bioavailability. Circulating resveratrol has a half-life of 8-14 minutes because it is rapidly metabolized in the liver and gut by sulfation and glucuronation. This metabolism

results in the formation of 3- and 4'-*O*-sulfate and 3-*O*-glucuronide conjugates and reduces the circulating plasma concentration of resveratrol (Figure 1.2).⁴⁷⁻⁵⁰ These primary metabolites of resveratrol have been shown to have far lower affinity for certain targets *in vitro*. For instance, COX1, COX2, and quinone reductase 2 (QR2) are inhibited by resveratrol; however, only COX1 and COX2 are inhibited by resveratrol-4'-*O*-sulfate. The resveratrol-3-*O*-sulfate and -3-*O*-glucuronide metabolites were found to only weakly inhibit COX1 and COX2, while none of the metabolites were found to inhibit QR2.⁴⁷ The serum half-life of total resveratrol metabolites was found to be 9.2 hours by Walle and colleagues, signifying that the *in vivo* exposure to metabolite forms of resveratrol is greater than exposure to resveratrol itself.⁵¹

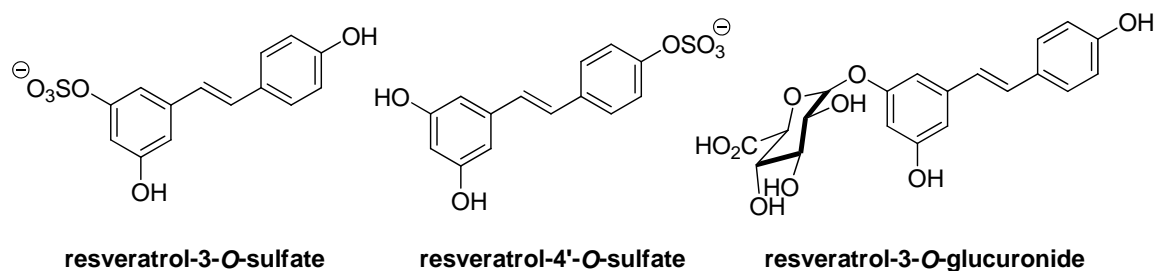


Figure 1.2. Metabolites of resveratrol

1.2.6. Targets of Resveratrol

Though resveratrol exerts a host of beneficial health effects, and there is a plethora of convoluted research about its targets and mechanisms, the complete story is still a mystery. The search for targets of resveratrol has been met with almost universal success; consequently, resveratrol has been shown to either inhibit or activate a variety of different enzymes and biological pathways.⁵² For example, resveratrol's anti-

inflammatory, cardioprotective, and chemopreventative activity has been linked to its ability to inhibit cyclo- and lipoxygenases,^{8, 53} while activation of Sir2/SIRT1 by resveratrol has been proposed to explain lifespan prolongation.^{13, 54} A sample of resveratrol's identified targets is shown in Table 1.2.

Because of the many direct targets of resveratrol that have been identified, elucidating which target is implicated in the treatment of a given disease state is unclear, complicating its use as a therapeutic lead. Additionally, resveratrol typically acts on its targets with concentrations in the micromolar range, and in many cases those targets may be acted on by other molecules with nanomolar concentrations.⁵² As an example, resveratrol inhibits cyclooxygenase-1 (COX1) with an IC_{50} of 15 μ M, while the diarylpyrazole SC-560 inhibits COX1 with an IC_{50} of 9 nM.⁵⁵ To date, the highest affinity target of resveratrol identified is the enzyme quinone reductase 2 (QR2), which resveratrol binds to with a dissociation constant (K_i) of 35 nM.⁵⁶

Table 1.2. Activity of resveratrol on various enzymes.

Enzyme Inhibited by Resveratrol	Enzymes Activated by Resveratrol
Cyclooxygenase-1 (ED_{50} = 15 μ M) ⁸	Quinone Reductase-1 (27 μ M*) ²⁹
Cyclooxygenase-2 (IC_{50} = 32 μ M) ⁵⁷	Sir2/SIRT1 (100 μ M**) ¹³
Lipoxygenases (IC_{50} = 3.7 μ M) ⁵²	AMP kinase (50 μ M**) ⁵⁸
Protein kinase C (IC_{50} = 40 μ M) ⁵⁹	Adenylyl cyclase (0.8 μ M**) ⁶⁰
IKK β (IC_{50} = 1 μ M) ⁶¹	
Ribonucleotide reductase (IC_{50} = 50 μ M) ⁶²	
NF- κ B (IC_{50} = 30 μ M) ⁶³	
Quinone reductase 2 (K_i = 35 nM) ⁵⁶	
Aromatase (IC_{50} = 25 μ M) ⁶⁴	

*concentration required to double activity, **resveratrol concentration tested

1.3. Quinone Reductase 2 (QR2)

Quinone reductase 2 (QR2) was discovered in 1961, when it was purified from bovine kidney, and is the second member of a small family of quinone reductases.⁶⁵ It was first described as a mammalian cytosolic FAD-dependent flavoprotein that catalyzed the oxidation of reduced *N*-ribosyl- and *N*-dihyronicotinamides by menadione and other quinone substrates.⁶⁵⁻⁶⁷ Interestingly, it was not found to catalyze the oxidation of the more common NAD(P)H or reduced nicotinamide mononucleotide (NMnH). After its initial discovery and characterization, it was generally forgotten about for the next 30 years. In 1990, QR2 was rediscovered by Jaiswal and coworkers in the process of their work cloning human QR1, when they isolated a second quinone oxidoreductase, which they termed NQO2.⁶⁸ It was not until 1997 that QR2 and NQO2 were reconciled to be the same enzyme by Zhao and coworkers.⁶⁹

1.3.1. QR1 vs. QR2 Comparison

The QR2 physiological homodimer of 231 amino acids per monomer is encoded for by the human QR2 gene located on chromosome 6p25 and is 43 residues shorter than QR1.^{70, 71} In contrast to QR1, which is known to be a cytoprotective detoxifying enzyme, the true in vivo function of QR2 is currently a mystery. The characterized function of QR1 is the deactivation of quinones via a two-electron reduction, producing hydroquinones that can be conjugated with glutathione or glucuronic acid and excreted from the body.⁷² QR2 has been shown to effect either the one-, two-, or four-electron reductions of quinones, quinone derivatives, some anti-malarial quinolones,^{73, 74} and certain nitro-containing compounds,⁷⁵ as well as being identified as the third melatonin

binding site.⁷⁶ In some cases, QR2 has been shown to catalyze the metabolic activation of quinones and anti-tumor drugs, producing reactive oxygen species and leading to cytotoxicity and cell death.⁷⁷⁻⁷⁹ Another difference between the two reductases is their cosubstrate specificity; QR1 is capable of using phosphorylated dihydronicotinamides as cosubstrates where QR2 is not, having been shown to use the reduced *N*-substituted nicotinamide analogues in vitro.⁷⁵ In addition, QR2 is a metalloenzyme, containing a zinc ion, the function of which has yet to be identified.⁶⁹ The two enzymes also have different tissue distribution profiles, where QR1 is ubiquitous in all tissue types⁸⁰ and QR2 tissue distribution appears to be highly dependent on the species investigated. In humans, QR2 expression is high in both skeletal muscle and the liver.^{70, 81}

Yet another distinction between the two reductases is their inhibitor profiles. A clear example of this is their opposite responses to resveratrol. Prochaska and coworkers found that resveratrol was able to increase QR1 activity with cultured mouse hepatoma (Hepa 1c1c7) cells at a concentration of 21 μM to double its enzymatic activity.²⁹ In contrast, resveratrol acts as a competitive inhibitor of QR2 against *N*-methyl-dihydronicotinamide (NMeH) with a K_i of 80 ± 20 nM and as an uncompetitive inhibitor of QR2 against menadione with a K_i of 0.9 ± 0.1 μM .⁴⁷

1.3.2. QR2 Catalytic Mechanism

QR2 operates via a classic ping-pong mechanism; first, the oxidized isoalloxazine ring of the FAD cofactor is reduced by accepting a hydride from the reduced nicotinamide, which forms the FADH₂-QR2 enzyme complex and releases the oxidized nicotinamide from the active site. The quinone substrate then enters the QR2 active site

and accepts a hydride from FADH₂, resulting in the two-electron reduction of the quinone substrate (Figure 1.3).^{74, 82} The QR2 active site is 17 Å long by 7 Å wide; three side of the active site are lined with hydrophobic amino acids, while the fourth side is solvent exposed. The two ends of the active site contain amino acids amenable for hydrogen bond formation (Gly174, Asn161, and Thr71).⁵⁶ These features of the QR2 active site, its narrow width and hydrophobic nature, allow only for the accommodation of molecules similar to resveratrol, molecules that can easily occupy essentially planar conformations. In addition, molecules that have been identified to bind tightly to QR2 are typically planar, polyaromatic, and have the ability to pi-stack with the isoalloxazine ring of FAD.^{83, 84}

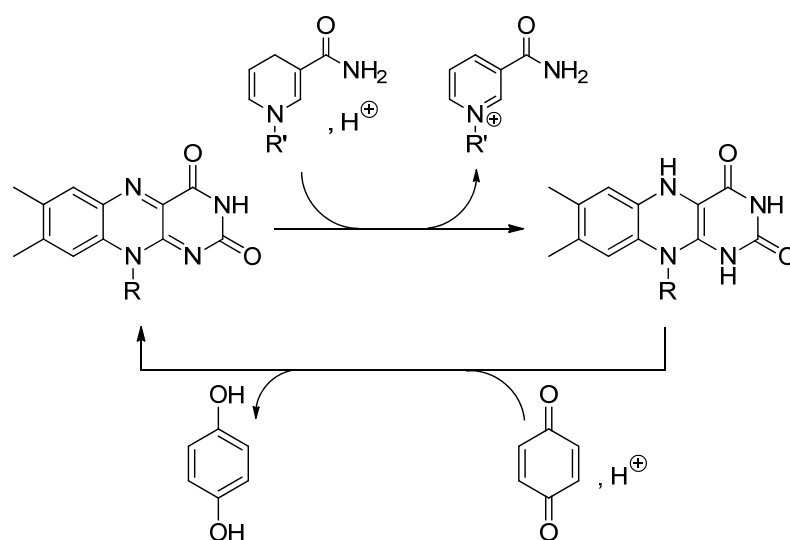


Figure 1.3. Mechanism of quinone reduction by QR2, where R = FAD chain, R' = alkyl.

1.3.3. Resveratrol and QR2

The mechanism by which resveratrol inhibits QR2 has been extensively studied. Resveratrol binds tightly in the active site of QR2, sitting parallel to the oxidized isoalloxazine ring of the bound FAD cofactor, in a perfectly flat conformation (Figure 1.4A). It is bound deep in the QR2 dimeric interface, filling a hydrophobic cleft (Figure 1.4B).⁵⁶ Each of the hydroxyl groups of resveratrol participate in stabilizing hydrogen bonding interactions with residues at the termini of the active site. The 4'-hydroxyl of resveratrol forms two water-mediated hydrogen bonds through ordered active site waters to Asp117 and Thr71. The 3-hydroxyl forms a direct hydrogen bond to Gly174 and the 5-hydroxyl forms a direct hydrogen bond to Asn161. The phenyl rings of resveratrol participate in van der Waals interactions with neighboring residues lining the interior of the active site cavity.

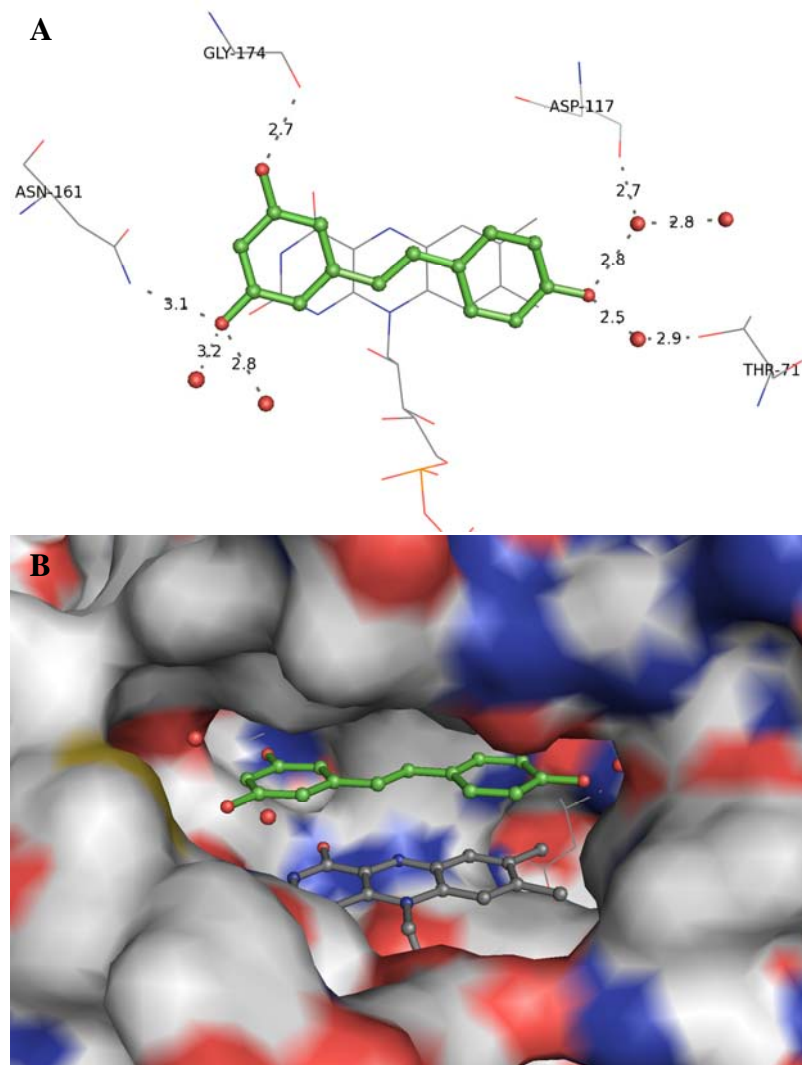


Figure 1.4. Resveratrol-QR2 complex (PDB: 1SG0) where resveratrol is shown in green, colored by atom type, and shown in ball and stick representation. Water molecules are shown as red spheres and distances are displayed by a grey dashed line labeled with the distance in Ångstroms (Å). (A) X-ray structure of resveratrol in complex with QR2, showing hydrogen bond network within QR2 active site, where the position of resveratrol parallel to the isoalloxazine ring of the FAD cofactor is displayed; (B) Resveratrol in QR2 active site, where QR2 is shown in grey surface representation and colored according to atom type and FAD cofactor is shown in grey ball and stick representation.⁵⁶

1.4. Interest in Resveratrol and its Targets

The biological activity of resveratrol – its ability to produce a vast assortment of beneficial health effects, not exert any known detrimental side effects, and the fact that it interacts with a host of targets – makes it an incredibly interesting research subject. There is much to be learned about resveratrol's interactions. One way to accomplish this is to make various structural modifications to resveratrol and determine what effect those modifications have on the molecule's activity. The work in the next two chapters of this thesis has been accomplished in an attempt to elucidate the structural and electronic features of resveratrol that make it such a unique molecule.

1.5. References

1. Stanley, L. L.; Mazier, M. J. P., Potential explanations for the French paradox. *Nutr. Res.* **1999**, *19* (1), 3-15.
2. Renaud, S.; Delorgeril, M., Wine, alcohol, platelets, and the French paradox for coronary heart-disease. *Lancet* **1992**, *339* (8808), 1523-1526.
3. Sun, A. Y.; Simonyi, A.; Sun, G. Y., The "French paradox" and beyond: neuroprotective effects of polyphenols. *Free Radical Biology and Medicine* **2002**, *32* (4), 314-318.
4. Takaoka, M. J., Of the phenolic substances of white hellebore (*Veratrum grandiflorum* Loes. fil.). *J. Faculty Sci. Hokkaido Imperial University* **1940**, *3*, 1-16.
5. Langcake, P.; Pryce, R. J., Production of resveratrol by *Vitis-Vinifera* and other members of vitaceae as a response to infection or injury. *Physiological Plant Pathology* **1976**, *9* (1), 77-86.
6. Langcake, P.; Pryce, R. J., The production of resveratrol and the viniferins by grapevines in response to ultraviolet irradiation. *Phytochemistry* **1977**, *16* (8), 1193-1196.
7. Siemann, E. H.; Creasy, L. L., Concentration of the phytoalexin resveratrol in wine. *Am. J. Enol. Vitic.* **1992**, *43* (1), 49-52.
8. Jang, M. S.; Cai, E. N.; Udeani, G. O.; Slowing, K. V.; Thomas, C. F.; Beecher, C. W. W.; Fong, H. H. S.; Farnsworth, N. R.; Kinghorn, A. D.; Mehta, R. G.; Moon, R. C.; Pezzuto, J. M., Cancer chemopreventive activity of resveratrol, a natural product derived from grapes. *Science* **1997**, *275* (5297), 218-220.
9. Bradamante, S.; Barenghi, L.; Villa, A., Cardiovascular protective effects of resveratrol. *Cardiovasc. Drug Rev.* **2004**, *22* (3), 169-188.
10. Wang, Q.; Xu, J. F.; Rottinghaus, G. E.; Simonyi, A.; Lubahn, D.; Sun, G. Y.; Sun, A. Y., Resveratrol protects against global cerebral ischemic injury in gerbils. *Brain Res.* **2002**, *958* (2), 439-447.
11. Sinha, K.; Chaudhary, G.; Gupta, Y. K., Protective effect of resveratrol against oxidative stress in middle cerebral artery occlusion model of stroke in rats. *Life Sci.* **2002**, *71* (6), 655-665.
12. Lee, S. M.; Yang, H.; Tartar, D. M.; Gao, B.; Luo, X.; Ye, S. Q.; Zaghoulani, H.; Fang, D., Prevention and treatment of diabetes with resveratrol in a non-obese mouse model of type 1 diabetes. *Diabetologia* *54* (5), 1136-1146.

13. Howitz, K. T.; Bitterman, K. J.; Cohen, H. Y.; Lamming, D. W.; Lavu, S.; Wood, J. G.; Zipkin, R. E.; Chung, P.; Kisielewski, A.; Zhang, L. L.; Scherer, B.; Sinclair, D. A., Small molecule activators of sirtuins extend *Saccharomyces cerevisiae* lifespan. *Nature* **2003**, *425* (6954), 191-196.
14. Valenzano, D. R.; Terzibasi, E.; Genade, T.; Cattaneo, A.; Domenici, L.; Cellerino, A., Resveratrol prolongs lifespan and retards the onset of age-related markers in a short-lived vertebrate. *Curr. Biol.* **2006**, *16* (3), 296-300.
15. Baur, J. A.; Sinclair, D. A., Therapeutic potential of resveratrol: the in vivo evidence. *Nat. Rev. Drug Discov.* **2006**, *5* (6), 493-506.
16. Goldberg, D. M.; Yan, J.; Ng, E.; Diamandis, E. P.; Karumanchiri, A.; Soleas, G.; Waterhouse, A. L., A Global survey of the trans-resveratrol concentrations in commercial wines. *Am. J. Enol. Vitic.* **1995**, *46* (2), 159-165.
17. Mark, L.; Nikfardjam, M. S. P.; Avar, P.; Ohmacht, R., A validated HPLC method for the quantitative analysis of trans-resveratrol and trans-piceid in Hungarian wines. *Journal of Chromatographic Science* **2005**, *43* (9), 445-449.
18. Vitrac, X.; Bornet, A.; Vanderlinde, R.; Valls, J.; Richard, T.; Delaunay, J. C.; Merillon, J. M.; Teissedre, P. L., Determination of stilbenes (delta-viniferin, trans-astringin, trans-piceid, cis- and trans-resveratrol, epsilon-viniferin) in Brazilian wines. *Journal of Agricultural and Food Chemistry* **2005**, *53* (14), 5664-5669.
19. Kiraly-Veghely, Z.; Tyihak, E.; Albert, L.; Nemeth, Z. I.; Katay, G., Identification and measurement of resveratrol and formaldehyde in parts of white and blue grape berries. *Acta Biologica Hungarica* **1998**, *49* (2-4), 281-289.
20. Burns, J.; Yokota, T.; Ashihara, H.; Lean, M. E. J.; Crozier, A., Plant foods and herbal sources of resveratrol. *Journal of Agricultural and Food Chemistry* **2002**, *50* (11), 3337-3340.
21. Creasy, L. L.; Coffee, M., Phytoalexin production potential of grape berries. *Journal of the American Society for Horticultural Science* **1988**, *113* (2), 230-234.
22. Wang, Y.; Catana, F.; Yang, Y. N.; Roderick, R.; van Breemen, R. B., An LC-MS method for analyzing total resveratrol in grape juice, cranberry juice, and in wine. *Journal of Agricultural and Food Chemistry* **2002**, *50* (3), 431-435.
23. Lyons, M. M.; Yu, C. W.; Toma, R. B.; Cho, S. Y.; Reiboldt, W.; Lee, J.; Van Breemen, R. B., Resveratrol in raw and baked blueberries and bilberries. *Journal of Agricultural and Food Chemistry* **2003**, *51* (20), 5867-5870.
24. Sanders, T. H.; McMichael, R. W.; Hendrix, K. W., Occurrence of resveratrol in edible peanuts. *Journal of Agricultural and Food Chemistry* **2000**, *48* (4), 1243-1246.

25. Sobolev, V. S.; Cole, R. J., trans-resveratrol content in commercial peanuts and peanut products. *Journal of Agricultural and Food Chemistry* **1999**, *47* (4), 1435-1439.
26. Tokusoglu, O.; Unal, M. K.; Yemis, F., Determination of the phytoalexin resveratrol (3,5,4'-trihydroxystilbene) in peanuts and pistachios by high-performance liquid chromatographic diode array (HPLC-DAD) and gas chromatography-mass Spectrometry (GC-MS). *Journal of Agricultural and Food Chemistry* **2005**, *53* (12), 5003-5009.
27. Callemien, D.; Jerkovic, V.; Rozenberg, R.; Collin, S., Hop as an interesting source of resveratrol for brewers: Optimization of the extraction and quantitative study by liquid chromatography/atmospheric pressure chemical ionization tandem mass spectrometry. *Journal of Agricultural and Food Chemistry* **2005**, *53* (2), 424-429.
28. Sharma, S.; Stutzman, J. D.; Kelloff, G. J.; Steele, V. E., Screening of potential chemopreventive agents using biochemical markers of carcinogenesis. *Cancer Res.* **1994**, *54* (22), 5848-5855.
29. Prochaska, H. J.; Santamaria, A. B., Direct measurement of NAD(P)H - quinone reductase from cells cultured in microtiter wells - a screening assay for anticarcinogenic enzyme inducers. *Analytical Biochemistry* **1988**, *169* (2), 328-336.
30. Wang, Z. R.; Huang, Y. Z.; Zou, J. G.; Cao, K. J.; Xu, Y. N.; Wu, J. M., Effects of red wine and wine polyphenol resveratrol on platelet aggregation in vivo and in vitro. *International Journal of Molecular Medicine* **2002**, *9* (1), 77-79.
31. Zini, R.; Morin, C.; Bertelli, A.; Bertelli, A. A. E.; Tillement, J. P., Effects of resveratrol on the rat brain respiratory chain. *Drugs under Experimental and Clinical Research* **1999**, *25* (2-3), 87-97.
32. Hamberg, M.; Svensson, J.; Samuelsson, B., Thromboxanes - new group of biologically active compounds derived from prostaglandin endoperoxides. *Proc. Natl. Acad. Sci. U. S. A.* **1975**, *72* (8), 2994-2998.
33. Moncada, S.; Gryglewski, R.; Bunting, S.; Vane, J. R., Enzyme isolated from arteries transforms prostaglandin endoperoxides to an unstable substance that inhibits platelet-aggregation. *Nature* **1976**, *263* (5579), 663-665.
34. Barger, J. L.; Walford, R. L.; Weindruch, R., The retardation of aging by caloric restriction: its significance in the transgenic era. *Experimental Gerontology* **2003**, *38* (11-12), 1343-1351.
35. Brachmann, C. B.; Sherman, J. M.; Devine, S. E.; Cameron, E. E.; Pillus, L.; Boeke, J. D., The Sir2 gene family, conserved from bacteria to humans, functions in silencing, cell-cycle progression, and chromosome stability. *Genes & Development* **1995**, *9* (23), 2888-2902.

36. Lin, S. J.; Defossez, P. A.; Guarente, L., Requirement of NAD and SIR2 for life-span extension by calorie restriction in *Saccharomyces cerevisiae*. *Science* **2000**, *289* (5487), 2126-2128.
37. Kaerberlein, M.; McVey, M.; Guarente, L., The SIR2/3/4 complex and SIR2 alone promote longevity in *Saccharomyces cerevisiae* by two different mechanisms. *Genes & Development* **1999**, *13* (19), 2570-2580.
38. Tissenbaum, H. A.; Guarente, L., Increased dosage of a sir-2 gene extends lifespan in *Caenorhabditis elegans*. *Nature* **2001**, *410* (6825), 227-230.
39. Rogina, B.; Helfand, S. L., Sir2 mediates longevity in the fly through a pathway related to calorie restriction. *Proc. Natl. Acad. Sci. U. S. A.* **2004**, *101* (45), 15998-16003.
40. Banks, A. S.; Kon, N.; Knight, C.; Matsumoto, M.; Gutierrez-Juarez, R.; Rossetti, L.; Gu, W.; Accili, D., SirT1 Gain of Function Increases Energy Efficiency and Prevents Diabetes in Mice. *Cell Metabolism* **2008**, *8* (4), 333-341.
41. Herranz, D.; Munoz-Martin, M.; Canamero, M.; Mulero, F.; Martinez-Pastor, B.; Fernandez-Capetillo, O.; Serrano, M., Sirt1 improves healthy ageing and protects from metabolic syndrome-associated cancer. *Nature Communications* *1*.
42. Donmez, G.; Guarente, L., Aging and disease: connections to sirtuins. *Aging Cell* *9* (2), 285-290.
43. Pearson, K. J.; Baur, J. A.; Lewis, K. N.; Peshkin, L.; Price, N. L.; Labinskyy, N.; Swindell, W. R.; Kamara, D.; Minor, R. K.; Perez, E.; Jamieson, H. A.; Zhang, Y.; Dunn, S. R.; Sharma, K.; Pleshko, N.; Woollett, L. A.; Csiszar, A.; Ikeno, Y.; Le Couteur, D.; Elliott, P. J.; Becker, K. G.; Navas, P.; Ingram, D. K.; Wolf, N. S.; Ungvari, Z.; Sinclair, D. A.; de Cabo, R., Resveratrol delays age-related deterioration and mimics transcriptional aspects of dietary restriction without extending life span. *Cell Metabolism* **2008**, *8* (2), 157-168.
44. Kaerberlein, M.; McDonagh, T.; Heltweg, B.; Hixon, J.; Westman, E. A.; Caldwell, S. D.; Napper, A.; Curtis, R.; DiStefano, P. S.; Fields, S.; Bedalov, A.; Kennedy, B. K., Substrate-specific activation of sirtuins by resveratrol. *J. Biol. Chem.* **2005**, *280* (17), 17038-17045.
45. Borra, M. T.; Smith, B. C.; Denu, J. M., Mechanism of human SIRT1 activation by resveratrol. *J. Biol. Chem.* **2005**, *280* (17), 17187-17195.
46. Park, S. J.; Ahmad, F.; Philp, A.; Baar, K.; Williams, T.; Luo, H. B.; Ke, H. M.; Rehmann, H.; Taussig, R.; Brown, A. L.; Kim, M. K.; Beaven, M. A.; Burgin, A. B.; Manganiello, V.; Chung, J. H., Resveratrol Ameliorates Aging-Related Metabolic Phenotypes by Inhibiting cAMP Phosphodiesterases. *Cell* *148* (3), 421-433.

47. Calamini, B.; Ratia, K.; Malkowski, M. G.; Cuendet, M.; Pezzuto, J. M.; Santarsiero, B. D.; Mesecar, A. D., Pleiotropic mechanisms facilitated by resveratrol and its metabolites. *Biochem. J.* **2010**, *429*, 273-282.
48. Boocock, D. J.; Patel, K. R.; Faust, G. E. S.; Normolle, D. P.; Marczylo, T. H.; Crowell, J. A.; Brenner, D. E.; Booth, T. D.; Gescher, A.; Steward, W. P., Quantitation of trans-resveratrol and detection of its metabolites in human plasma and urine by high performance liquid chromatography. *J. Chromatogr. B* **2007**, *848* (2), 182-187.
49. De Santi, C.; Pietrabissa, A.; Mosca, F.; Pacifici, G. M., Glucuronidation of resveratrol, a natural product present in grape and wine, in the human liver. *Xenobiotica* **2000**, *30* (11), 1047-1054.
50. De Santi, C.; Pietrabissa, A.; Spisni, R.; Mosca, F.; Pacifici, G. M., Sulphation of resveratrol, a natural compound present in wine, and its inhibition by natural flavonoids. *Xenobiotica* **2000**, *30* (9), 857-866.
51. Walle, T.; Hsieh, F.; DeLegge, M. H.; Oatis, J. E.; Walle, U. K., High absorption but very low bioavailability of oral resveratrol in humans. *Drug Metabolism and Disposition* **2004**, *32* (12), 1377-1382.
52. Pirola, L.; Frojdo, S., Resveratrol: One molecule, many targets. *IUBMB Life* **2008**, *60* (5), 323-332.
53. Kimura, Y.; Okuda, H.; Arichi, S., Effects of stilbenes on arachidonate metabolism in leukocytes. *Biochimica Et Biophysica Acta* **1985**, *834* (2), 275-278.
54. Wood, J. G.; Rogina, B.; Lavu, S.; Howitz, K.; Helfand, S. L.; Tatar, M.; Sinclair, D., Sirtuin activators mimic caloric restriction and delay ageing in metazoans. *Nature* **2004**, *430* (7000), 686-689.
55. Smith, C. J.; Zhang, Y.; Koboldt, C. M.; Muhammad, J.; Zweifel, B. S.; Shaffer, A.; Talley, J. J.; Masferrer, J. L.; Seibert, K.; Isakson, P. C., Pharmacological analysis of cyclooxygenase-1 in inflammation. *Proc. Natl. Acad. Sci. U. S. A.* **1998**, *95* (22), 13313-13318.
56. Buryanovskyy, L.; Fu, Y.; Boyd, M.; Ma, Y. L.; Hsieh, T. C.; Wu, J. M.; Zhang, Z. T., Crystal structure of quinone reductase 2 in complex with resveratrol. *Biochemistry* **2004**, *43* (36), 11417-11426.
57. Subbaramaiah, K.; Michaluart, P.; Chung, W. J.; Tanabe, T.; Telang, N.; Dannenberg, A. J., Resveratrol inhibits cyclooxygenase-2 transcription in human mammary epithelial cells. In *Cancer Prevention: Novel Nutrient and Pharmaceutical Developments*, Bradlow, H. L.; Fishman, J.; Osborne, M. P., Eds. New York Acad Sciences: New York, 1999; Vol. 889, pp 214-223.

58. Baur, J. A.; Pearson, K. J.; Price, N. L.; Jamieson, H. A.; Lerin, C.; Kalra, A.; Prabhu, V. V.; Allard, J. S.; Lopez-Lluch, G.; Lewis, K.; Pistell, P. J.; Poosala, S.; Becker, K. G.; Boss, O.; Gwinn, D.; Wang, M. Y.; Ramaswamy, S.; Fishbein, K. W.; Spencer, R. G.; Lakatta, E. G.; Le Couteur, D.; Shaw, R. J.; Navas, P.; Puigserver, P.; Ingram, D. K.; de Cabo, R.; Sinclair, D. A., Resveratrol improves health and survival of mice on a high-calorie diet. *Nature* **2006**, *444* (7117), 337-342.
59. Atten, M. J.; Godoy-Romero, E.; Attar, B. M.; Milson, T.; Zopel, M.; Holian, O., Resveratrol regulates cellular PKC alpha and delta to inhibit growth and induce apoptosis in gastric cancer cells. *Invest. New Drugs* **2005**, *23* (2), 111-119.
60. El-Mowafy, A. M.; Alkhalaf, M., Resveratrol activates adenylyl-cyclase in human breast cancer cells: a novel, estrogen receptor-independent cytostatic mechanism. *Carcinogenesis* **2003**, *24* (5), 869-873.
61. Kundu, J. K.; Shin, Y. K.; Kim, S. H.; Surh, Y. J., Resveratrol inhibits phorbol ester-induced expression of COX-2 and activation of NF-kappa B in mouse skin by blocking I kappa B kinase activity. *Carcinogenesis* **2006**, *27* (7), 1465-1474.
62. Fontecave, M.; Lepoivre, M.; Elleingand, E.; Gerez, C.; Guittet, O., Resveratrol, a remarkable inhibitor of ribonucleotide reductase. *Febs Letters* **1998**, *421* (3), 277-279.
63. Holmes-McNary, M.; Baldwin, A. S., Chemopreventive properties of trans-resveratrol are associated with inhibition of activation of the I kappa B kinase. *Cancer Res.* **2000**, *60* (13), 3477-3483.
64. Wang, Y.; Leung, L. K., Pharmacological concentration of resveratrol suppresses aromatase in JEG-3 cells. *Toxicology Letters* **2007**, *173* (3), 175-180.
65. Liao, S.; Williamsashman, H. G., Enzymatic oxidation of some non-phosphorylated derivatives of dihydronicotinamide. *Biochem. Biophys. Res. Commun.* **1961**, *4* (3), 208-&.
66. Liao, S.; Williamsashman, H. G., Inhibition of enzymatic oxidation of some dihydropyridines by polycyclic aromatic hydrocarbons. *Biochem. Pharmacol.* **1961**, *6* (1-2), 53-&.
67. Liao, S.; Dulaney, J. T.; Williamsashman, H. G., Purification and properties of a flavoprotein catalyzing oxidation of reduced ribosyl nicotinamide. *J. Biol. Chem.* **1962**, *237* (9), 2981-&.
68. Jaiswal, A. K.; Burnett, P.; Adesnik, M.; McBride, O. W., Nucleotide and deduced amino-acid-sequence of a human CDNA (NQO2) corresponding to a 2nd member of the NAD(P)H - quinone oxidoreductase gene family - extensive polymorphism at the NQO2 gene locus on chromosome-6. *Biochemistry* **1990**, *29* (7), 1899-1906.

69. Zhao, Q. J.; Yang, X. L.; Holtzclaw, W. D.; Talalay, P., Unexpected genetic and structural relationships of a long-forgotten flavoenzyme to NAD(P)H:quinone reductase (DT-diaphorase). *Proc. Natl. Acad. Sci. U. S. A.* **1997**, *94* (5), 1669-1674.
70. Long, D. J.; Jaiswal, A. K., NRH : quinone oxidoreductase2 (NQO2). *Chemico-Biological Interactions* **2000**, *129* (1-2), 99-112.
71. Jaiswal, A. K.; Bell, D. W.; Radjendirane, V.; Testa, J. R., Localization of human NQO1 gene to chromosome 16q22 and NQO2-6p25 and associated polymorphisms. *Pharmacogenetics* **1999**, *9* (3), 413-418.
72. Vella, F.; Gilles, F. A.; Delagrangé, P.; Boutin, J. A., NRH : quinone reductase 2: An enzyme of surprises and mysteries. *Biochem. Pharmacol.* **2005**, *71* (1-2), 1-12.
73. Graves, P. R.; Kwiek, J. J.; Fadden, P.; Ray, R.; Hardeman, K.; Coley, A. M.; Foley, M.; Haystead, T. A. J., Discovery of novel targets of quinoline drugs in the human purine binding proteome. *Molecular Pharmacology* **2002**, *62* (6), 1364-1372.
74. Kwiek, J. J.; Haystead, T. A. J.; Rudolph, J., Kinetic mechanism of quinone oxidoreductase 2 and its inhibition by the antimalarial quinolines. *Biochemistry* **2004**, *43* (15), 4538-4547.
75. Wu, K. B.; Knox, R.; Sun, X. Z.; Joseph, P.; Jaiswal, A. K.; Zhang, D.; Deng, P. S. K.; Chen, S., Catalytic properties of NAD(P)H:quinone oxidoreductase-2 (NQO2), a dihydronicotinamide riboside dependent oxidoreductase. *Arch. Biochem. Biophys.* **1997**, *347* (2), 221-228.
76. Mailliet, F.; Ferry, G.; Vella, F.; Thiam, K.; Delagrangé, P.; Boutin, J. A., Organs from mice deleted for NRH : quinone oxidoreductase 2 are deprived of the melatonin binding site MT3. *Febs Letters* **2004**, *578* (1-2), 116-120.
77. Celli, C. M.; Tran, N.; Knox, R.; Jaiswal, A. K., NRH : quinone oxidoreductase 2 (NQO2) catalyzes metabolic activation of quinones and anti-tumor drugs. *Biochem. Pharmacol.* **2006**, *72* (3), 366-376.
78. Jamieson, D.; Tung, A. T. Y.; Knox, R. J.; Boddy, A. V., Reduction of mitomycin C is catalysed by human recombinant NRH : quinone oxidoreductase 2 using reduced nicotinamide adenine dinucleotide as an electron donating co-factor. *Br. J. Cancer* **2006**, *95* (9), 1229-1233.
79. Knox, R. J.; Jenkins, T. C.; Hobbs, S. M.; Chen, S. A.; Melton, R. G.; Burke, P. J., Bioactivation of 5-(aziridin-1-yl)-2,4-dinitrobenzamide (CB 1954) by human NAD(P)H quinone oxidoreductase 2: A novel co-substrate-mediated antitumor prodrug therapy. *Cancer Res.* **2000**, *60* (15), 4179-4186.

80. Talalay, P.; Fahey, J. W.; Holtzclaw, W. D.; Prester, T.; Zhang, Y., Chemoprotection against cancer by Phase 2 enzyme induction. *Toxicology Letters* **1995**, *82-83* (0), 173-179.
81. Jaiswal, A. K., Human NAD(P)H - quinone oxidoreductase(2) - gene structure, activity, and tissue-specific expression. *J. Biol. Chem.* **1994**, *269* (20), 14502-14508.
82. Li, R. B.; Bianchet, M. A.; Talalay, P.; Amzel, L. M., The 3-dimensional structure of NAD(P)H - quinone reductase, a flavoprotein involved in cancer chemoprotection and chemotherapy - mechanism of the 2-electron reduction. *Proc. Natl. Acad. Sci. U. S. A.* **1995**, *92* (19), 8846-8850.
83. Foster, C. E.; Bianchet, M. A.; Talalay, P.; Faig, M.; Amzel, L. M., Structures of mammalian cytosolic quinone reductases. *Free Radical Biology and Medicine* **2000**, *29* (3-4), 241-245.
84. Zhou, Z.; Fisher, D.; Spidel, J.; Greenfield, J.; Patson, B.; Fazal, A.; Wigal, C.; Moe, O. A.; Madura, J. D., Kinetic and Docking Studies of the Interaction of Quinones with the Quinone Reductase Active Site. *Biochemistry* **2003**, *42* (7), 1985-1994.

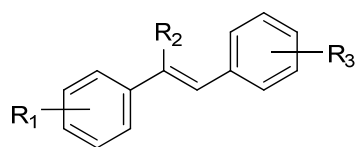
CHAPTER TWO:
QSAR DETERMINATION FOR COX1, COX2, NF- κ B, AND QR2 RESVERATROL
ANALOGUE MODELS

2.1. Previous Work

To begin to address the problems with using resveratrol as a therapeutic lead, previous Lipton Research Group member Dr. SooSung Kang synthesized a small library of 78 resveratrol analogues. These resveratrol analogues were designed to probe the different steric and electronic requirements of the central olefin and aryl rings of resveratrol. To do this, several electron-donating (OH, OMe, and NMe₂) and electron-withdrawing (F, CF₃, and NO₂) as well as naphthyl substituents were chosen to decorate the aryl rings. Four substituents (H, Me, Et, and CF₃) were chosen to investigate the steric and electron demands of the central olefin. The design, synthesis, and evaluation of this library against COX1, COX2, and NF- κ B has been previously published.¹

These analogues were tested for COX1, COX2, and NF- κ B inhibition by the research laboratory of Prof. John Pezzuto of the Department of Medicinal Chemistry and Molecular Pharmacology at Purdue University. The COX1 assay was accomplished using an initial screen for COX1 inhibition of each of the resveratrol analogues at a concentration of 10 μ g/ml. Analogues that showed at least 50%

enzymatic inhibition of COX1 at that concentration were then reassayed in triplicate to determine an IC_{50} value and standard deviation. The COX2 assay was carried out similarly to the COX1 assay. Inhibition of NF- κ B was determined using a luciferase reporter gene assay where the resveratrol analogues were initially screened at a concentration of 20 μ g/ml. The library members that showed more than 50% inhibition at that concentration were then reassayed in duplicate to determine an IC_{50} value and standard deviation. Library members were tested for QR2 inhibition by Dr. Barbara Calamini and Prof. Andrew Mesecar of the Center for Pharmaceutical Biotechnology and Department of Medicinal Chemistry and Pharmacognosy, College of Pharmacy at The University of Illinois at Chicago. Briefly, the enzymatic activity of QR2 at steady-state was determined using an assay where NMeH (*N*-methyldihydronicotinamide) was used as a co-substrate and menadione was used as the quinone substrate, and the activity of QR2 was followed by monitoring the decrease in absorbance of NMeH at 360 nm. The resveratrol analogues were tested at 100 μ M and IC_{50} values were determined for compounds that showed greater than 50% inhibition of QR2 at this concentration. The results of this library's inhibition of COX1, COX2, NF- κ B, and QR2 are summarized in Table 2.1.

Table 2.1. Inhibition of COX1, COX2, NF- κ B, and QR2 by first generation resveratrol analogue library.

L.M. ^a	R ₁	R ₂	R ₃	IC ₅₀ (μM)			
				COX1	COX2	NF- κ B	QR2
Res	4-OH	H	3,5-(OH) ₂	0.83	0.99	16.1	11.5
2.1a	4-OH	H	3,4-(OH) ₂	--	--	12.7	6.0
2.1b	4-OH	H	3,5-(OMe) ₂	0.70	0.82	19.5	5.1
2.1c	3,4-(OH) ₂	H	4-OMe	--	--	12.2	9.3
2.1d	3,4-(OH) ₂	H	3-F	11.5	--	10.3	20.8
2.1e	3,4-(OH) ₂	H	4-CF ₃	--	--	--	14.2
2.1f	4-OMe	H	3,5-(OMe) ₂	--	--	28.3	14.6
2.1g	3,5-(OMe) ₂	H	3,4-(OMe) ₂	--	--	--	37.1
2.1h	3,5-(OMe) ₂	H	4-F	--	--	37.5	4.6
2.1i	3,5-(OMe) ₂	H	2-Naphthyl	--	--	18.8	0.73
2.1j	3,4-(OMe) ₂	H	3-OMe	--	--	17.3	6.8
2.1k	3,4-(OMe) ₂	H	4-NMe ₂	--	--	--	13.0
2.1l	3,4-(OMe) ₂	H	2-Naphthyl	--	--	--	5.5
2.1m	4-OH	Me	3,5-(OH) ₂	1.9	1.57	--	39.0
2.1n	4-OH	Me	4-CF ₃	--	--	--	2.8
2.1o	3,5-(OH) ₂	Me	4-OH	1.9	1.78	26.2	4.8
2.1p	4-OMe	Me	3,5-(OH) ₂	12.4	16.0	35.2	12.0
2.1q	4-OMe	Me	3,5-(OMe) ₂	--	--	27.1	20.1
2.1r	4-OMe	Me	3,4-(OMe) ₂	--	--	--	6.7
2.1s	3,4-(OMe) ₂	Me	3,5-(OH) ₂	11.4	--	13.1	33.7
2.1t	3,4-(OMe) ₂	Me	3,5-(OMe) ₂	--	--	--	9.9
2.1u	3,5-(OMe) ₂	CF ₃	4-OMe	7.8	--	--	13.0
2.1v	3-CF ₃	CF ₃	3,4-(OMe) ₂	--	--	25.5	0.18

Table 2.1, continued

L.M. ^a	R ₁	R ₂	R ₃	IC ₅₀ (μM)			
				COX1	COX2	NF-κB	QR2
2.1w	3,5-(OH) ₂	Et	4-NMe ₂	0.99	--	--	10.9
2.1x	3,4-(OMe) ₂	Et	3,5-(OMe) ₂	--	--	27.2	16.3
2.1y	4-OH	CF ₃	3,5-(OH) ₂	--	--	--	--
2.1z	4-OMe	CF ₃	3,5-(OH) ₂	--	--	--	--
2.1aa	3-CF ₃	CF ₃	3,5-(OMe) ₂	--	--	31.9	--
2.1ab	4-F	CF ₃	3,5-(OMe) ₂	3.0	--	39.0	--
2.1ac	4-OMe	CF ₃	3,5-(OMe) ₂	--	--	37.8	--
2.1ad	3,5-(OH) ₂	H	4-OMe	25.8	19.6	--	--
2.1ae	3,5-(OH) ₂	H	3,4-(OMe) ₂	0.29	21.3	--	--
2.1af	3,5-(OH) ₂	H	3-F	16.5	--	--	--
2.1ag	3,5-(OH) ₂	H	4-F	51.3	--	52.1	--
2.1ah	3,5-(OH) ₂	H	4-Me ₂ N	29.7	--	12.9	--
2.1ai	3,5-(OH) ₂	H	4-NO ₂	2.2	31.6	--	--
2.1aj	3,5-(OH) ₂	H	2-Naphthyl	18.4	--	--	--
2.1ak	3,5-(OH) ₂	H	4-CF ₃	17.8	--	--	--
2.1al	3,4-(OH) ₂	H	4-F	--	--	17.9	--
2.1am	3,4-(OH) ₂	H	4-Me ₂ N	--	--	14.8	--
2.1an	3,4-(OH) ₂	H	2-Naphthyl	--	--	6.9	--
2.1ao	4-OMe	H	3,4-(OMe) ₂	--	--	52.0	--
2.1ap	3,5-(OMe) ₂	H	3-F	--	--	--	--
2.1aq	3,5-(OMe) ₂	H	4-Me ₂ N	--	--	--	--
2.1ar	3,5-(OMe) ₂	H	4-NO ₂	10.1	5.94	--	--
2.1as	3,5-(OMe) ₂	H	4-CF ₃	--	--	--	--
2.1at	3,4-(OMe) ₂	H	3-F	3.2	--	38.8	--
2.1au	3,4-(OMe) ₂	H	4-NO ₂	--	--	--	--
2.1av	3,4-(OMe) ₂	H	4-CF ₃	--	--	34.7	--
2.1aw	4-OH	Me	3,4-(OH) ₂	--	--	21.3	--
2.1ax	4-OH	Me	3,5-(OMe) ₂	--	--	--	--
2.1ay	4-OH	Me	4-Me ₂ N	36.3	0.47	--	--

Table 2.1, continued

L.M. ^a	R ₁	R ₂	R ₃	IC ₅₀ (μM)			
				COX1	COX2	NF-κB	QR2
2.1az	3,5-(OH) ₂	Me	3,4-(OMe) ₂	10.6	12.8	--	103.8
2.1ba	3,5-(OH) ₂	Me	3-F	10.5	--	--	--
2.1bb	3,5-(OH) ₂	Me	4-F	--	--	--	--
2.1bc	3,5-(OH) ₂	Me	4-Me ₂ N	10.9	--	--	--
2.1bd	3,5-(OH) ₂	Me	2-Naphthyl	--	--	42.3	--
2.1be	3,5-(OH) ₂	Me	4-CF ₃	10.7	1.74	--	--
2.1bf	4-OMe	Me	2-Naphthyl	--	--	48.2	--
2.1bg	4-Cl	Me	3,5-(OH) ₂	5.3	--	39.2	--
2.1bh	4-Cl	Me	3,4-(OH) ₂	--	--	37.5	--
2.1bi	3-F	Me	3,5-(OH) ₂	4.9	2.54	--	--
2.1bj	4-Me ₂ N	Me	3,5-(OH) ₂	0.97	--	34.2	--
2.1bk	4-Me ₂ N	Me	3,4-(OH) ₂	--	--	--	--
2.1bl	4-Me ₂ N	Me	3,5-(OMe) ₂	32.6	--	--	--
2.1bm	4-OH	Et	3,5-(OH) ₂	--	--	--	--
2.1bn	4-OH	Et	3,5-(OMe) ₂	--	--	--	--
2.1bo	3,5-(OH) ₂	Et	3,4-(OMe) ₂	9.7	--	--	--
2.1bp	3,5-(OH) ₂	Et	3-F	5.4	--	--	--
2.1bq	3,5-(OH) ₂	Et	4-F	--	--	--	--
2.1br	3,5-(OH) ₂	Et	2-Naphthyl	--	--	--	--
2.1bs	3,5-(OH) ₂	Et	4-CF ₃	7.4	2.2	--	--
2.1bt	4-Cl	Et	3,5-(OH) ₂	11.6	--	38.3	--
2.1bu	4-Cl	Et	3,4-(OH) ₂	--	--	--	--
2.1bv	3-F	Et	3,5-(OH) ₂	3.5	17.7	25.7	--
2.1bw	2-Naphthyl	Et	3,5-(OH) ₂	0.17	3.3	--	--
2.1bx	4-CF ₃	Et	3,5-(OH) ₂	30.5	14.8	--	--
2.1by	4-CF ₃	Et	3,4-(OH) ₂	--	--	--	--

^aL.M. = library member

2.2. Structure-Activity Relationships (SARs)

Twenty-five library members were found to inhibit COX1 over 50% at a concentration of 10 $\mu\text{g/ml}$. Of those twenty-five, eight had IC_{50} values similar to or better than resveratrol: **2.1b**, **2.1m**, **2.1o**, **2.1w**, **2.1ae**, **2.1ai**, **2.1bj**, and **2.1bw**. Examination of the potent inhibitors proves that a resorcinol ring is present in all of the compounds; however, in **2.1b** it is methylated. This may be a consequence of the free-hydroxyls forming stabilizing hydrogen-bonds within the COX1 active site. Additionally, an electron-rich aryl ring may be required for potent inhibition. Five of the eight potent inhibitors had substituted central alkenes, possibly indicating that a perfectly planar structure is not required for inhibition of COX1. Further evidence to support this hypothesis comes the fact that the inhibitors **2.1o** and **2.1m**, which only differ by the location of the alkene-methyl group relative to the resorcinol ring, have the same IC_{50} value of 1.90 μM . Additional support of this hypothesis is found in the most potent COX1 inhibitor in the library, compound **2.1bw**, which has an ethyl-group functionalizing its central alkene. Comparison of **2.1bw** to the compound **2.1aj**, an analogue of **2.1bw** that lacks the central-alkene ethyl substituent, proves that the ethyl group is required for potent inhibition as **2.1aj** is 100-fold less active than **2.1bw**. Finally, it appears that the ring opposite the resorcinol is able to tolerate a wide variety of substitution, albeit most of the rings are relatively electron-rich. From these results, the compound **2.1bc** was identified for selective inhibition of COX1.

Seventeen library members were found to inhibit COX2 over 50% at a concentration of 10 $\mu\text{g/ml}$. Of those seventeen, seven had IC_{50} values similar to or better than resveratrol: **2.1b**, **2.1m**, **2.1o**, **2.1ay**, **2.1be**, **2.1bi**, and **2.1bw**. Four of the analogues

were also good inhibitors of COX1: **2.1b**, **2.1m**, **2.1o**, and **2.1bw**. Five of the seven inhibitors had a resorcinol ring; however, in **2.1b** it was methylated. Again, this may indicate that the free resorcinol hydroxyls are important for hydrogen-bonding within the active site. Possibly of more consequence, all of the potent COX2 inhibitors have at least one very electron-rich aryl ring. Six of the seven best inhibitors had a substituted central alkene, indicating that possibly COX2 also recognizes a form of resveratrol that is not completely planar.

Twenty-six of the seventy-eight compounds tested were found to inhibit NF- κ B. Seven of the active inhibitors had IC₅₀ values similar to or better than resveratrol: **2.1a**, **2.1c**, **2.1d**, **2.1s**, **2.1ah**, **2.1am**, and **2.1an**. Six of the most potent inhibitors had unsubstituted central alkenes, and the seventh (**2.1s**) had a methyl substituent, indicating that for potent inhibition of NF- κ B, less steric bulk around the central olefin is required. Additionally, this finding points to a planar binding conformation of resveratrol. All of the most active compounds were found to contain a catechol ring, and with the exception of **2.1s**, all of the catechol hydroxyls are free. Again, this may signify that free hydroxyls are required for hydrogen-bonding within the NF- κ B active site.

Twenty-six of the seventy-eight library members were found to inhibit QR2. Of those twenty-six, thirteen showed inhibition similar to or better than resveratrol: **2.1a**, **2.1b**, **2.1c**, **2.1h**, **2.1i**, **2.1j**, **2.1l**, **2.1n**, **2.1o**, **2.1r**, **2.1t**, **2.1v**, and **2.1w**. The two most active compounds **2.1i** and **2.1v** were substantially more potent than resveratrol and had IC₅₀ values greater than 20 μ M for COX1, COX2, and NF- κ B, giving them at least 30-fold selectivity for QR2. Six of the thirteen potent compounds were found to have substituted central olefins, indicating that the active site of QR2 either (a) accommodates

a non-planar structure of resveratrol, or (b) the alkene-substituted molecules are able to adopt a different binding conformation than resveratrol. Examination of the crystal structure of resveratrol bound to QR2 (Chapter 1, Figure 1.4) indicates that there may be room for the alkene-substituent on the solvent exposed side of the QR2 active site. Seven of the most active compounds did not have free hydroxyl groups, which may imply that the stabilizing hydrogen-bonds resveratrol makes within the QR2 active site are not rigorously required for QR2 inhibition, or that the library members lacking hydroxyl groups that inhibit QR2 potentially bind in a different conformation or location.

These initial data from the work for Dr. SooSung Kang, the Pezzuto lab, and the Mesecar lab resulted in at least one compound for each enzyme target that had activity superior to resveratrol. Additionally, some initial SARs for the interactions of the compounds with the targets were generated, producing hypothetical pharmacophore models. To maximize the benefit of these SAR models, and to more fully elucidate the importance of the physical attributes of the analogues that increase their potency toward their respective targets, we set out to determine quantitative structure-activity relationships (QSARs) for each system. Herein, we describe the use of QSARs and 3D-QSARs to develop quantitative models for the interaction of the resveratrol analogues with COX1, COX2, NF- κ B, and QR2.

2.3. Quantitative Structure-Activity Relationships (QSARs)

Quantitative structure-activity relationships (QSARs) use the similarity principle, the observation that chemically similar compounds tend to have similar biological activity, to try and understand the quantitative correlation between the structural and electronic elements of molecules that dictate their biological activities. In order to do this, various molecular descriptors are used. Molecular descriptors are the structural and electronic factors of a compound that can be quantified to describe a specific molecular property of the compound. The molecular descriptors chosen for the analysis of the seventy-eight resveratrol analogues were the Hammett parameter (σ), the Taft steric parameter (E_s), and the hydrophobic parameter (π). These parameters were chosen to describe the electronic, steric, and hydrophobic properties of the compounds, respectively. Stepwise regression was then used to determine QSARs.

2.3.1. Molecular Descriptors

The Hammett parameter (σ) was originally described by Louis P. Hammett in 1937.² Hammett observed that the position and electronic nature of a benzoic acid substituent had a measurable effect on the acidity of benzoic acid; when a substituent was electron donating, acidity decreased, and when a substituent was electron withdrawing, acidity increased. Hammett was able to quantify this effect with the parameters σ_{meta} and σ_{para} , where $\sigma = \log(K_a/K_a^0)$ and K_a is the acidity constant of the substituted benzoic acid, K_a^0 is the acidity constant of unsubstituted benzoic acid (Figure 2.1). Negative values of σ indicate a substituent is electron-donating, while positive values of σ indicate a

substituent is electron-withdrawing. The σ value for hydrogen, no matter the position, is always zero.

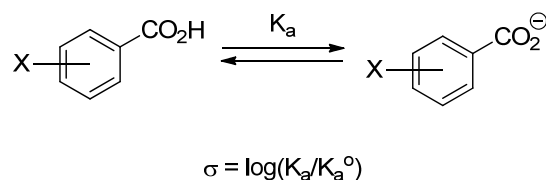


Figure 2.1. Determination of Hammett parameter.

The Taft steric parameter (E_S) was described by Robert W. Taft Jr. in 1952.^{3, 4} Taft proposed his parameter as a modification to the Hammett equation, as a way to factor in the effect of steric bulk of a substituent on reaction rate. To determine E_S , Taft investigated the rate of acid-catalyzed methyl ester hydrolysis (Figure 2.2), where $E_S = (1/\delta)\log(k_s/k_{CH_3})$ and δ is the reaction constant describing susceptibility to steric effects ($\delta = 1$ for reference reaction ($R = CH_3$)), k_s is the rate of the investigated reaction, k_{CH_3} is the rate of the reference reaction. All substituents have a negative value of E_S except hydrogen, and the more sterically bulky a substituent is, the more negative the value of E_S is.

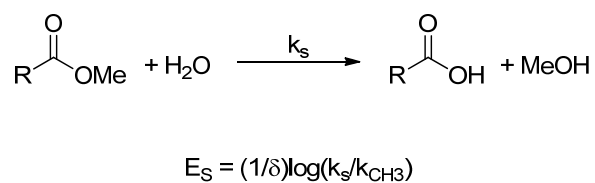


Figure 2.2. Determination of Taft steric parameter.

The hydrophobic parameter (π) describes how hydrophobic or hydrophilic a particular substituent is. The hydrophobic parameter is defined from the partition coefficient (P) of a molecule, where $P = [\text{drug}]_{\text{octanol}}/[\text{drug}]_{\text{water}}$. Applying the logarithm, this equation becomes: $\log P = \log[\text{drug}]_{\text{octanol}} - \log[\text{drug}]_{\text{water}}$. The particular contribution of a substituent, the hydrophobic parameter (π), is arrived then arrived at by the equation: $\pi_x = \log P_{\text{substituted compound}} - \log P_{\text{parent compound}}$, or $\pi_x = \log(P_{RX}/P_{RH})$. Positive values of π indicate a substituent that is more hydrophobic than hydrogen, negative values of π indicate a substituent that is less hydrophobic than hydrogen, where $\pi = 0$ for hydrogen. Table 2.2 is a compilation of the molecular descriptors used in the determination of QSAR models.

Table 2.2. Molecular descriptors used for the construction of QSAR models.

Substituent	σ_m	σ_p	E_S	π
OH	0.12	-0.37	-0.55	-0.67
OMe	0.12	-0.27	-0.55	-0.02
NMe₂	-0.16	-0.83	-1.71*	0.18
F	0.34	0.06	-0.55	0.14
Cl	0.37	0.23	-0.97	0.71
CF₃	0.43	0.54	-2.4	0.88
NO₂	0.71	0.78	-2.52	-0.28
H	0	0	0	0
Me	-0.07	-0.17	-1.24	0.56
Et	-0.07	-0.15	-1.31	1.02
2-Naphthyl	0.04	0.04	-1.31**	1.32

* E_S unavailable for NMe₂, E_S for *i*-Pr was used, ** E_S unavailable for 2-Naphthyl, E_S for Et was used

2.3.2. Stepwise Regression

Each resveratrol analogue in the library had seven possible positions of substitution and each position had three molecular descriptors, resulting in a total of twenty-one descriptors per analogue (Figure 2.3). Because of the way the compounds were tested for inhibition of each enzyme, IC₅₀ data was only available for compounds that were moderate to good inhibitors of each enzyme – and not for the compounds that inhibited each enzyme poorly or not at all. This was unfortunate because information about molecules that show poor inhibition is of equal importance as information about molecules that show good inhibition for the generation of a good QSAR.

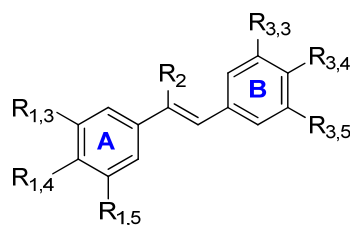


Figure 2.3. Seven possible positions of substitution for each resveratrol analogue.

Stepwise regression is a regression model that selects the included predictive variables by forward selection, backward elimination, or bidirectional elimination. The QSARs reported herein were determined by the use of forward selection stepwise regression. This was done to preclude a QSAR that was overdetermined, as there were a large number of descriptors for each system (twenty-one) and a small number of molecules in each set. In general, each QSAR was arrived at by testing each variable individually. For each QSAR, the variable that gave the best correlation with the data

was used as the starting variable. An iterative process followed in which every variable was tested and the variable that gave the best correlation was added to the QSAR. This process was continued until there was either no improvement in the QSAR or until the *F*-test determined the correlation was not meaningful at a 95% confidence interval. For every QSAR, the figures in parentheses are the standard errors associated with the coefficients, *n* represents the number of data points upon which the equation is based, *r* is the correlation coefficient, and *s* is the standard deviation from the regression equation.

2.3.3. COX1 QSAR

Of the thirty-six resveratrol analogues that were found to inhibit COX1, thirty-three contained a resorcinol or methylated resorcinol ring. For this reason, the distribution of values of the molecular descriptors in some positions on the resveratrol skeleton was not great enough to establish a meaningful correlation with the IC₅₀ data. To circumvent this issue, we attempted aligning the compounds in such a way as to place all of the resorcinol rings in the same chemical space and only examine the effect of substitution on one ring and the central alkene; however, this attempt was not a success as the position of the alkene substituent varied with respect to the resorcinol ring.

2.3.4. COX2 QSAR

Stepwise regression on the molecular descriptors of the seventeen molecules that were found to inhibit COX2 resulted in the QSAR model, Equation 2.1.

$$\begin{aligned} \log(1/IC_{50}) = & 1.77(\pm 0.67)R_{1,3\pi} + 1.97(\pm 1.11)R_{1,4\sigma_p} - 1.36(\pm 0.65)R_{1,4\pi} - 0.92(\pm 0.78)R_{1,5\pi} \\ & - 16.6(\pm 3.22)R_{1,5E_S} - 1.27(\pm 0.65)R_{2\pi} - 0.57(\pm 0.38)R_{2E_S} - 8.55(\pm 1.66)R_{3,4\sigma_p} - \\ & 4.40(\pm 0.88)R_{3,4E_S} - 20.7(\pm 4.33)R_{3,5\pi} - 14.5(\pm 2.75) \\ n = 17, r^2 = 0.91, s = 0.29, F = 5.929, F_{0.05}(10, 6) = 4.06 \end{aligned} \quad \text{Eq. 2.1. COX2 QSAR}$$

The QSAR model derived for COX2 signified that substitution at the 3,3 position of the “B” ring of the analogue was not required for good inhibition. Additionally, the initial SARs were supported in the QSAR. First, the QSAR model indicated that a relatively large, hydrophobic alkene substituent will increase inhibition of COX2. Second, the QSAR model indicated an electron-donating substituent was important at the 3,4 position of the “B” ring, supporting our observation that at least one electron rich ring is required for good inhibition. A pictorial representation of the COX2 QSAR result is shown in Figure 2.4.

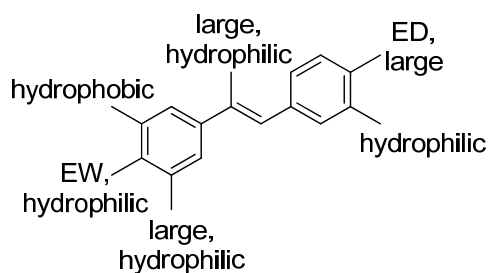


Figure 2.4. Pictorial representation of COX2 QSAR.

2.3.5. NF-κB QSAR

Stepwise regression on the molecular descriptors of the thirty-four molecules that were found to inhibit NF-κB resulted in the QSAR model, Equation 2.2.

$$\begin{aligned} \log(1/IC_{50}) = & - 0.16(\pm 0.05)R_{1,3}E_S - 0.19(\pm 0.09)R_{1,4}\sigma_p + 0.11(\pm 0.04)R_2E_S - \\ & 1.55(\pm 1.22)R_{3,3}\sigma_m - 0.63(\pm 0.25)R_{3,3}E_S + 0.52(\pm 0.32)R_{3,4}\sigma_p - 0.60(\pm 0.17)R_{3,4}\pi - \\ & 1.58(\pm 0.17) \end{aligned}$$

$n = 34, r^2 = 0.66, s = 0.15, F = 7.08, F_{0.05}(7, 26) = 2.39$ Eq. 2.2. NF-κB QSAR

The QSAR model derived for NF-κB inhibition supports some of our initial SARs. First, it appears substitution at the 1,5 position of the “A” ring is not required for good inhibition of NF-κB. This finding from the QSAR model is supported by the trend in the inhibitory data, where all of the most active NF-κB inhibitors had a catechol ring. Second, in support of our initial SAR observation that an unsubstituted central-olefin is preferred, the QSAR for NF-κB indicates that a small alkene-substituent will increase inhibition of NF-κB. A pictorial representation of the NF-κB QSAR result is shown in Figure 2.5.

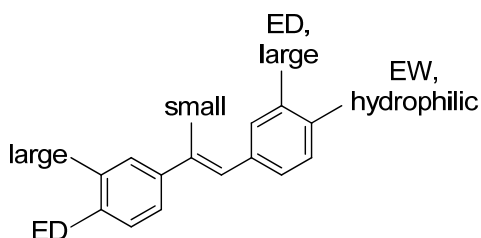


Figure 2.5. Pictorial representation of NF-κB QSAR.

2.3.6. QR2 QSAR

Stepwise regression on the molecular descriptors of the twenty-six molecules that were found to inhibit QR2 resulted in the QSAR model, Equation 2.3.

$$\begin{aligned} \log(1/IC_{50}) = & 1.08(\pm 0.31)R_{1,3}\pi + 0.31(\pm 0.27) R_{1,3}E_S - 0.47(\pm 0.30)R_{1,4}\pi + \\ & 3.01(\pm 1.43)R_{2}\sigma_m + 11.9(\pm 5.79)R_{3,3}\sigma_m + 4.36(\pm 1.28)R_{3,3}\pi - 3.90(\pm 1.21)R_{3,4}\pi - \\ & 2.74(\pm 0.94)R_{3,4}E_S + 12.4(\pm 4.92)R_{3,5}\sigma_m - 3.75(\pm 1.36)R_{3,5}\pi - 3.78(\pm 1.13) \\ n = 26, r^2 = 0.75, s = 0.36, F = 4.40, F_{0.05}(10, 15) = 2.54 \end{aligned} \quad \text{Eq. 2.3. QR2 QSAR}$$

The QSAR model determined for QR2 indicates that it is important that one side of the analogue have hydrophilic residues and the other hydrophobic residues. The way the QSAR data was input, the positions 1,3 and 3,3 positions appear to dictate hydrophobic substituents. Taking into consideration the known structure of the QR2 active site, rotation about the central sp^3 bonds of the stilbene model yields a conformation of the analogues that agrees with the known structural information (Figure 2.6). Thus, the QSAR model dictates that small hydrophobic substituents should be placed on the side of the stilbene that will interact with the hydrophobic side of the active site and hydrophilic substituents should be placed on the side of the stilbene that will interact with the solvent exposed side of the QR2 active site. The QSAR model also signifies that an electron-withdrawing substituent is preferred on the central alkene, something the most potent QR2 inhibitor in the library, **2.1v**, also has.

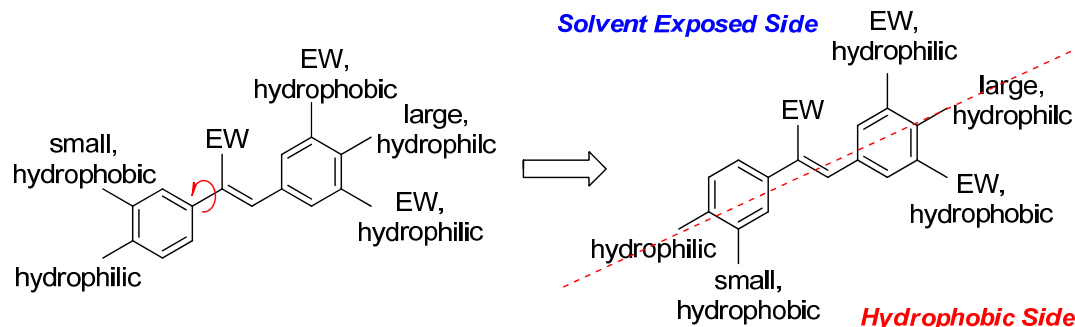


Figure 2.6. Pictorial representation of QR2 QSAR.

2.4. 3D-QSAR

Though the developed QSAR models resulted in some preliminary correlations between the structural elements of our analogues and their biological activities, as well as supporting our observed SARs, they were by no means conclusive. The QSARs were constructed using only the compounds that had inhibitory concentrations within a range of 0.17 to 103.8 μM , as the enzymatic inhibition data for the less active analogues was not available. Each QSAR was derived from a small set of structurally similar compounds, where the true alignment of the rings, and the substituents on the rings, in each of the enzyme's active sites was unknown. These facts greatly increased the likelihood of chance correlations within each of the models. Additionally, the 1D-QSARs generated were not able to account for any conformational effects that may be critical for protein-ligand association.

In an attempt to further clarify the properties of the analogues that dictated their biological activity toward the given targets, we turned our attention to the development of 3D-QSAR models. 3D-QSARs are incredibly useful for representing the binding site of a target by mapping the physicochemical properties of the ligands onto a surface or grid

that surrounds the ligand molecules, which are superimposed in 3D space. This type of 3D-QSAR model interacts simultaneously with all ligands and represents an average of all of the modeled compounds. Implementing 3D-QSARs was of particular interest to us as we reasoned they would generate 3D models of the binding sites of COX1, COX2, and NF- κ B by looking at 3D properties of the ligands. Additionally, 3D-QSARs would facilitate quantification of the interactions between the analogues and protein at an atomic level by modeling the electrostatic forces, hydrogen bonds, and van der Waals interactions that were important in the ligands.

We set out to determine 3D-QSARs in collaboration with Gregory Wilson and Prof. Markus Lill of the Department of Medicinal Chemistry and Molecular Pharmacology at Purdue University. The 3D structures of all active resveratrol analogues were generated using MacroModel and optimized in aqueous solution on the basis of the AMBER* force field. The most potent resveratrol analogue identified for each of the four targets was used as the template for alignment for the other bioactive analogues in that set. The software *Symposar*, developed by Lill and colleagues, was used to align the ligands in each of the four data sets.⁵ *Symposar* does this by first aligning the query molecule in 2D space on the template based on substructure similarity, followed by alignment in 3D space based on similarity of physiochemical fields. In this way, *Symposar* is capable of yielding a superposition of the molecules in configurations relative to each other that would be expected in their bioactive conformations. The software *Raptor*, also developed by Lill and colleagues, was then used to run the 3D-QSAR simulations based on the prepared data sets.⁶

The 3D-QSAR generated for QR2 is displayed in Figure 2.7. The highest affinity ligand, **2.1v**, was used as the template for alignment. The test set was composed of ligands **2.1b**, **2.1c**, **2.1d**, **2.1h**, **2.1l**, **2.1q**, **2.1s**, and **2.1w** (Figure 2.7, A). All other ligands with bioactivity toward QR2 were used in the training set. The alignment produced by Symposar (Figure 2.7, B) was then used to generate a 3D-QSAR using Raptor, which is displayed both pictorially and graphically. The regions in blue represent hydrogen-bond donor character; the regions in red represent hydrogen-bond acceptor character and the regions colored yellow represent hydrophobic character (Figure 2.7, C). A graph plotting the predicted versus experimental affinity is also displayed, where the data points colored green are the compounds in the training set and the data points colored red are the compounds in the test set (Figure 2.7, D).

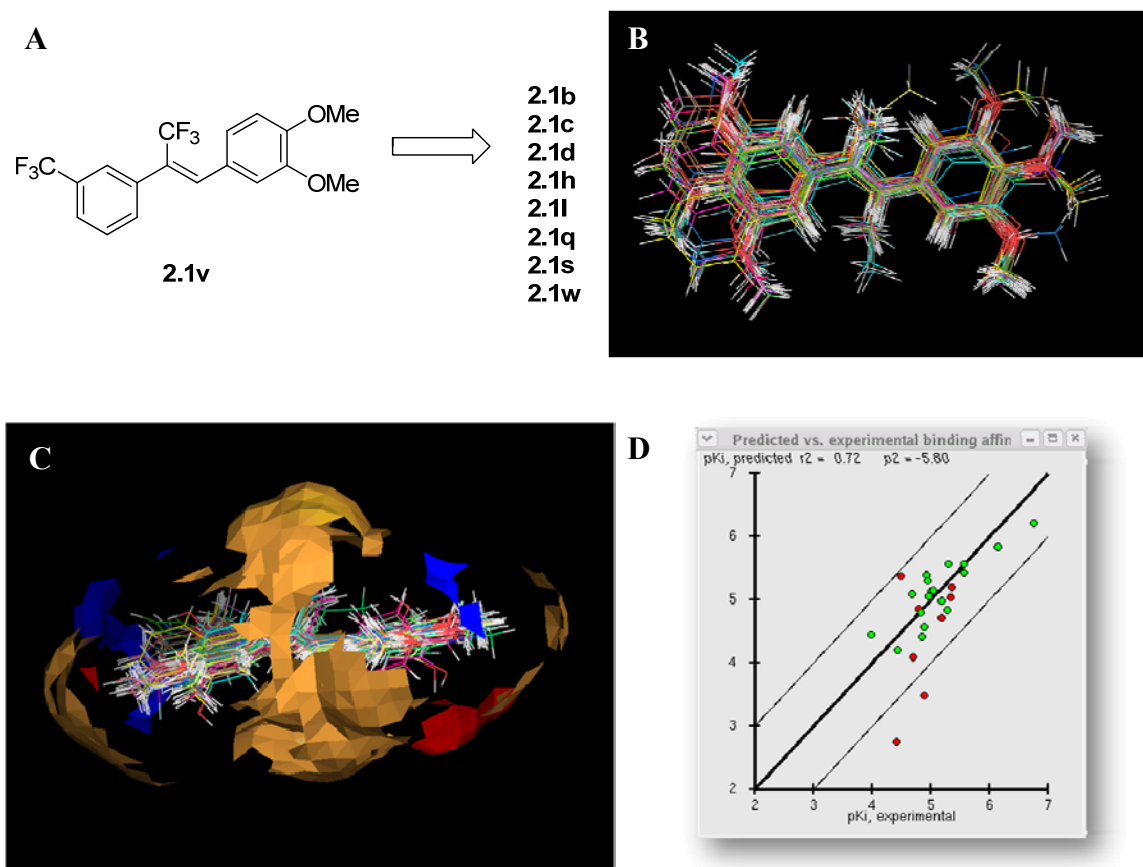


Figure 2.7. 3-D QSAR for QR2; (A) Template ligand **2.1v** was used for the alignment of the training set. The test set molecules are shown. (B) Symposar alignment of molecules in training set. (C) Common 3D features of active site determined by Raptor model, where blue indicates hydrogen-bond donor character, red indicates hydrogen-bond acceptor character, and yellow indicates hydrophobic character. (D) Graph plotting the predicted vs. experimental affinity of the analogues, where the molecules in the training set are shown in green and the molecules in the test set are shown in red.

Similar 3D-QSAR models were determined for COX1, COX2, and NF- κ B. Unfortunately, none of the 3D-QSAR models were useful to explain the observed bioactivity of the resveratrol analogues toward their respective targets. This was clear as the 3D-QSARs for each of the targets could not accurately predict the activity of the molecules in their respective test sets (see Figure 2.7, D). This led us to believe our

assumption that all of the analogues shared a common binding orientation was erroneous. Additionally, the construction of QSARS (1D- or 3D-) for compounds containing a stilbene skeleton is a particular challenge due to the inherent pseudo-symmetry of these types of molecules.

2.5. Conclusions

The 1D- and 3D-QSAR models generated for the resveratrol analogues' activity toward COX1, COX2, NF- κ B, and QR2 were largely unsuccessful for the determination and prediction of the structural and electronic factors of the molecules that produced good enzymatic inhibition. The poor QSARs generated from the data sets can be explained by three factors: first, the QSARs were constructed using only compounds that were identified as good inhibitors of their respective targets. These compounds had a quite narrow range of IC₅₀ values, from 0.17 to 103.8 μ M. Second, the QSARs were derived from a small, structurally similar set of compounds. This greatly increases the possibility of chance correlations within each of the models. Third, because the nature of the stilbene skeleton of resveratrol, the symmetry of the compounds was an uncontrollable variable when aligning them for the construction of QSAR models. There was no way to determine how the compounds truly aligned in the active site of each of the targets, if indeed they did align in a common binding pose at all.

2.6. References

1. Kang, S. S.; Cuendet, M.; Endringer, D. C.; Croy, V. L.; Pezzuto, J. M.; Lipton, M. A., Synthesis and biological evaluation of a library of resveratrol analogues as inhibitors of COX-1, COX-2 and NF- κ B. *Bioorganic & Medicinal Chemistry* **2009**, *17* (3), 1044-1054.
2. Hammett, L. P., The Effect of Structure upon the Reactions of Organic Compounds. Benzene Derivatives. *Journal of the American Chemical Society* **1937**, *59* (1), 96-103.
3. Taft, R. W., The Dependence of the Rate of Hydration of Isobutene on the Acidity Function, H_0 , and the Mechanism for Olefin Hydration in Aqueous Acids. *Journal of the American Chemical Society* **1952**, *74* (21), 5372-5376.
4. Taft, R. W., Polar and Steric Substituent Constants for Aliphatic and o-Benzoate Groups from Rates of Esterification and Hydrolysis of Esters¹. *Journal of the American Chemical Society* **1952**, *74* (12), 3120-3128.
5. Lill, M. A.; Vedani, A., Combining 4D pharmacophore generation and multidimensional QSAR: Modeling ligand binding to the bradykinin B-2 receptor. *Journal of Chemical Information and Modeling* **2006**, *46* (5), 2135-2145.
6. Lill, M. A.; Vedani, A.; Dobler, M., Raptor: Combining dual-shell representation, induced-fit simulation, and hydrophobicity scoring in receptor modeling: Application toward the simulation of structurally diverse ligand sets. *Journal of Medicinal Chemistry* **2004**, *47* (25), 6174-6186.

CHAPTER THREE:
DESIGN, SYNTHESIS, AND EVALUATION OF SUBSTITUTED RESVERATROL
ANALOGUES FOR THE INHIBITION OF QUINONE REDUCTASE 2 (QR2) AS
CHEMOPREVENTATIVE AGENTS

3.1. Design of QR2 Inhibitors

The overall goal of the research reported herein was the synthesis and identification of novel analogues of resveratrol to serve as leads for future chemopreventative agents. We embarked on the present work with the aim of identifying new resveratrol analogues that displayed either increased selectivity or potency toward QR2. Our objectives were two-fold in this research. First, we desired to find analogues of resveratrol that lacked the 3- and 4'-hydroxyl groups of resveratrol, therefore negating the biological deactivation of resveratrol by its metabolism in vivo. Second, we wished to further investigate exactly what structural features of resveratrol were pertinent for potent inhibition of QR2. We set out to accomplish this through the synthesis and testing of two different sets of resveratrol analogues. One set in which the 3,5,4'-substitution pattern of resveratrol was held constant and only the central alkene was functionalized, and a second set in which the central alkene was replaced completely by an amide, and the substitution pattern on the aryl rings was varied.

3.1.1. First Generation Influences

Of the 78 first generation resveratrol analogues tested for inhibition of QR2, 24 were found to actively inhibit the enzyme. Of those, ten had IC_{50} values lower than resveratrol (Chapter 2, Table 2.1). Six of those ten lack the 3- and 4'-hydroxyl substituents required for metabolic sulfation and glucuronation (**2.1h**, **2.1i**, **2.1j**, **2.1l**, **2.1r**, and **2.1v**). Interestingly, two of the more potent analogues (**2.1i** and **2.1l**) have naphthyl substituents, which may allow for a greater pi-stacking interaction with the isoalloxazine ring of the active site FAD cofactor.

The most potent inhibitor of the series, compound **2.1v**, has both a highly electron-deficient central alkene and aryl ring as a consequence of two trifluoromethyl substituents. Interestingly, of the other six analogues in the 78-member first generation library that had trifluoromethyl alkene substituents,¹ only one was active, compound **2.1u**, which has *two electron-rich aryl rings*. Examination of the other analogues with trifluoromethyl alkene substituents does not show a clear pattern for QR2 inhibition. For instance, while compound **2.1u** was found to be an active inhibitor of QR2, compound **2.1ac** did not show inhibition of QR2 (Figure 3.1). These two compounds differ only in the position of the dimethylresorcinol ring relative to the trifluoromethyl alkene substituent. Comparing the most potent analogue in the library, **2.1v**, to compound **2.1aa**, the only difference is that the 4-methoxy substituent has migrated to the 3-position. However, this change is significant enough to effectively deactivate the most potent compound of the first generation library. Additionally, the analogue **2.1y** which has the exact aryl substitution pattern of resveratrol was not found to be active. Thus, in

this case, substitution of the central olefin of resveratrol with a trifluoromethyl group resulted in the deactivation of the compound.

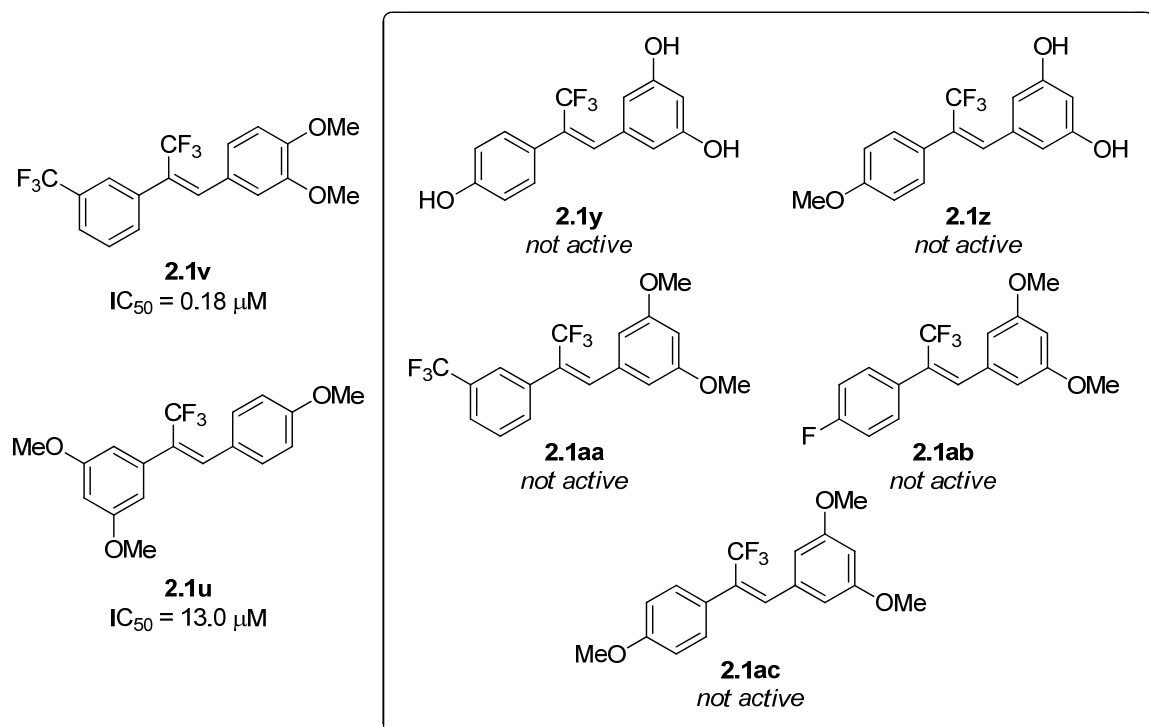


Figure 3.1. First generation resveratrol analogues with trifluoromethyl alkene substituents. Compounds not found to potently inhibit QR2 are boxed.

3.1.2. Design of Second Generation Resveratrol Analogue Library

To investigate this complex interplay between the position of the alkene substituent and the substitution pattern on the aryl rings, we envisioned a second generation resveratrol analogue library composed of two sets of molecules; one set where the substitution pattern of the aryl rings was held constant and various electron-withdrawing groups were placed at the central alkene, and a second set where the alkene substitution was held constant and various substitutions were made on the aryl rings. We

set out to accomplish this through the synthesis of a set of olefin-substituted resveratrol analogues and a set of benzanilide resveratrol analogues (Figure 3.2).

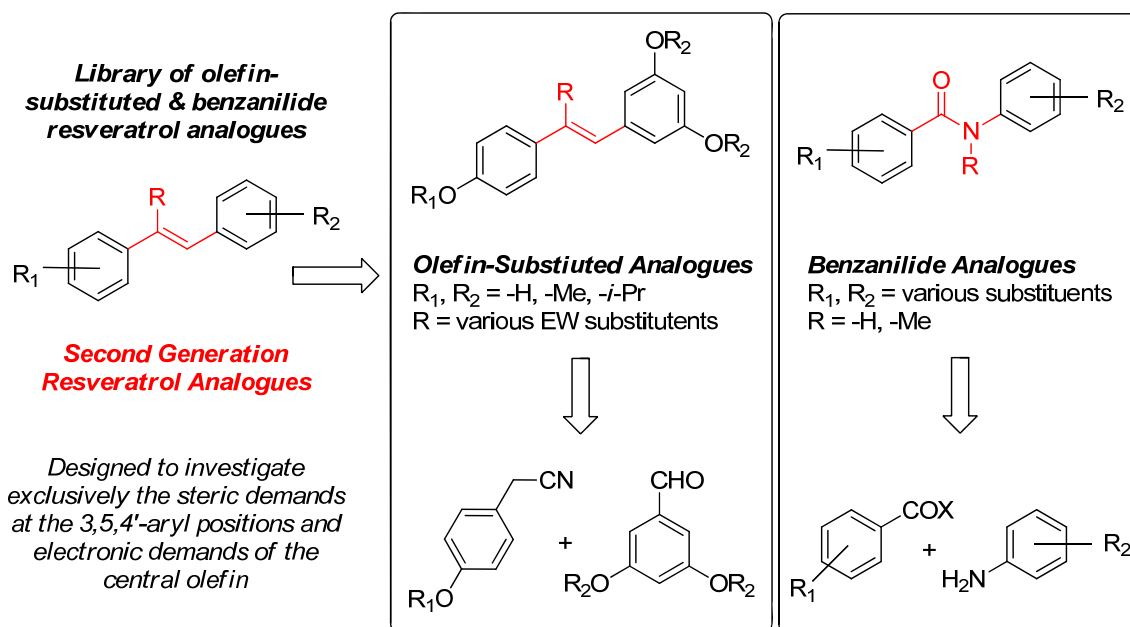


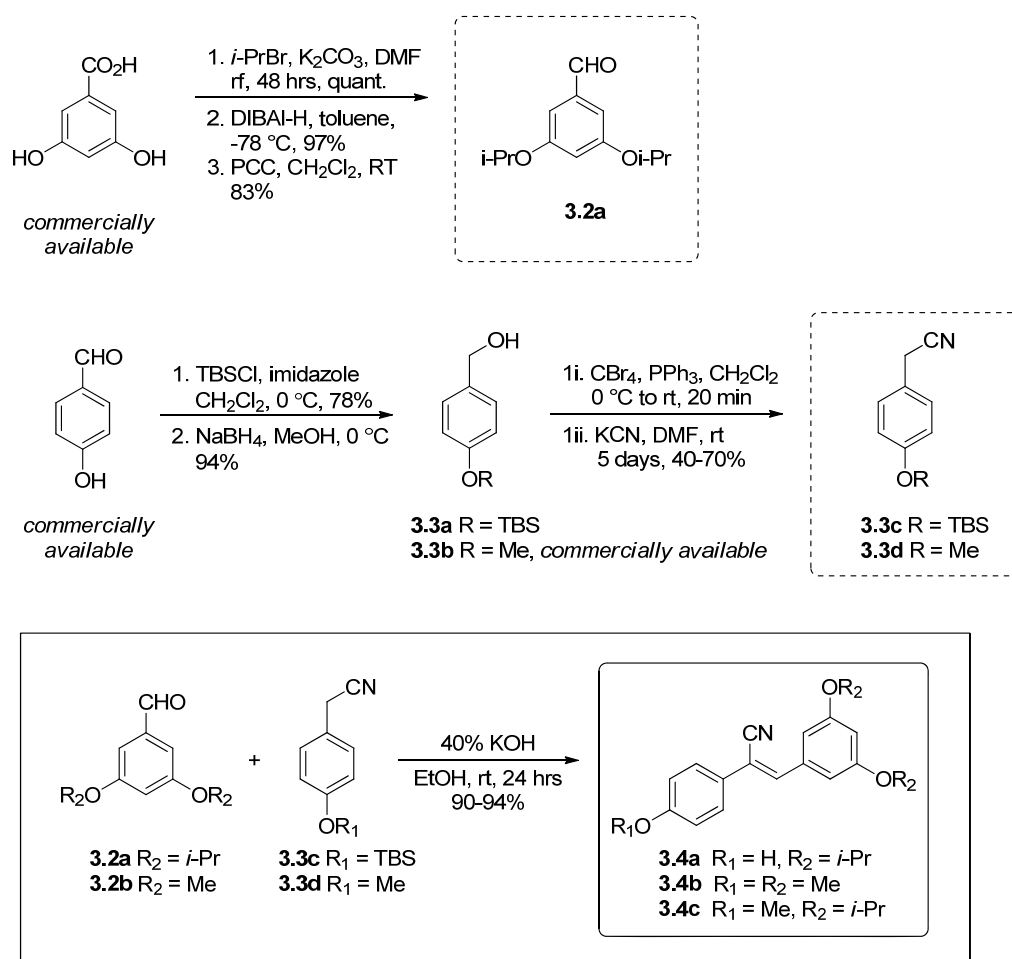
Figure 3.2. Design of second generation resveratrol analogue library.

3.2 Construction of Second Generation Library

3.2.1. Construction of Olefin-Substituted Resveratrol Analogue Set

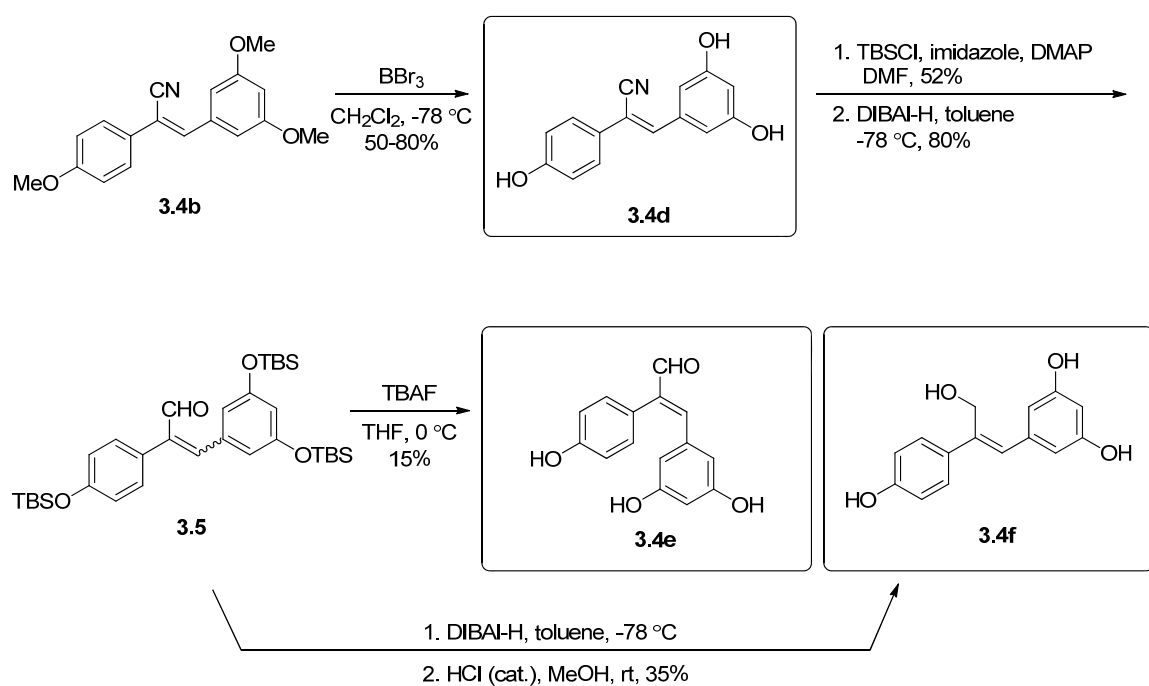
To investigate the role of substitution at the central alkene of resveratrol, the ability of the QR2 active site to accommodate aryl ethers at the traditional 3,5,4'-positions of resveratrol, and the conformational effect of *E/Z*-isomerism on QR2 inhibition, a small set of 21 olefin-substituted resveratrol analogues was synthesized. This was accomplished through the formation of three key nitrile resveratrol analogues that were amenable to further synthetic transformations (Scheme 3.1, analogues **3.4a-**

3.4c). The analogues **3.4a-3.4c** were produced in gram quantities with high yields by the condensation of the appropriately substituted aldehyde (**3.2a** or **3.2b**) with the appropriately substituted phenylacetonitrile (**3.3c** or **3.3d**).^{2, 3} These starting materials were either commercially available or were arrived at through the simple chemistry shown in Scheme 3.1. Compound **3.4a** was produced by the condensation of aldehyde **3.2a** with phenylacetonitrile **3.3c** under which conditions the phenol of **3.3c** was liberated.



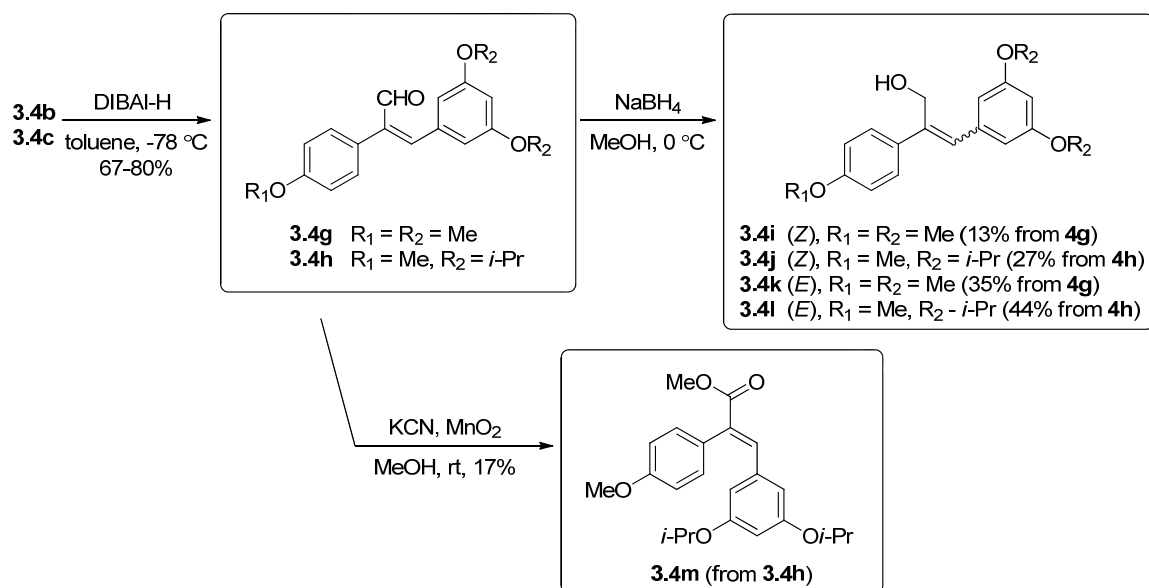
Scheme 3.1. Construction of starting materials **3.2a**, **3.3c**, and **3.3d** and condensation reaction forming key nitrile analogues **3.4a-3.4c**.

With the key nitriles in hand, the synthesis of the eighteen remaining olefin-substituted structural analogues of resveratrol commenced. Deprotection of **3.4b** by treatment with boron tribromide (Scheme 3.2) yielded the (*Z*)-nitrile analogue **3.4d**, which upon protection of the free phenols as *tert*-butyldimethylsilyl ethers and reduction of the nitrile, resulted in a mixture of the (*E*)- and (*Z*)-aldehydes **3.5**. Treatment of this mixture **3.5** with tetra-*n*-butylammonium fluoride resulted in the aldehyde **3.4e** as a single *E* isomer, where the *Z* isomer was not detected. Further reduction of the mixture **3.5** by treatment with diisobutylaluminum hydride and subsequent exposure to dilute hydrochloric acid in methanol gave the *Z* isomer alcohol **3.4f**, where the *E* isomer was not detected.



Scheme 3.2. Synthesis of analogues **3.4d**-**3.4f**.

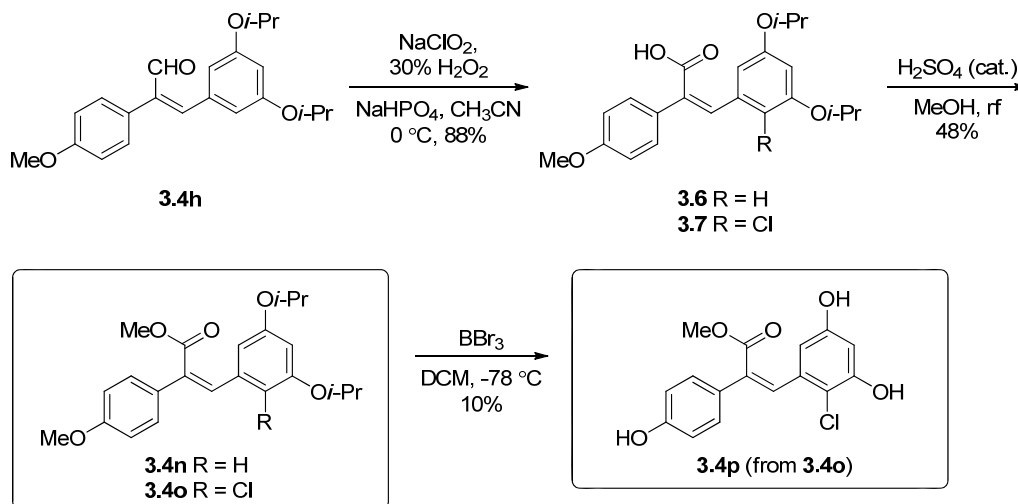
Reduction of both (*Z*)-nitriles **3.4b** and **3.4c** using diisobutylaluminum hydride gave rise to the (*Z*)-aldehyde analogues **3.4g** and **3.4h**. Additional reduction of the aldehydes by treatment with sodium borohydride yielded mixtures of both the (*Z*)- and (*E*)-alcohols, which were easily separated by flash chromatography, yielding the four resveratrol analogues **3.4i**, **3.4j**, **3.4k**, and **3.4l**. Oxidation of the aldehyde **3.4h** by treatment with manganese dioxide and potassium cyanide in methanol resulted only in the isolation of the (*E*)-methyl ester resveratrol analogue **3.4m** (Scheme 3.3).⁴



Scheme 3.3. Synthesis of analogues **3.4g-3.4m**.

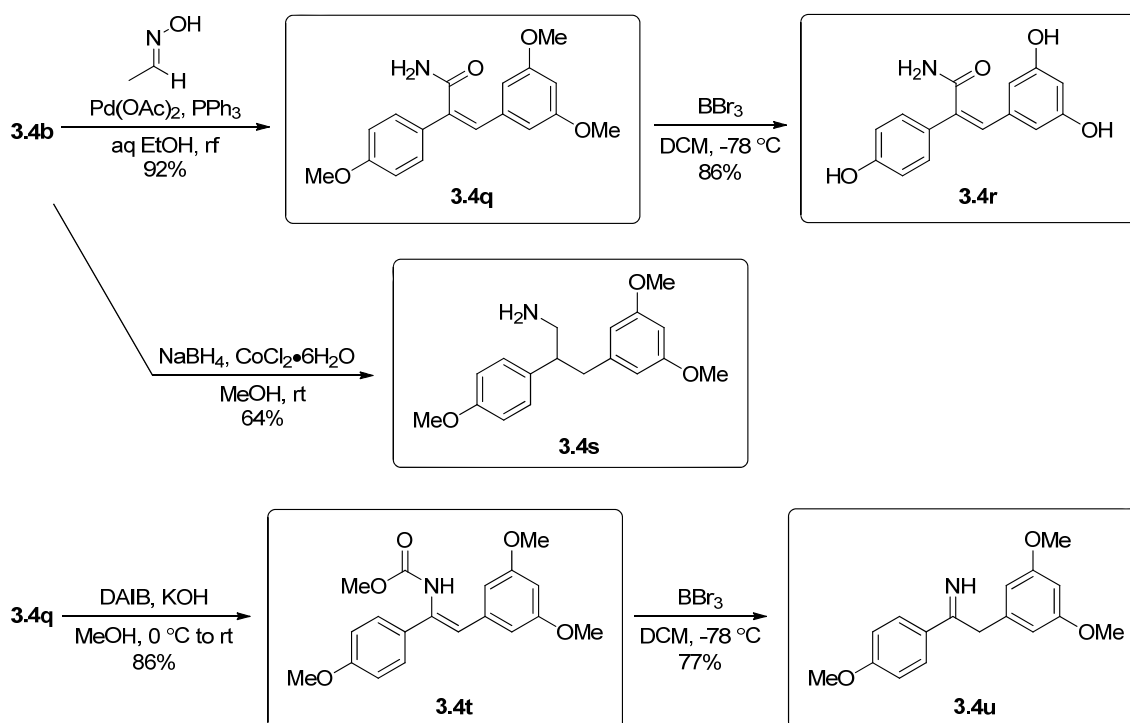
A Pinnick-type oxidation of the aldehyde **3.4h** using sodium chlorite-hydrogen peroxide was employed to yield an inseparable mixture of the desired (*Z*)-carboxylic acid **3.6** and the chlorinated byproduct **3.7**, which was formed by reaction with hypochlorite generated in situ.⁵ Fischer esterification was used to resolve the mixture of **3.6** and **3.7**,

resulting in the two esters (*Z*)- **3.4n** and (*Z*)- **3.4o** which could be separated by flash chromatography. Finally, treatment of **3.4o** with boron tribromide resulted in the liberation of the phenols, yielding the desired (*Z*)-ester analogue **3.4p** (Scheme 3.4).



Scheme 3.4. Synthesis of analogues **3.4n-3.4p**.

A palladium-catalyzed hydration of the nitrile **3.4b** was used to obtain the (*Z*)-amide **3.4q**, which - when treated with boron tribromide - produced the (*Z*)-amide analogue **3.4r** in good yield (Scheme 3.5).⁶ Concomitant reduction of the nitrile and the olefin was achieved by exposure of **3.4b** to sodium borohydride and cobalt chloride hexahydrate, resulting in the amine analogue **3.4s**.⁷ An oxidative Hofmann rearrangement of **3.4q** was effected using (diacetoxyiodo)benzene, which resulted in the (*Z*)-methyl carbamate **3.4t**. Treatment of the carbamate with boron tribromide resulted in the imine analogue **3.4u**.



Scheme 3.5. Synthesis of analogues **4q-4s**.

3.2.2. Construction of Benzanilide Resveratrol Analogue Set

Former Lipton research group member Dr. SooSung Kang carried out the synthesis of a set of 26 substituted benzanilide resveratrol analogues. The synthesis of these analogues was accomplished using standard amide bond forming techniques by reaction of the appropriately activated benzoic acid derivative with a substituted aniline. These analogues were designed to investigate the effect of complete substitution of the central alkene of resveratrol. The effect of methylation of the amide and phenols, as well as the position of the resorcinol ring relative to the amide nitrogen was investigated by benzanilide analogues **3.8a-3.8e**. The complete second generation resveratrol analogue library is shown in Figure 3.3.

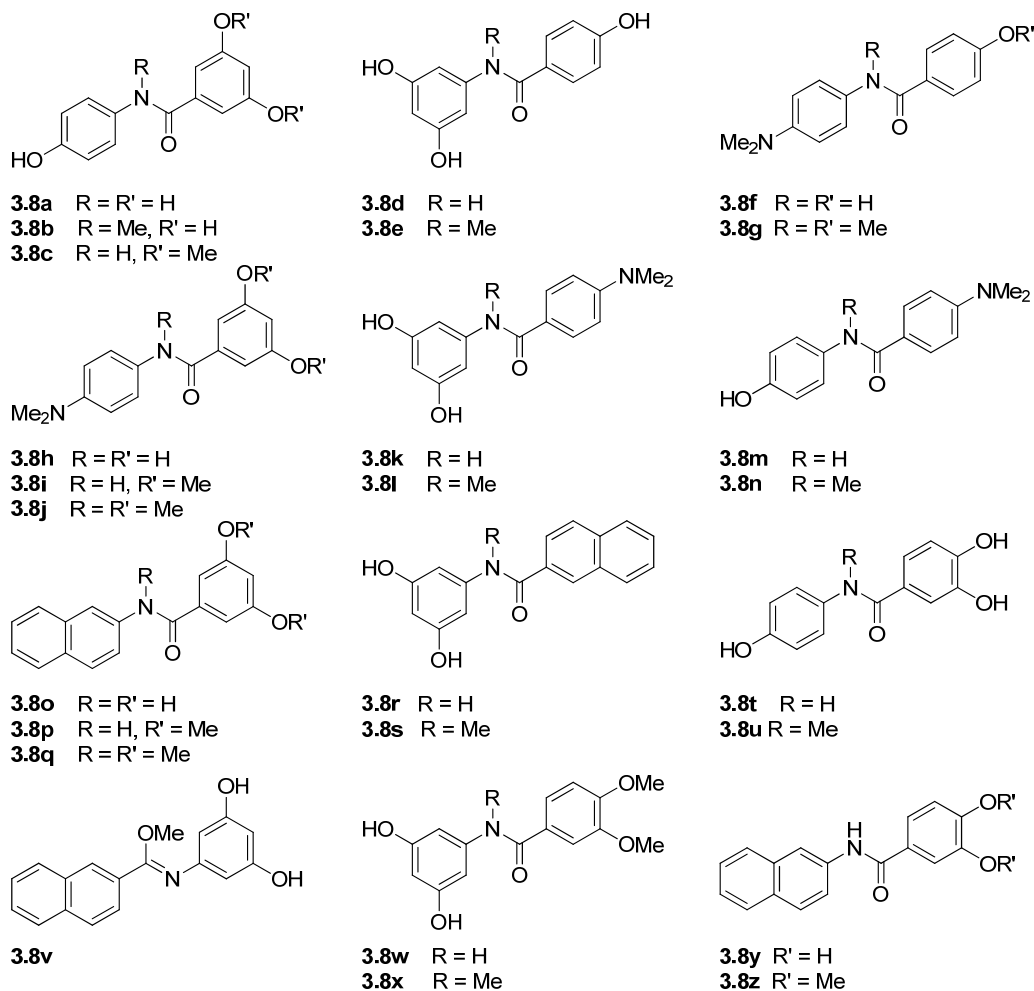
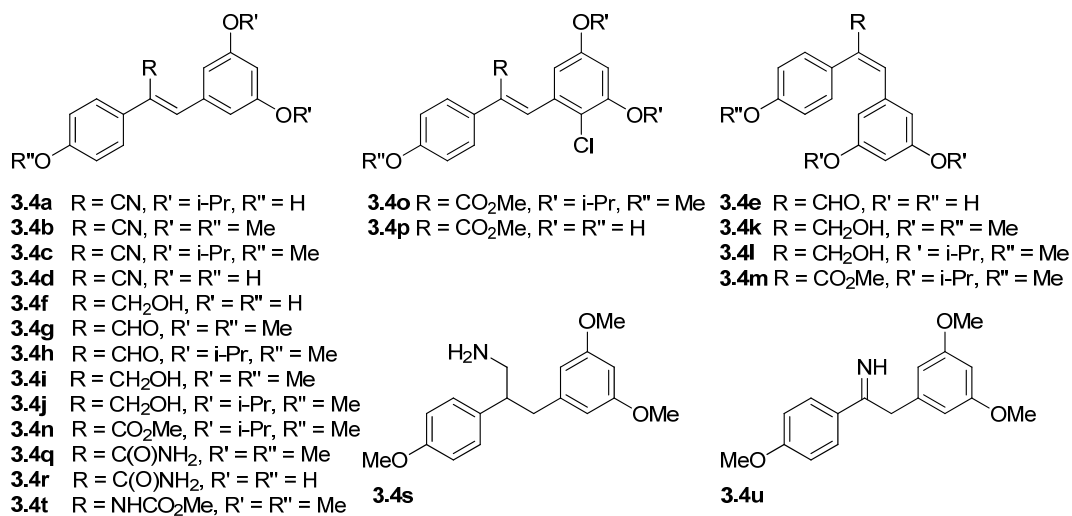


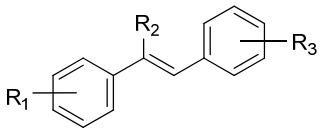
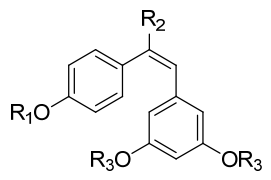
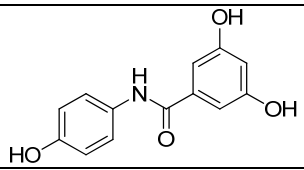
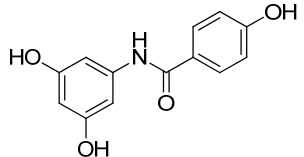
Figure 3.3. Complete second generation resveratrol analogue library; (*Top*) Olefin-substituted resveratrol analogues, (*Bottom*) Benzanilide resveratrol analogues.

3.3. Results of Second Generation Resveratrol Analogue Library

3.3.1. Biological Evaluation

The ability of the second generation resveratrol analogues to inhibit QR2 was determined by Dr. Katherine Jensen and Prof. Andrew Mesecar of the Department of Biological Sciences at Purdue University. Briefly, the enzymatic activity of QR2 at steady-state was determined using an assay where NMeH (*N*-methylidihydronicotinamide) was used as a co-substrate and MTT ((3-(4,5-Dimethylthiazol-2-yl)-2,5-diphenyltetrazolium bromide)) was used as the “quinone” substrate, and the activity of QR2 was followed by monitoring the increase in formazan product at 612 nm.^{8,9} The resveratrol analogues were screened for activity at 100 μ M and IC₅₀ values were determined for compounds that showed greater than 50% inhibition of QR2 at this concentration. The ability of the second-generation analogues to inhibit QR2 is displayed in Table 3.1.

Table 3.1. Inhibition of QR2 by olefin-substituted and benzanilide resveratrol analogues.

Structure	L.M. ^a	R ₁	R ₂	R ₃	IC ₅₀ (μM)
	Res	4-OH	H	3,5-(OH) ₂	6.9 ± 0.4
	3.4b	4-OMe	CN	3,5-(OMe) ₂	31.6 ± 4.3
	3.4d	4-OH	CN	3,5-(OH) ₂	5.9 ± 0.3
	3.4f	4-OH	CH ₂ OH	3,5-(OH) ₂	5.1 ± 0.3
	3.4g	4-OMe	CHO	3,5-(OMe) ₂	24.2 ± 1.3
3.4r	4-OH	CONH ₂	3,5-(OH) ₂	9.3 ± 1.9	
	3.4e	H	CHO	H	25.5 ± 3.5
	3.4k	Me	CH ₂ OH	Me	27.5 ± 4.9
	3.8a	-	-	-	27.6 ± 4.6
	3.8d	-	-	-	16.8 ± 1.3

^aL.M. = library member

Nine of the forty-seven second generation resveratrol analogues showed inhibition of QR2 over 50% at 100 μM and subsequently the IC₅₀ values of those compounds were determined. Of those nine compounds, two compounds (**3.4d** and **3.4f**) inhibited QR2 with IC₅₀ values comparable to that of resveratrol, while the remaining seven compounds were slightly weaker inhibitors of QR2 than resveratrol (6.9 ± 0.4 μM). Of the remaining compounds, ten showed weak inhibition of QR2 (between 20-50% at 100 μM); **3.4i**, **3.4p**, **3.4q**, **3.4s**, **3.4t**, **3.8c**, **3.8i**, **3.8m**, **3.8t**, and **3.8z**. The remaining twenty-nine analogues showed minimal inhibition of QR2 (<20% at 100 μM).

Six of the analogues found to inhibit QR2 strongly had free phenolic hydroxyl groups, while the remaining three had phenolic methyl ethers (**3.4b**, **3.4g**, and **3.4k**). From the second generation library's IC_{50} data, inhibitory activity of the analogues appears to decrease as steric bulk associated with the aryl rings increases. An example of this is the series **3.4a-3.4d**. The nitrile analogue **3.4d** with free phenolic hydroxyls was found to inhibit QR2 with an IC_{50} of $5.9 \pm 0.3 \mu\text{M}$ and 88.8% maximal inhibition. The nitrile analogue **3.4b**, which differs from **3.4d** only in that the phenolic hydroxyl groups have been substituted for methyl ethers, was found to inhibit QR2 with a six-fold increase in IC_{50} value of $31.6 \pm 4.3 \mu\text{M}$ and 57.4% inhibition. Extending this trend further, the nitrile analogues **3.4a** and **3.4c**, where the phenolic methyl ethers of **3.4d** have been replaced by more sterically bulky isopropyl ethers, do not show inhibition of QR2 above 20% at 100 μM (Figure 3.4). The same trend can be observed in the comparison of analogues **3.4f** and **3.4i**. This trend may be a result of the sterically bulky aryl ethers reducing the ability of the analogue to bind in the QR2 active site in the same orientation as resveratrol, thus reducing the ability of the molecule to form stabilizing hydrogen bonds to the ordered active site water molecules and key residues (*vide supra*).

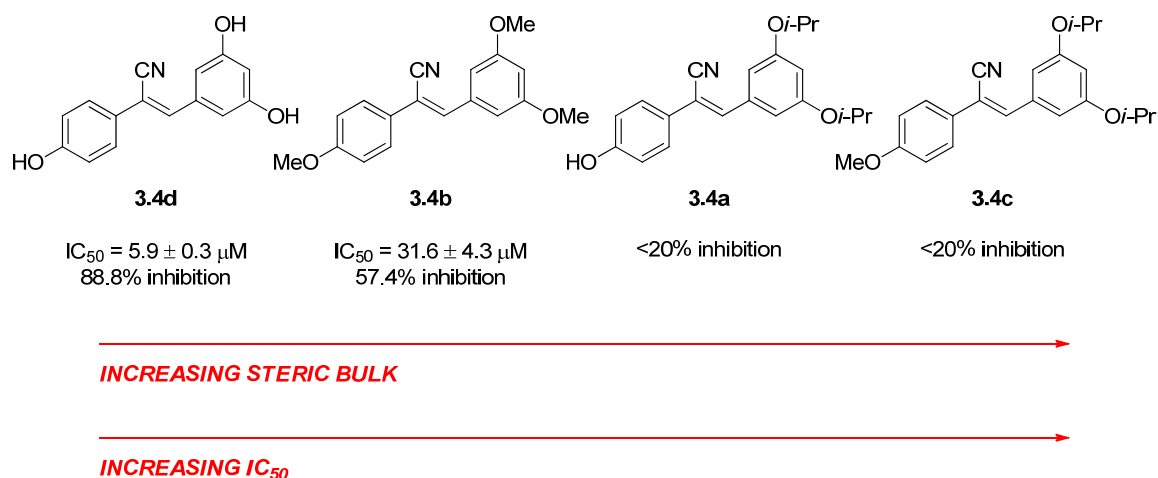


Figure 3.4. Correlation of increased steric bulk with increased IC_{50} as shown by **3.4a-3.4d**.

The trend illustrated in Figure 3.4 appears only to be consistent with the analogues of the second generation library and may heavily depend on the nature of the alkene substituent. For example, comparison of resveratrol to the first generation analogue **2.1f** shows only a modest increase in IC_{50} as a result of complete substitution of hydroxy for methoxy substituents ($IC_{50} = 11.5 \pm 3.2 \mu\text{M}$ for resveratrol vs. $IC_{50} = 14.6 \pm 4.3 \mu\text{M}$ for **2.1a**). In contrast, comparison of first generation analogues **2.1m** and **2.1q** shows that substitution of the methoxy substituents for hydroxy substituents has the opposite effect in this case, actually improving IC_{50} value ($IC_{50} = 39.0 \pm 17.2 \mu\text{M}$ for **2.1m** vs. $IC_{50} = 20.1 \pm 0.1$ for **2.1q**). Possibly the methyl-substituted central olefins of **2.1m** and **2.1q** dictate an alternate binding conformation of the analogues in the QR2 active site, and that binding in this alternative conformation is assisted by the sterically bulky (and hydrophobic) aryl ethers.

Two of the analogues, **3.4e** and **3.4k**, found to inhibit QR2 above 50% were of the *E* configuration, more closely resembling *cis*-resveratrol. This is significant as the *trans*-geometry is known to be the more bioactive form of the compound. An interesting trend among the allylic alcohol analogue series **3.4f**, **3.4i**, and **3.4k** can be inferred from the IC₅₀ data. The compound **3.4f**, which is of the *Z* configuration, was found to be the most potent inhibitor in our second-generation library, having an IC₅₀ of 5.1 ± 0.3 μM and 87.4% inhibition at 100 μM. Replacing the free phenolic hydroxyls of **3.4f** with methyl ethers, as in compound **3.4i**, drastically reduces the inhibitory potency of the analogue, lowering its inhibition at 100 μM from 87.4% to 27.7%, a finding consistent with the observation that steric bulk associated with the aryl rings has a detrimental effect on inhibition. However, comparing analogue **3.4i** to **3.4k**, where the single difference between the compounds is their geometry (**3.4i** is of the *Z* configuration while **3.4k** is of the *E* configuration), reveals that this trend can be negated by configuration. Thus, isomerization of **3.4i** to **3.4k** increases inhibition of QR2 to 57.2% (Figure 3.5). To the best of our knowledge, this is the first report of a *cis*-resveratrol analogue having greater inhibition of QR2 than its *trans*-configured counterpart.

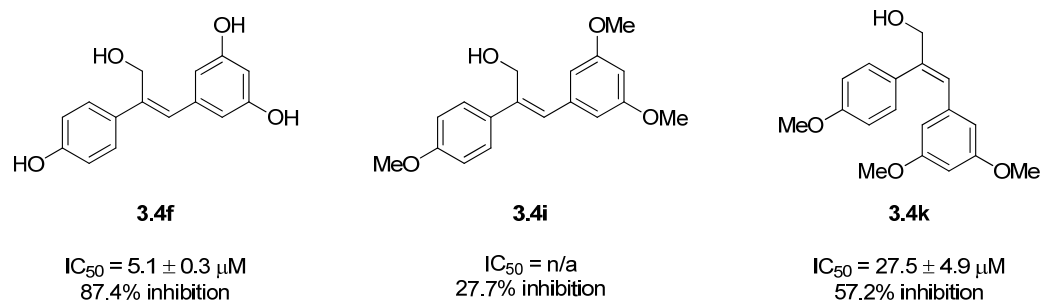


Figure 3.5. Effect of configuration on inhibition of QR2.

Of the twenty-six benzanilide resveratrol analogues, two were found to inhibit QR2, **3.8a** and **3.8d**. Interestingly, these two analogues have the same aryl substitution pattern as resveratrol and have secondary amide cores. None of the benzanilide analogues with the tertiary, methyl amide core showed inhibition of QR2 above 20%. Comparison of the IC₅₀s of **3.8a** and **3.8d** shows that the position of the amide nitrogen relative to the resorcinol ring has an observable effect on inhibition of QR2. When the amide nitrogen is bound directly to the resorcinol ring, the IC₅₀ is decreased by approximately 40% ($16.8 \pm 1.3 \mu\text{M}$ for **3.8d** compared to $27.6 \pm 4.6 \mu\text{M}$ for **3.8a**). Additionally, only phenolic hydroxyls appear to be tolerated in the benzanilide resveratrol analogue set, and even then, only at the traditional 3,5,4'-positions of resveratrol. This is illustrated by the comparison of **3.8a** to **3.8t**, where the 3-hydroxyl has been moved to the 4-position; this 2.7Å difference in the position the hydroxyl group is enough to decrease the inhibition of QR2 from 59.7% average inhibition for **3.8a** to 49.9% average inhibition for **3.8t**. Substituting the phenols of the resorcinol ring of **3.8a** for methyl ethers, as in benzanilide analogue **3.8c**, reduces inhibition of QR2 from 59.7% average inhibition to 43.2% average inhibition. Comparing **3.8a** to **3.8f** and **3.8d** to **3.8k** shows that the replacement of the 4'-hydroxyl group with a 4'-dimethylamino group eliminates inhibition of QR2. This is of consequence as previous reports have shown that the replacement of the 4'-hydroxyl group of resveratrol with a 4'-amino group can increase QR2 inhibition.^{9,10}

Of the eight second generation, naphthyl-substituted benzanilide analogues, only one was found to moderately inhibit QR2, analogue **3.8z** (30.5% average inhibition at 100 μM). The first generation analogue **2.11** differs only from **3.8z** in that it has a central

alkene instead of an amide; however, this difference results in **2.11** being a potent inhibitor of QR2, having an IC_{50} of 5.5 μ M. The naphthyl-substituted analogue **2.1i** was the second most active inhibitor of the first generation library, having an IC_{50} of 0.7 μ M. In comparison, the second generation benzanilide analogue **3.8p** showed no inhibition of QR2 at 100 μ M.

3.3.2. Structural Evaluation of Second Generation Resveratrol Analogue Inhibitors

To illuminate the structural factors beneath the trends seen in the inhibitory data of the second generation analogues, a series of X-ray crystal structures was determined for six of the nine most potent compounds. One of the goals behind the acquisition of the structural data was to better understand why the *E* configured analogue **3.4k** was a more potent inhibitor of QR2 than its corresponding *Z* isomer **3.4i**. Therefore, complete X-ray crystallographic data sets of inhibitors **3.4d**, **3.4f**, **3.4k**, **3.4r**, **3.8a**, and **3.8d** in complex with QR2 were collected in collaboration with Dr. Katherine Jensen and Prof. Andrew Mesecar and the structure of each complex was subsequently determined.

All structures were determined to 1.40-1.63Å resolution (Figure 3.6). The resveratrol analogues are shown in green, colored according to atom type, and shown in ball and stick representation. Water molecules are shown as red spheres, with hydrogen bonds shown as grey dashes with distances (Å) labeled. The FAD cofactor is shown in grey lines and colored according to atom type. Electron density omit maps ($F_o - F_c$) are shown in grey mesh and contoured to 3.0 σ around the ligand only. The binding orientation of each resveratrol analogue was the same in both active sites of the QR2 dimer, therefore only one active site is shown for clarity.

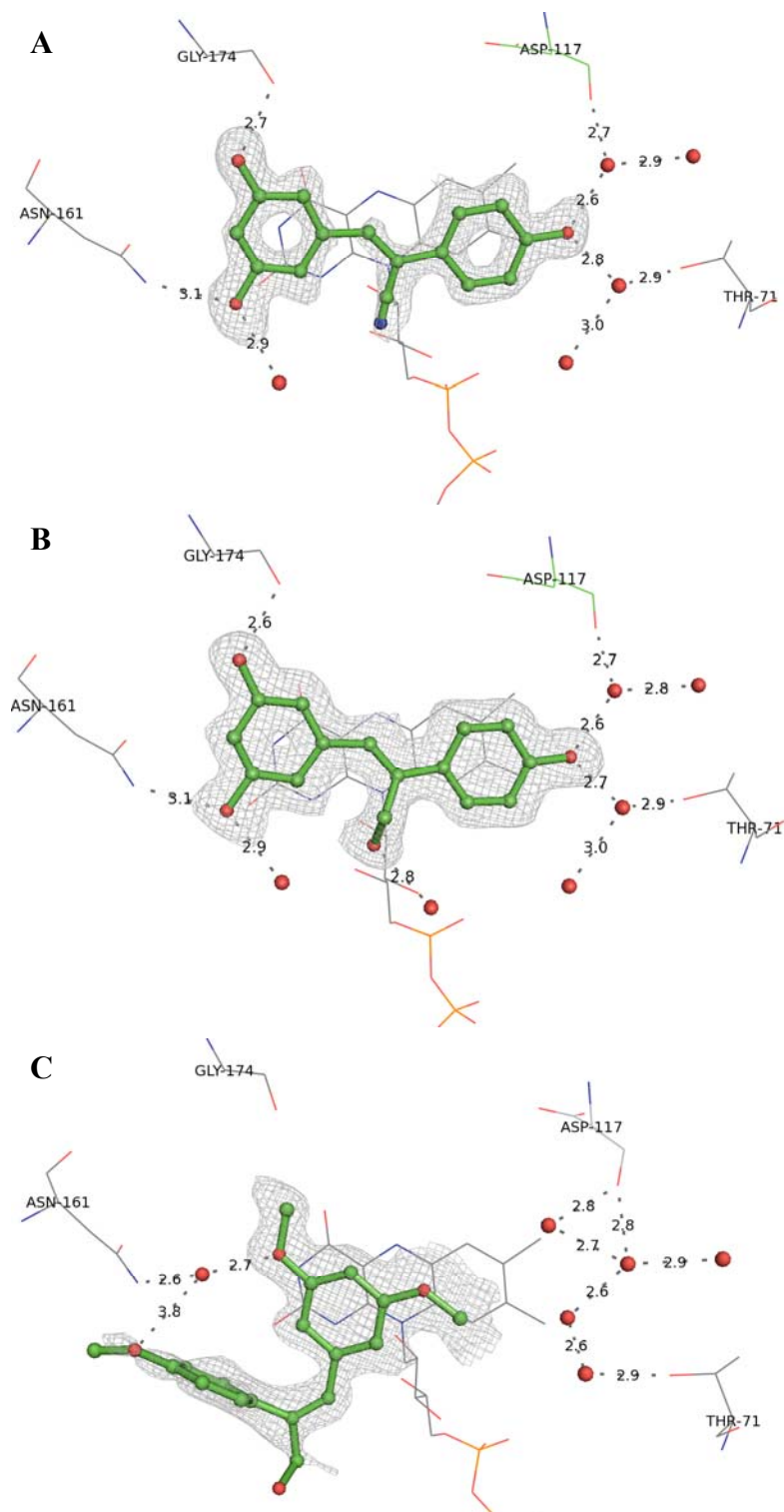


Figure 3.6. X-ray crystal structures of (A) **3.4d**, (B) **3.4f**, (C) **3.4k**, (D) **3.4r**, (E) **3.8a**, and (F) **3.8d** in complex with QR2.

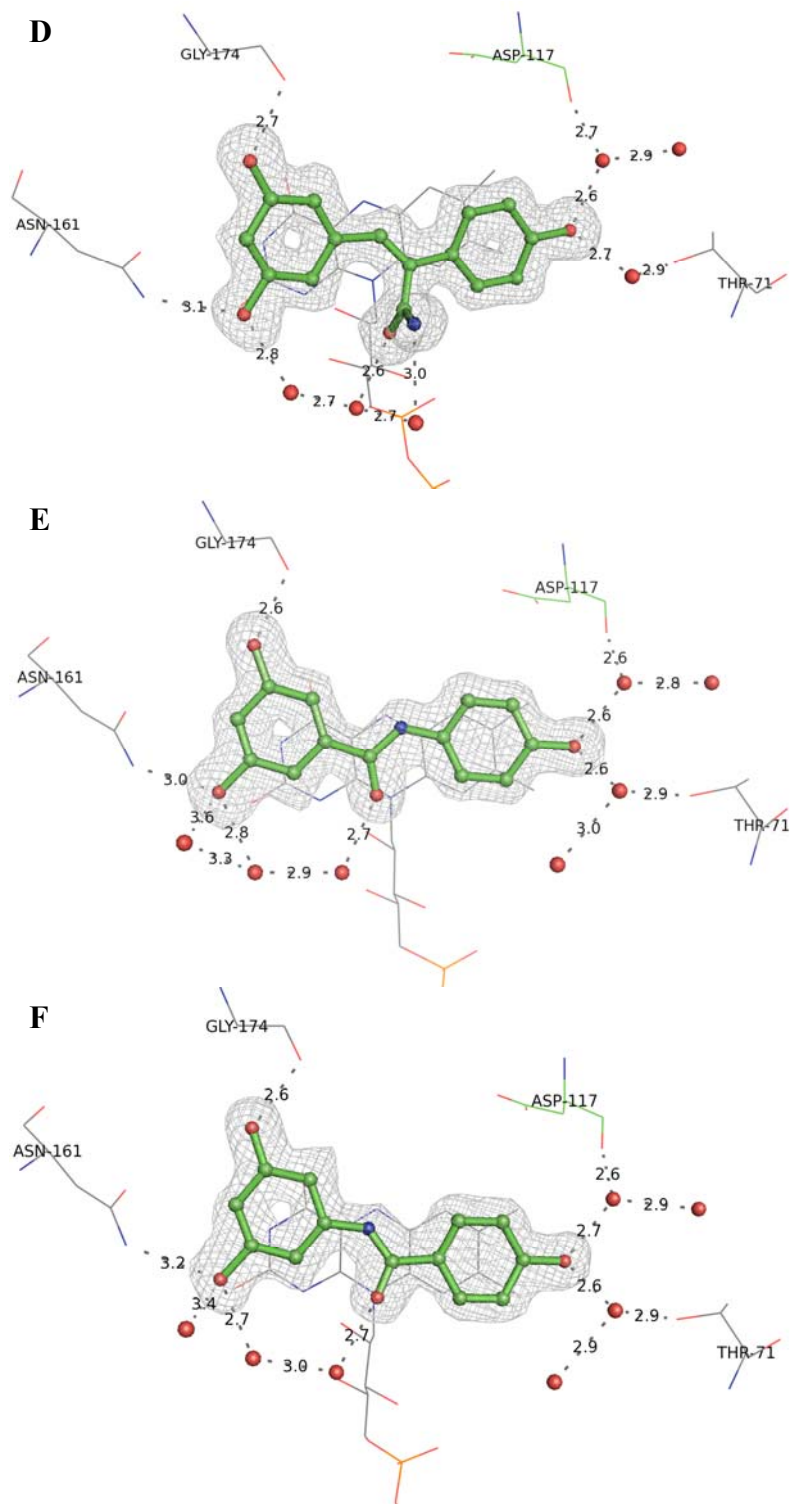


Figure 3.6 (cont).

Examination of the X-ray crystal structures of the *Z* configured analogues **3.4d**, **3.4f**, **3.4r**, **3.8a**, and **3.8d** in complex with QR2 confirms that they bind in almost identical conformations, placing their resorcinol and 4'-substituted aryl rings in the same chemical space within the active site, taking advantage of the same stabilizing interactions (Figure 3.6). All of the alkene substituents are positioned toward the solvent-exposed side of the active site and all of these analogues bind in the same conformation as resveratrol, utilizing the same hydrogen bonds to the same ordered active site water molecules and amino acids in the QR2 active site. This finding may explain the trend among the second generation library where increasing steric bulk associated with the aryl rings decreases the inhibitory ability of the molecule. Substitution of the aryl hydroxyl substituents for more sterically bulky alkyl aryl ethers may change this preferred binding orientation within the QR2 active site, thus disfavoring the utilization of the ordered hydrogen bonding network by the compound. In support of this hypothesis, strong electron density of analogue **3.4b** was not observed in the QR2 active site, suggesting that the inhibitor was present only at partial occupancy.

This hypothesis is also supported by our observations regarding the series **3.4f**, **3.4i**, and **3.4k** (Figure 3.5). The most active analogue of our second generation library, **3.4f**, is of the *Z* configuration and has free hydroxyl substituents at the traditional 3,5,4'-positions of resveratrol, which easily participate in the well-characterized hydrogen-bonding network within the QR2 active site. In contrast, the analogue **3.4i**, which is only different from **3.4f** in that it has methyl aryl ethers in the 3,5,4'-positions, did not show great enough inhibition of QR2 to determine an IC_{50} , serving as further evidence that increasing the size of the 3,5,4'-substituents is not easily accommodated by the QR2

active site. The *E* configured isomer of **3.4i**, the analogue **3.4k**, was found not only to be a potent inhibitor of QR2, but also to inhibit QR2 in a completely novel binding orientation. This orientation is entirely distinct from the binding orientations of the *Z* configured analogues, where only the dimethylresorcinol ring of **3.4k** occupies the same molecular space as the other (*Z*)-conformation analogues (Figure 3.6, C). The dimethylresorcinol ring of **3.4k** is positioned parallel to the isoalloxazine ring of the FAD cofactor, possibly participating in a favorable pi-stacking interaction (Figure 3.7, A). In this novel binding orientation **3.4k** does not utilize the same stabilizing hydrogen bonding interactions as the other compounds, instead only forming two hydrogen bonds from the 3- and 4'-methoxy oxygen atoms to a single water molecule which is further anchored through a hydrogen bonding interaction to Asn161. The opposite end of the active site is not occupied by the molecule – instead, there are two new water molecules present, one of which occupies the same molecular space and participates in the same hydrogen bonding network as the 4'-hydroxyl of the *Z* configured resveratrol analogues. Combining the novel structure of **3.4k** in the QR2 active site, and the partial electron density observed for **3.4b** in the QR2 active site, we hypothesize that, for the QR2 active site to accommodate sterically bulky aryl substituents, the molecules must rotate 90° from their preferred binding orientation to allow for the stacking of at least one aryl ring on the isoalloxazine ring. Whether this rotation is possible depends on the nature of the aryl substituents and the orientation of the active site water molecules.

The two most active benzanilide analogues, **3.8a** and **3.8b** (Figure 3.6, E & F), are oriented within the QR2 active site to position all three of their hydroxyl substituents in the same chemical space as those of resveratrol. They participate in identical hydrogen

bonding networks and utilize the same residues as resveratrol for stabilization. The carbonyl groups of the benzanilide cores of each analogue are positioned to interact with the solvent exposed side of the active site and participate in a hydrogen bonding network that can be extended to the 3-hydroxyl (Figure 3.7, B).

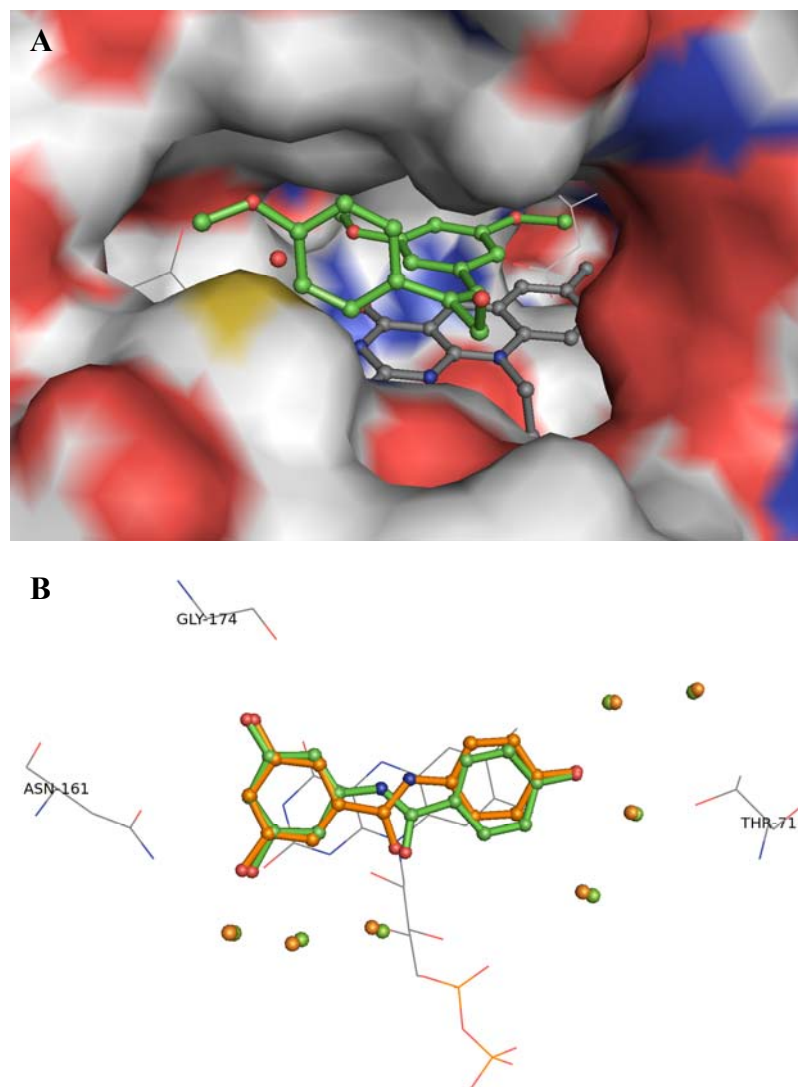


Figure 3.7. (A) Crystal structure of inhibitor **3.4k** bound in the QR2 active site; where QR2 is shown in grey surface representation, and **3.4k** and the FAD cofactor are shown in green and grey, respectively and all are colored according to atom type. (B) Superposition of X-ray structures of **3.8a** (orange ball and stick) and **3.8d** (green ball and stick) in complex with QR2, where active site waters are shown as non-bonding spheres, are colored according to ligand, and are identical between the two compounds.

3.4. Conclusions

Two generations of resveratrol analogues were designed, synthesized, and tested for the inhibition of QR2. This was carried out to explore the types of modifications that could be implemented to increase the selectivity and potency of resveratrol toward QR2, and in an attempt to discover analogues of resveratrol that lacked the 3- and 4'-hydroxyl substituents required for metabolic deactivation. The first generation of analogues was designed to investigate the effect of various substitutions at the both the central alkene and aryl rings of resveratrol. Twenty-four of the seventy-eight first generation analogues were found to inhibit QR2 with ten being more potent inhibitors than resveratrol. Five of the ten most active first generation analogues lacked the metabolically sensitive 3- and 4'-hydroxyl substituents. Based on the results of the first generation, a second generation of analogues was designed to investigate specifically the role of substitution at the central olefin of resveratrol. A total library of forty-seven resveratrol analogues was synthesized and nine compounds from this second generation library were found to inhibit QR2. Two of the second generation analogues had comparable activity to resveratrol while the remaining seven analogues were slightly less potent. Because of the unique nature of these nine compounds, X-ray crystal structures of six of the active analogues were determined. From these X-ray crystallographic studies, were learned that the *Z* configured resveratrol analogues share a common binding conformation, utilizing the same hydrogen bonding network within the QR2 active site as resveratrol. Ultimately, these studies resulted in the identification of a novel binding orientation of our analogue **3.4k**, which is the first example of an *E* configured resveratrol analogue bound in the QR2 active site.

3.5 References

1. Kang, S. S.; Cuendet, M.; Endringer, D. C.; Croy, V. L.; Pezzuto, J. M.; Lipton, M. A., Synthesis and biological evaluation of a library of resveratrol analogues as inhibitors of COX-1, COX-2 and NF- κ B. *Bioorganic & Medicinal Chemistry* **2009**, *17* (3), 1044-1054.
2. Meyers, M. J.; Sun, J.; Carlson, K. E.; Marriner, G. A.; Katzenellenbogen, B. S.; Katzenellenbogen, J. A., Estrogen Receptor- \hat{I}^2 Potency-Selective Ligands: Structure-Activity Relationship Studies of Diarylpropionitriles and Their Acetylene and Polar Analogues. *Journal of Medicinal Chemistry* **2001**, *44* (24), 4230-4251.
3. Knoevenagel, E., Condensation von Malonsäure mit aromatischen Aldehyden durch Ammoniak und Amine. *Berichte der deutschen chemischen Gesellschaft* **1898**, *31* (3), 2596-2619.
4. Lai, G.; Anderson, W. K., A Simplified Procedure for the Efficient Conversion of Aromatic Aldehydes into Esters. *Synthetic Communications* **1997**, *27* (7), 1281-1283.
5. Dalcanale, E.; Montanari, F., Selective oxidation of aldehydes to carboxylic acids with sodium chlorite-hydrogen peroxide. *The Journal of Organic Chemistry* **1986**, *51* (4), 567-569.
6. Kim, E. S.; Lee, H. S.; Kim, J. N., An efficient synthesis of Baylis-Hillman adducts of acrylamide: Pd-catalyzed hydration of Baylis-Hillman adducts of acrylonitrile. *Tetrahedron Letters* **2009**, *50* (46), 6286-6289.
7. Satoh, T.; Suzuki, S.; Suzuki, Y.; Miyaji, Y.; Imai, Z., Reduction of organic compounds with sodium borohydride-transition metal salt systems : Reduction of organic nitrile, nitro and amide compounds to primary amines. *Tetrahedron Letters* **1969**, *10* (52), 4555-4558.
8. Maiti, A.; Reddy, P. V. N.; Sturdy, M.; Marler, L.; Pegan, S. D.; Mesecar, A. D.; Pezzuto, J. M.; Cushman, M., Synthesis of Casimiroin and Optimization of Its Quinone Reductase 2 and Aromatase Inhibitory Activities. *Journal of Medicinal Chemistry* **2009**, *52* (7), 1873-1884.

9. Kondratyuk, T. P.; Park, E.-J.; Marler, L. E.; Ahn, S.; Yuan, Y.; Choi, Y.; Yu, R.; van Breemen, R. B.; Sun, B.; Hoshino, J.; Cushman, M.; Jermihov, K. C.; Mesecar, A. D.; Grubbs, C. J.; Pezzuto, J. M., Resveratrol derivatives as promising chemopreventive agents with improved potency and selectivity. *Molecular Nutrition & Food Research* **2011**, *55* (8), 1249-1265.
10. Sun, B.; Hoshino, J.; Jermihov, K.; Marler, L.; Pezzuto, J. M.; Mesecar, A. D.; Cushman, M., Design, synthesis, and biological evaluation of resveratrol analogues as aromatase and quinone reductase 2 inhibitors for chemoprevention of cancer. *Bioorganic & Medicinal Chemistry* **2010**, *18* (14), 5352-5366.

CHAPTER FOUR:
DE NOVO DESIGN, SYNTHESIS, AND EVALUATION OF SUBSTITUTED
PHENOTHIAZINES AS INHIBITORS OF THE CLASS-II HMG-COENZYME A
REDUCTASE ENZYME FOR THE DEVELOPMENT OF NOVEL
ANTIBACTERIALS

4.1 Introduction: Antibiotic-Resistant Bacteria

Penicillin was discovered in 1928 by the Scottish biologist Sir Alexander Fleming upon returning to his untidy laboratory after an extended vacation at his country house. As he sorted through a stack of Petri dishes, he noticed one that had been contaminated with a blue-green mold and that colonies of *Staphylococcus aureus* near the mold were being dissolved. Interested, Fleming grew pure cultures of the mold and identified it to be from the *Penicillium* genus; he found that the mold produced a substance capable of killing various disease-causing bacteria. He named the substance penicillin and published his work in the British *Journal of Experimental Pathology* in 1929, but was never able to isolate the compound in large quantity.¹ In 1940, the researchers Howard Walter Florey and Ernst Boris Chain of the Radcliffe Infirmary in Oxford determined how to isolate and concentrate penicillin. After several clinical trials, their team developed methods for mass production and distribution of the antibiotic in 1945. The discovery and implementation of penicillin in the twentieth century by Florey, Chain, and Fleming revolutionized modern medicine, and in 1945 the three shared the Nobel Prize in Medicine for their work.

4.1.1 Current Demand for New Antibacterials

Bacteria are constantly evolving in ways to negate the impact of environmental stresses, including antimicrobials. As a result, antibiotic resistance has become a phenomenal problem in the twenty-first century as drug-resistant organisms have acquired resistance to many or all of the antimicrobials on the market. In 2002, the U.S. Centers for Disease Control and Prevention (CDC) estimated no less than 90,000 U.S. deaths due to bacterial infections – more than half of which were caused by bacteria resistant to one or more generally used antibiotic. In October of 2007, the CDC reported at least 100,000 serious bacterial infections a year in the U.S. due to methicillin-resistant *Staphylococcus aureus* (MRSA), with close to 19,000 related fatalities – a number higher than the HIV/AIDS U.S. death toll that same year.² As a consequence, there is a continuous need for new antibacterials as the inevitable rise of bacterial resistance will undo the usefulness of currently used antibiotics.³ To compound the problem, two factors have served as a disincentive for the development of novel antimicrobials. First, the nature of antibiotics dictates that they are used only for a short period of time, days to weeks, whereas other drugs used to treat chronic illnesses like depression or high cholesterol can be taken for years or even decades.⁴ Second, the use of newly approved antibiotics is often limited to the treatment of individuals with cases of serious bacterial infections. This is done in an attempt to prolong the effective lifetime of the new drug by limiting its exposure to bacteria. Thus, only the most severe cases of all those who could potentially benefit from the new antibiotic are able to use it.⁵ Furthermore, a drug that may take over a decade to develop could no longer be clinically useful in just a couple of years as a result of antibacterial resistance. The combination of these factors has resulted

in the decline of antibiotic discovery and development while antibiotic resistance is increasing.

This discovery disincentive has resulted in identification of only four new classes of antibiotics since the 1960s, four classes that have not made a major contribution to antibiotic therapy as a whole. In addition, with the exception of the carbapenems in 1985, all of the antibiotics between the 1960s and 2000 approved for clinical use have been synthetic derivatives of previously used scaffolds. As an example, four scaffolds are responsible for 73% of new antibacterials between 1981 and 2005, the cephalosporins, penicillins, quinolones, and macrolides.⁶ This has led to a forty-year innovation gap in the drug pipeline (Figure 4.1).

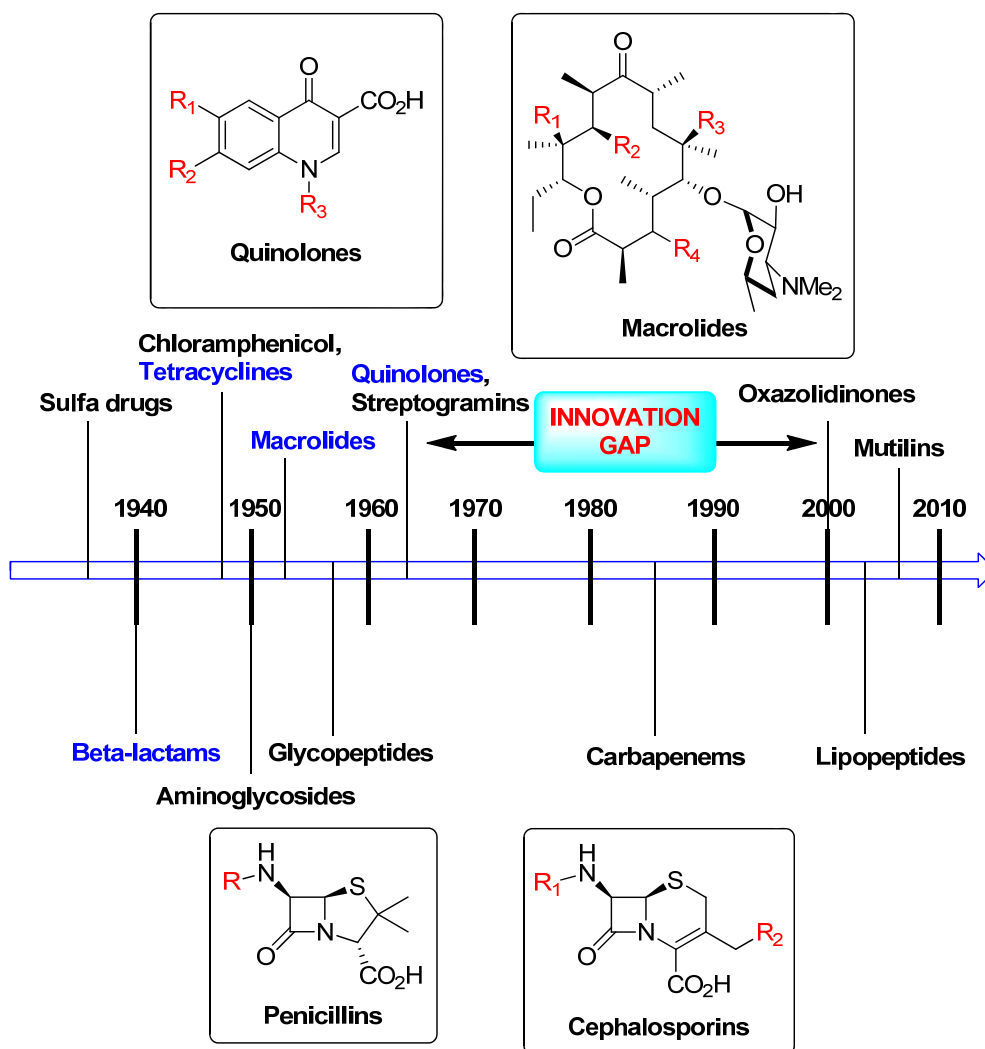


Figure 4.1. Innovation gap in antibacterial drug discovery pipeline.

The late 1980s witnessed the start of an exodus of the pharmaceutical companies from antibiotic development. Originally, fifteen major pharmaceutical companies were involved in antibiotic discovery programs. Today, of those fifteen, eight companies have fully abandoned their discovery programs while two more have significantly reduced their research efforts. Only five companies with antibiotic discovery programs remain, GlaxoSmithKline, Novartis, AstraZeneca, Merck, and Pfizer.² Accordingly, almost all

new antibiotics, and those currently in the pipeline for Gram-positive bacteria, are second- or higher-generation drugs. The combination of all of these factors has led to a desperate need for the development of novel antibacterials and synthetic scaffolds.

4.1.2. Methicillin-Resistant *Staphylococcus Aureus* (MRSA)

Discovered in the 1880s, *Staphylococcus aureus* is a Gram-positive Firmicutes bacterium that colonizes the skin and mucosal surfaces in the nose and human respiratory tract of up to 30% of the population. Though it is not always pathogenic, when it moves beyond its commensal locations, it may cause a variety of infections including boils, necrotizing pneumonia, post-operative wound infections, joint infections, and endocarditis.^{2,7} Before the discovery and use of penicillin in the early 1940s, *S. aureus* infections were fatal in approximately 80% of cases.⁷

In Gram-positive bacteria, penicillin and other β -lactam antibiotics function by inhibiting the transpeptidase activity of penicillin-binding proteins (PBPs), which are a class serine acyltransferases that cross-link the peptidoglycan that forms the bacterial cell wall. The β -lactam antibiotics bind to the PBP's catalytic cleft, forming a covalent association with an active site serine. This covalent β -lactam-enzyme complex is stable and only hydrolyzed at a very slow rate, thus reducing the amount of peptidoglycan cross-linking that can occur.⁸ Ultimately, these antibiotics cause a disruption in the synthesis of the peptidoglycan layer and consequently bacterial death. By 1942, the first strains of penicillin-resistant *S. aureus* were discovered in hospitals. This resistance arose as a consequence of the bacteria acquiring a plasmid that encoded for penicillinase, a β -lactamase enzyme first described by Abraham and Chain in 1940 that deactivates

penicillin and other β -lactams by hydrolysis of the lactam.⁹ In the past half-century, close to 80% of all *S. aureus* isolates found have been penicillin-resistant.

To counteract the growing resistance of *S. aureus* to penicillin in the 1950s, the pharmaceutical industry developed a variety of semisynthetic penicillin variants designed to be resistant to hydrolysis by penicillinase. As a result, methicillin was developed and introduced in 1959 (Figure 4.2). By 1961, European hospitals had identified the first *S. aureus* strains that were resistant to methicillin.¹⁰ *S. aureus* resistance to methicillin is a result of the presence of the *mecA* gene, which encodes for the 78 k-Da penicillin-binding protein 2a (PBP2a). The β -lactam antibiotics are not able to bind to PBP2a; therefore, they cannot disrupt the synthesis of the peptidoglycan layer and bacterial cell wall synthesis is maintained.⁷ Thus, MRSA was born and continues today to be a major cause of nosocomial infections worldwide.

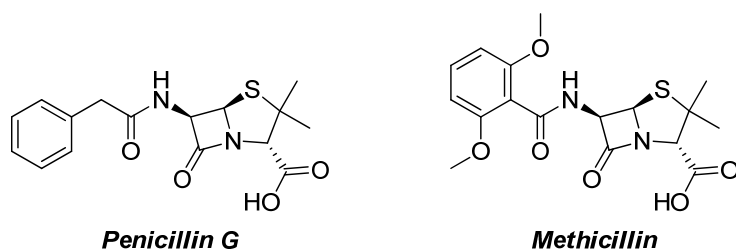


Figure 4.2. Structures of penicillin and methicillin.

4.1.3. Vancomycin-Resistant *Enterococcus* (VRE)

Enterococci are Gram-positive Firmicutes bacteria. Dozens of *Enterococcus* species are known; however, there are two common commensal types of enterococci that reside in human intestines, *E. faecalis* and *E. faecium*. These two species are also

responsible for the majority of human infections, where *E. faecalis* accounts for 80-90% of clinical isolates and *E. faecium* accounts for 5-15%, while the remaining other *Enterococcus* species account for less than 5%.¹¹

Beginning in the late 1970s, enterococci began to be identified as a major player in nosocomial infections. Enterococci are intrinsically resistant to several antimicrobials including moderate concentrations of β -lactams, low concentrations of aminoglycosides, clindamycin, cephalosporins, fluoroquinolones, sulphonamides, and trimethoprim-sulfamethoxazole.¹² Enterococci also have an amazing ability to acquire resistance to all currently available antibiotics, either through mutation or by exchange of plasmids and transposons.¹³ Accordingly, enterococci have acquired resistance to high concentrations of β -lactams, high concentrations of aminoglycosides, glycopeptides, tetracycline, erythromycin, fluoroquinolones, rifampin, chloramphenicol, fusidic acid, and nitrofurantoin.

Until recently, vancomycin was the only drug that could be reliably used to treat bacterial infections caused by multi-drug resistant enterococci. Vancomycin is a tricyclic glycopeptide antibiotic that was discovered in 1953 when it was isolated from the actinomycete *Amycolatopsis orientalis* and is often used as the “antibiotic of last resort.” Vancomycin exerts its bactericidal effect by binding to peptides containing D-alanyl-D-alanine, the substrate of peptidoglycan synthetase, thus disrupting peptidoglycan polymerization.¹² It has been in use for over 30 years, and until recently, vancomycin-resistance was relatively rare.

The first strains of vancomycin-resistant *Enterococcus* (VRE) were isolated in England and France in 1986 and, after only one year, VRE was isolated in the U.S.¹⁴

Since then, five phenotypes of vancomycin resistance have been described in enterococci: VanA-VanE.¹¹ VanA and VanB are the most clinically important of the phenotypes, and both are frequently found in *E. faecalis* and *E. faecium*. The VanA phenotype shows high resistance to vancomycin and the semisynthetic glycopeptide antibiotic teicoplanin. Exposure of the VanA phenotype to antimicrobial agents triggers the synthesis of multiple proteins that work together to prevent the binding of vancomycin to its peptide substrates, thus conferring resistance. The VanB phenotype enterococci show resistance to vancomycin but not teicoplanin.¹² Between the years 1989 and 1993, the National Nosocomial Infections Surveillance System (NNIS) reported an increase from 0.3 to 7.9% of enterococcal isolates containing VRE from intensive care units (ICUs). By 2000, of the 2575 enterococcal isolates tested from ICUs, the percentage containing VRE had risen to 26.3%.¹⁵

4.2. Targeting MRSA and VRE

The overall aim of this research is the development of novel antibacterial compounds, compounds having previously unused scaffolds and that function through new modes of action, for the treatment of MRSA, VRE, and other pathogenic Gram-positive bacteria. The Class II 3-hydroxy-3-methylglutaryl coenzyme A reductase (II-HMGR) enzyme was selected as the target for the development of novel antibacterials. The high druggability of II-HMGR makes it an appealing target; it is essential for the survival of Gram-positive cocci, it is highly conserved among staphylococcal, streptococcal, and enterococcal pathogens, it is distinct from the Class I HMGR of

humans, absent in a large quantity of other commensal bacteria, and harbors an active site region amenable to small molecule binding.

4.2.1. 3-Hydroxy-3-Methylglutaryl Coenzyme A Reductase (HMGR)

The HMGR enzyme catalyzes the first committed step in the mevalonate pathway, which is the biological pathway used by humans, other eukaryotes, archaea, and Gram-positive cocci for the biosynthesis of isopentenyl diphosphate (isopentenyl pyrophosphate). Isopentenyl diphosphate (IPP) is an essential precursor for the synthesis of isoprenoids. In bacteria, IPP is used in the construction of undecaprenol, a lipid carrier that is crucially involved in cell wall biosynthesis. Other products of IPP include the menaquinones and ubiquinones which are involved in electron transport.¹⁶ Two pathways for the synthesis of IPP have been identified. The mevalonate pathway is the more common of the two, while the glyceraldehyde 3-phosphate/pyruvate (GAP) pathway is less common and is employed by Gram-negative bacteria.¹⁷

The mevalonate pathway was described by Joseph Goldstein and Michael Brown in 1970 when it was first identified in eukaryotic cells.¹⁸ This pathway ultimately results in the production of IPP from the linking of three acetyl coenzyme A (acetyl-CoA) units. First, the enzyme acetyl-CoA transferase joins two acetyl-CoA units. The addition of a third acetyl-CoA unit is then catalyzed by HMG-CoA synthase, forming 3-hydroxy-3-methylglutaryl coenzyme A (HMG-CoA). A series of biological reactions involving the reduction of HMG-CoA to mevalonate, phosphorylation, decarboxylation, and dehydration eventually results in the formation of IPP (Figure 4.3).

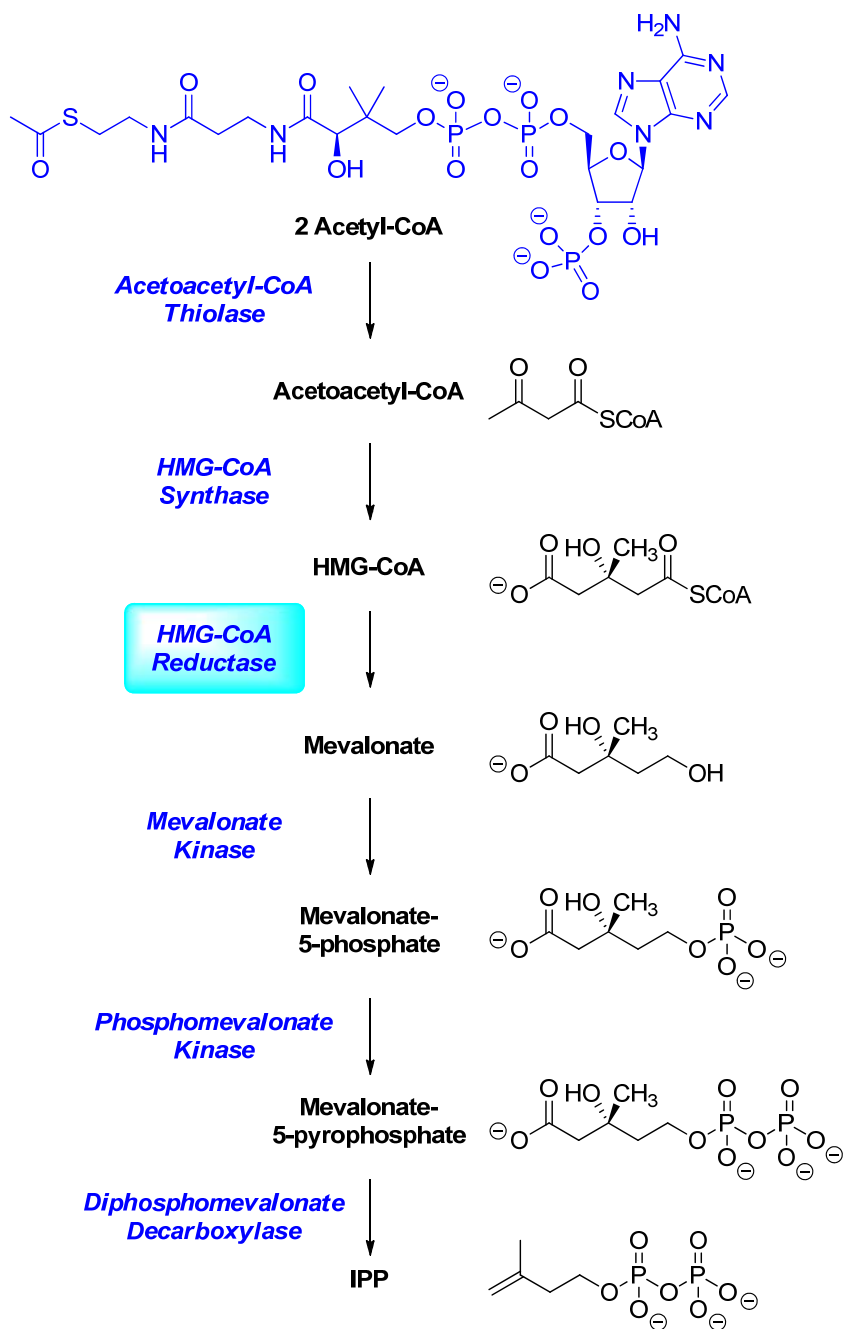


Figure 4.3. Mevalonate pathway.

HMG-CoA reductase is the best characterized enzyme in the mevalonate pathway. It is a four-electron oxidoreductase that catalyzes the reductive deacylation of (*S*)-HMG-CoA to (*R*)-mevalonate, a reaction that occurs in three parts, where the first and third part are reductive. There are four conserved catalytic residues that are crucial for HMGR function as determined by site-directed mutagenesis: a histidine,^{19, 20} aspartate,²¹ glutamate, and lysine.²² The role of the histidine is the protonation of the departing CoA thiolate, which reduces the ability of the sulfur to attack the bound mevaldehyde intermediate, an event that would subsequently hinder the overall reaction. The other residues, the catalytic lysine, aspartate, and glutamate, function through a hydrogen bond network that interacts with the carbonyl group of HMG-CoA and stabilizes the mevaldyl-CoA and mevaldehyde enzyme-bound intermediates (Figure 4.4).

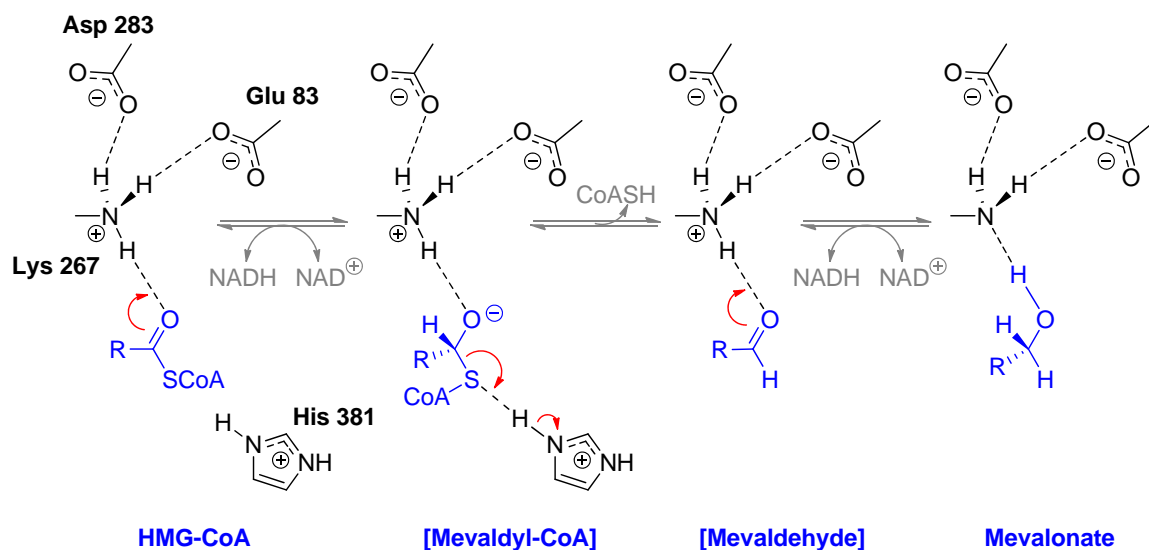


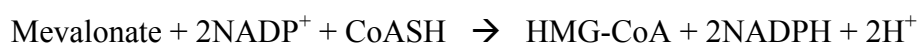
Figure 4.4. Proposed reaction mechanism for *P. mevalonii* HMG-CoA reductase.¹⁷

The difference between the two classes of HMGRs (Class I for humans and eukaryotes, Class II for prokaryotes) resides in the placement of the active site lysine, which is only conserved within the two classes and is present on different structural elements.¹⁷ The eukaryotic I-HMGRs contain a highly conserved C-terminal catalytic domain and a weakly conserved, membrane-bound N-terminal domain that is made of two to eight transmembrane helices. Unlike the I-HMGRs, II-HMGRs do not contain a membrane-bound N-terminal domain. Both I- and II-HMGRs form obligate dimers that associate into a tetramer in the human form and a dimer or hexamer in the bacterial form, where the overall fold of both classes of HMGR are similar and have the active site located at the dimer interface. The catalytic domains of both I- and II-HMGRs are analogous, where the positions and orientations of the key catalytic residues are conserved between Class I- and II-HMGRs. The catalytic area of the I-HMGR is composed of three domains: a helical N-terminal domain (N-domain), a larger central domain (L-domain), and a small domain (S-domain) that resides within the L-domain. The II-HMGRs contain all of the domains of the I-HMGRs in addition to a fourth domain, the C-terminal helical domain. This C-terminal domain is known as the ‘flap domain’ and is only ordered upon binding of the substrate and cofactor. When the substrate and cofactor bind to HMGR, a helical domain (a single helix in Class I and three helices in Class II HMGRs) folds over the active site. In the Class I HMGRs, this single helix delivers the critical lysine to the active site, a feature known as the ‘*cis*-loop’. In contrast, in the Class II HMGRs, this critical catalytic lysine is always present in the active site, residing on a well-defined helix.²³

These differences in the structures and catalytic sites of I- and II-HMGRs create a therapeutic window for targeting II-HMGR. An example of this are the well known statin drugs, used to treat high cholesterol in humans through the inhibition I-HMGR. Lovastatin inhibits hamster I-HMGR with a K_i of 5 nM. Against the II-HMGRs of *S. aureus*, *E. faecalis*, and *P. mevalonii*, Lovastatin has K_i 's of 320, 500, and 530 μ M, respectively.²⁴

4.3. Previous Work

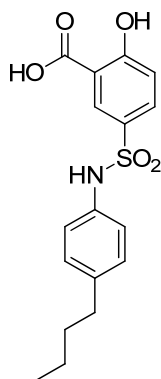
The Stauffacher Research Group of the Department of Biological Sciences at Purdue University produced and purified the II-HMGR enzyme from *E. faecalis* to be used as a target for an initial high throughput screen to identify inhibitors for II-HMGR.²⁵ The *E. faecalis* II-HMGR enzyme was chosen as the target for the screen as it was the most stable and easily purified enzyme of the pathogens of interest. The purified enzyme was sent to the Southern Research Institute (SRI) in Birmingham, AL where a high throughput screen of 305,000 compounds was performed to identify II-HMGR inhibitors. Inhibitor ability was determined using an assay that monitored the reverse reaction of II-HMGR by following the conversion of NADP to NADPH at 340 nm (Equation 4.1).



Equation 4.1. Reverse reaction of II-HMGR (non-physiological direction).

This high throughput screen of 305,000 commercially available compounds resulted in the identification of 27 small molecules that inhibited II-HMGR in the non-physiological direction with IC_{50} values less than 250 μ M. These 27 small molecules

were re-assayed at Purdue against II-HMGR from *E. faecalis* and *P. mevalonii* where seven of the compounds were found to inhibit II-HMGR in the non-physiological direction with IC_{50} values less than 250 μ M. Structural studies were then undertaken for these seven compounds, where only one of the seven identified inhibitors was found to show electron density when soaked into *P. mevalonii* II-HMGR crystals, resulting in the identification of the compound 5-(*N*-(4-butylphenyl)sulfamoyl)-2-hydroxybenzoic acid (*N*-bsha). Subsequently, the X-ray crystal structure of the *N*-bsha-*E. faecalis* II-HMGR complex was determined and *N*-bsha was found to competitively inhibit *E. faecalis* II-HMGR with an IC_{50} of 50 μ M in the physiological direction and 5 μ M in the non-physiological direction (Figure 4.5).



***N*-bsha**

E. faecalis II-HMGR

(physiological direction) IC_{50} = 50 μ M

(non-physiological direction) IC_{50} = 5 μ M

Figure 4.5. Structure of lead compound *N*-bsha.

The X-ray crystal structure of the *N*-bsha-*E. faecalis* II-HMGR complex shows that *N*-bsha binds in the active site of II-HMGR, utilizing the same chemical space as mevalonate (Figure 4.6, A&B). *N*-bsha forms several direct and water-mediated stabilizing hydrogen-bonds from each of its heteroatoms to key residues within the II-HMGR active site, including two of the residues that are functional in the catalytic mechanism, Asn213 and Glu86. The orientation of *N*-bsha within the II-HMGR active site is such that the butylphenyl group of *N*-bsha is in a position to effectively block the closing of the C-terminal flap domain, inhibiting catalysis. Comparison of the *N*-bsha-*E. faecalis* II-HMGR complex and a complex of *E. faecalis* II-HMGR bound with an HMG-CoA analogue shows that the carboxylate groups of each compound are aligned in the active site, allowing for the hydrogen-bonding interaction of each carboxylate with Arg257. Furthermore, the phenol ring of *N*-bsha shares the same chemical space as the hydroxymethylglutamate of HMG-CoA and the sulfonamide of *N*-bsha imitates the amide of HMG-CoA resulting in very little reorganization of the II-HMGR active site upon binding of *N*-bsha.

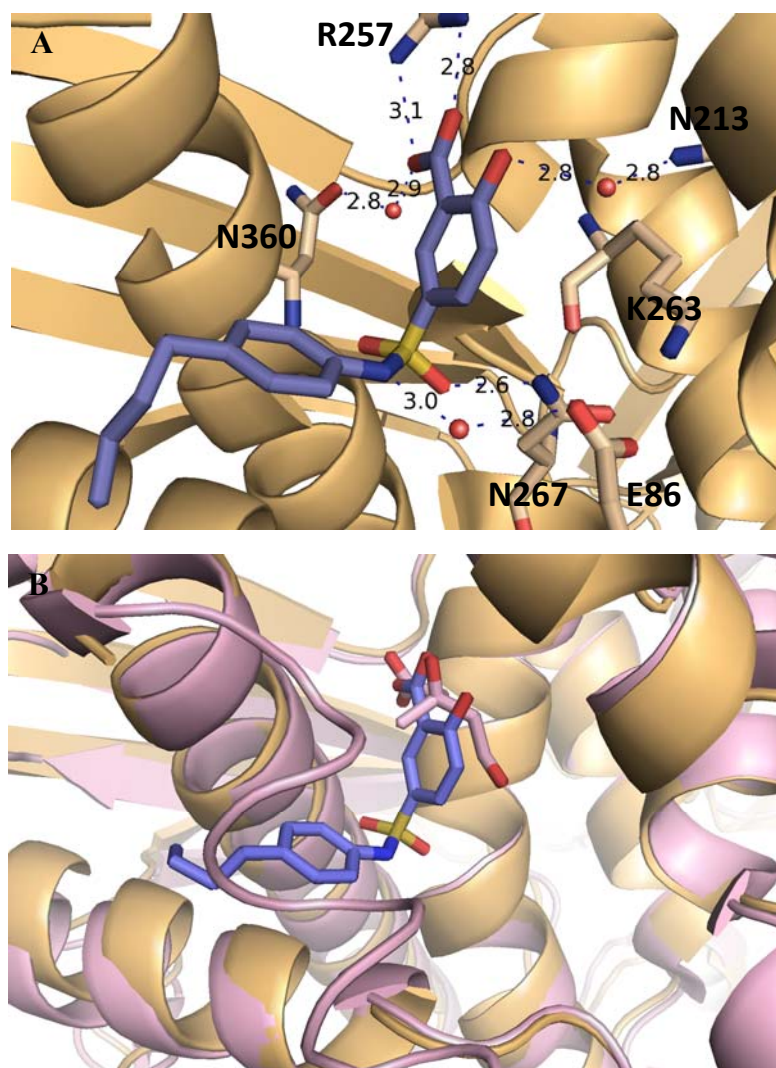


Figure 4.6. (A) X-ray crystal structure of *N*-bsha bound in *E. faecalis* II-HMGR active site showing key hydrogen-bonding network, where *N*-bsha is shown in blue and colored by atom type, waters are shown as red spheres, and the critical active site residues are shown as sticks and colored by atom type. (B) Superposition of *E. faecalis* II-HMGR (light yellow) and *P. mevalonii* II-HMGR (light pink, PDB: 1QAY), where mevalonate is shown in light pink and colored by atom type.

4.4 De Novo Design of II-HMGR Inhibitors

Using the structural features elucidated by the X-ray crystal structure of the inhibited *E. faecalis* II-HMGR active site, we set out to discover novel inhibitors of II-HMGR through a strategy of *de novo* design and *in silico* screening.

4.4.1. Tandem Design Approach: e-LEA3D and AutoDock Vina (ADV)

A tandem design approach was utilized for the design of novel II-HMGR inhibitors. The initial *de novo* design was performed using the e-LEA3D web server and the results of the *de novo* design were evaluated *in silico* using the docking program AutoDock Vina (ADV). The e-LEA3D web server is a program that utilizes a fragment-based approach for the generation of original drug candidates.²⁶ This fragment-based approach employs a genetic algorithm that optimizes a combination of chemical fragments by evolving a population of molecules over several generations. A scoring function that incorporates various user-defined molecular properties and the protein-ligand docking score calculated by the program PLANTS is used to assess the fitness of each candidate within a population.²⁷ Only the most fit combinations are used in the next generation.

The binding site from the X-ray crystal structure of *P. mevalonii* II-HMGR complexed with HMG-CoA (PDB: 1R31) was used to define the region for fragment-based design. The *P. mevalonii* II-HMGR was used as the enzyme structure uploaded to the e-LEA3D web server for fragment-based design, as the X-ray crystal structure of *E. faecalis* II-HMGR in complex with *N*-bsha was not yet published. Residues K267 and T264 of *P. mevalonii* II-HMGR were chosen to define the binding region around which

ligand design was based. The K267 residue was chosen due to its critical function in the II-HMGR mechanism (*vide supra*) and the T264 residue was chosen as a result of its prime location within the interior of the II-HMGR active site. The *P. mevalonii* II-HMGR residues K267 and T264 correspond to the *E. faecalis* II-HMGR residues K263 and T260. Fifteen generations of twenty candidates each were produced by e-LEA3D, where the binding site radius was limited to 15 Å around the specified amino acid and the molecular weight of the candidates produced was limited so as not to exceed 469 Da.

The results produced by e-LEA3D were assessed using ADV, a program for the molecular docking and virtual screening of compounds *in silico*.^{28,29} The output of ADV was evaluated in three ways. First, the predicted orientation of the candidate relative to the II-HMGR active site was examined. The defined search space for ADV, the space in the II-HMGR enzyme available for ADV to dock the candidate, was defined to encompass an entire half of the II-HMGR enzyme. Because II-HMGR is a homodimer, each side is essentially identical and the enzyme has two identical active sites. Therefore, by defining the search space as half of the II-HMGR homodimer, ADV was essentially allowed to dock the candidate anywhere on II-HMGR. Here, the binding orientation is used to refer to the placement of the docked candidate relative into the II-HMGR active site. Nine binding orientations were produced for each candidate, and candidates that had better binding orientations were candidates that were oriented in or near the II-HMGR active site as predicted by ADV. Second, ADV uses a scoring function that is tuned to recognize promising conformations of the candidate molecule in the II-HMGR enzyme, and ADV uses this scoring function to predict the binding affinity of the candidate. This output, produced in kcal/mol, is different for each predicted binding conformation and

orientation of a given candidate. Candidates with better scores have lower binding affinities. Third, the binding conformation is used here to refer to the conformation of the molecule when docked in the enzyme.

The results of the initial e-LEA3D *de novo* design were evaluated by ADV for two reasons; first, ADV was used as a means to “double-check” the results of e-LEA3D and second, it provided a method to validate that the candidates produced by e-LEA3D for *P. mevalonii* II-HMGR would also be active against *E. faecalis* II-HMGR. To determine these two things, the predicted orientation, binding conformation, and binding affinity produced by ADV were all taken into consideration. The candidates from the initial e-LEA3D design that had the best binding affinities and most promising orientations predicted by ADV were then carried forward and subjected to further modifications, this time using the functionalization feature of e-LEA3D to decorate the molecules at user-specified positions that were identified by the analysis of the candidate’s predicted binding orientations produced by ADV.

The functionalization results produced by e-LEA3D from the second design step were then evaluated with ADV. Again, ADV was used to assess the predicted orientation, binding conformation, and binding affinity of the functionalized candidates. The candidates with the best predicted binding affinities and most selective predicted binding orientations were then subjected to further user-specified functionalization. These user-specified modifications were made to confer further selectivity to the candidate, and the success of the various functionalizations was determined by ADV. Three candidate scaffolds were arrived at through this design approach: a phenothiazine

scaffold, a quinoline scaffold, and an indole scaffold. A pictorial representation of this iterative design approach is shown in Figure 4.7.

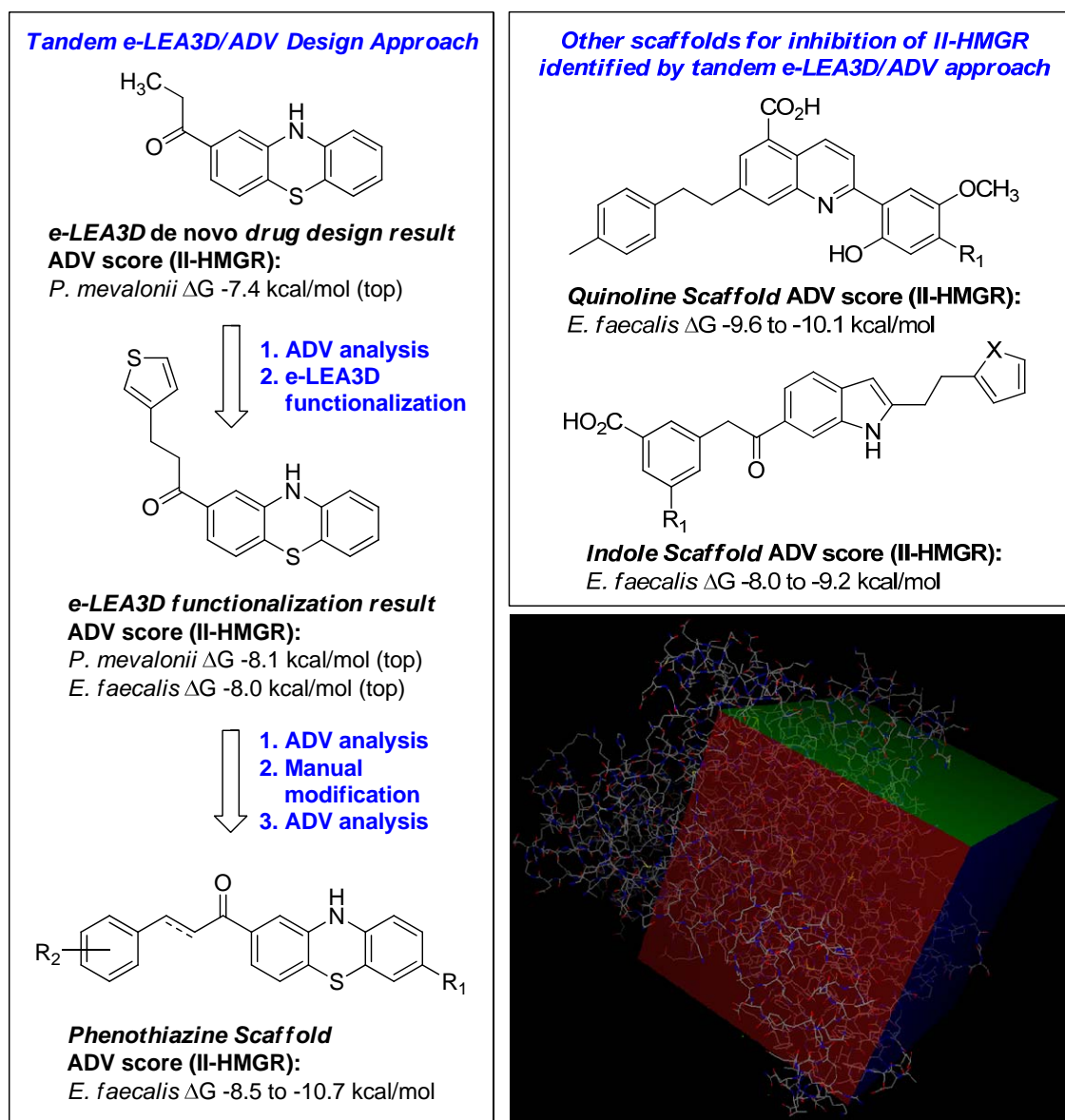


Figure 4.7. (Left) Pictorial representation of tandem e-LEA3D/ADV design approach, (Top Right) Other scaffolds arrived at through tandem design approach, (Bottom Right) Available search space defined for ADV.

4.4.2. Validation of ADV Results

To test the validity of the docking results produced by ADV for the candidate inhibitors, ADV was used to predict the binding conformation of the known II-HMGR inhibitor *N*-bsha in *E. faecalis* II-HMGR. Starting from the unbound structures of the II-HMGR enzyme and *N*-bsha, where the rotatable bonds, torsion angles, and position of *N*-bsha had been randomized prior to docking, ADV was able to correctly predict the actual binding conformation of *N*-bsha to within a small margin of difference. Thus, the scoring function utilized by ADV correctly identified the true binding conformation of *N*-bsha actually determined by the X-ray crystal structure, recognizing this binding pose as an energy minimum. The predicted binding conformation overlaid with the actual crystal structure of *N*-bsha are shown in Figure 4.8, A.

The predicted binding affinity produced by ADV for the top scored binding pose of *N*-bsha (Figure 4.8) was -7.0 kcal/mol. Using Equation 4.2, this predicted binding affinity (ΔG) can be used to predict the dissociation constant (K_i) for *N*-bsha and *E. faecalis* II-HMGR to be roughly 8 μ M. Though the actual K_i for *N*-bsha and *E. faecalis* II-HMGR has not been determined, the K_i for *N*-bsha and *S. aureus* II-HMGR has been determined by the Stauffacher group to be 71 μ M in the non-physiological direction, roughly an order of magnitude higher than that predicted. The predicted binding affinity produced by ADV for the top binding pose of the designed phenothiazine **4.40** was -10.1 kcal/mol, which corresponds to a predicted K_i of roughly 43 nM (Figure 4.8, B & C).

$$K_i = e^{(\Delta G/k_B T)} \text{ where } k_B T[300K] = 0.596165 \text{ kcal/mol}$$

Equation 4.2. Prediction of K_i .

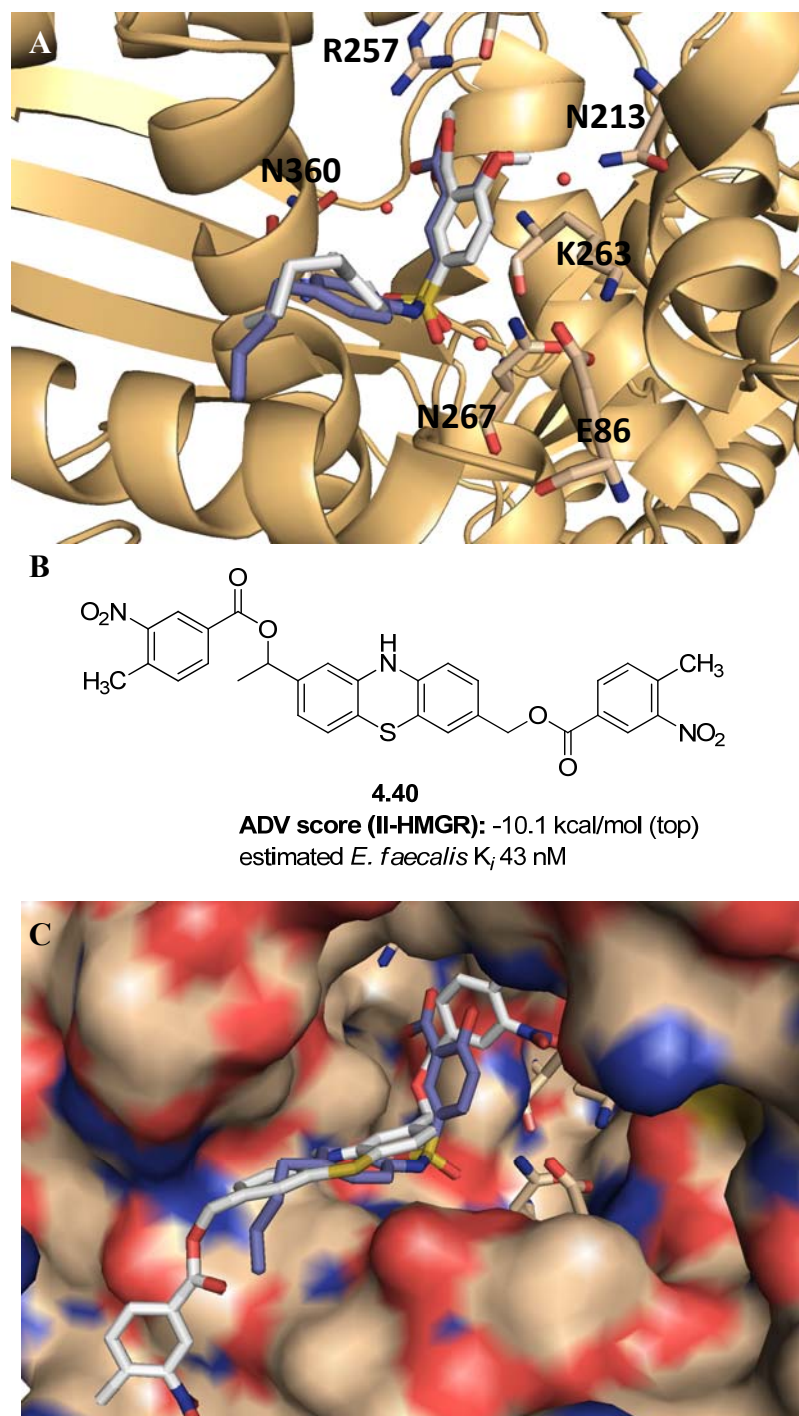
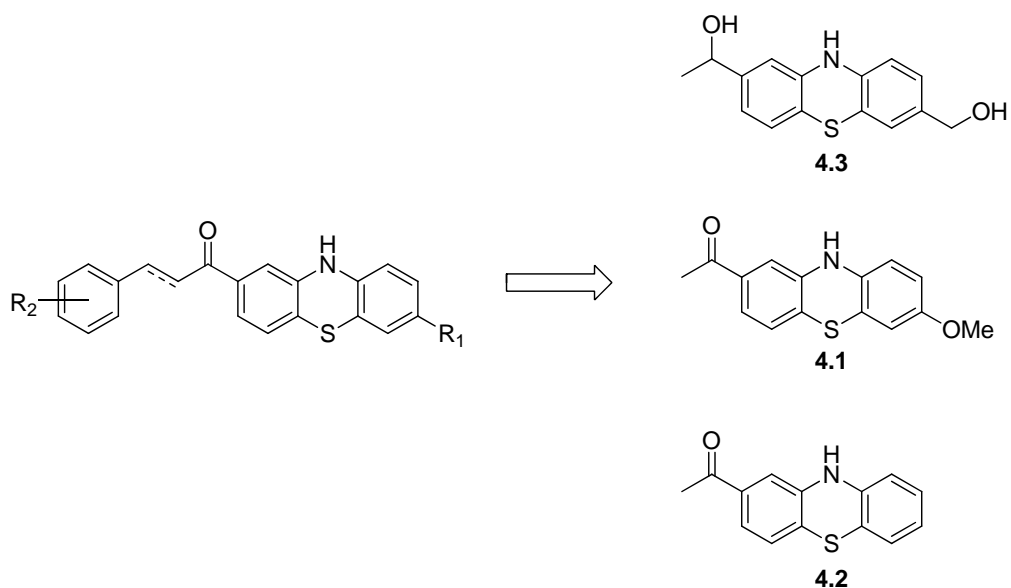


Figure 4.8. (A) Validation of ADV exercise, predicted and actual binding conformation of *N*-bsha in *E. faecalis* II-HMGR, where the blue *N*-bsha molecule is the actual binding conformation determined by X-ray crystal structure and the white *N*-bsha molecule is the predicted binding conformation produced by ADV. (B) Designed phenothiazine compound **4.40**. (C) Overlay of predicted fourth binding mode of **4.40** superimposed on X-ray crystal structure of *N*-bsha.

4.5. Construction of Substituted Phenothiazine Library

Based on our *de novo* design and *in silico* screening work, we set out to synthesize a small library of substituted phenothiazines for the inhibition of II-HMGR. The phenothiazines synthesized were derivatives of the general structure shown in Figure 4.7, and were selected for synthesis based on their docking score, synthetic accessibility, and availability of starting materials. To construct the phenothiazine library, we envisioned the formation of three phenothiazine cores amenable to functionalization, **4.1**, **4.2**, and **4.3** (Scheme 4.1).

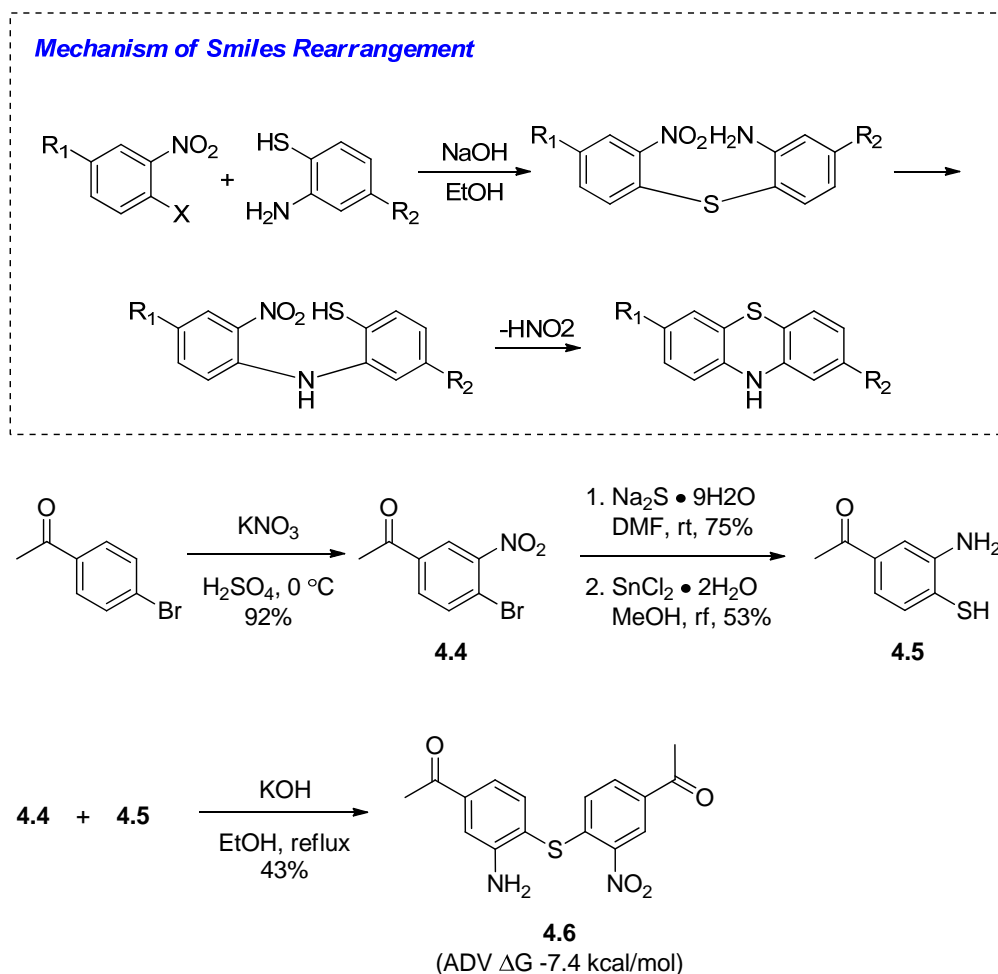


Scheme 4.1. Retrosynthetic route toward phenothiazine library.

4.5.1. Attempted Synthesis of Phenothiazine Cores

4.5.1.1. Smiles Rearrangement

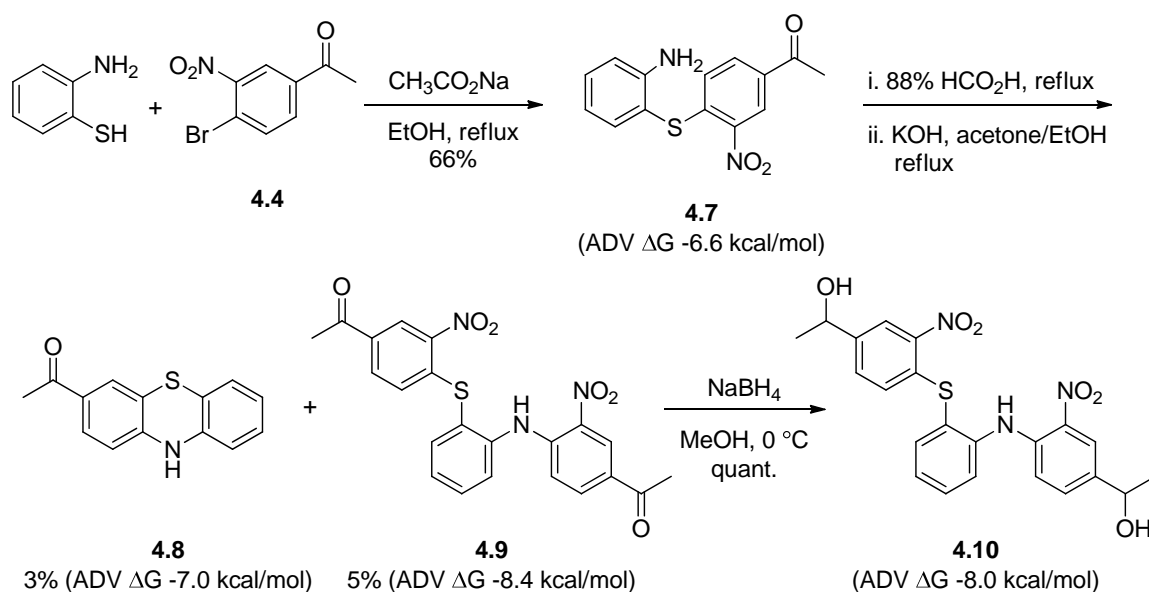
We first set out to accomplish the synthesis of the phenothiazine cores by a Smiles rearrangement, the mechanism of which is shown in Scheme 4.2.³⁰⁻³³ Envisioning that reaction of the *o*-nitro bromide **4.4** with the *o*-amino thiophenol **4.5** would result in the phenothiazine in one synthetic step, we set out to synthesize these molecules. The two reactants **4.4** and **4.5** were obtained by derivatization of the same commercially available starting material. The *o*-nitro bromide **4.4** was formed by the nitration of 4-bromoacetophenone using potassium nitrate in sulfuric acid and the *o*-amino thiophenol **4.5** was obtained by treatment of **4.4** with sodium sulfide followed by reduction of the nitro group with stannous chloride. With the two desired reactants in hand, we attempted to affect the Smiles rearrangement using the established procedure, by treatment with potassium hydroxide in refluxing ethanol. To our dismay, this reaction did not produce the desired phenothiazine, and the only product isolated from the reaction mixture was the sulfide **4.6** (Scheme 4.2, bottom). Presumably, this reaction did not proceed to the phenothiazine because the aryl ring containing the nitro moiety was not sufficiently electron deficient. Though the sulfide obtained was not the desired compound, we were curious as to whether this derivative could inhibit II-HMGR. Analysis of **4.6** using ADV produced a predicted binding affinity of -7.4 kcal/mol for the best scored binding pose, and had a predicted binding conformation in the same chemical space in II-HMGR as *N*-bsha.



Scheme 4.2. (Top) Mechanism of Smiles rearrangement. (Bottom) Synthesis of reactants and first attempt at production of phenothiazine core via Smiles rearrangement.

We then turned our attention to a slightly modified synthetic route to the phenothiazine, still employing the similar reactants.³² Treatment of the commercially available *o*-aminothiophenol and **4.4** with sodium acetate in refluxing ethanol produced the desired sulfide **4.7**, which was predicted by ADV to have a binding affinity of -6.6 kcal/mol. The amine was then formylated, increasing its acidity, and treated with potassium hydroxide in a refluxing mixture of acetone and ethanol. This reaction produced the desired phenothiazine **4.8** in very low yield as well as a number of other

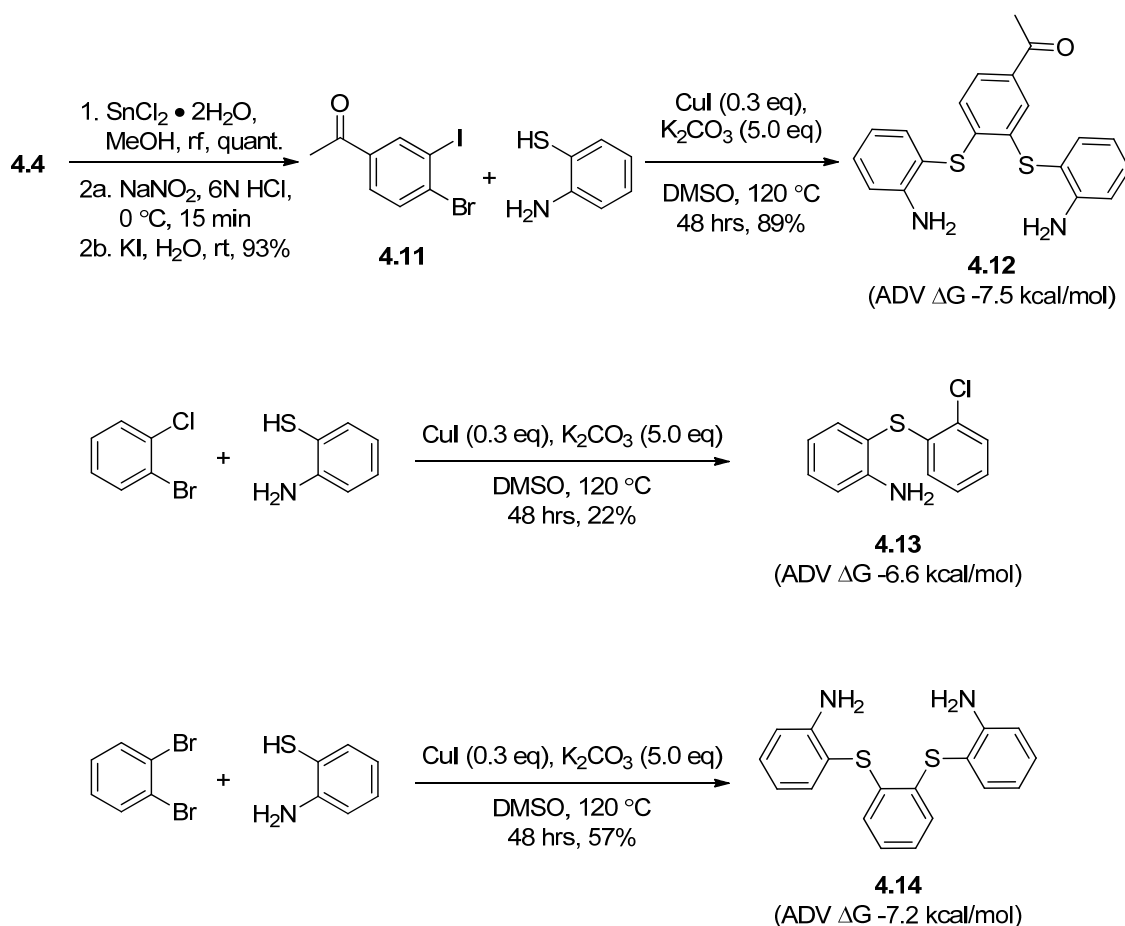
products including the byproduct **4.9** which arose as a result of the di-substitution of *o*-aminothiophenol. Again, ADV was used to predict the ability of the synthesized compounds to inhibit II-HMGR and, to our surprise, the byproduct **4.9** had a predicted binding affinity of -8.4 kcal/mol for its top scored binding pose. An analogue of **4.9** was then synthesized by reduction of the carbonyls using sodium borohydride, resulting in the desired compound **4.10** (Scheme 4.3). Though the modified Smiles rearrangement resulted in the desired phenothiazine core, it could not be optimized to give reliable results in higher yields and was therefore not a suitable synthetic route.



Scheme 4.3. Modified Smiles rearrangement resulting in compounds **4.7-4.10**.

4.5.1.2. CuI-Catalyzed Cascade C-S and C-N Bond Formation

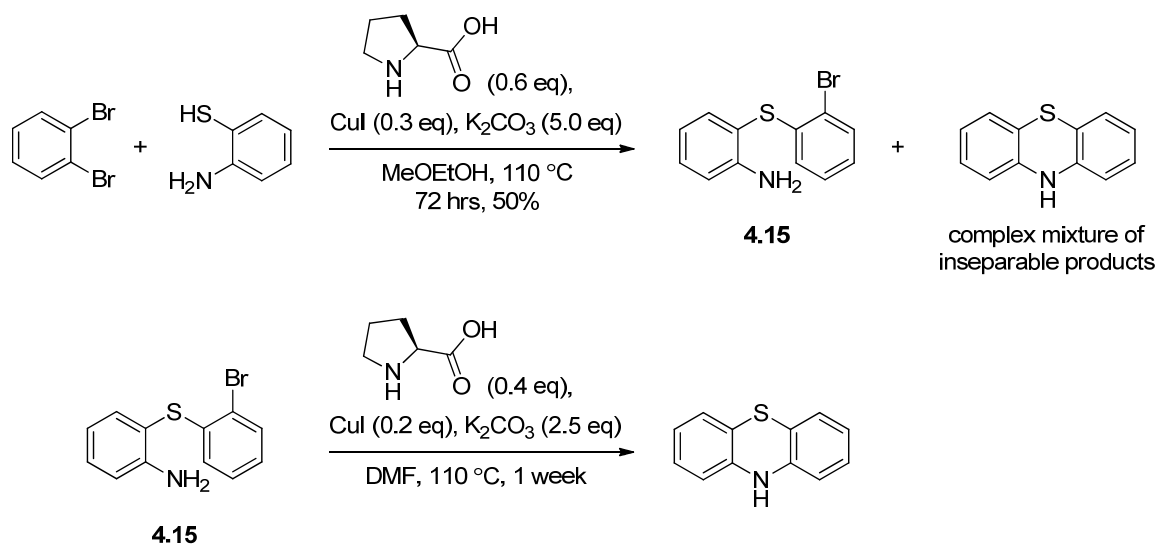
Turning toward a new synthetic route, we sought to employ a copper-catalyzed cascade C-S and C-N bond forming reaction.³⁴ The starting materials for this reaction were again synthesized from the same commercially available 4-bromoacetophenone. Reduction of the nitro moiety of **4.4** with stannous chloride followed by diazotization and substitution using potassium iodide resulted in the *o*-dihalide **4.11**. Reaction of **4.11** with the commercially available *o*-aminothiophenol following the reported ligand-free protocol of Dai,³⁴ with freshly recrystallized Cu^(I)I and potassium carbonate in dimethylsulfoxide at 120 °C for 48 hours under an inert atmosphere, did not yield the desired phenothiazine. Instead the bis-sulfide **4.12** was obtained in 89% yield. This result was rationalized as a consequence of the two very labile carbon-halogen bonds. Thinking that reducing the lability of these bonds would promote the desired intramolecular cascade reaction over the two intermolecular S-C couplings, the reaction was carried out again using the two commercially available substrates, *o*-bromochlorobenzene and *o*-aminothiophenol. Unfortunately, this attempt was not met with success; instead, the reaction stopped after formation of the sulfide **4.13**, and C-N bond formation did not take place, indicating that the C-Cl bond was not labile enough to promote the intramolecular coupling. In a final attempt at this ligand-free protocol, the commercially available *o*-dibromobenzene was reacted with *o*-aminothiophenol. Here, the two C-Br bonds proved too labile and the intermolecular reaction was again favored, producing the bis-sulfide **4.14**. All of the byproducts produced from these coupling attempts were analyzed using ADV and their predicted binding affinities are shown in Scheme 4.4.



Scheme 4.4. Attempts at ligand-free CuI-catalyzed cascade C-S and C-N bond formation.

After our many failures at employing the ligand-free CuI-catalyzed route toward the phenothiazine, we attempted the use of L-proline as a ligand to promote the reaction.³⁵ However, subjecting the commercially available *o*-dibromide and *o*-aminothiophenol to the conditions shown in Scheme 4.5 using L-proline as a ligand did not result in the desired phenothiazine in pure form. Instead, the sulfide **4.15** was obtained in 50% yield along with a complex mixture of products that appeared to contain the phenothiazine, but from which it could not be purified. Finally, re-subjecting the sulfide **4.15** to the coupling conditions produced phenothiazine by NMR analysis of the crude

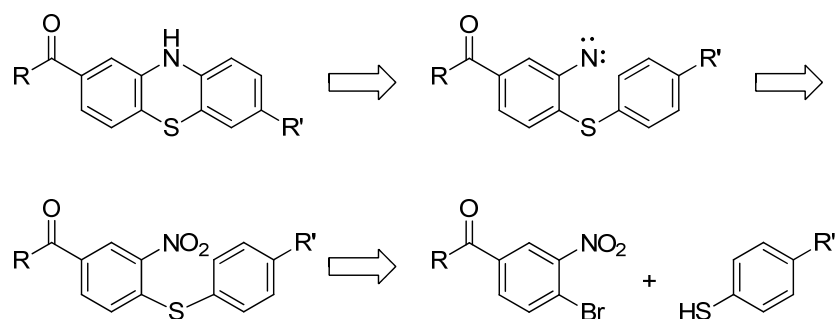
reaction mixture; however, because of the long reaction times and inconsistency of the results, we set out to find an alternative synthetic route to access the phenothiazine cores (Scheme 4.5).



Scheme 4.5. CuI-catalyzed coupling using L-proline as a ligand.

4.5.2. The Cadogan Reaction: Synthesis of First Phenothiazine Set

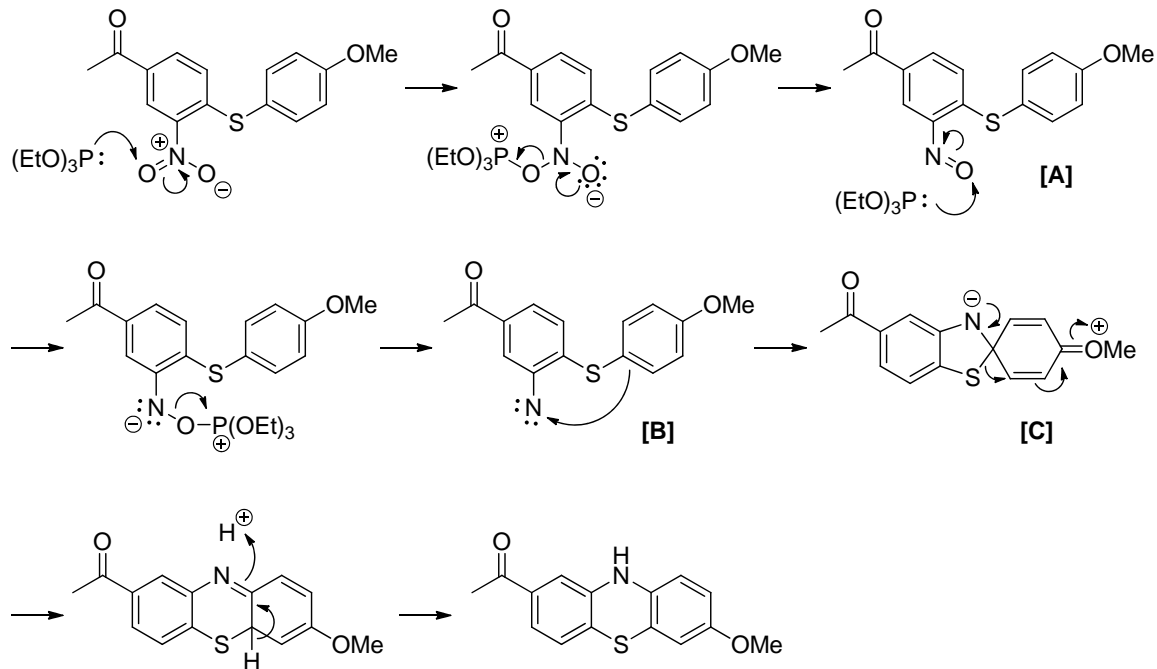
After the various, detailed failures in our synthetic efforts towards the phenothiazines cores, we envisioned effecting the formation of the phenothiazine through a new route - the formation of an electrophilic nitrogen (Scheme 4.6). We had learned through our previous failures that the sulfide was easy to access, and therefore we thought to create a sulfide starting material that bore a nitrogen-containing functionality that could eventually react as an electrophile in an aromatic substitution reaction, forming the phenothiazine. A literature search of such reaction types resulted in the discovery of the Cadogan reaction.



Scheme 4.6. Intended formation of phenothiazine via reactive nitrene intermediate.

The Cadogan reaction was first reported in 1966 and is an underutilized method for the synthesis of phenothiazines, as most phenothiazines are currently synthesized by various coupling reactions.^{36, 37} These reactions employ metal catalysts, various ligands, are extremely sensitive to air and moisture, have long reactions times, and often times have variable results (*vide supra*). In contrast, the Cadogan reaction uses easily accessible starting materials and inexpensive reagents, is only mildly air sensitive, and consistently results in the desired phenothiazine product in moderate to good yields depending on the substitution pattern of the starting materials.

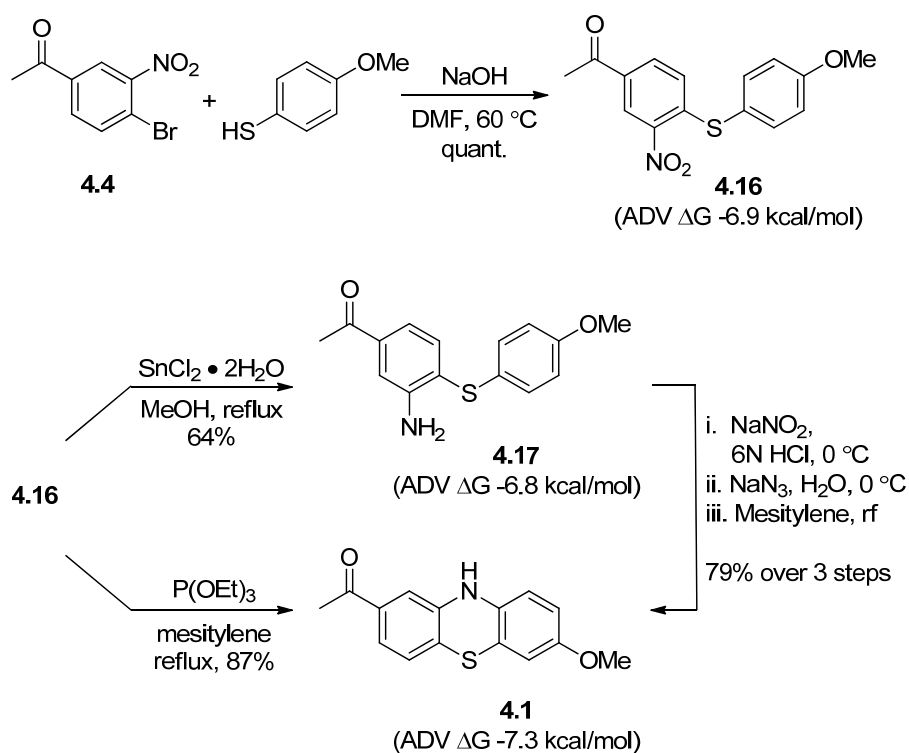
The Cadogan reaction employs the reductive cyclization of an aromatic nitro compound using triethylphosphite to generate a nitrene in situ; the mechanism of this rearrangement is shown in Scheme 4.7. First, attack of triethylphosphite on the nitro group followed by elimination of triethyl phosphate produces the nitroso compound **[A]**. Attack of a second molecule of triethylphosphite on the nitroso moiety followed by alpha-elimination produces the nitrene intermediate **[B]**. Electrophilic aromatic substitution at the ipso-carbon of the sulfide then gives the cyclic intermediate **[C]**, which rearranges and produces the phenothiazine upon tautomerization.



Scheme 4.7. Mechanism of Cadogan reaction.

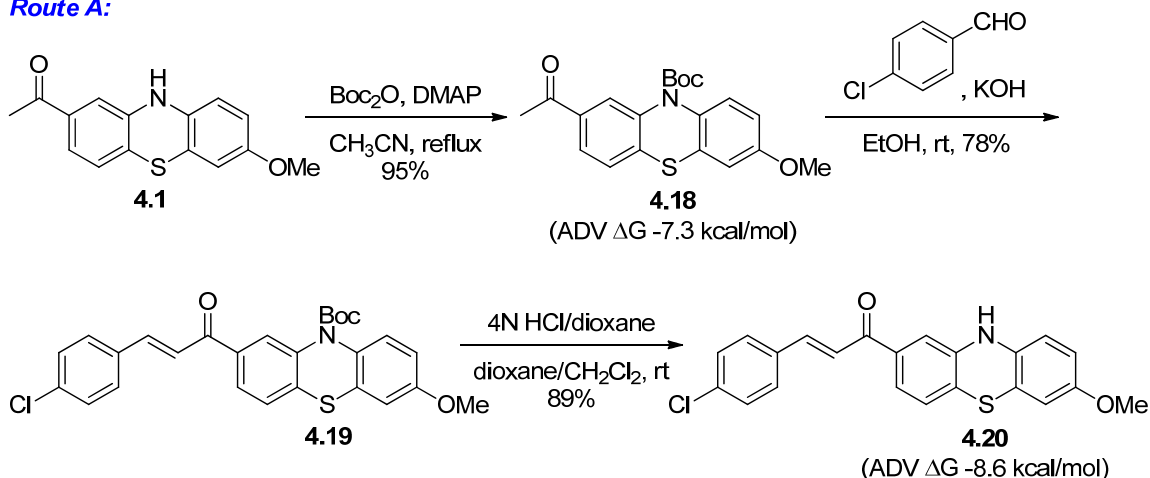
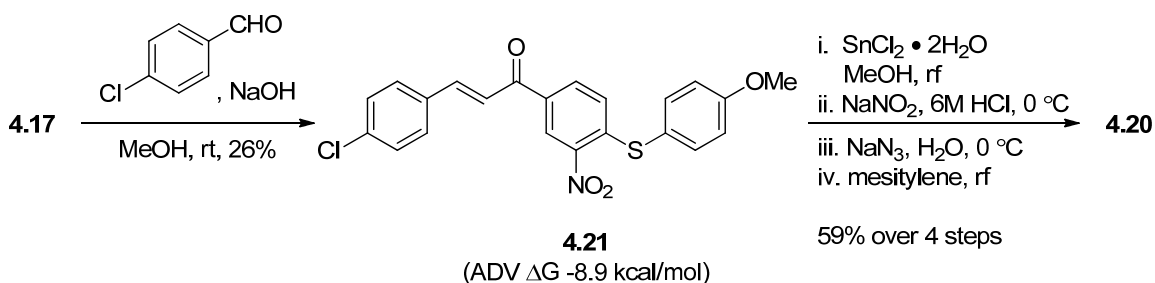
We set out to produce the Cadogan cyclization in two ways from the same sulfide (4.16). First, we sought to generate the reactive nitrene via treatment of **4.16** with triethylphosphite. Second, we explored thermal decomposition of the corresponding azide to the nitrene. With this synthetic plan in hand, the sulfide **4.16** was synthesized by the reaction of **4.4** and commercially available 4-methoxythiophenol in quantitative yield. Our first attempt at the Cadogan reaction utilized the original synthetic procedure, where the starting material was refluxed in triethylphosphite. However, this resulted in a complex reaction mixture that appeared to contain the desired phenothiazine as well as several ethylated byproducts. A variant of Cadogan's original procedure was then employed, where mesitylene was used as the reaction solvent and the sulfide **4.16** was

treated with six equivalents of triethylphosphite under reflux conditions. To our delight, the desired phenothiazine **4.1** was obtained in good yield. Concurrently, we were working towards accessing the same phenothiazine by means of thermally decomposing an azide. Treatment of **4.16** with stannous chloride resulted in the desired amine **4.17** in moderate yield, which upon diazotization, formation of the azide, and refluxing of the azide in mesitylene also gave the desired phenothiazine **4.1** in good yield over three steps (Scheme 4.8).



Scheme 4.8. Formation of **4.17** via generation of a reactive nitrene.

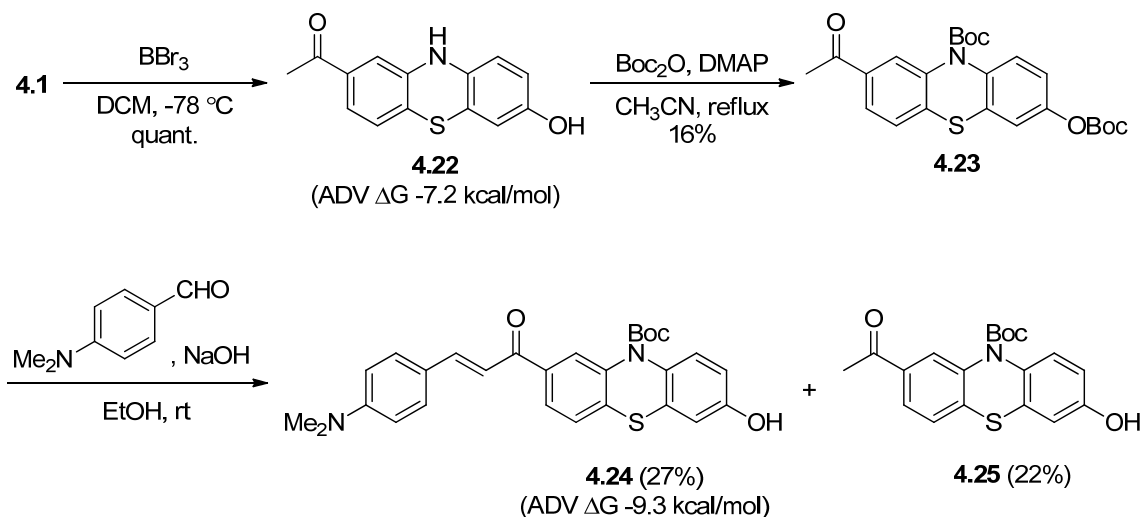
With the first desired phenothiazine core in hand, the synthesis of the library commenced. Two different routes toward the same “one-armed” phenothiazine were undertaken simultaneously to expedite the process. The first route entailed the protection of the secondary amine of **4.1** with a *tert*-butyl carbamate, yielding **4.18**. Aldol condensation of **4.18** with 4-chlorobenzaldehyde resulted in the intermediate **4.19**, which upon treatment with 4 N HCl/dioxane gave the desired functionalized phenothiazine **4.20** (Route A, Scheme 4.9). Meanwhile, starting from sulfide **4.17**, aldol condensation with 4-chlorobenzaldehyde yielded the functionalized sulfide **4.21**. Reduction of the nitro group with stannous chloride followed by diazotization and treatment with sodium azide resulted in formation of the azide, which was subsequently thermally decomposed to the nitrene to affect the Cadogan reaction and yield the same “one-armed” phenothiazine **4.20** (Route B, Scheme 4.9).

Route A:**Route B:**

Scheme 4.9. Two successful routes toward the same “one-armed” phenothiazine **4.20**.

Of the two available routes toward the synthesis of the functionalized phenothiazines, Route A (Scheme 4.9) was chosen for the construction of the remaining phenothiazine library members as it required fewer synthetic steps and gave the products in higher overall yields. A second “one-armed” phenothiazine was synthesized with the **4.1** core structure, using a modified Route A. Treatment of **4.1** with boron tribromide resulted in the free phenolic phenothiazine **4.22** in quantitative yield. Treatment of **4.21** with di-*tert*-butyl dicarbonate gave the di-protected product **4.23**, which upon Aldol condensation with 4-dimethylaminobenzaldehyde resulted in the “one-armed”

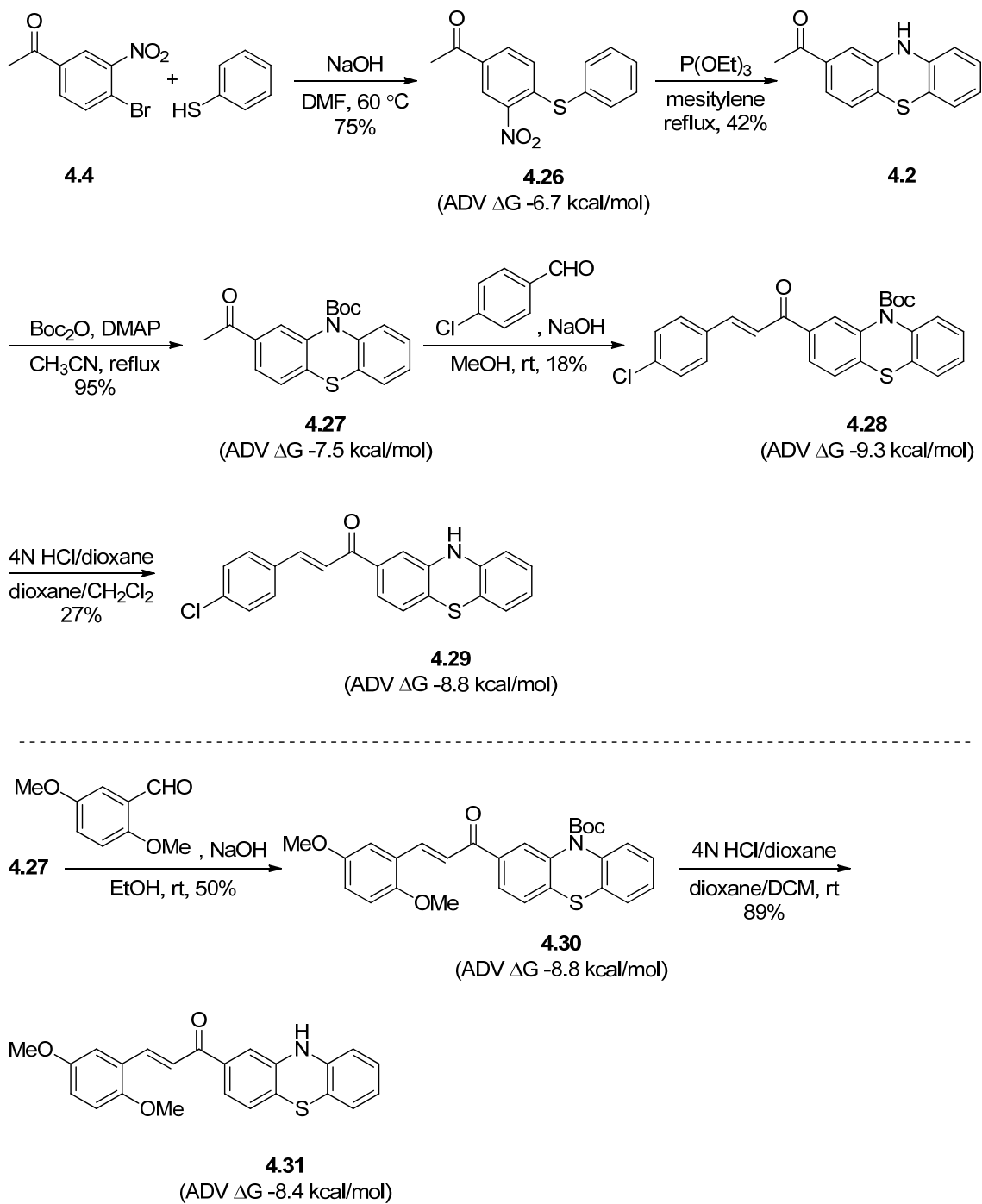
phenothiazine product **4.24** where the phenol was liberated under those reaction conditions. Additionally, the phenothiazine **4.25** was recovered in 22% yield (Scheme 4.10).



Scheme 4.10. Synthesis of “one-armed” phenothiazine **4.24**.

With the two phenothiazine analogues **4.20** and **4.24** from the **4.1** phenothiazine core in hand, we set out to synthesize a set of analogues arrived at from the phenothiazine core **4.2**. The sulfide **4.26** was obtained in 75% yield from the reaction of **4.4** and commercially available thiophenol. Subsequent, Cadogan cyclization of sulfide **4.26** resulted in the phenothiazine core **4.2** in 75% yield, a slightly lower yield than that obtained for phenothiazine core **4.1**. This result was not entirely unexpected as the absence of the methoxy group of **4.1** dictates a less electron rich aryl ring of **4.2**. Protection of the amine of **4.2** as a *tert*-butyl carbamate resulted in **4.27**, which was followed by aldol condensation with 4-chlorobenzaldehyde to give library member **4.28**.

Deprotection of the amine subsequently produced phenothiazine **4.29** (Scheme 4.11, top). Another series of “one-armed” phenothiazines was accomplished by the condensation of **4.27** with 2,4-dimethoxybenzaldehyde, yielding **4.30** in 50% yield. Deprotection of the amine gave analogue **4.31** (Scheme 4.11, bottom).



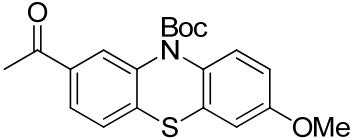
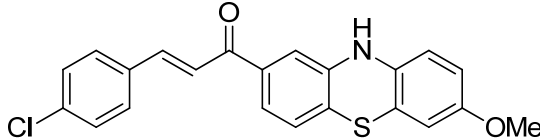
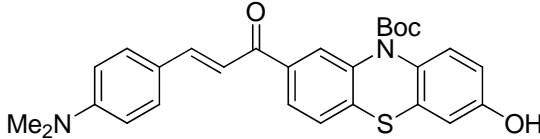
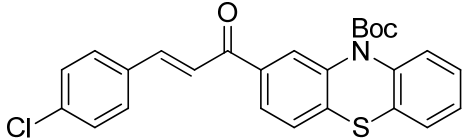
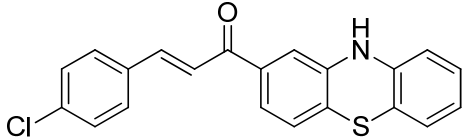
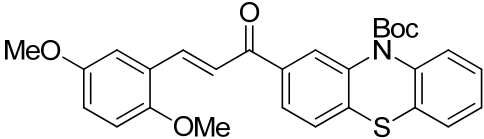
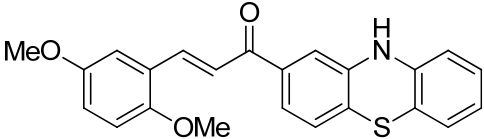
Scheme 4.11. (Top) Synthesis of phenthiazines **4.2**, **4.26-4.28**. (Bottom) Synthesis of phenthiazines **4.29** and **4.30**.

4.5.3. Biological Evaluation of First Phenothiazine Set

At this point, six desired “one-armed” phenothiazines had been synthesized: **4.20**, **4.24**, **4.28**, **4.29**, **4.30**, and **4.31**. These phenothiazines had predicted binding affinities between -8.4 and -9.3 kcal/mol by ADV. In addition, another seventeen molecules including twelve byproducts and intermediates and five phenothiazine cores had been synthesized that had been screened *in silico* for *E. faecalis* II-HMGR binding using ADV. These other compounds **4.1**, **4.6-4.10**, **4.12**, **4.13**, **4.14-4.18**, **4.21**, **4.22**, **4.26**, and **4.27** had predicted binding affinities between -6.6 and -8.9 kcal/mol by ADV; therefore, these compounds were submitted with the six phenothiazines to be assayed for inhibition of II-HMGR.

The twenty-three compounds were assayed for II-HMGR inhibition by Dr. Calvin Steussy of the Stauffacher Research Group of the Department of Biological Sciences at Purdue University. Briefly, enzymatic inhibition of *E. faecalis* II-HMGR was determined spectroscopically, where the disappearance of NADPH was monitored at 340 nm, in the physiological direction where HMG-CoA was converted to mevalonate. To our delight, all six of the “one-armed” phenothiazines were found to decrease *E. faecalis* II-HMGR activity by at least twenty percent. Compound **4.24** was found to decrease *E. faecalis* II-HMGR activity sufficiently enough for an IC₅₀ value to be determined. None of the byproducts or intermediates tested were found to be inhibitors of *E. faecalis* II-HMGR. This data is summarized in Table 4.1.

Table 4.1. Inhibition of *E. faecalis* II-HMGR by first phenothiazine set.

Structure	L.M. ^a	ADV ΔG (kcal/mol)	% Average Inhibition	IC ₅₀ (μM)
	4.18	-7.3	24.9 ± 5.9	n/d
	4.20	-8.6	21.0 ± 3.0	n/d
	4.24	-9.3	83.3 ± 1.4	130
	4.28	-9.3	19.0 ± 5.6	n/d
	4.29	-8.8	35.9 ± 11.5	n/d
	4.30	-8.8	39.2 ± 9.0	n/d
	4.31	-8.4	31.9 ± 4.0	n/d

^aL.M. = library member, n/d = not determined.

Compound **4.24** was found to inhibit *E. faecalis* II-HMGR in the physiological direction with an IC_{50} of 130 μ M. Interestingly, compound **4.24** also had the best predicted binding affinity of the compounds screened by ADV, -9.3 kcal/mol. The predicted binding conformation produced by ADV for compound **4.24** is shown in Figure 4.9. The aldol fragment of **4.24** occupies the same chemical space within the II-HMGR active site as *N*-bsha while the phenothiazine core fragment occupies space not utilized by *N*-bsha. The *tert*-butyl carbamate moiety of **4.24** extends out toward the solvent exposed side of the active site. Attempts at obtaining an X-ray crystal structure of **4.24** complexed with *E. faecalis* II-HMGR are currently in progress.

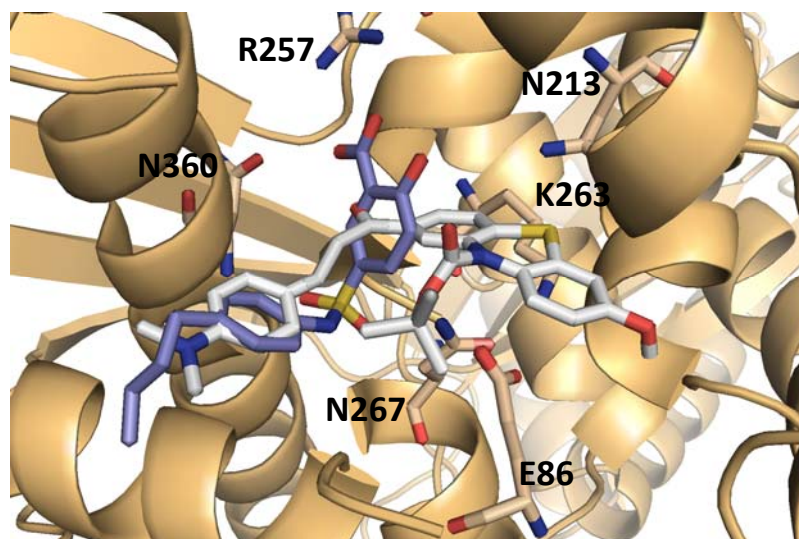
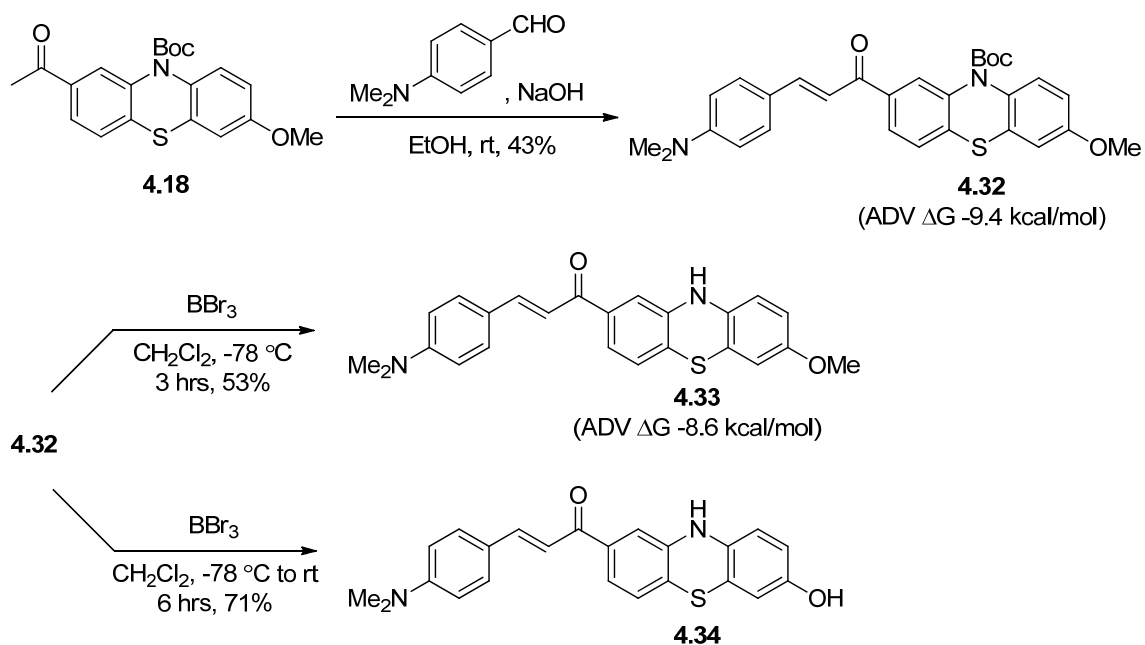


Figure 4.9. Predicted binding conformation of **4.24** ($IC_{50} = 130 \mu$ M) produced by ADV, where **4.24** is shown in white and colored by atom type, *N*-bsha shown in blue and colored by atom type, the *E. faecalis* II-HMGR enzyme is shown in light orange and the residues involved in catalysis or hydrogen bonding interaction to *N*-bsha are shown as sticks and labeled accordingly.

The initial inhibition results of the designed phenothiazines were very promising. The strength of our tandem *de novo* design and *in silico* screening approach can be fully appreciated by a comparison to the high-throughput screening method. When inhibitors of *E. faecalis* II-HMGR were initially sought, a commercial library of 305,000 compounds was screened for II-HMGR inhibition. From that library of 305,000 compounds, one compound was found as a lead inhibitor, *N*-bsha; a success rate of 0.0003%. In contrast, from the six designed phenothiazines that were assayed for II-HMGR inhibition, the compound **4.24** arose as a lead inhibitor; a 16.7% success rate.

4.5.4. Synthesis of Second Phenothiazine Set

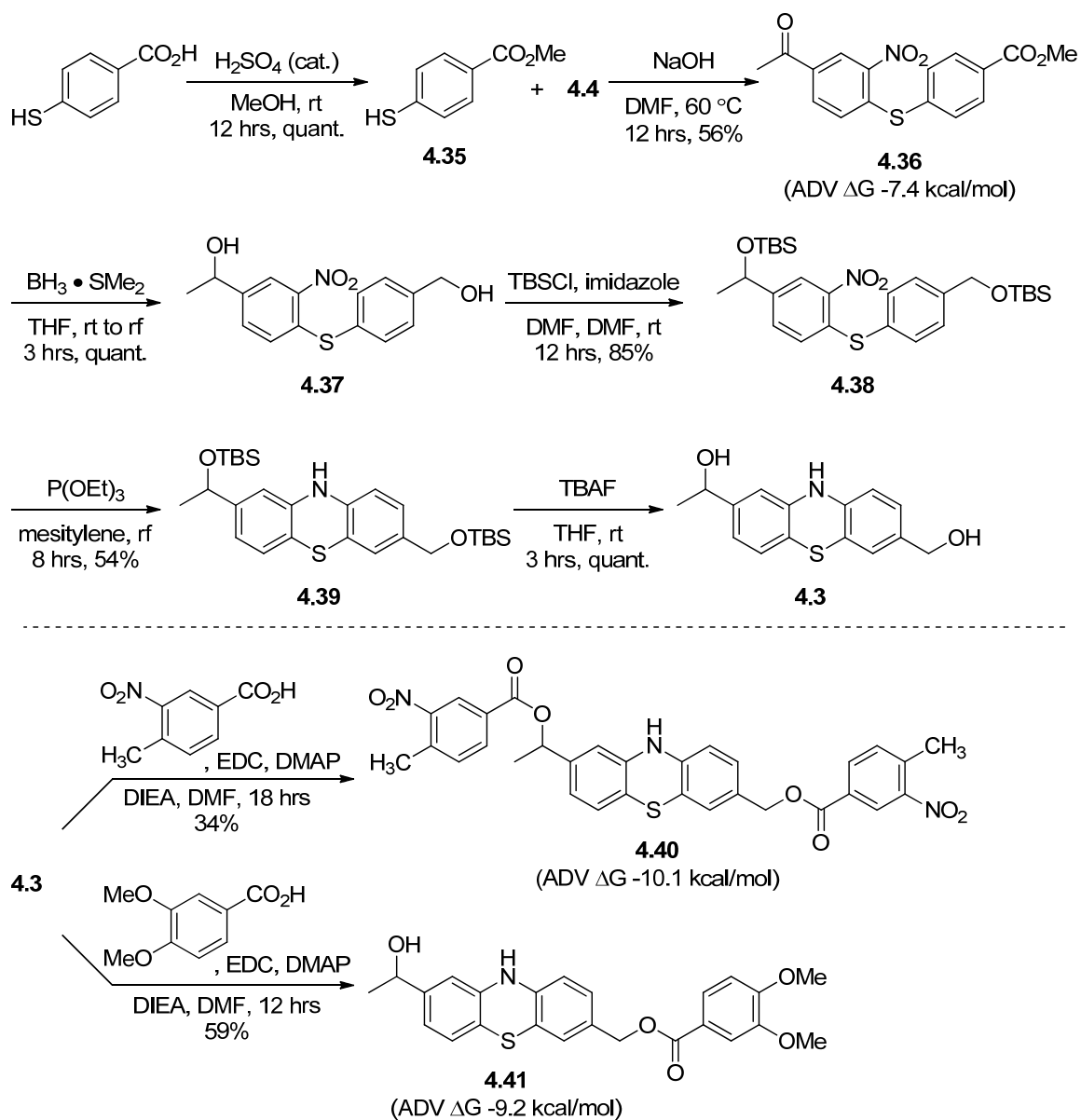
Based on the results of the first set of phenothiazine compounds submitted for testing, we set out to synthesize two variants of **4.24** while attempts at obtaining structural data for **4.24** complexed with II-HMGR were underway. In order to elucidate what aspects of **4.24** were important for II-HMGR inhibition, we synthesized two analogues: **4.32** and **4.33**. Starting from **4.18**, aldol condensation with 4-dimethylaminobenzaldehyde yielded the variant **4.32**, where the importance of the free phenol of **4.24** on inhibition of II-HMGR could be investigated. Deprotection of the amine of **4.32** using boron tribromide resulted in the analogue **4.33**, where the effect of the free amine could be examined. Subjecting **4.32** to boron tribromide for longer reaction times resulted in the analogue **4.34**; unfortunately, no amount of purification was able to isolate **4.34** in sufficient purity to test for II-HMGR inhibition (Scheme 4.12).



Scheme 4.12. Synthesis of **4.24** variants, **4.32-4.34**.

We then turned our attention to the synthesis of the phenthiazine core **4.3**. Starting from the commercially available 4-mercaptobenzoic acid, Fischer esterification yielded the ester **4.35** in quantitative yield. The sulfide **4.36** was formed in lower yield than that seen for the previous sulfides, presumably as a consequence of the electron-withdrawing ester. The Cadogan reaction was attempted directly from the sulfide intermediate **4.36**; however, the desired phenthiazine was not obtained and the reaction only resulted in a complex mixture. We rationalized this again as a consequence of the electron-withdrawing ester and thought to get around this problem by reduction of the ester to the alcohol. Thus, the ester was subjected to saponification conditions and the acid was obtained in quantitative yield. We then sought to take advantage of the known increased rate of reduction of an acid over a ketone by borane-dimethylsulfide complex, and therefore subjected the acid form of **4.36** to those conditions. To our dismay, our

molecule had the opposite reactivity, and the ketone was reduced in the presence of the acid, seemingly as a result of the electron-withdrawing nitro group. We were left with no choice but to reduce both the ketone and ester to the corresponding alcohols, a reaction that was also accomplished by treatment with borane-dimethylsulfide complex in refluxing tetrahydrofuran, yielding **4.37**. With **4.37** in hand, we tried to obtain the phenothiazine core **4.3** directly through the Cadogan reaction, but the free alcohols were not tolerated and a complex reaction mixture obtained. Silyl ether protection of the alcohols was carried out by treatment of **4.37** with *tert*-butyldimethylsilyl chloride, which resulted in the protected compound **4.38**. Fortunately, when **4.38** was subjected to the conditions of the Cadogan reaction, the desired phenothiazine **4.39** was formed, albeit in lower yield than the **4.1** and **4.2** phenothiazine cores. Finally, deprotection of the alcohols was accomplished by treatment with tetrabutylammonium fluoride yielding the phenothiazine core **4.3** (Scheme 4.13, top). The functionalized phenothiazines **4.40** and **4.41** were then obtained by coupling of the appropriate benzoic acid with **4.3** using EDC mediated coupling (Scheme 4.23, bottom).

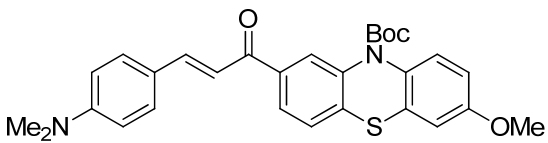
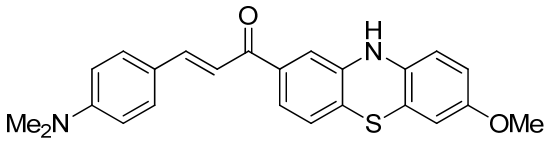
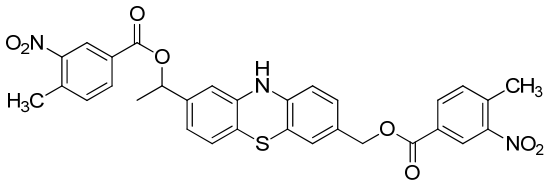
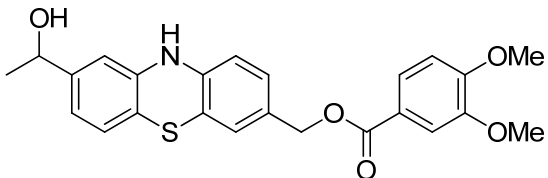


Scheme 4.13. (Top) Synthetic route toward phenothiazine core 4.3. (Bottom) Synthesis of phenothiazines 4.40 and 4.41.

4.5.5. Biological Evaluation of Second Phenothiazine Set

The four phenothiazines **4.32**, **4.33**, **4.40**, and **4.41** were submitted to Dr. Calvin Steussy for determination of II-HMGR inhibition using the same conditions as described previously. The sulfide **4.36** was also assayed for *E. faecalis* II-HMGR inhibition. Gratifyingly, all of the phenothiazines were found to decrease *E. faecalis* II-HMGR activity, though none as potently as **4.24**. This data is summarized in Table 4.2.

Table 4.2. Inhibition of *E. faecalis* II-HMGR by second phenothiazine set.

Structure	L.M. ^a	ADV ΔG (kcal/mol)	% Average Inhibition	IC ₅₀ (μM)
	4.32	-9.4	26.9 \pm 2.8	n/d
	4.33	-8.6	19.2 \pm 4.7	n/d
	4.40	-10.1	11.6 \pm 5.1	n/d
	4.41	-9.2	9.2 \pm 6.1	n/d

^aL.M. = library member, n/d = not determined.

A comparison of phenothiazines **4.24**, **4.32**, and **4.33** prove that both the *tert*-butyl carbamate and free phenol are required for good inhibition of *E. faecalis* II-HMGR. Whether all the compounds bind to *E. faecalis* II-HMGR in similar conformations and whether the free phenol of **4.24** and the phenyl methyl ethers of **4.32** and **4.33** occupy the same molecular space in the enzyme is a mystery. Interestingly, the “two-armed” phenothiazine **4.40**, which had the best binding affinity predicted by ADV, did not show potent inhibition of *E. faecalis* II-HMGR, possibly as a consequence of the absence of a free hydroxyl able to make stabilizing hydrogen bonds within the enzymatic binding cavity.

4.6. Conclusions

With the overall goal of discovering novel small molecule inhibitors of the II-HMGR enzyme, a *de novo* design strategy was used that incorporated a tandem computational approach consisting of two programs: the e-LEA3D web server and the docking program ADV. From this tandem design approach, we identified three molecular scaffolds with the potential for II-HMGR inhibition. Based on the results of our *de novo* design and *in silico* screening strategy, we set out to synthesize a set of phenothiazine compounds.

Two sets of compounds were successfully synthesized that combined contained nine “one-armed” phenothiazines, one “two-armed” phenothiazine, five phenothiazine cores, and thirteen sulfides that were either intermediates or byproducts that ADV scored highly. The enzymatic inhibition of *E. faecalis* II-HMGR by each set of phenothiazine compounds was determined. At 100 mM concentration, all ten of the designed phenothiazines were found to decrease *E. faecalis* II-HMGR activity, between 10 and 83%. This work resulted in the successful identification of the novel compound **4.24**, which was found to inhibit *E. faecalis* II-HMGR with an IC₅₀ of 130 μM in the physiological direction. Attempts at obtaining an X-ray crystal structure of **4.24** complexed with *E. faecalis* II-HMGR are currently underway. This work represents a successful strategy for the *de novo* identification of II-HMGR inhibitors.

4.7. Future Directions

In the future, the X-ray crystal structure of **4.24** in complex with *E. faecalis* II-HMGR will be determined. Based on that structural information, **4.24** will be modified accordingly in an attempt to confer more selectivity and potency to the molecule. Additionally, sets of compounds derived from the quinoline and indole scaffolds may be synthesized.

4.8. References

1. Fleming, A., On the antibacterial action of cultures of a penicillium, with special reference to their use in the isolation of *B. Influenzae*. *Brit. J. Exp. Pathol.* **1929**, *10* (3), 226-236.
2. Taubes, G., The bacteria fight back. *Science* **2008**, *321* (5887), 356-361.
3. Fischbach, M. A.; Walsh, C. T., Antibiotics for Emerging Pathogens. *Science* **2009**, *325* (5944), 1089-1093.
4. Nathan, C.; Goldberg, F. M., The profit problem in antibiotic R&D. *Nat. Rev. Drug Discov.* **2005**, *4* (11), 887-891.
5. Nathan, C., Antibiotics at the crossroads. *Nature* **2004**, *431* (7011), 899-902.
6. Newman, D. J.; Cragg, G. M., Natural products as sources of new drugs over the last 25 years. *J. Nat. Prod.* **2007**, *70* (3), 461-477.
7. Deurenberg, R. H.; Vink, C.; Kalenic, S.; Friedrich, A. W.; Bruggeman, C. A.; Stobberingh, E. E., The molecular evolution of methicillin-resistant *Staphylococcus aureus*. *Clin. Microbiol. Infect.* **2007**, *13* (3), 222-235.
8. Macheboeuf, P.; Contreras-Martel, C.; Job, V.; Dideberg, O.; Dessen, A., Penicillin binding proteins: key players in bacterial cell cycle and drug resistance processes. *Fems Microbiol. Rev.* **2006**, *30* (5), 673-691.
9. Duthie, E. S., The production of penicillinase by organisms of the subtilis group. *Brit. J. Exp. Pathol.* **1944**, *25* (3), 96-100.
10. Barber, M., Methicillin-resistant *Staphylococci*. *Journal of Clinical Pathology* **1961**, *14* (4), 385-&.
11. Cetinkaya, Y.; Falk, P.; Mayhall, C. G., Vancomycin-resistant enterococci. *Clinical Microbiology Reviews* **2000**, *13* (4), 686-+.
12. Chavers, L. S.; Moser, S. A.; Benjamin, W. H.; Banks, S. E.; Steinhauer, J. R.; Smith, A. M.; Johnson, C. N.; Funkhouser, E.; Chavers, L. P.; Stamm, A. M.; Waites, K. B., Vancomycin-resistant enterococci: 15 years and counting. *Journal of Hospital Infection* **2003**, *53* (3), 159-171.
13. Clewell, D. B., Movable genetic elements and antibiotic-resistance in enterococci. *Eur. J. Clin. Microbiol. Infect. Dis.* **1990**, *9* (2), 90-102.
14. Leclercq, R.; Derlot, E.; Duval, J.; Courvalin, P., Plasmid-mediated resistance to vancomycin and teicoplanin in enterococcus-faecium. *New England Journal of Medicine* **1988**, *319* (3), 157-161.

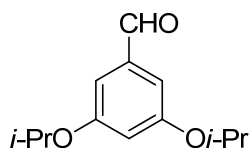
15. System, N., National Nosocomial Infections Surveillance (NNIS) System report, data summary from January 1992-June 2001, issued August 2001. *American Journal of Infection Control* **2001**, 29 (6), 404-421.
16. Wilding, E. I.; Brown, J. R.; Bryant, A. P.; Chalker, A. F.; Holmes, D. J.; Ingraham, K. A.; Iordanescu, S.; Chi, Y. S.; Rosenberg, M.; Gwynn, M. N., Identification, evolution, and essentiality of the mevalonate pathway for isopentenyl diphosphate biosynthesis in gram-positive cocci. *J. Bacteriol.* **2000**, 182 (15), 4319-4327.
17. Hedl, M.; Taberner, L.; Stauffacher, C. V.; Rodwell, V. W., Class II 3-hydroxy-3-methylglutaryl coenzyme A reductases. *J. Bacteriol.* **2004**, 186 (7), 1927-1932.
18. Goldstein, J. L.; Brown, M. S., Regulation of the mevalonate pathway. *Nature* **1990**, 343 (6257), 425-430.
19. Darnay, B. G.; Rodwell, V. W., His865 is the catalytically important histidyl residue of Syrian hamster 3-hydroxy-3-methylglutaryl-coenzyme A reductase. *J. Biol. Chem.* **1993**, 268 (12), 8429-35.
20. Darnay, B. G.; Wang, Y.; Rodwell, V. W., Identification of the catalytically important histidine of 3-hydroxy-3-methylglutaryl-coenzyme A reductase. *J. Biol. Chem.* **1992**, 267 (21), 15064-70.
21. Frimpong, K.; Rodwell, V. W., Catalysis by Syrian hamster 3-hydroxy-3-methylglutaryl-coenzyme A reductase. Proposed roles of histidine 865, glutamate 558, and aspartate 766. *J. Biol. Chem.* **1994**, 269 (15), 11478-83.
22. Bochar, D. A.; Stauffacher, C. V.; Rodwell, V. W., Investigation of the Conserved Lysines of Syrian Hamster 3-Hydroxy-3-methylglutaryl Coenzyme A Reductase. *Biochemistry* **1999**, 38 (48), 15848-15852.
23. Istvan, E. S., Bacterial and mammalian HMG-CoA reductases: related enzymes with distinct architectures. *Curr. Opin. Struct. Biol.* **2001**, 11 (6), 746-751.
24. Hedl, M.; Rodwell, V. W., Inhibition of the Class II HMG-CoA reductase of *Pseudomonas mevalonii*. *Protein Sci.* **2004**, 13 (6), 1693-1697.
25. Sutherlin, A.; Hedl, M.; Sanchez-Neri, B.; Burgner, J. W.; Stauffacher, C. V.; Rodwell, V. W., Enterococcus faecalis 3-hydroxy-3-methylglutaryl coenzyme A synthase, an enzyme of isopentenyl diphosphate biosynthesis. *J. Bacteriol.* **2002**, 184 (15), 4065-4070.
26. Douguet, D., e-LEA3D: a computational-aided drug design web server. *Nucleic Acids Res.* 38, W615-W621.

27. Korb, O.; Stutzle, T.; Exner, T. E., Empirical Scoring Functions for Advanced Protein-Ligand Docking with PLANTS. *Journal of Chemical Information and Modeling* **2009**, *49* (1), 84-96.
28. Trott, O.; Olson, A. J., Software News and Update AutoDock Vina: Improving the Speed and Accuracy of Docking with a New Scoring Function, Efficient Optimization, and Multithreading. *J. Comput. Chem.* *31* (2), 455-461.
29. Morris, G. M.; Huey, R.; Lindstrom, W.; Sanner, M. F.; Belew, R. K.; Goodsell, D. S.; Olson, A. J., AutoDock4 and AutoDockTools4: Automated Docking with Selective Receptor Flexibility. *J. Comput. Chem.* **2009**, *30* (16), 2785-2791.
30. Dixit, R. G., Naveen; Gautam D.C., Synthesis of 10H-Phenothiazines, their Sulfones and Ribofuranosides as Potential Chemotherapeutic Agents. *Jordan Journal of Chemistry* **2008**, *3* (4), 357-365.
31. Massie, S. P., The Chemistry of Phenothiazine. *Chemical Reviews* **1954**, *54* (5), 797-833.
32. Sharma, P. R.; Gupta, V.; Gautam, D. C.; Gupta, R. R., Synthesis of phenothiazines via Smiles rearrangement. *Heterocyclic Communications* **2002**, *8* (2), 195-198.
33. Schmidt, D. M.; Bonvicino, G. E., The Halogen-activated Smiles rearrangement. *2. The Journal of Organic Chemistry* **1984**, *49* (9), 1664-1666.
34. Dai, C.; Sun, X. F.; Tu, X. Z.; Wu, L.; Zhan, D.; Zeng, Q. L., Synthesis of phenothiazines via ligand-free CuI-catalyzed cascade C-S and C-N coupling of aryl ortho-dihalides and ortho-aminobenzenethiols. *Chemical Communications* *48* (43), 5367-5369.
35. Ma, D.; Geng, Q.; Zhang, H.; Jiang, Y., Assembly of Substituted Phenothiazines by a Sequentially Controlled CuI/L-Proline-Catalyzed Cascade C-S and C-N Bond Formation. *Angewandte Chemie International Edition* *49* (7), 1291-1294.
36. Cadogan, J. I. G.; Mackie, R. K.; Todd, M. J., Reductive cyclization of nitro-compounds by triethyl phosphite - new synthesis of phenothiazines and anthranils. *Chemical Communications* **1966**, (15), 491-&.
37. Cadogan, J. I. G.; Kulik, S.; Thomson, C.; Todd, M. J., Reduction of nitro-compounds and nitroso-compounds by trivalent phosphorus reagents. *Journal of the Chemical Society C-Organic* **1970**, (18), 2437.

APPENDICES

Appendix A: Experimental Procedures

All reagents (chemicals) were purchased from Sigma or Acros and used without further purification. Solvents were purified by passage through a solvent column composed of activated alumina and a supported copper redox catalyst. Infrared spectra were obtained using a ThermoNicolet Nexus 470 FT-IR spectrometer with OMNIC software package. Mass spectral analyses were performed using a Waters Micromass ZQ with ESI-MS injection port utilizing MassLynx V4.1 software package. Analytical thin-layer chromatography was performed on Sorbent Technologies Glass Backed Silica Gel HL TLC Plates w/UV254. Flash chromatography was performed with Sorbent Technologies 200-400 mesh silica gel. ^1H NMR spectra were obtained at 300, 400, 500, or 800 MHz and ^{13}C NMR spectra were obtained at 75, 100, 125, or 200 MHz, using Varian Inova30, Bruker ARX400, Bruker Avance DRX500, or Bruker AV-III-800 spectrometers, respectively. *E/Z* isomerism was determined by Nuclear Overhauser Effect experiments. All compounds were purified by flash chromatography to >90% purity by ^1H NMR.

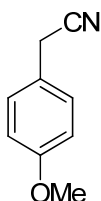


3,5-diisopropoxybenzaldehyde (3.2a).

A mixture of 3,5-dihydroxybenzoic acid (1.00 g, 6.49 mmol), potassium carbonate (4.04 g, 29.2 mmol) and isopropyl bromide (3.65 mL, 38.93 mmol) in 12 mL dimethylformamide was heated to reflux for 4 days. After cooling to room temperature, 6 mL water and 6 mL 2M hydrochloric acid were added to dissolve the carbonate and acidify the reaction mixture. The aqueous layer was extracted with ethyl acetate (3 x 20 mL) and the combined organic layers were dried over magnesium sulfate, filtered and concentrated to yield 3,5-diisopropoxybenzoic acid as a clear oil that was used without further purification.

A 0.54 M solution of DIBAL-H in dichloromethane (4.66 mL, 2.52 mmol) was added to a solution of 3,5-diisopropoxybenzoic acid (282 mg, 1.01 mmol) in toluene (5 mL) at -78 °C. The reaction mixture was allowed to stir for 45 minutes at that temperature before quenching with 5% aqueous hydrochloric acid (1 mL). After warming to room temperature, the reaction mixture was diluted with water and the aqueous layer was extracted with ethyl acetate (3 x 5 mL), the combined organic layers were dried over magnesium sulfate, filtered and concentrated to yield a mixture of 3,5-diisopropoxybenzaldehyde and (3,5-diisopropoxyphenyl)methanol in 97% combined yield. 3,5-Diisopropoxybenzaldehyde: $^1\text{H-NMR}$ (400 MHz, CDCl_3) δ (ppm): 9.77 (1H, s), 6.86 (2H, d, $J = 2.31$), 6.57 (1H, t, $J = 2.31$), 4.48 (2H, m, $J = 6.15$), 1.24 (6H, d, $J =$

6.16). ^{13}C NMR (100 MHz, CDCl_3) δ (ppm): 191.72, 159.44, 110.10, 108.33, 70.03, 21.72.

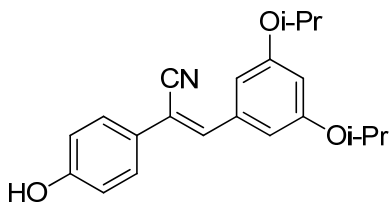


2-(4-Methoxyphenyl)acetonitrile (3.3d).

Triphenyl phosphine (1.14 g, 4.34 mmol) was added portion-wise to a solution of (4-methoxyphenyl)methanol (300 mg, 2.17 mmol) and carbon tetrabromide (1.22 g, 3.69 mmol) in anhydrous dichloromethane (7.2 mL) at 0 °C. The reaction mixture was stirred at that temperature for 20 minutes then concentrated to yield a viscous oil which was dissolved in 10 mL of 50% hexanes 50% ethyl acetate. The precipitate was filtered off and the filtrate concentrated. The residue was taken up in dimethylformamide (7.2 mL) and potassium cyanide (0.99 g, 15.2 mmol) was added. The reaction mixture was allowed to stir for 90 minutes before quenching with saturated aqueous sodium bicarbonate (10 mL). The aqueous layer was extracted with ethyl acetate (3 x 10 mL) and the combined organic layers were washed with brine, dried over magnesium sulfate, filtered and concentrated. The crude product was purified by flash chromatography using 20% ethyl acetate 80% hexanes to yield the pure product **3** in 45% yield. ^1H -NMR (300 MHz, CDCl_3) δ (ppm): 7.19 (2H, d, $J = 8.38$), 6.86 (2H, d, $J = 8.38$), 3.74 (3H, s), 3.61 (2H, s). ^{13}C NMR (75 MHz, CDCl_3) δ (ppm): 159.15, 129.01, 121.89, 118.42, 114.35, 55.18, 22.50.

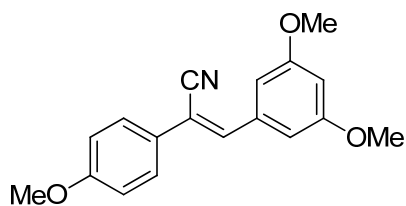
General Procedure for Aldol Condensation (3.4a-3.4c).

Aqueous 40% potassium hydroxide (0.23 mL/mmol nitrile) was diluted with absolute ethanol (0.46 mL/mmol nitrile) and added at room temperature to a solution of the appropriate aldehyde (1.1 equivalents) and nitrile (1.0 equivalent) in absolute ethanol (0.35 mL/mmol nitrile). The reaction was then allowed to stir at room temperature for 12-24 hours before concentrating. The resulting yellow residue was taken up in water and ethyl acetate and dilute hydrochloric acid was added to neutralize the aqueous layer. The aqueous layer was then extracted with ethyl acetate and the combined organic layers were washed with brine, dried over magnesium sulfate, filtered and concentrated to yield the crude product. Purification by flash chromatography yielded the pure nitrile products in 80-95% yield.



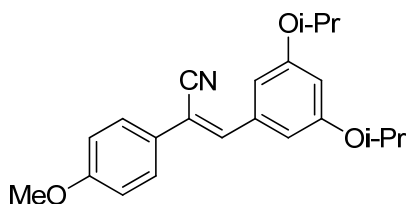
(Z)-3-(3,5-diisopropoxyphenyl)-2-(4-hydroxyphenyl)acrylonitrile (3.4a).

General procedure for Aldol condensation was used in combination with **3.2a** and 2-(4-((*tert*-butyldimethylsilyl)oxy)phenyl)acetonitrile (28%). ¹H-NMR (300 MHz, CDCl₃) δ (ppm): 7.56 (2H, d, J = 8.71), 7.31 (1H, s), 6.98 (2H, d, J = 2.15), 6.90 (2H, d, J = 8.71), 6.50 (1H, t, J = 2.15), 5.06 (1H, s), 4.58 (2H, m, J = 6.05), 1.36 (12H, d, J = 2.05). ESIMS(+) *m/z* 338 (M + H), 360 (M + Na), 376 (M + K).



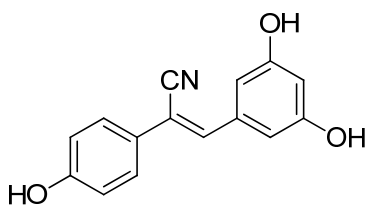
(Z)-3-(3,5-dimethoxyphenyl)-2-(4-methoxyphenyl)acrylonitrile (3.4b).

General procedure for Aldol condensation was used in combination with 3,5-dimethoxybenzaldehyde and **3.3d** (95%). $^1\text{H-NMR}$ (300 MHz, CDCl_3) δ (ppm): 7.61 (2H, d, $J = 8.91$), 7.34 (1H, s), 7.04 (2H, d, $J = 2.13$), 6.96 (2H, d, $J = 8.91$), 6.53 (1H, t, 2.13), 3.85 (9H, s). $^{13}\text{C NMR}$ (75 MHz, CDCl_3) δ (ppm): 160.73, 160.32, 139.83, 135.47, 127.16, 126.59, 118.11, 114.27, 111.14, 106.71, 102.65, 55.28. ESIMS(+) m/z 318 (M + Na).



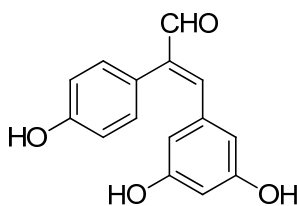
(Z)-3-(3,5-diisopropoxyphenyl)-2-(4-methoxyphenyl)acrylonitrile (3.4c).

General procedure for Aldol condensation was used in combination with **3.2a** and **3.3d** (92%). $^1\text{H-NMR}$ (300 MHz, CDCl_3) δ (ppm): 7.56 (2H, d, $J = 8.83$), 7.32 (1H, s), 7.01 (2H, d, $J = 1.86$), 6.94 (2H, d, $J = 8.83$), 6.51 (1H, t, 1.86), 4.58 (2H, m, $J = 6.04$), 3.81 (3H, s), 1.37 (12H, d, $J = 6.04$). $^{13}\text{C NMR}$ (75 MHz, CDCl_3) δ (ppm): 160.31, 159.15, 140.24, 135.45, 127.19, 126.79, 118.08, 114.30, 110.98, 108.30, 108.24, 106.13, 70.07, 70.01, 55.25, 21.96. ESIMS(+) m/z 352 (M + H), 374 (M + Na), 390 (M + K).



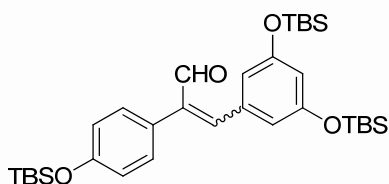
(Z)-3-(3,5-dihydroxyphenyl)-2-(4-hydroxyphenyl)acrylonitrile (3.4d).

A 1.0 M solution of boron tribromide in dichloromethane (2.34 mL, 2.34 mmol) was added slowly to a solution of **3.4b** (138 mg, 0.46 mmol) in dichloromethane (2.3 mL) at -78 °C under nitrogen atmosphere. The reaction was allowed to stir at room temperature for four hours before cooling to -78 °C and quenching with an aqueous solution of saturated sodium bicarbonate (2 mL). The reaction mixture was warmed to room temperature and the aqueous layer was extracted with ethyl acetate (3 x 2 mL). The combined organic layers were washed with saturated sodium bicarbonate (3 x 5 mL), water (1 x 5 mL), and brine (1 x 5 mL) before being dried over magnesium sulfate, filtered, and concentrated. The pure product was obtained in 80% yield after purification by flash chromatography using 50% ethyl acetate 50% hexanes. ¹H-NMR (400 MHz, CD₃OD) δ (ppm): 7.52 (2H, d, J = 8.70), 7.42 (1H, s), 6.85 (2H, d, J = 8.70), 6.82 (2H, d, J = 2.02), 6.33 (1H, t, J = 2.02). ¹³C NMR (100 MHz, CD₃OD) δ (ppm): 159.85, 141.34, 137.32, 128.35, 127.07, 119.17, 116.86, 111.91, 108.56, 105.58. IR ν_{\max} 3216 (OH), 2227 (CN) cm⁻¹.



(E)-3-(3,5-dihydroxyphenyl)-2-(4-hydroxyphenyl)acrylaldehyde (3.4e).

A 1.0 M solution of tetrabutylammonium fluoride solution in THF (0.15 mL, 0.15 mmol) was added to a solution of **3.5** (29 mg, 0.05 mmol) in THF (0.25 mL) at 0 °C. The reaction was allowed to stir overnight before quenching with saturated ammonium chloride. The aqueous layer was extracted with ethyl acetate (3 x 3 mL) and the combined organic layers were washed with brine, dried over magnesium sulfate, filtered and concentrated. The pure product **4e** was obtained in 15% yield after flash chromatography using 50% ethyl acetate 50% hexanes. ¹H-NMR (400 MHz, CD₃OD:CDCl₃ 50:50) δ (ppm): 9.44 (1H, s), 7.03 (1H, s), 6.81 (2H, d, J = 8.59), 6.63 (2H, d, J = 8.59), 6.07 (2H, s). ¹³C NMR (100 MHz, CD₃OD) δ (ppm): 195.25, 157.48, 157.33, 151.12, 140.98, 135.65, 130.39, 123.78, 115.27, 109.10, 104.54. ESIMS(+) *m/z* 257 (M + H).

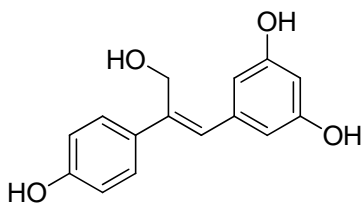


3-(3,5-bis((tert-butyldimethylsilyl)oxy)phenyl)-2-(4-((tert-butyldimethylsilyl)oxy)phenyl)-acrylaldehyde (3.5).

Tert-Butyldimethylsilyl chloride (202 mg, 1.34 mmol) and imidazole (228 mg, 3.35 mmol) were added to a stirred solution of **3.4d** (94 mg, 0.37 mmol) in

dimethylformamide (2 mL) at 0 °C. The reaction mixture was warmed to room temperature. After stirring overnight, the reaction mixture was diluted with water and extracted with ethyl acetate (3 x 5 mL). The combined organic layers were then washed with brine, dried over magnesium sulfate, filtered and concentrated to yield the protected nitrile in 52% yield after flash chromatography using 5% ethyl acetate 95% hexanes.

A 0.54 M solution of DIBAL-H in hexanes (0.31 mmol, 0.57 mL) was added slowly to the protected nitrile (155 mg, 0.26 mmol) in toluene (1.3 mL) at 0 °C under nitrogen atmosphere. After 40 minutes the reaction was quenched by addition of methanol (0.32 mL) and water (0.31 mL), warmed to room temperature and stirred for an additional 3 hours. The reaction mixture was diluted with water and the aqueous phase was extracted with ethyl acetate (3 x 5 mL). The combined organic layers were washed with brine, dried over magnesium sulfate, filtered and concentrated. Flash chromatography using 5% ethyl acetate 95% hexanes yielded the pure aldehyde product **3.5** in 80% yield. (*Z*)-**5**: ¹H-NMR (300 MHz, CDCl₃) δ (ppm): 9.71 (1H, s), 7.20 (1H, s), 7.05 (2H, d, J = 8.41), 6.85 (2H, s, J = 8.41), 6.39 (2H, d, J = 2.18), 6.29 (1H, t, J = 2.18), 1.00 (12H, s), 0.92 (18H, s), 0.23 (6H, s), 0.08 (9H, s). (*E*)-**3.5**: ¹H-NMR (300 MHz, CDCl₃) δ (ppm): 10.10 (1H, 1), 7.70 (1H, s), 7.39 (2H, d, J = 8.38), 6.94 (2H, d, J = 8.38), 6.50 (2H, d, J = 2.07), 6.41 (1H, t, J = 2.07), 1.00 (12H, s), 0.92 (18H, s), 0.23 (6H, s), 0.08 (9H, s). ¹³C NMR (75 MHz, CDCl₃) δ (ppm): 192.46, 156.47, 145.57, 140.63, 135.76, 129.80, 128.96, 127.20, 119.85, 115.32, 113.12, 25.56, 18.13.



(Z)-5-(3-hydroxy-2-(4-hydroxyphenyl)prop-1-en-1-yl)benzene-1,3-diol (3.4f).

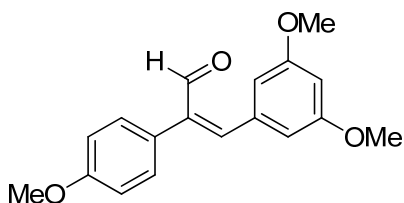
A 0.54 M solution of DIBAL-H in hexanes (0.7 mmol, 0.12 mL) was added slowly to **3.5** (40 mg, 0.07 mmol) in toluene (.4 mL) at -78 °C under nitrogen atmosphere. The reaction was allowed to warm to room temperature and stirred for 4 hours. The reaction was quenched by addition of methanol (0.12 mL) and 0.1 N HCl (0.12 mL) at -78 °C. The reaction mixture was diluted with water and the aqueous phase was extracted with ethyl acetate (3 x 5 mL). The combined organic layers were washed with brine, dried over magnesium sulfate, filtered and concentrated. Flash chromatography using 5% ethyl acetate 95% hexanes yielded the pure protected alcohol in 55% yield.

The protected alcohol (15 mg, 0.04 mmol) was dissolved in methanol (0.5 mL) and a catalytic amount of hydrochloric acid was added. The reaction was allowed to stir until all of the starting material had disappeared from TLC. The reaction mixture was then concentrated. The residue was taken up in ethyl acetate and water, and the aqueous phase was extracted with ethyl acetate (3 x). The combined organic layers were washed with brine, dried over magnesium sulfate, filtered and concentrated. The product **4f** was obtained in 35% yield after purification by flash chromatography using 70% ethyl acetate 30% hexanes. ¹H-NMR (400 MHz, CD₃OD) δ (ppm): 7.43 (2H, d, J = 8.64), 6.78 (2H, d, J = 8.64), 6.73 (1H, s), 6.37 (2H, d, J = 2.13), 6.19 (1H, t, J = 2.13), 4.59 (2H, s). ¹³C

NMR (100 MHz, CD₃OD) δ (ppm): 159.33, 158.05, 141.01, 140.74, 133.78, 130.22, 128.76, 116.09, 109.11, 108.50, 102.42, 101.57, 84.02, 60.22.

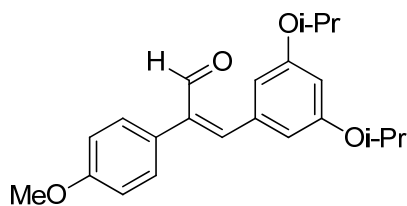
General Procedure for Nitrile Reduction (**3.4g**, **3.4h**).

A 0.54 M solution of DIBAL-H in hexanes (2.0 equivalents) was added slowly to a solution of the appropriate nitrile (1.0 equivalent) in toluene (0.2 M) at -78 °C. The reaction mixture was stirred at that temperature for four hours before quenching with water and ethyl acetate. The organic layer was washed (3x) with dilute hydrochloric acid. The combined aqueous layers were extracted with ethyl acetate (3x) and the combined organic layers were washed with brine, dried over magnesium sulfate, filtered and concentrated. The desired aldehyde products were obtained in 67-80% yield after flash chromatography.



(*Z*)-3-(3,5-dimethoxyphenyl)-2-(4-methoxyphenyl)acrylaldehyde (**3.4g**).

General procedure for nitrile reduction was used starting from **3.4b** (67%). ¹H-NMR (400 MHz, CDCl₃) δ (ppm): 9.75 (1H, s), 7.28 (1H, s), 7.15 (2H, d, J = 8.71), 6.96 (2H, d, J = 8.71), 6.41 (3H, s), 3.83 (3H, s), 3.59 (6H, s). ¹³C NMR (100 MHz, CDCl₃) δ (ppm): 194.16, 160.36, 159.56, 149.81, 141.68, 135.80, 130.70, 125.30, 114.23, 108.37, 102.83, 55.23, 55.06.

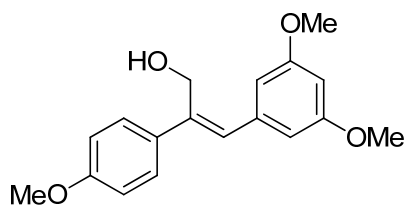


(Z)-3-(3,5-diisopropoxyphenyl)-2-(4-methoxyphenyl)acrylaldehyde (3.4h).

General procedure for nitrile reduction was used starting from **3.4c** (80%). ¹H-NMR (300 MHz, CDCl₃) δ (ppm): 10.13 (1H, s), 7.73 (1H, s), 7.37 (2H, d, J = 8.77), 6.94 (2H, d, J = 8.77), 6.49 (3H), 4.54 (2H, m, J = 6.04), 3.84 (3H, s), 1.35 (12H, d, J = 6.04). ¹³C NMR (75 MHz, CDCl₃) δ (ppm): 192.58, 159.69, 158.88, 145.96, 140.65, 135.82, 129.89, 128.43, 113.72, 109.81, 104.68, 70.07, 55.22, 21.94.

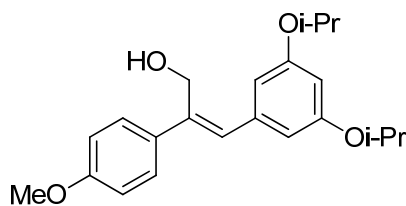
General Procedure for Aldehyde Reduction (3.4i-3.4l).

Sodium borohydride (1.2 equivalents) was added portion-wise to a stirred solution of the appropriate aldehyde (1.0 equivalent) in methanol (0.2 M) at 0 °C. The reaction mixture was concentrated under reduced pressure after 30 min. The residue was dissolved in CH₂Cl₂ and extracted with H₂O, and the aqueous layer was washed with CH₂Cl₂ (3x). The combined organic layers were washed with H₂O (3x) and brine, dried over MgSO₄, filtered and concentrated. Purification by flash chromatography afforded the pure alcohol products in 13-44% yield.



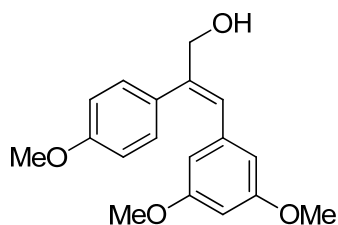
(Z)-3-(3,5-dimethoxyphenyl)-2-(4-methoxyphenyl)prop-2-en-1-ol (3.4i).

General procedure for aldehyde reduction as used from **3.4g** (13%). $^1\text{H-NMR}$ (300 MHz, CDCl_3) δ (ppm): 7.53 (2H, d, $J = 8.82$), 6.94 (2H, d, $J = 8.82$), 6.85 (1H, s), 6.57 (2H, d, $J = 2.16$), 6.42 (1H, t, $J = 2.16$), 4.70 (2H, s), 3.84 (3H, s), 3.82 (6H, s). ^{13}C NMR (100 MHz, CDCl_3) δ (ppm): 160.63, 159.32, 139.94, 139.00, 132.70, 129.62, 127.68, 114.01, 106.80, 99.44, 60.39, 55.29.



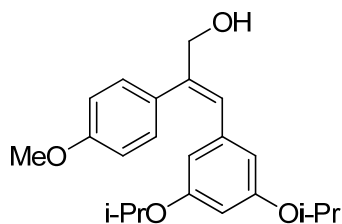
(Z)-3-(3,5-diisopropoxyphenyl)-2-(4-methoxyphenyl)prop-2-en-1-ol (3.4j).

General procedure for aldehyde reduction was used from **3.4h** (27%). $^1\text{H-NMR}$ (400 MHz, CDCl_3) δ (ppm): 7.52 (2H, d, $J = 8.71$), 6.93 (2H, d, $J = 8.71$), 6.82 (1H, s), 6.53 (2H, d, $J = 2.16$), 6.39 (1H, t, $J = 2.16$), 4.70 (2H, s), 4.54 (2H, m, $J = 6.07$), 3.84 (3H, s), 1.34 (12H, d, $J = 6.07$). ^{13}C NMR (100 MHz, CDCl_3) δ (ppm): 159.25, 158.92, 139.60, 138.86, 132.80, 129.84, 127.66, 113.98, 108.49, 102.90, 69.87, 60.39, 55.25, 22.03.



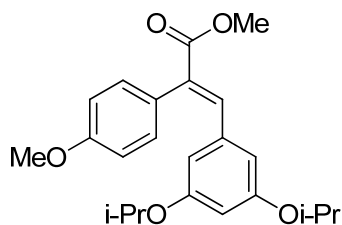
(E)-3-(3,5-dimethoxyphenyl)-2-(4-methoxyphenyl)prop-2-en-1-ol (3.4k).

General procedure for aldehyde reduction was used from **3.4g** (35%). ¹H-NMR (300 MHz, CDCl₃) δ (ppm): 7.17 (2H, d, J = 8.77), 6.88 (2H, d, J = 8.77), 6.59 (1H, s), 6.24 (1H, t, J = 2.23), 6.20 (2H, d, J = 2.23), 4.43 (2H, s), 3.80 (3H, s), 3.56 (6H, s). ¹³C NMR (75 MHz, CDCl₃) δ (ppm): 160.05, 158.97, 141.52, 138.37, 130.47, 129.86, 126.01, 114.09, 106.98, 99.50, 68.36, 55.17, 54.88.



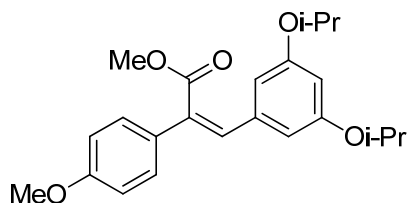
(E)-3-(3,5-diisopropoxyphenyl)-2-(4-methoxyphenyl)prop-2-en-1-ol (3.4l).

General procedure for aldehyde reduction was used from **3.4h** (44%). ¹H-NMR (300 MHz, CDCl₃) δ (ppm): 7.17 (2H, d, J = 8.63), 6.88 (2H, d, J = 8.63), 6.56 (1H, s), 6.21 (1H, t, J = 2.02), 6.16 (2H, d, J = 2.02), 4.41 (2H, s), 4.19 (2H, m, J = 6.05), 1.17 (12H, d, J = 6.05).



(E)-methyl 3-(3,5-diisopropoxyphenyl)-2-(4-methoxyphenyl)acrylate (3.4m).

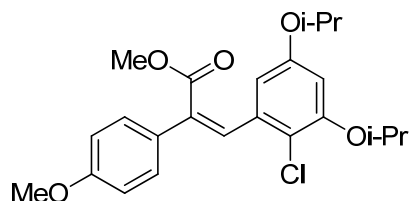
To a stirred solution of **3.4h** (64 mg, 0.18 mmol) in methanol (1.8 mL) was added potassium cyanide (59 mg, 0.91 mmol) and manganese dioxide (317 mg, 3.65 mmol). After six days, the reaction mixture was diluted with dichloromethane and filtered through a celite pad. The combined organic layers were washed with brine, dried over magnesium sulfate, filtered and concentrated. Flash chromatography using 10% ethyl acetate 90% hexanes afforded the pure product in 17% yield. $^1\text{H-NMR}$ (300 MHz, CDCl_3) δ (ppm): 7.72 (1H, s), 7.16 (2H, d, $J = 8.70$), 6.92 (2H, d, $J = 8.70$), 6.29 (1H, t, $J = 2.22$), 6.20 (2H, d, $J = 2.22$), 4.16 (2H, m, $J = 6.06$), 3.81 (3H, s), 3.79 (3H, s), 1.17 (12H, d, $J = 6.06$).



(Z)-methyl 3-(3,5-diisopropoxyphenyl)-2-(4-methoxyphenyl)acrylate (3.4n).

See procedure for **3.4o** (34%). $^1\text{H-NMR}$ (400 MHz, CDCl_3) δ (ppm): 7.37 (2H, d, 8.86), 6.91 (2H, d, $J = 8.86$), 6.85 (1H, s), 6.49 (2H, d, $J = 2.11$), 6.38 (1H, t, $J = 2.11$), 4.50 (2H, m, $J = 6.07$), 3.83 (3H, s), 3.80 (3H, s), 1.33 (12H, d, $J = 6.07$). $^{13}\text{C NMR}$ (100

MHz, CDCl₃) δ (ppm): 170.24, 159.71, 159.02, 137.48, 134.37, 129.44, 129.23, 127.52, 114.06, 107.71, 104.14, 69.92, 55.26, 52.17, 22.03, 21.90.

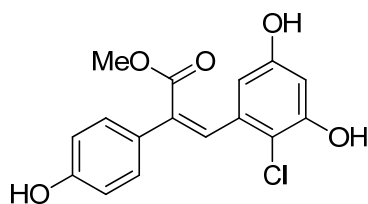


(Z)-methyl 3-(2-chloro-3,5-diisopropoxyphenyl)-2-(4-methoxyphenyl)acrylate (3.4o).

Sodium chlorite (66 mg, 0.73 mmol) in water (0.73 mL) was added drop-wise to a mixture of **3.4h** (185 mg, 0.52 mmol) in acetonitrile (0.54 mL), monosodium phosphate (108 mg, 0.78 mmol) in water (0.25 mL) and 30% hydrogen peroxide (0.07 mL) at 0 °C. The reaction was then allowed to stir for 48 hours at room temperature before addition of a saturated solution of sodium thiosulfate. The aqueous phase was then extracted with ethyl acetate (3 x 5 mL). The combined organic layers were washed with brine, dried over magnesium sulfate, filtered and concentrated to afford an inseparable mixture of (Z)-3-(3,5-diisopropoxyphenyl)-2-(4-methoxyphenyl)acrylic acid and (Z)-3-(2-chloro-3,5-diisopropoxyphenyl)-2-(4-methoxyphenyl)acrylic acid in 81-88% yield.

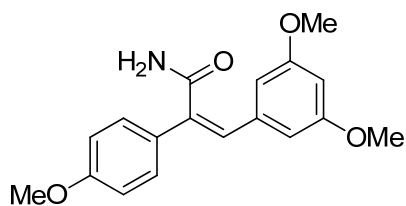
The above mixture of acids was dissolved in methanol (2.33 mL) and a catalytic amount of concentrated sulfuric acid was added. The reaction mixture was then refluxed for 48 hours, cooled to room temperature and concentrated. The residue was taken up in ethyl acetate and water, and the aqueous layer was extracted with ethyl acetate (3 x 8 mL). The combined organic layers were washed with brine, dried over magnesium sulfate, filtered and concentrated to yield a mixture of **3.4o** and **3.4n**, which were separated by flash chromatography using 49% petroleum ether, 49% toluene, 1% t-

butanol to yield **3.4o** in 34% yield and **3.4n** in 14% yield. $^1\text{H-NMR}$ (400 MHz, CDCl_3) δ (ppm): 7.42 (2H, d, $J = 8.84$), 7.15 (1H, s), 6.92 (2H, d, $J = 8.84$), 6.55 (1H, d, $J = 2.63$), 6.47 (1H, d, $J = 2.63$), 4.51 (1H, m, $J = 6.03$), 4.46 (1H, m, $J = 6.05$), 3.83 (3H, s), 3.71 (3H, s), 1.39 (6H, d, $J = 6.05$), 1.33 (6H, d, $J = 6.03$). $^{13}\text{C NMR}$ (100 MHz, CDCl_3) δ (ppm): 169.70, 159.88, 156.63, 154.38, 136.10, 135.85, 128.97, 127.97, 127.73, 115.50, 114.03, 106.95, 104.71, 71.99, 70.39, 55.27, 52.04, 21.97. ESIMS m/z 441 ($\text{M} + \text{Na}$). IR ν_{max} 1726 (CO) cm^{-1} .



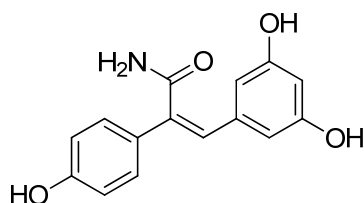
(Z)-methyl 3-(2-chloro-3,5-dihydroxyphenyl)-2-(4-hydroxyphenyl)acrylate (3.4p).

A 1.0 M solution of boron tribromide in dichloromethane ((0.60 mL, 0.60 mmol) was added slowly to a solution of **3.4o** (50 mg, 0.12 mmol) in dry dichloromethane (0.60 mL) at $-78\text{ }^\circ\text{C}$. The reaction was gradually allowed to warm to room temperature. After six hours the reaction mixture was cooled to $-78\text{ }^\circ\text{C}$ and quenched with saturated sodium bicarbonate. The aqueous layer was extracted with ethyl acetate (3 x 5 mL) and the combined organic layers were washed with brine, dried over magnesium sulfate, filtered and concentrated. The pure product was obtained in 10% yield after flash chromatography using 50% ethyl acetate 50% hexanes. $^1\text{H-NMR}$ (400 MHz, CD_3OD) δ (ppm): 7.80 (1H, s), 6.94 (2H, d, $J = 8.67$), 6.69 (2H, d, $J = 8.67$), 6.26 (1H, d, $J = 2.70$), 5.84 (1H, d, $J = 2.70$). $^{13}\text{C NMR}$ (100 MHz, CD_3OD) δ (ppm): 170.02, 158.35, 157.17, 155.04, 137.90, 136.51, 135.48, 132.47, 128.87, 115.98, 112.88, 110.09, 104.76, 52.77.



(Z)-3-(3,5-dimethoxyphenyl)-2-(4-methoxyphenyl)acrylamide (3.4q).

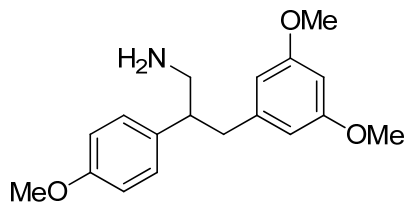
A mixture of **3.4b** (45 mg, 0.15 mmol), acetaldoxime (0.02 mL, 0.30 mmol), palladium acetate (3 mg, 0.02 mmol), and triphenylphosphine (8 mg, 0.03 mmol) in aqueous ethanol (0.5 mL, 1:4 water:ethanol) was heated to reflux for three hours under nitrogen atmosphere. The reaction mixture was diluted with ethanol, filtered through a celite pad, washed with dichloromethane, and the combined organic layers were concentrated. The pure product was obtained in 92% yield after purification by flash chromatography using 40% ethyl acetate 60% hexanes. $^1\text{H-NMR}$ (300 MHz, CDCl_3) δ (ppm): 7.34 (2H, d, $J = 8.91$), 6.79 (2H, d, $J = 8.91$), 6.70 (1H, s), 6.57 (2H, d, $J = 2.06$), 6.28 (1H, t, $J = 2.06$), 3.86 (2H, s), 3.71 (3H, s), 3.66 (6H, s). $^{13}\text{C NMR}$ (100 MHz, CDCl_3) δ (ppm): 173.13, 160.51, 159.62, 137.32, 137.24, 129.21, 127.30, 126.65, 113.92, 106.17, 100.24, 55.05.



(Z)-3-(3,5-dihydroxyphenyl)-2-(4-hydroxyphenyl)acrylamide (3.4r).

A 1.0 M solution of boron tribromide in dichloromethane ((0.94 mL, 0.94 mmol) was added slowly to a solution of **3.4q** (50 mg, 0.13 mmol) in dry dichloromethane (0.60

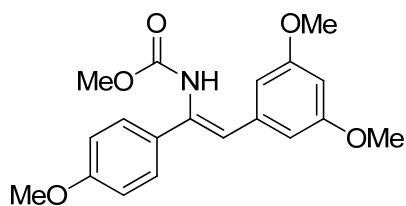
mL) at $-78\text{ }^{\circ}\text{C}$. The reaction was gradually allowed to warm to room temperature. After four hours the reaction mixture was cooled to $-78\text{ }^{\circ}\text{C}$ and quenched with saturated sodium bicarbonate. The aqueous layer was extracted with ethyl acetate (3 x 5 mL) and the combined organic layers were washed with brine, dried over magnesium sulfate, filtered and concentrated. The pure product was obtained in quantitative yield after flash chromatography using 60% ethyl acetate 40% hexanes. $^1\text{H-NMR}$ (400 MHz, CD_3OD) δ (ppm): 7.38(2H, d, $J = 8.66$), 6.79 (2H, d, $J = 8.66$), 6.70 (1H, s), 6.52 (2H, s), 6.19 (1H, s). ^{13}C NMR (100 MHz, CD_3OD) δ (ppm): 175.86, 159.43, 158.82, 139.17, 138.47, 130.03, 128.45, 126.91, 116.43, 108.12, 103.31.



3-(3,5-dimethoxyphenyl)-2-(4-methoxyphenyl)propan-1-amine (3.4s).

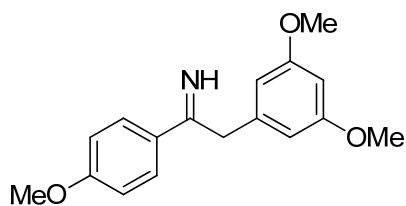
To a mixture of **3.4b** (20 mg, 0.07 mmol) cobalt chloride hexahydrate (32 mg, 0.14 mmol) in anhydrous methanol (0.5 mL) was added sodium borohydride (26 mg, 0.68 mmol) portionwise. After stirring overnight a second portion of sodium borohydride was added. After one hour, an aqueous solution of 3N HCl was added to the reaction mixture until it became clear in appearance. The aqueous layer was then extracted with ether (3 x) to remove any remaining nitrile. The aqueous layer was then made alkaline using ammonium hydroxide (pH = 10) and extracted with ethyl acetate (3 x 5 mL). The combined organic layers were washed with brine, dried over magnesium sulfate, filtered and concentrated. The pure product was obtained in 64% yield after purification by flash

chromatography using 5% methanol 95% dichloromethane. $^1\text{H-NMR}$ (400 MHz, CDCl_3) δ (ppm): 7.09 (2H, d, $J = 8.57$), 6.84 (2H, d, $J = 8.57$), 6.26 (1H, t, $J = 2.17$), 6.21 (2H, d, $J = 2.17$), 3.78 (3H, s), 3.71 (6H, s), 2.96-2.81 (5H, m). $^{13}\text{C NMR}$ (100 MHz, CDCl_3) δ (ppm): 160.42, 158.22, 142.46, 134.57, 128.82, 113.89, 107.01, 97.93, 55.11, 49.88, 46.82, 41.15.



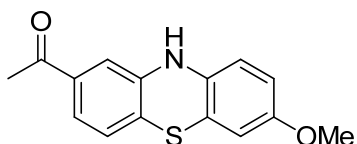
(Z)-methyl (2-(3,5-dimethoxyphenyl)-1-(4-methoxyphenyl)vinyl)carbamate (3.4t).

Potassium hydroxide (14 mg, 0.26 mmol) was added to **3.4q** (32 mg, 0.10 mmol) in anhydrous methanol (1.25 mL) at room temperature under nitrogen atmosphere. Once a clear reaction mixture was obtained, (diacetoxyiodo)benzene (33 mg, 0.10 mmol) was added in one portion. The reaction mixture was concentrated after three hours and the crude residue as taken up in water and dichloromethane. The aqueous phase was extracted with dichloromethane (3 x 5 mL) and the combined organic layers were washed with brine, dried over magnesium sulfate, filtered and concentrated. The pure product was obtained in 86% yield after purification by flash chromatography using 30% ethyl acetate 70% hexanes. $^1\text{H-NMR}$ (400 MHz, CDCl_3) δ (ppm): 7.44 (2H, d, $J = 8.80$), 6.91 (2H, d, $J = 8.80$), 6.58 (2H, d, $J = 2.20$), 6.37 (1H, t, $J = 2.20$), 6.20 (1H, s), 3.83 (3H, s), 3.78 (6H, s), 3.67 (3H, s). $^{13}\text{C NMR}$ (100 MHz, CDCl_3) δ (ppm): 160.84, 159.85, 154.67, 137.66, 135.13, 130.56, 127.38, 118.19, 113.72, 106.30, 99.55, 55.20, 52.51.



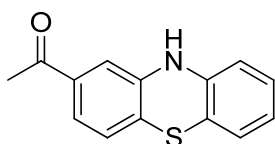
2-(3,5-dimethoxyphenyl)-1-(4-methoxyphenyl)ethanimine (3.4u).

A 1.0M solution of boron tribromide in dichloromethane (0.66 mL, 0.66 mmol) was added slowly to a solution of **3.4t** (30 mg, 0.09 mmol) in dichloromethane (0.5 mL) at -78 °C under nitrogen atmosphere. The reaction was allowed to stir at room temperature for four hours before cooling to -78 °C and quenching with an aqueous solution of saturated sodium bicarbonate (2 mL). The reaction mixture was warmed to room temperature and the aqueous layer was extracted with ethyl acetate (3 x 2 mL). The combined organic layers were washed with saturated sodium bicarbonate (3 x 5 mL), water (1 x 5 mL), and brine (1 x 5 mL) before being dried over magnesium sulfate, filtered, and concentrated. The pure product was obtained in 77% yield after purification by flash chromatography using 30% ethyl acetate 70% hexanes. ¹H-NMR (400 MHz, CDCl₃) δ (ppm): 7.99 (2H, d, J = 8.97), 6.92 (2H, d, J = 8.97), 6.43 (2H, d, J = 2.26), 6.34 (1H, t, J = 2.26), 4.15 (2H, s), 3.85 (3H, s), 3.76 (6H, s). ¹³C NMR (100 MHz, CDCl₃) δ (ppm): 195.94, 163.45, 160.83, 137.07, 130.90, 129.50, 113.70, 107.32, 98.76, 55.37, 55.20, 45.53. ESIMS(+) *m/z* 272 (M + H), 294 (M + Na).



1-(7-methoxy-10H-phenothiazin-2-yl)ethanone (4.1).

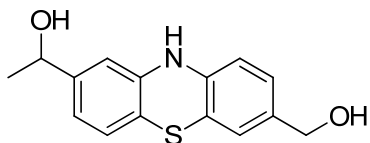
To a solution of **4.16** (1.0 eq.) in mesitylene (0.5 M) under N₂ atmosphere at ambient temperature was added triethylphosphite (6.0 eq.) slowly. The reaction mixture was then refluxed for 5 hours. After cooling to ambient temperature, the reaction mixture was diluted with toluene and concentrated as much as possible. Under no circumstance was the phenothiazine product dissolved in a chlorinated solvent. The crude residue was purified directly by flash chromatography using 20% ethyl acetate 80% hexanes and the pure product was isolated as an orangish brown flaky solid in 87% yield. ¹H-NMR (800 MHz, d⁶-DMSO) δ (ppm): 8.56 (1H (NH), s), 7.32 (1H, dd, J = 1.82, 7.98), 7.17 (1H, J = 1.82), 7.03 (1H, d, J = 7.98), 6.62 (2H, m), 6.58 (1H, d, J = 2.40), 3.67 (3H, s), 2.48 (3H, s). ¹³C NMR (75 MHz, d⁶-DMSO:CD₃OD 3:1) δ (ppm): 196.69, 154.83, 142.56, 136.02, 134.51, 125.81, 122.66, 121.41, 116.41, 114.93, 113.08, 112.26, 111.44, 54.94, 25.83. ESIMS(+) *m/z* 272 (M + H), 294 (M + Na). IR ν_{\max} 3342.68 (NH), 1666.04 (CO) cm⁻¹.



1-(10H-phenothiazin-2-yl)ethanone (4.2).

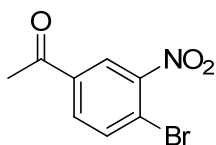
The procedure for compound **4.1** was followed starting from the sulfide **4.26**. The desired phenothiazine product was isolated in 42% yield after purification. ¹H-NMR (400 MHz, CD₃OD) δ (ppm): 7.35 (1H, dd, J = 1.79, 8.01), 7.16 (1H, d, J = 1.79), 6.94

(2H, m), 6.84 (1H, dd, $J = 1.35, 7.70$), 6.74 (1H, m), 6.60 (1H, dd, $J = 1.05, 7.93$), 2.49 (3H, s).



1-(7-(hydroxymethyl)-10H-phenothiazin-2-yl)ethanol (4.3).

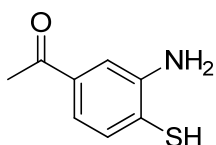
The protected phenothiazine **4.39** (1.0 eq.) in anhydrous THF (0.2 M) was added a 1.0 M solution of TBAF in THF dropwise (4.0 eq.), with vigorous stirring. The reaction mixture turned light brown and was allowed to stir at ambient temperature for 3 hours before it was diluted with water and extracted with ethyl acetate (3X). The combined organic layers were washed with brine, dried over magnesium sulfate, and concentrated. The crude product was used without further purification. $^1\text{H-NMR}$ (800 MHz, d^6 -DMSO) δ (ppm): 8.52 (1H (NH), s), 6.92 (1H, dd, $J = 1.42, 8.03$), 6.86 (1H, s), 6.84 (1H, d, $J = 7.91$), 6.74 (1H, d, $J = 1.42$), 6.70 (1H, dd, $J = 1.48, 7.91$), 6.64 (1H, d, $J = 8.03$), 4.57 (1H, m), 4.31 (2H, s), 1.27 (3H, d, $J = 6.45$).



1-(4-bromo-3-nitrophenyl)ethanone (4.4).

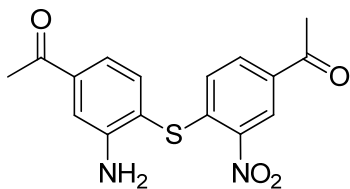
A solution of commercially available 4-bromoacetophenone (1.0 eq) in sulfuric acid (4 ml/mmol of 4-bromoacetophenone) was cooled to 0 °C and potassium nitrate (1.1 eq.) was added portionwise at that temperature. After 6 hrs, the reaction was SLOWLY

poured onto a mixture of ice and water and the pure product crashed out as a white solid. After vacuum filtration the desired compound **4.4** was isolated in 92% yield. $^1\text{H-NMR}$ (300 MHz, CDCl_3) δ (ppm): 8.33 (1H, d, $J = 2.00$), 7.97 (1H, dd, $J = 2.00, 8.34$), 7.85 (1H, d, $J = 8.34$), 2.63 (3H, s). $^{13}\text{C-NMR}$ (75 MHz, CDCl_3) δ (ppm): 194.69, 149.84, 136.80, 135.55, 131.96, 124.99, 119.54, 26.47.



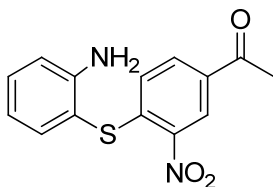
1-(3-amino-4-mercaptophenyl)ethanone (4.5).

To a solution of **4.4** (1.0 eq.) in DMF (0.4 M) was added sodium sulfide nonahydrate (2.0 eq.). The reaction was allowed to stir overnight before diluting with water and acidifying with 1 N HCl to pH 1-2. At this point, the sulfide product precipitated and was collected by vacuum filtration as an organish yellow solid in 75% yield. The sulfide was then dissolved in anhydrous methanol (0.2 M) and stannous chloride dihydrate (5.0 eq.) was added. The reaction mixture was refluxed until starting material disappeared from TLC. After cooling to room temperature, the reaction mixture was rotovapped onto a small amount of silica gel and used directly on the flash chromatography column for purification with 50% ethyl acetate 50% hexanes, giving the product in 53% yield. $^1\text{H-NMR}$ (300 MHz, CDCl_3) δ (ppm): 7.25 (2H, m), 7.12 (1H, d, $J = 8.05$), 4.48 (2H, bs), 2.54 (3H, s).



1-(4-((4-acetyl-2-aminophenyl)thio)-3-nitrophenyl)ethanone (4.6).

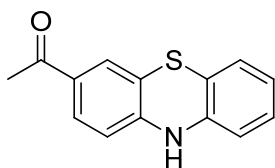
To a stirred suspension of **4.5** (1.0 eq.) and sodium hydroxide (1.0 eq.) in absolute ethanol (0.5 M) was added an alcoholic solution of **4.4** (1.0 eq.). The reaction mixture was refluxed for four hours before it was concentrated. The crude residue was diluted with water and extracted with ethyl acetate (3X). The combined organic layers were washed with brine, dried over magnesium sulfate, and concentrated. The crude residue was purified by flash chromatography using a gradient column from 20%-40% ethyl acetate 80%-60% hexanes to give the product in 43% yield. $^1\text{H-NMR}$ (400 MHz, CDCl_3) δ (ppm): 8.82 (1H, d, $J = 1.78$), 7.72 (1H, dd, $J = 1.78, 8.53$), 7.55 (1H, d, $J = 7.95$), 7.42 (1H, d, $J = 1.45$), 7.36 (1H, dd, $J = 1.68, 7.95$), 6.90 (1H, d, $J = 8.53$), 4.44 (2H, s), 2.62 (3H, s), 2.61 (3H, s). $^{13}\text{C-NMR}$ (100 MHz, CDCl_3) δ (ppm): 197.67, 194.91, 149.29, 144.97, 141.86, 140.60, 137.84, 134.26, 132.28, 127.57, 126.13, 118.70, 116.41, 114.66, 26.76, 26.42. IR ν_{max} 3462.69 (NH), 3360.43 (NH) cm^{-1} .



1-(4-((2-aminophenyl)thio)-3-nitrophenyl)ethanone (4.7).

Commercially available 2-aminobenzenethiol (1.0 eq.) was dissolved in absolute ethanol (0.5 M) containing sodium acetate (1.0 eq.) in a round bottom flask that had been

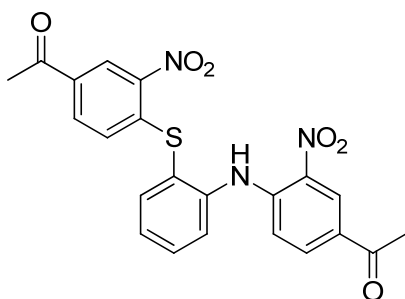
flame dried under N₂ atmosphere. A solution of **4.4** (1.0 eq.) in absolute ethanol (1 M) was then added and the reaction mixture was refluxed under N₂ atmosphere for 6 hours. After cooling to ambient temperature, the reaction mixture was diluted with dichloromethane and concentrated to an orange residue. The residue was taken up in water and extracted with ethyl acetate (3X). The combined organic extracts were washed with brine, dried over magnesium sulfate, and concentrated. The product was purified by flash chromatography using 20% ethyl acetate and 80% hexanes, giving the product in 66% yield. ¹H-NMR (300 MHz, CDCl₃) δ (ppm): 8.44 (1H, d, J = 1.90), 7.89 (1H, dd, J = 1.90, 8.53), 7.40 (1H, dd, J = 1.46, 7.67), 7.34 (1H, m), 6.93 (1H, d, J = 8.53), 6.85 (1H, dd, J = 0.91, 8.21), 6.81 (1H, dd, J = 1.18, 7.53), 2.59 (3H, s). ¹³C-NMR (75 MHz, CDCl₃) δ (ppm): 195.13, 149.26, 144.75, 143.29, 137.46, 133.81, 132.68, 132.15, 127.61, 125.99, 119.28, 115.72, 111.05, 26.41. IR ν_{max} 3480.25 (NH), 3375.31 (NH), 1681.64 (CO) cm⁻¹.



1-(10H-phenothiazin-3-yl)ethanone (4.8).

Compound **4.6** (1.0 eq.) was refluxed in 88% formic acid for five hours before it was cooled to room temperature and poured onto ice. The yellow precipitate was collected by vacuum filtration and dissolved in acetone (0.6 M). The solution was heated to reflux and an alcoholic solution of potassium hydroxide (0.4 eq.) was added. The reaction was heated for 30 minutes and another aliquot of potassium hydroxide was

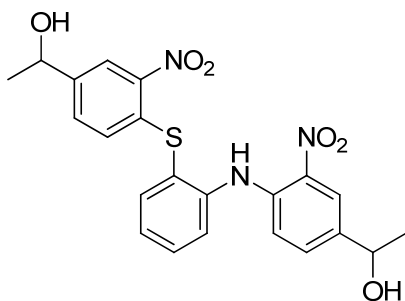
added. The reaction mixture was then refluxed for 12 hours before it was cooled to room temperature and poured onto ice. After the ice melted, the aqueous layer was extracted with ethyl acetate (3X). The combined organic extracts were washed with brine, dried over magnesium sulfate, and concentrated. The reaction mixture yielded a variety of products, two of which were purified by flash chromatography using a gradient of 100% dichloromethane ramped to 3% methanol 97% dichloromethane. $^1\text{H-NMR}$ (300 MHz, CDCl_3) δ (ppm): 9.80 (1H, s), 8.78 (1H, d, $J = 2.07$), 7.93 (1H, dd, $J = 1.89, 9.02$), 7.65 (1H, dd, $J = 1.27, 7.83$), 7.32 (1H, m), 7.22 (1H, m), 6.92 (1H, d, $J = 9.02$), 2.59 (3H, s). ESIMS(+) m/z 242 ($M + H$), 264 ($M + \text{Na}$), 280 ($M + \text{K}$). IR ν_{max} 3480.25 (NH), 3375.31 (NH), 1681.64 (CO) cm^{-1} .



1-(4-((2-((4-acetyl-2-nitrophenyl)amino)phenyl)thio)-3-nitrophenyl)ethanone (4.9).

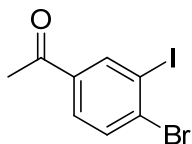
This product was isolated from the reaction mixture described for compound **4.8** in 5% yield. $^1\text{H-NMR}$ (300 MHz, CDCl_3) δ (ppm): 9.82 (1H (NH), s), 8.75 (1H, d, $J = 1.82$), 8.69 (1H, d, $J = 2.03$), 7.99 (1H, dd, $J = 2.00, 9.01$), 7.87 (1H, dd, $J = 1.91, 8.50$), 7.81 (1H, d, $J = 7.48$), 7.64 (2H, m), 7.41 (1H, m), 7.29 (1H, d, $J = 9.01$), 6.92 (1H, d, $J = 8.50$), 2.59 (3H, s), 2.56 (3H, s). $^{13}\text{C-NMR}$ (75 MHz, CDCl_3) δ (ppm): 194.79, 194.54, 145.00, 143.80, 142.31, 140.86, 138.21, 134.55, 134.38, 132.89, 132.25, 128.13, 127.81,

127.32, 126.17, 124.43, 115.51, 26.42, 26.02. ESIMS(+) m/z 452 (M + H), 474 (M + Na), 490 (M + K). IR ν_{\max} 3288.83 (NH) cm^{-1} .

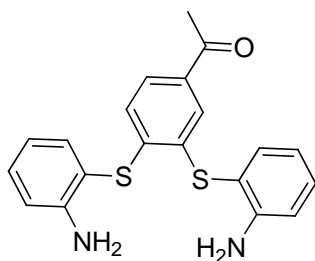


1-(4-((2-((4-(1-hydroxyethyl)-2-nitrophenyl)amino)phenyl)thio)-3-nitrophenyl)ethanol (4.10).

Compound **4.9** (1.0 eq.) was dissolved in anhydrous methanol (0.2 M) and sodium borohydride (4.0 eq.) was added portionwise. The reaction mixture was allowed to stir for one hour before it was concentrated. The crude residue was taken up in dilute hydrochloric acid and extracted with dichloromethane (3X). The combined organic layers were washed with brine, dried over magnesium sulfate, and concentrated. The pure product was obtained in quantitative yield after purification by flash chromatography using 40% ethyl acetate 60% hexanes. $^1\text{H-NMR}$ (300 MHz, CDCl_3) δ (ppm): 9.28 (1H (NH), s), 8.09 (1H, t, $J = 2.04$), 8.02 (1H, m), 7.79 (1H, m), 7.52 (2H, m), 7.38 (1H, m), 7.30 (1H, dd, $J = 2.06, 6.71$), 7.16 (1H, d, $J = 8.80$), 6.86 (1H, d, $J = 8.32$), 4.83 (2H, m), 1.47 (3H, d, $J = 6.45$), 1.43 (3H, d, $J = 6.47$). $^{13}\text{C-NMR}$ (75 MHz, CDCl_3) δ (ppm): 145.89, 144.59, 141.40, 139.96, 137.60, 136.24, 134.57, 133.01, 132.89, 131.23, 130.65, 128.41, 125.86, 125.37, 124.13, 123.20, 122.66, 116.38, 68.96, 68.55, 24.88, 24.64. IR ν_{\max} 3313.10 (NH) cm^{-1} .

**1-(4-bromo-3-iodophenyl)ethanone (4.11).**

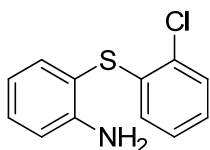
Compound **4.4** (1.0 eq.) was dissolved in anhydrous methanol (0.2 M) and stannous chloride dihydrate (5.0 eq.) was added. The reaction mixture was refluxed under N₂ atmosphere for two hours before it was cooled to room temperature and poured onto ice. The pH was adjusted to 7-8 using sodium bicarbonate and the aqueous layer was extracted with ethyl acetate (3X). The combined organic layers were washed with brine, dried over magnesium sulfate, and concentrated. The crude amine was then dissolved in 6 N HCl (1 M) and sodium nitrite (1.1 eq.) was then added slowly at 0 °C and the reaction was stirred at that temperature for 15 minutes. A solution of potassium iodide (3.5 eq.) in water (1 M) was then slowly added to the reaction mixture and it was stirred overnight. The reaction mixture was extracted with ether (3X) and the combined organic layers were washed with brine, 2 N NaOH, saturated Na₂S₂O₃, water, and brine. The organic layer was dried over magnesium sulfate and concentrated to give the pure product in 93% yield. ¹H-NMR (300 MHz, CDCl₃) δ (ppm): 8.34 (1H, d, J = 1.98), 7.71 (1H, dd, J = 1.98, 8.31), 7.65 (1H, d, J = 8.31), 2.54 (3H, s).



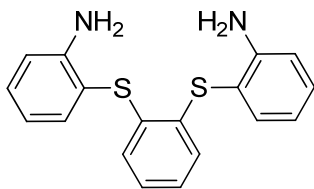
1-(3,4-bis((2-aminophenyl)thio)phenyl)ethanone (4.12).

Copper iodide (0.3 eq.) and potassium carbonate (5.0 eq.) were weighed into a seal tube flask that was subsequently flushed with argon. To the flask were added 2-aminothiophenol (1.1 eq.), **4.11** (1.0 eq.), and dimethylsulfoxide (0.2 M). The reaction vessel was then heated to 120 °C for 48 hours. After cooled to room temperature, the reaction mixture was diluted with ethyl acetate and washed with water. The aqueous layer was extracted with ethyl acetate (3X) and the combined organic layers were washed with brine, dried over magnesium sulfate, and concentrated. Flash chromatography using 20% ethyl acetate and 80% hexanes of the crude residue resulted in **4.12** in 89% yield.

$^1\text{H-NMR}$ (300 MHz, CDCl_3) δ (ppm): 7.47 (4H, m), 7.26 (2H, m), 6.77 (5H, m), 4.30 (4H (NH), s), 2.34 (3H, s). $^{13}\text{C-NMR}$ (75 MHz, CDCl_3) δ (ppm): 196.80, 149.07, 148.69, 142.46, 137.44, 136.66, 134.52, 133.99, 131.81, 131.29, 127.87, 126.06, 125.51, 118.88, 115.53, 113.65, 112.17, 26.25. ESIMS(+) m/z 367 (M + H), 389 (M + Na). IR ν_{max} 3464.58 (NH), 3427.24 (NH), 1673.82 (CO) cm^{-1} .

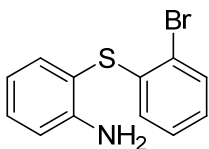
**2-((2-chlorophenyl)thio)aniline (4.13).**

A three-neck round bottom flask was flame dried under argon gas, evacuated, and backfilled with argon. Copper iodide (0.3 eq.) and potassium carbonate (5.0 eq.) and dimethylsulfoxide (0.2 M) were then added. The reaction vessel was evacuated and backfilled with argon. The commercially available starting materials 2-aminothiophenol (1.1 eq.) and 2-chlorobromobenzene (1.0 eq) were then added. The reaction vessel was then heated to 120 °C for 48 hours. After cooled to room temperature, the reaction mixture was diluted with ethyl acetate and washed with water. The aqueous layer was extracted with ethyl acetate (3X) and the combined organic layers were washed with brine, dried over magnesium sulfate, and concentrated. Flash chromatography using 20% ethyl acetate 80% hexanes resulted in the product in 22% yield. ¹H-NMR (300 MHz, CDCl₃) δ (ppm): 7.47 (1H, dd, J = 1.53, 7.65), 7.32 (2H, m), 7.06 (2H, m), 6.81 (2H, m), 6.65 (1H, m). ¹³C-NMR (75 MHz, CDCl₃) δ (ppm): 149.15, 137.84, 135.90, 131.67, 130.85, 129.41, 127.07, 126.07, 125.91, 118.86, 115.33, 112.33. IR ν_{\max} 3460.47 (NH), 3364.73 (NH) cm⁻¹.



2,2'-(1,2-phenylenebis(sulfaneydiyl))dianiline (4.14).

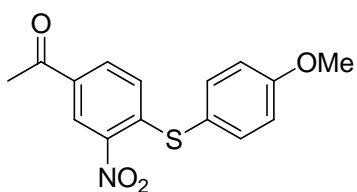
Followed procedure for **4.13** with 2-aminothiophenol and 1,2-dibromobenzene. The product was isolated in 57% yield after flash chromatography with 10% ethyl acetate 90% hexanes. $^1\text{H-NMR}$ (300 MHz, CDCl_3) δ (ppm): 7.48 (2H, dd, $J = 1.55, 8.00$), 7.26 (2H, ddd, $J = 1.55, 9.34$), 7.00 (2H, m), 6.88 (2H, m), 6.79 (4H, m), 4.27 (4H (NH), s). $^{13}\text{C-NMR}$ (75 MHz, CDCl_3) δ (ppm): 148.71, 136.94, 134.87, 130.98, 127.52, 126.35, 118.72, 115.37, 114.41. IR ν_{max} 3320.58 (NH) cm^{-1} .



2-((2-bromophenyl)thio)aniline (4.15).

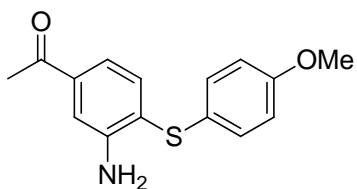
A three-neck round bottom flask was flame dried under argon gas, evacuated, and backfilled with argon. Copper iodide (0.3 eq.) and potassium carbonate (5.0 eq.) and 2-methoxyethanol (0.2 M) were then added. The reaction vessel was evacuated and backfilled with argon. The commercially available starting materials 2-aminothiophenol (1.1 eq.) and 1,2-dibromobenzene (1.0 eq.) were then added. The reaction vessel was then heated to 110 °C for 48 hours. After cooled to room temperature, the reaction mixture was diluted with ethyl acetate and washed with water. The aqueous layer was extracted with ethyl acetate (3X) and the combined organic layers were washed with brine, dried

over magnesium sulfate, and concentrated. Flash chromatography using 20% ethyl acetate 80% hexanes resulted in the product in 50% yield. $^1\text{H-NMR}$ (300 MHz, CDCl_3) δ (ppm): 7.54 (1H, dd, $J = 1.35, 7.87$), 7.48 (1H, dd, $J = 1.52, 7.61$), 7.31 (1H, m), 7.11 (1H, td, $J = 1.35, 7.65$), 6.98 (1H, td, $J = 1.60, 7.61$), 6.82 (2H, m), 6.64 (1H, dd, $J = 1.60, 7.93$), 4.26 (2H (NH), s). $^{13}\text{C-NMR}$ (75 MHz, CDCl_3) δ (ppm): 149.12, 137.82, 132.71, 131.75, 127.71, 126.15, 120.58, 118.91, 115.40, 112.91. IR ν_{max} 3320.58 (NH) cm^{-1} .



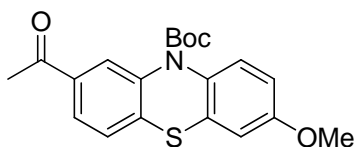
1-(4-((4-methoxyphenyl)thio)-3-nitrophenyl)ethanone (4.16).

A solution of 4-methoxythiophenol (1.05 eq.), **4.4** (1.0 eq.), and sodium hydroxide (1.0 eq.) was heated in DMF (0.4 M) at 60 °C for 12 hours. The reaction was cooled to room temperature, and poured into saturated aqueous lithium chloride. The aqueous layer was then extracted with ethyl acetate (3X). The combined organic layers were washed with saturated aqueous lithium chloride (5X), dried over magnesium sulfate, and concentrated. The crude residue was purified by flash chromatography using 15% ethyl acetate 85% hexanes, to give the product in quantitative yield. $^1\text{H-NMR}$ (300 MHz, CDCl_3) δ (ppm): 8.70 (1H, d, $J = 1.95$), 7.83 (1H, dd, $J = 1.95, 8.59$), 7.44 (2H, d, $J = 8.79$), 6.99 (2H, d, $J = 8.79$), 6.97 (1H, d, $J = 8.59$), 3.85 (3H, s), 2.57 (3H, s). $^{13}\text{C-NMR}$ (75 MHz, CDCl_3) δ (ppm): 195.04, 161.40, 146.58, 143.87, 137.43, 133.34, 131.77, 127.94, 125.70, 119.81, 115.84, 55.40, 26.37. IR ν_{max} 1680.32 (CO) cm^{-1} .



1-(3-amino-4-((4-methoxyphenyl)thio)phenyl)ethanone (4.17).

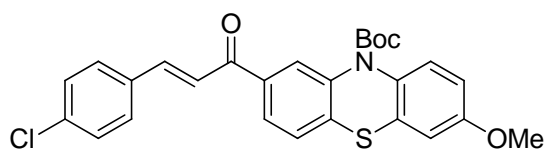
A solution of **4.16** (1.0 eq.) and stannous chloride dihydrate (5.0 eq.) in anhydrous methanol was refluxed for 6 hours. It was cooled to room temperature and poured onto ice. The pH was adjusted to 7-8 using sodium bicarbonate and the aqueous layer was extracted with ethyl acetate (3X). The combined organic layers were washed with brine, dried over magnesium sulfate, and concentrated. The desired amine was purified by flash chromatography using 40% ethyl acetate 60% hexanes and obtained in 64% yield. $^1\text{H-NMR}$ (300 MHz, CDCl_3) δ (ppm): 7.31 (1H, m), 7.24 (4H, m), 6.85 (2H, d, $J = 6.85$), 3.79 (3H, s), 2.54 (3H, s). $^{13}\text{C-NMR}$ (75 MHz, CDCl_3) δ (ppm): 197.77, 159.17, 146.15, 137.41, 133.29, 132.10, 124.95, 124.00, 118.63, 114.97, 114.24, 55.27, 26.57. IR ν_{max} 3425.46 (NH), 3351.24 (NH), 1673.32 (CO) cm^{-1} .



tert-butyl 2-acetyl-7-methoxy-10H-phenothiazine-10-carboxylate (4.18).

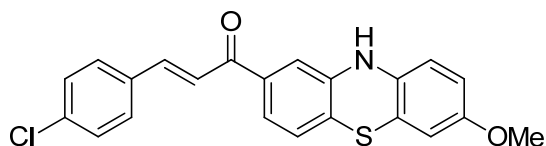
A solution of **4.1** (1.0 eq.), di-*tert*-butyl dicarbonate (6.0 eq.), and DMAP (1.0 eq.) was refluxed in acetonitrile (0.2 M) for 8 hours. After cooling to room temperature, the reaction mixture was poured into water and extracted with ethyl acetate (3X). The combined organic layers were washed with brine, dried over magnesium sulfate, and

concentrated. The pure product was obtained in 95% yield after flash chromatography using 5% ethyl acetate 95% hexanes. $^1\text{H-NMR}$ (300 MHz, CD_3OD) δ (ppm): 8.08 (1H, d, $J = 1.72$), 7.80 (1H, dd, $J = 1.82, 8.20$), 7.46 (1H, d, $J = 8.20$), 7.41 (1H, d, $J = 8.77$), 6.90 (2H, dt, $J = 2.72, 8.77$), 3.79 (3H, s), 2.60 (3H, s), 1.47 (9H, s). $^{13}\text{C-NMR}$ (100 MHz, CDCl_3) δ (ppm): 196.66, 157.59, 152.32, 138.96, 138.07, 135.54, 131.78, 130.81, 127.82, 127.14, 126.98, 125.48, 113.23, 111.59, 82.24, 55.52, 28.05, 26.52. IR ν_{max} 3425.46 (NH), 3351.24 (NH), 1673.32 (CO) cm^{-1} .



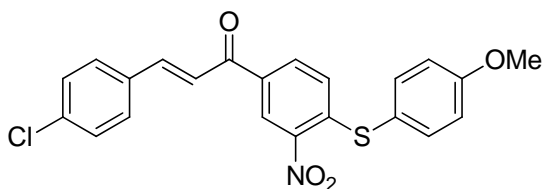
(E)-tert-butyl-2-(3-(4-chlorophenyl)acryloyl)-7-methoxy-10H-phenothiazine-10-carboxylate (4.19).

To a solution of **4.18** (1.0 eq.) and 4-chlorobenzaldehyde (1.0 eq.) in absolute ethanol (0.4 M) was added a solution of potassium hydroxide (1.0 eq.) in ethanol (0.4 m). The reaction was allowed to stir for 24 hours before water was added. The aqueous layer was extracted with ethyl acetate (3X). The combined organic layers were washed with brine, dried over magnesium sulfate, and concentrated. The crude residue was used without further purification. $^1\text{H-NMR}$ (300 MHz, CDCl_3) δ (ppm): 8.15 (1H, s), 7.72 (3H, m), 7.44 (4H, m), 6.85 (2H, m), 3.80 (3H, s), 1.49 (9H, s).



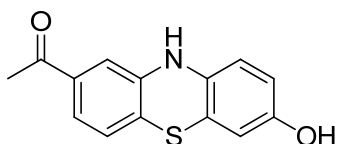
(E)-3-(4-chlorophenyl)-1-(7-methoxy-10H-phenothiazin-2-yl)prop-2-en-1-one (4.20).

To a solution of **4.19** (1.0 eq.) in dichloromethane (10 ml/mmol) was added a 4N solution of hydrochloric acid in dioxane (20 eq.). The reaction was stirred at room temperature for 12 hours. The reaction was diluted with ethyl acetate and washed with 1 N sodium hydroxide (3X), water (2X), brine (2X), dried over magnesium sulfate, and concentrated. The crude residue was purified by flash chromatography using 20% ethyl acetate 80% hexanes to afford the pure product in 89% yield. $^1\text{H-NMR}$ (800 MHz, d^6 -DMSO) δ (ppm): 8.60 (1H (NH), s), 7.91 (2H, d, $J = 8.49$), 7.82 (1H, d, $J = 15.63$), 7.70 (1H, d, $J = 15.63$), 7.61 (1H, dd, $J = 1.81, 8.04$), 7.54 (2H, d, $J = 8.49$), 7.28 (1H, d, $J = 1.81$), 7.10 (1H, d, $J = 8.04$), 6.62 (3H, m), 3.67 (3H, s). $^{13}\text{C-NMR}$ (200 MHz, d^6 -DMSO) δ (ppm): 188.47, 155.31, 143.30, 142.74, 137.26, 135.54, 134.98, 134.16, 130.98, 129.46, 126.62, 123.59, 123.13, 122.63, 116.78, 115.75, 114.01, 113.12, 112.15, 55.91. IR ν_{max} 3354.84 (NH), 1655.53 (CO) cm^{-1} .



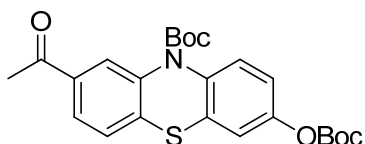
**(E)-3-(4-chlorophenyl)-1-(4-((4-methoxyphenyl)thio)-3-nitrophenyl)prop-2-en-1-one
(4.21).**

To a stirred solution of sulfide **4.16** (1.0 eq.) and 4-chlorobenzaldehyde (1.0 eq.) in absolute methanol (1.3 M) was added a solution of a solution of sodium hydroxide (1.3 eq.) in absolute methanol (1.3 M) dropwise. The resulting mixture was stirred at room temperature for 12 hours, water was added and the aqueous layer was extracted with ethyl acetate (3X). The combined organic layers were washed with brine, dried over magnesium sulfate, and concentrated. The crude product was purified by flash chromatography giving the desired sulfide in 26% yield. $^1\text{H-NMR}$ (400 MHz, CDCl_3) δ (ppm): 8.86 (1H, d, $J = 1.84$), 7.97 (1H, dd, $J = 1.84, 8.61$), 7.80 (1H, d, $J = 15.59$), 7.58 (2H, d, $J = 8.49$), 7.51 (2H, d, $J = 8.73$), 7.46 (1H, d, $J = 15.59$), 7.40 (2H, d, $J = 8.49$), 7.04 (2H, d, $J = 8.73$), 6.96 (1H, d, $J = 8.60$), 3.89 (3H, s). $^{13}\text{C-NMR}$ (100 MHz, CDCl_3) δ (ppm): 186.71, 161.48, 146.68, 144.48, 144.04, 137.53, 136.90, 134.29, 132.84, 132.21, 129.71, 129.28, 128.20, 125.72, 120.70, 120.04, 115.89, 55.42. IR ν_{max} 1588.61 (CO) cm^{-1} .



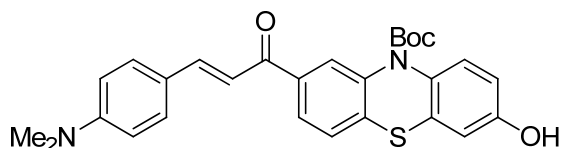
1-(7-hydroxy-10H-phenothiazin-2-yl)ethanone (4.22).

To a solution of **4.18** (1.0 eq.) in anhydrous dichloromethane (0.2 M) under N₂ atmosphere at -78 °C was added a solution of 1.0 M boron tribromide in dichloromethane (2.5 eq.) dropwise. The reaction mixture was allowed to stir for 6 hours. The reaction mixture was cooled back to -78 °C and quenched with saturated sodium bicarbonate and methanol. The aqueous layer was extracted with ethyl acetate (3X). The combined organic layers were washed with saturated sodium bicarbonate (4X) and brine (3X). The combined organic layers were then dried over magnesium sulfate and concentrated. The crude residue was purified by flash chromatography using 30% ethyl acetate 70% hexanes, giving the pure product in quantitative yield. ¹H-NMR (400 MHz, CDCl₃) δ (ppm): 8.41 (1H, d, J = 1.80), 8.05 (1H, dd, J = 1.80, 8.35), 7.62 (1H, d, J = 9.91), 7.53 (1H, d, J = 8.37), 6.95 (1H, dd, J = 2.05, 9.91), 6.77 (1H, d, J = 2.05), 2.68 (3H, s). ¹³C-NMR (100 MHz, CDCl₃) δ (ppm): 182.35, 147.95, 147.27, 139.70, 138.90, 136.50, 135.50, 134.12, 133.95, 129.47, 128.85, 125.32, 120.91, 26.45. IR ν_{max} 1675.26 (CO) cm⁻¹.



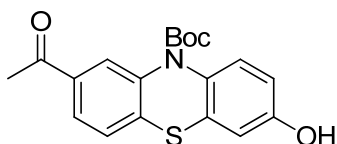
***tert*-butyl-2-acetyl-7-((*tert*-butoxycarbonyl)oxy)-10H-phenothiazine-10-carboxylate (4.23).**

To a solution of **4.22** (1.0 eq.) in anhydrous acetonitrile (0.2 M) was added di-*tert*-butyl dicarbonate (6.0 eq.) and DMAP (1.0 eq.) and the reaction mixture was refluxed under N₂ atmosphere for 24 hours. The reaction mixture was allowed to cool to room temperature and poured into water. The aqueous layer was extracted with ethyl acetate (3X). The combined organic layers were washed with brine, dried over magnesium sulfate, and concentrated. The crude residue was purified by flash chromatography using 10% ethyl acetate 90% hexanes to afford the pure product in 16% yield. ¹H-NMR (400 MHz, CDCl₃) δ (ppm): 8.04 (1H, d, J = 1.62), 7.74 (1H, dd, J = 1.62, 8.15), 7.51 (1H, d, J = 8.77), 7.39 (1H, d, J = 8.15), 7.19 (1H, d, J = 2.59), 7.10 (1H, dd, J = 2.59, 8.77), 2.61 (3H, s), 1.55 (9H, s), 1.49 (2H, s). ¹³C-NMR (100 MHz, CDCl₃) δ (ppm): 196.60, 151.97, 151.35, 148.66, 138.54, 137.80, 135.73, 131.92, 127.67, 127.24, 126.97, 125.69, 119.95, 83.93, 82.67, 60.29, 28.04, 27.56. IR ν_{max} 1675.26 (CO) cm⁻¹.



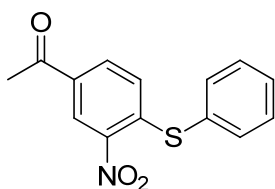
(E)-tert-butyl-2-(3-(4-(dimethylamino)phenyl)acryloyl)-7-hydroxy-10H-phenothiazine-10-carboxylate (4.24).

To a solution of **4.23** (1.0 eq.) and 4-dimethylaminobenzaldehyde (1.0 eq.) in absolute ethanol (1.3 M) was added a solution of sodium hydroxide (1.3 eq.) in ethanol (1.3 M). The resulting mixture was stirred at room temperature for 24 hours, water was added and the aqueous layer was extracted with ethyl acetate (3X). The combined organic layers were washed with brine, dried over magnesium sulfate, and concentrated. The crude product was purified by flash chromatography giving the desired phenothiazine **4.24** in 27% yield and compound **4.25** in 22% yield. $^1\text{H-NMR}$ (800 MHz, CDCl_3) δ (ppm): 8.15 (1H, d, $J = 1.57$), 7.85 (1H, d, $J = 15.41$), 7.82 (1H, dd, $J = 1.70$, 8.09), 7.58 (2H, d, $J = 8.85$), 7.44 (1H, d, $J = 8.09$), 8.71 (1H, d, $J = 8.71$), 7.33 (1H, d, $J = 15.41$), 6.82 (1H, d, $J = 2.71$), 6.76 (1H, dd, $J = 2.72$, 8.71), 6.73 (2H, d, $J = 8.85$), 3.09 (6H, s), 1.53 (9H, s). $^{13}\text{C-NMR}$ (200 MHz, CDCl_3) δ (ppm): 189.28, 153.95, 152.73, 152.19, 146.39, 139.04, 137.64, 137.02, 132.39, 130.98, 130.59, 128.04, 127.18, 125.75, 122.60, 116.34, 114.50, 113.69, 111.86, 82.45, 40.15, 28.22. IR ν_{max} 3316.24 (OH), 1521.55 (CO) cm^{-1} .



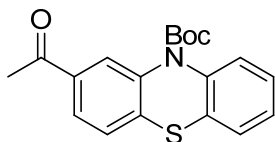
tert-butyl 2-acetyl-7-hydroxy-10H-phenothiazine-10-carboxylate (4.25).

See procedure for **4.24**. $^1\text{H-NMR}$ (800 MHz, CDCl_3) δ (ppm): 8.10 (1H, d, $J = 1.69$), 7.77 (1H, dd, $J = 1.81, 8.15$), 7.43 (1H, d, $J = 8.15$), 7.39 (1H, d, $J = 8.71$), 6.81 (1H, d, $J = 2.74$), 6.76 (1H, dd, $J = 2.76, 8.71$), 2.63 (3H, s), 1.52 (9H, s).



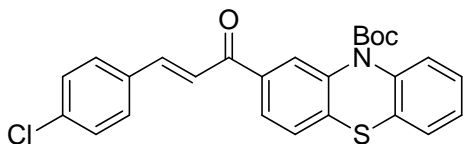
1-(3-nitro-4-(phenylthio)phenyl)ethanone (4.26).

A solution of thiophenol (1.05 eq.), **4.4** (1.0 eq.), and sodium hydroxide (1.0 eq.) was heated in DMF (0.4 M) at 60 °C for 12 hours. The reaction was cooled to room temperature, and poured into saturated aqueous lithium chloride. The aqueous layer was then extracted with ethyl acetate (3X). The combined organic layers were washed with saturated aqueous lithium chloride (5X), dried over magnesium sulfate, and concentrated. The crude residue was purified by flash chromatography using 10% ethyl acetate 90% hexanes, to give the product in 75% yield. $^1\text{H-NMR}$ (400 MHz, CDCl_3) δ (ppm): 8.76 (1H, d, $J = 1.85$), 7.87 (1H, dd, $J = 1.85, 8.59$), 7.58 (2H, m), 7.52 (3H, m), 6.91 (1H, d, $J = 8.59$). $^{13}\text{C-NMR}$ (100 MHz, CDCl_3) δ (ppm): 195.00, 145.57, 144.25, 135.84, 133.62, 131.84, 130.53, 130.33, 129.75, 128.25, 125.77, 26.38. IR ν_{max} 1682.39 (CO) cm^{-1} .



tert-butyl 2-acetyl-10H-phenothiazine-10-carboxylate (4.27).

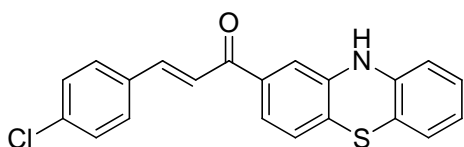
A solution of **4.2** (1.0 eq.), di-*tert*-butyl dicarbonate (6.0 eq.), and DMAP (1.0 eq.) was refluxed in acetonitrile (0.2 M) for 8 hours. After cooling to room temperature, the reaction mixture was poured into water and extracted with ethyl acetate (3X). The combined organic layers were washed with brine, dried over magnesium sulfate, and concentrated. The pure product was obtained in 95% yield after flash chromatography using 5% ethyl acetate 95% hexanes. $^1\text{H-NMR}$ (400 MHz, CDCl_3) δ (ppm): 8.10 (1H, d, $J = 1.70$), 7.73 (1H, dd, $J = 1.70, 8.18$), 7.54 (1H, d, $J = 8.10$), 7.39 (1H, d, $J = 8.18$), 7.31 (2H, m), 7.16 (1H, td, $J = 1.03, 7.60$), 2.59 (3H, s), 1.49 (9H, s). $^{13}\text{C-NMR}$ (100 MHz, CDCl_3) δ (ppm): 196.65, 152.07, 138.61, 138.36, 138.04, 135.57, 130.69, 127.32, 127.24, 127.20, 127.03, 126.91, 126.29, 125.60, 82.47, 28.05, 26.54. IR ν_{max} 1794.75 (CO) cm^{-1} .



(E)-tert-butyl-2-(3-(4-chlorophenyl)acryloyl)-10H-phenothiazine-10-carboxylate (4.28).

To a solution of **4.27** (1.0 eq.) and 4-chlorobenzaldehyde (1.0 eq.) in absolute methanol (0.4 M) was added a solution of sodium hydroxide (1.0 eq.) in methanol (0.4 M). The reaction was allowed to stir for 24 hours before water was added. The aqueous layer was extracted with ethyl acetate (3X). The combined organic layers were washed

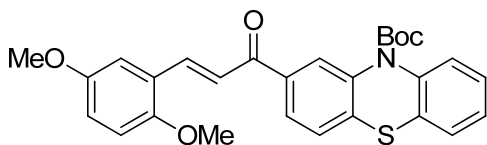
with brine, dried over magnesium sulfate, and concentrated. The crude residue was purified by flash chromatography to give the pure product **4.28** in 18% yield. $^1\text{H-NMR}$ (800 MHz, CDCl_3) δ (ppm): 8.20 (1H, s), 8.10 (1H, d, $J = 8.10$), 7.82 (1H, d, $J = 15.67$), 7.62 (2H, d, $J = 8.33$), 8.08 (1H, d, $J = 8.10$), 7.50 (1H, d, $J = 15.67$), 4.49 (1H, d, $J = 7.76$), 7.44 (2H, d, $J = 8.33$), 7.38 (1H, d, $J = 7.76$), 7.34 (1H, m), 7.22 (1H, m), 1.53 (9H, s). $^{13}\text{C-NMR}$ (200 MHz, CDCl_3) δ (ppm): 188.86, 152.25, 143.72, 138.81, 138.40, 138.17, 136.58, 136.53, 133.36, 130.81, 129.67, 129.31, 127.46, 127.36, 127.04, 126.42, 125.93, 122.13, 82.64, 28.19. IR ν_{max} 1711.37 (CO) cm^{-1} .



(E)-3-(4-chlorophenyl)-1-(10H-phenothiazin-2-yl)prop-2-en-1-one (4.29).

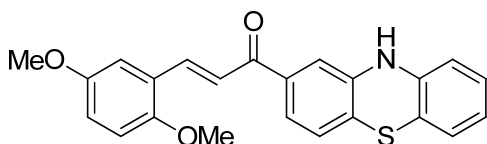
To a solution of **4.28** (1.0 eq.) in dichloromethane (10 ml/mmol) was added a 4N solution of hydrochloric acid in dioxane (20 eq.). The reaction was stirred at room temperature for 12 hours. The reaction was diluted with ethyl acetate and washed with 1 N sodium hydroxide (3X), water (2X), brine (2X), dried over magnesium sulfate, and concentrated. The crude residue was purified by flash chromatography using 20% ethyl acetate 80% hexanes to afford the pure product in 27% yield. $^1\text{H-NMR}$ (800 MHz, $\text{d}^6\text{-DMSO}$) δ (ppm): 8.80 (1H, s), 7.92 (2H, d, $J = 8.41$), 7.83 (1H, d, $J = 15.61$), 7.71 (1H, d, $J = 15.61$), 7.65 (1H, dd, $J = 1.47, 8.05$), 7.54 (2H, d, $J = 8.41$), 7.31 (1H, d, $J = 1.47$), 7.10 (1H, d, $J = 8.05$), 7.02 (1H, m), 6.93 (1H, m), 6.78 (1H, m), 6.67 (1H, d, $J = 7.92$). $^1\text{H-NMR}$ (200 MHz, $\text{d}^6\text{-DMSO}$) δ (ppm): 188.39, 142.77, 142.65, 141.58, 137.24,

135.55, 135.02, 134.17, 130.99, 129.46, 128.51, 126.77, 126.62, 124.27, 123.11, 122.61, 115.66, 115.09, 113.35. IR ν_{\max} 3346.88 (NH), 1652.07 (CO) cm^{-1} .



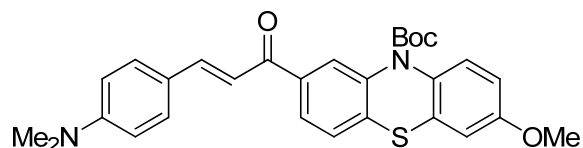
(E)-tert-butyl-2-(3-(2,5-dimethoxyphenyl)acryloyl)-10H-phenothiazine-10-carboxylate (4.30).

To a solution of **4.27** (1.0 eq.) and 2,5-dimethoxybenzaldehyde (1.0 eq.) in absolute methanol (0.4 M) was added a solution of sodium hydroxide (1.0 eq.) in methanol (0.4 m). The reaction was allowed to stir for 24 hours before water was added. The aqueous layer was extracted with ethyl acetate (3X). The combined organic layers were washed with brine, dried over magnesium sulfate, and concentrated. The crude residue was purified by flash chromatography to give the pure product **4.30** in 50% yield. $^1\text{H-NMR}$ (400 MHz, CDCl_3) δ (ppm): 8.17 (1H, d, $J = 1.64$), 8.10 (1H, d, $J = 15.81$), 7.81 (1H, dd, $J = 1.64, 8.16$), 7.58 (2H, m), 7.44 (1H, d, $J = 8.16$), 7.35 (1H, m), 7.31 (1H, m), 7.18 (2H, m), 6.95 (1H, dd, $J = 3.00, 9.00$), 6.88 (1H, d, $J = 9.00$), 3.88 (3H, s), 3.82 (3H, s), 1.51 (9H, s). $^{13}\text{C-NMR}$ (100 MHz, CDCl_3) δ (ppm): 189.42, 153.43, 153.35, 152.13, 140.40, 138.67, 138.12, 137.74, 136.91, 130.83, 127.31, 127.21, 126.88, 126.24, 125.88, 124.37, 122.59, 117.25, 113.82, 112.41, 82.42, 56.03, 55.77, 28.07. IR ν_{\max} 1710.23 (CO) cm^{-1} .



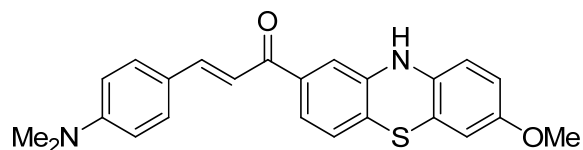
(E)-3-(2,5-dimethoxyphenyl)-1-(10H-phenothiazin-2-yl)prop-2-en-1-one (4.31).

To a solution of **4.30** (1.0 eq.) in dichloromethane (10 ml/mmol) was added a 4N solution of hydrochloric acid in dioxane (20 eq.). The reaction was stirred at room temperature for 12 hours. The reaction was diluted with ethyl acetate and washed with 1 N sodium hydroxide (3X), water (2X), brine (2X), dried over magnesium sulfate, and concentrated. The crude residue was purified by flash chromatography using 20% ethyl acetate 80% hexanes to afford the pure product in 89% yield. $^1\text{H-NMR}$ (800 MHz, $\text{d}^6\text{-DMSO}$) δ (ppm): 8.80 (1H, s), 7.99 (1H, d, $J = 15.71$), 7.78 (1H, d, $J = 15.71$), 7.62 (1H, dd, $J = 1.79, 8.02$), 7.51 (1H, d, $J = 2.60$), 7.31 (1H, d, $J = 1.79$), 7.09 (1H, d, $J = 7.96$), 7.06 (2H, m), 7.02 (1H, td, $J = 1.39, 7.84$), 6.93 (1H, dd, $J = 1.21, 7.64$), 6.78 (1H, td, $J = 1.21, 7.64$), 6.68 (dd, $J = 1.09, 7.96$), 3.86 (3H, s), 3.80 (3H, s). $^{13}\text{C-NMR}$ (200 MHz, $\text{d}^6\text{-DMSO}$) δ (ppm): 188.56, 153.74, 153.21, 142.63, 141.63, 138.59, 137.48, 128.49, 126.76, 126.60, 123.98, 123.96, 123.03, 122.59, 122.34, 118.61, 115.70, 115.08, 113.54, 113.39, 113.12, 56.64, 56.19. IR ν_{max} 3332.24 (NH), 1646.26 (CO) cm^{-1} .



(E)-tert-butyl-2-(3-(4-(dimethylamino)phenyl)acryloyl)-7-methoxy-10H-phenothiazine-10-carboxylate (4.32).

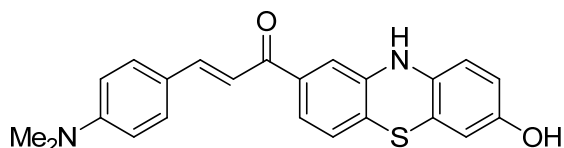
To a solution of **4.18** (1.0 eq.) and 4-dimethylaminobenzaldehyde (1.0 eq.) in absolute ethanol (1.3 M) was added a solution of sodium hydroxide (1.3 eq.) in ethanol (1.3 M). The resulting mixture was stirred at room temperature for 24 hours, water was added and the aqueous layer was extracted with ethyl acetate (3X). The combined organic layers were washed with brine, dried over magnesium sulfate, and concentrated. The crude product was purified by flash chromatography giving the desired phenothiazine **4.32** in 27% yield. $^1\text{H-NMR}$ (400 MHz, CDCl_3) δ (ppm): 8.14 (1H, s), 7.81 (2H, m), 7.55 (2H, 8.25), 7.43 (2H, m), 7.31 (1H, $J = 15.40$), 6.84 (2H, m), 6.68 (2H, d, $J = 8.26$), 3.78 (3H, s), 3.03 (6H, s), 1.50 (9H, s). $^1\text{H-NMR}$ (100 MHz, CDCl_3) δ (ppm): 188.94, 157.55, 152.44, 152.02, 146.09, 138.93, 137.54, 136.81, 132.08, 131.02, 130.44, 127.84, 127.03, 125.60, 122.46, 116.20, 113.18, 111.73, 111.62, 82.17, 55.56, 40.01, 28.11. IR ν_{max} 1709.67 (CO) cm^{-1} .



(E)-3-(4-(dimethylamino)phenyl)-1-(7-methoxy-10H-phenothiazin-2-yl)prop-2-en-1-one (4.33).

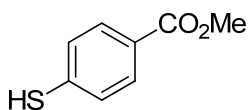
A 1.0 M solution of boron tribromide in dichloromethane (6.0 eq.) was added to a solution of **4.32** (1.0 eq.) in dichloromethane (0.2 M) under N₂ atmosphere at -78 °C. The reaction was allowed to stir at that temperature for 3 hours before quenching with saturated sodium bicarbonate and methanol. The aqueous layer was extracted with ethyl acetate (3X) and the combined organic layers were washed with saturated sodium bicarbonate (4X) and brine (1X), dried over magnesium sulfate, and concentrated. The pure product was obtained after flash chromatography using 50% ethyl acetate 50% hexanes in 53% yield. ¹H-NMR (800 MHz, d⁶-DMSO) δ (ppm): 8.57 (1H, s), 7.68 (2H, d, J = 8.85), 7.66 (1H, d, J = 15.33), 7.53 (1H, dd, J = 1.69, 8.01), 7.49 (1H, d, J = 15.33), 7.28 (1H, d, J = 1.69), 7.06 (1H, d, J = 8.01), 6.75 (2H, d, J = 8.85), 6.62 (3H, m), 3.67 (3H, s), 3.02 (6H, s). ¹³C-NMR (200 MHz, d⁶-DMSO) δ (ppm): 188.01, 155.27, 152.47, 145.43, 143.21, 138.20, 135.18, 134.92, 131.16, 126.50, 122.42, 122.10, 116.95, 116.30, 115.70, 113.95, 113.19, 112.24, 112.15, 55.90. IR ν_{max} 3331.26 (NH), 1726.18 (CO) cm⁻¹.

1.



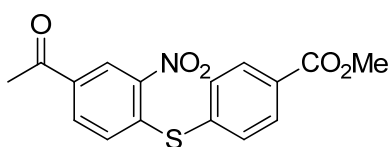
(E)-3-(4-(dimethylamino)phenyl)-1-(7-hydroxy-10H-phenothiazin-2-yl)prop-2-en-1-one (4.34).

A 1.0 M solution of boron tribromide in dichloromethane (6.0 eq.) was added to a solution of **4.32** (1.0 eq.) in dichloromethane (0.2 M) under N₂ atmosphere at -78 °C. The reaction was allowed to stir at that temperature for 6 hours before quenching with saturated sodium bicarbonate and methanol. The aqueous layer was extracted with ethyl acetate (3X) and the combined organic layers were washed with saturated sodium bicarbonate (4X) and brine (1X), dried over magnesium sulfate, and concentrated. The pure product was obtained after flash chromatography using 50% ethyl acetate 50% hexanes in 71% yield. ¹H-NMR (800 MHz, d⁶-DMSO) δ (ppm): 9.07 (1H (NH), s), 8.46 (1H (OH), s), 7.66 (3H, m), 7.49 (2H, m), 7.28 (1H, s), 7.04 (1H, d, J = 7.88), 6.74 (2H, d, J = 8.62), 6.54 (1H, d, J = 8.46), 6.47 (1H, dd, J = 2.19, 8.46), 6.40 (1H, d, J = 1.99), 3.01 (6H, s). ¹³C-NMR (200 MHz, d⁶-DMSO) δ (ppm): 188.05, 153.17, 152.45, 145.37, 143.51, 138.13, 133.75, 131.13, 126.45, 122.52, 122.46, 121.82, 116.63, 116.33, 115.85, 114.94, 113.29, 113.10, 112.23, 40.17.



methyl 4-mercaptobenzoate (4.35).

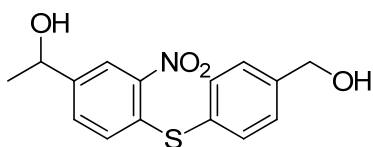
4-mercaptobenzoic acid (1.0 M) was dissolved in anhydrous methanol (0.2 M) and a catalytic amount of sulfuric acid was added. The reaction mixture was then refluxed for 6 hours. After cooling to room temperature, the methanol was evaporated and the residue was taken up in water and ethyl acetate. The aqueous layer was extracted with ethyl acetate (3X) and the combined organic layers were washed with brine, dried over magnesium sulfate, and concentrated to yield the product in quantitative yield and sufficient purity for subsequent reactions. $^1\text{H-NMR}$ (300 MHz, CDCl_3) δ (ppm): 7.88 (2H, d, $J = 8.22$), 7.27 (2H, d, $J = 8.22$), 3.89 (3H, s). $^{13}\text{C-NMR}$ (75 MHz, CDCl_3) δ (ppm): 166.34, 138.14, 130.02, 127.91, 126.91, 52.03.



methyl 4-((4-acetyl-2-nitrophenyl)thio)benzoate (4.36).

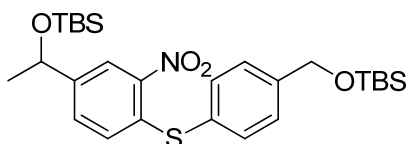
A solution of thiophenol (1.05 eq.), **4.4** (1.0 eq.), and sodium hydroxide (1.0 eq.) was heated in DMF (0.4 M) at 60 °C for 12 hours. The reaction was cooled to room temperature, and poured into saturated aqueous lithium chloride. The aqueous layer was then extracted with ethyl acetate (3X). The combined organic layers were washed with saturated aqueous lithium chloride (5X), dried over magnesium sulfate, and concentrated. The crude residue was purified by flash chromatography using 10% ethyl acetate 90%

hexanes, to give the product in 56% yield. $^1\text{H-NMR}$ (400 MHz, CDCl_3) δ (ppm): 8.74 (1H, d, $J = 1.54$), 8.13 (2H, d, $J = 8.11$), 7.87 (1H, dd, $J = 1.54, 8.55$), 7.64 (2H, d, $J = 8.11$), 6.93 (1H, d, $J = 8.55$), 3.94 (3H, s), 2.59 (3H, s). $^{13}\text{C-NMR}$ (100 MHz, CDCl_3) δ (ppm): 194.83, 165.95, 144.75, 143.79, 135.74, 135.33, 134.12, 131.97, 131.12, 128.56, 125.73, 52.41, 26.36. IR ν_{max} 1714.47 (CO) cm^{-1} .



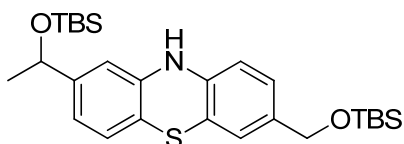
1-(4-((4-(hydroxymethyl)phenyl)thio)-3-nitrophenyl)ethanol (4.37).

To a solution of **4.36** (1.0 eq.) in THF (0.2 M) at room temperature under N_2 atmosphere was added a 10.0 M solution of borane dimethylsulfide complex in THF (3.6 eq.) dropwise. The mixture was heated to reflux for three hours before it was cooled to room temperature and the solvent was evaporated. The residue was taken up in water and extracted with ethyl acetate (3X). The combined organic layers were washed with brine, dried over magnesium sulfate, and concentrated. The crude residue was purified by flash chromatography using 50% ethyl acetate 50% hexanes. $^1\text{H-NMR}$ (400 MHz, CDCl_3) δ (ppm): 8.23 (1H, d, $J = 1.63$), 7.56 (2H, d, $J = 8.09$), 7.47 (2H, d, $J = 8.09$), 7.35 (1H, dd, $J = 1.69, 8.48$), 6.84 (1H, d, $J = 8.48$), 4.92 (1H, q, $J = 6.43$), 4.79 (2H, s), 1.48 (3H, d, $J = 6.43$).



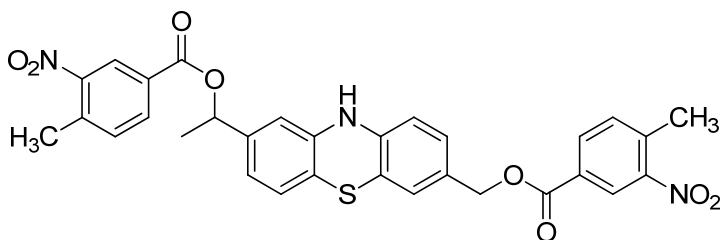
tert-butyl((4-((4-(1-((tert-butyl)dimethylsilyl)oxy)ethyl)-2-nitrophenyl)thio)benzyl)oxydimethylsilane (4.38).

To a solution of **4.37** (1.0 eq.) in DMF (0.2 M) was added TBSCl (4.0 eq.), imidazole (8.0 eq.), and DMAP (1.0 eq.). The reaction mixture was allowed to stir at room temperature for 14 hours. The reaction mixture was then poured into saturated lithium chloride (aq.) and the organic layer was extracted with ethyl acetate (3X). The combined organic layers were then washed with saturated lithium chloride (aq., 5X), dried over magnesium sulfate, and concentrated. The crude residue was purified by flash chromatography using 5% ethyl acetate 95% hexanes to give the pure product in 85% yield. $^1\text{H-NMR}$ (300 MHz, CDCl_3) δ (ppm): 8.20 (1H, d, $J = 1.64$), 7.55 (2H, d, $J = 8.16$), 7.44 (2H, d, $J = 8.16$), 7.31 (1H, dd, $J = 1.64, 8.49$), 6.81 (1H, d, $J = 8.49$), 4.87 (1H, q, $J = 6.35$), 4.82 (2H, s), 1.39 (3H, d, $J = 6.35$), 0.97 (9H, s), 0.90 (9H, s), 0.15 (6H, s), 0.07 (3H, s), -0.01 (3H, s). $^{13}\text{C-NMR}$ (75 MHz, CDCl_3) δ (ppm): 144.45, 143.49, 137.46, 135.64, 130.21, 129.01, 127.99, 127.31, 122.14, 69.31, 64.36, 26.89, 25.96, 25.80, 18.44, 18.17, -4.72, -4.80, -5.19.



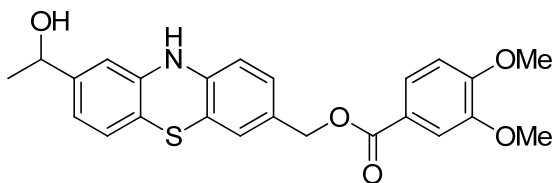
2-(1-((tert-butyldimethylsilyl)oxy)ethyl)-7-(((tert-butyldimethylsilyl)oxy)methyl)-10H-phenothiazine (4.39).

To a solution of **4.38** (1.0 eq.) in mesitylene (0.5 M) under N₂ atmosphere at ambient temperature was added triethylphosphite (6.0 eq.) slowly. The reaction mixture was then refluxed for 5 hours. After cooling to ambient temperature, the reaction mixture was diluted with toluene and concentrated as much as possible. Under no circumstance was the phenothiazine product dissolved in a chlorinated solvent. The crude residue was purified directly by flash chromatography using 10% ethyl acetate 90% hexanes and the pure product was isolated as an orangish brown flaky solid in 54% yield. ¹H-NMR (800 MHz, d⁶-DMSO) δ (ppm): 8.57 (1H, s), 6.92 (1H, dd, J = 1.86, 8.09), 6.85 (1H, d, J = 8.45), 6.84 (1H, d, J = 1.86), 6.71 (2H, m), 6.66 (1H, d, J = 8.08), 4.75 (1H, q, J = 6.33), 4.52 (2H, s), 6.33 (3H, d, J = 6.33), 0.89 (9H, s), 0.88 (9H, s), 0.06 (6H, s), 0.06 (3H, s), -0.01 (3H, s).



(8-(1-((4-methyl-3-nitrobenzoyl)oxy)ethyl)-10H-phenothiazin-3-yl)methyl-4-methyl-3-nitrobenzoate (4.40).

To a stirred solution of 4-methyl-3-nitrobenzoic acid (8.0 eq.), DIEA (8.0 eq.), and DMAP (2.0 eq.) in DMF (0.4 M) was added EDC (3.0 eq.) at 0 °C. After 30 minutes, **4.39** (1.0 eq.) was added. The reaction mixture was allowed to stir for 24 hours. The reaction mixture was then poured into saturated lithium chloride (aq.) and the organic layer was extracted with ethyl acetate (3X). The combined organic layers were then washed with saturated lithium chloride (aq., 5X), dried over magnesium sulfate, and concentrated. The crude residue was purified by flash chromatography using 15% ethyl acetate 85% hexanes to give the pure product in 34%. ¹H-NMR (800 MHz, d⁶-DMSO) δ (ppm): 8.75 (1H, s), 8.47 (1H, d, J = 1.71), 8.43 (1H, d, J = 1.71), 8.18 (1H, dd, J = 1.75, 7.95), 8.14 (1H, dd, J = 1.75, 7.98), 7.70 (1H, d, J = 8.07), 7.66 (1H, d, J = 8.03), 7.12 (1H, dd, J = 1.86, 8.18), 7.06 (1H, d, J = 1.75), 6.93 (1H, d, J = 7.94), 6.88 (1H, dd, J = 1.64, 8.02), 6.76 (1H, d, J = 1.64), 6.68 (1H, d, J = 8.18), 5.93 (1H, q, J = 6.54), 5.19 (2H, s), 2.61 (3H, s), 2.59 (3H, s), 1.59 (3H, d, J = 6.54). ¹³C-NMR (200 MHz, d⁶-DMSO) δ (ppm): 164.40, 163.71, 149.46, 149.39, 142.40, 142.29, 141.50, 138.85, 138.75, 134.13, 134.10, 133.75, 129.55, 129.37, 129.27, 128.92, 127.30, 126.83, 125.39, 125.35, 120.04, 116.77, 116.21, 114.79, 112.31, 73.40, 66.95, 22.33, 20.22. IR ν_{\max} 3360.12 (NH), 1717.81 (CO) cm⁻¹.



(8-(1-hydroxyethyl)-10H-phenothiazin-3-yl)methyl 3,4-dimethoxybenzoate (4.41).

To a stirred solution of 3,4-dimethoxybenzoic acid (8.0 eq.), DIEA (8.0 eq.), and DMAP (2.0 eq.) in DMF (0.4 M) was added EDC (3.0 eq.) at 0 °C. After 30 minutes, **4.39** (1.0 eq.) was added. The reaction mixture was allowed to stir for 24 hours. The reaction mixture was then poured into saturated lithium chloride (aq.) and the organic layer was extracted with ethyl acetate (3X). The combined organic layers were then washed with saturated lithium chloride (aq., 5X), dried over magnesium sulfate, and concentrated. The crude residue was purified by flash chromatography using 15% ethyl acetate 85% hexanes to give the pure product in 59%. ¹H-NMR (800 MHz, d⁶-DMSO) δ (ppm): 8.67 (1H, s), 7.60 (1H, dd, J = 2.01, 8.44), 7.44 (1H, d, J = 2.01), 7.09 (1H, dd, J = 1.89, 8.12), 7.07 (1H, d, J = 8.44), 7.02 (1H, d, J = 1.89), 6.85 (1H, d, J = 7.82), 6.74 (1H, d, J = 1.58), 6.72 (1H, dd, J = 1.58, 8.04), 6.69 (1H, d, J = 8.12), 5.13 (3H, s), 4.57 (1H, m), 3.84 (3H, s), 3.81 (3H, s), 1.27 (3H, d, J = 6.45). ¹³C-NMR (200 MHz, d⁶-DMSO) δ (ppm): 165.88, 153.50, 148.92, 147.80, 142.63, 142.04, 129.99, 128.54, 127.03, 126.25, 123.72, 122.27, 119.59, 117.02, 114.70, 114.19, 112.12, 112.06, 111.61, 68.01, 66.03, 56.19, 56.01, 26.21. IR ν_{\max} 3345.27 (NH), 1707.39 (CO) cm⁻¹.

Appendix B: NMR, ESI-MS, and IR Spectra

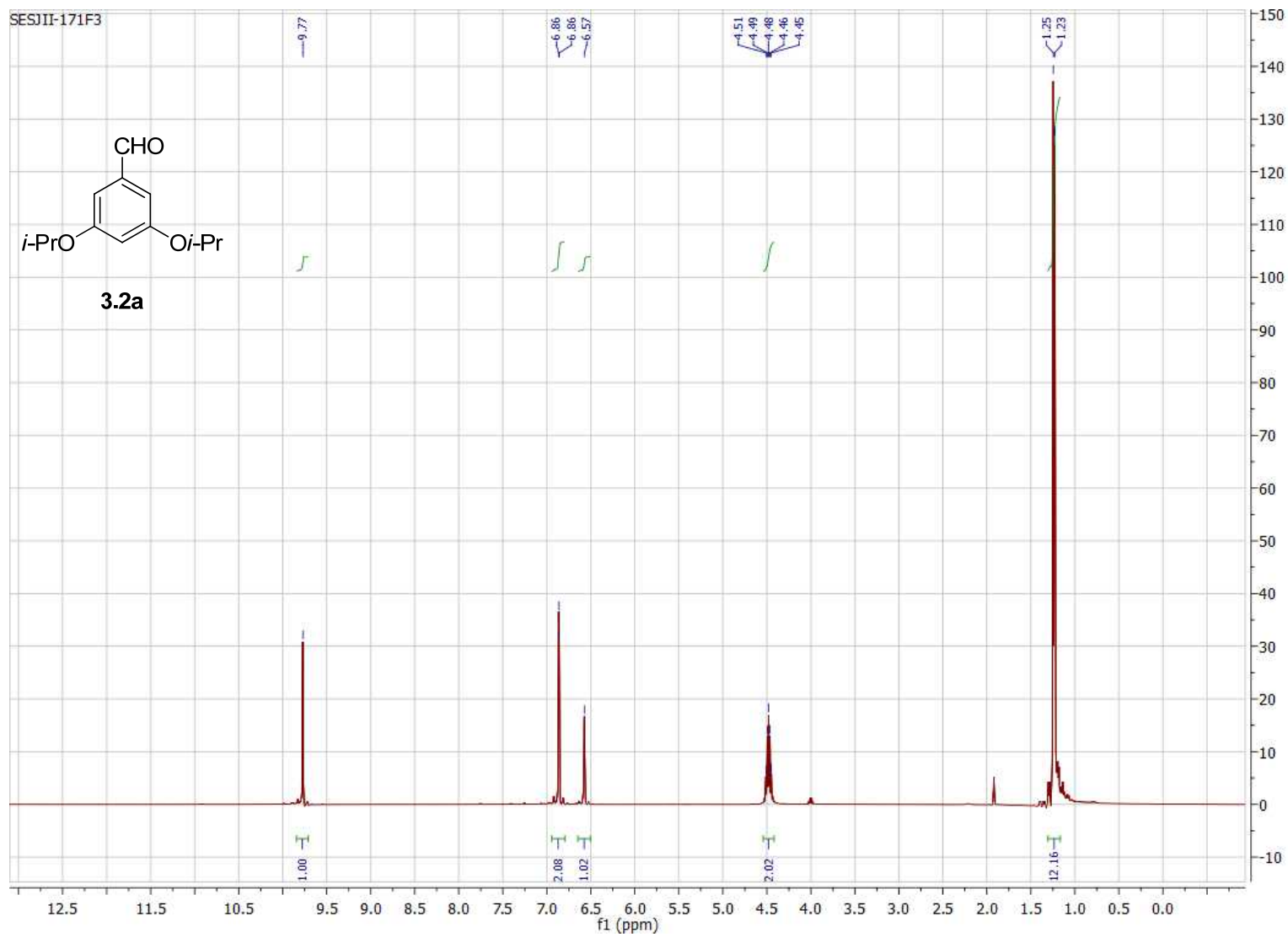


Figure B.1. 400 MHz ^1H NMR of compound **3.2a** in CDCl_3 .

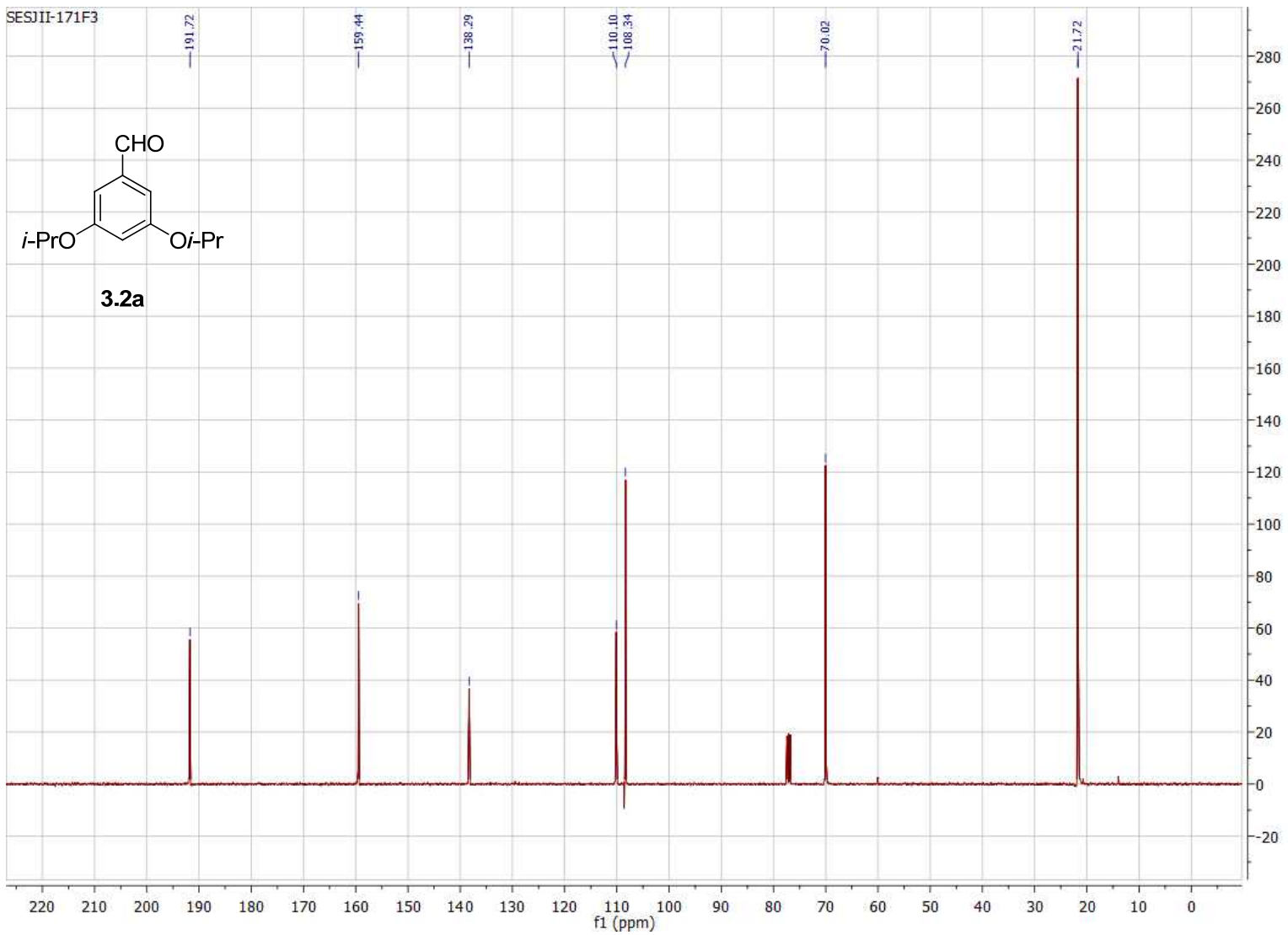


Figure B.2. 100 MHz ^{13}C NMR of compound **3.2a** in CDCl_3 .

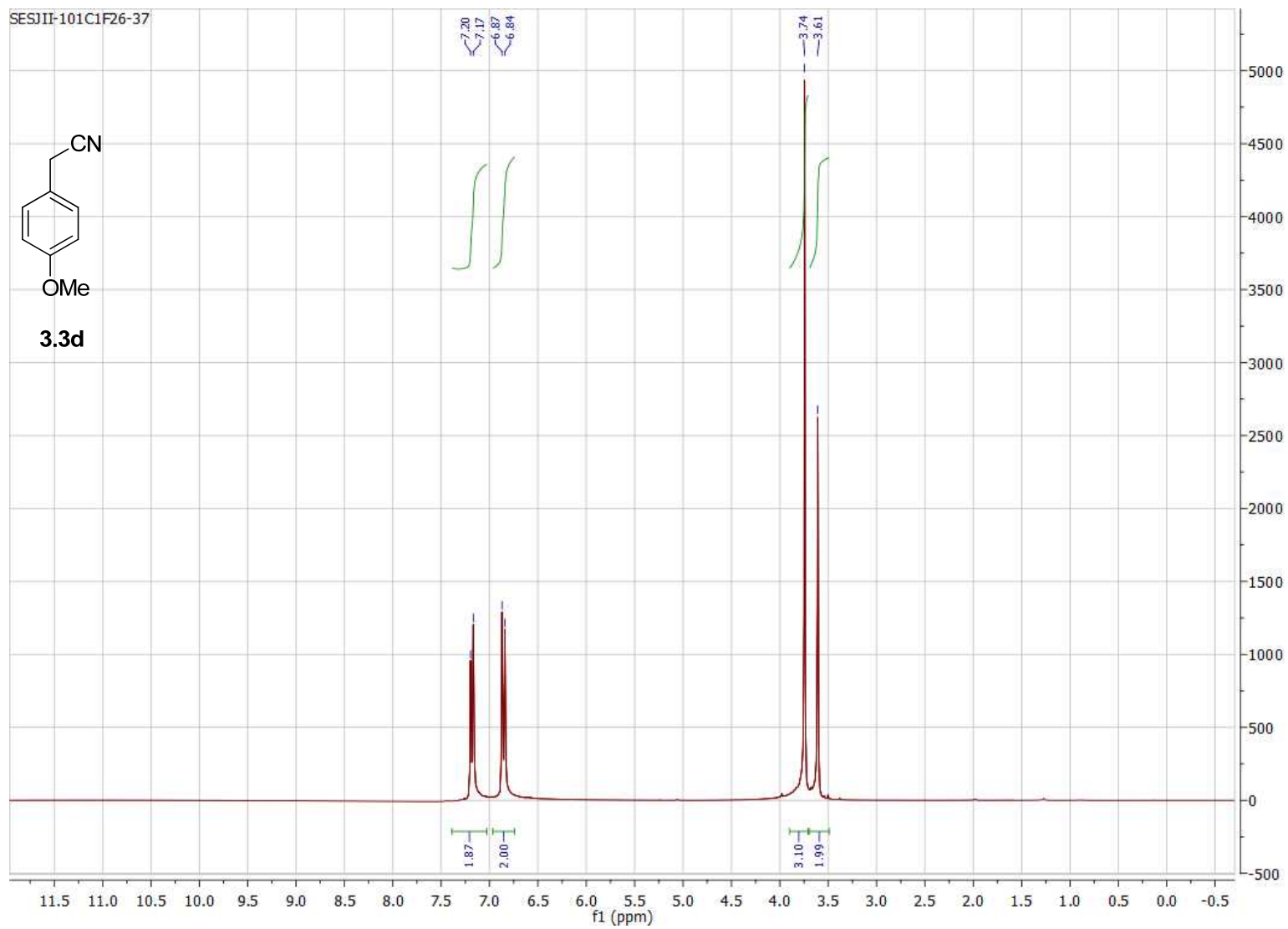


Figure B.3. 300 MHz ^1H NMR of compound **3.3d** in CDCl_3 .

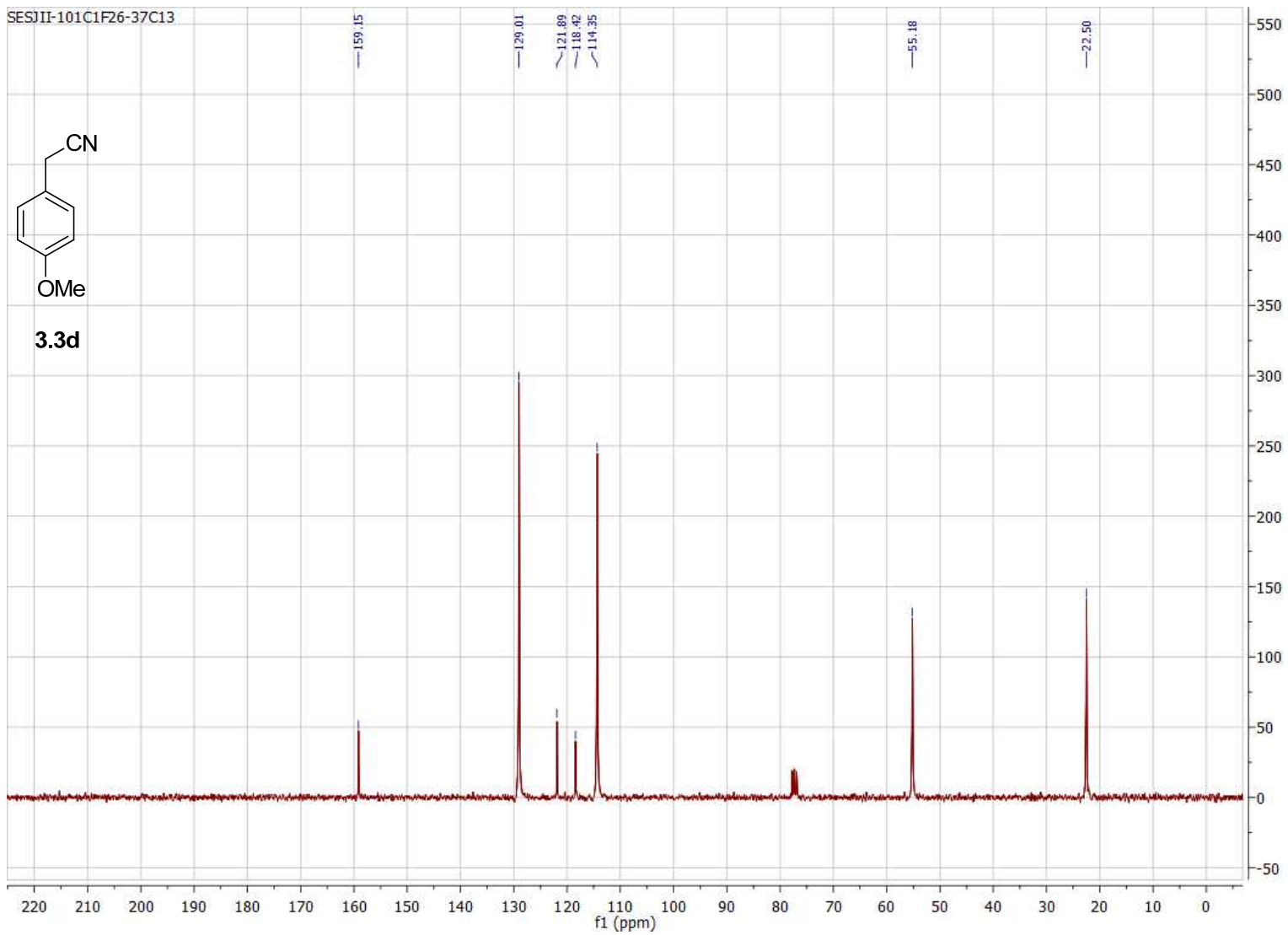


Figure B.4. 75 MHz ^{13}C NMR of compound **3.3d** in CDCl_3 .

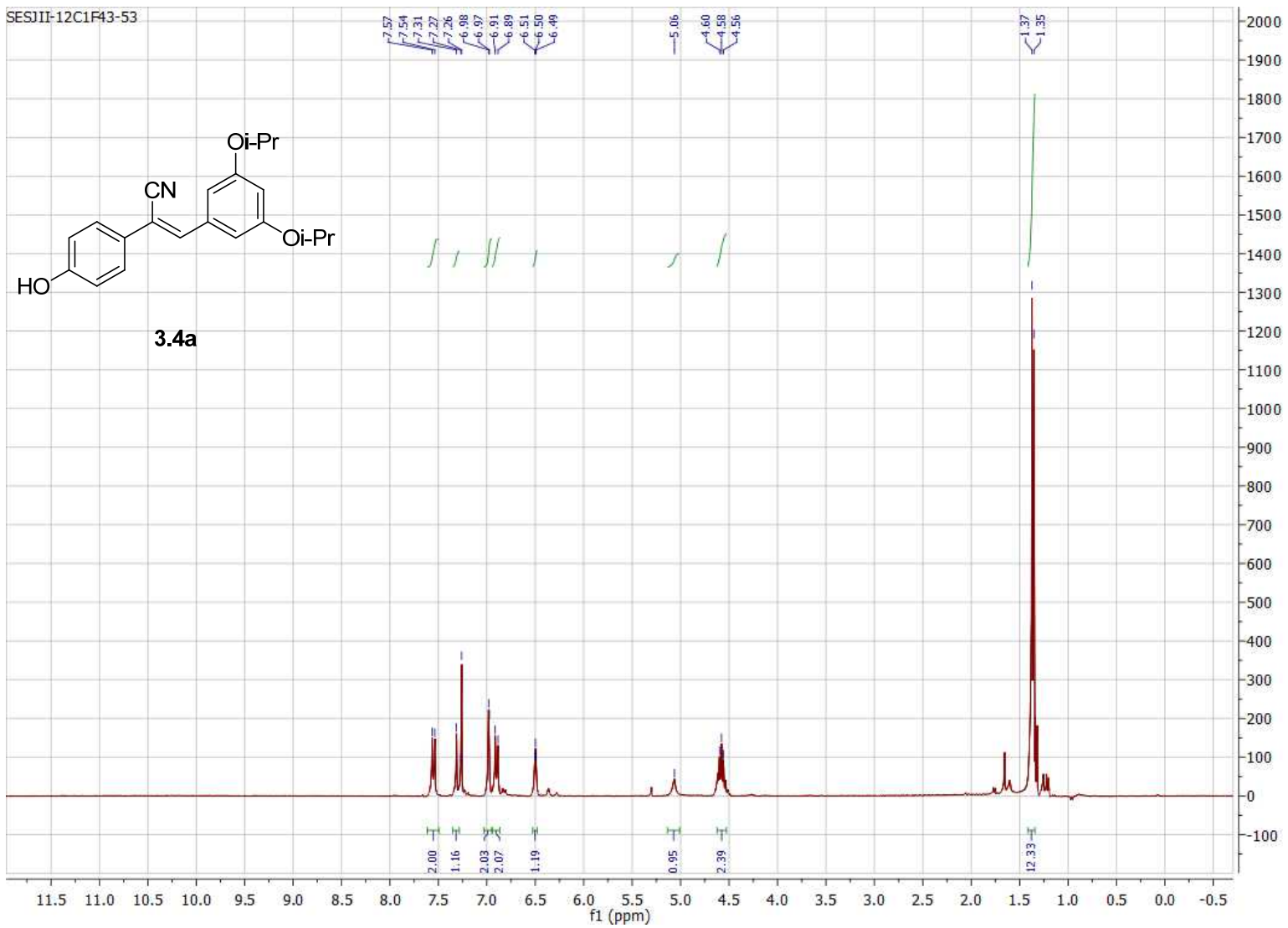


Figure B.5. 300 MHz ^1H NMR of compound **3.4a** in CDCl_3 .

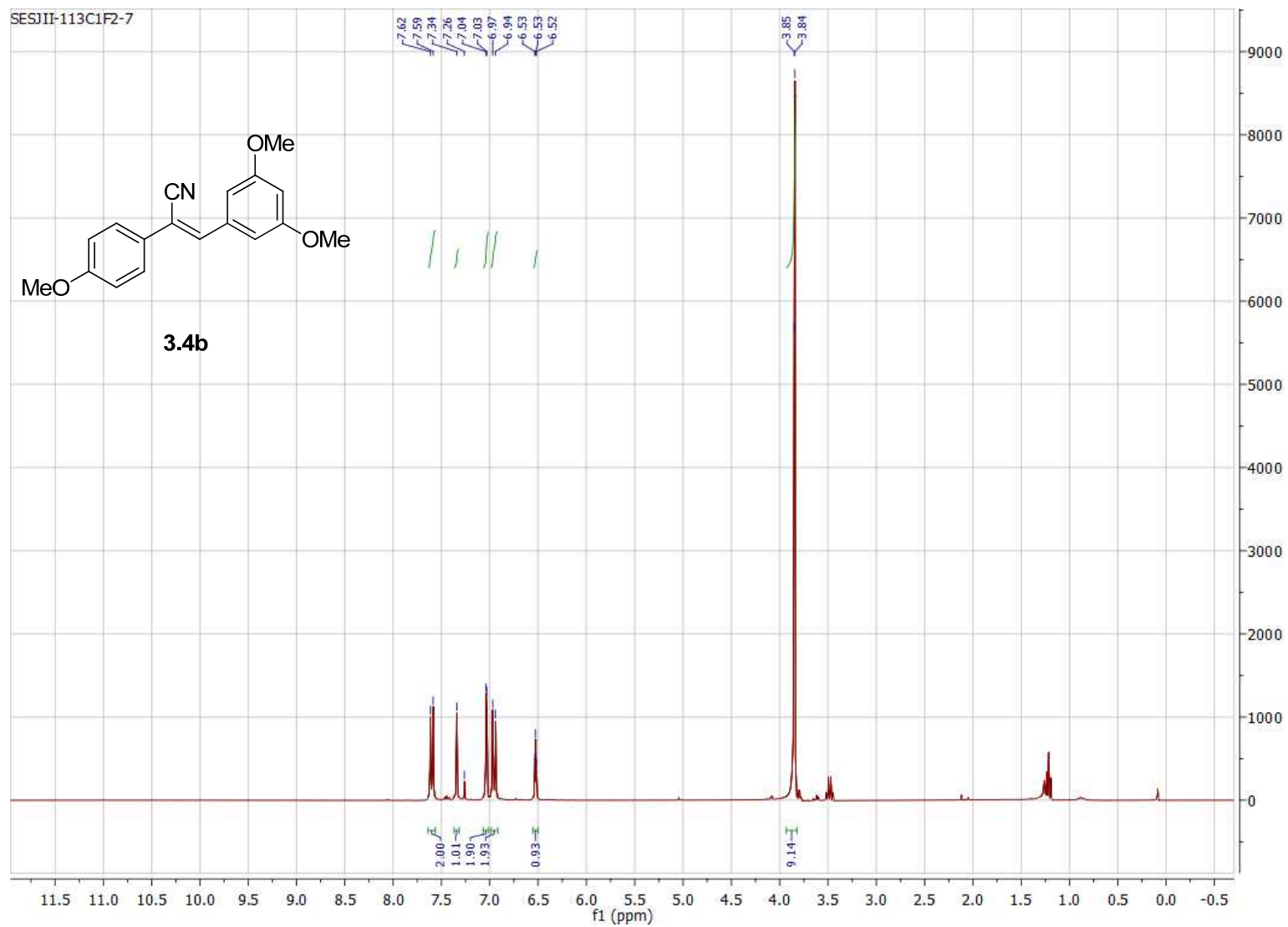


Figure B.6. 300 MHz ¹H NMR of compound **3.4b** in CDCl₃.

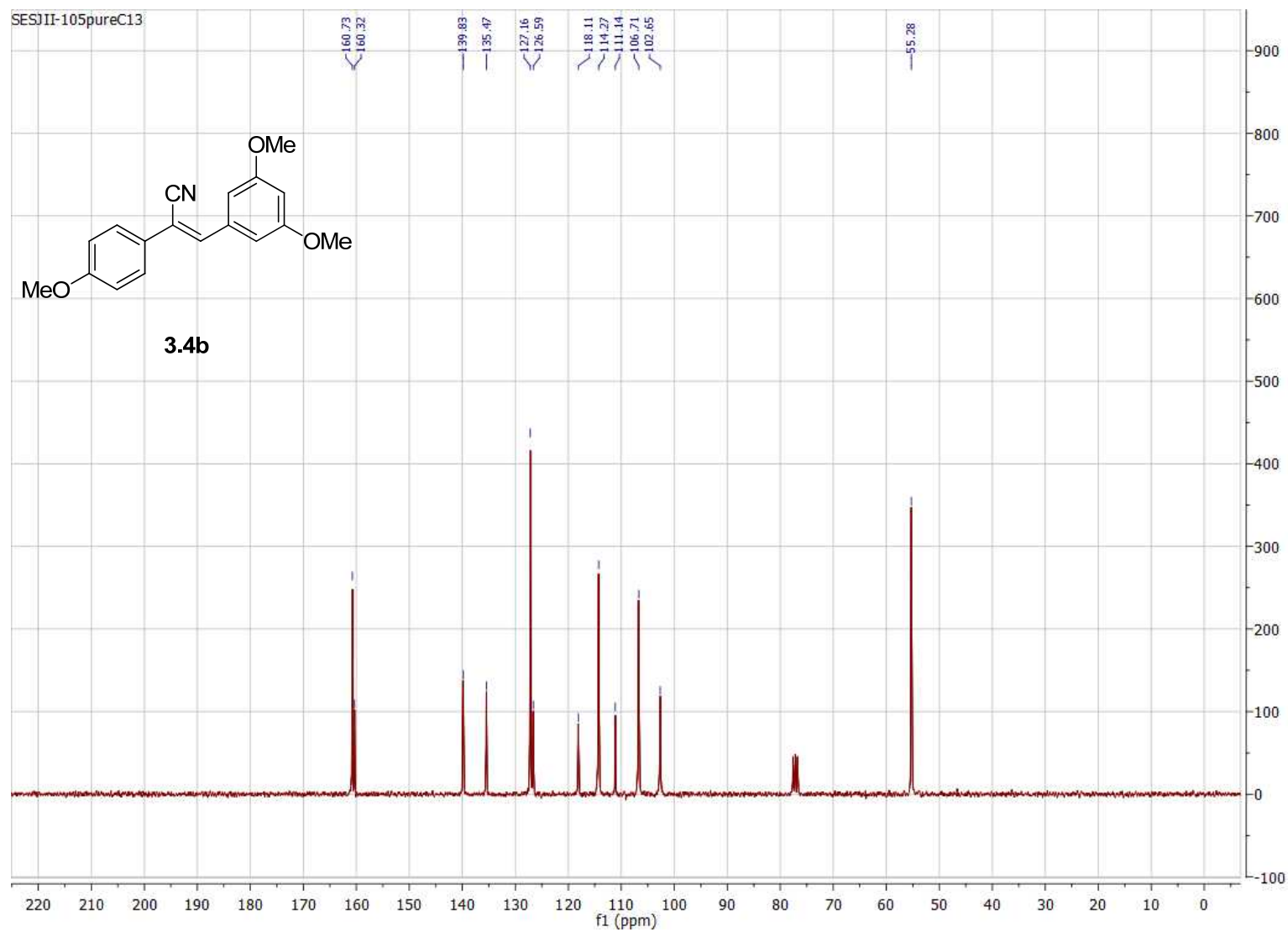


Figure B.7. 75 MHz ^{13}C NMR of compound **3.4b** in CDCl_3 .

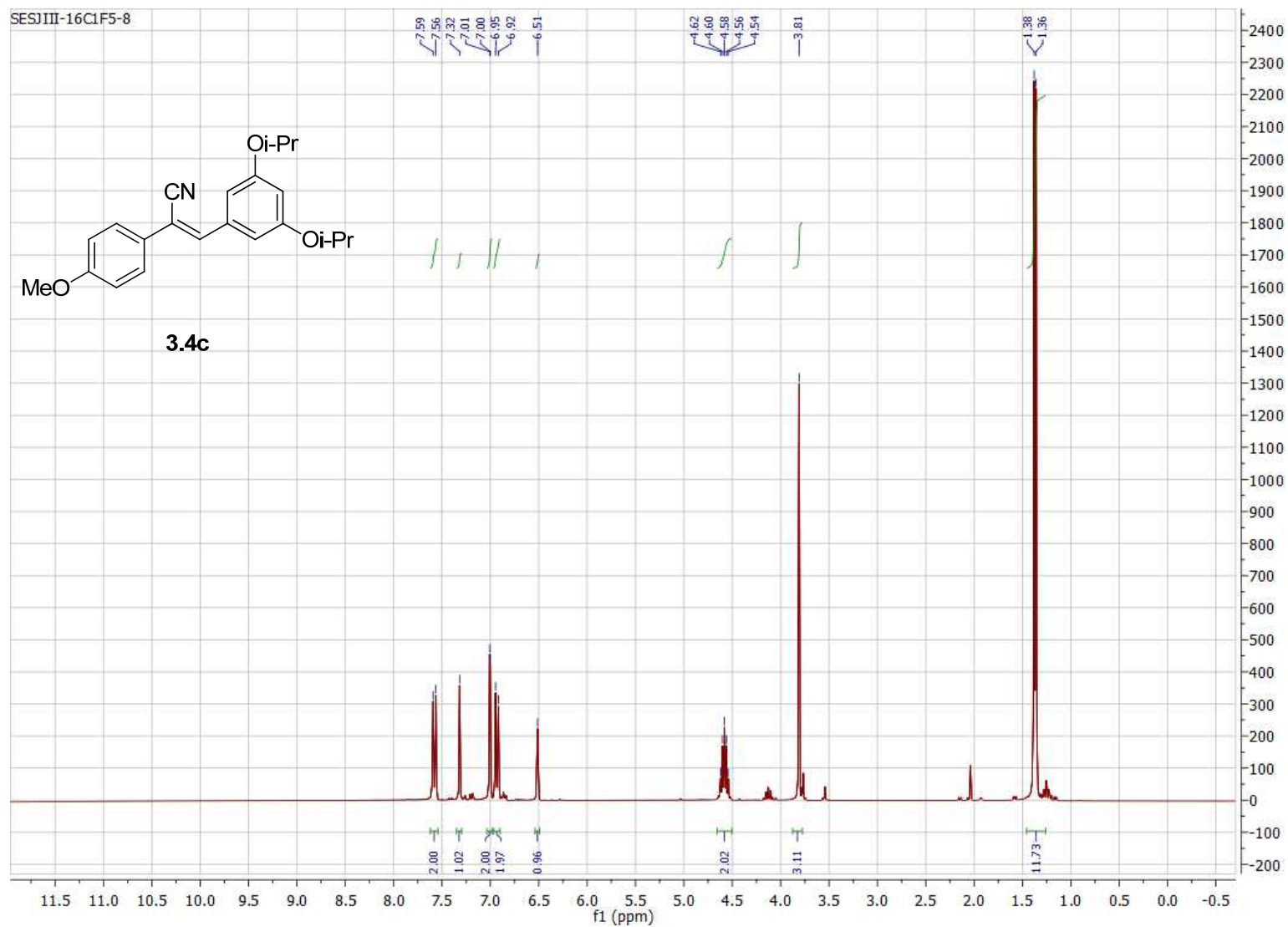


Figure B.8. 300 MHz ^1H NMR of compound **3.4c** in CDCl_3 .

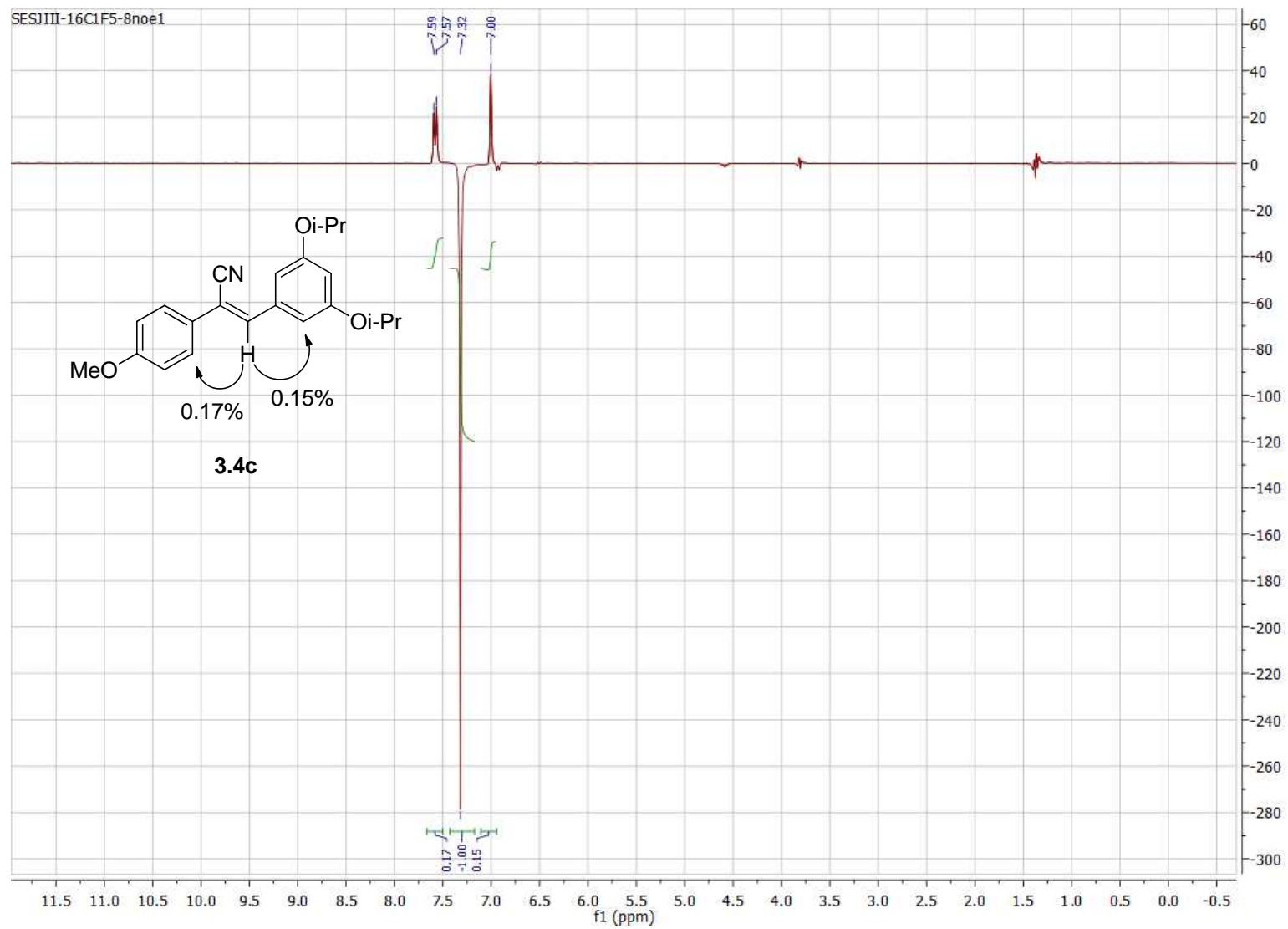


Figure B.9. 300 MHz nOe ^1H NMR of compound **3.4c** in CDCl_3 .

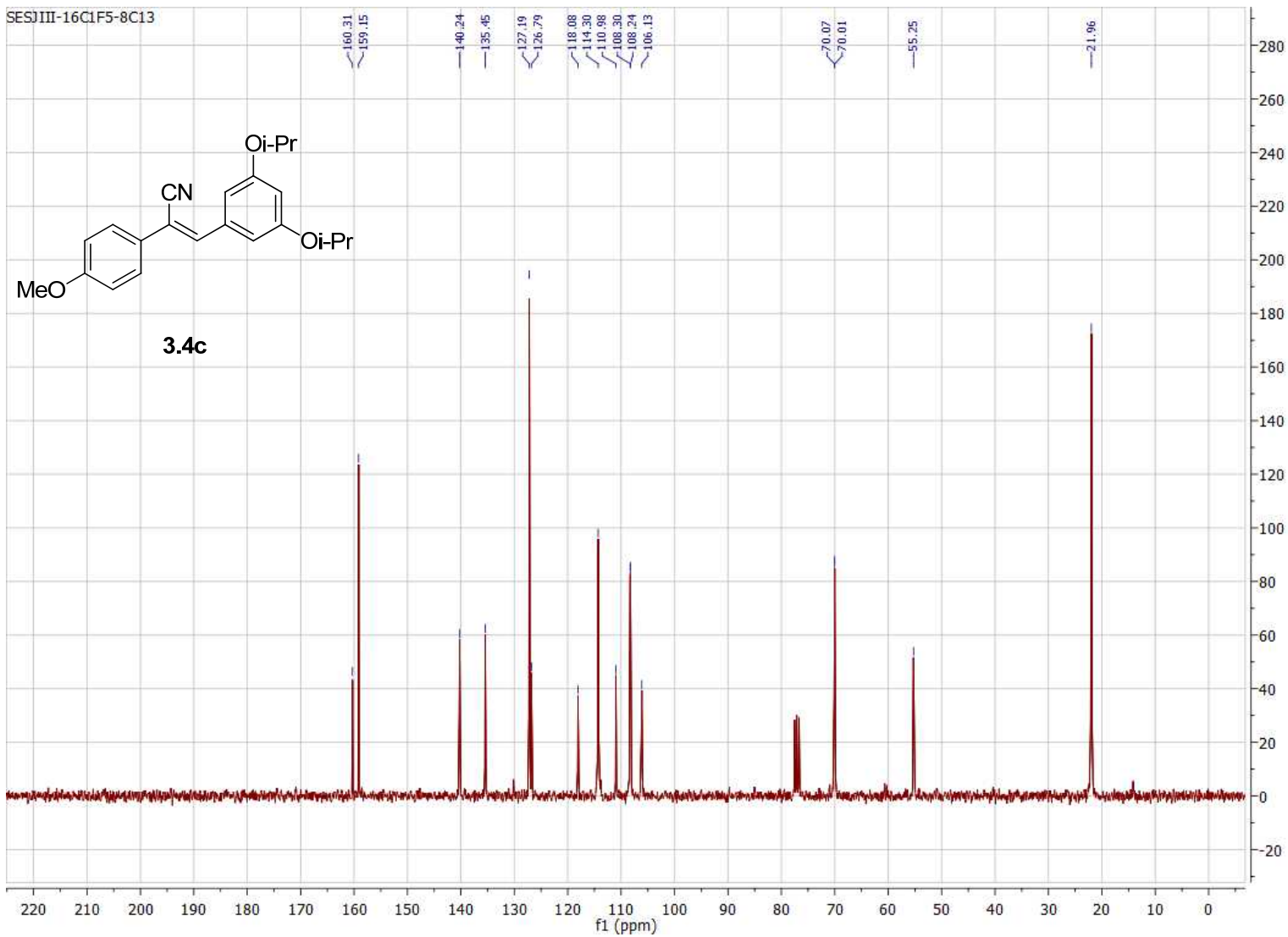


Figure B.10. 75 MHz ^{13}C NMR of compound **3.4c** in CDCl_3 .

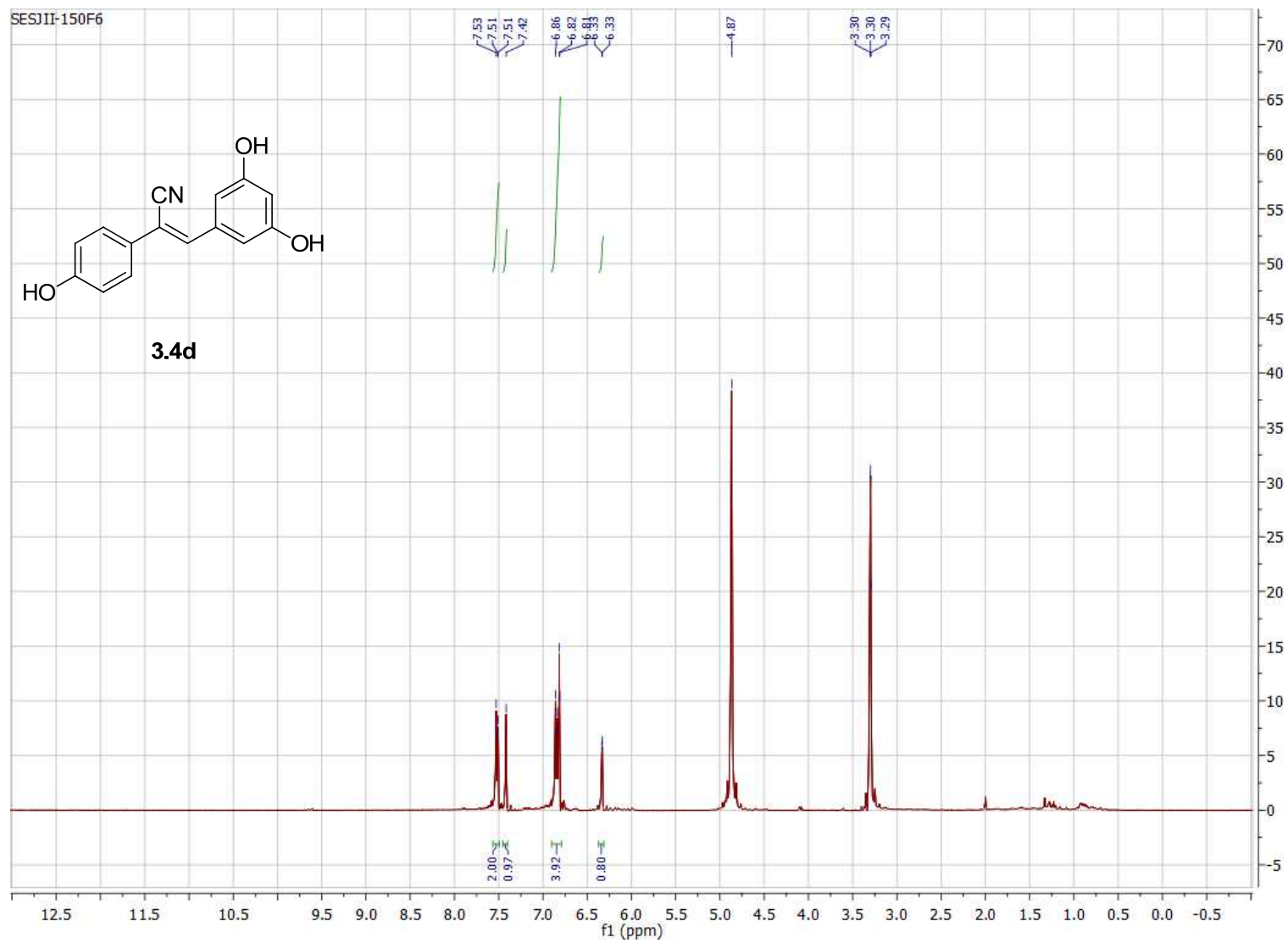


Figure B.11. 400 MHz ^1H NMR of compound **3.4d** in CD_3OD .

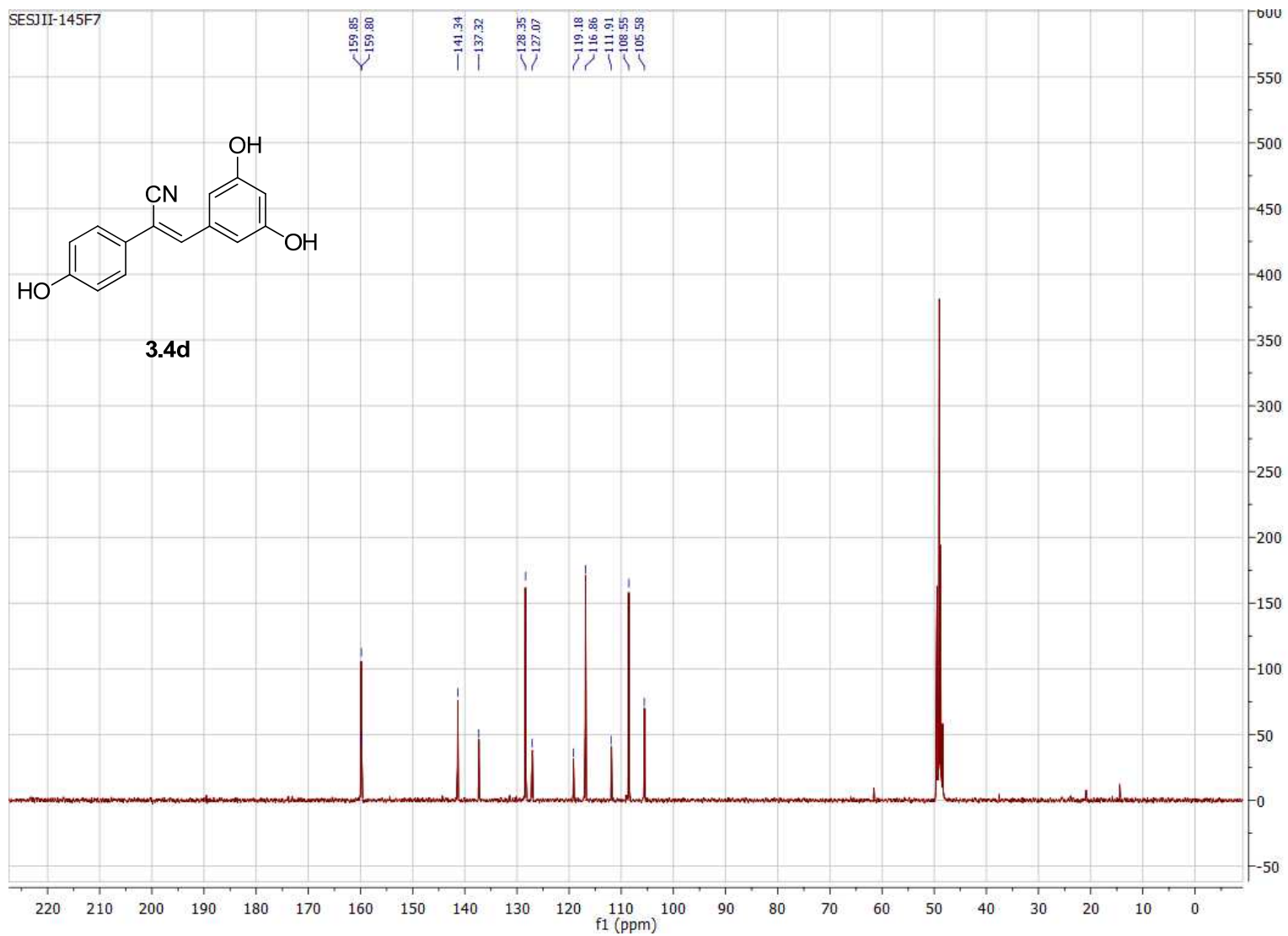


Figure B.12. 100 MHz ^{13}C NMR of compound **3.4d** in CD_3OD .

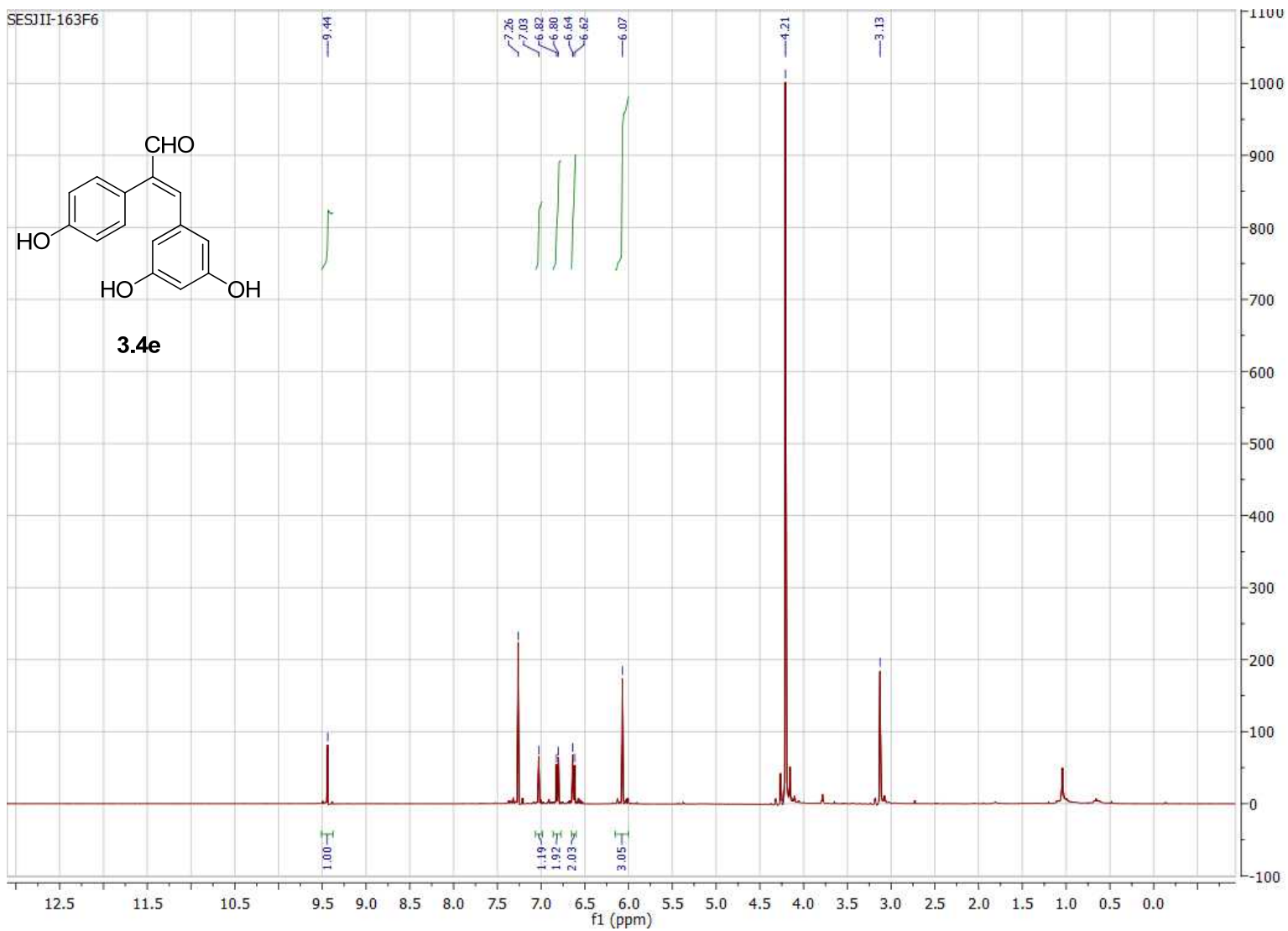


Figure B.13. 400 MHz ^1H NMR of compound **3.4e** in CD_3OD .

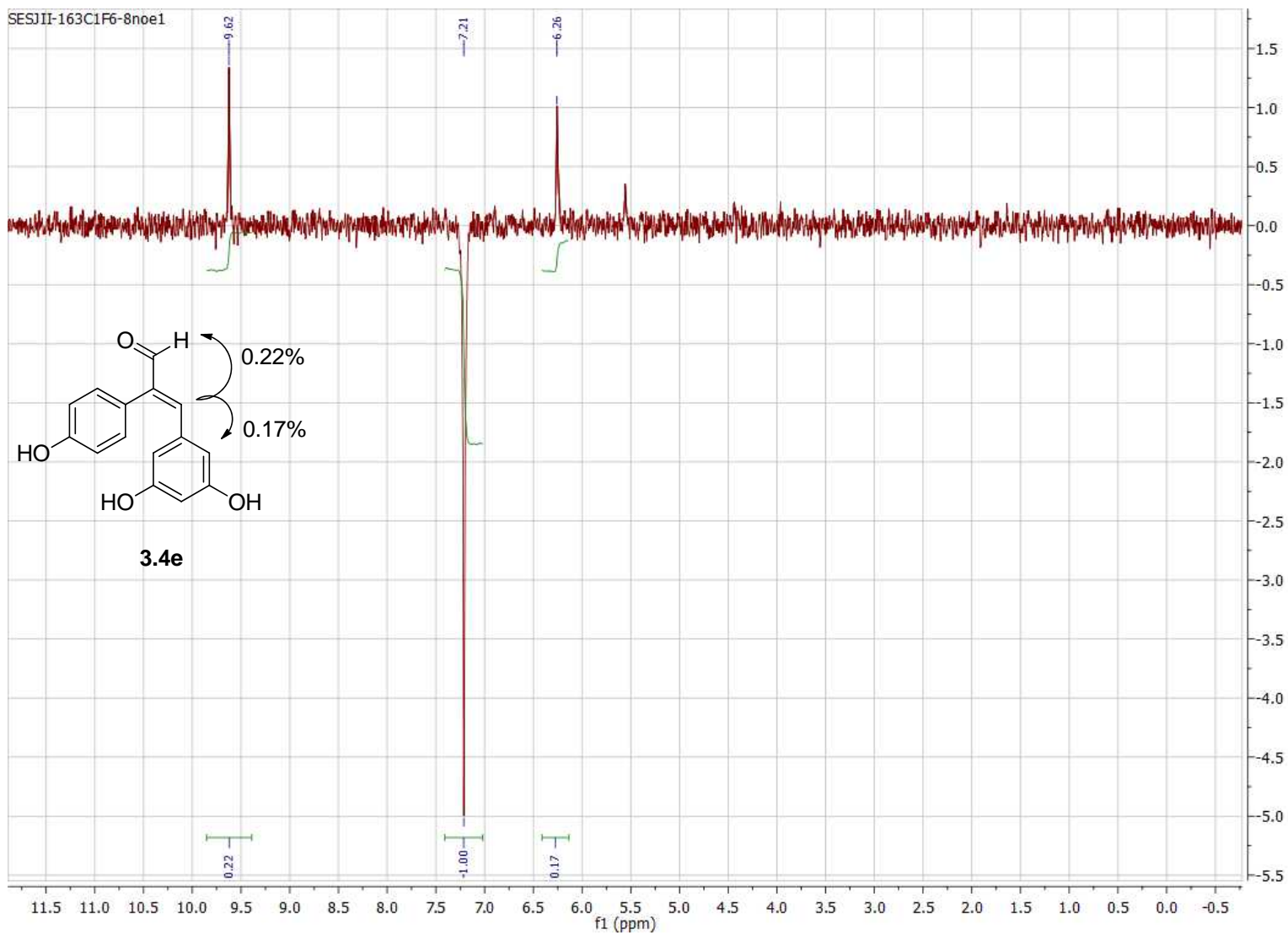


Figure B.14. 400 MHz nOe ^1H NMR of compound **3.4e** in CD_3OD .

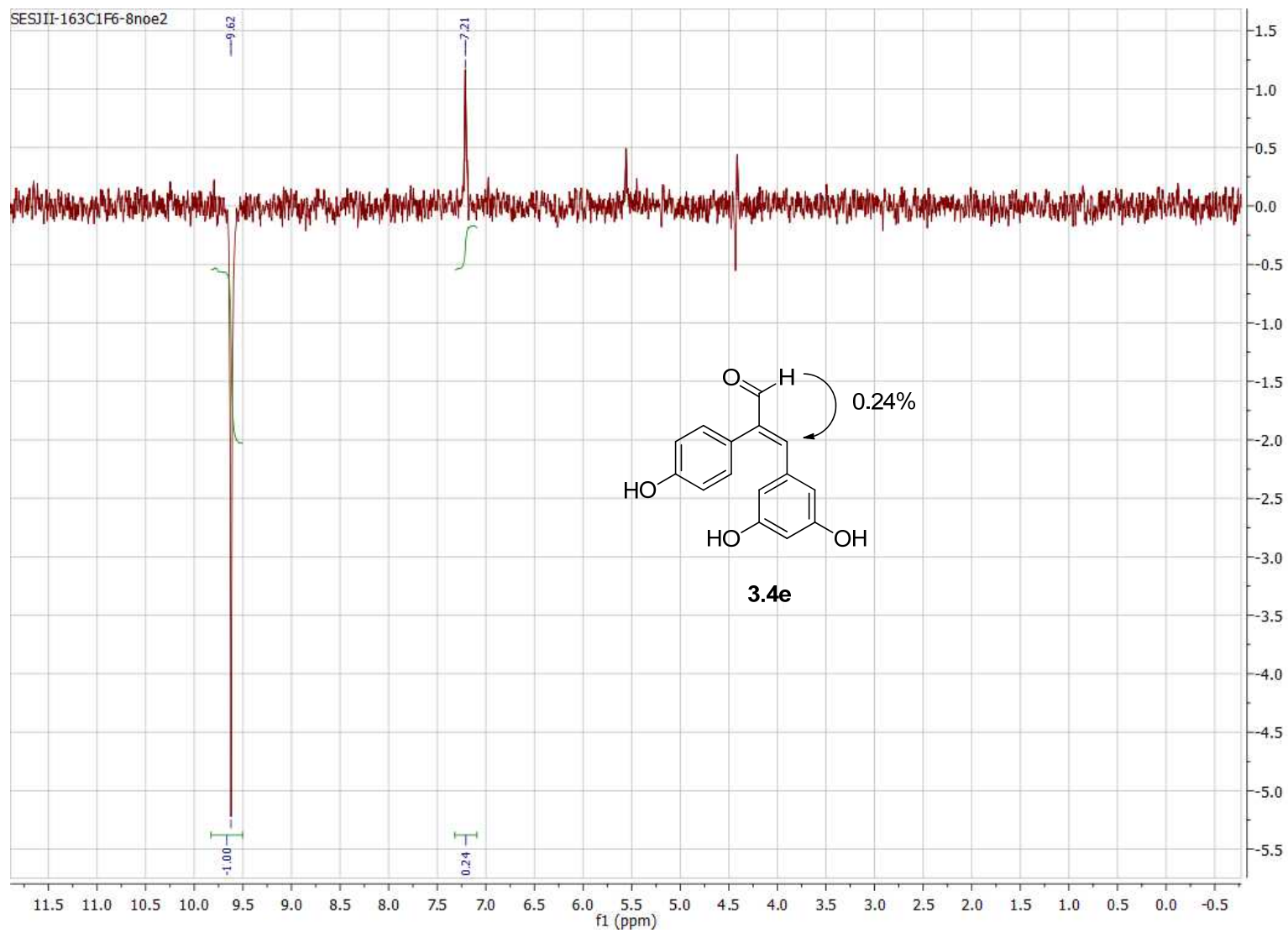


Figure B.15. 400 MHz nOe ^1H NMR of compound **3.4e** in CD_3OD .

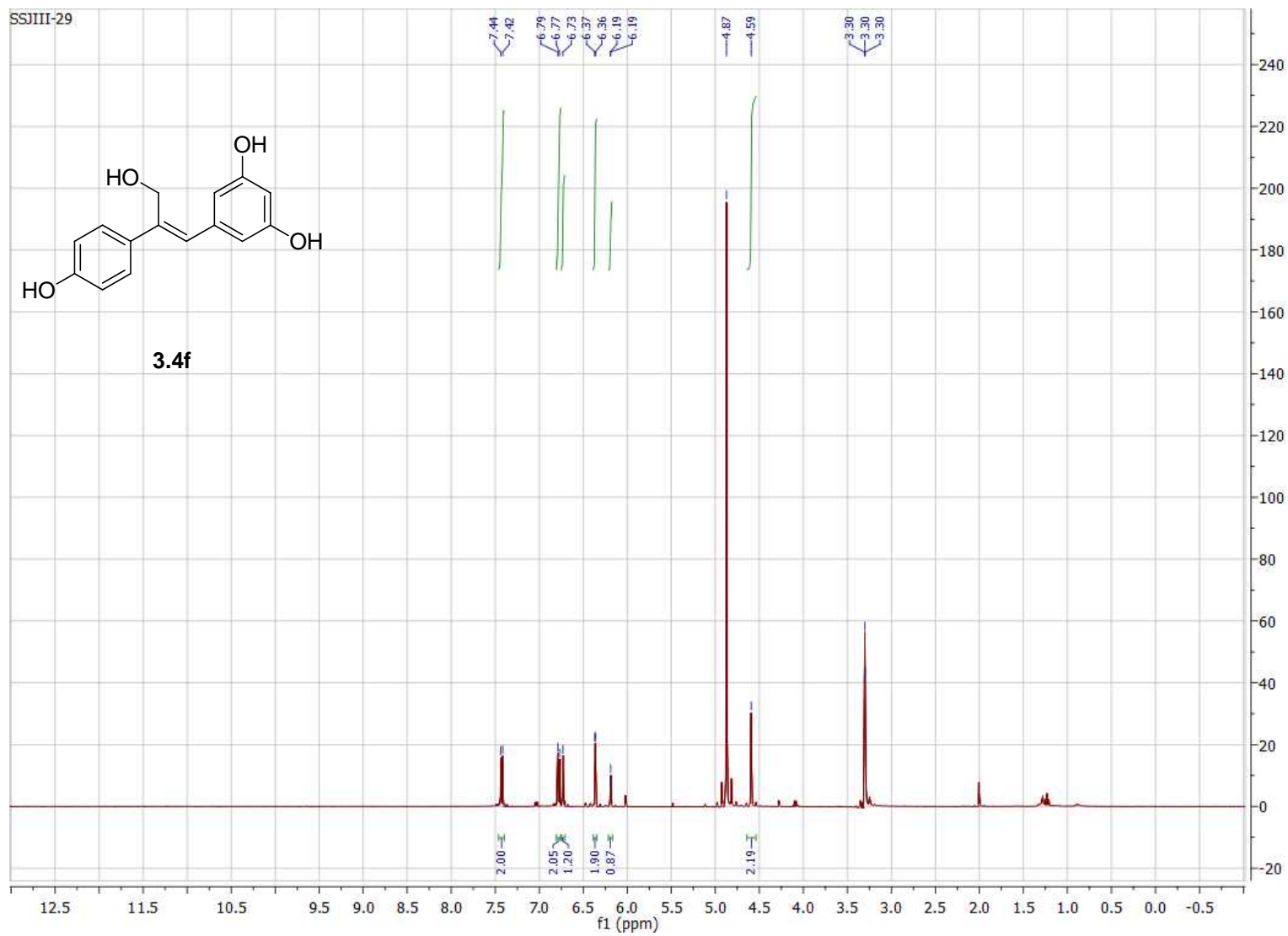


Figure B.16. 400 MHz ^1H NMR of compound **3.4f** in CD_3OD .

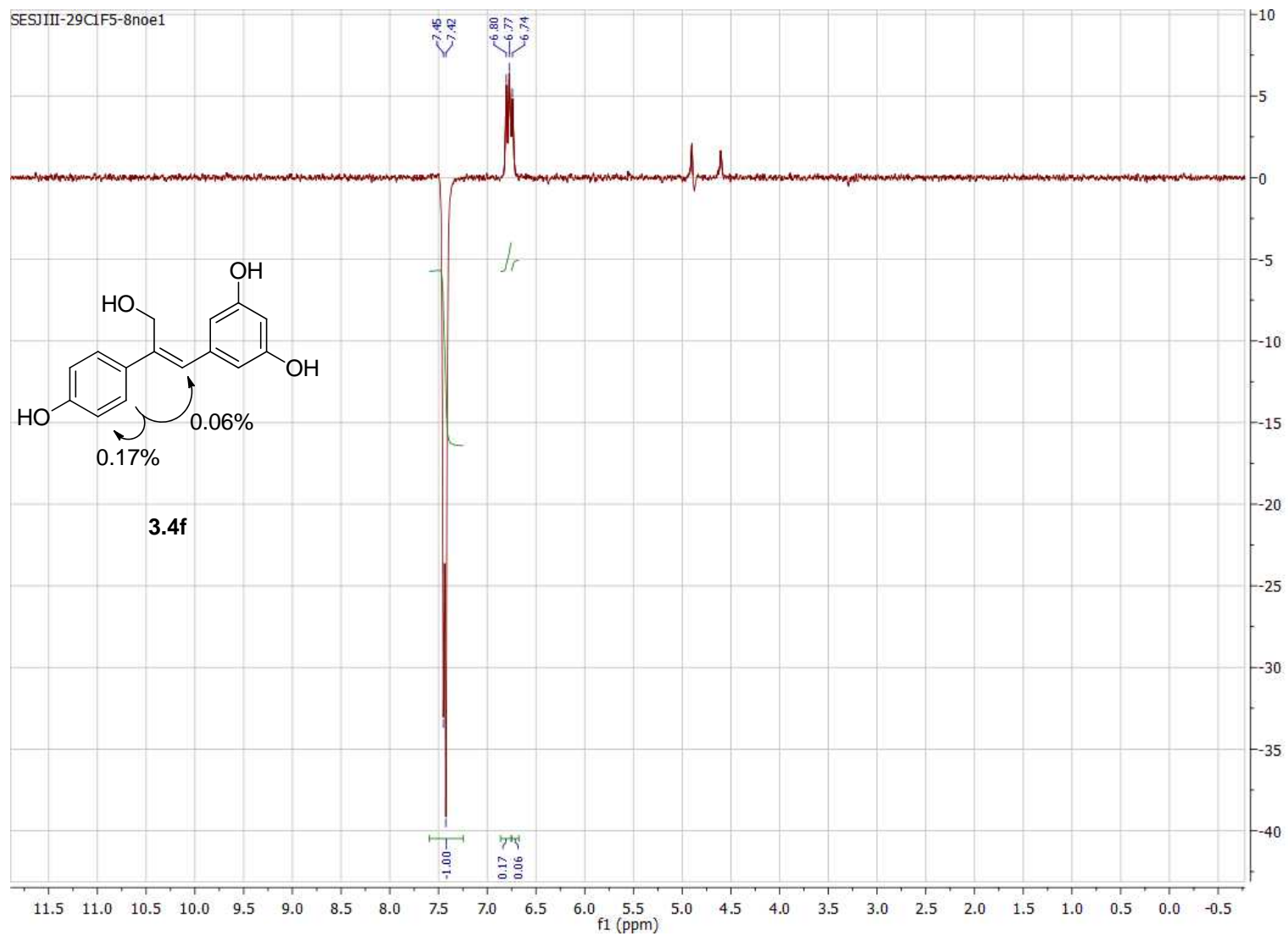


Figure B.17. 400 MHz nOe ^1H NMR of compound **3.4f** in CD_3OD .

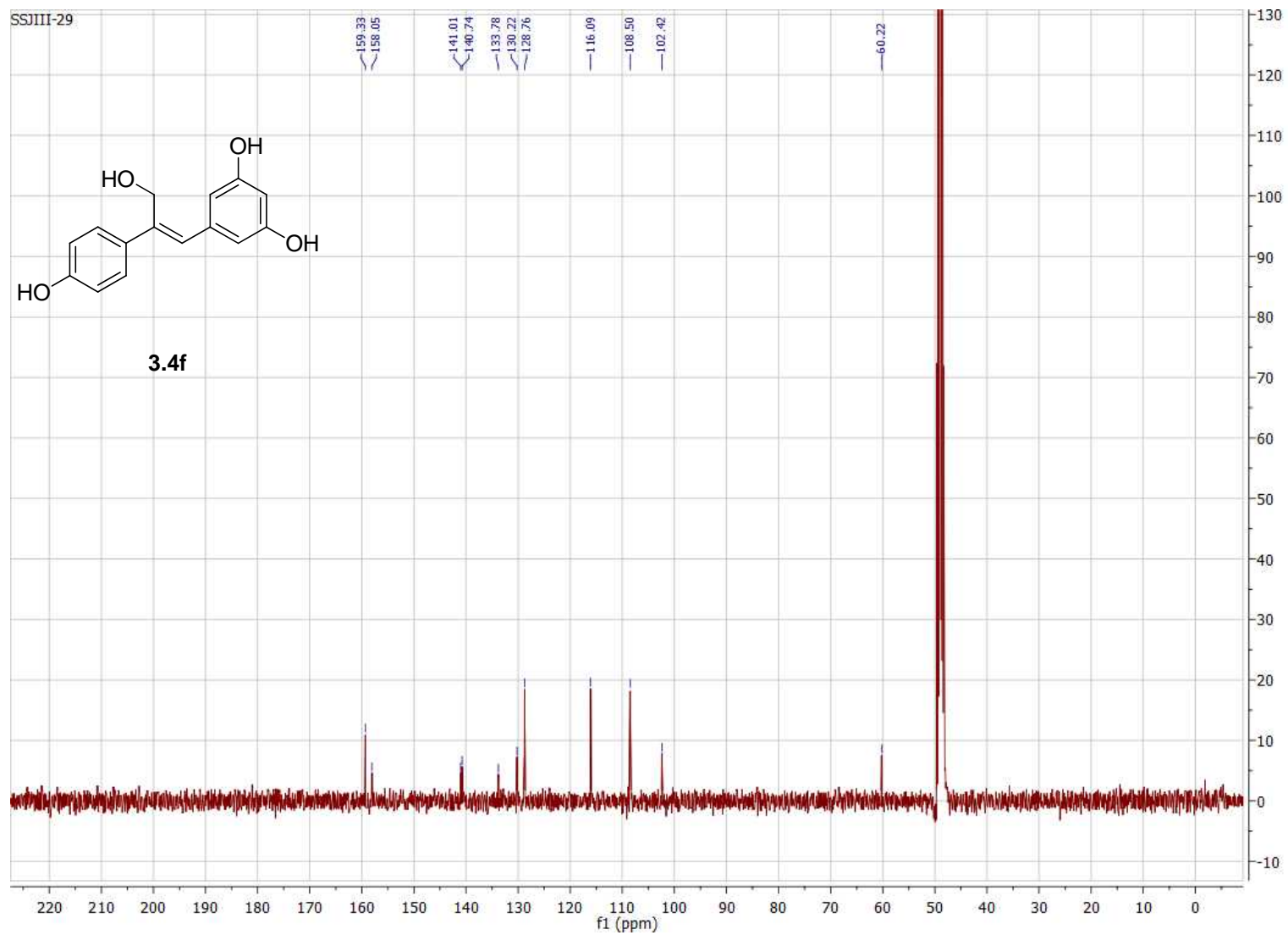


Figure B.18. 100 MHz ^{13}C NMR of compound **3.4f** in CD_3OD .

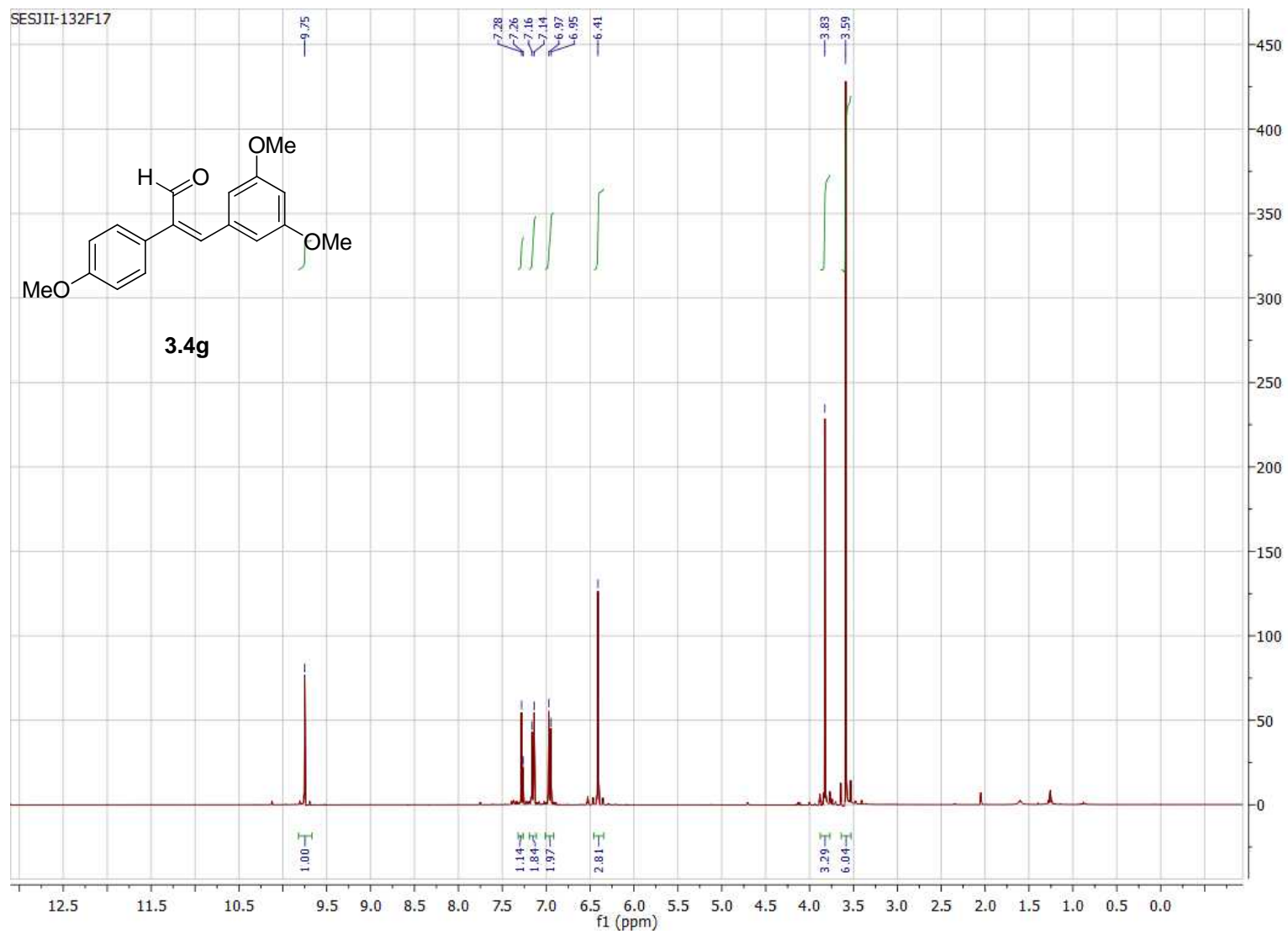


Figure B.19. 400 MHz ^1H NMR of compound **3.4g** in CDCl_3 .

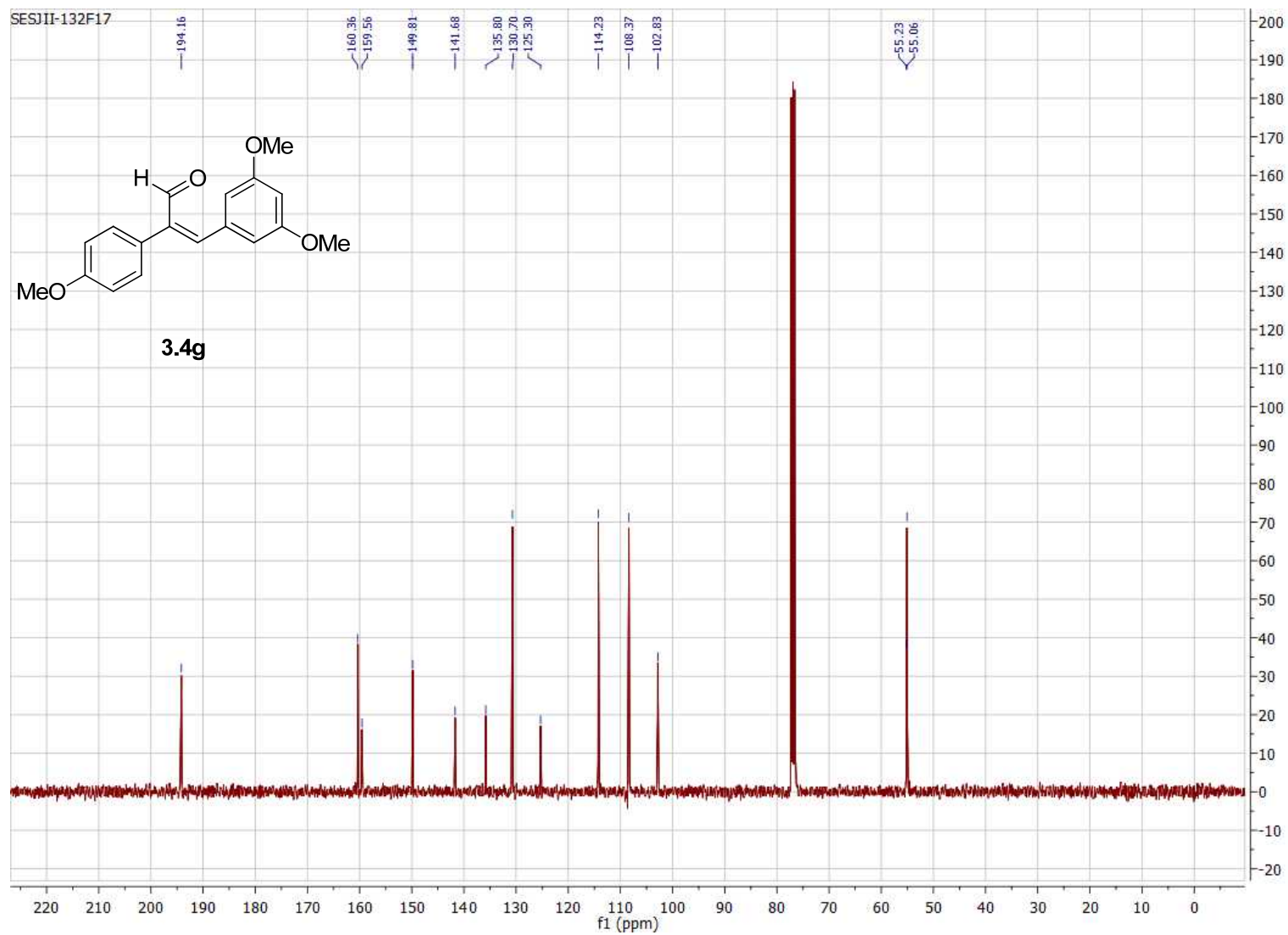


Figure B.20. 100 MHz ^{13}C NMR of compound **3.4g** in CDCl_3 .

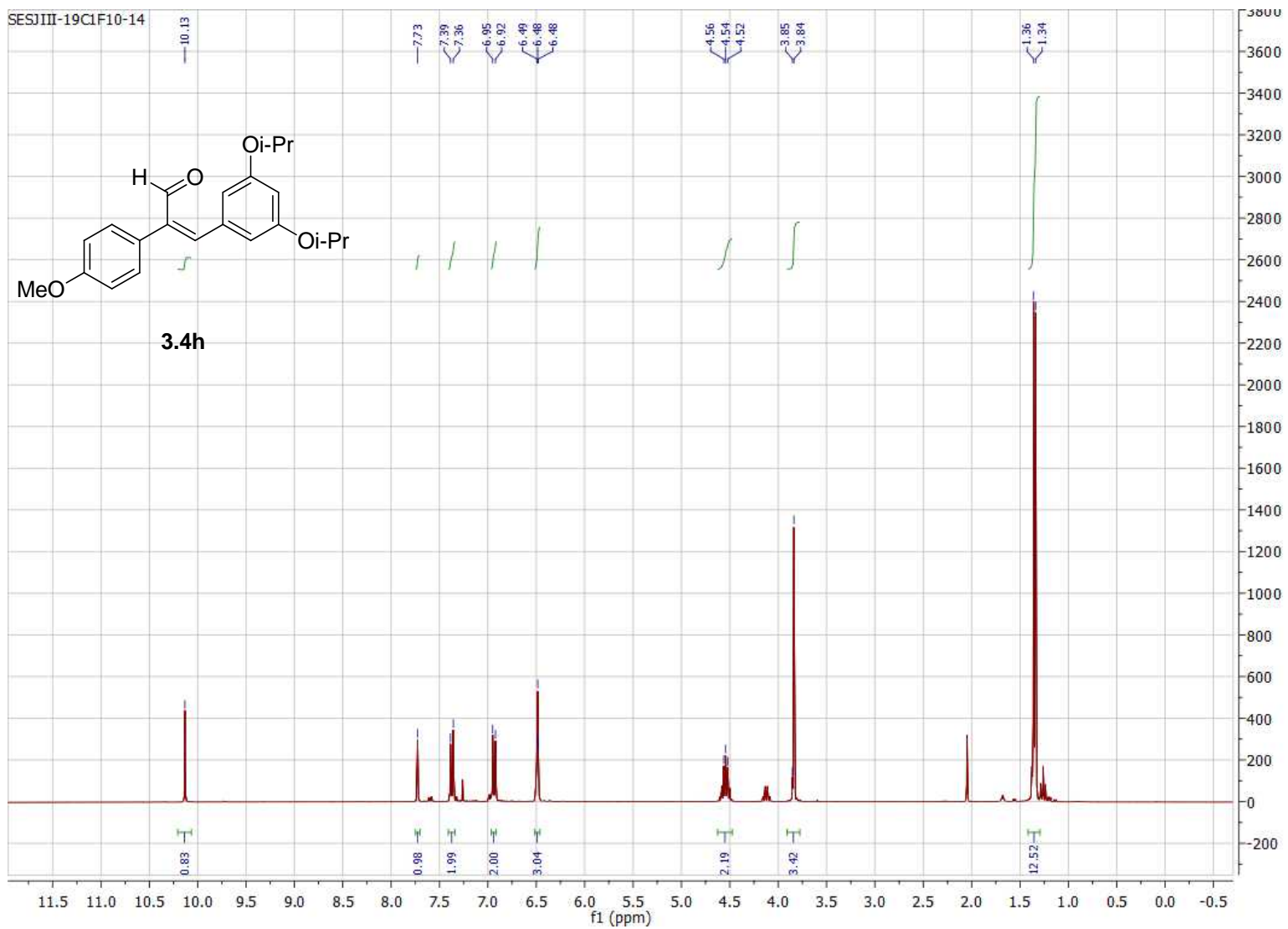


Figure B.21. 300 MHz ^1H NMR of compound **3.4h** in CDCl_3 .

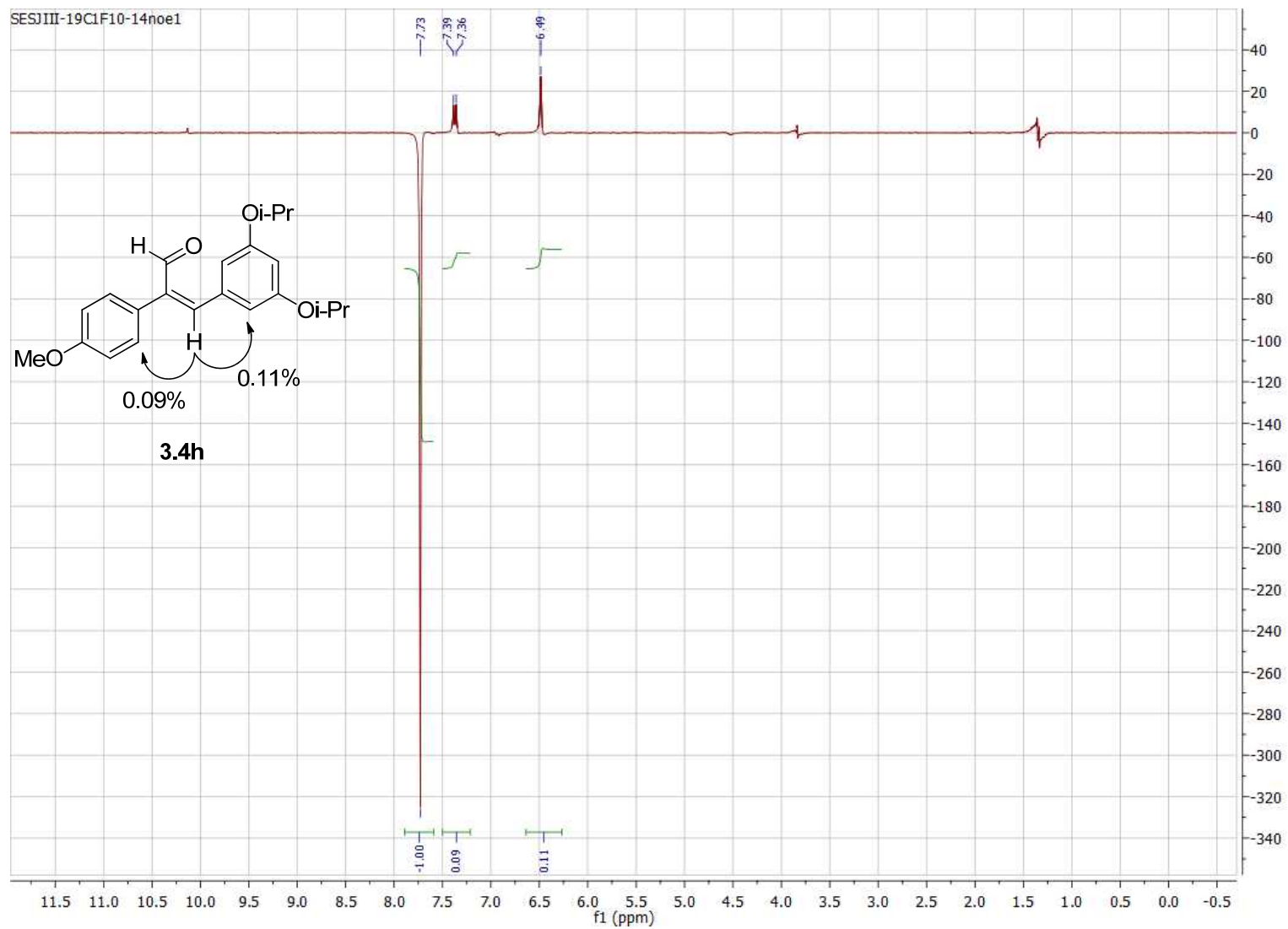


Figure B.22. 300 MHz nOe ^1H NMR of compound **3.4h** in CDCl_3 .

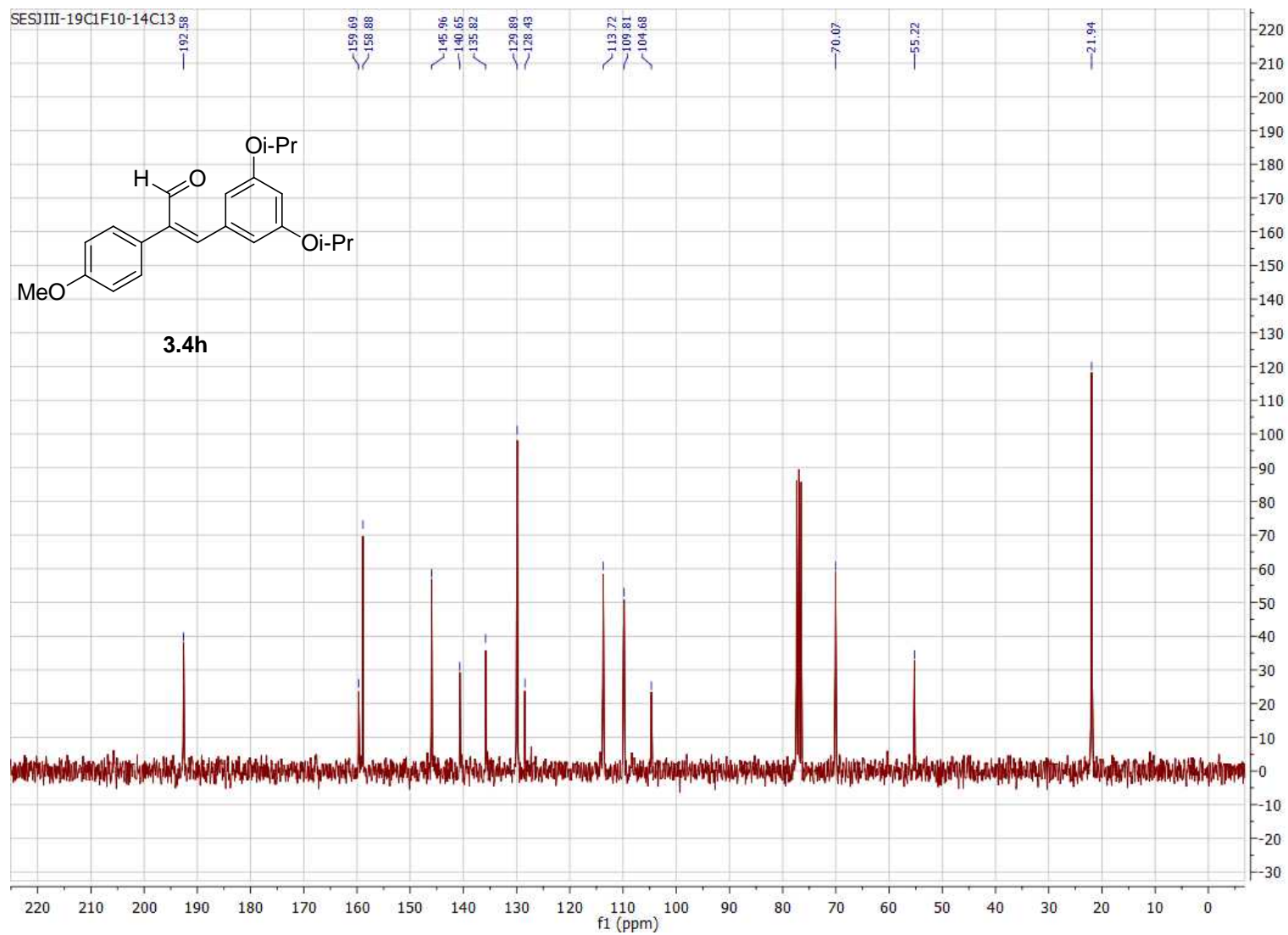


Figure B.23. 75 MHz ^{13}C NMR of compound **3.4h** in CDCl_3 .

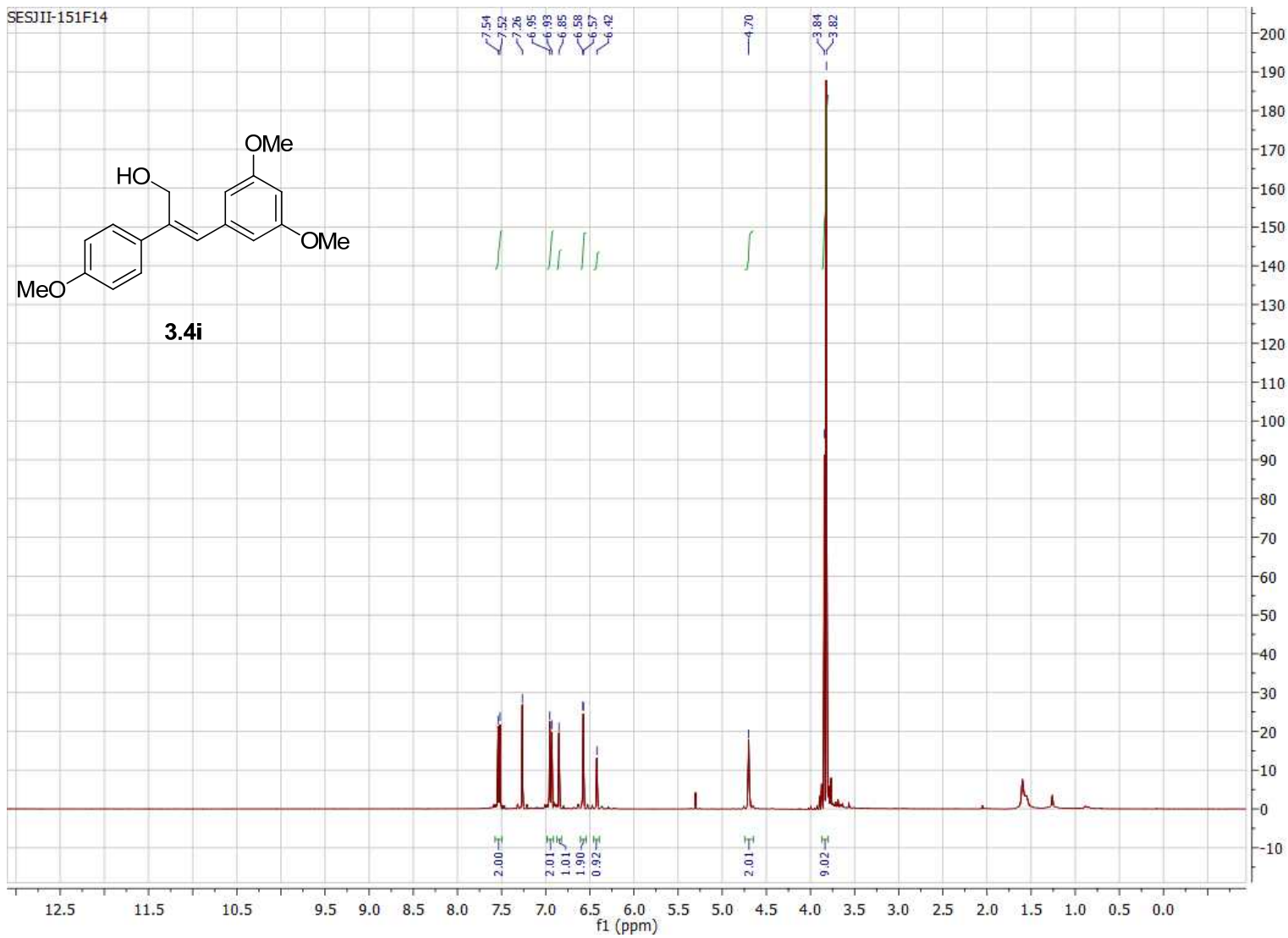


Figure B.24. 300 MHz ^1H NMR of compound **3.4i** in CDCl_3 .

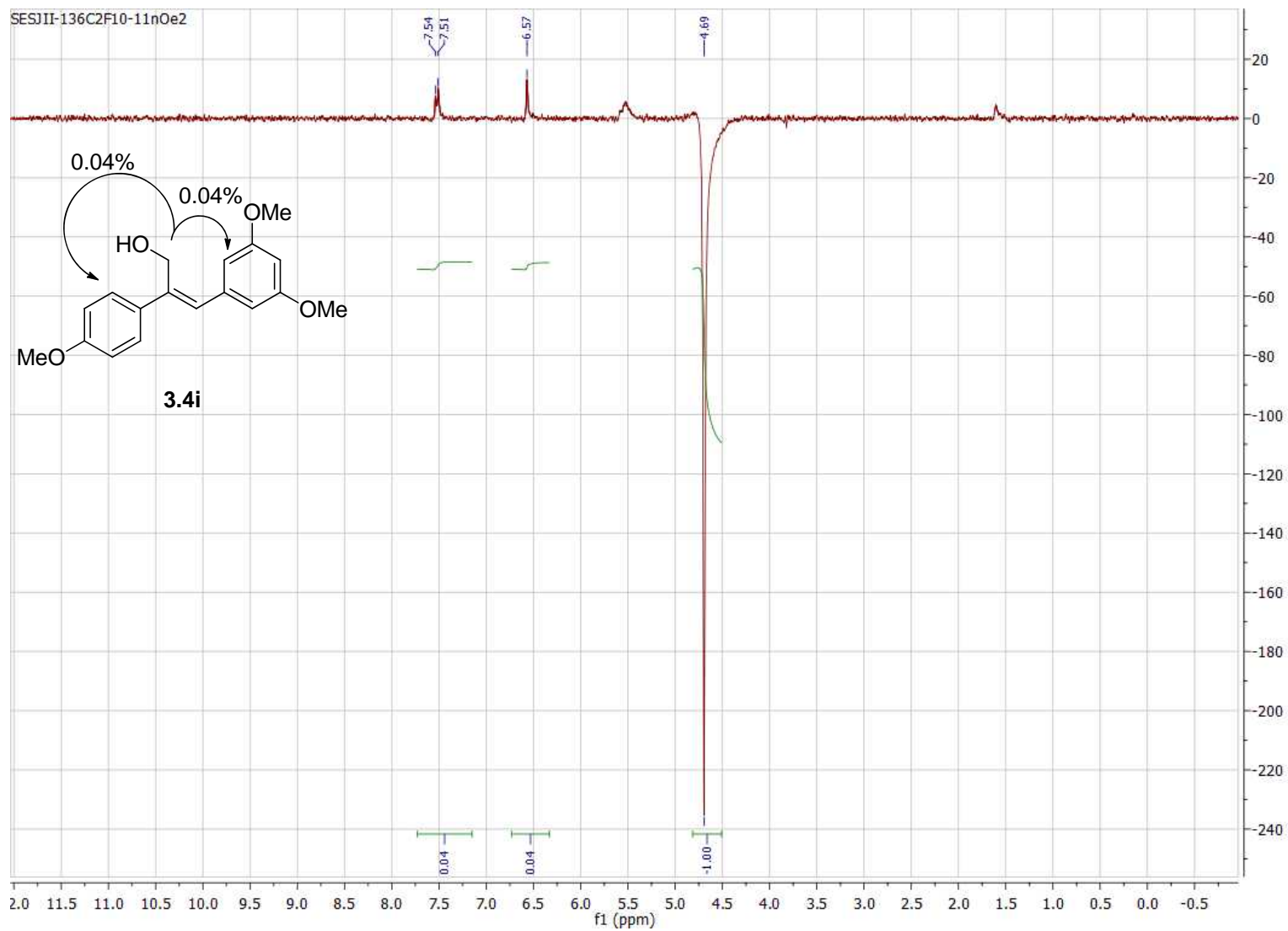


Figure B.25. 300 MHz nOe ^1H NMR of compound **3.4i** in CDCl_3 .

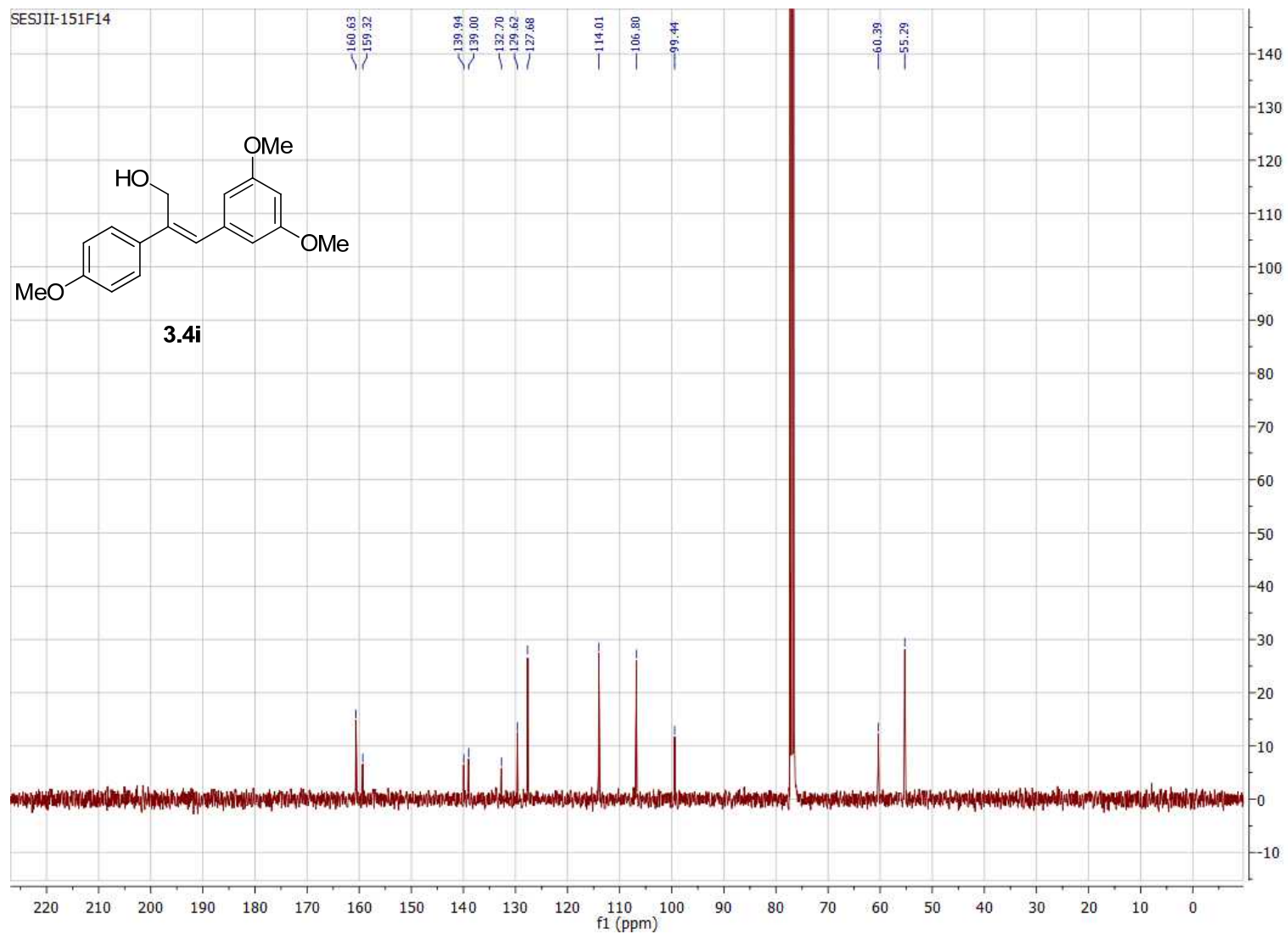


Figure B.26. 100 MHz ¹³C NMR of compound **3.4i** in CDCl₃.

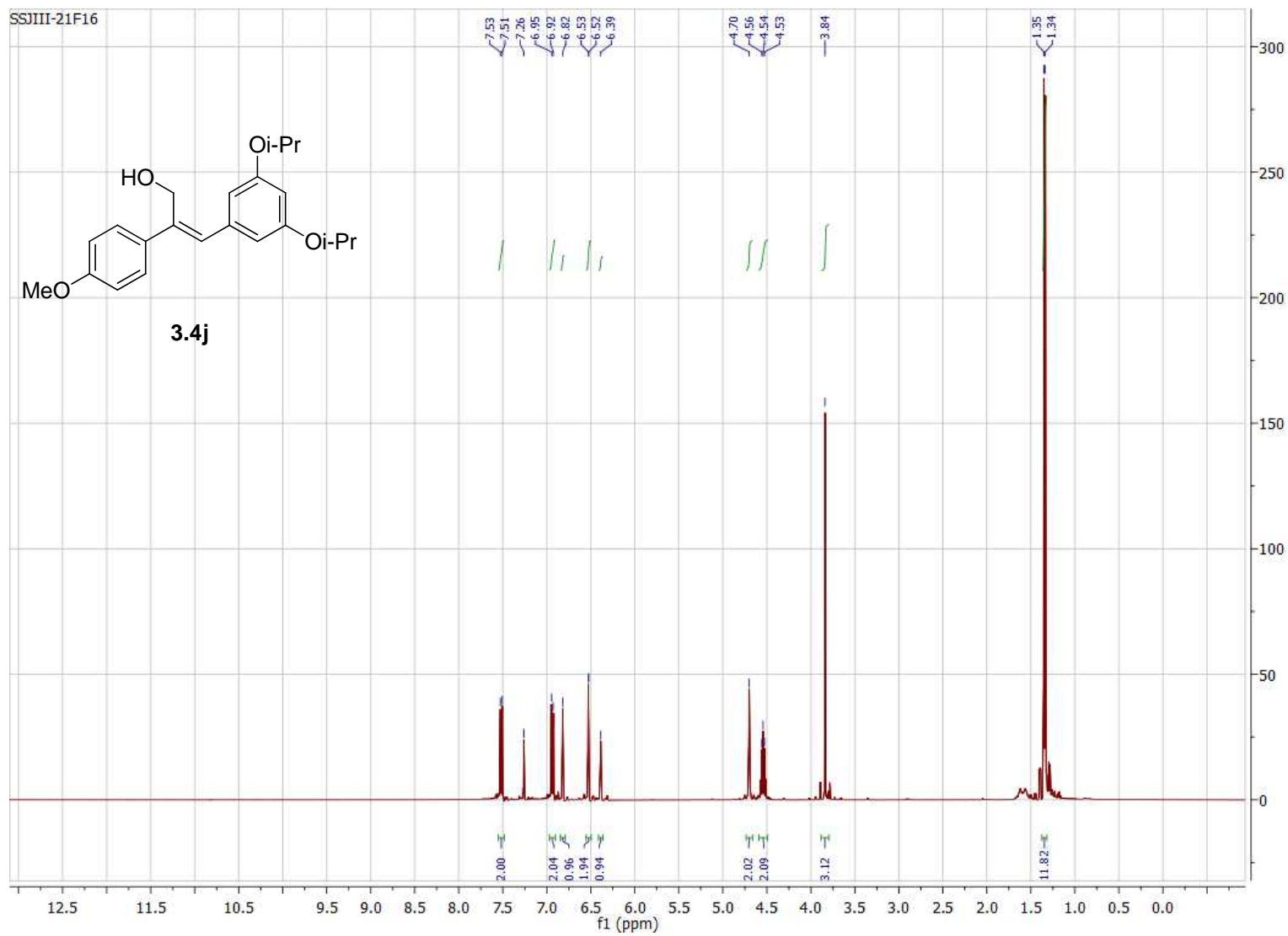


Figure B.27. 400 MHz ^1H NMR of compound **3.4j** in CDCl_3 .

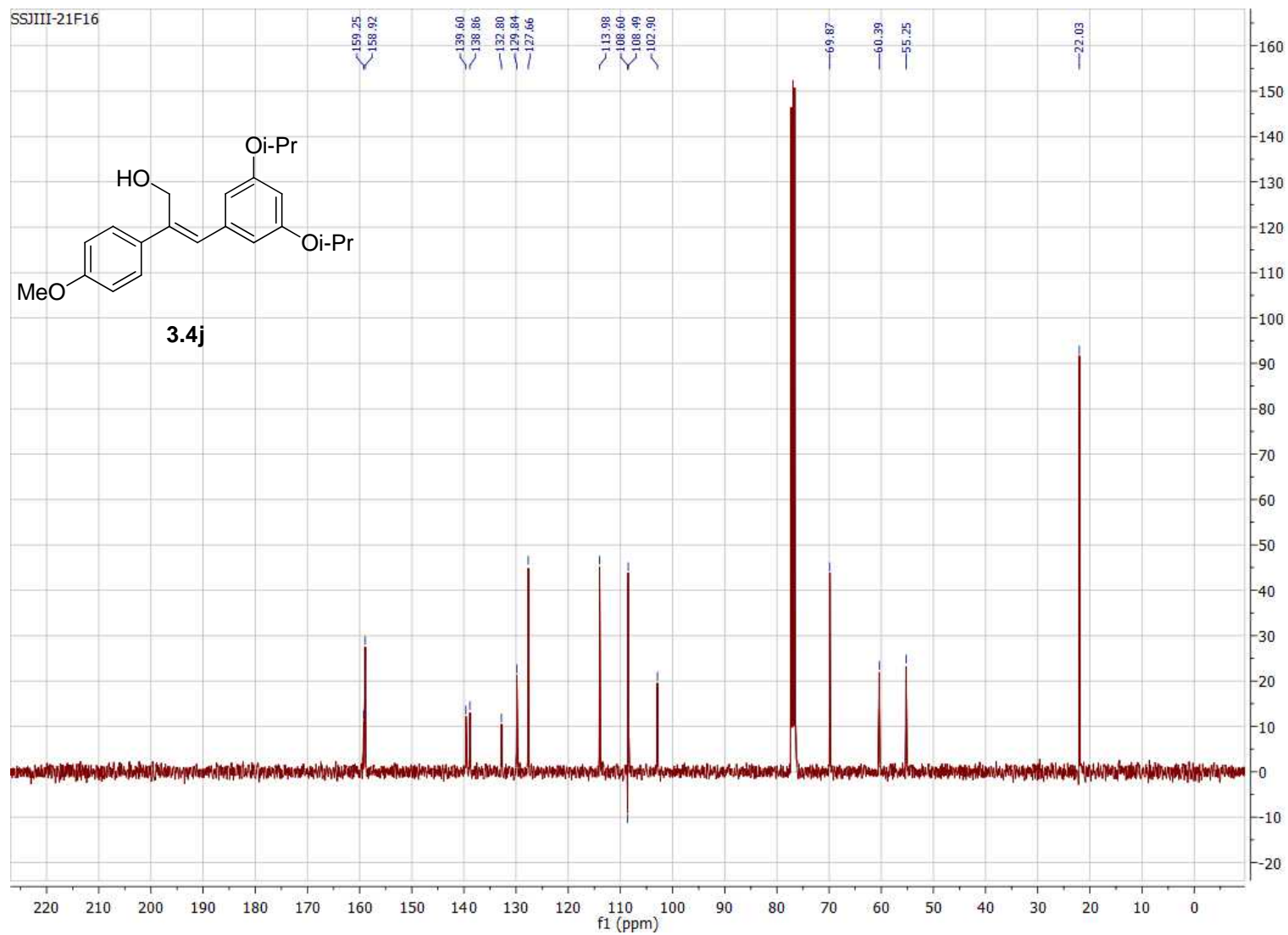


Figure B.28. 100 MHz ^{13}C NMR of compound **3.4j** in CDCl_3 .

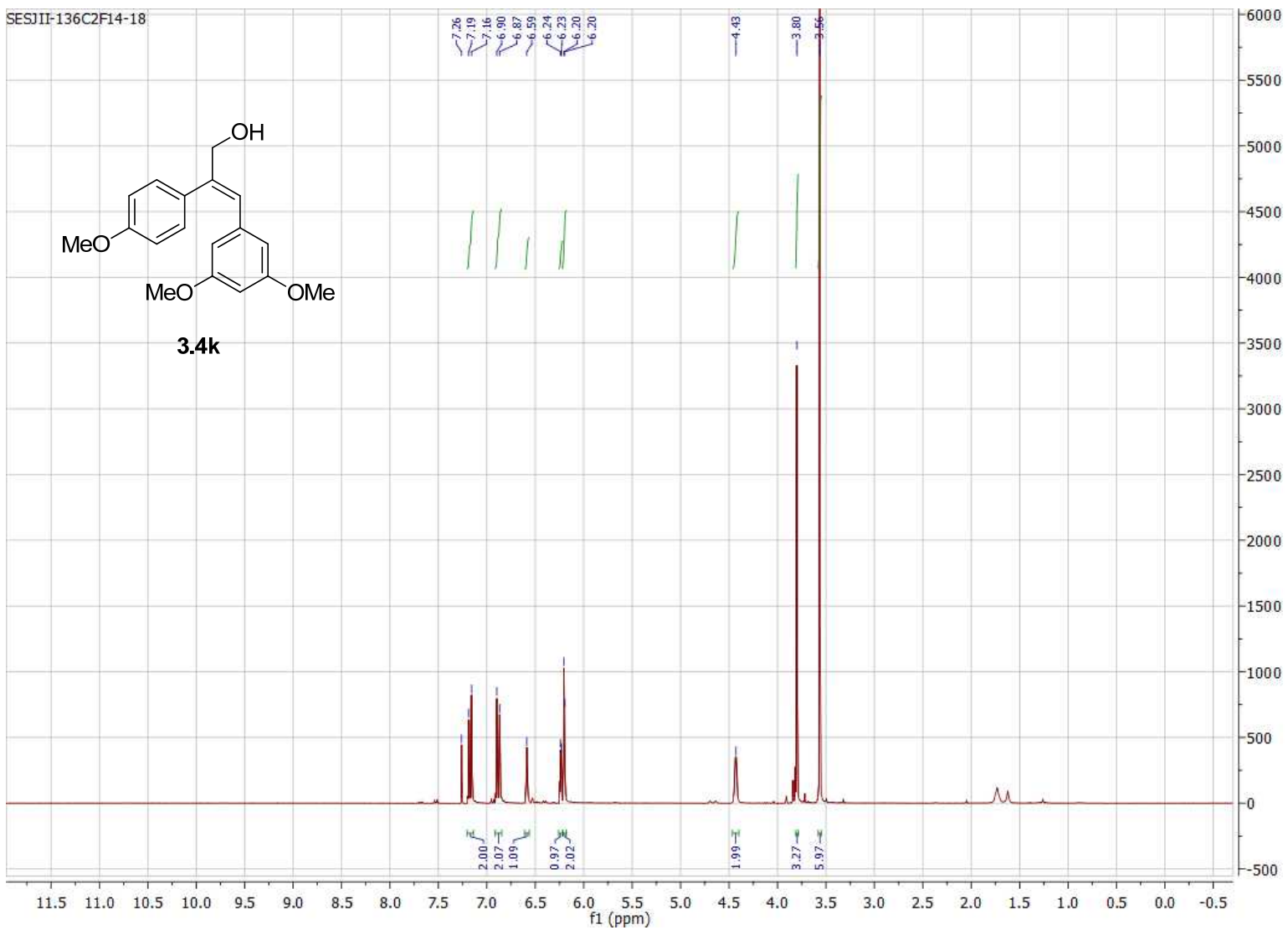


Figure B.29. 300 MHz ¹H NMR of compound **3.4k** in CDCl₃.

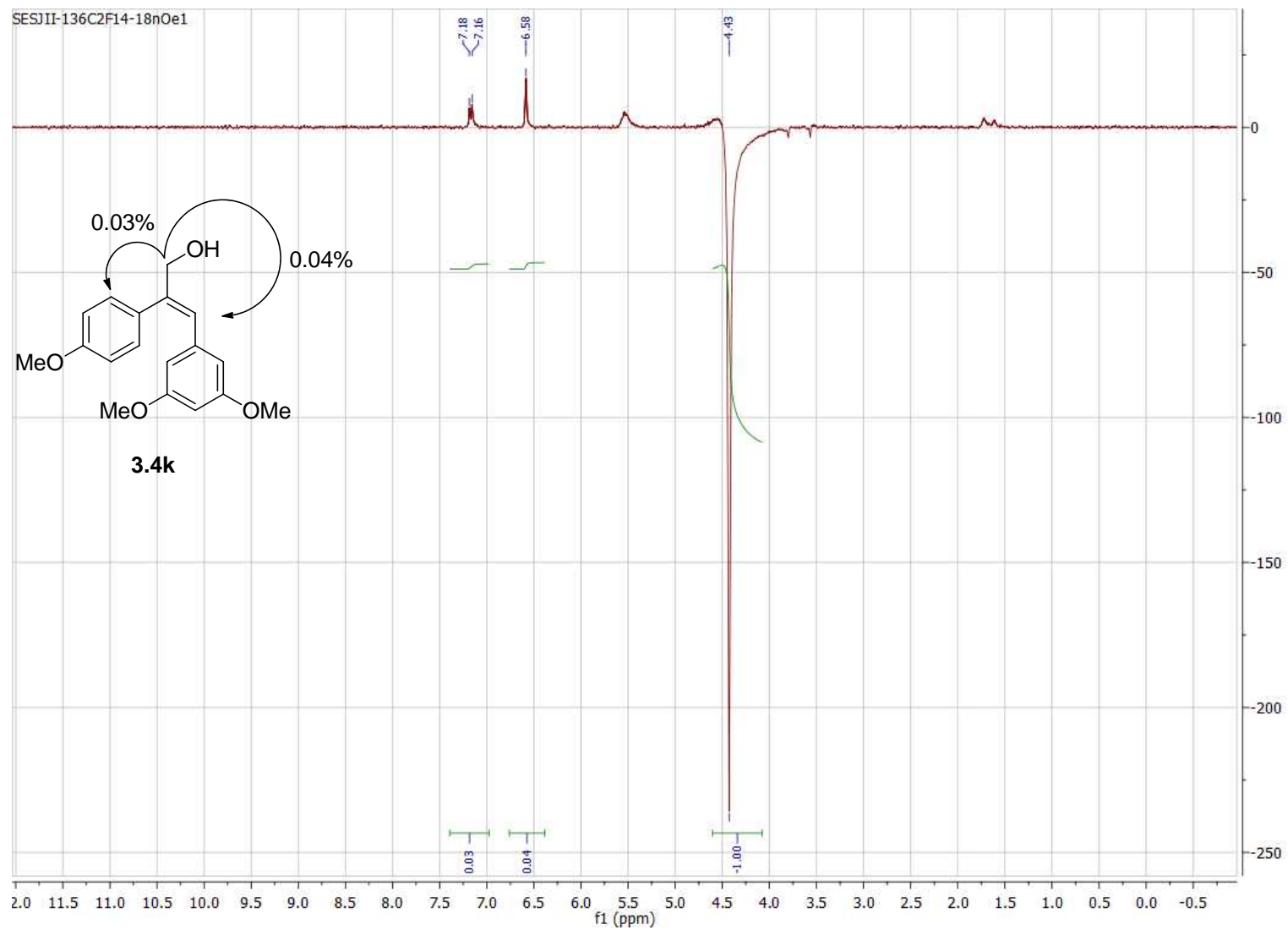


Figure B.30. 300 MHz nOe ^1H NMR of compound **3.4k** in CDCl_3 .

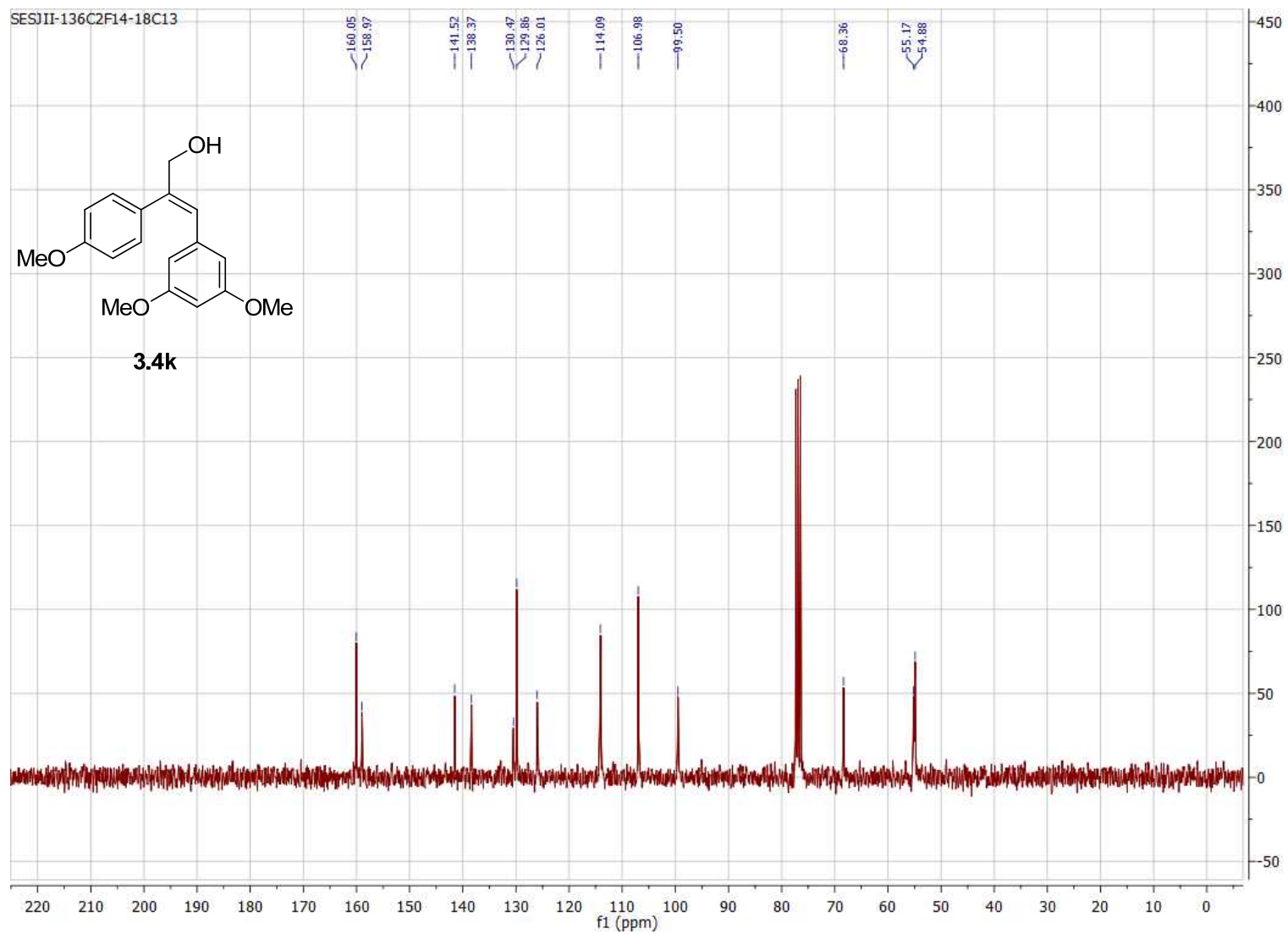


Figure B.31. 75 MHz ^{13}C NMR of compound **3.4k** in CDCl_3 .

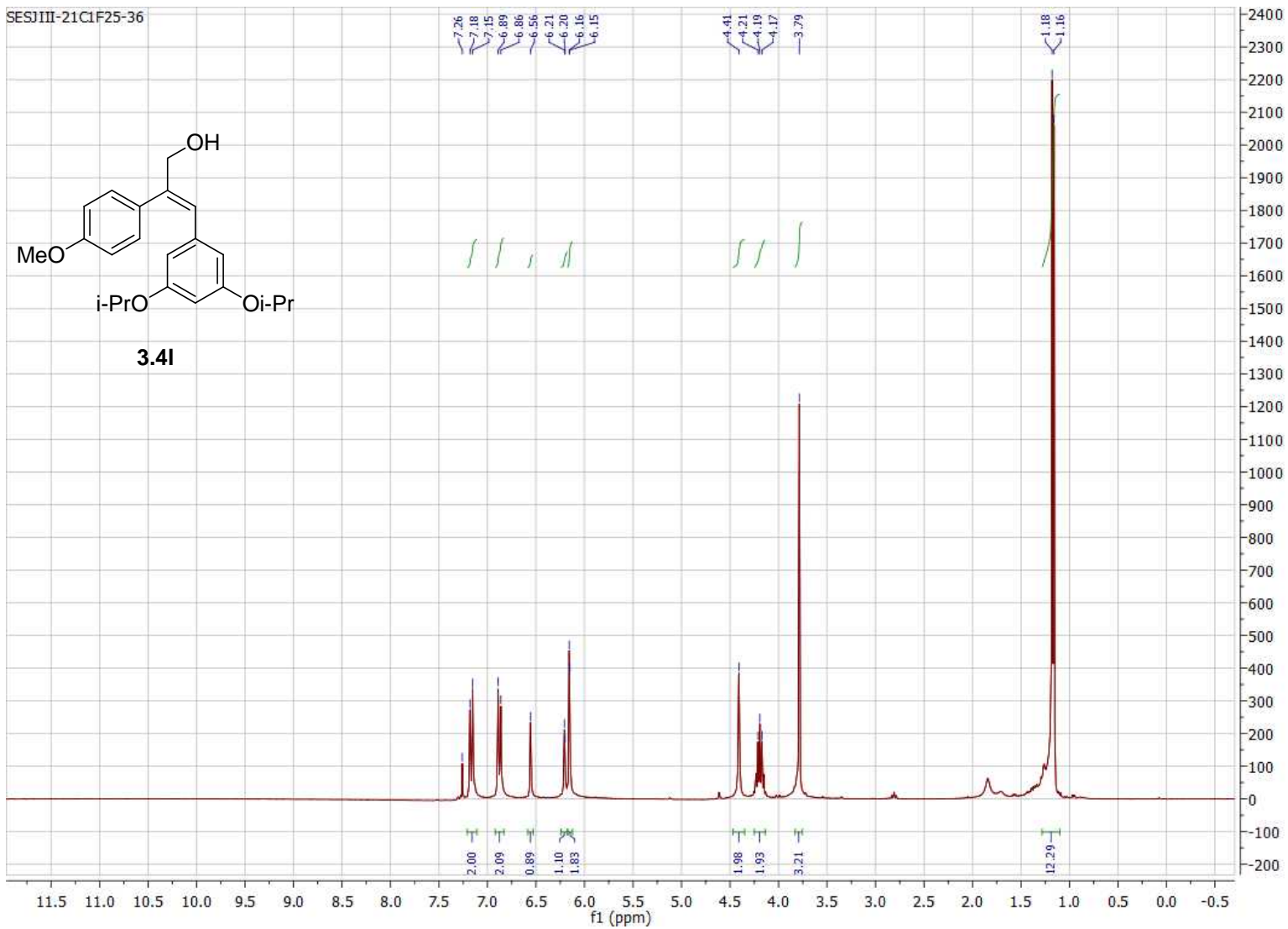


Figure B.32. 300 MHz ¹H NMR of compound **3.4I** in CDCl₃.

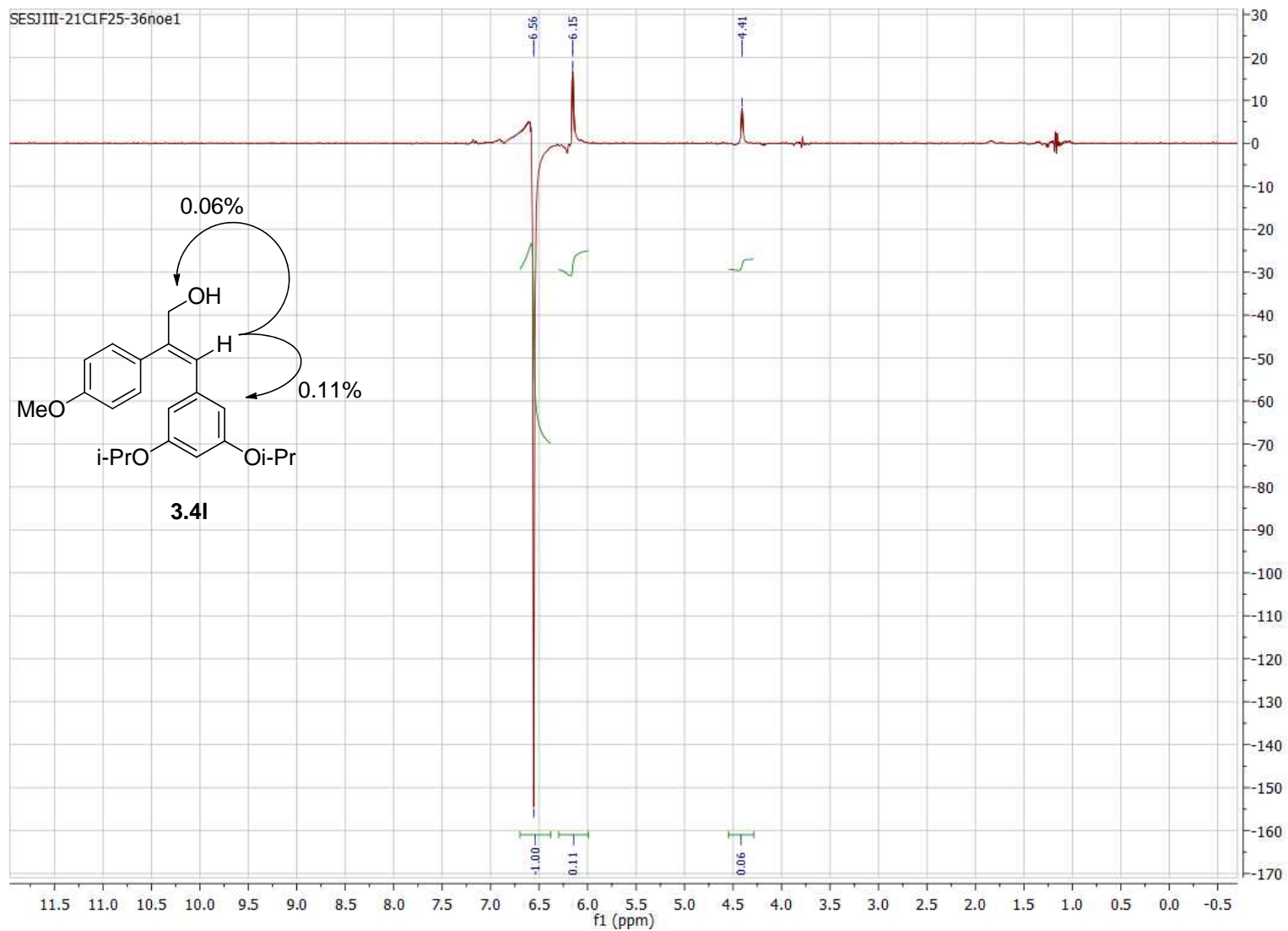


Figure B.33. 300 MHz nOe ^1H NMR of compound **3.4I** in CDCl_3 .

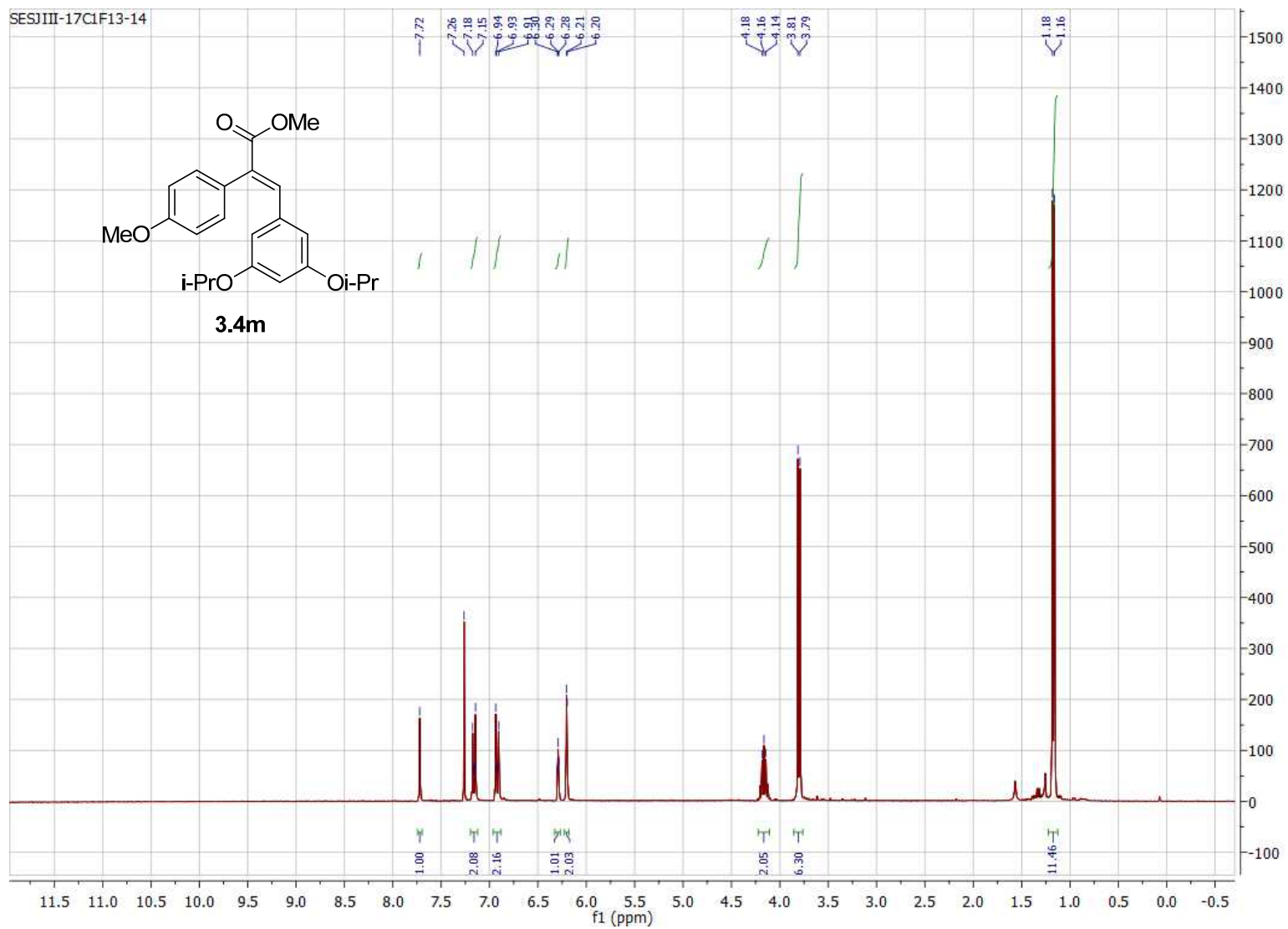


Figure B.34. 300 MHz ¹H NMR of compound **3.4m** in CDCl₃.

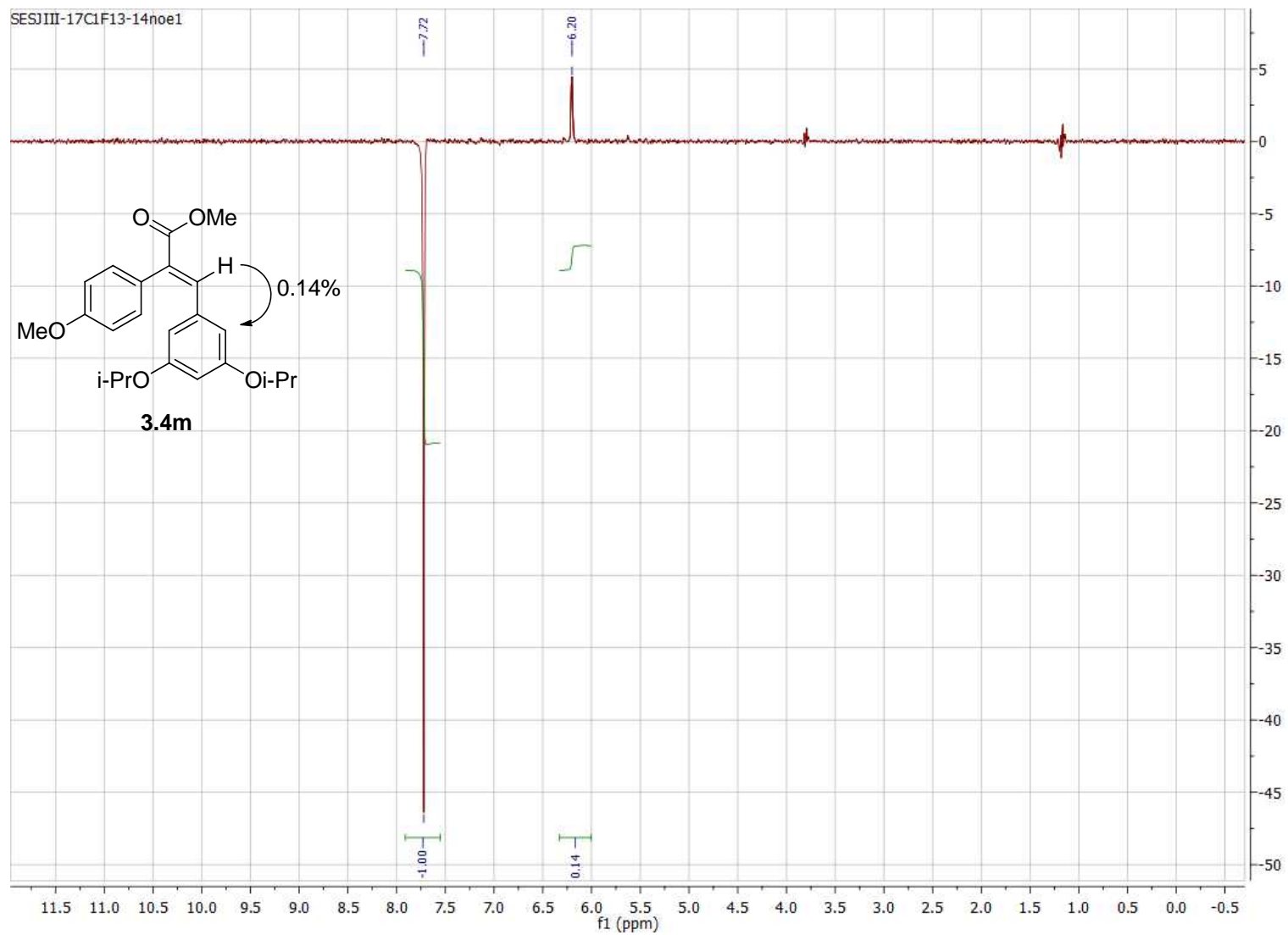


Figure B.35. 300 MHz nOe ^1H NMR of compound **3.4m** in CDCl_3 .

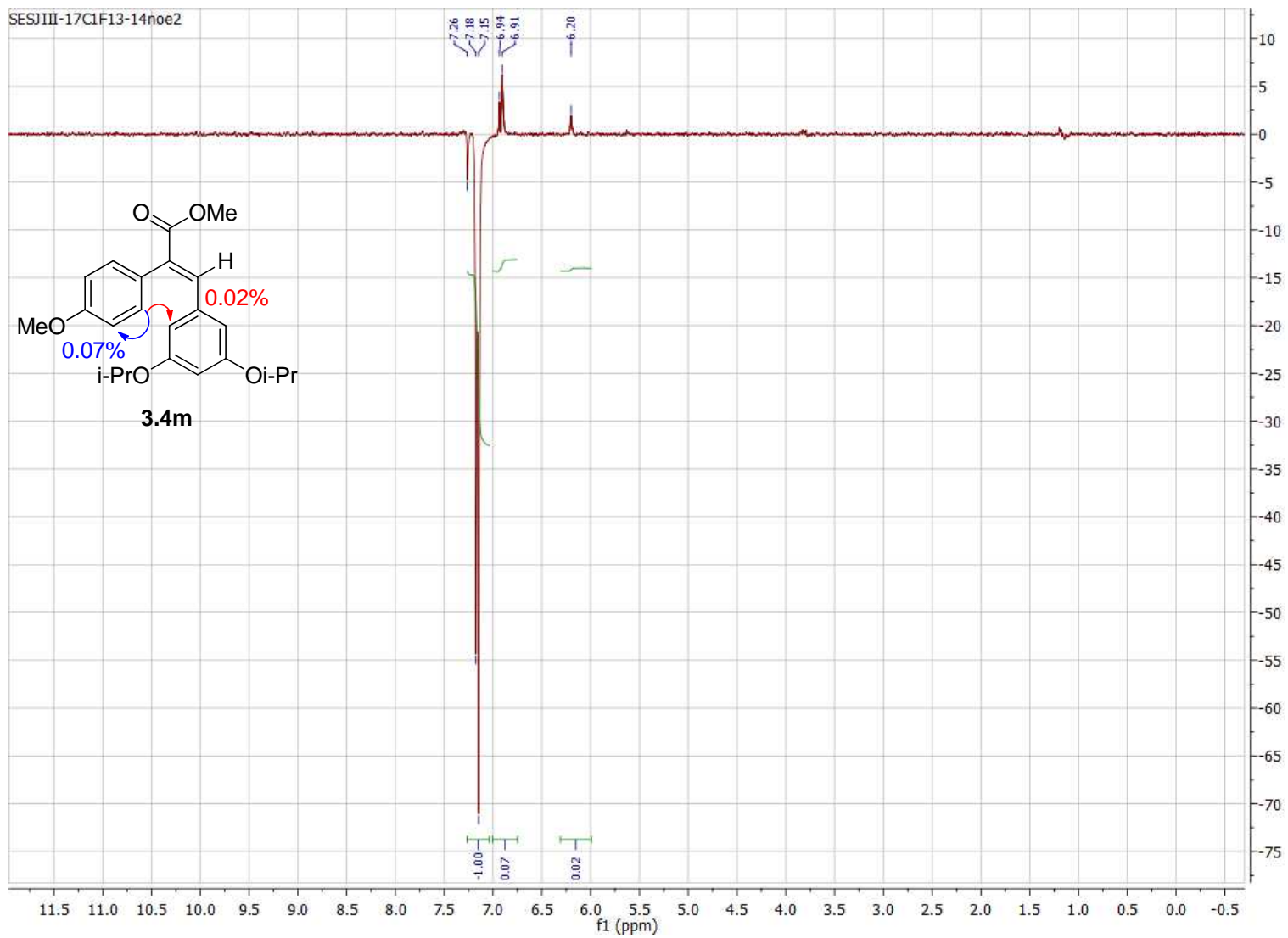


Figure B.36. 300 MHz nOe ^1H NMR of compound **3.4m** in CDCl_3 .

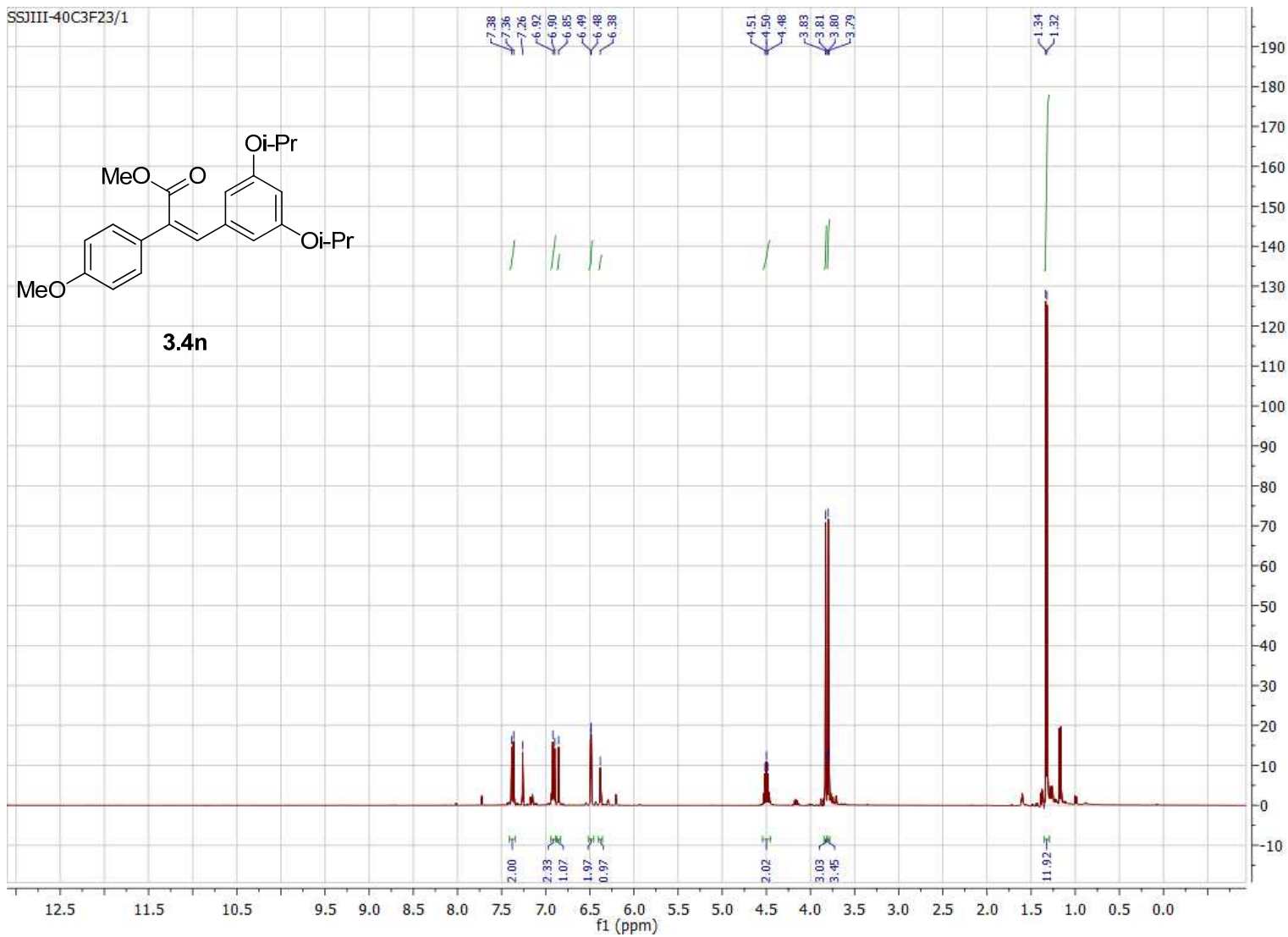


Figure B.37. 400 MHz ^1H NMR of compound **3.4n** in CDCl_3 .

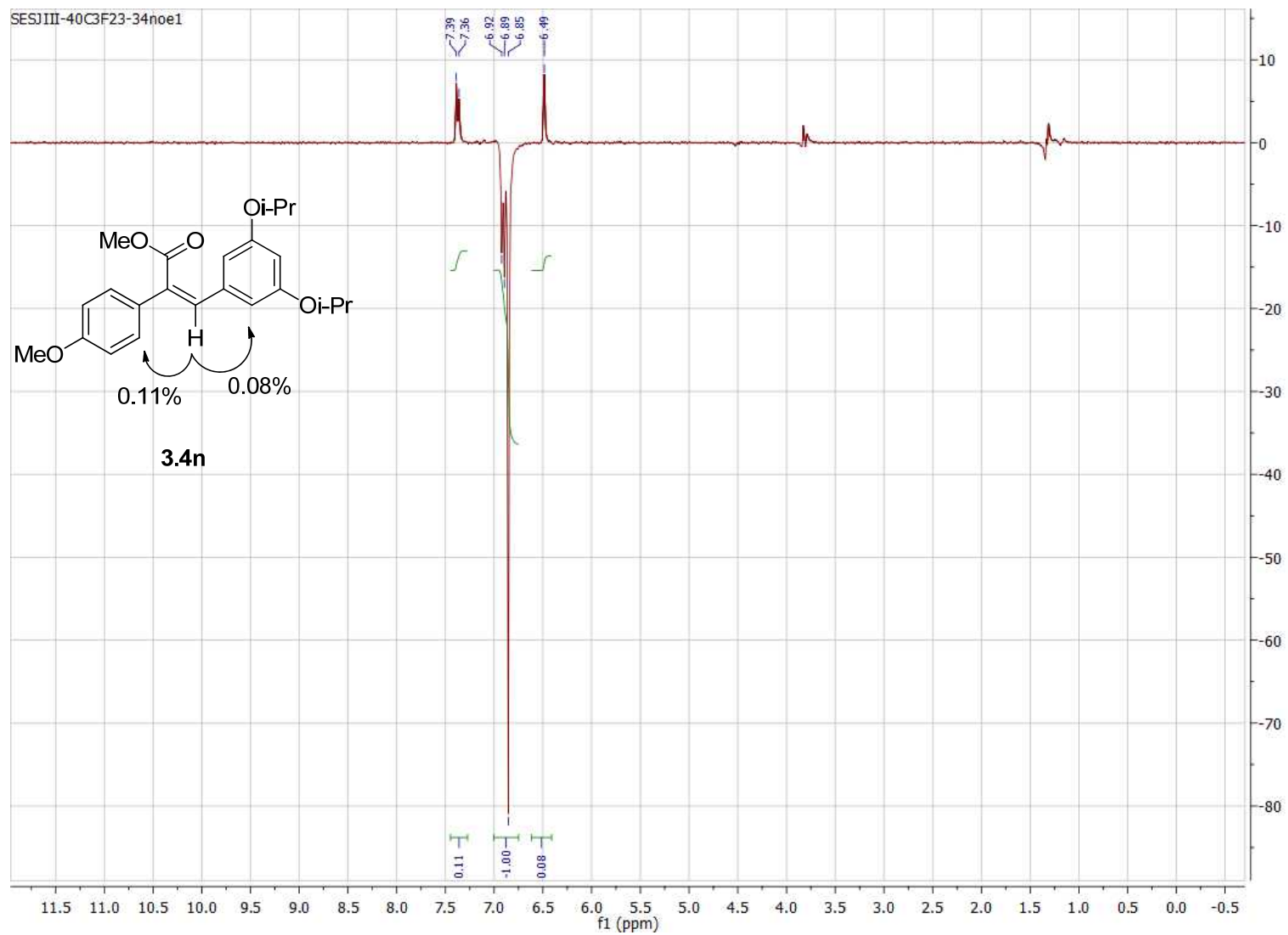


Figure B.38. 300 MHz nOe ^1H NMR of compound **3.4n** in CDCl_3 .

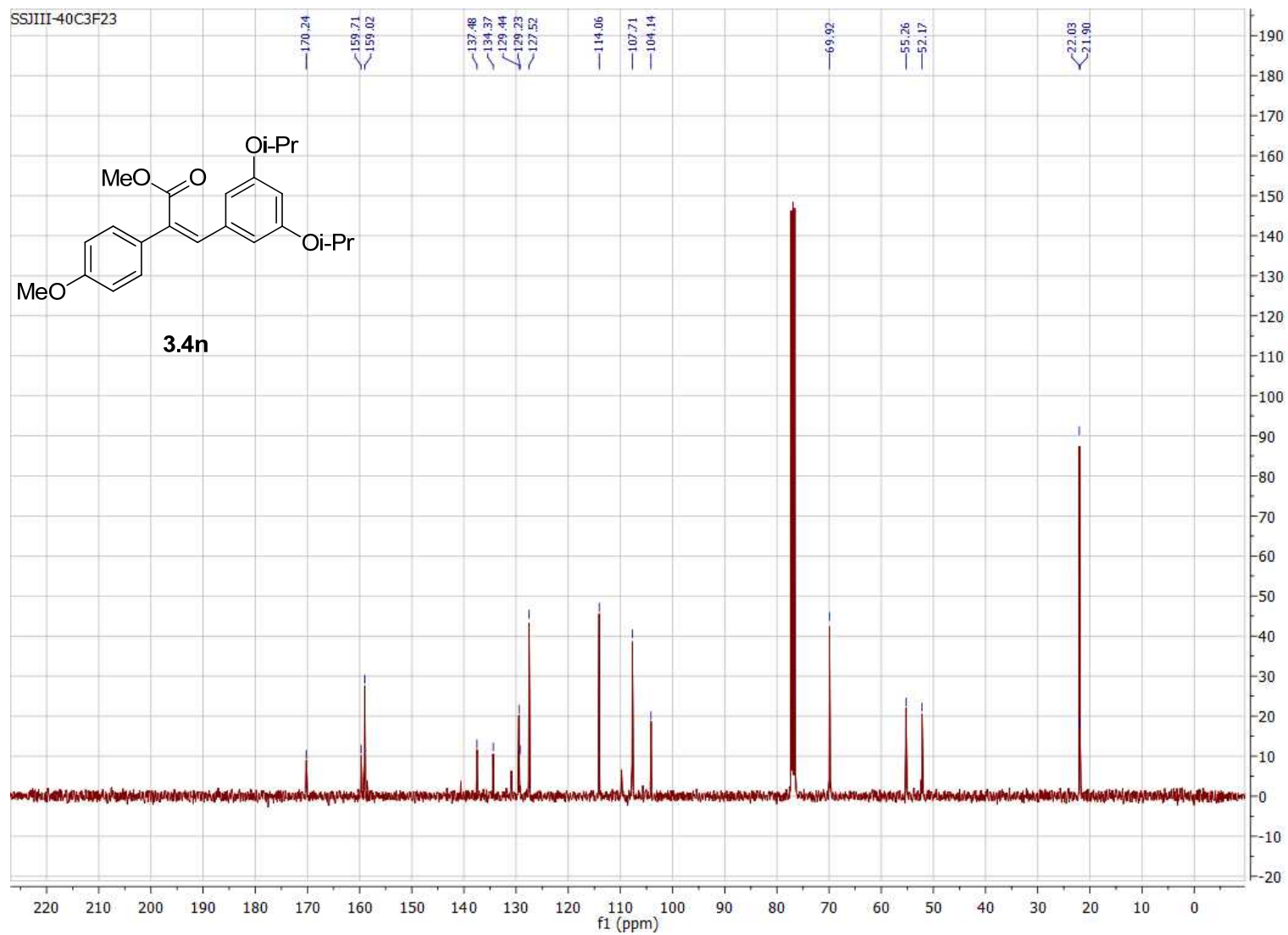


Figure B.39. 100 MHz ^{13}C NMR of compound **3.4n** in CDCl_3 .

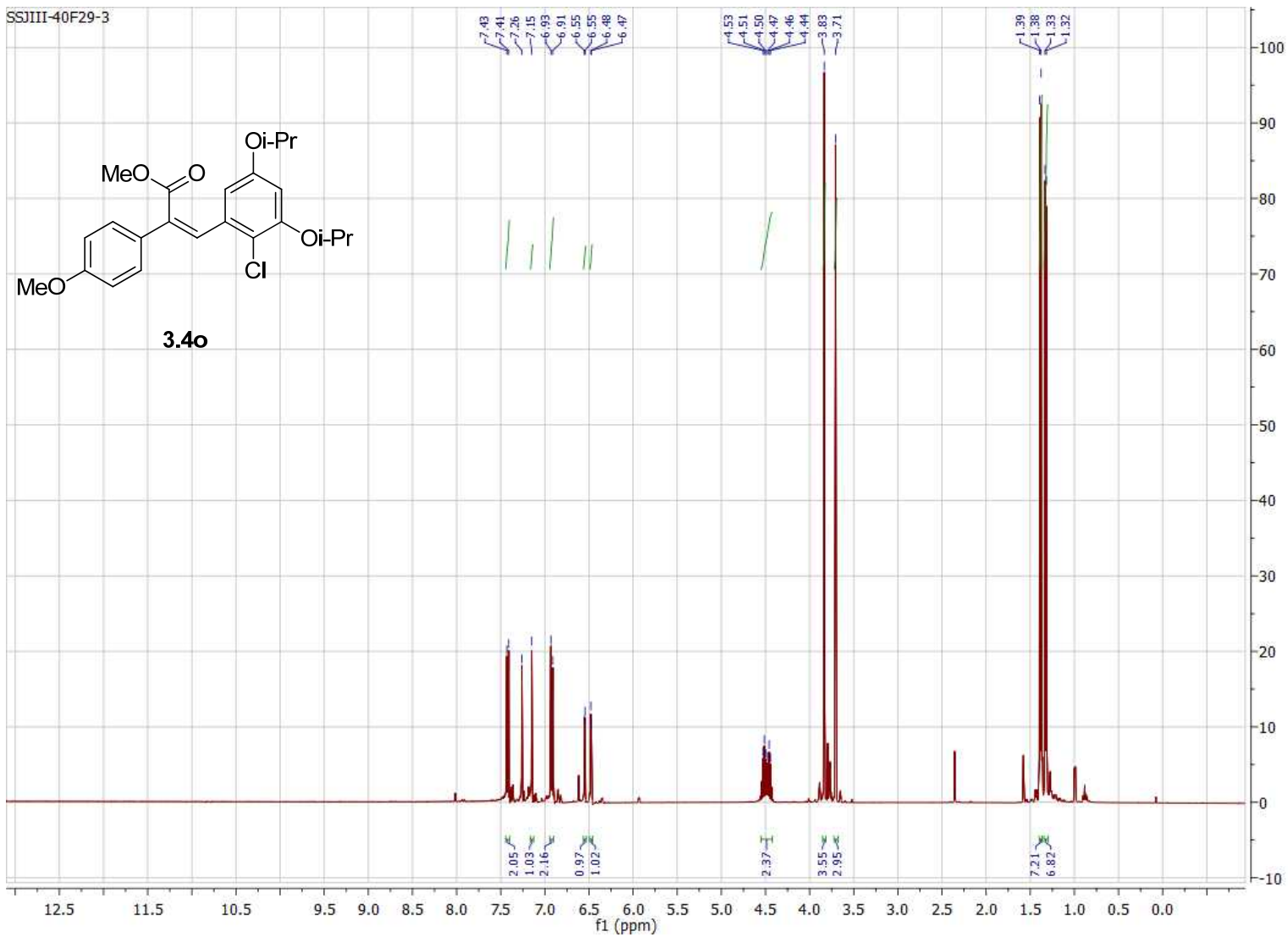


Figure B.40. 400 MHz ¹H NMR of compound **3.4o** in CDCl₃.

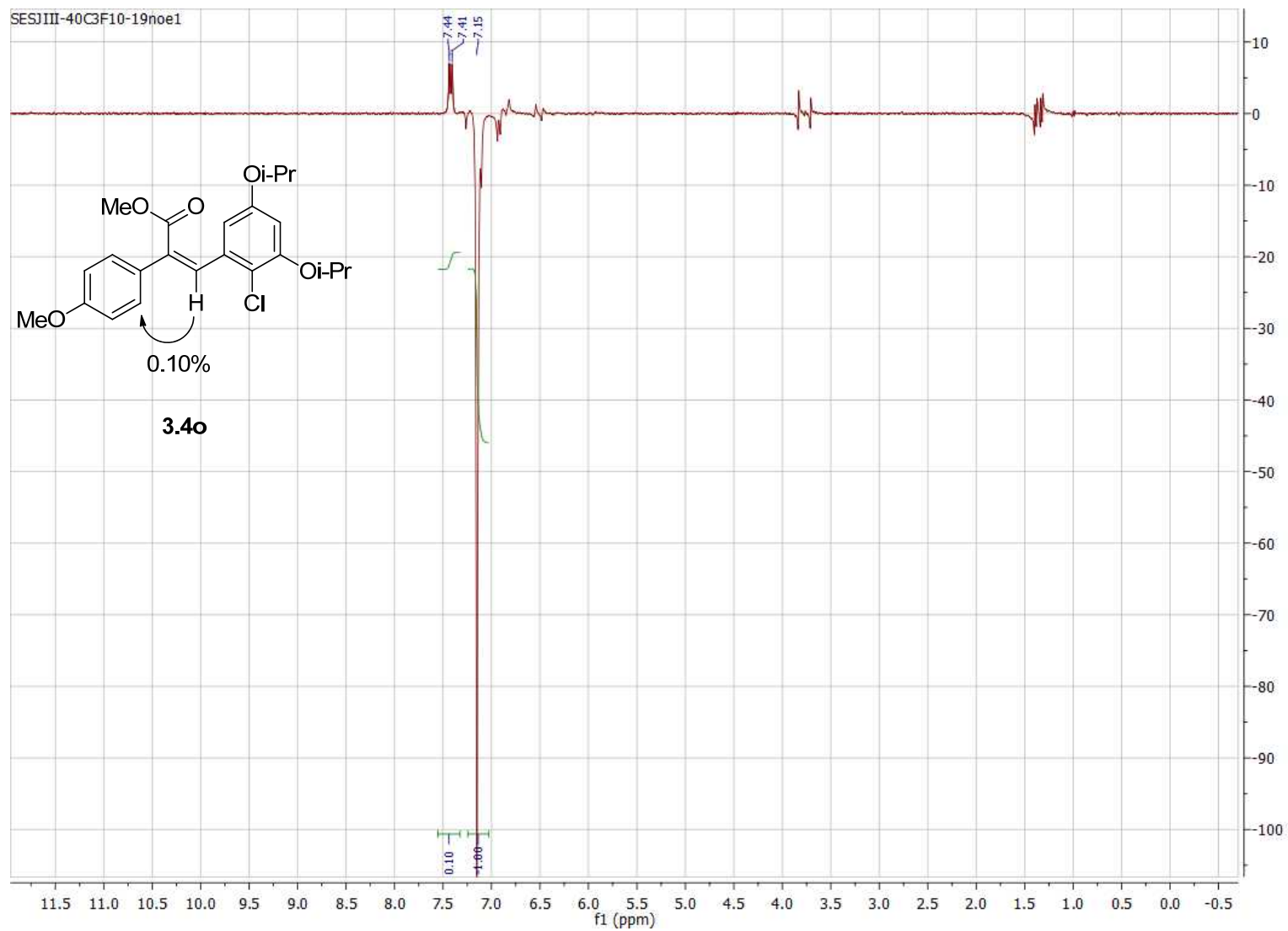


Figure B.41. 300 MHz nOe ^1H NMR of compound **3.4o** in CDCl_3 .

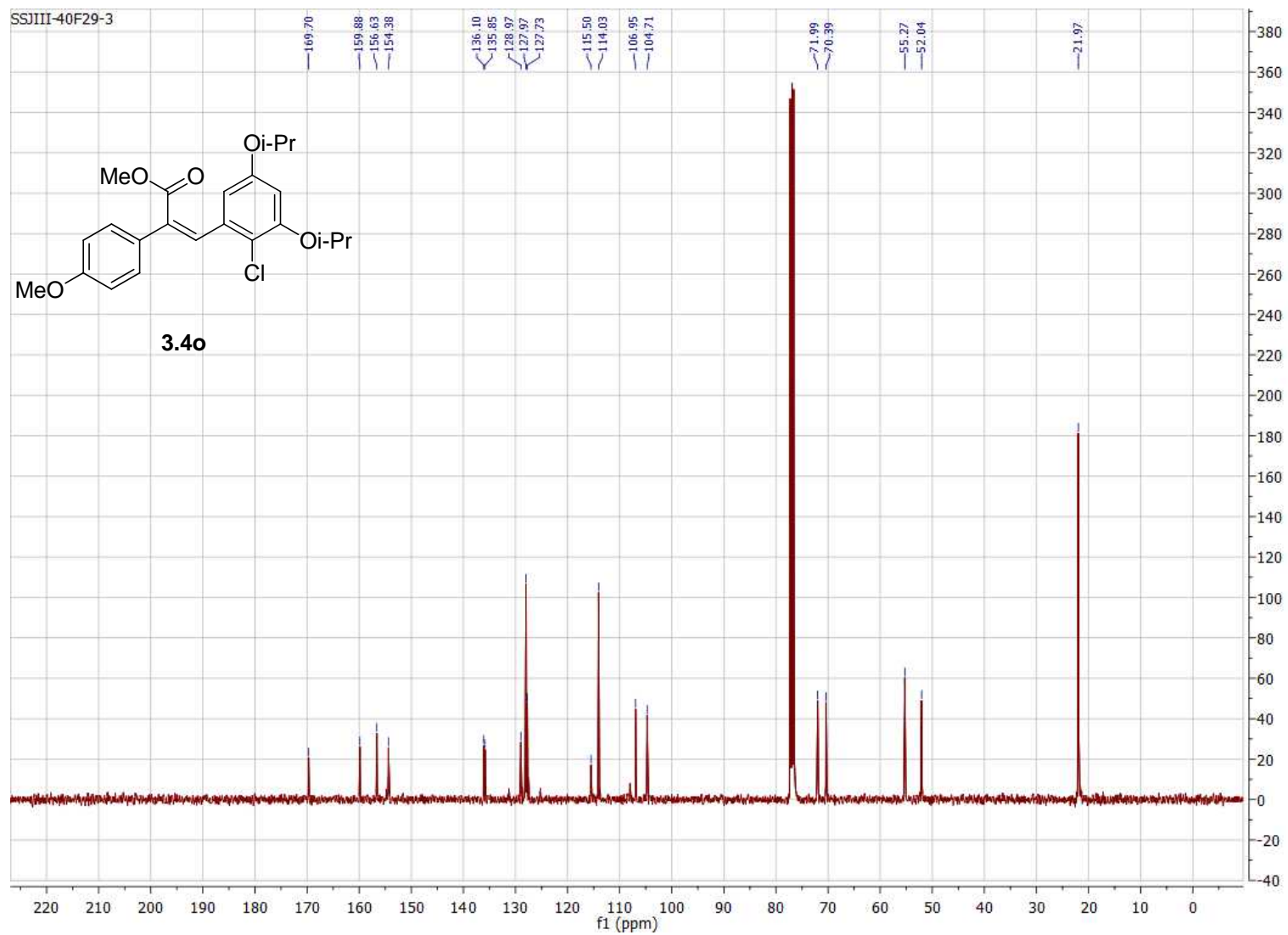


Figure B.42. 100 MHz ^{13}C NMR of compound **3.4o** in CDCl_3 .

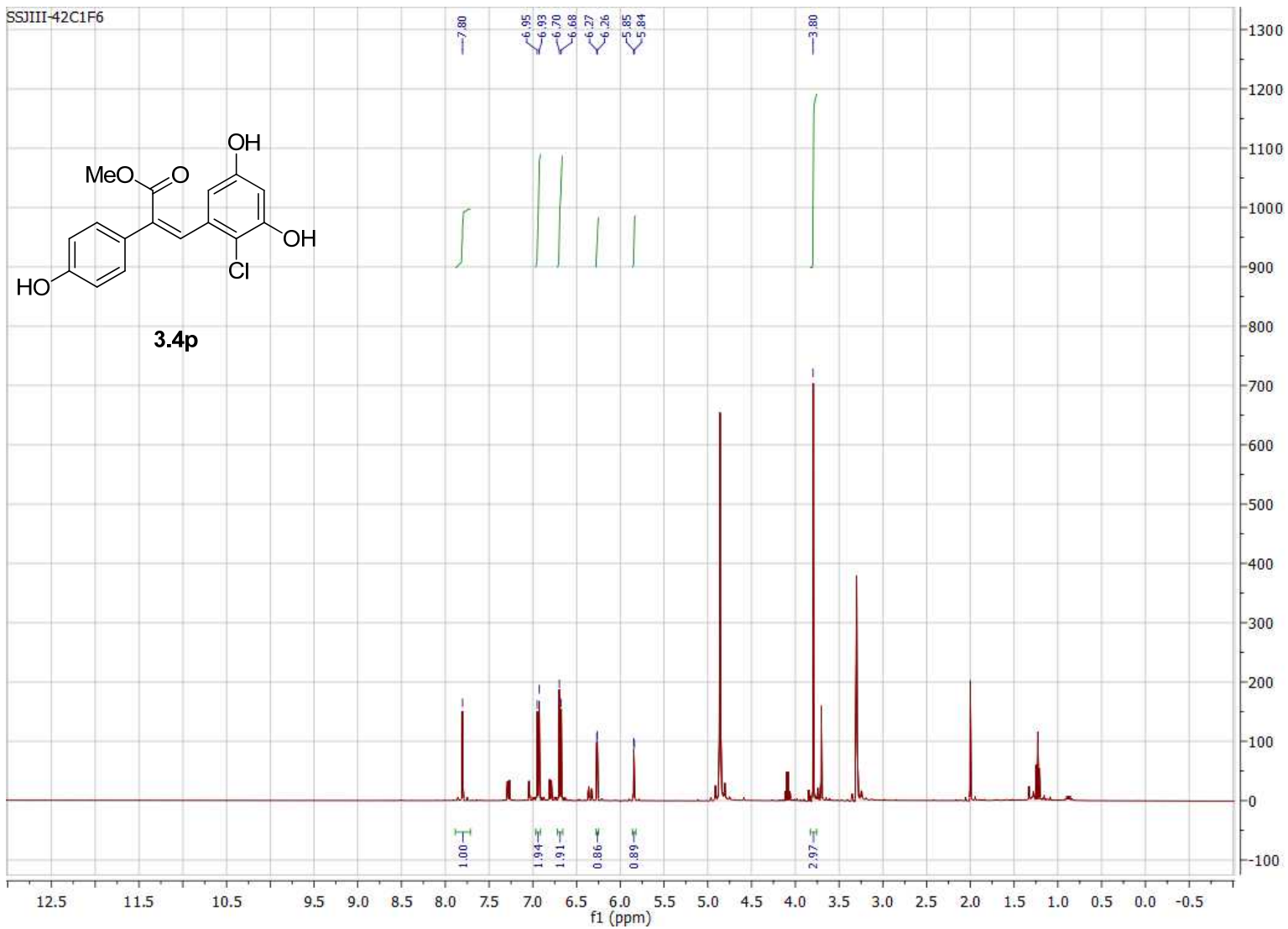


Figure B.43. 400 MHz ^1H NMR of compound **3.4p** in CD_3OD .

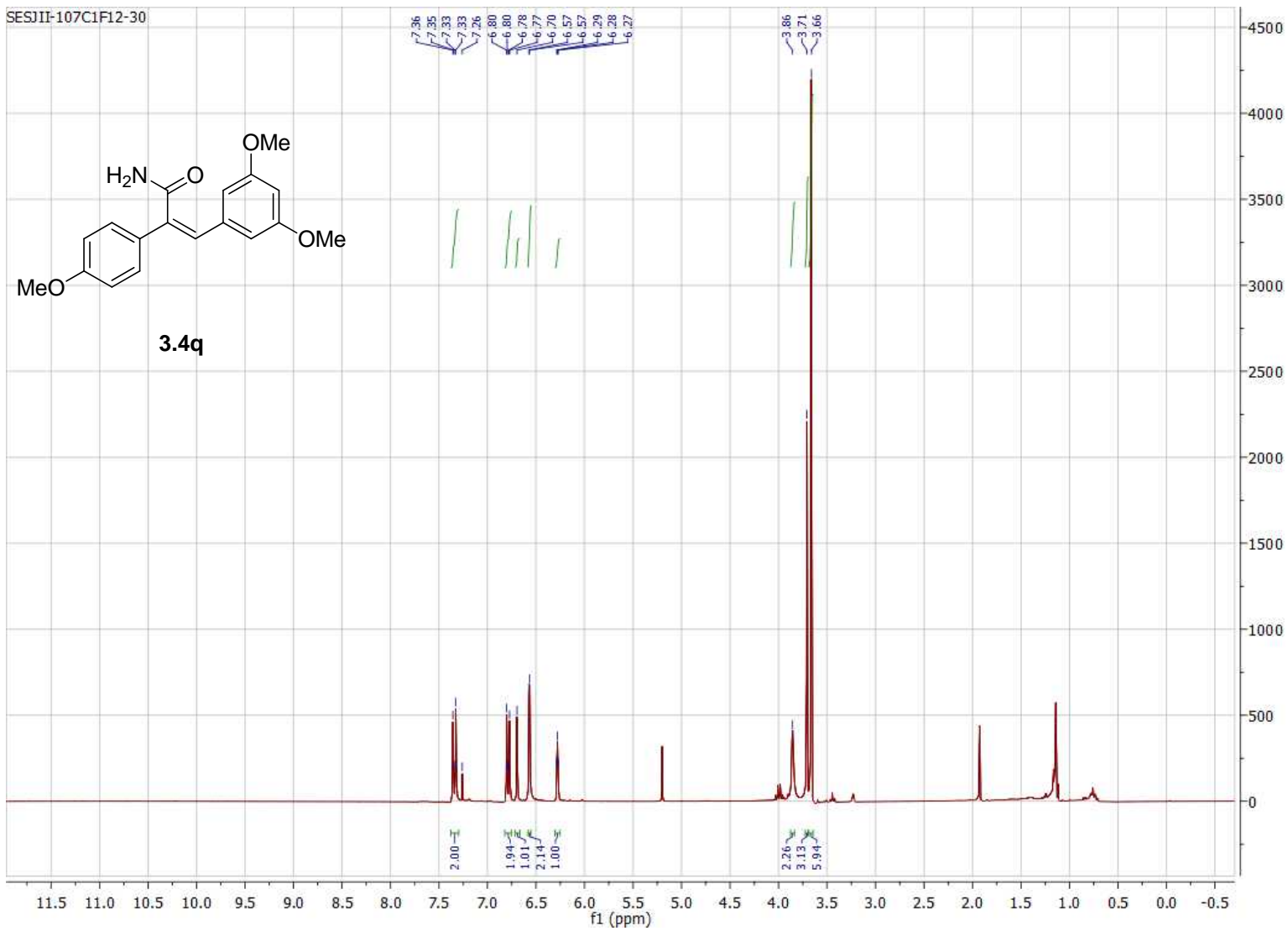


Figure B.44. 300 MHz ^1H NMR of compound **3.4q** in CDCl_3 .

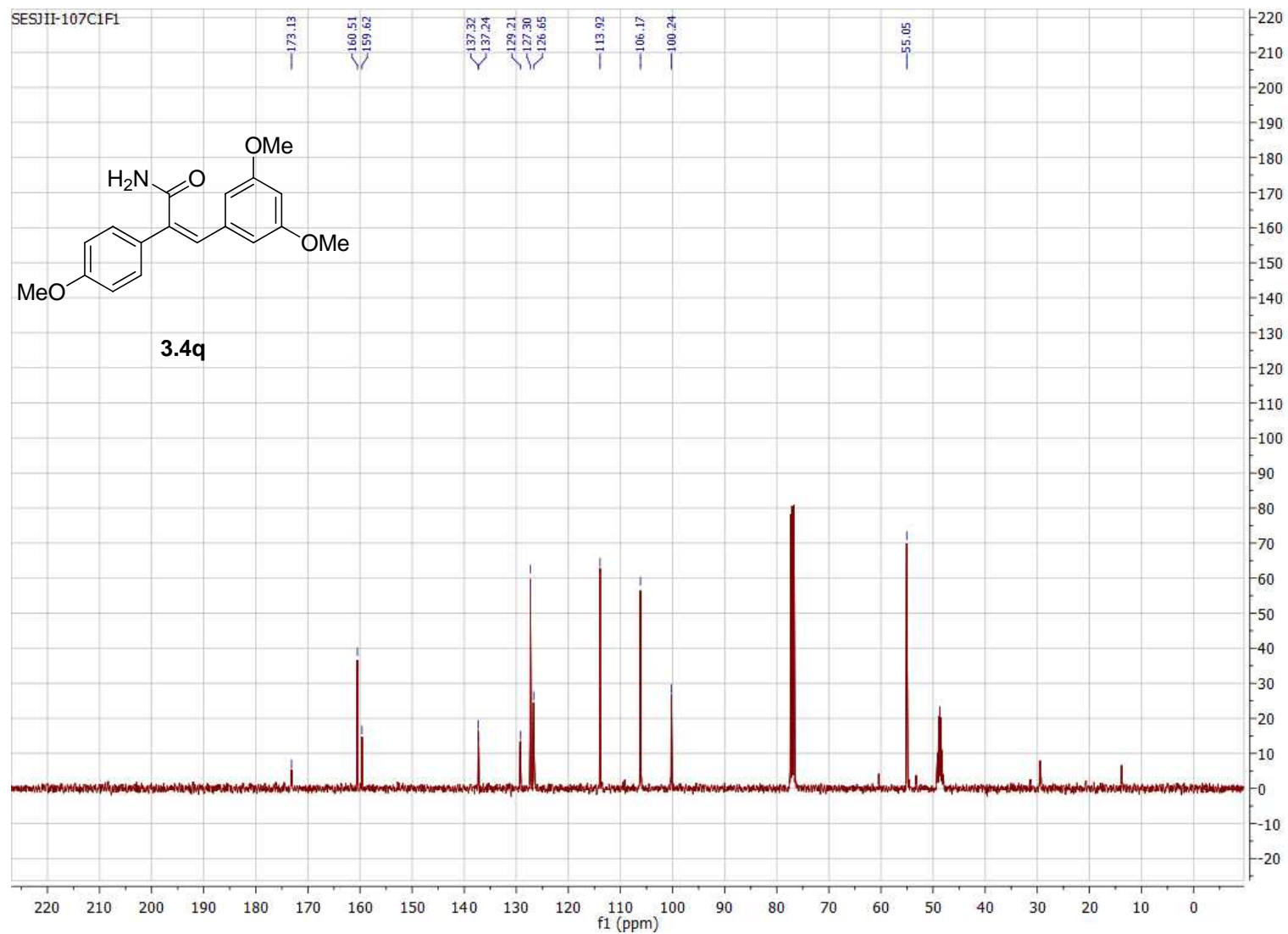


Figure B.45. 100 MHz ^{13}C NMR of compound **3.4q** in CDCl_3 .

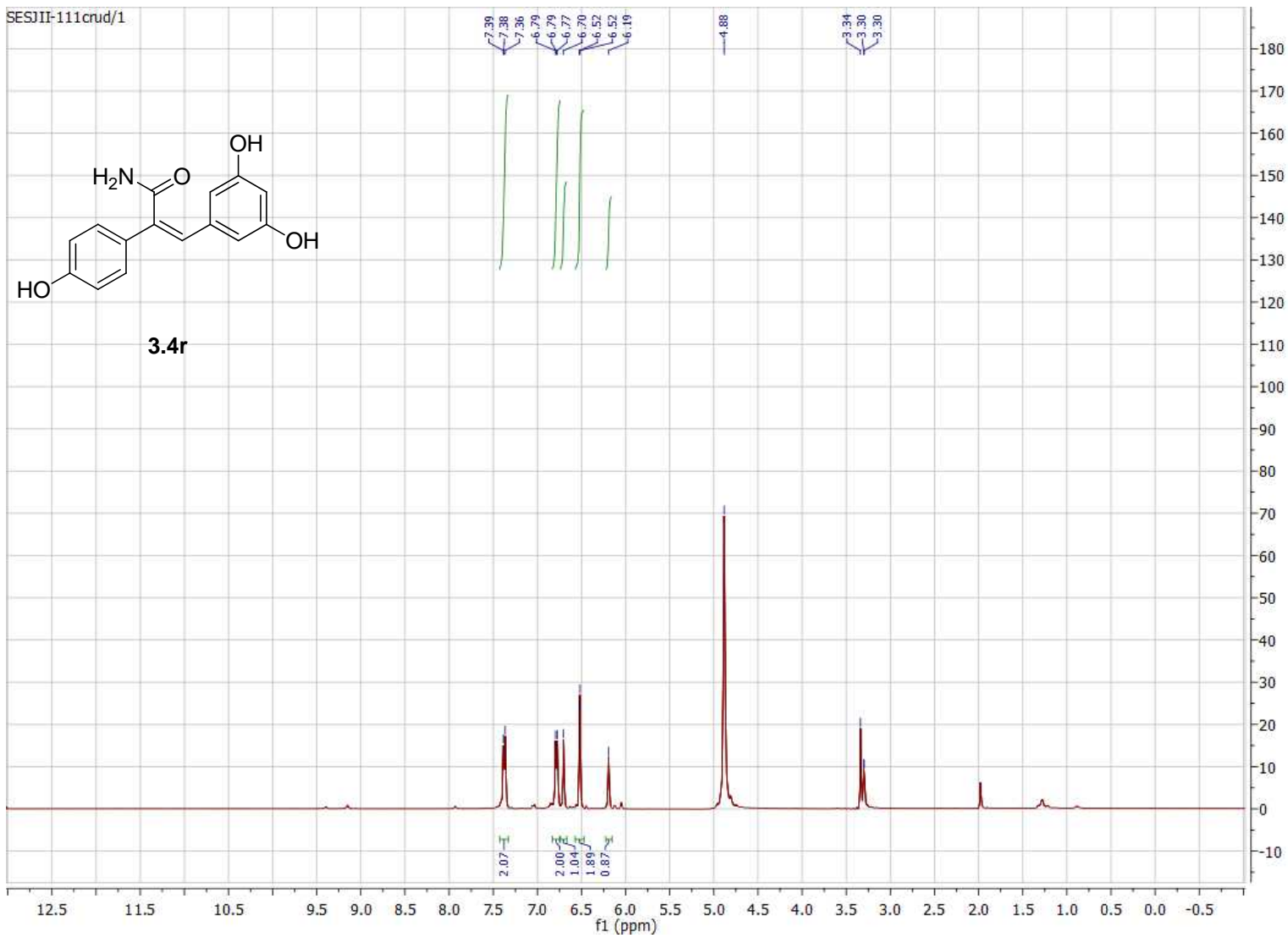


Figure B.46. 400 MHz ^1H NMR of compound **3.4r** in CD_3OD .

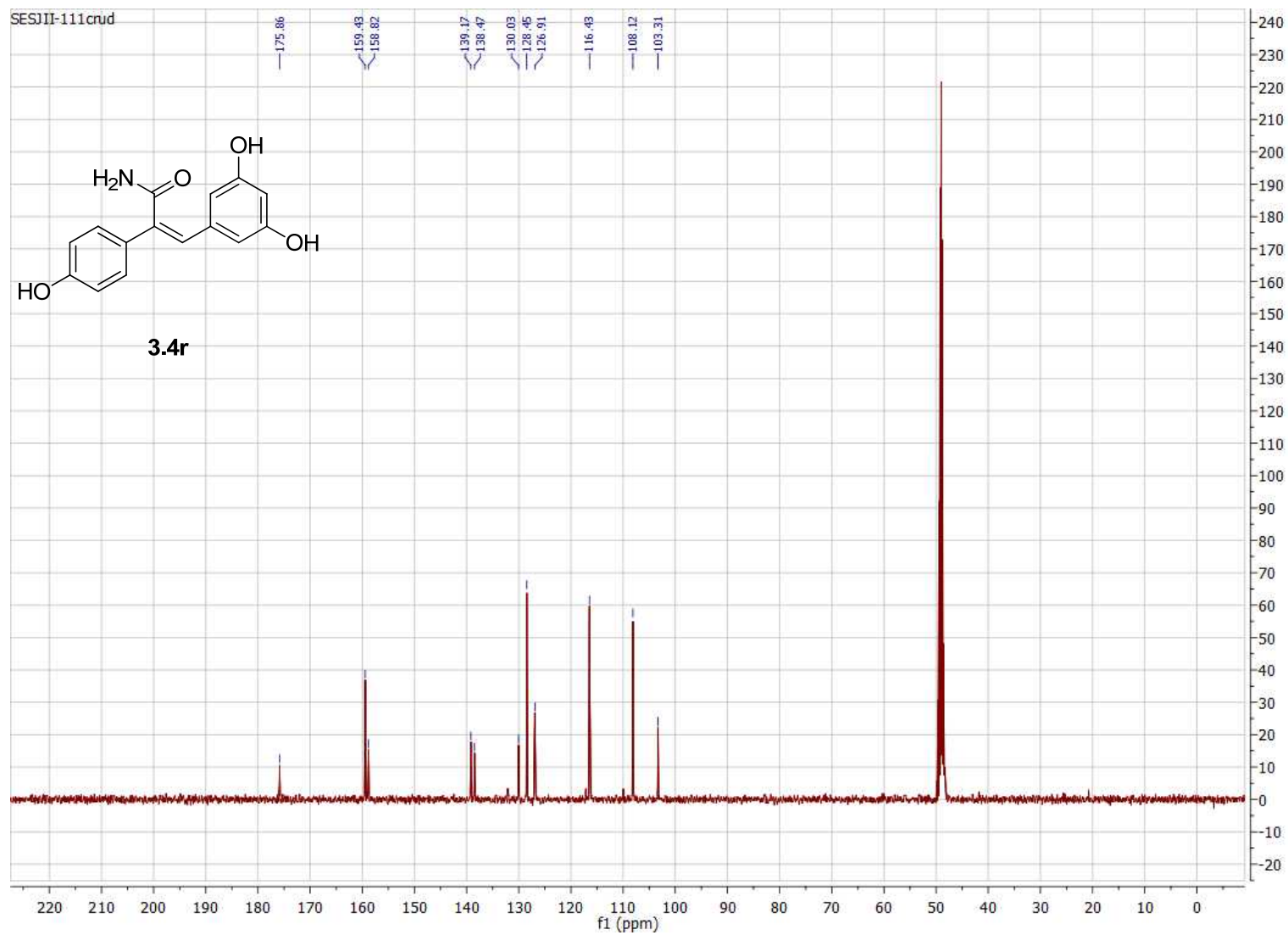


Figure B.47. 100 MHz ^{13}C NMR of compound **3.4r** in CD_3OD .

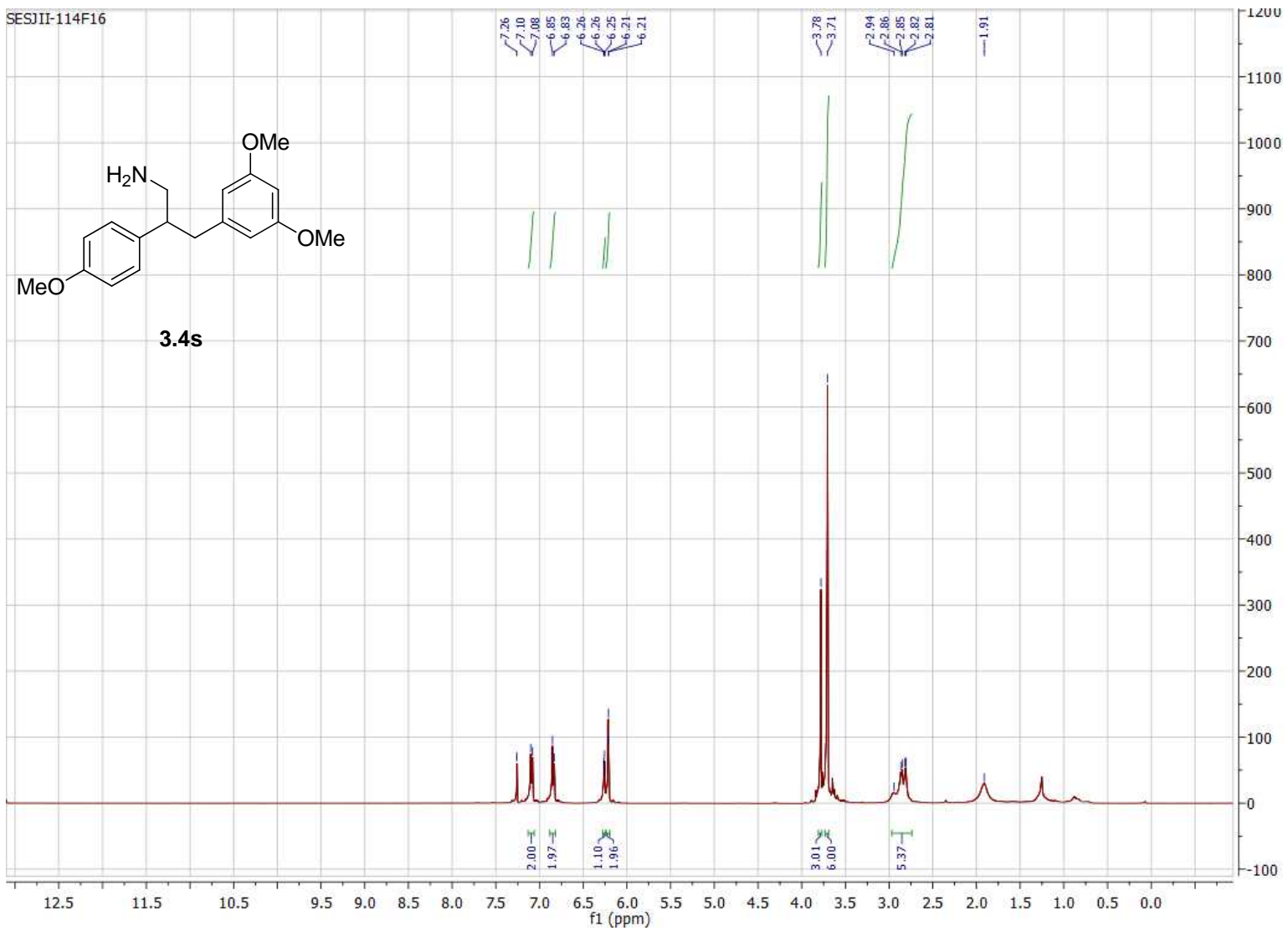


Figure B.48. 400 MHz ^1H NMR of compound **3.4s** in CDCl_3 .

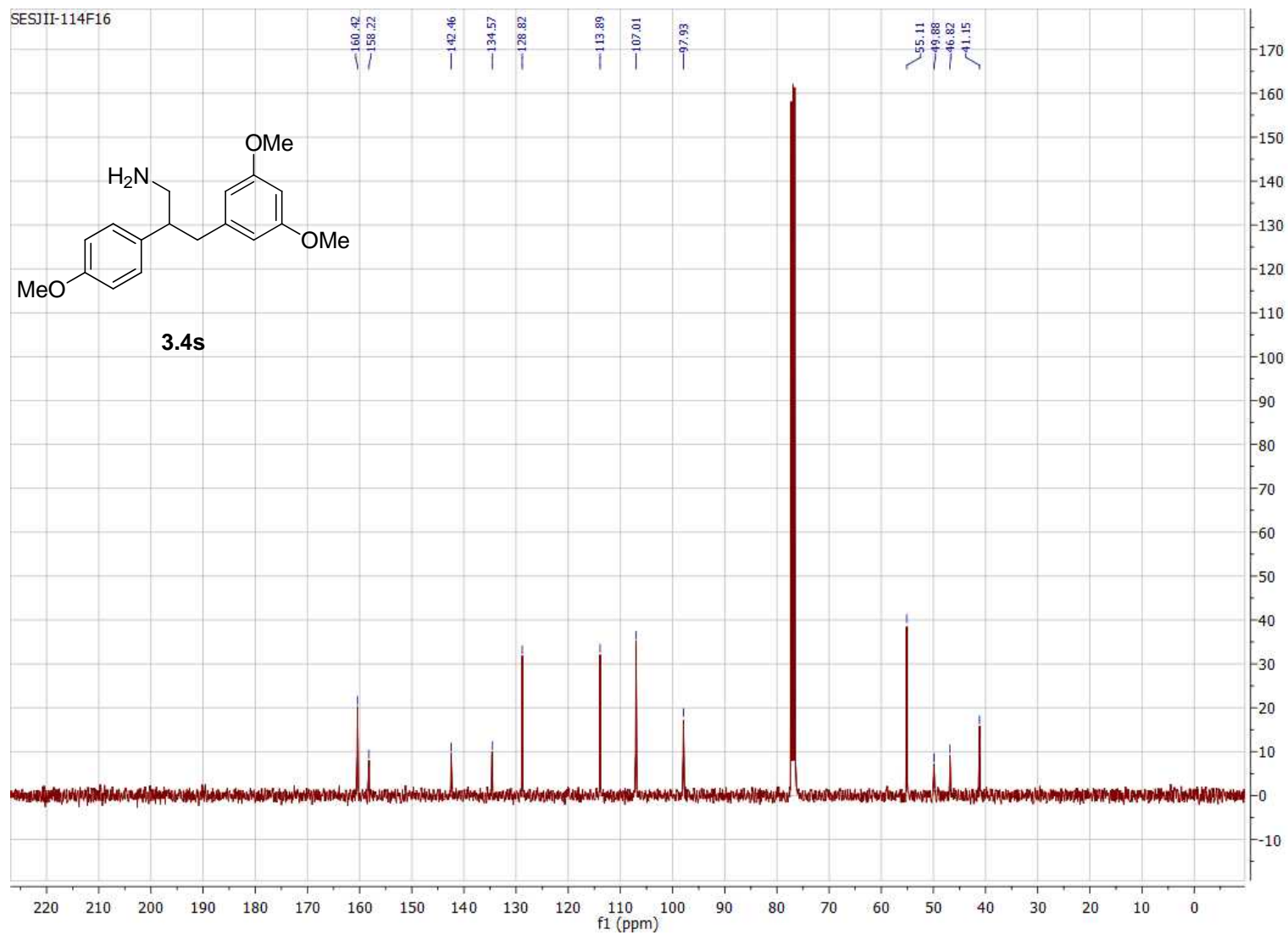


Figure B.49. 100 MHz ^{13}C NMR of compound **3.4s** in CDCl_3 .

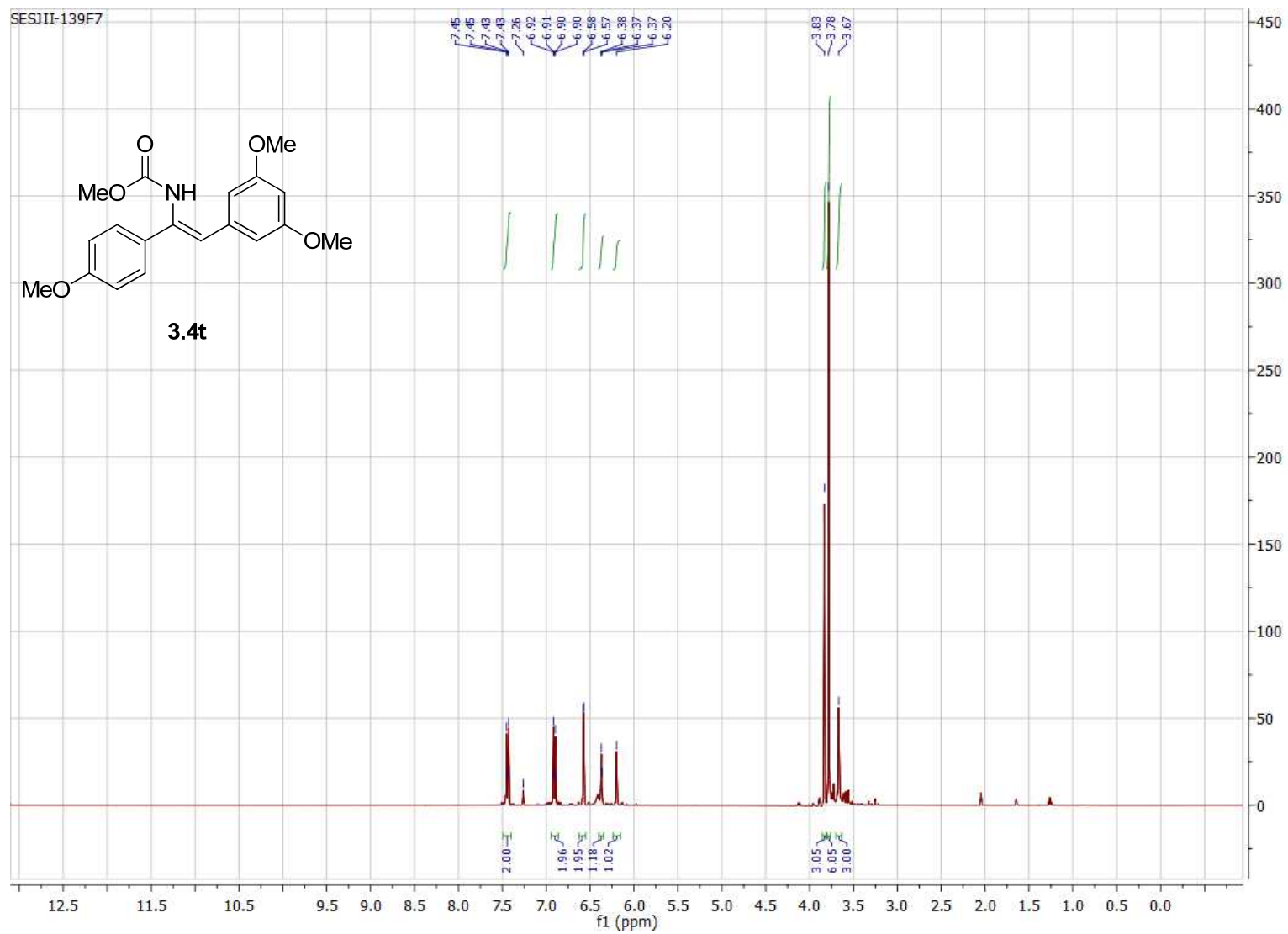


Figure B.50. 400 MHz ^1H NMR of compound **3.4t** in CDCl_3 .

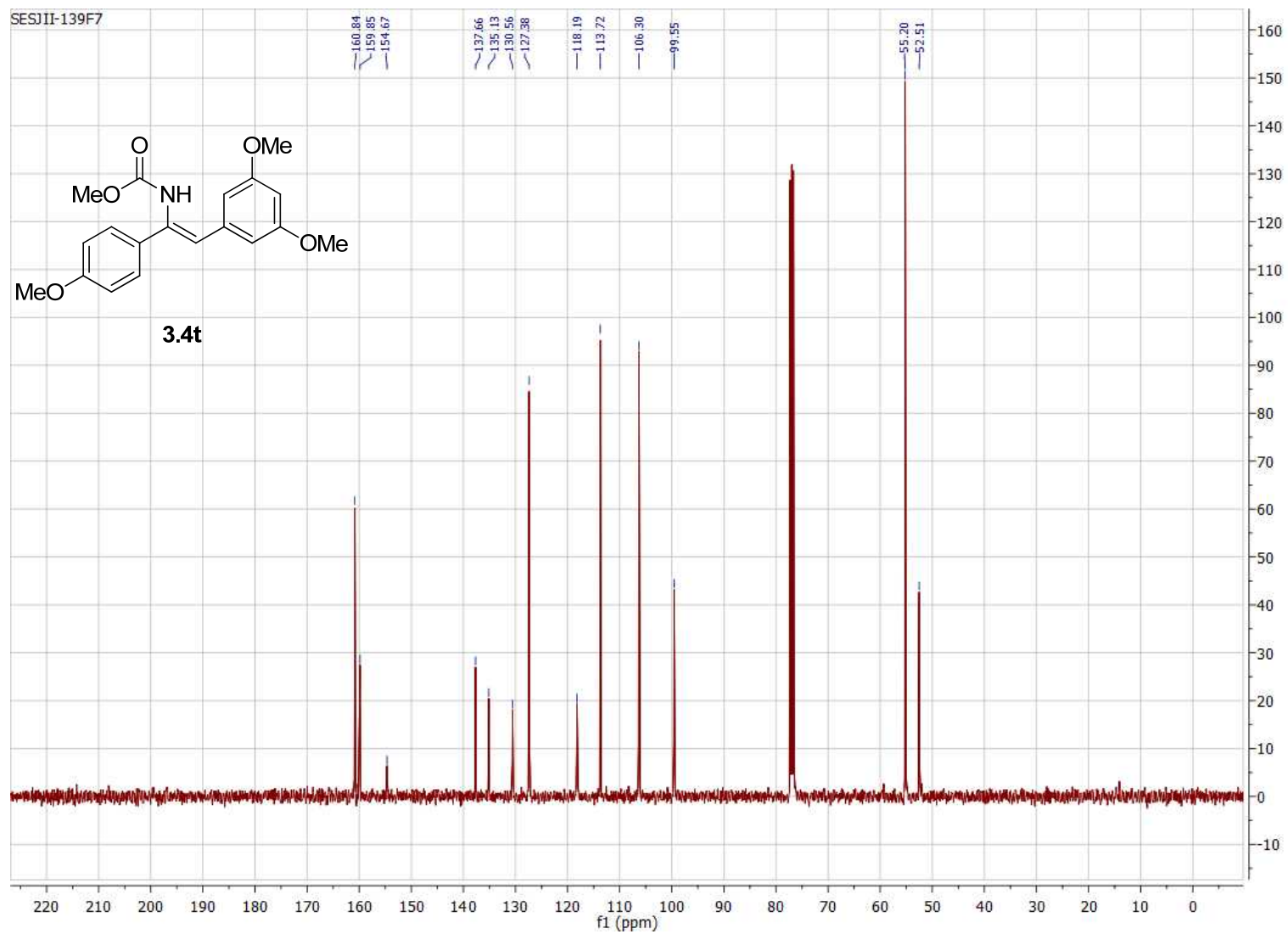


Figure B.51. 100 MHz ^{13}C NMR of compound **3.4t** in CDCl_3 .

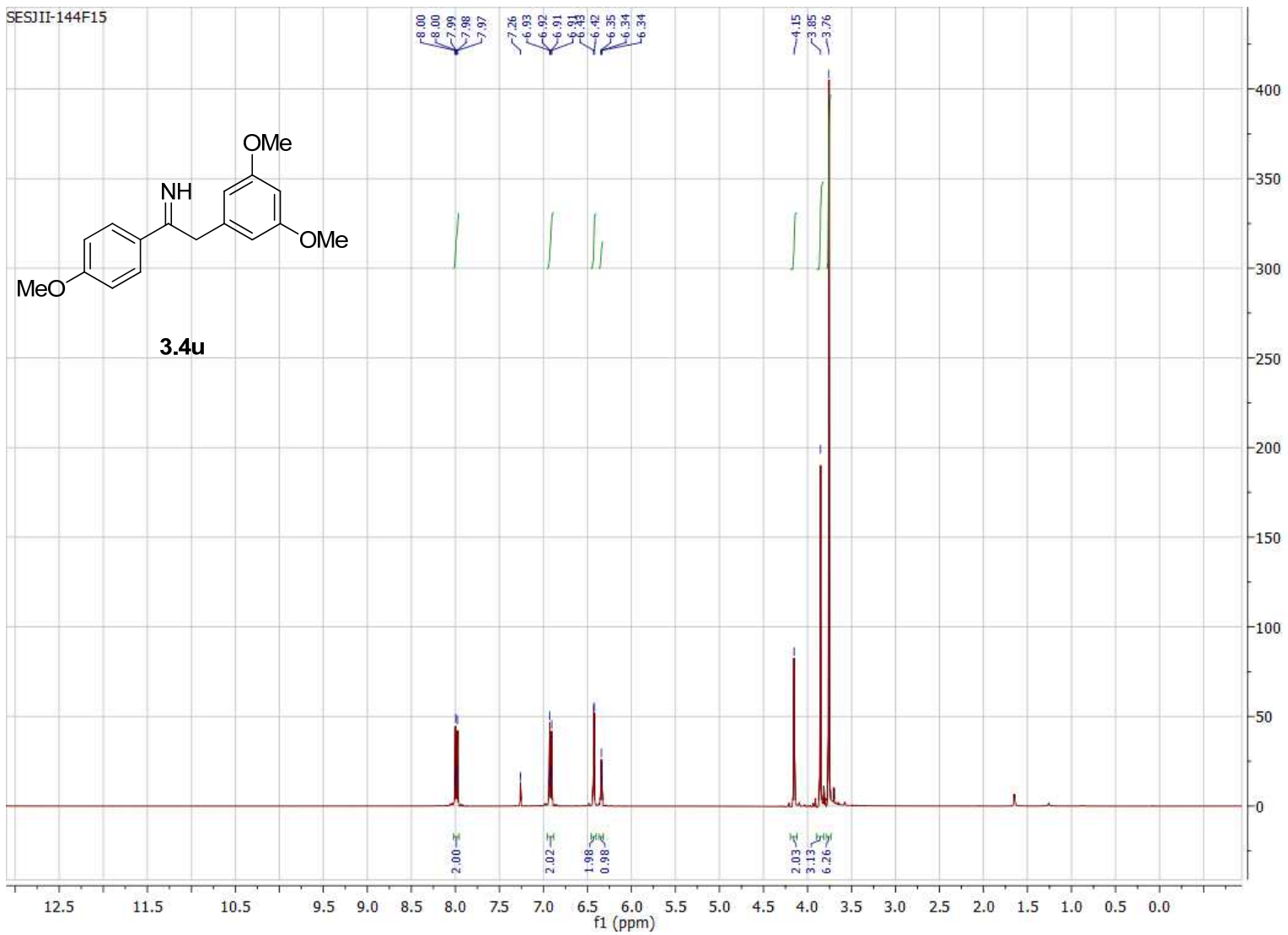


Figure B.52. 400 MHz ^1H NMR of compound **3.4u** in CDCl_3 .

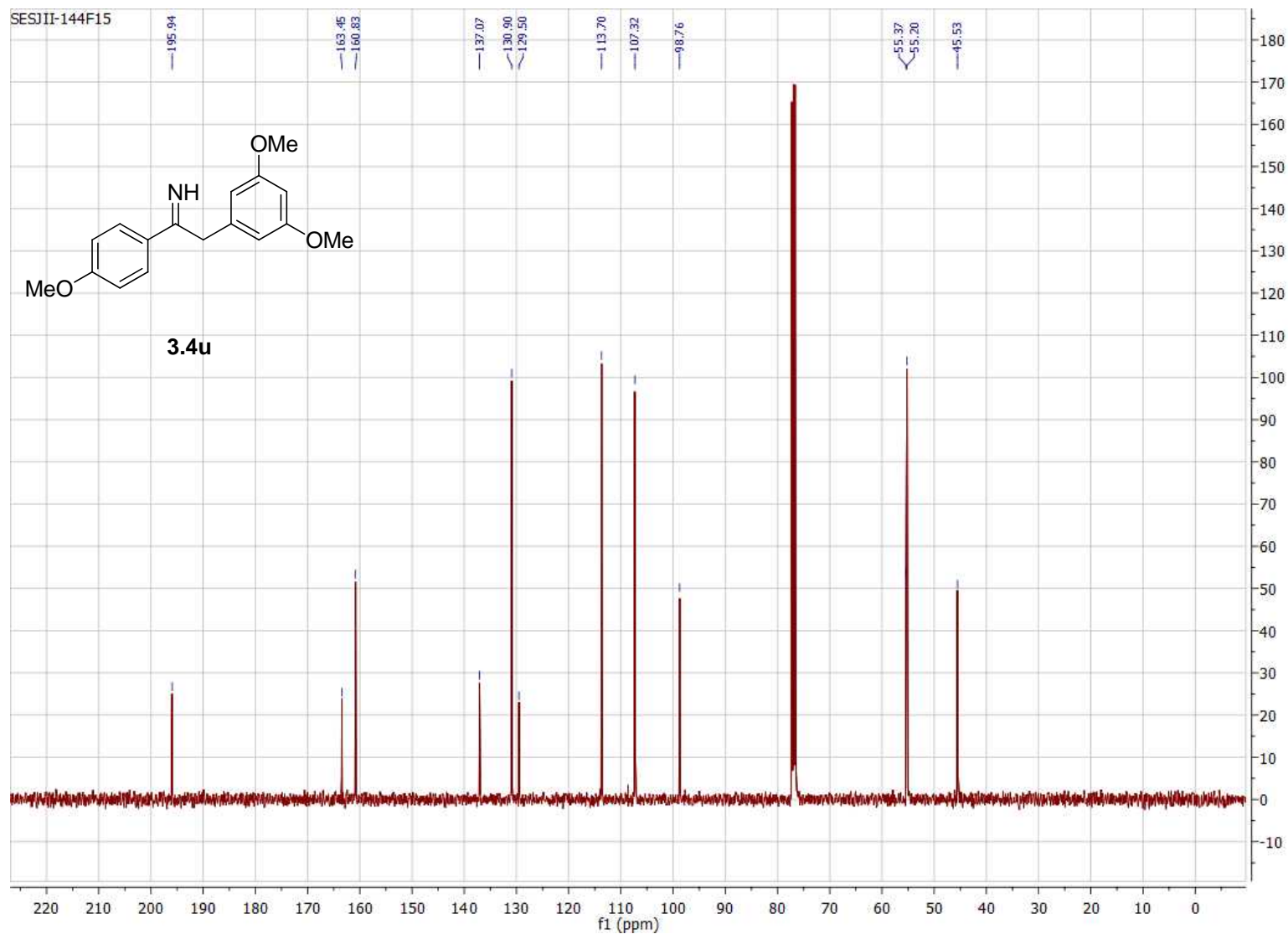


Figure B.53. 100 MHz ^{13}C NMR of compound **3.4u** in CDCl_3 .

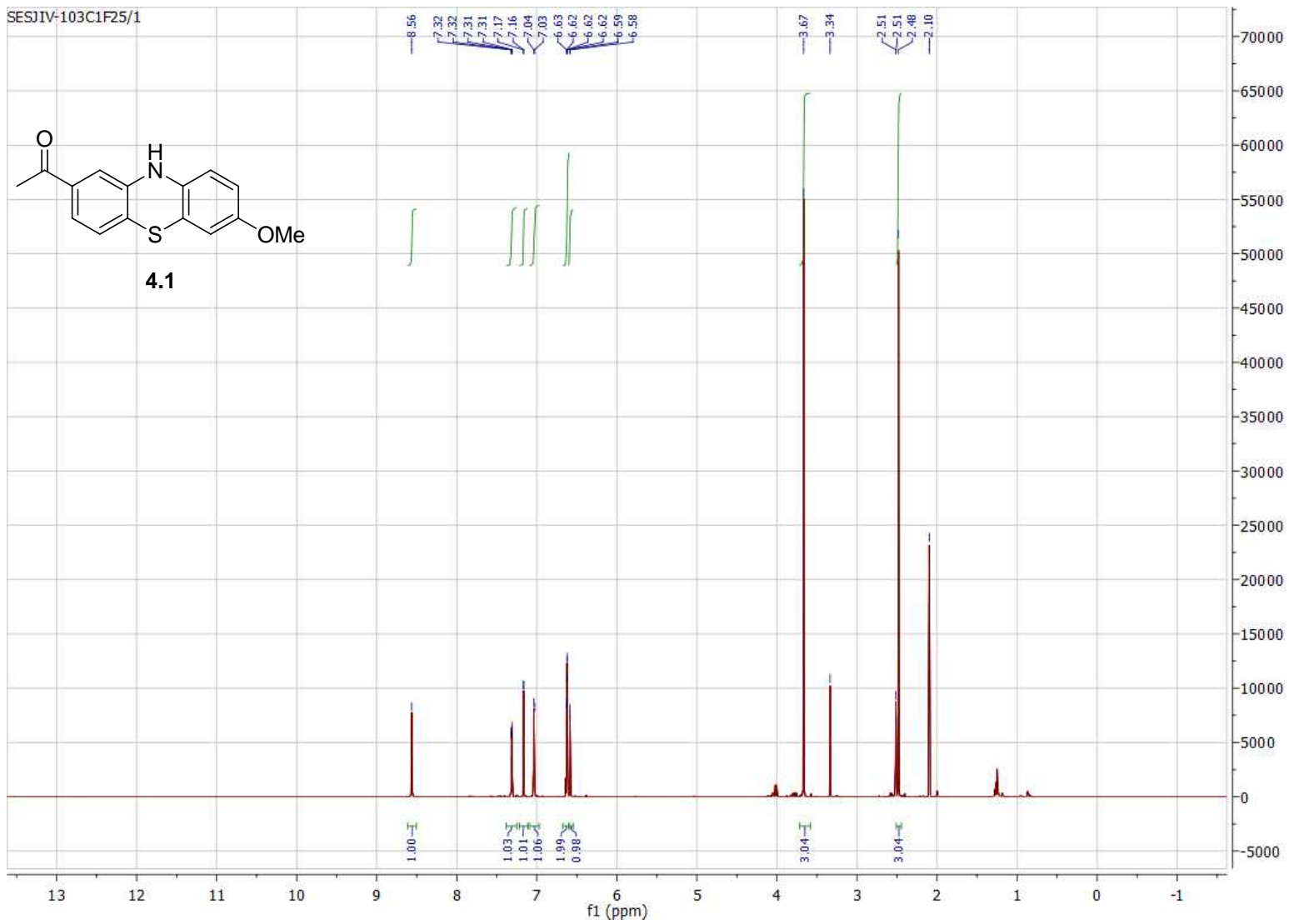


Figure B.54. 800 MHz ^1H NMR of compound **4.1** in d^6 -DMSO.

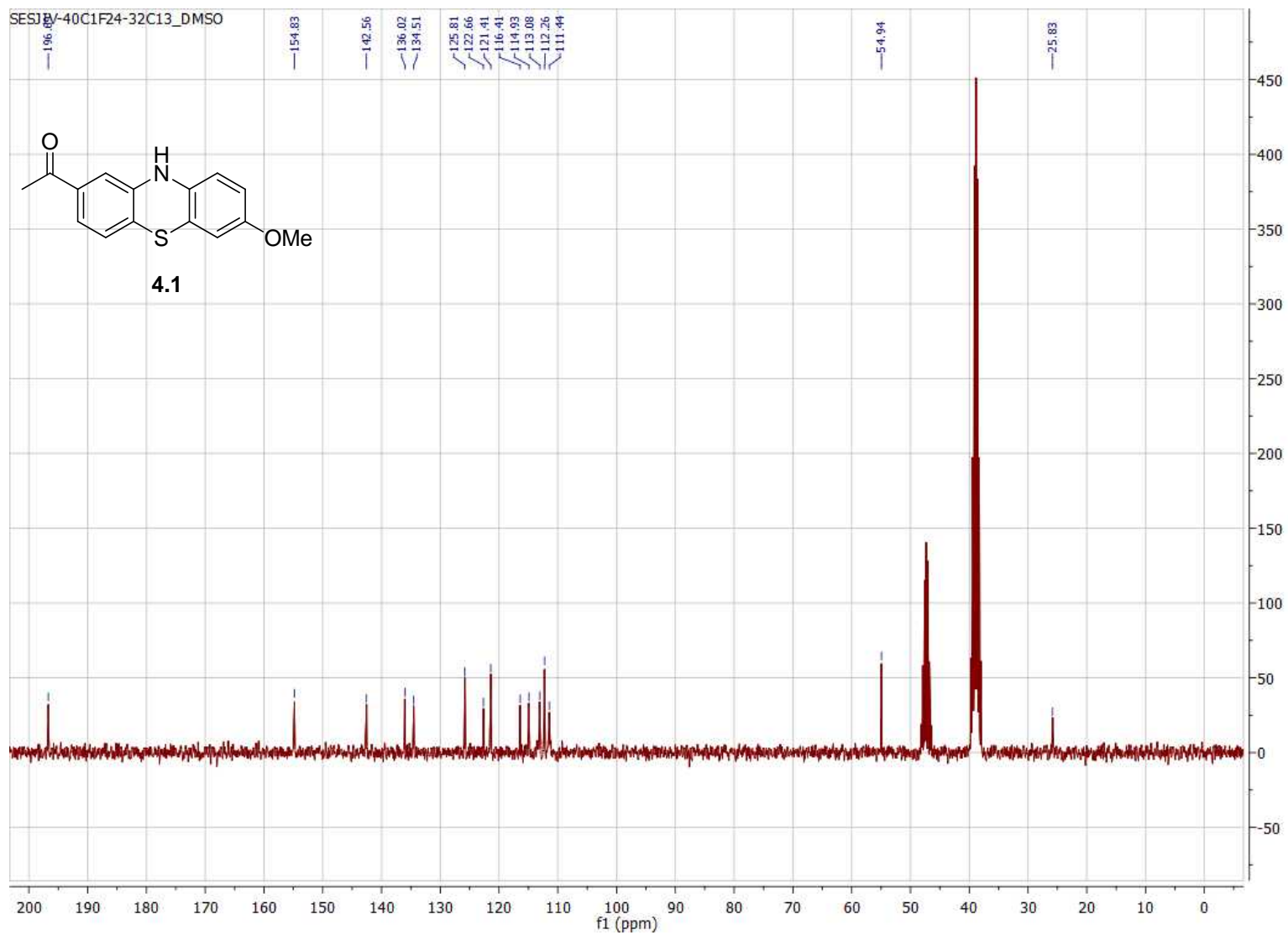


Figure B.55. 75 MHz ^{13}C NMR of compound **4.1** in d^6 -DMSO: CD_3OD .

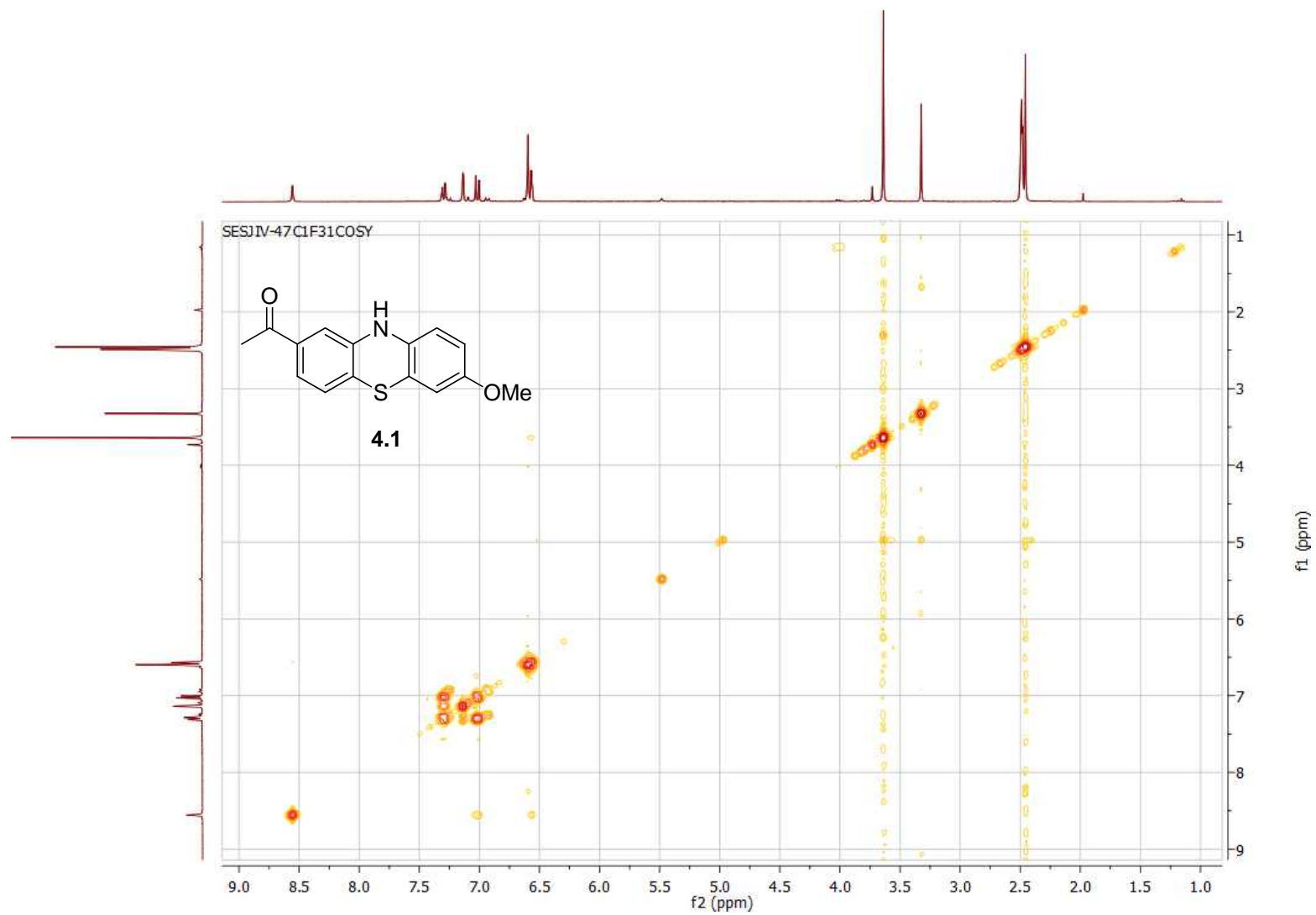


Figure B.56. 800 MHz COSY NMR of compound **4.1** in d^6 -DMSO:CD₃OD.

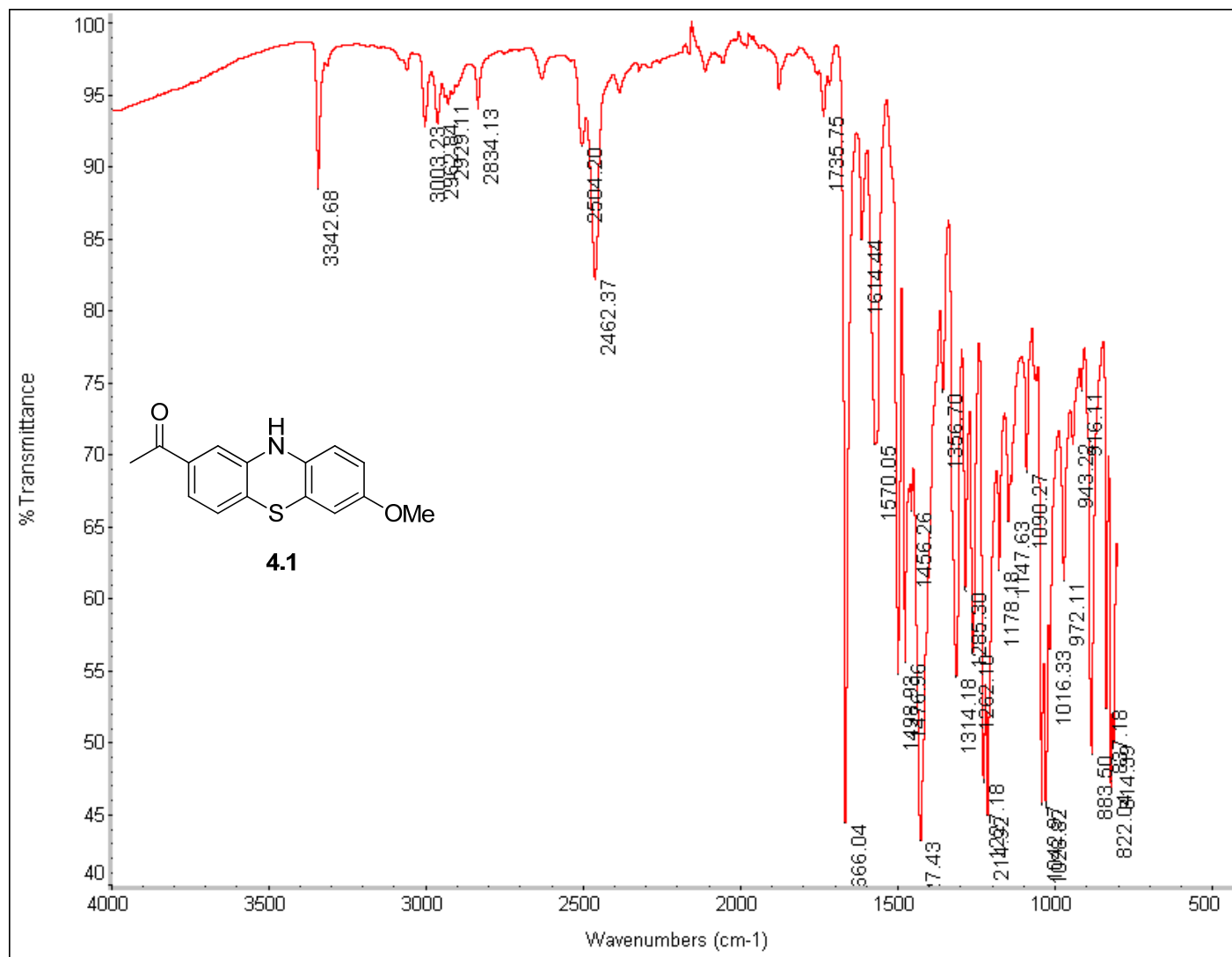


Figure B.57. FTIR of compound 4.1.

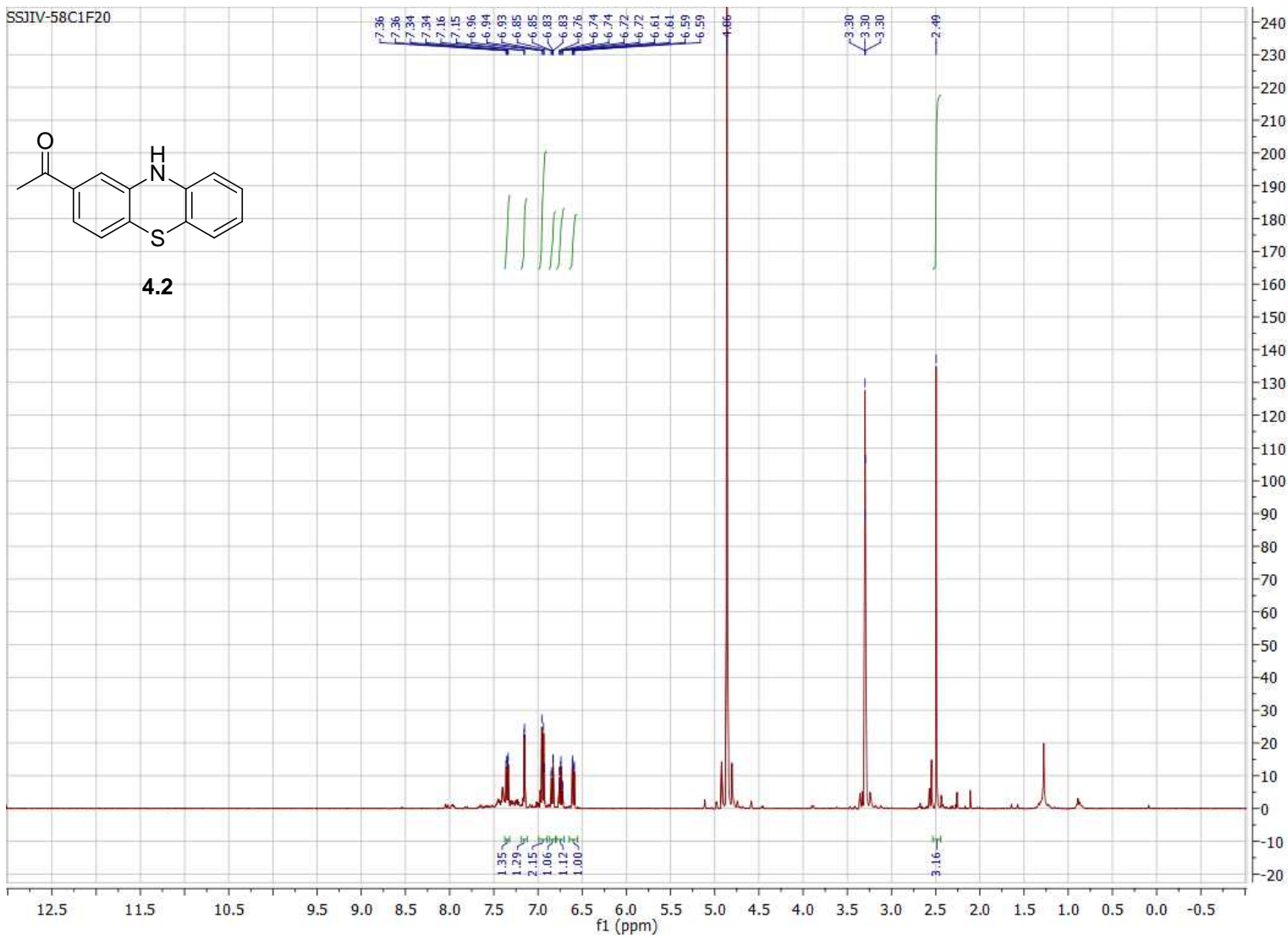


Figure B.58. 400 MHz ^1H NMR of compound **4.2** in CD_3OD .

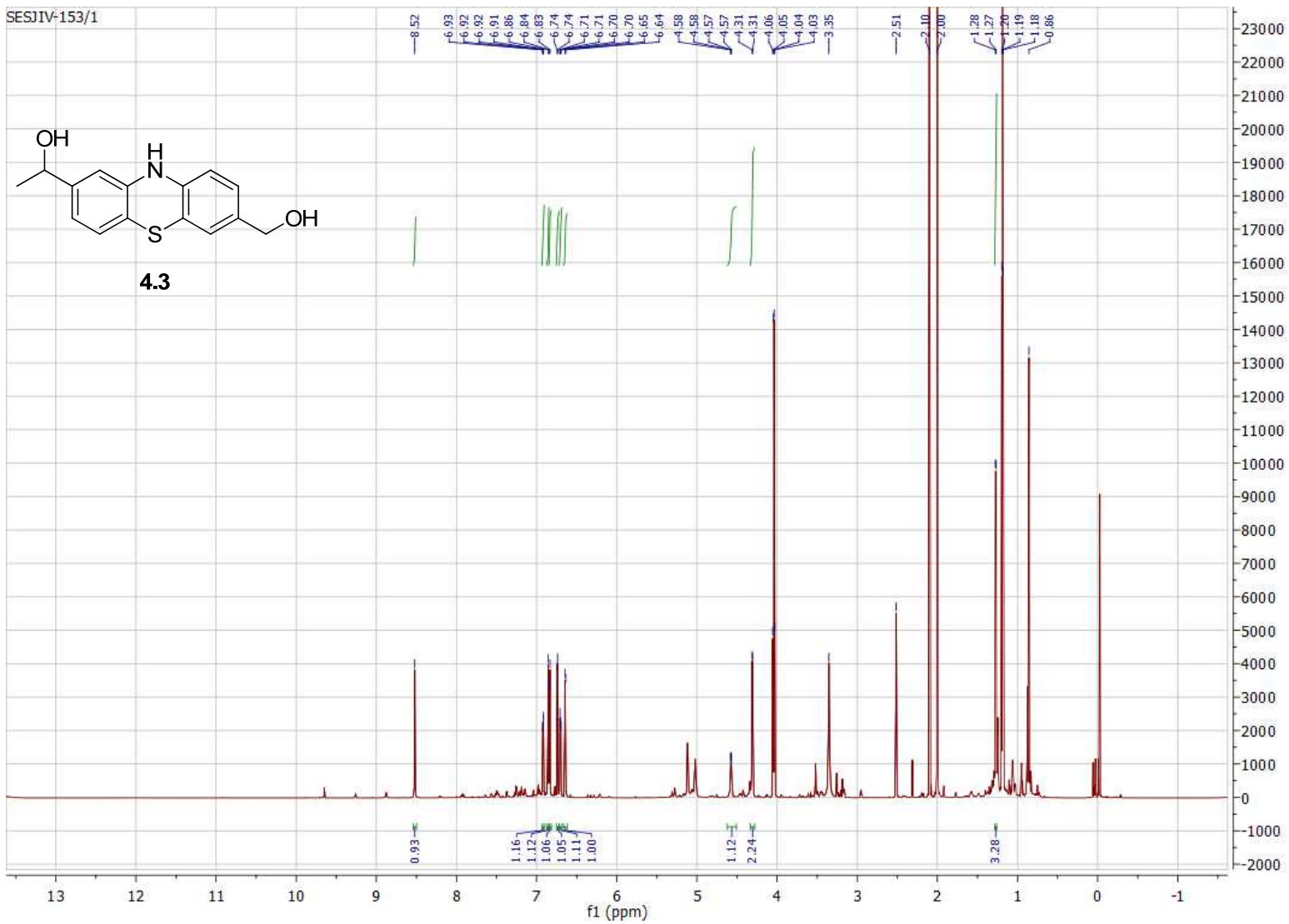


Figure B.59. 800 MHz ^1H NMR of crude compound **4.3** in d^6 -DMSO.

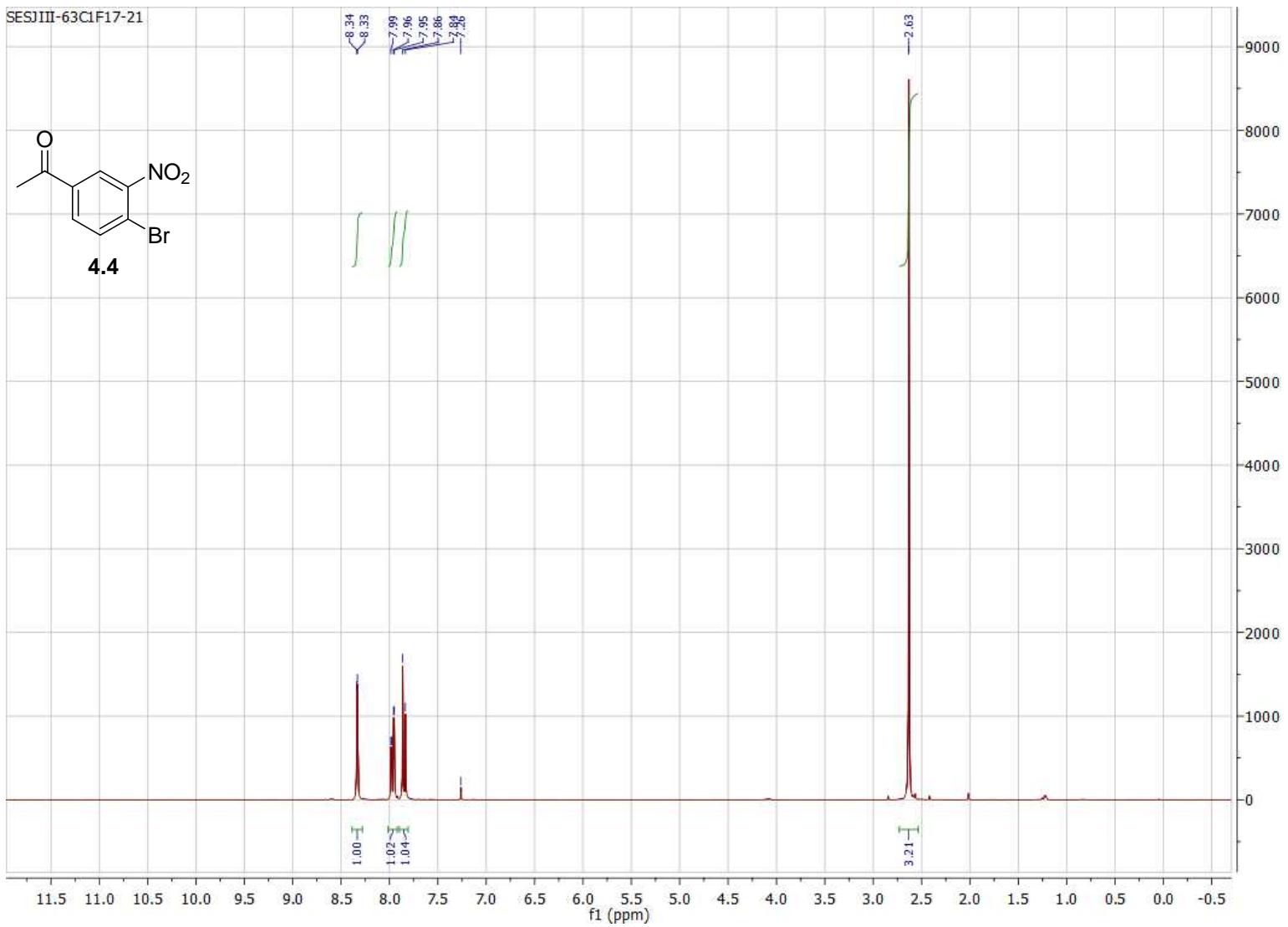


Figure B.60. 300 MHz ^1H NMR of compound **4.4** in CDCl_3 .

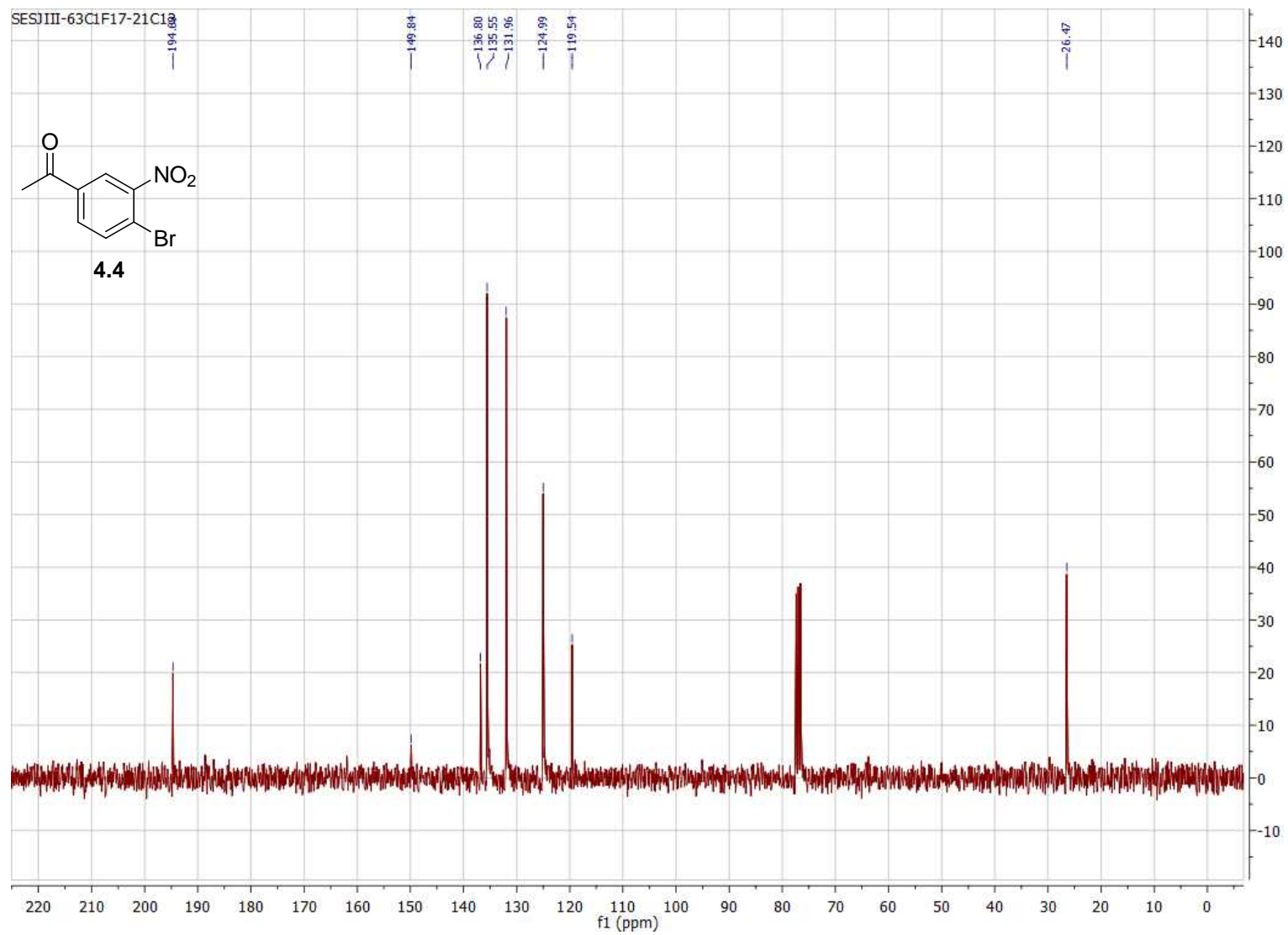


Figure B.61. 300 MHz ^{13}C NMR of compound **4.4** in CDCl_3 .

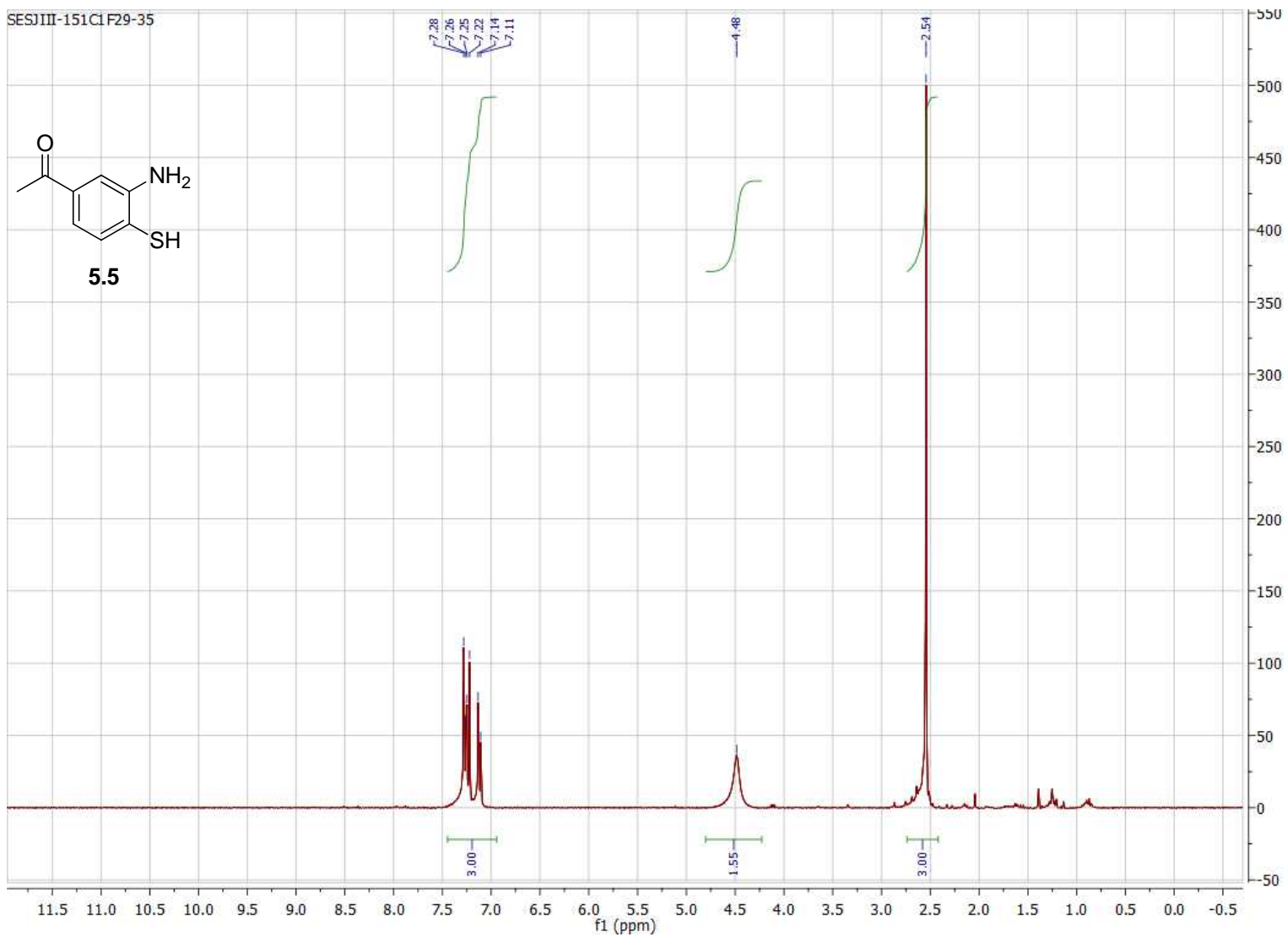


Figure B.62. 300 MHz ^1H NMR of compound **4.5** in CDCl_3 .

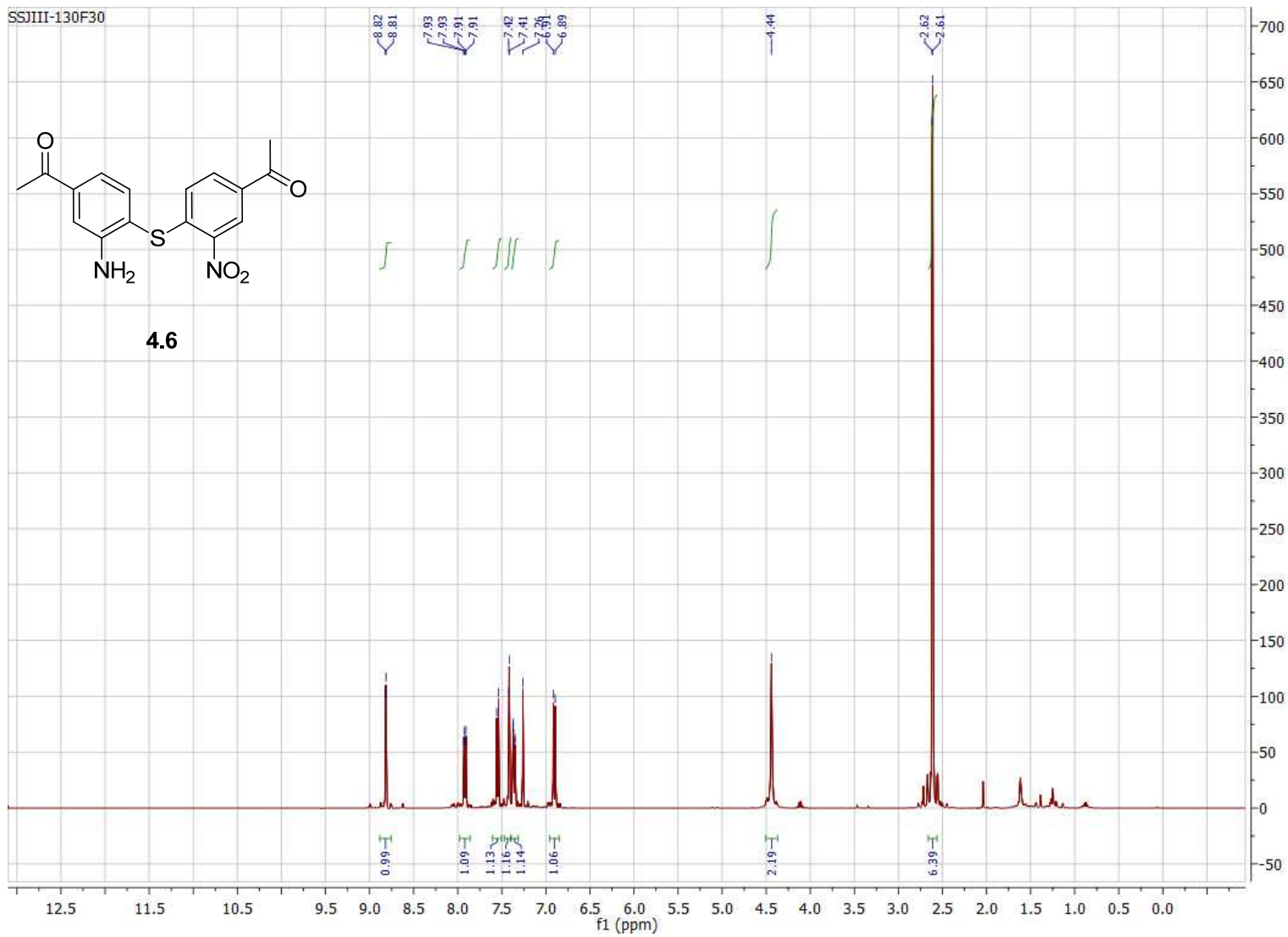


Figure B.63. 400 MHz ^1H NMR of compound **4.6** in CDCl_3 .

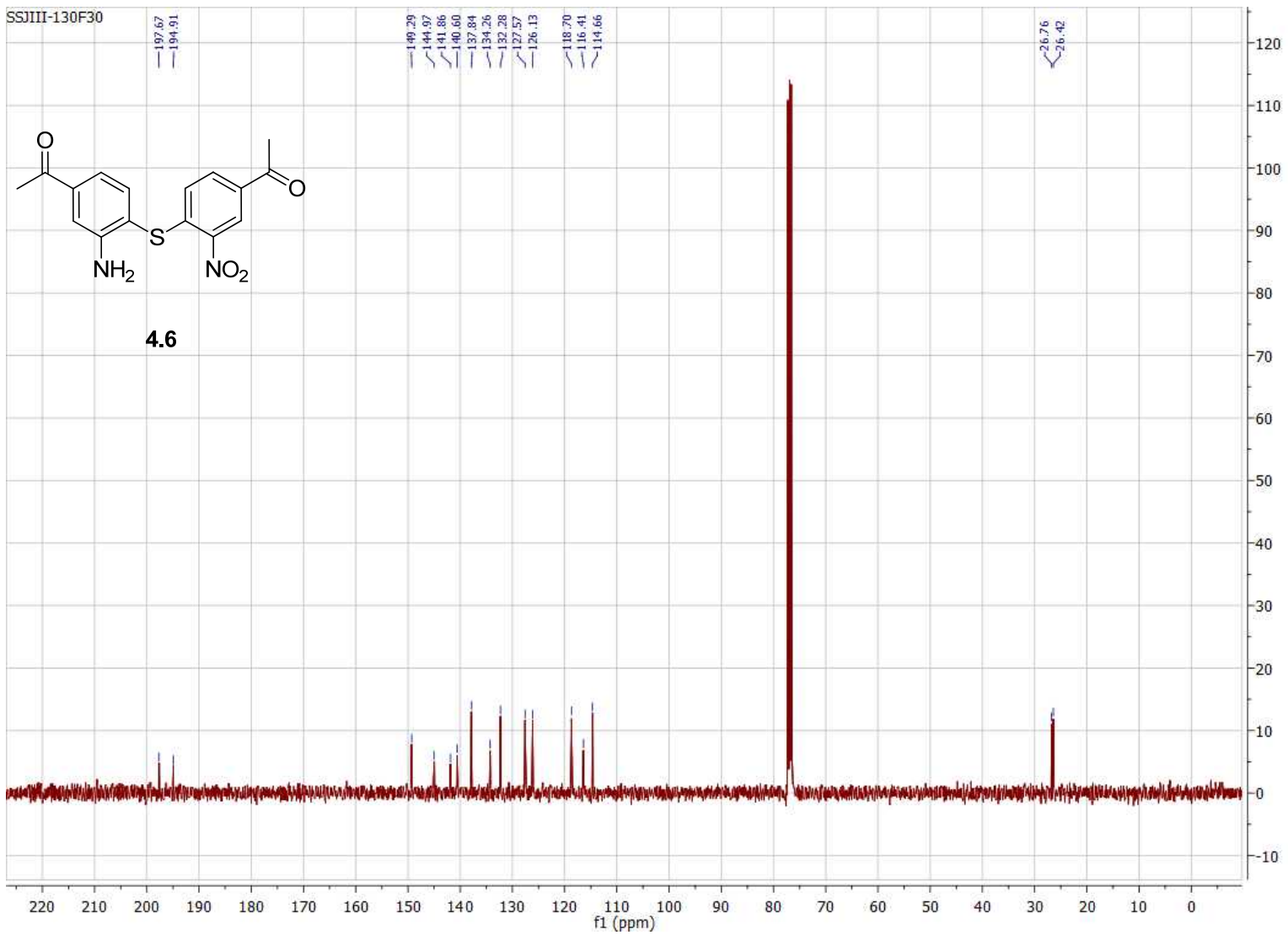


Figure B.64. 100 MHz ^{13}C NMR of compound **4.6** in CDCl_3 .

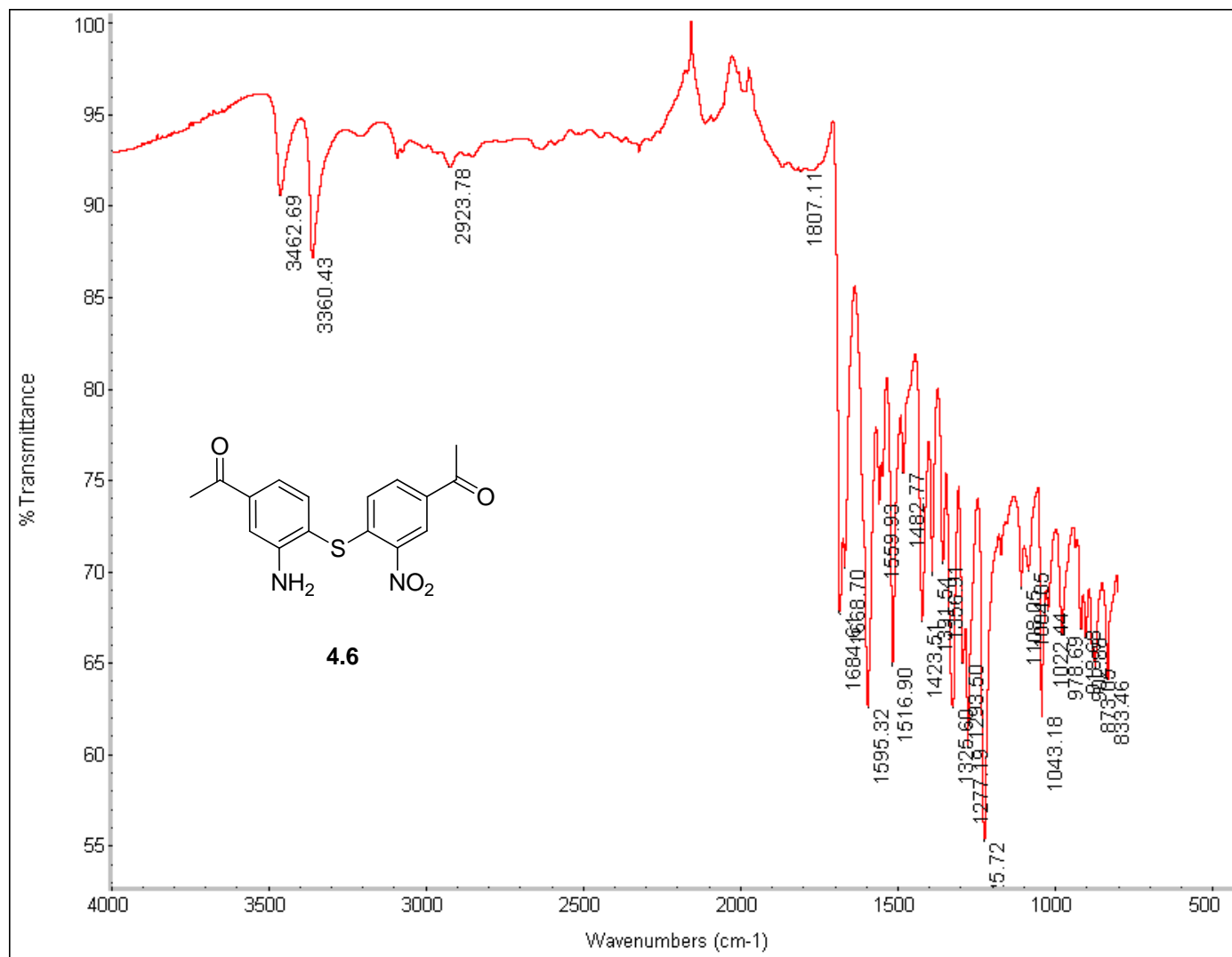


Figure B.65. FTIR of compound 4.6.

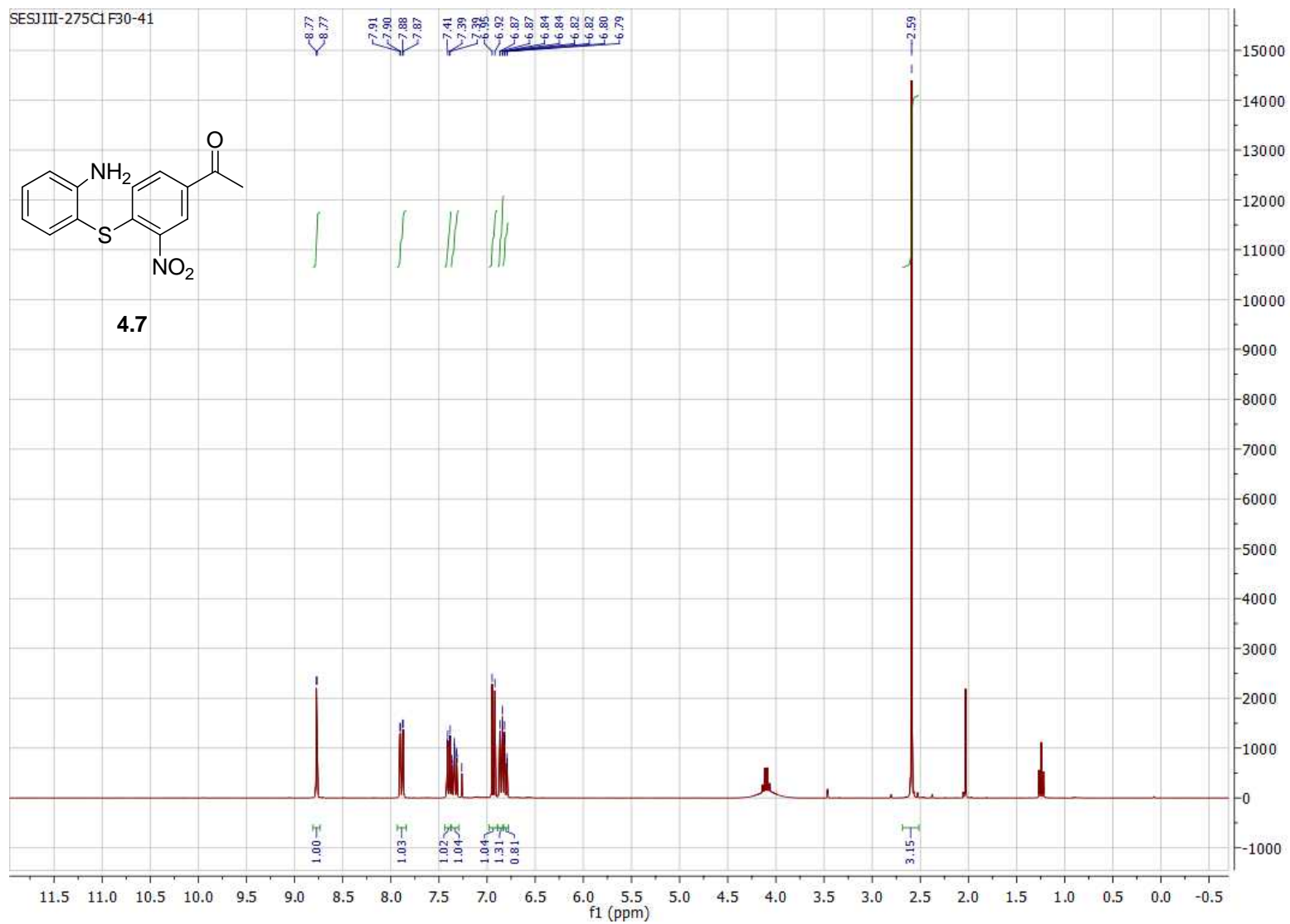


Figure B.66. 300 MHz ^1H NMR of compound **4.7** in CDCl_3 .

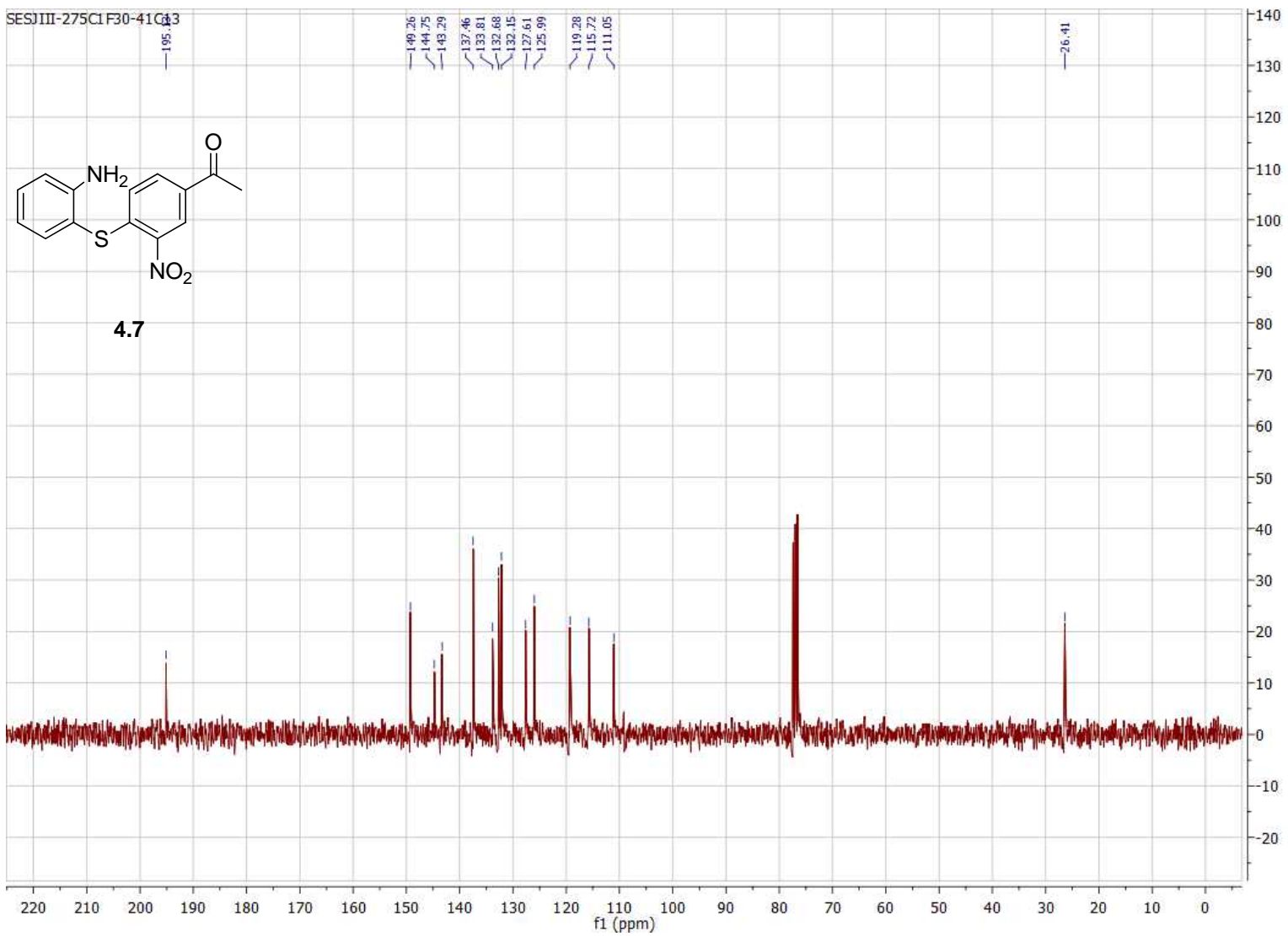


Figure B.67. 75 MHz ^{13}C NMR of compound **4.7** in CDCl_3 .

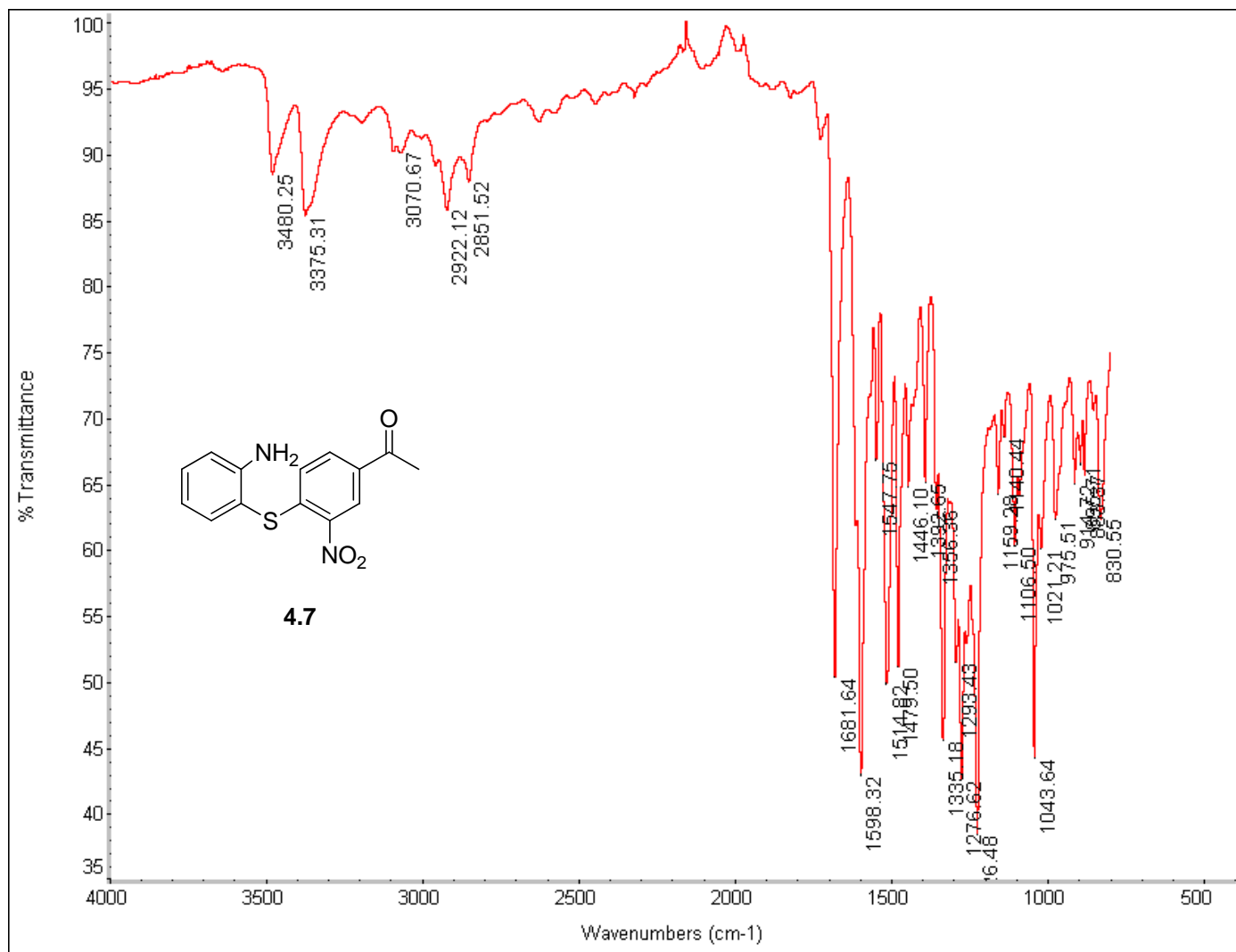


Figure B.68. FTIR compound 4.7.

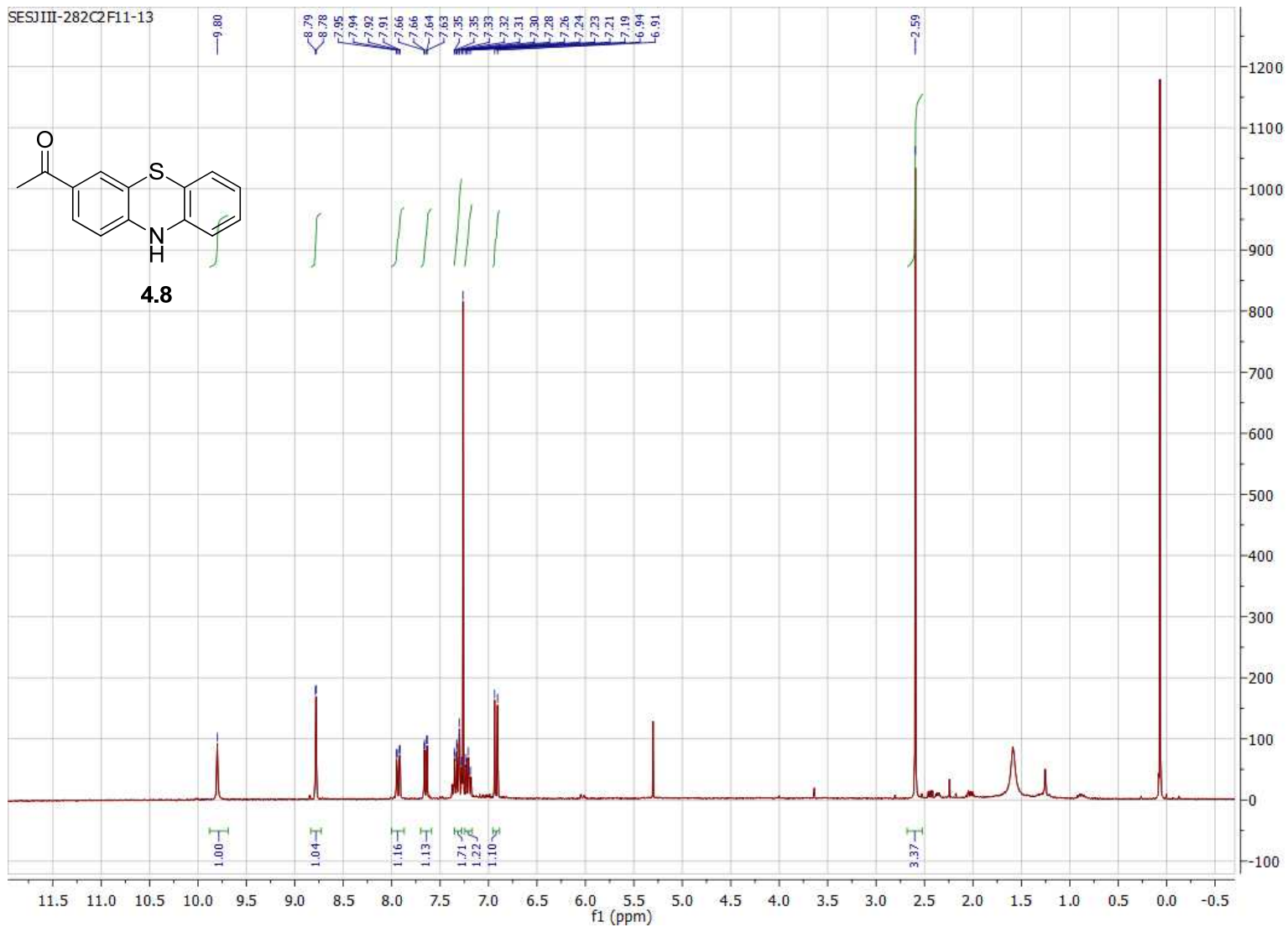


Figure B.69. 300 MHz ^1H NMR of compound **4.8** in CDCl_3 .

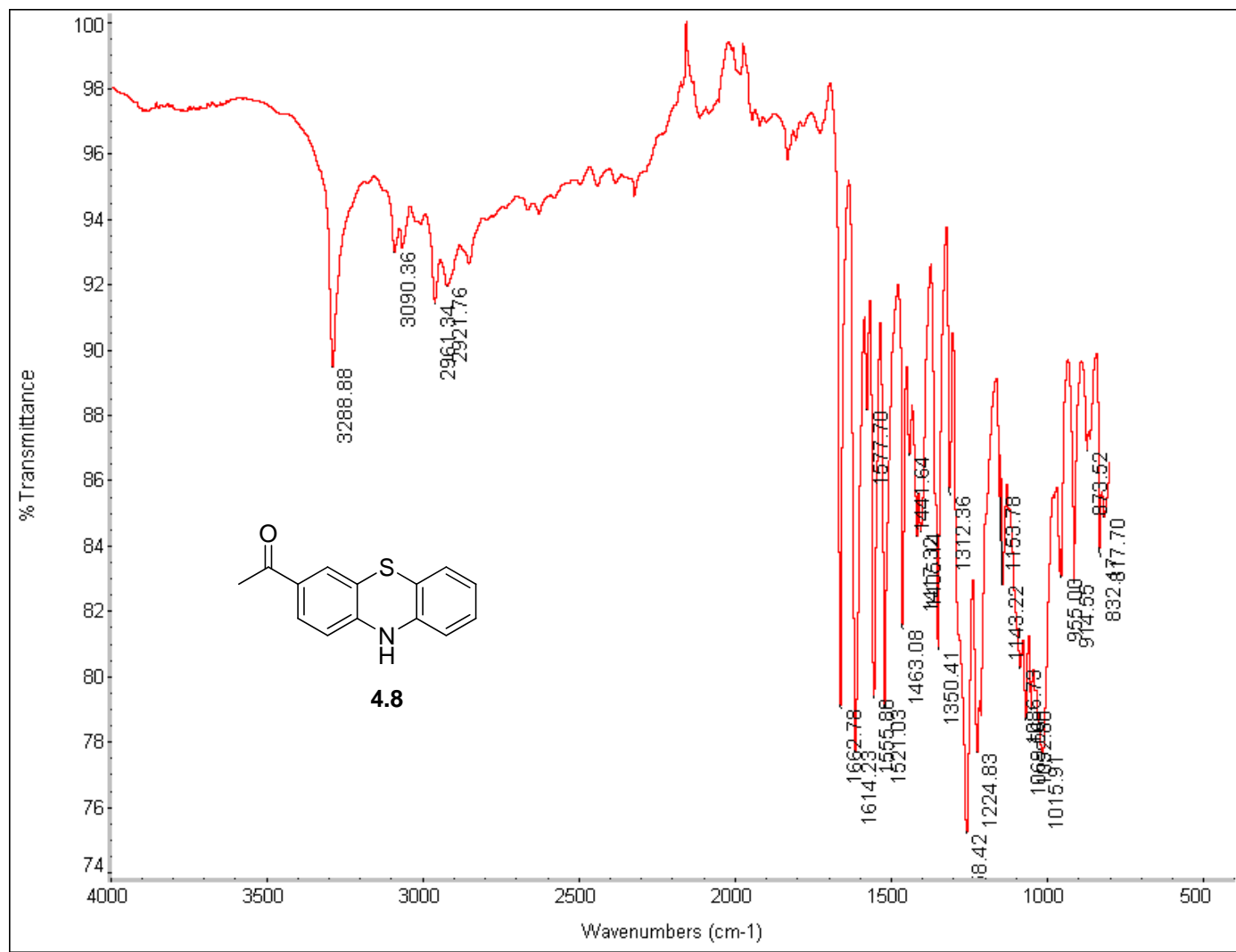


Figure B.70. FTIR of compound 4.8.

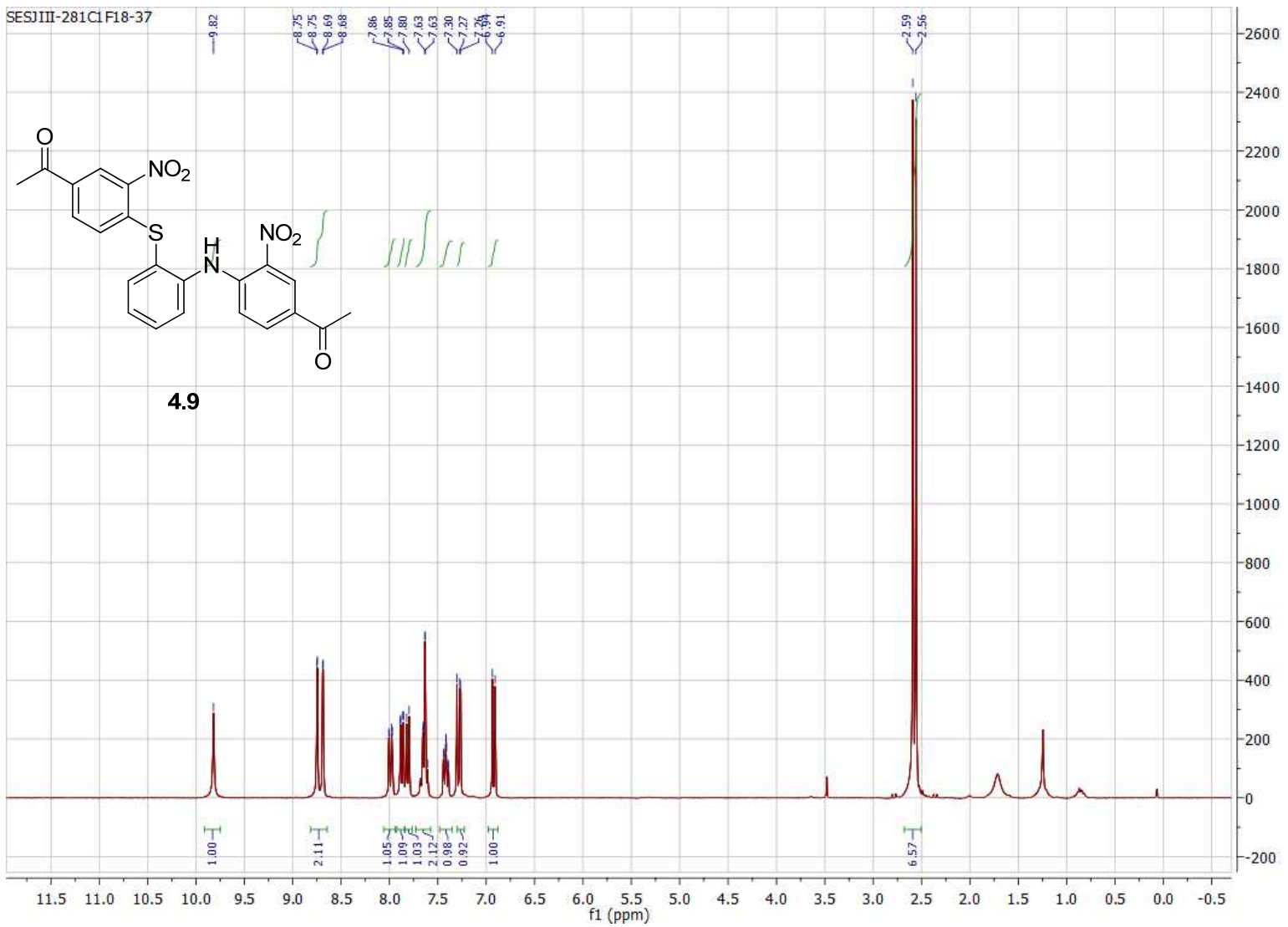


Figure B.71. 300 MHz ^1H NMR of compound **4.9** in CDCl_3 .

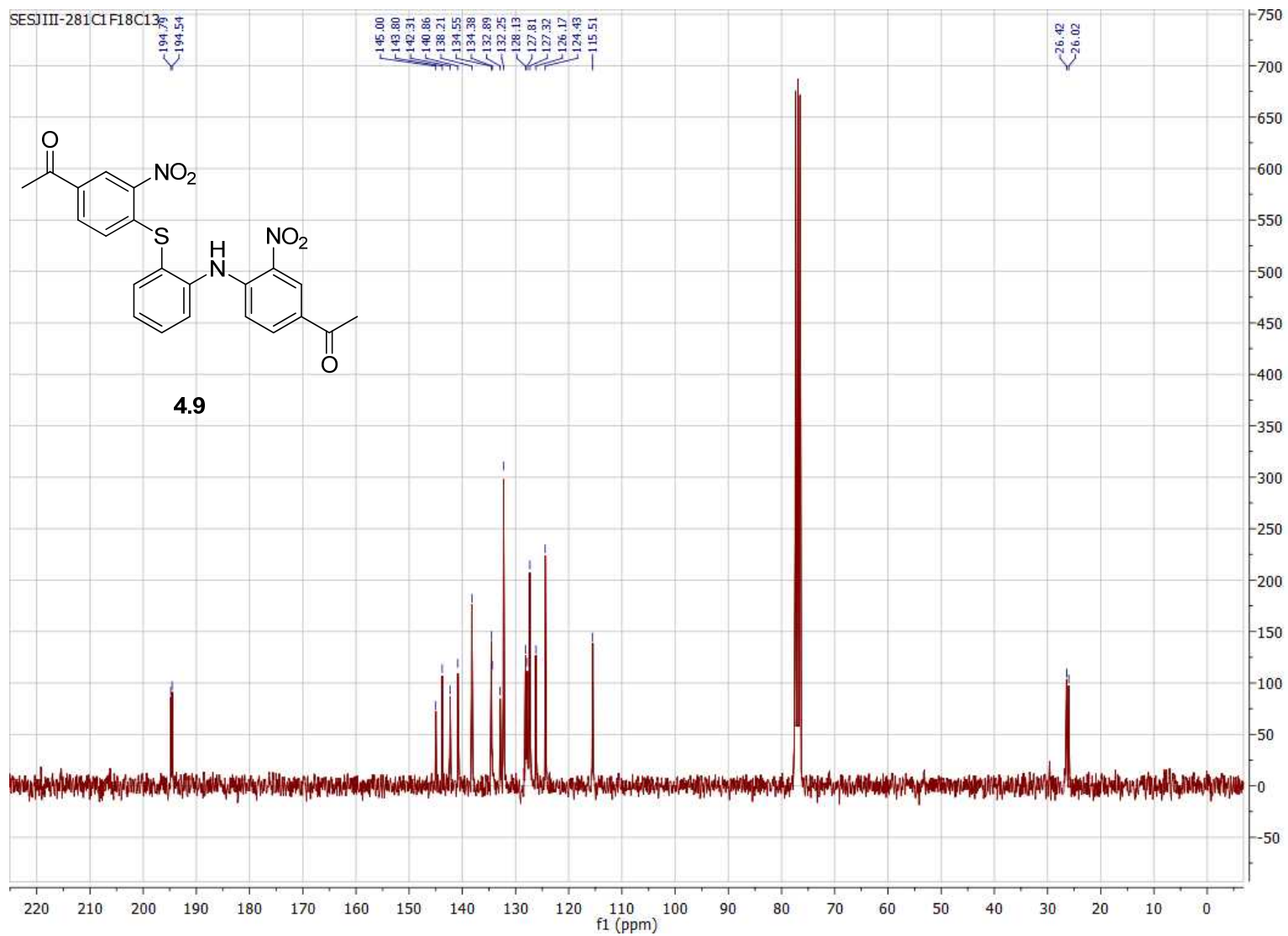


Figure B.72. 75 MHz ^{13}C NMR of compound **4.9** in CDCl_3 .

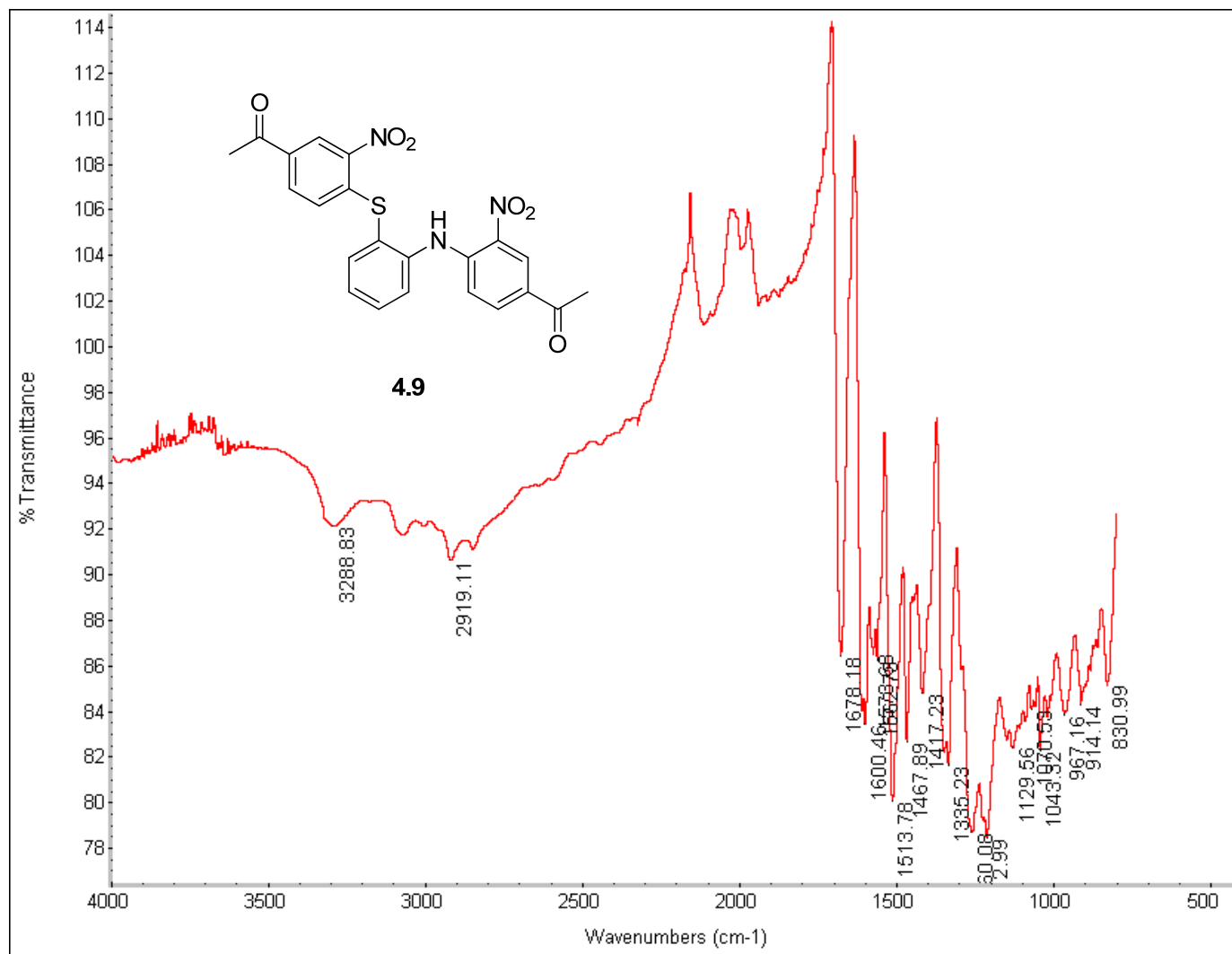


Figure B.73. FTIR of compound 4.9.

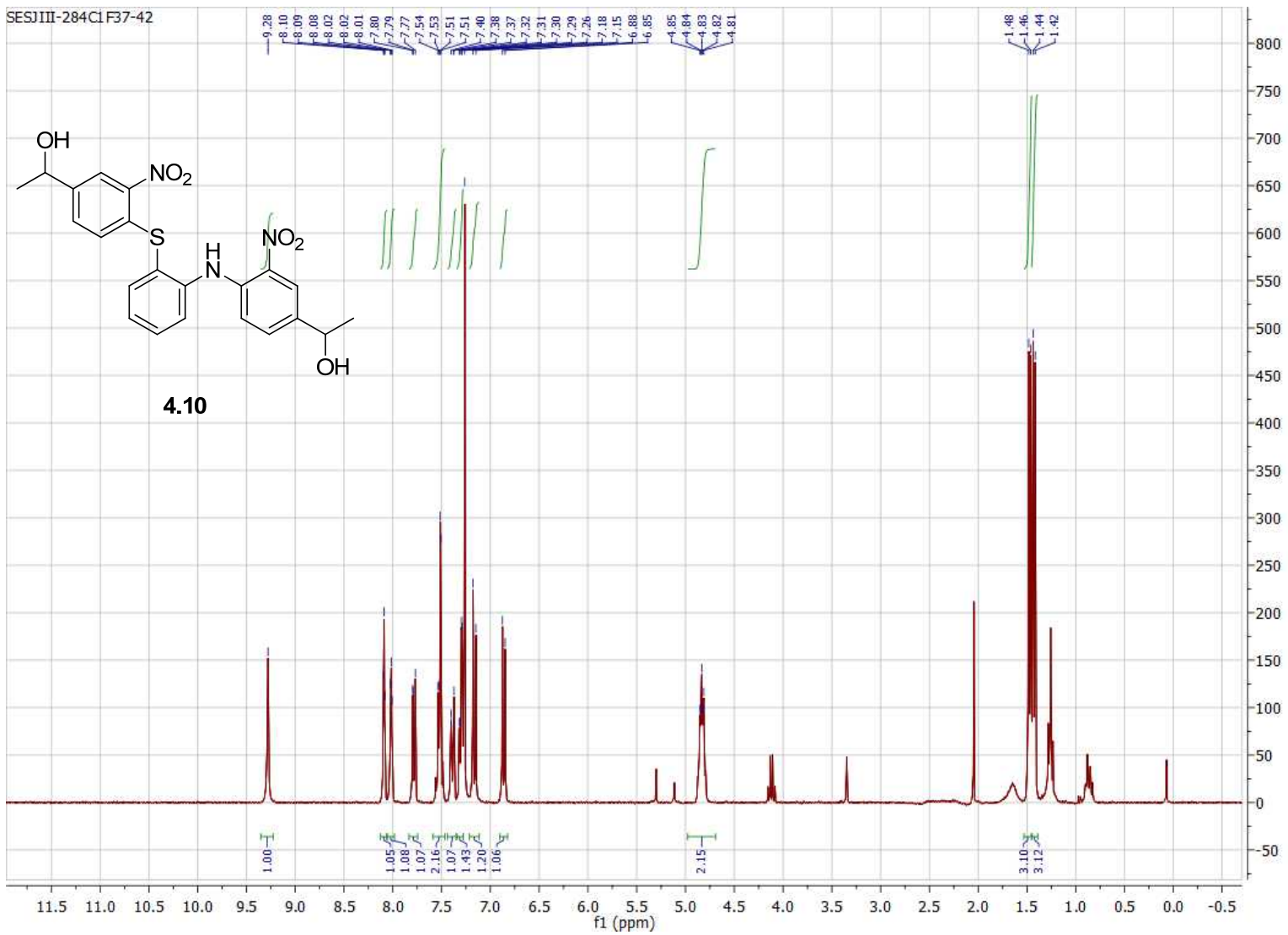


Figure B.74. 300 MHz ^1H NMR of compound **4.10** in CDCl_3 .

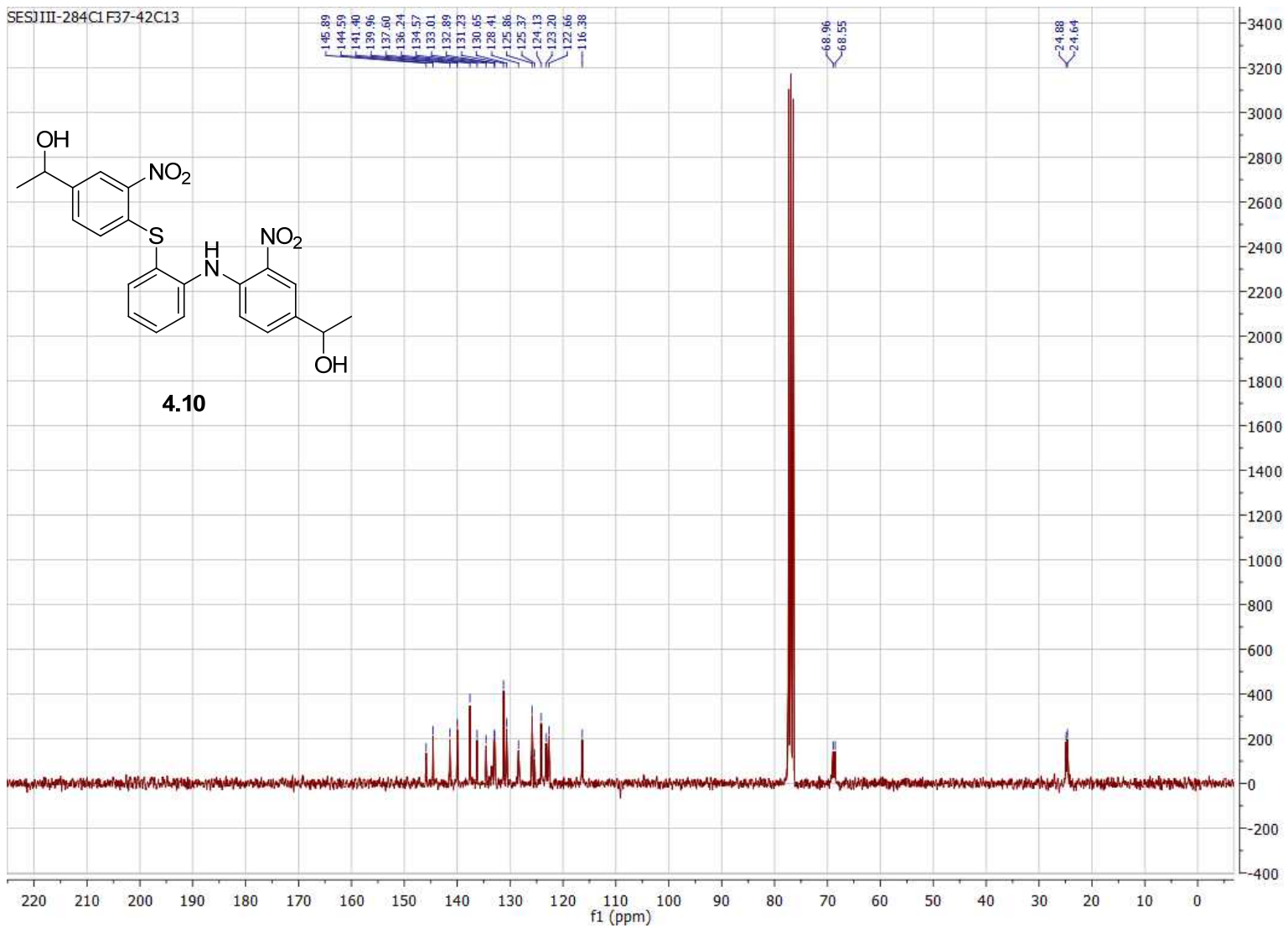


Figure B.75. 75 MHz ^{13}C NMR of compound **4.10** in CDCl_3 .

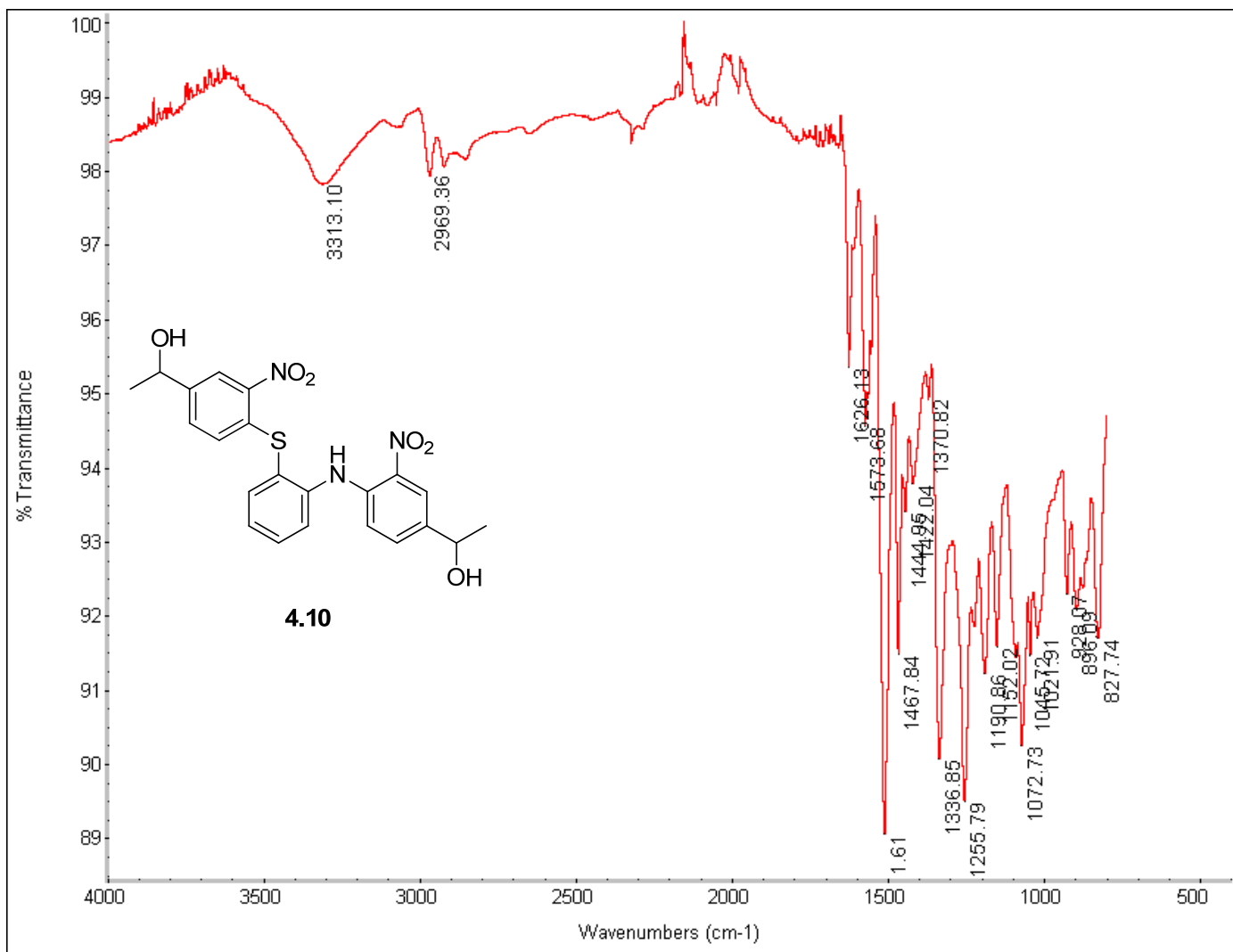


Figure B.76. FTIR of compound 4.10.

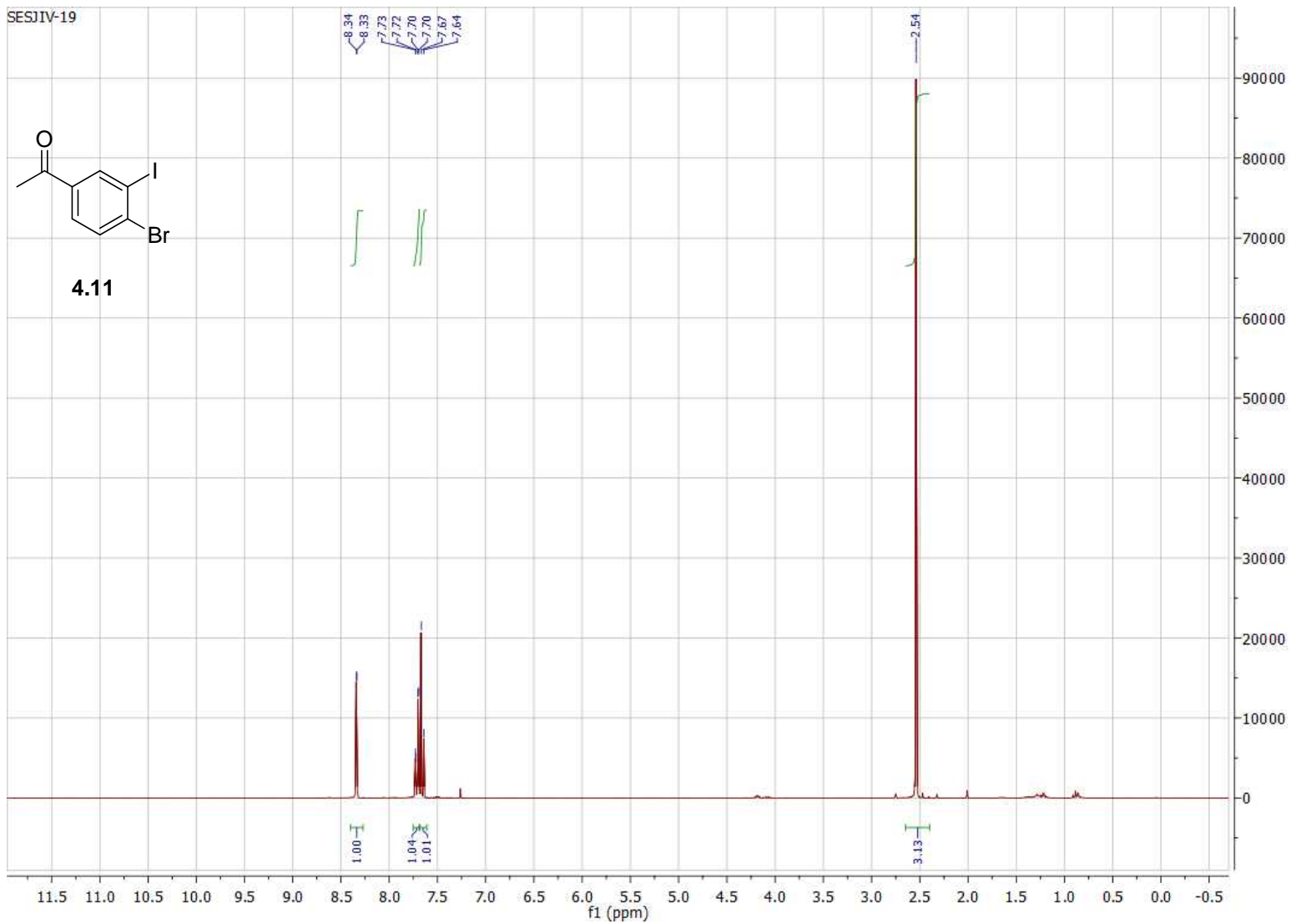


Figure B.77. 300 MHz ^1H NMR of compound **4.11** in CDCl_3 .

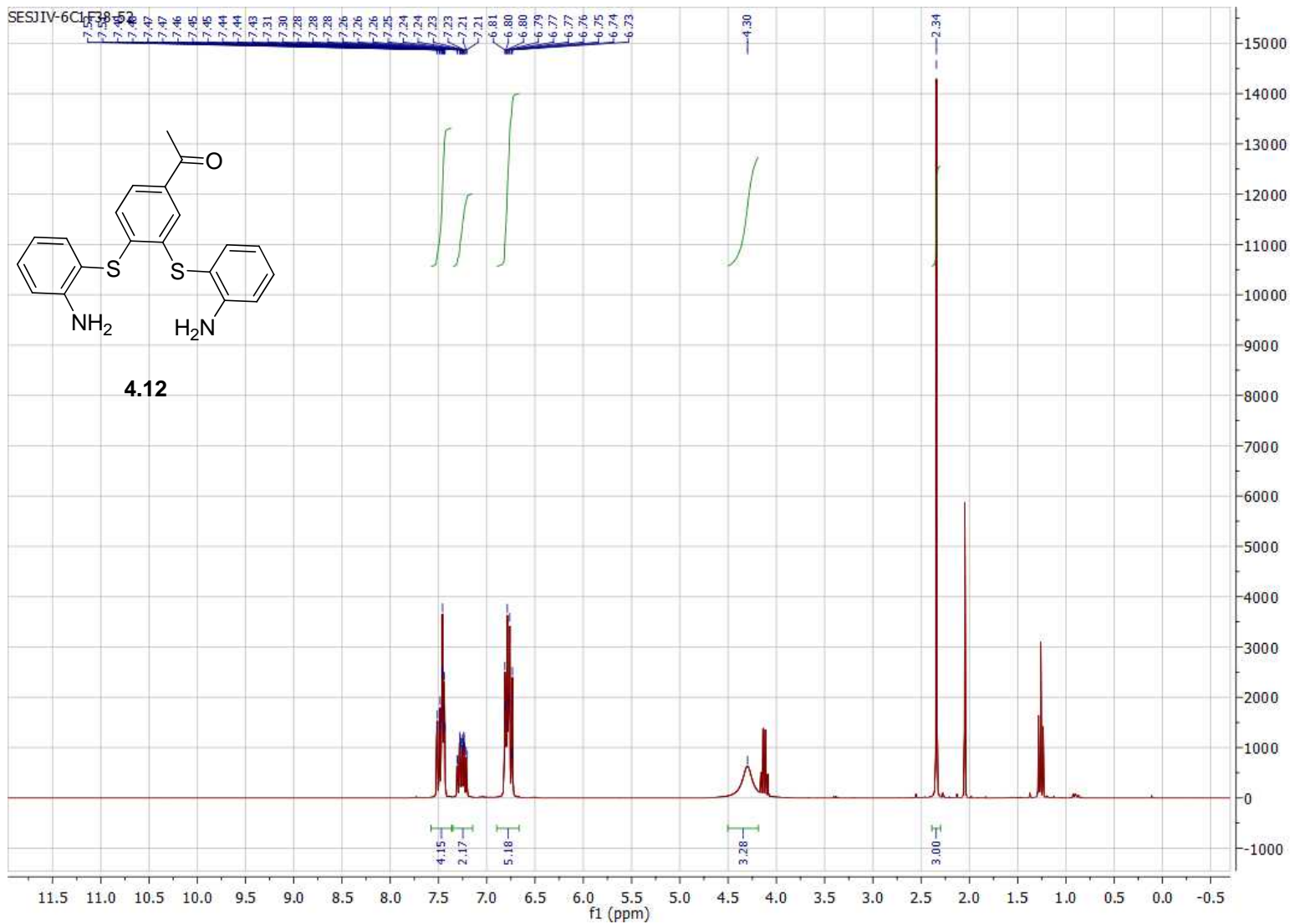


Figure B.78. 300 MHz ¹H NMR of compound **4.12** in CDCl₃.

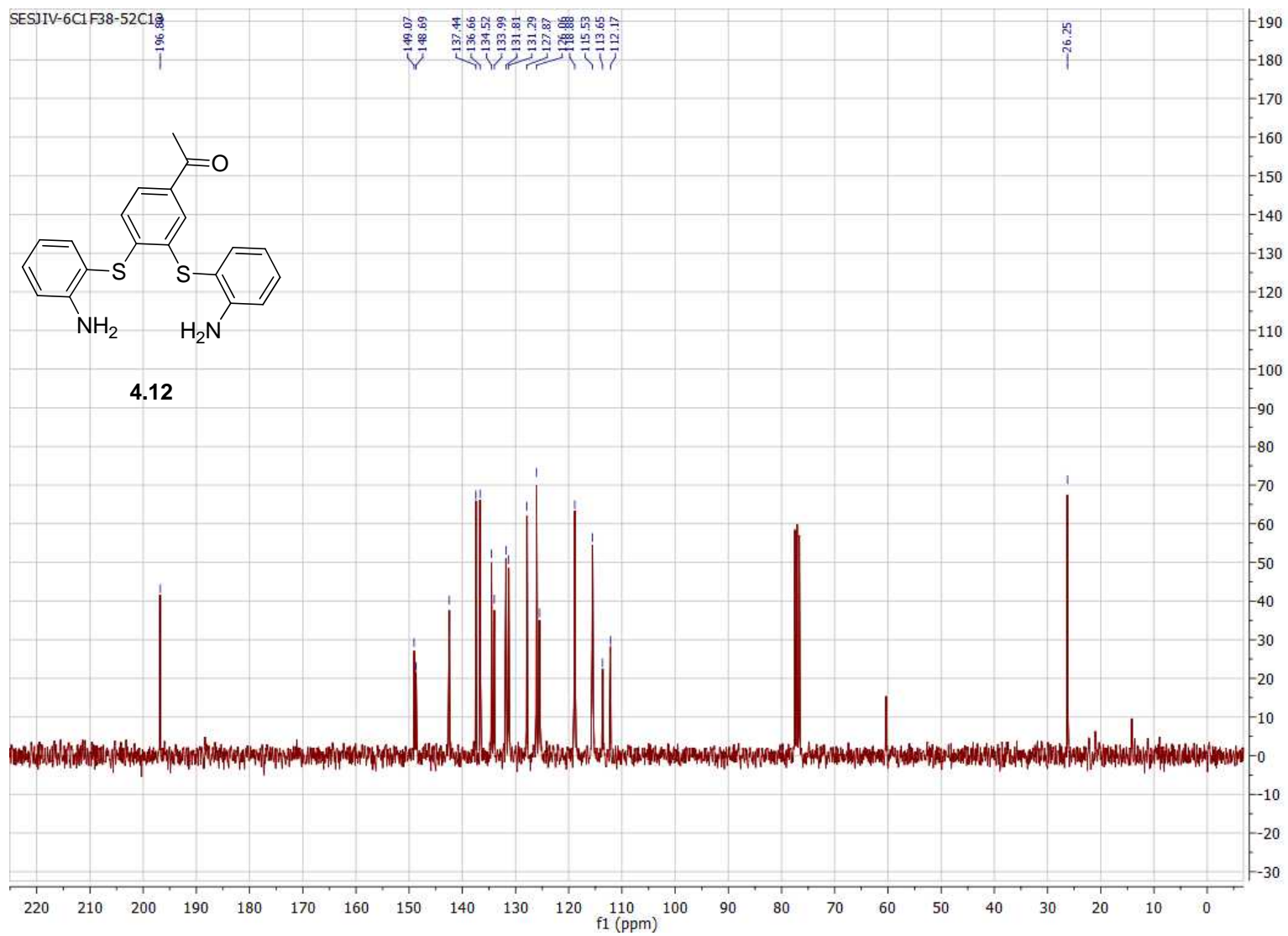


Figure B.79. 75 MHz ¹³C NMR of compound **4.12** in CDCl₃.

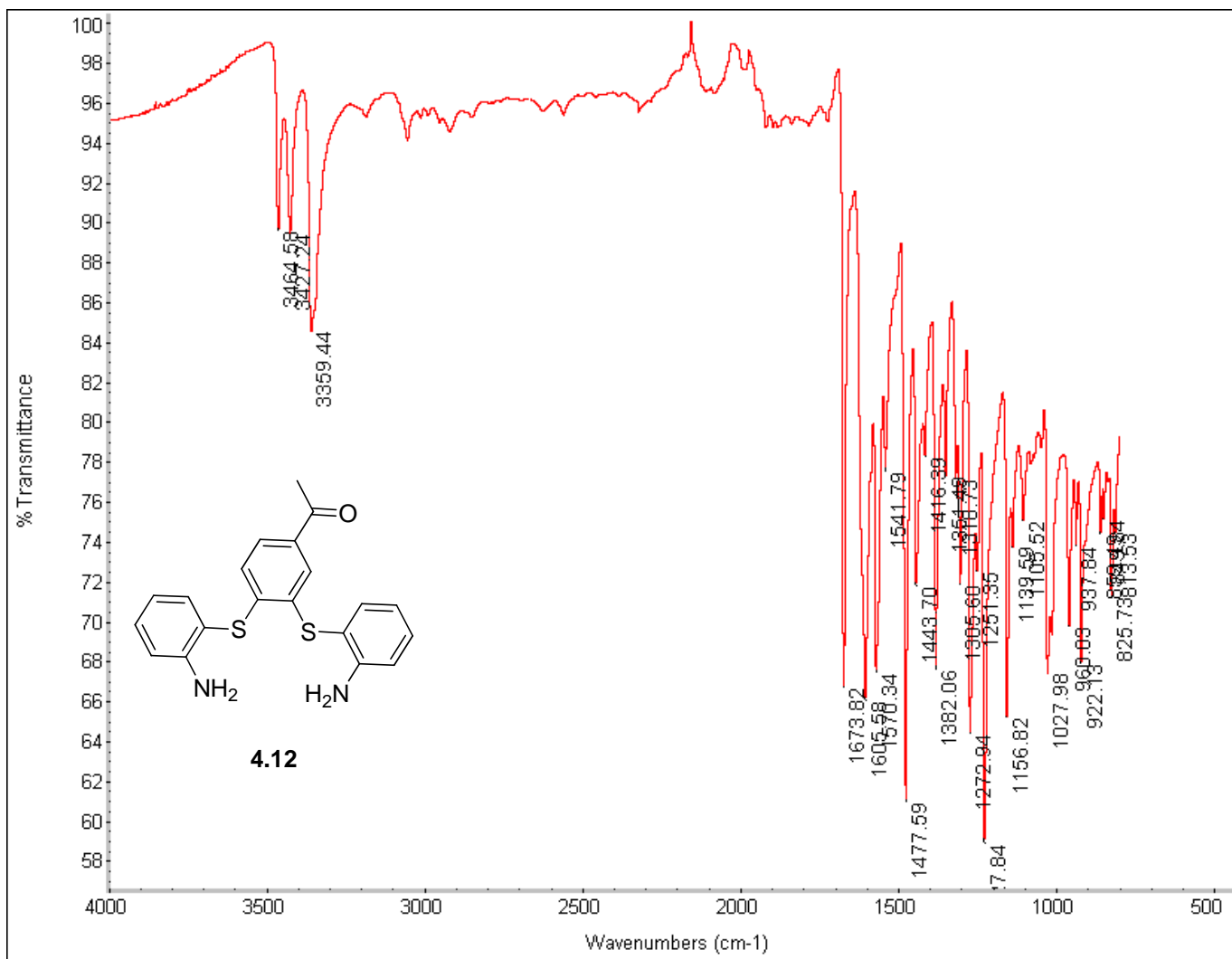


Figure B.80. FTIR of compound 4.12.

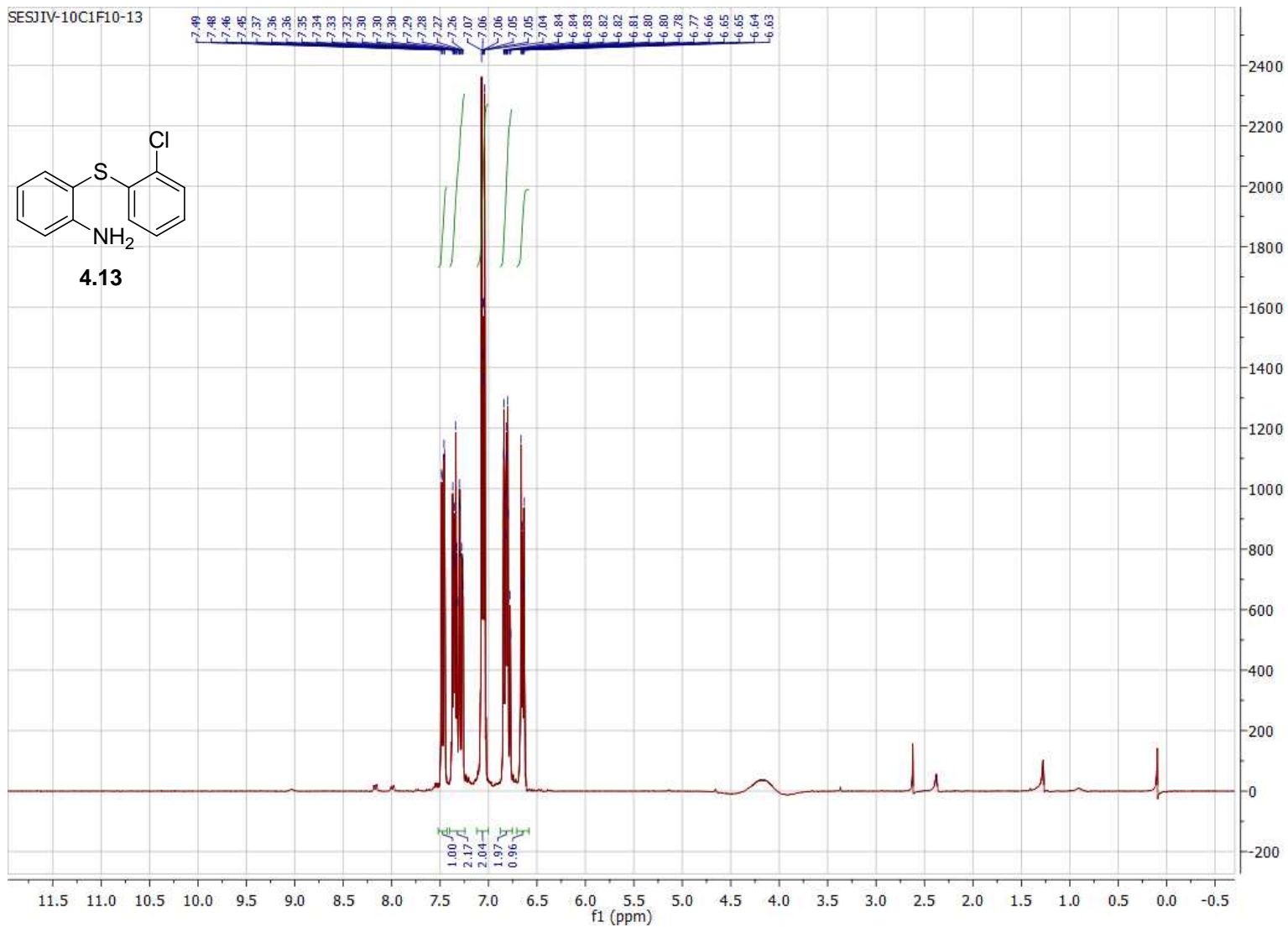


Figure B.81. 300 MHz ^1H NMR of compound **4.13** in CDCl_3 .

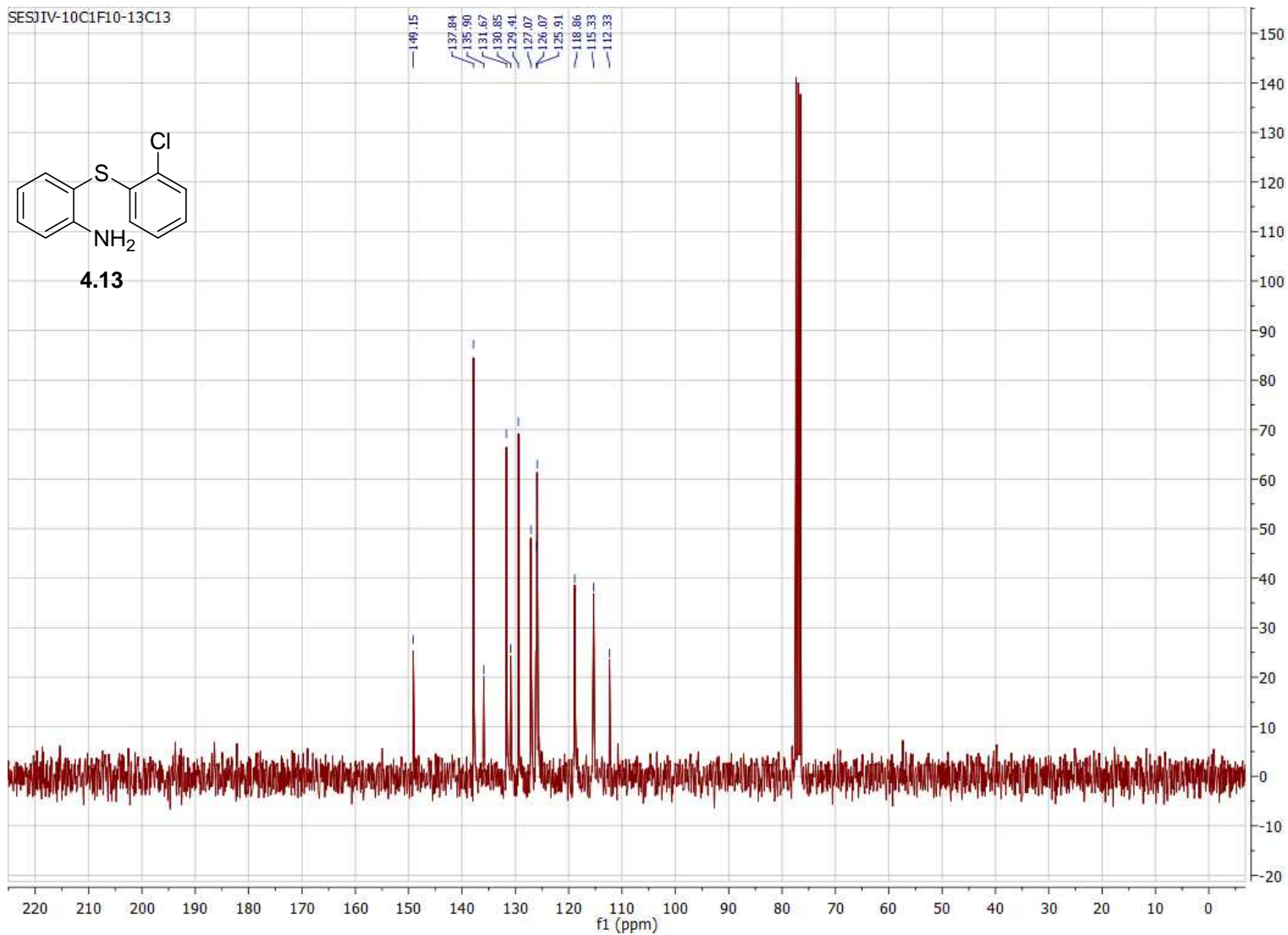


Figure B.82. 75 MHz ^{13}C NMR of compound **4.13** in CDCl_3 .

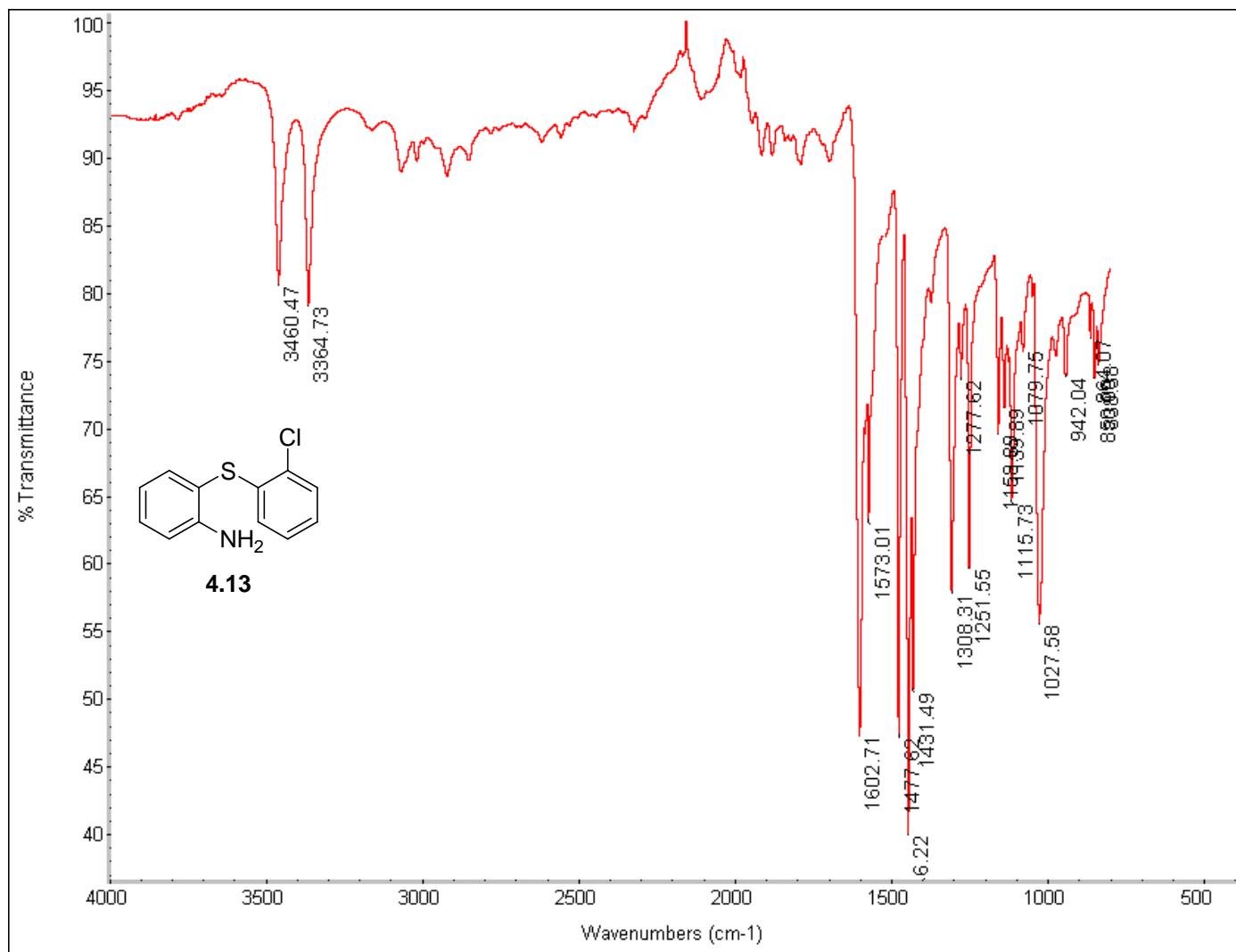


Figure B.83. FTIR of compound **4.13**.

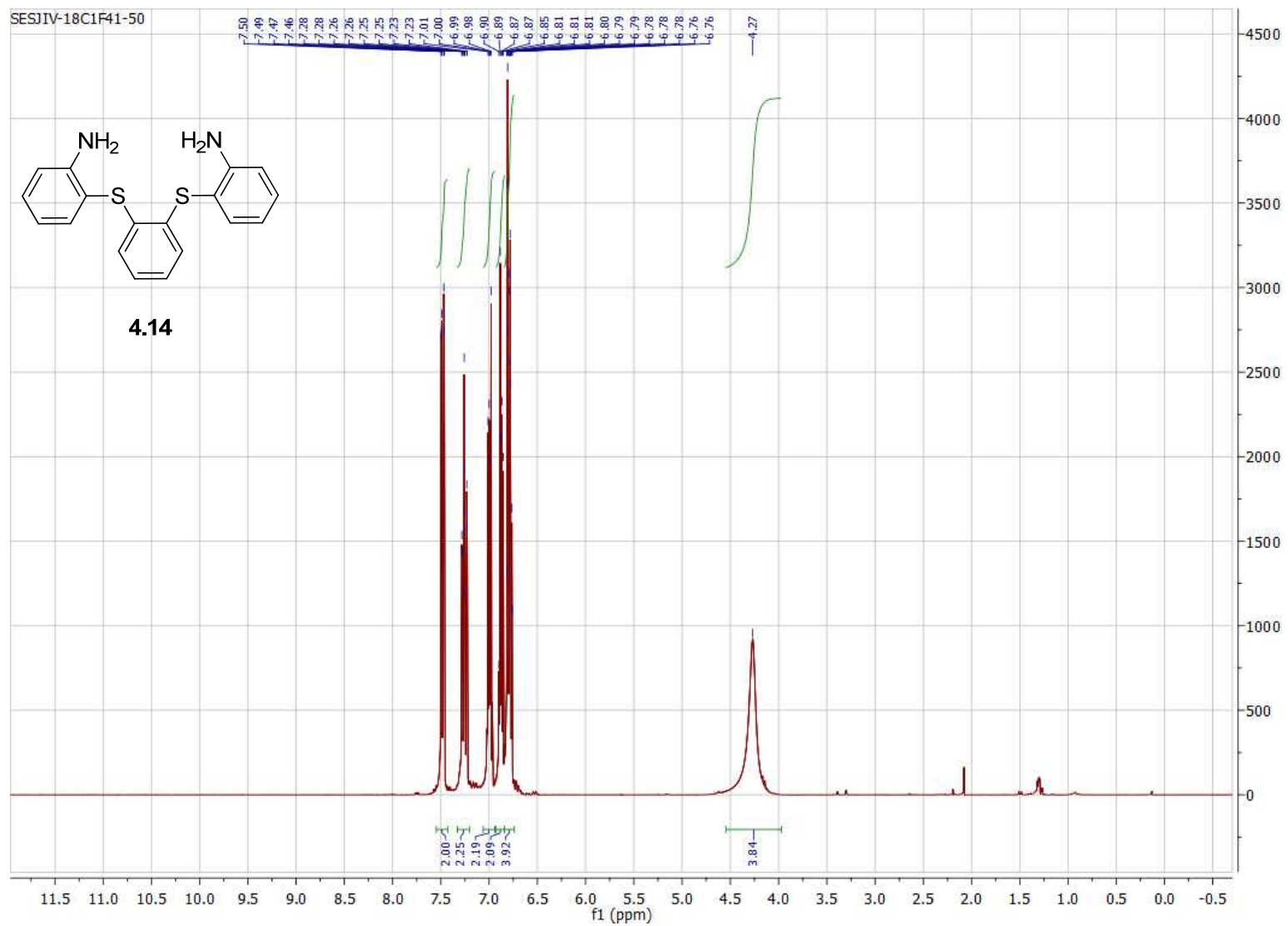


Figure B.84. 300 MHz ^1H NMR of compound **4.14** in CDCl_3 .

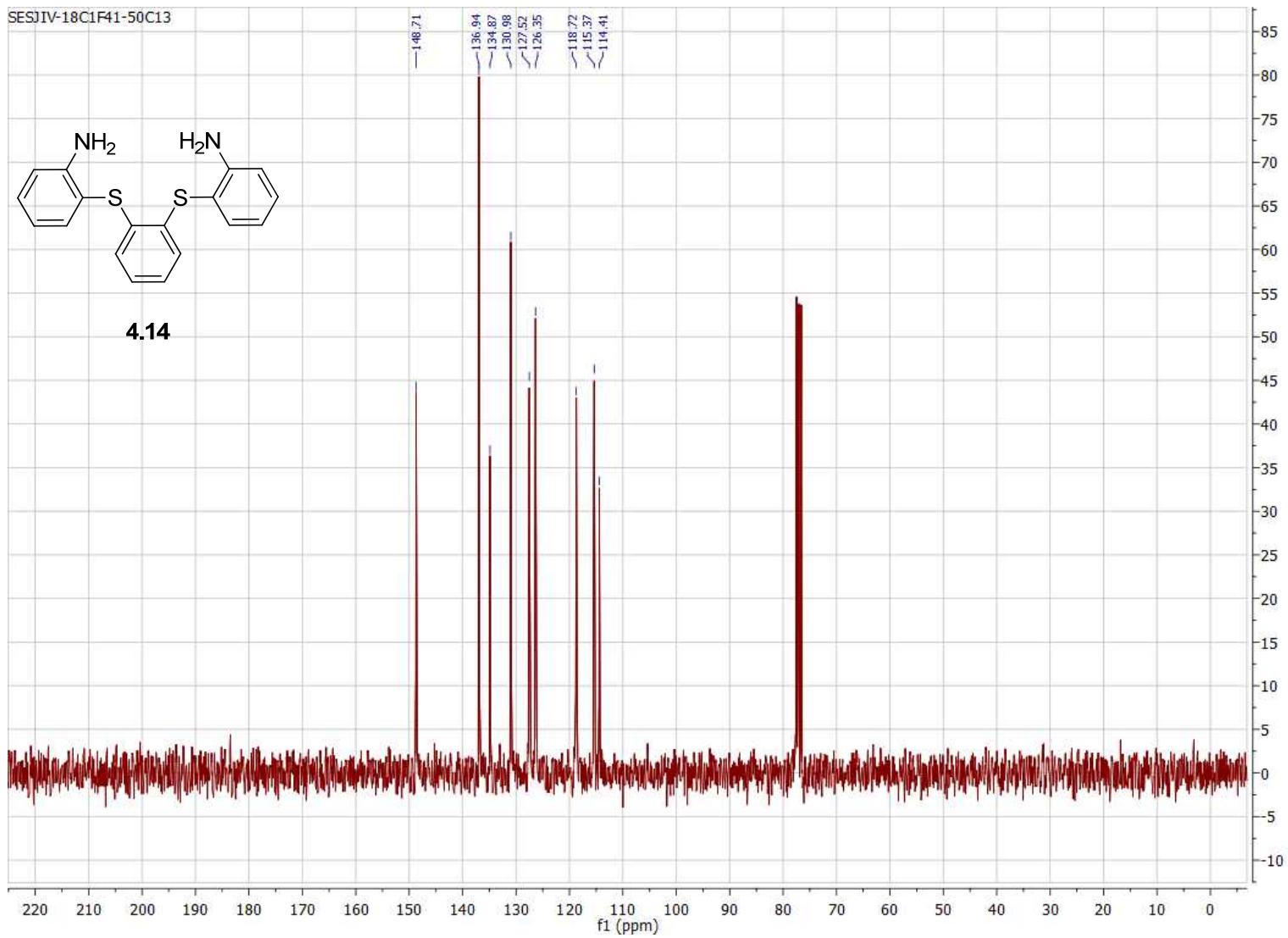


Figure B.85. 75 MHz ^{13}C NMR of compound **4.14** in CDCl_3 .

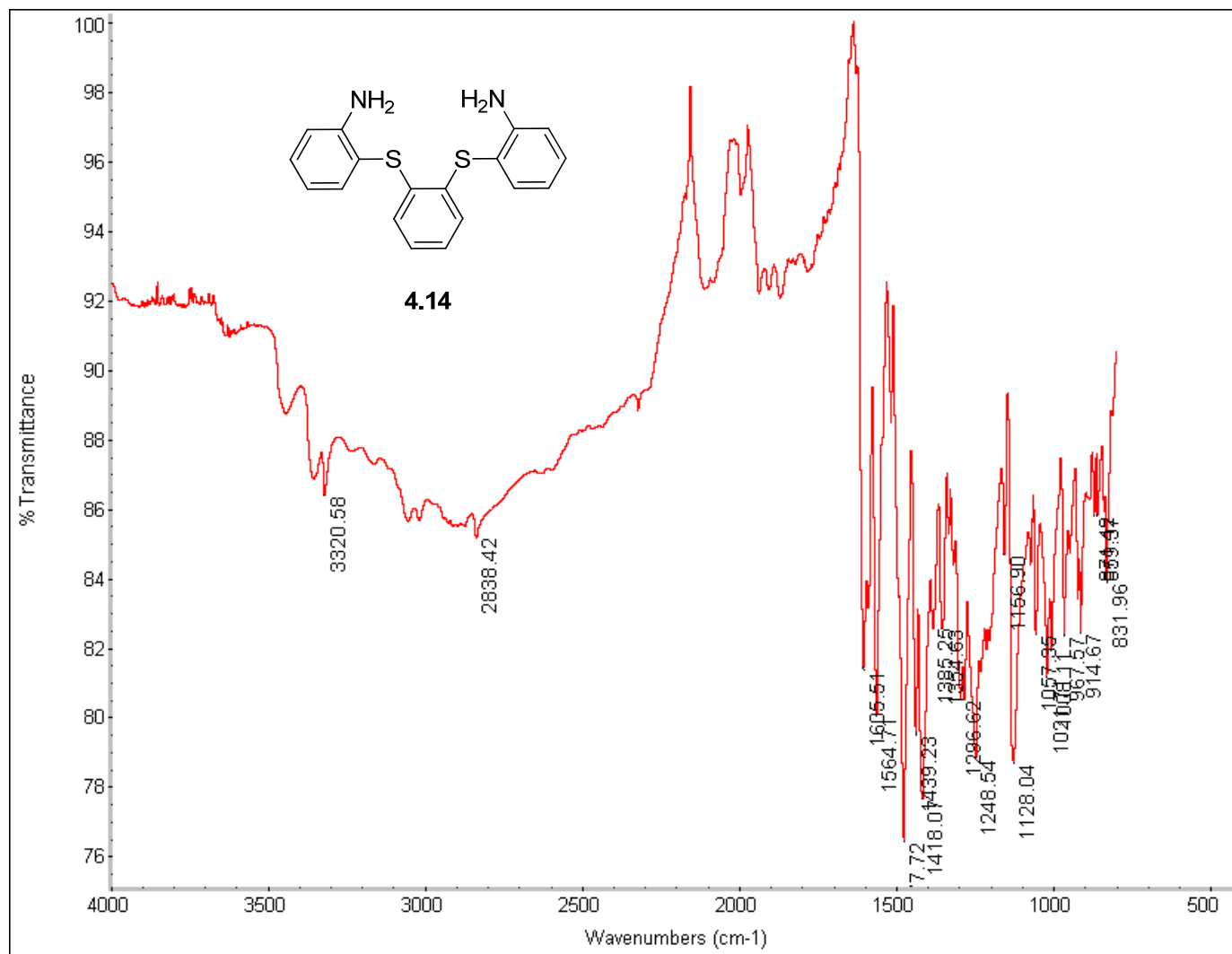


Figure B.86. FTIR of compound **4.14**.

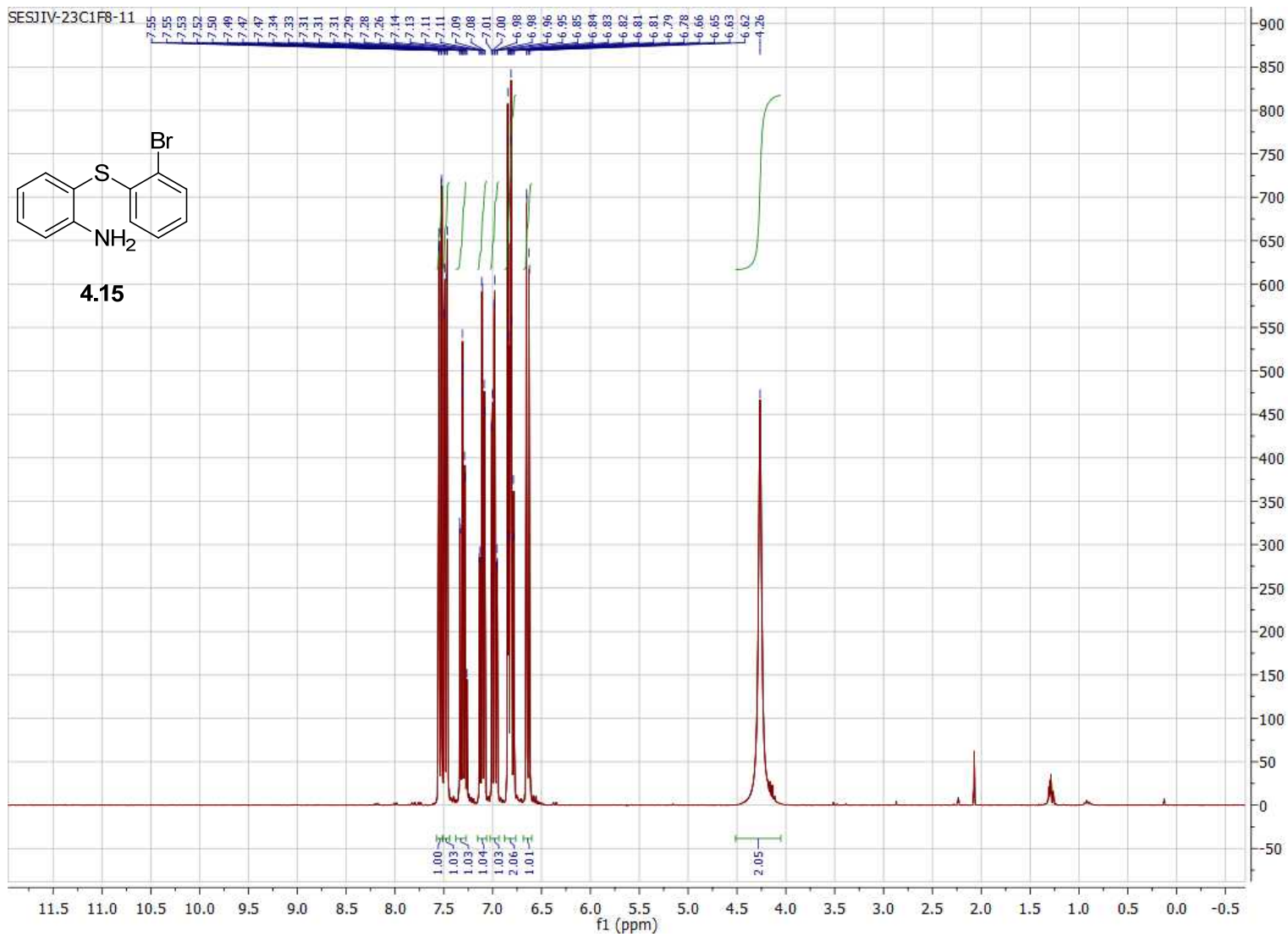


Figure B.87. 300 MHz ^1H NMR of compound **4.15** in CDCl_3 .

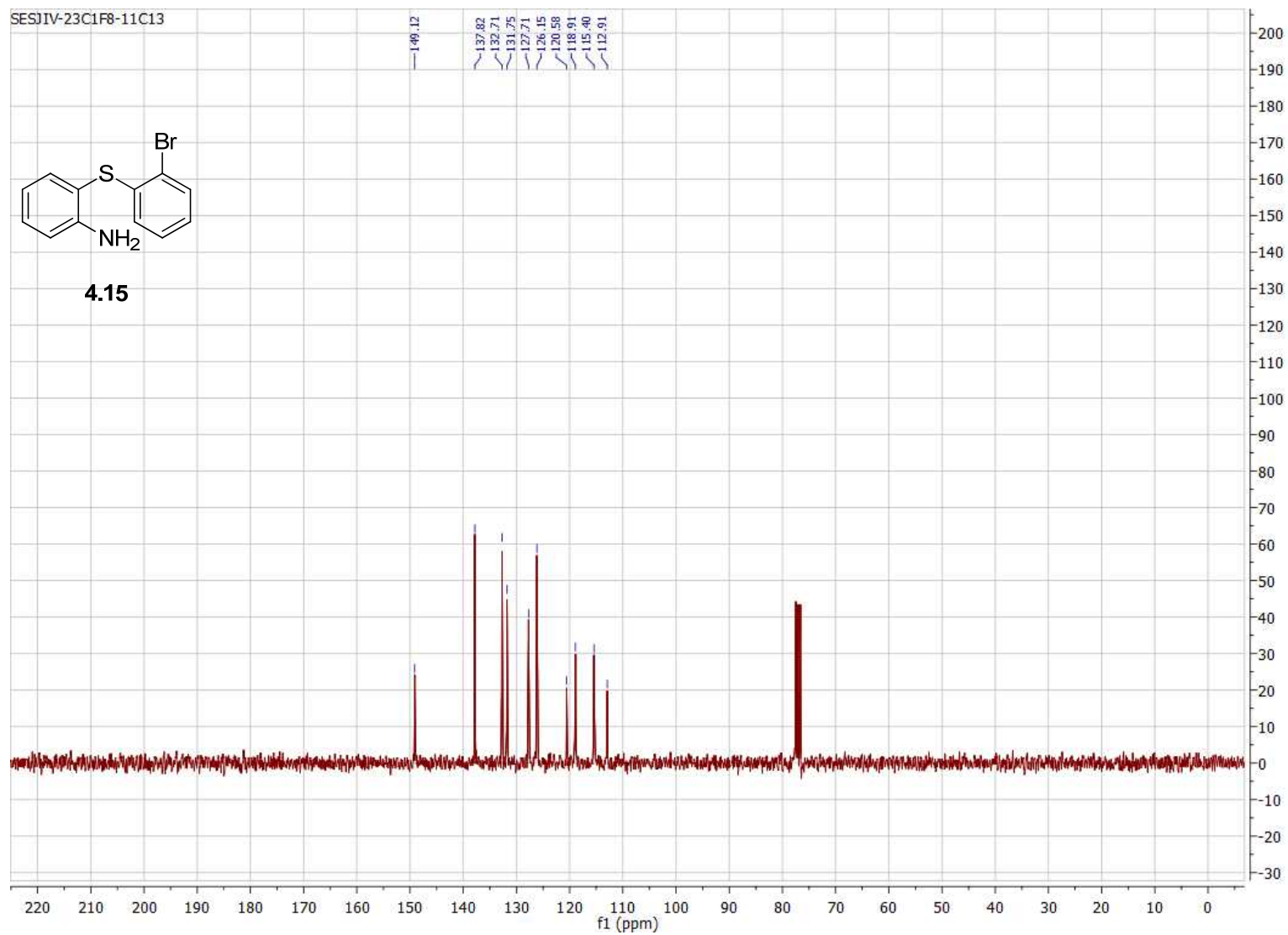


Figure B.88. 75 MHz ^{13}C NMR of compound **4.15** in CDCl_3 .

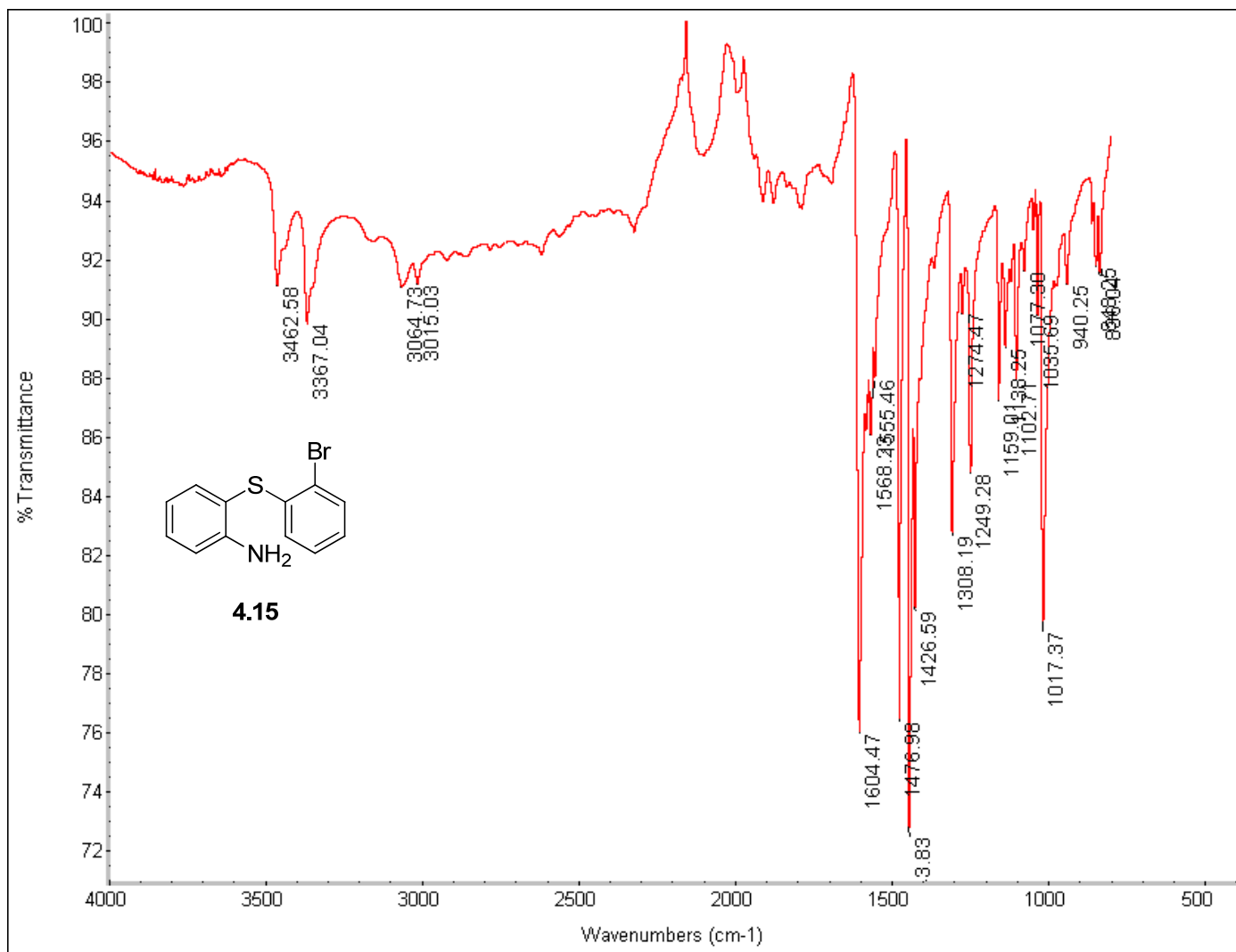


Figure B.89. FTIR of compound 4.15.

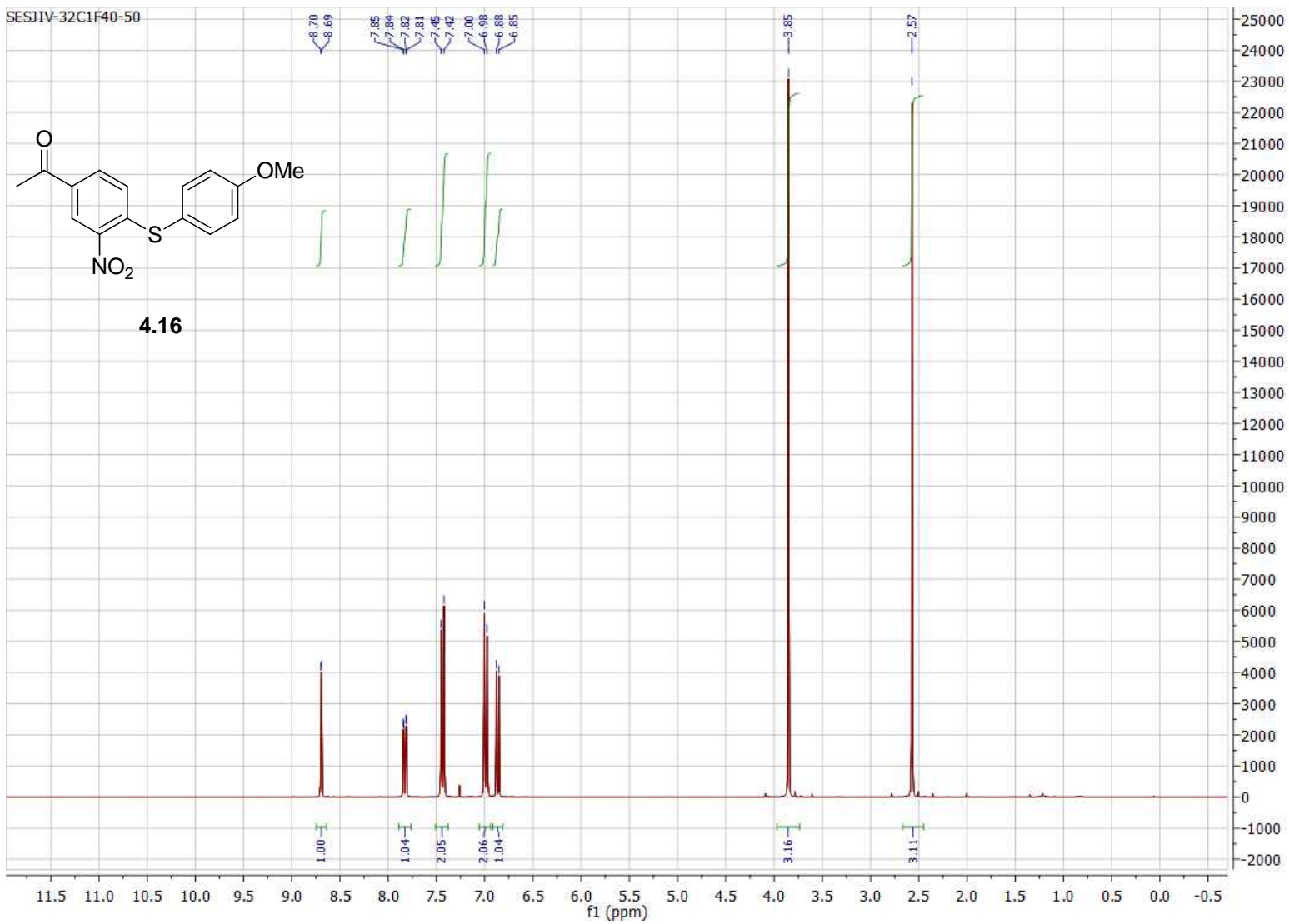


Figure B.90. 300 MHz ^1H NMR of compound **4.16** in CDCl_3 .

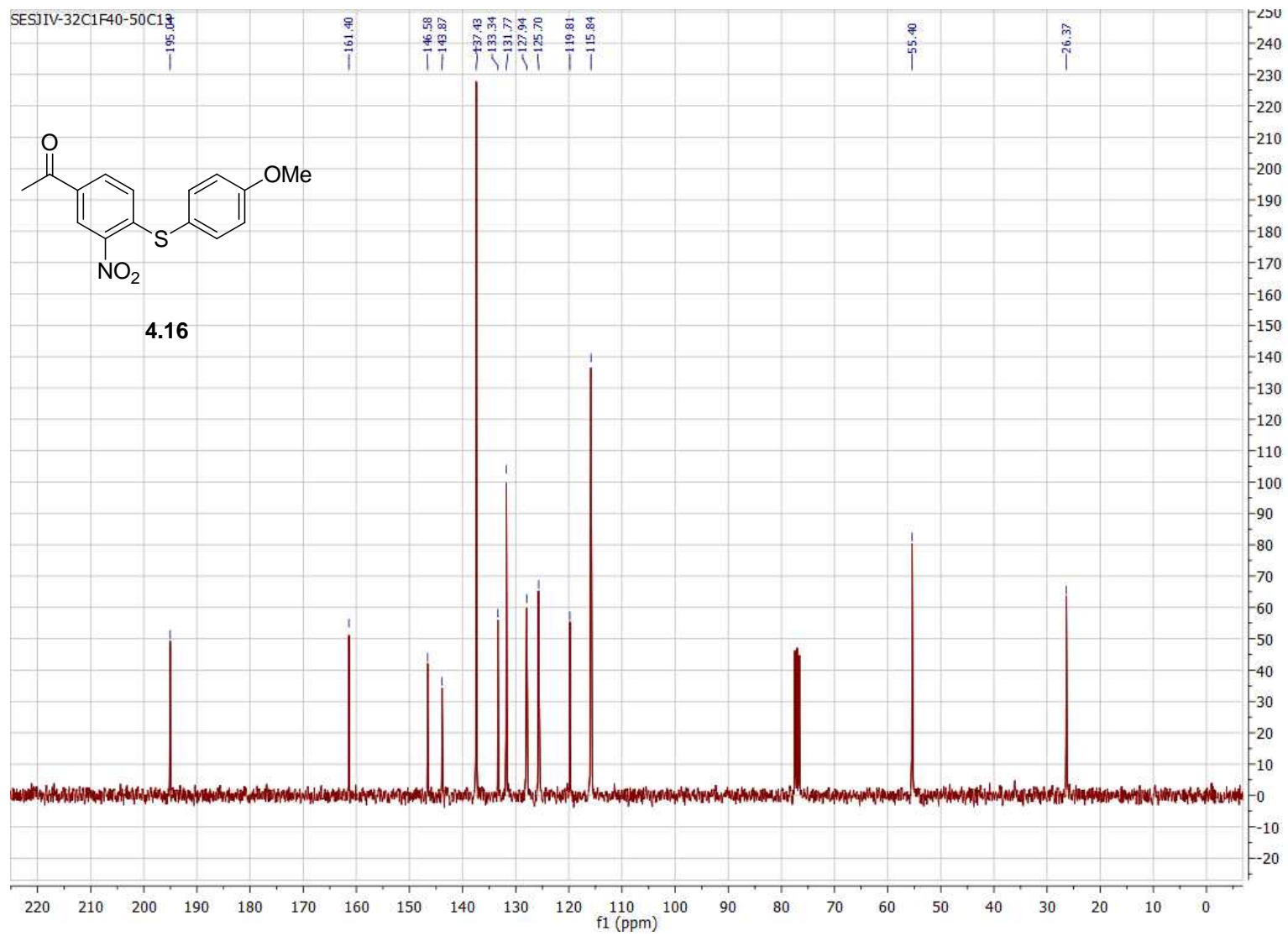


Figure B.91. 75 MHz ^{13}C NMR of compound **4.16** in CDCl_3 .

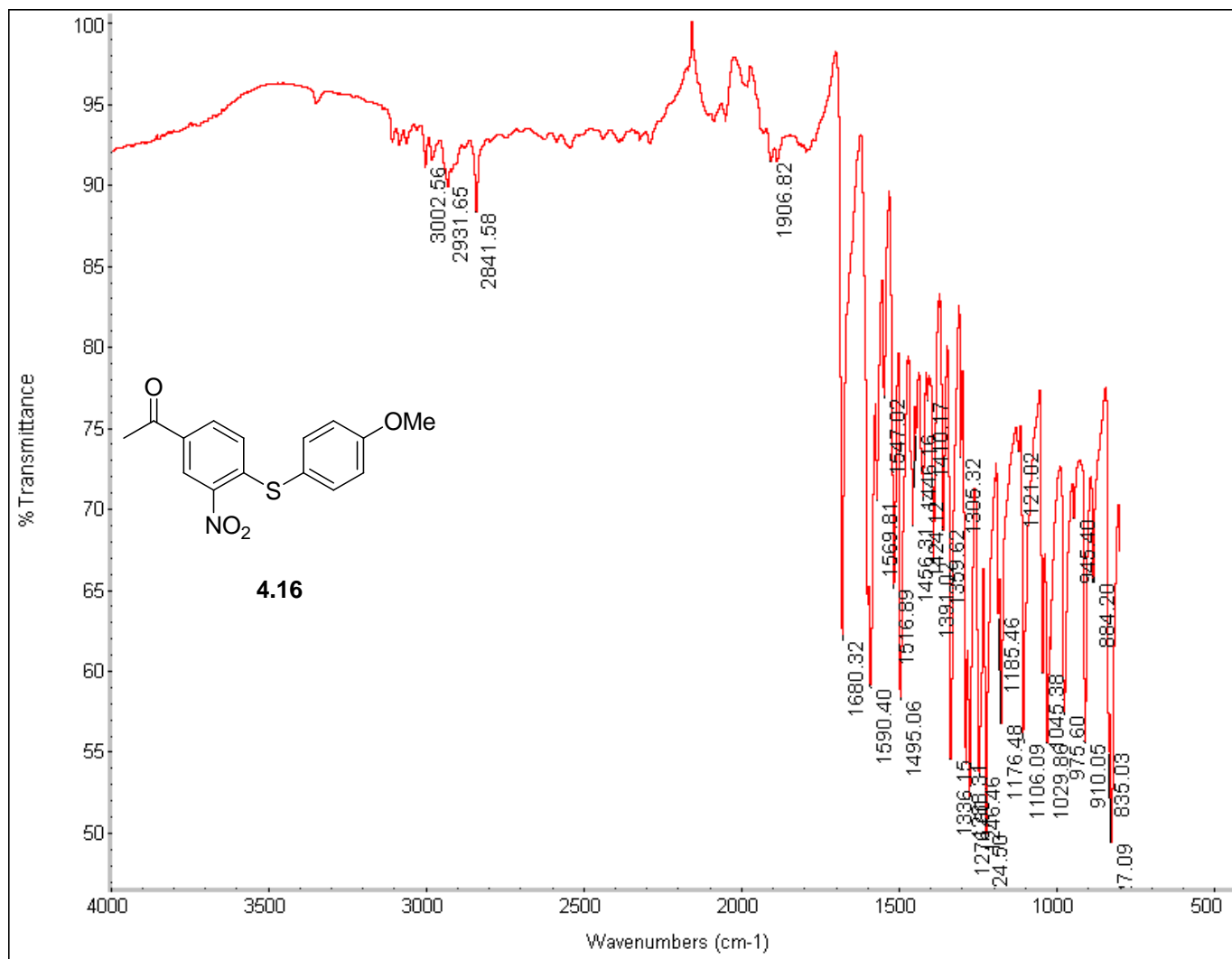


Figure B.92. FTIR of compound **4.16**.

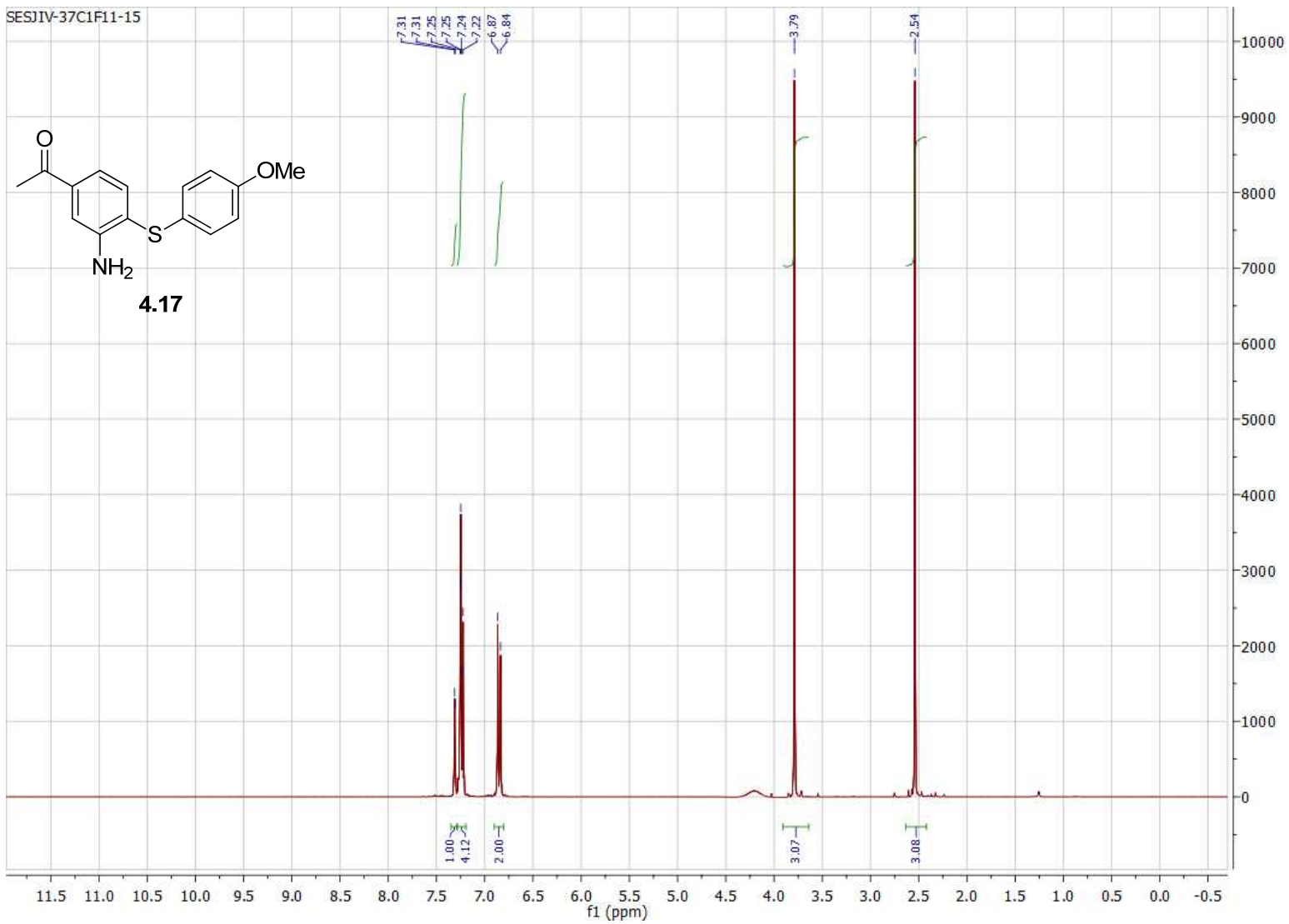


Figure B.93. 300 MHz ^1H NMR of compound **4.17** in CDCl_3 .

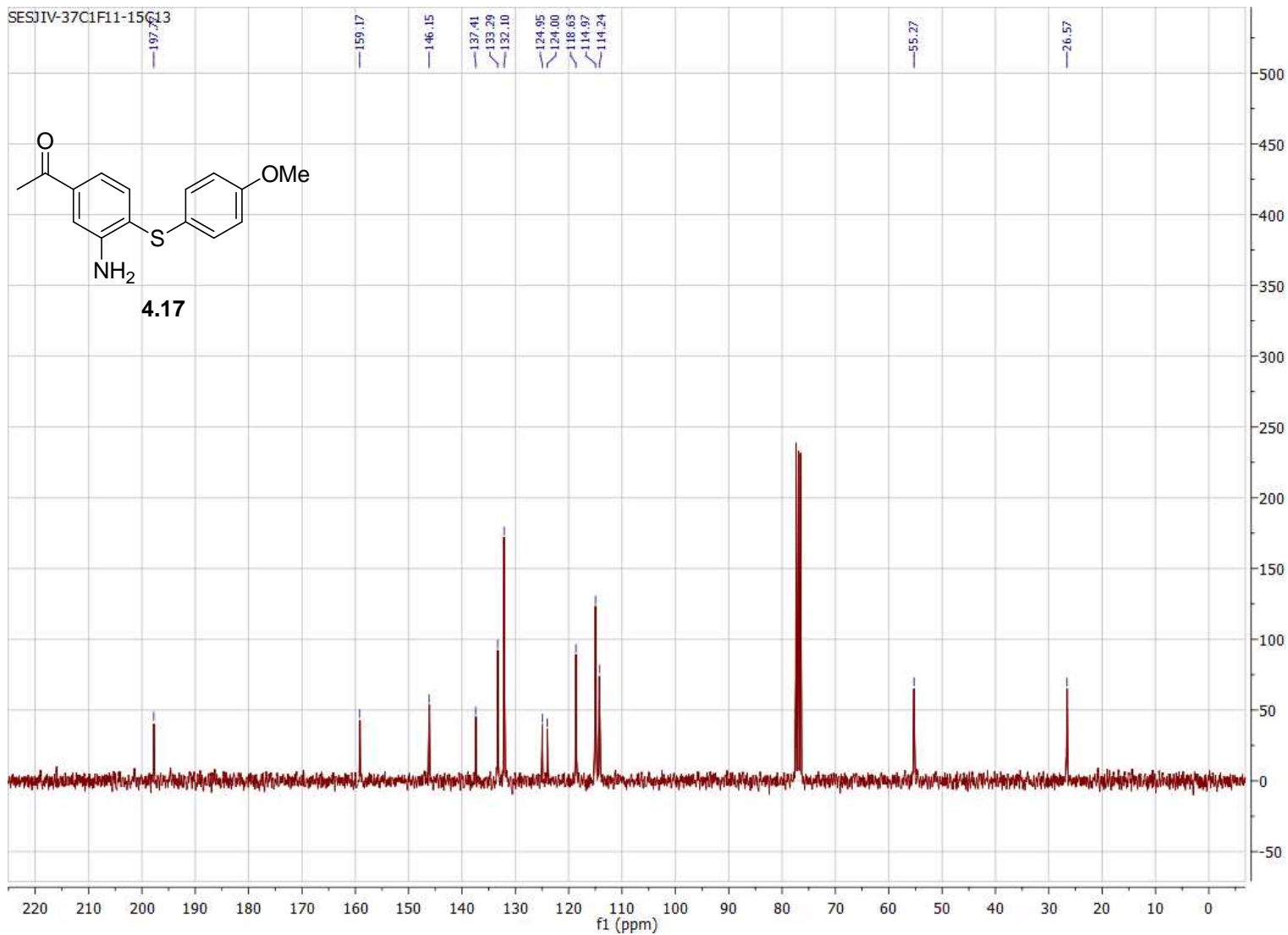


Figure B.94. 75 MHz ^{13}C NMR of compound **4.17** in CDCl_3 .

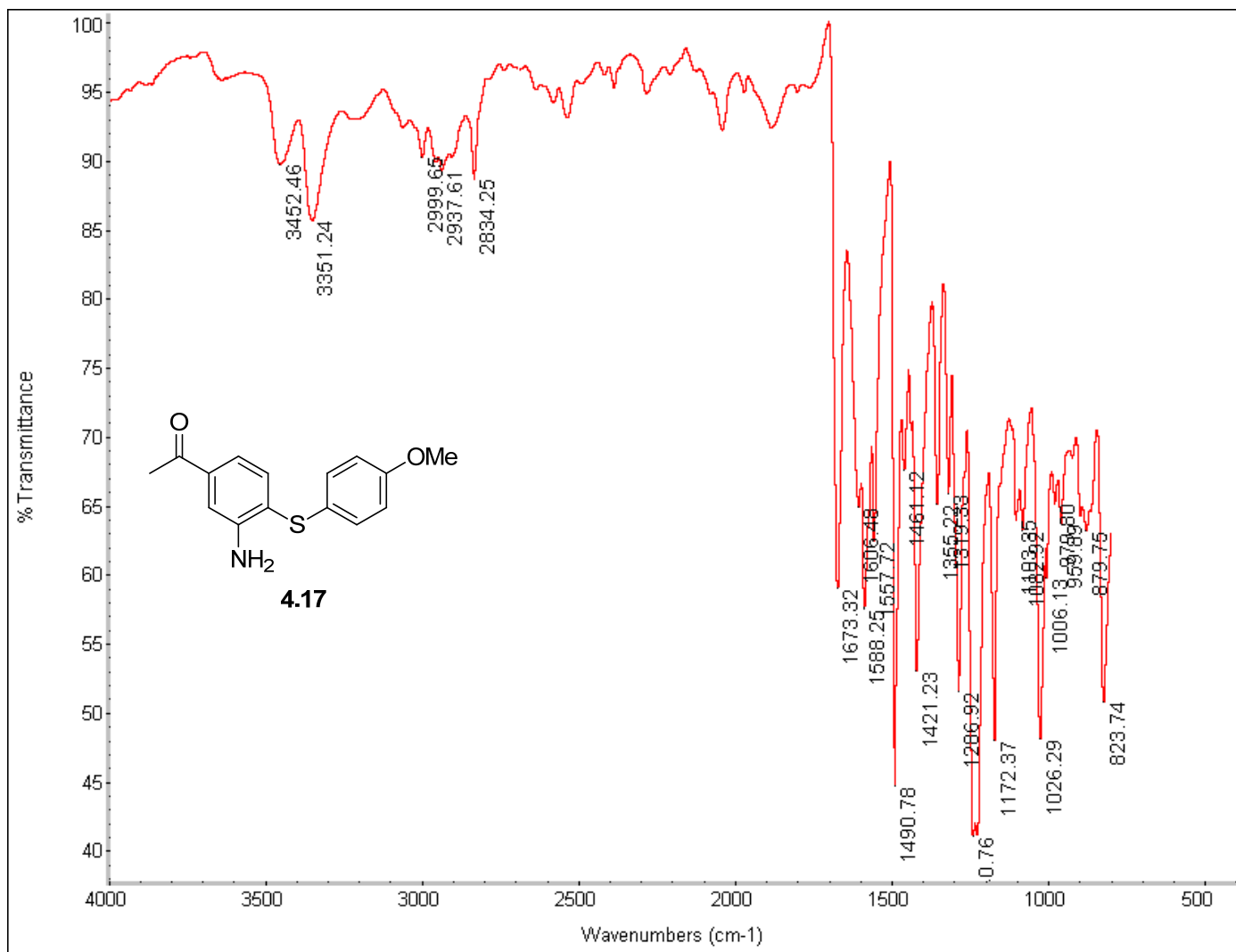


Figure B.95. FTIR of compound 4.17.

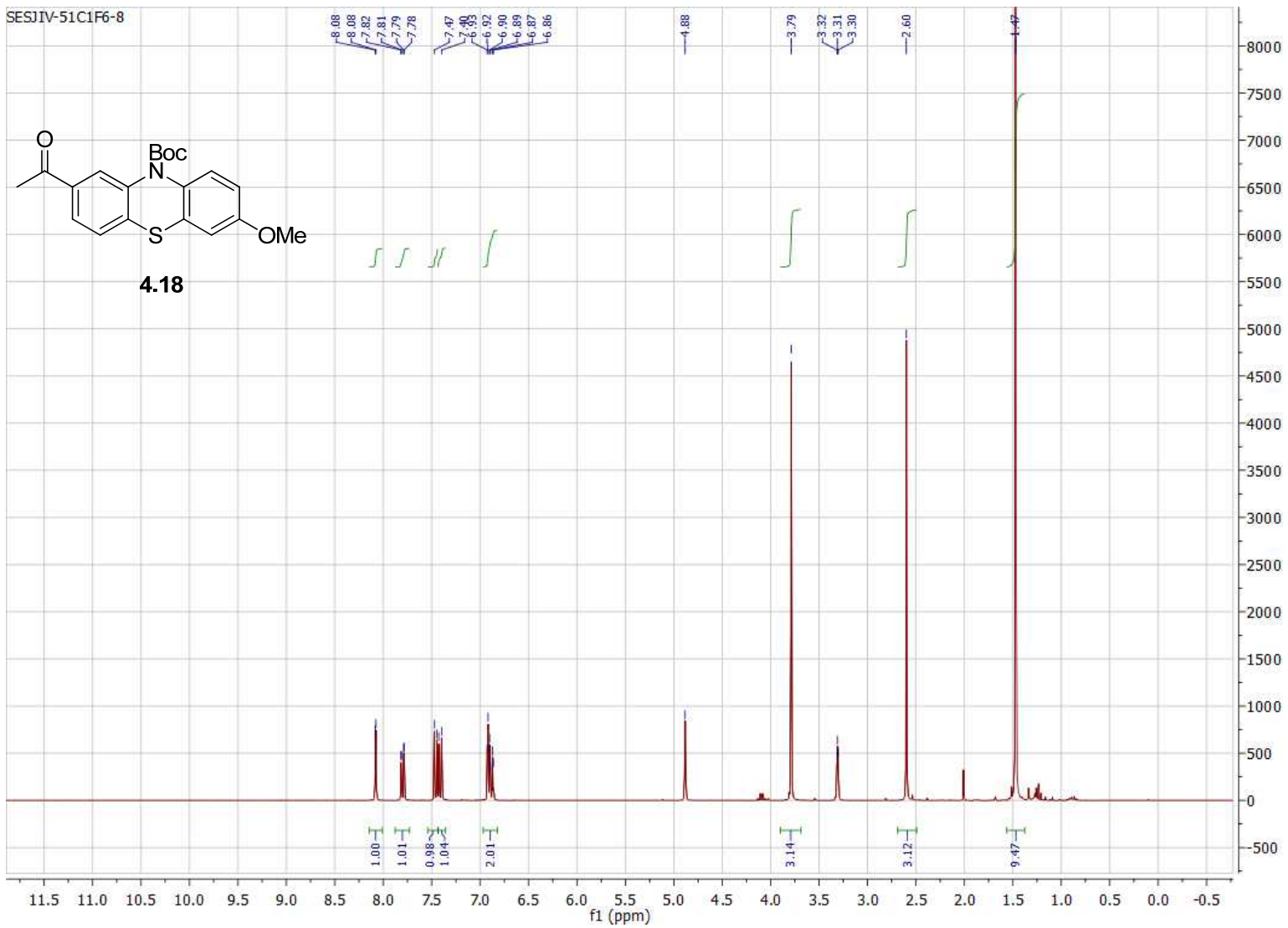


Figure B.96. 300 MHz ¹H NMR of compound **4.18** in CD₃OD.

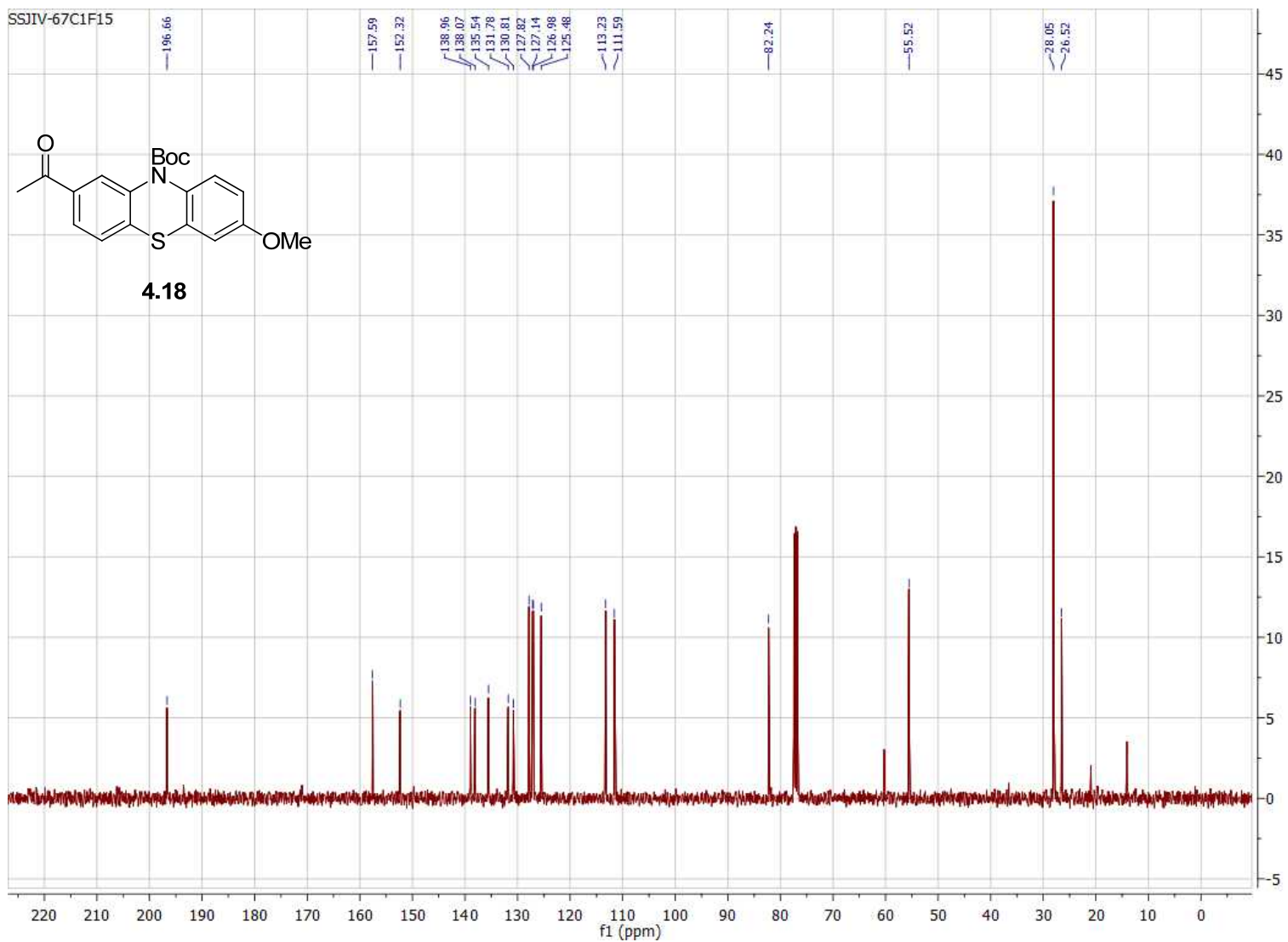


Figure B.97. 100 MHz ^{13}C NMR of compound **4.18** in CDCl_3 .

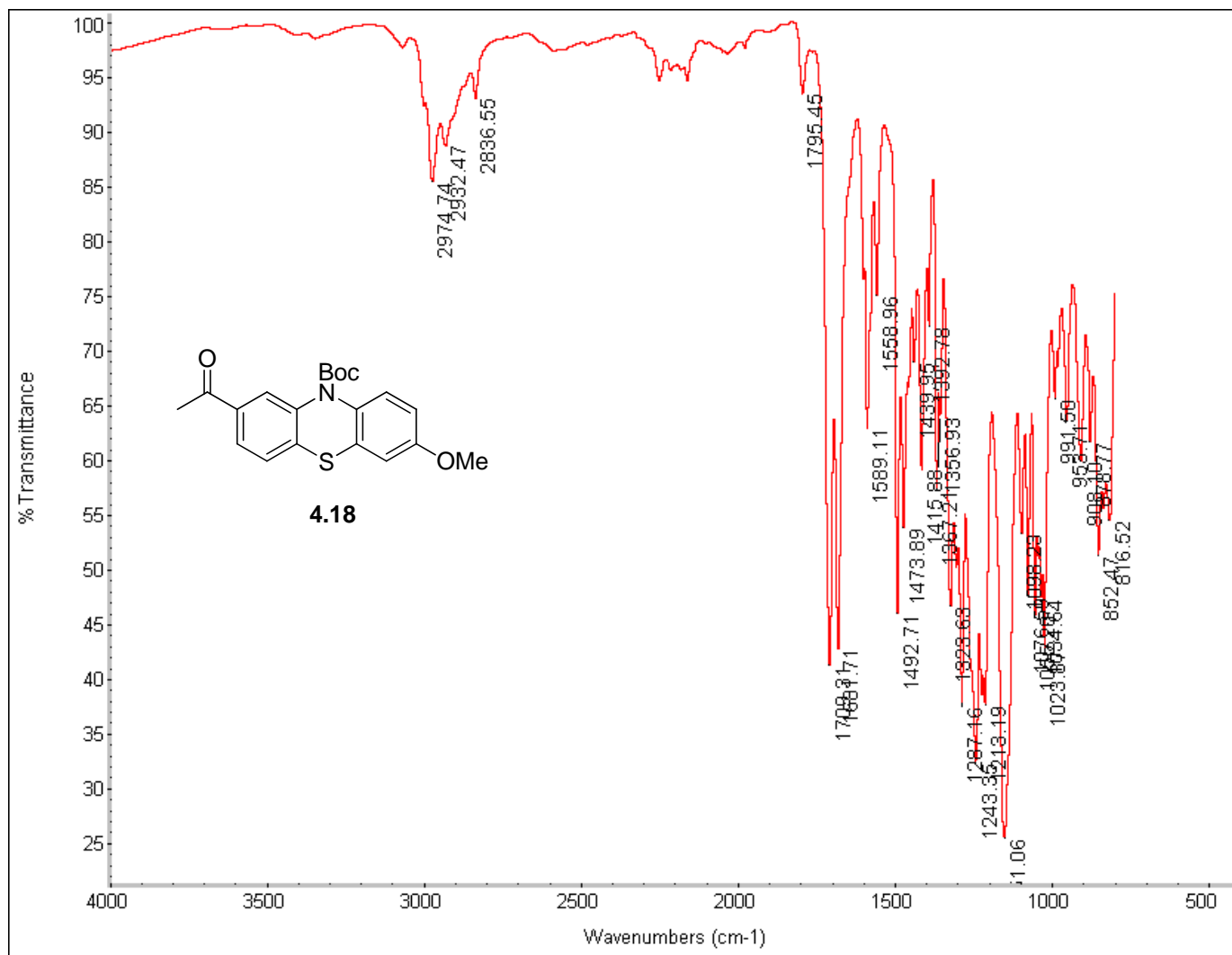


Figure B.98. FTIR of compound 4.18.

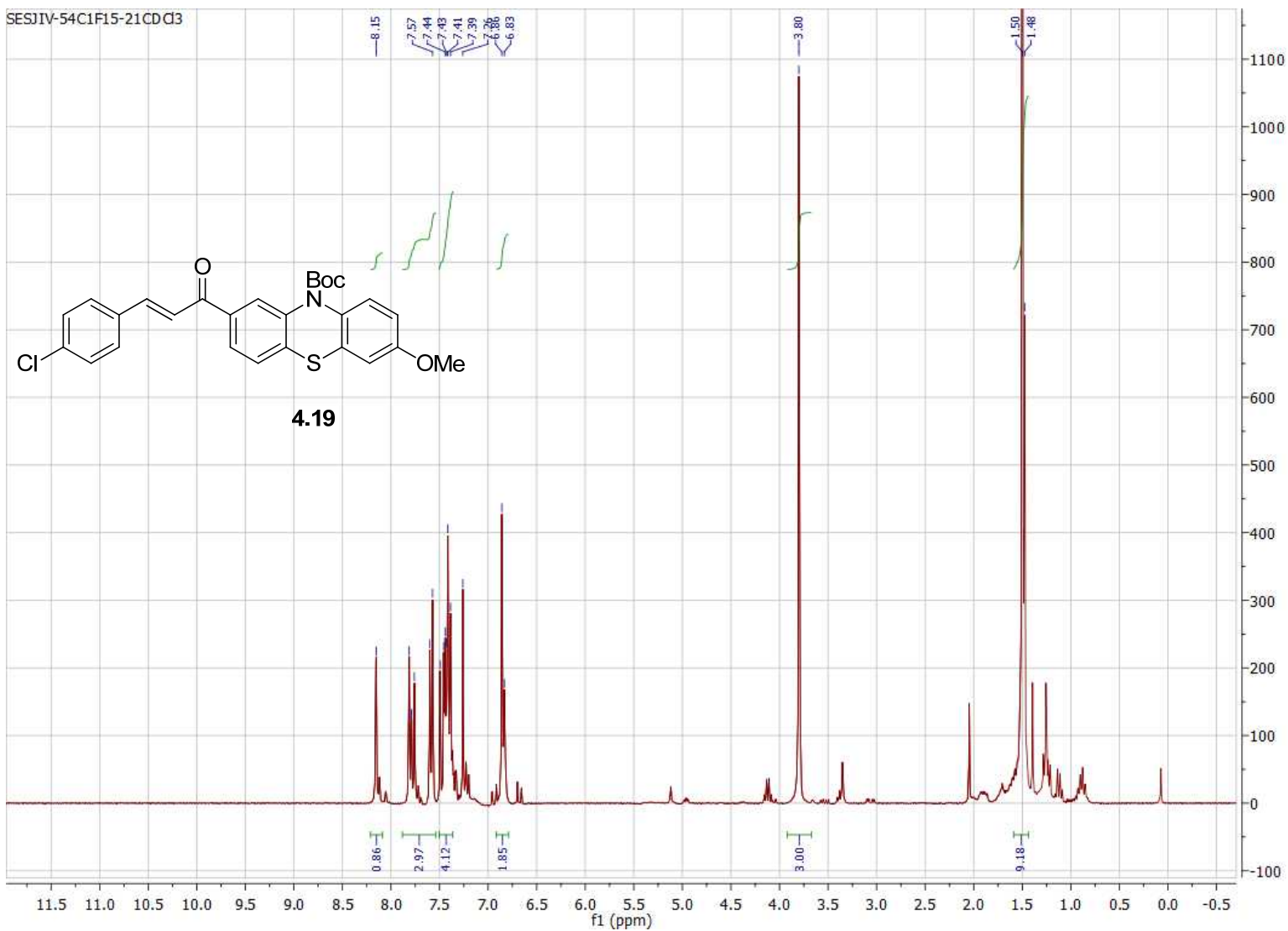


Figure B.99. 300 MHz ^1H NMR of crude compound **4.19** in CDCl_3 .

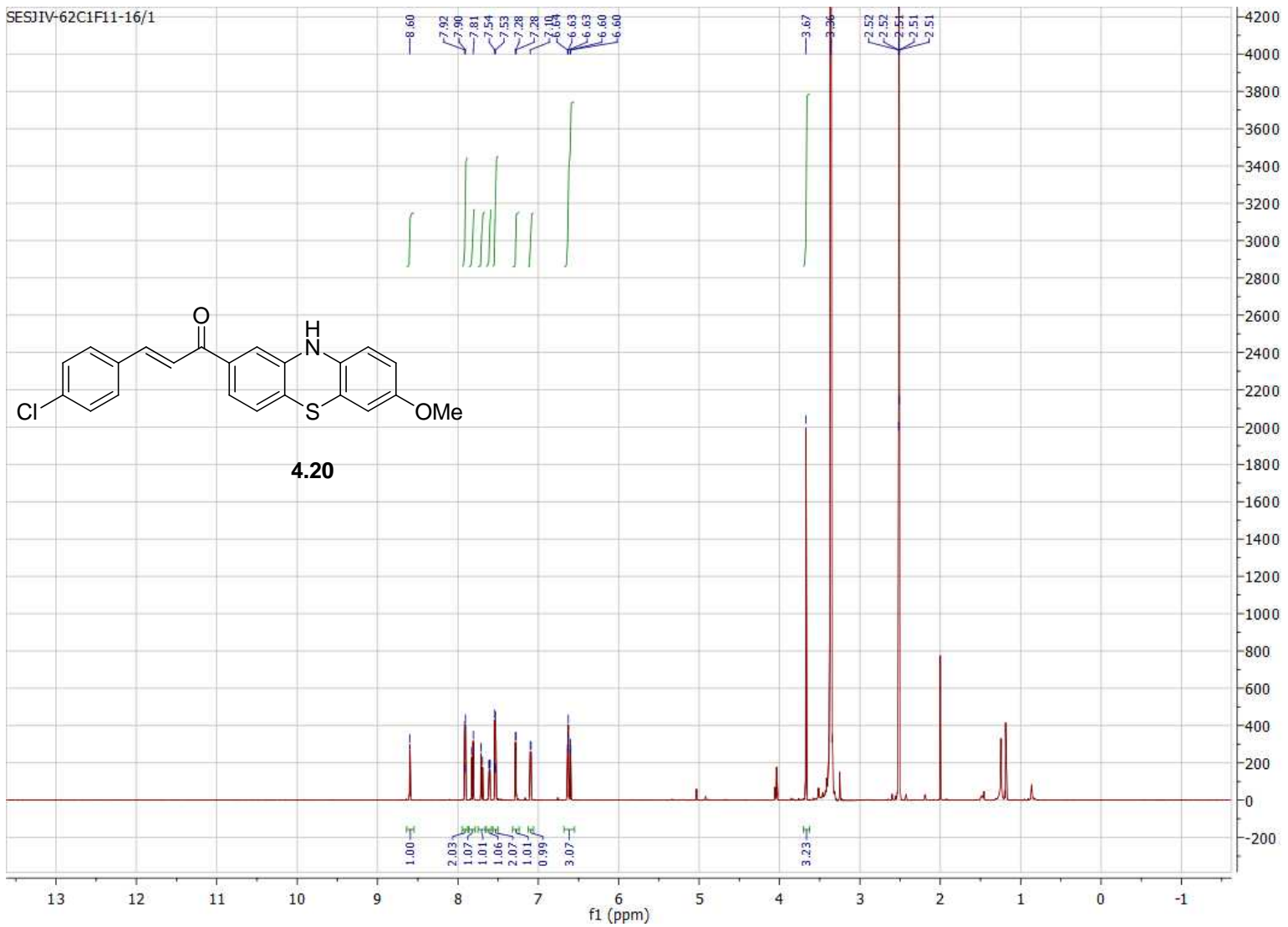


Figure B.100. 800 MHz ^1H NMR of compound **4.20** in d^6 -DMSO.

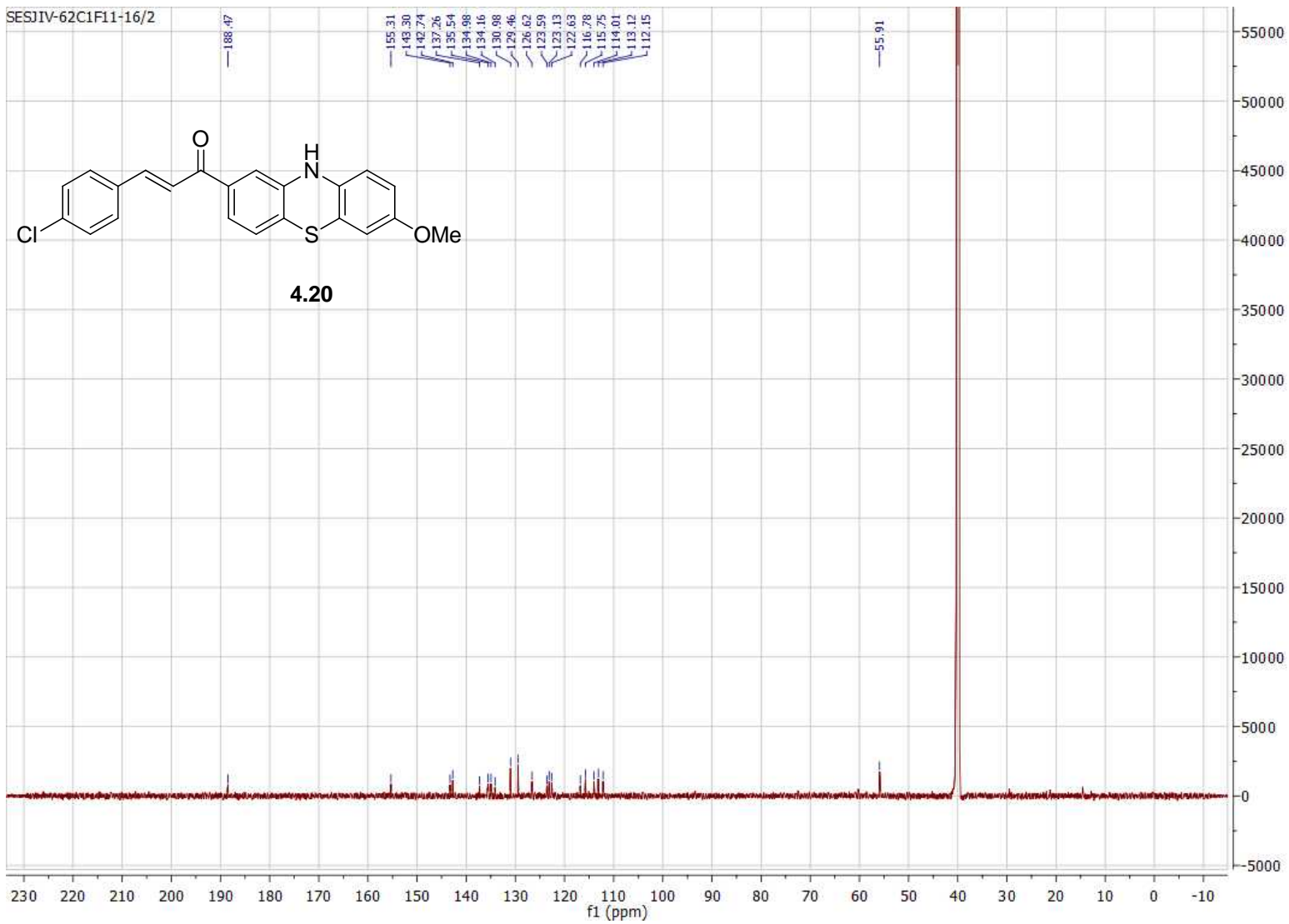


Figure B.101. 200 MHz ^1H NMR of compound **4.20** in d^6 -DMSO.

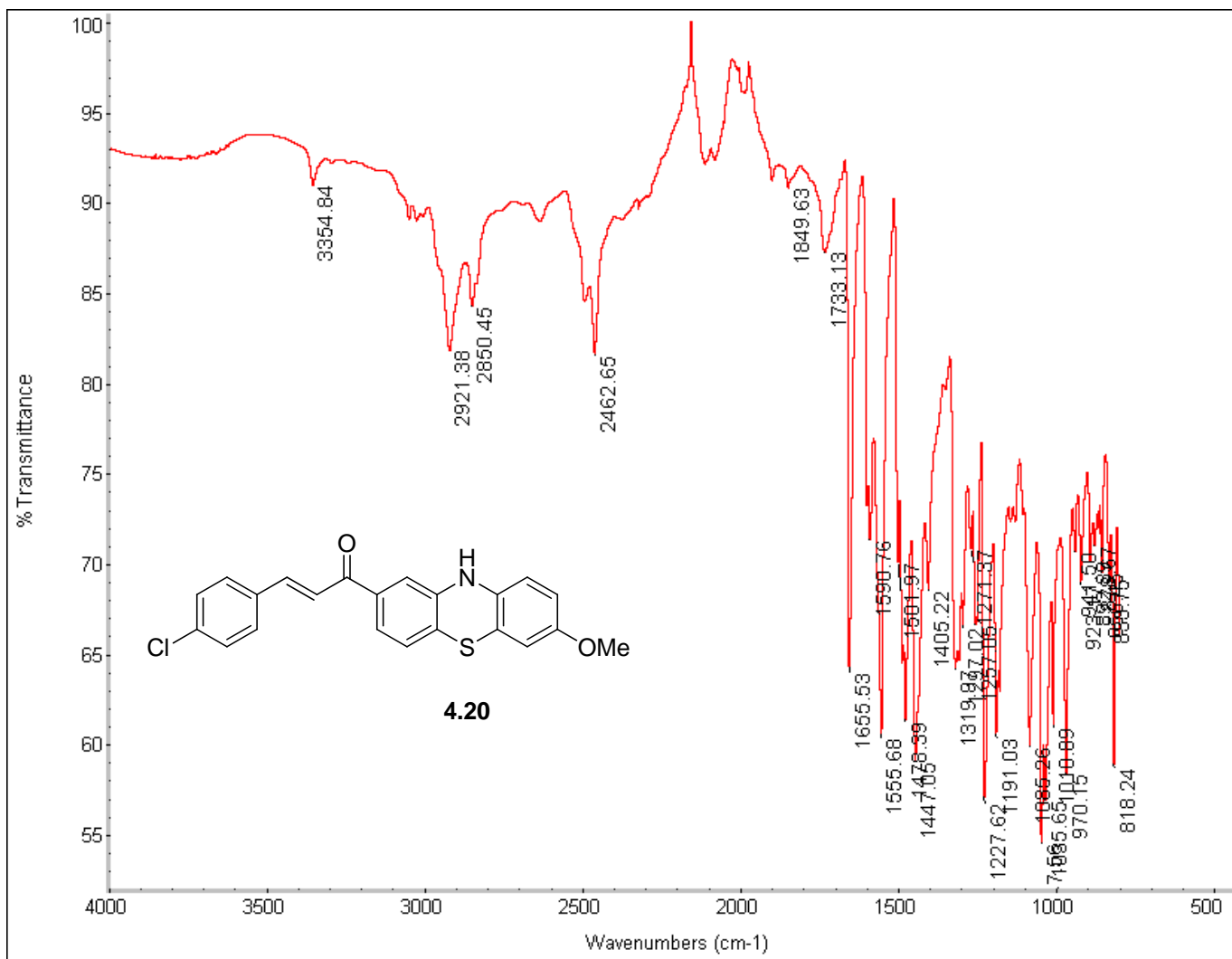


Figure B.102. FTIR of compound 4.20.

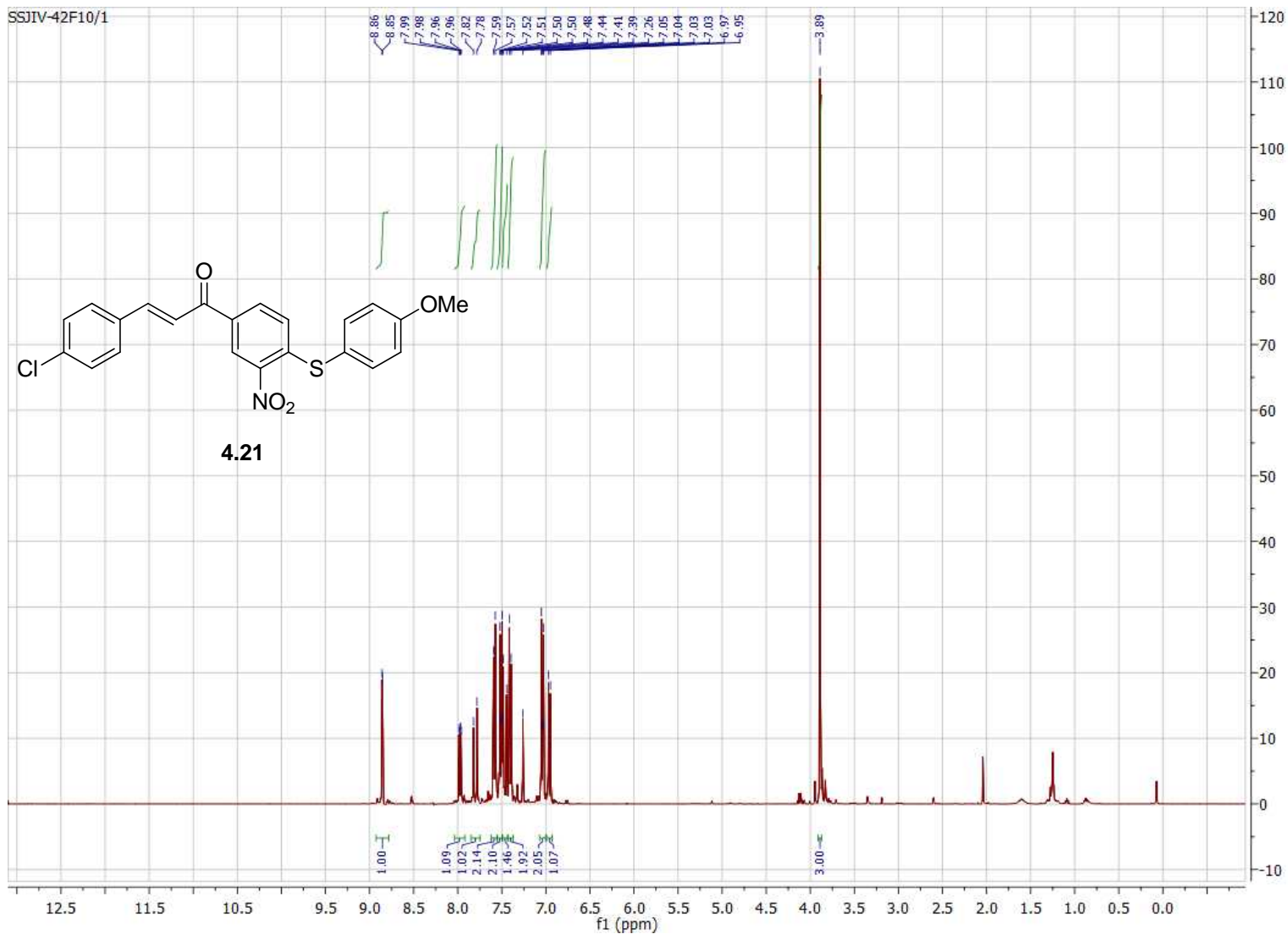


Figure B.103. 400 MHz ^1H NMR of compound **4.21** in CDCl_3 .

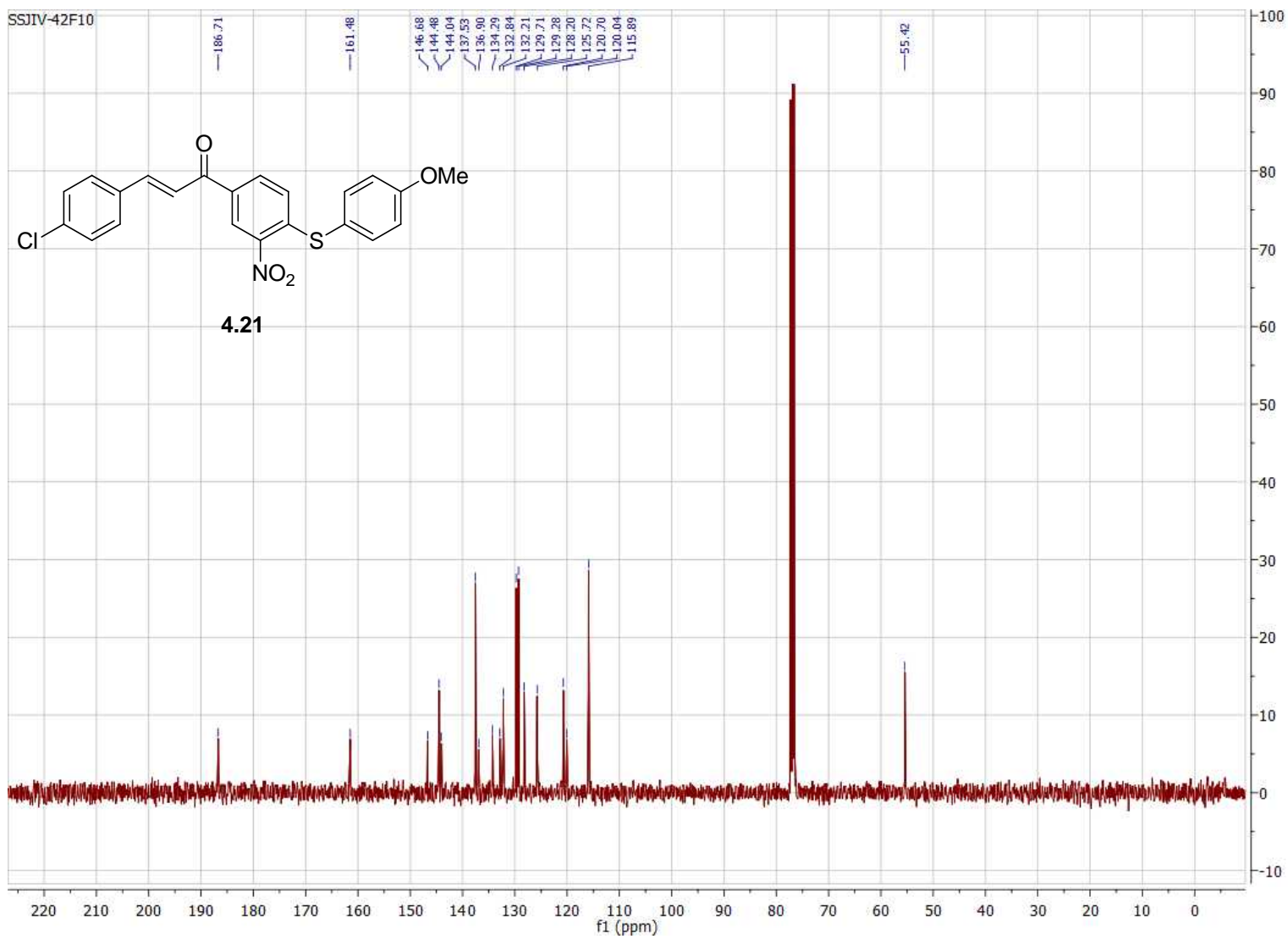


Figure B.104. 100 MHz ^{13}C NMR of compound **4.21** in CDCl_3 .

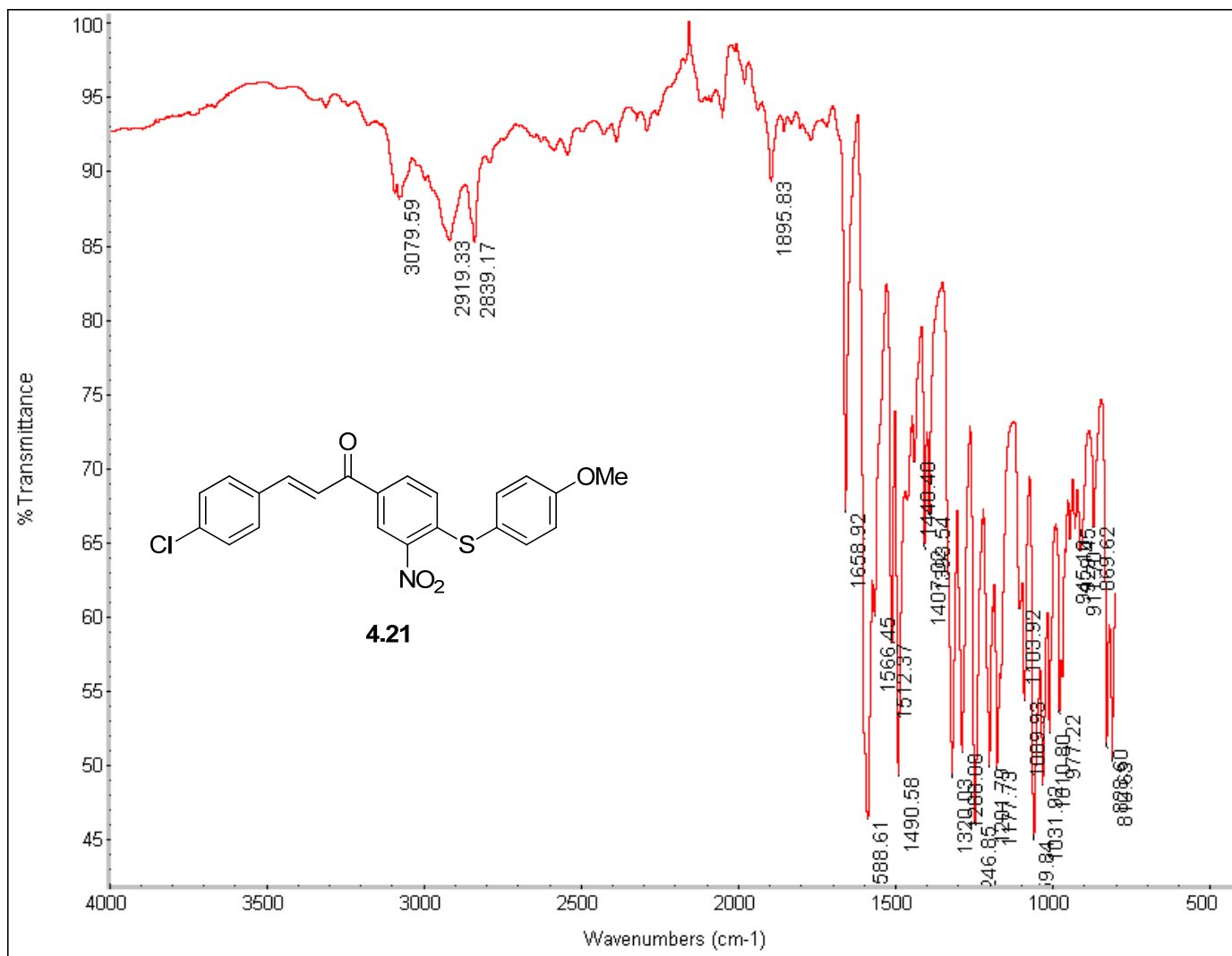


Figure B.105. FTIR of compound 4.21.

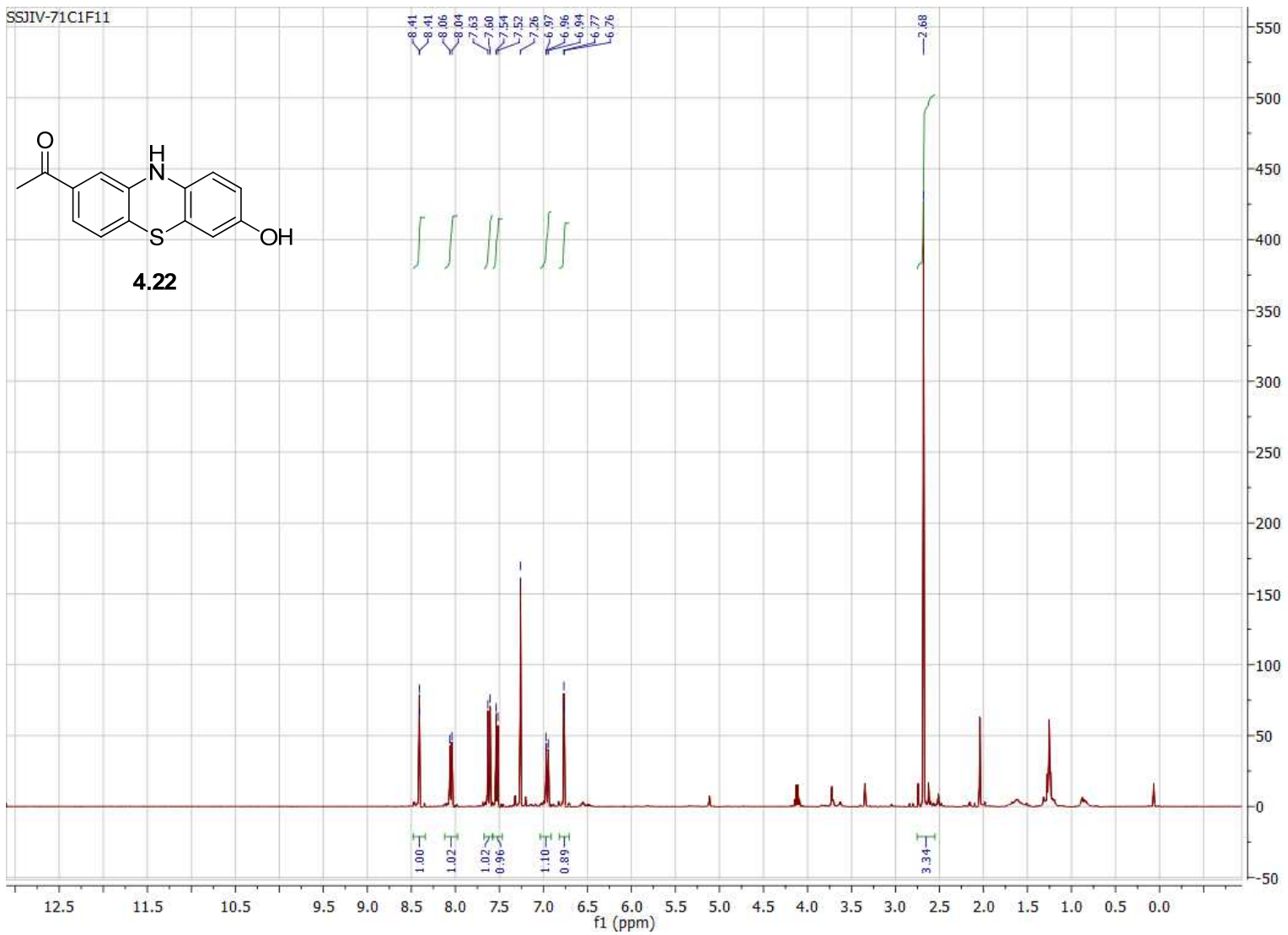
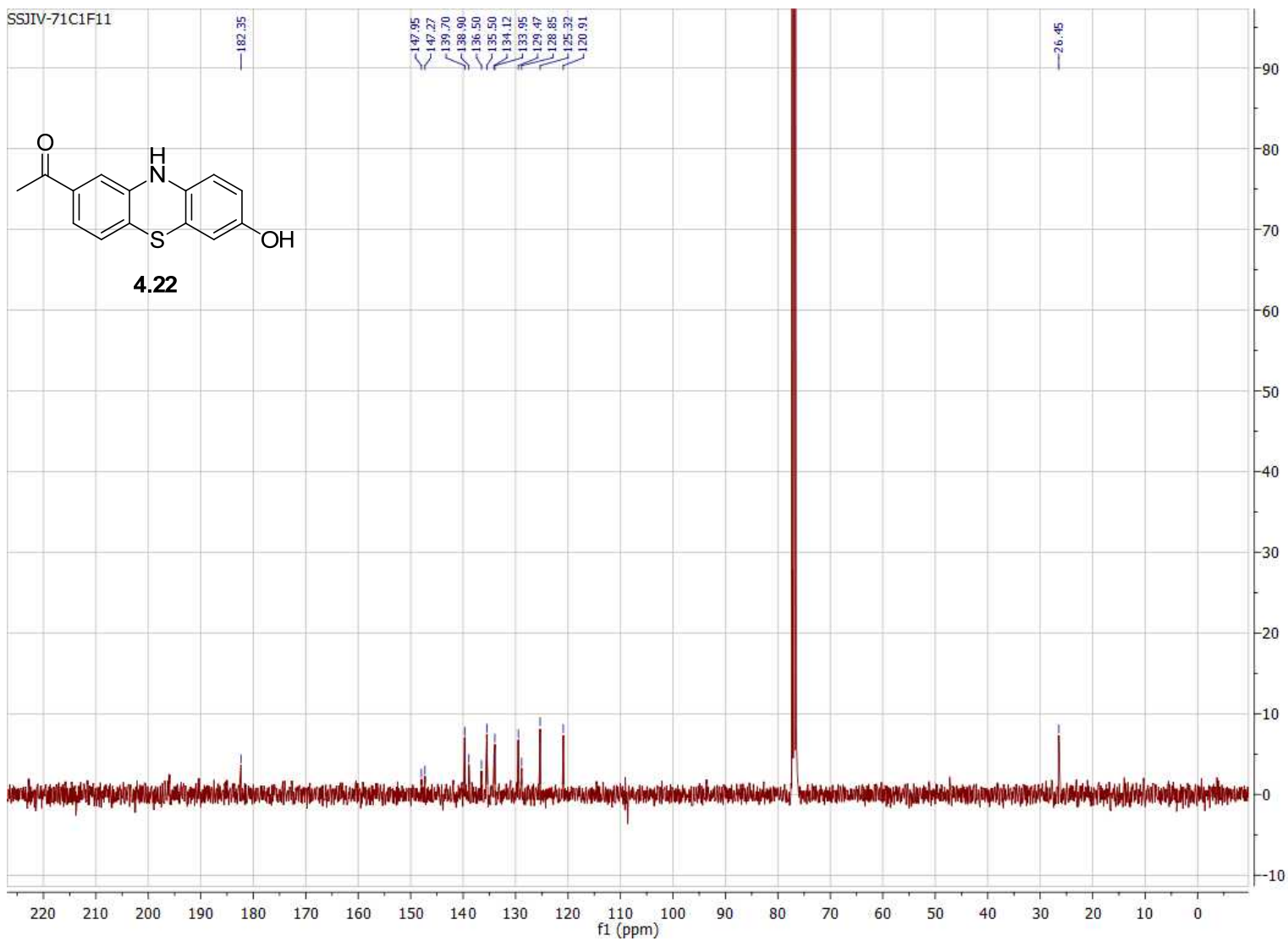


Figure B.106. 400 MHz ^1H NMR of compound **4.22** in CDCl_3 .



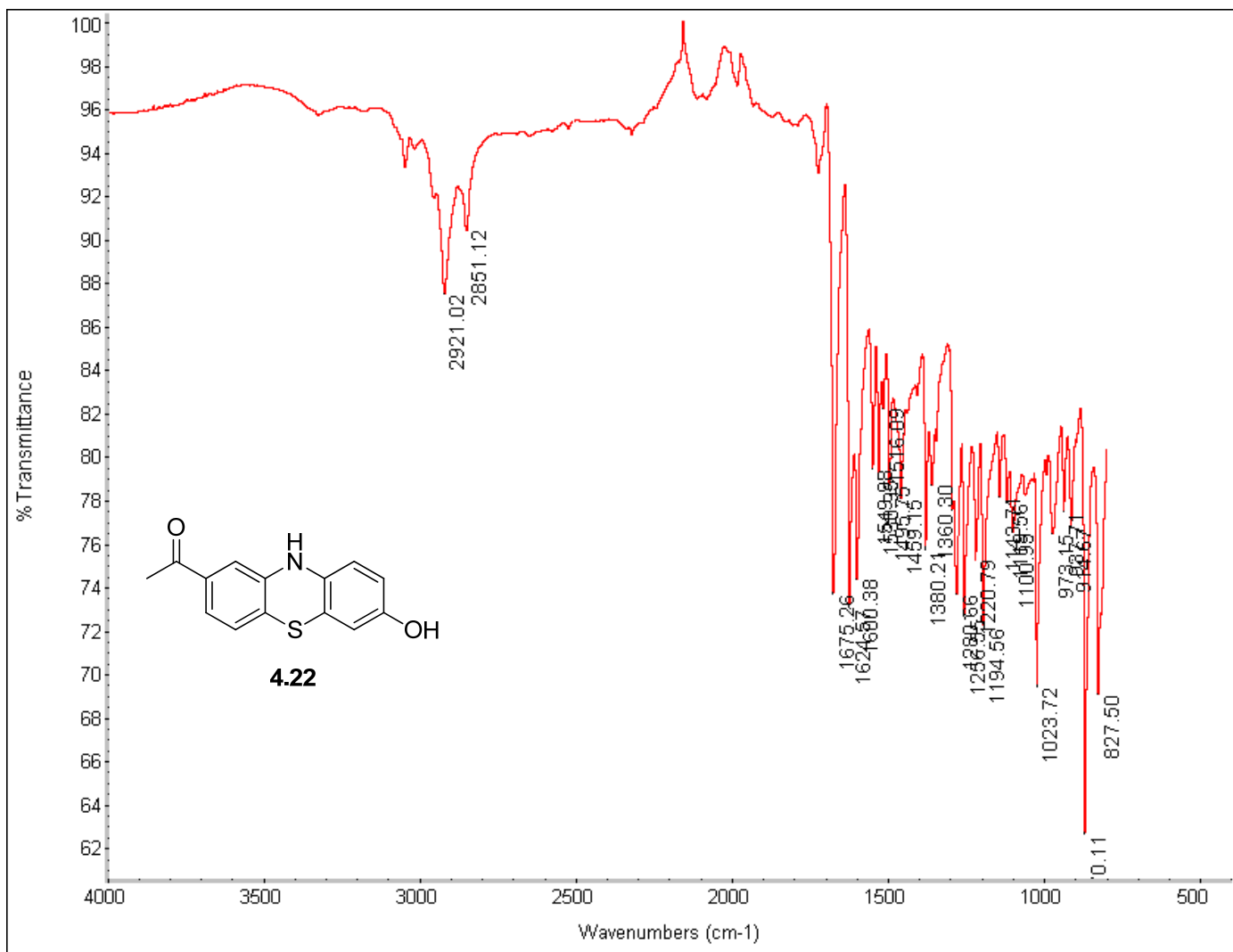


Figure B.108. FTIR of compound 4.22.

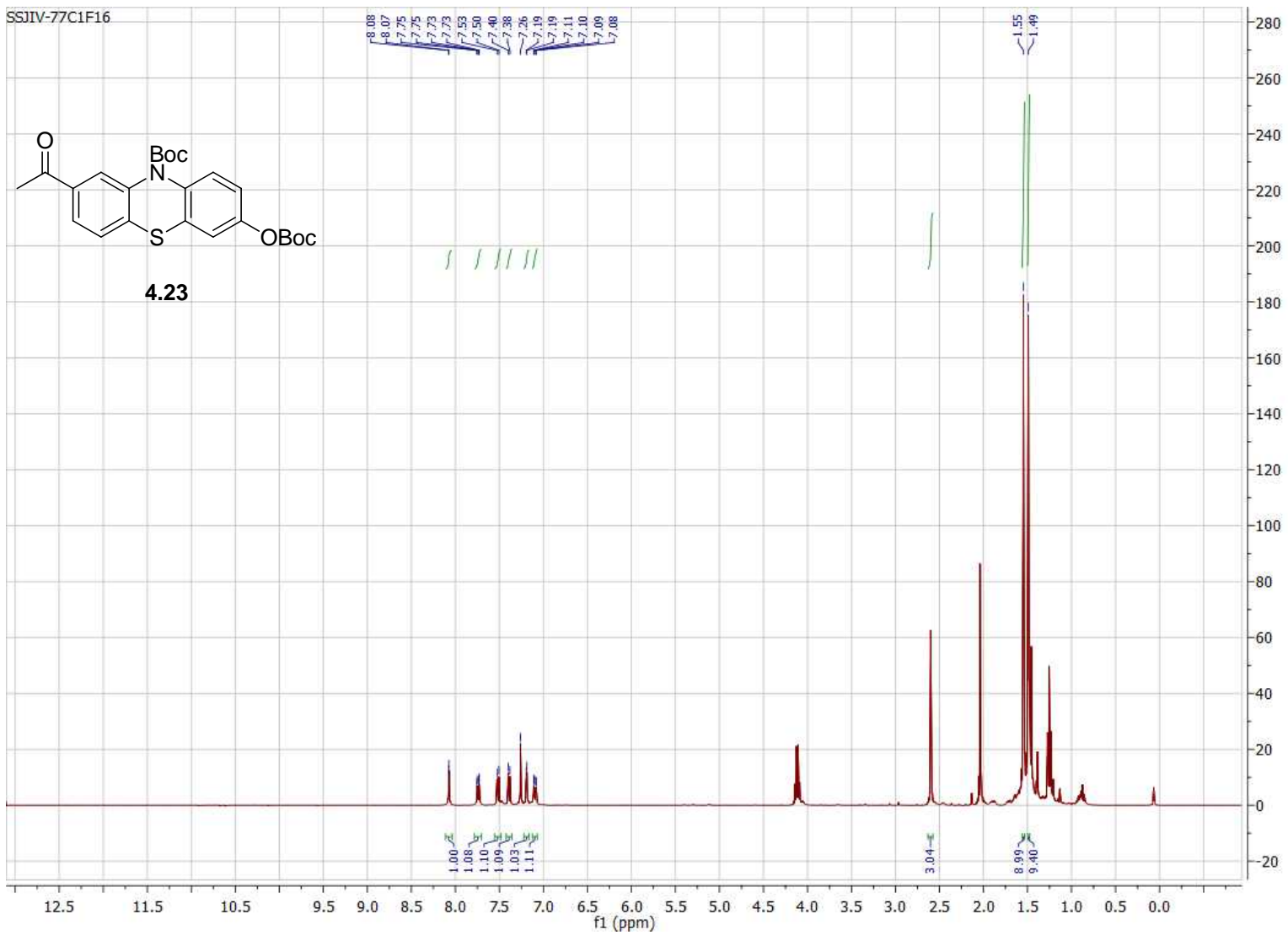


Figure B.109. 400 MHz ^1H NMR of compound **4.23** in CDCl_3 .

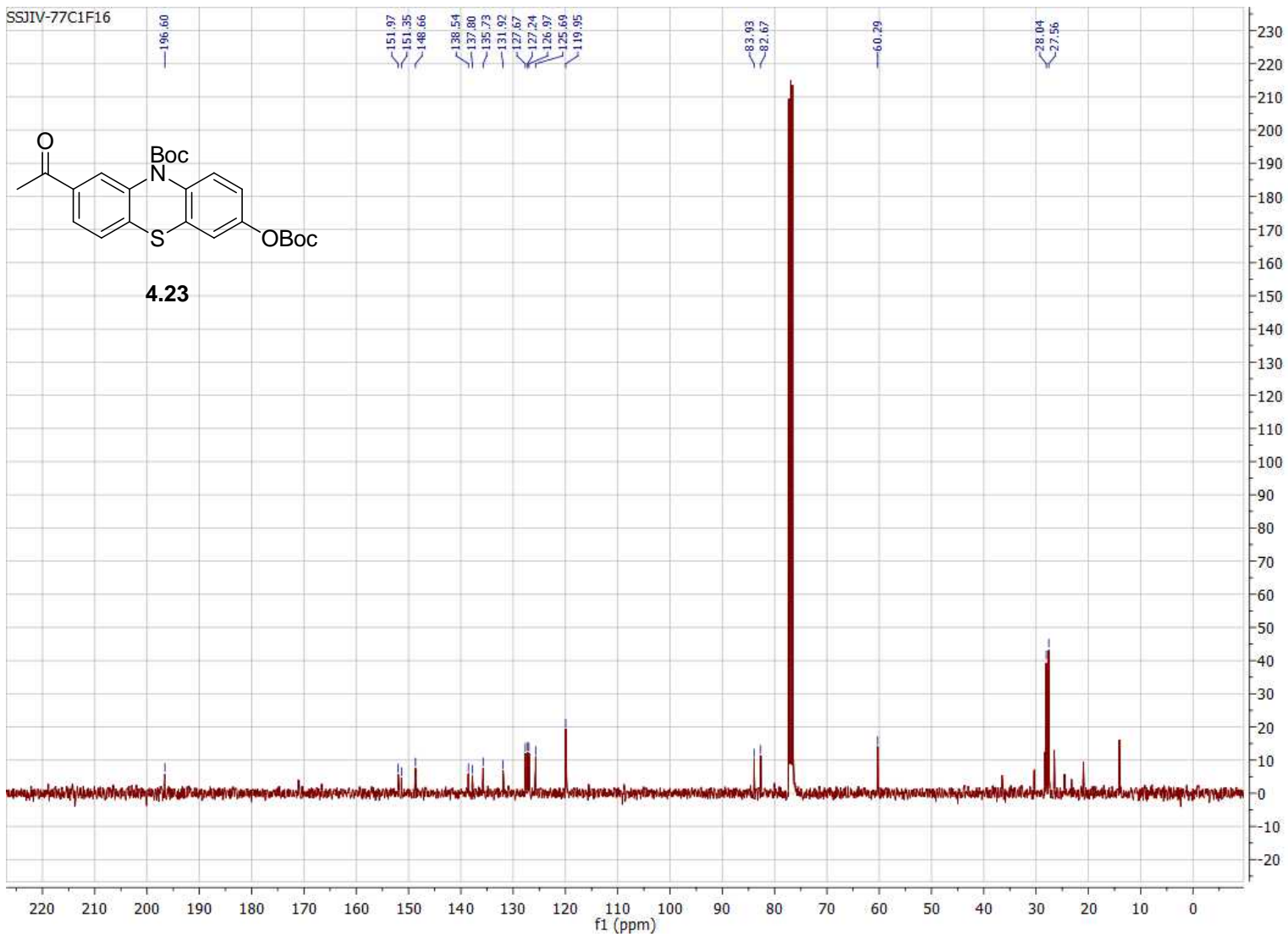


Figure B.110. 100 MHz ¹³C NMR of compound **4.23** in CDCl₃.

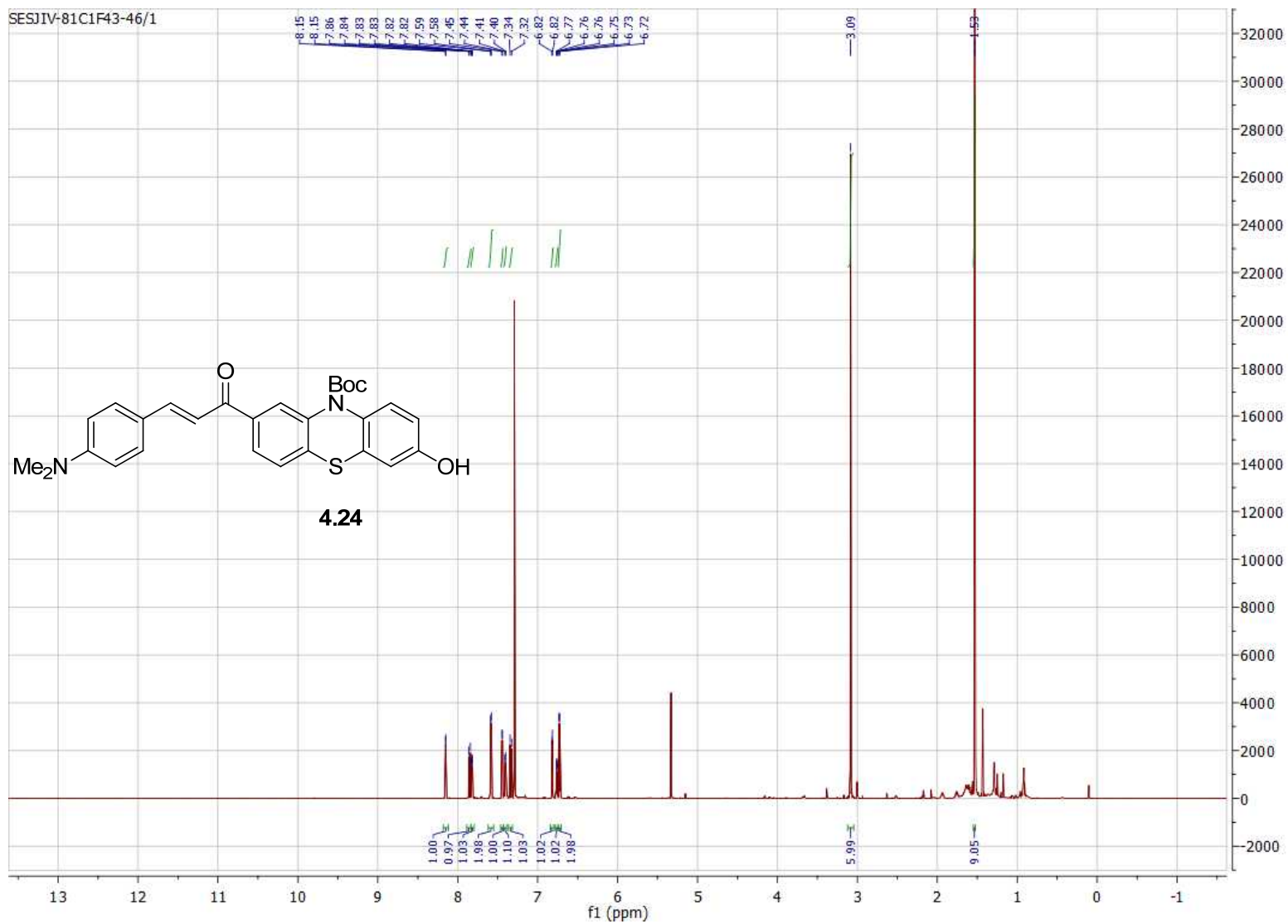


Figure B.111. 800 MHz ^1H NMR of compound **4.24** in CDCl_3 .

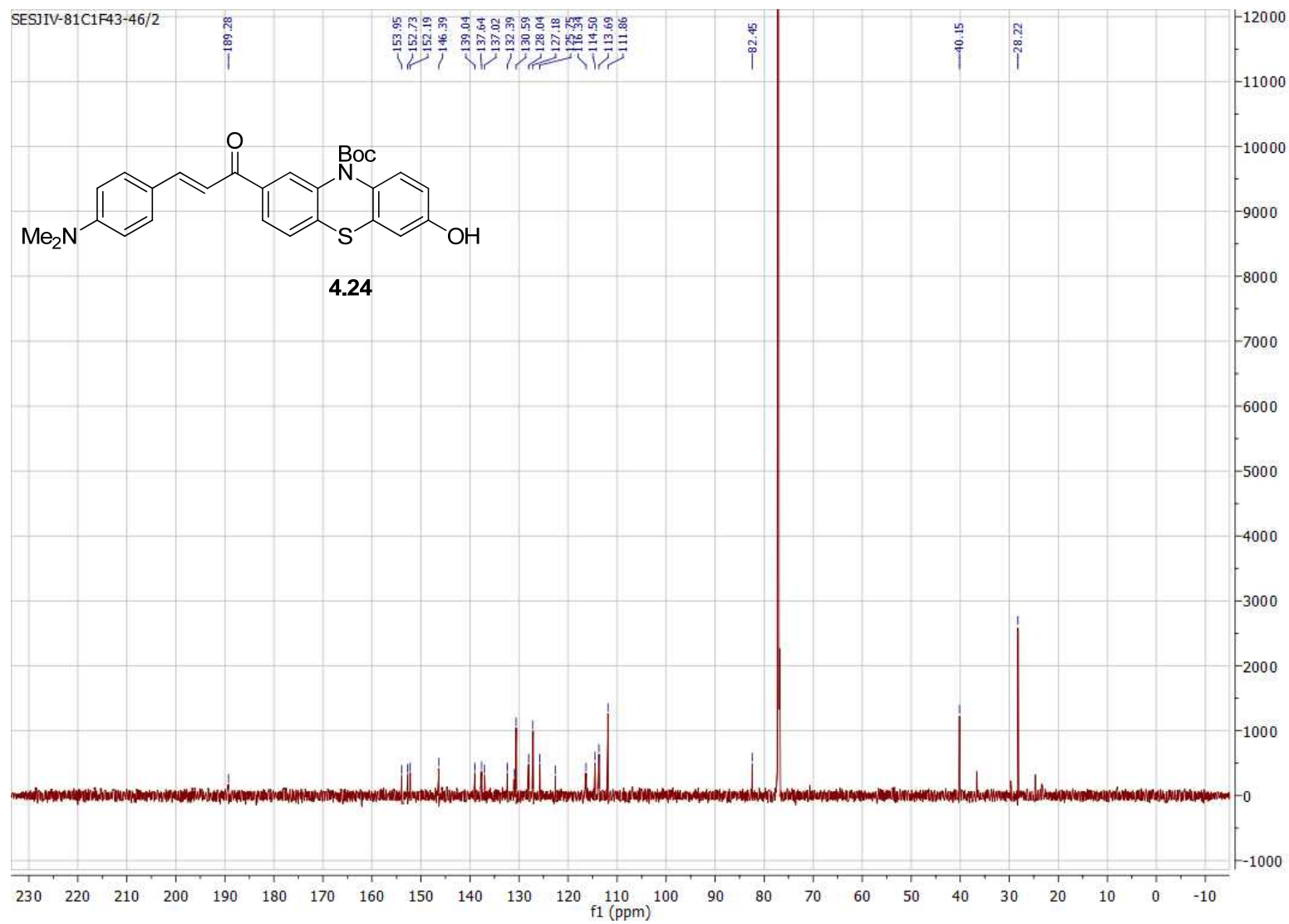


Figure B.112. 200 MHz ^{13}C NMR of compound **4.24** in CDCl_3 .

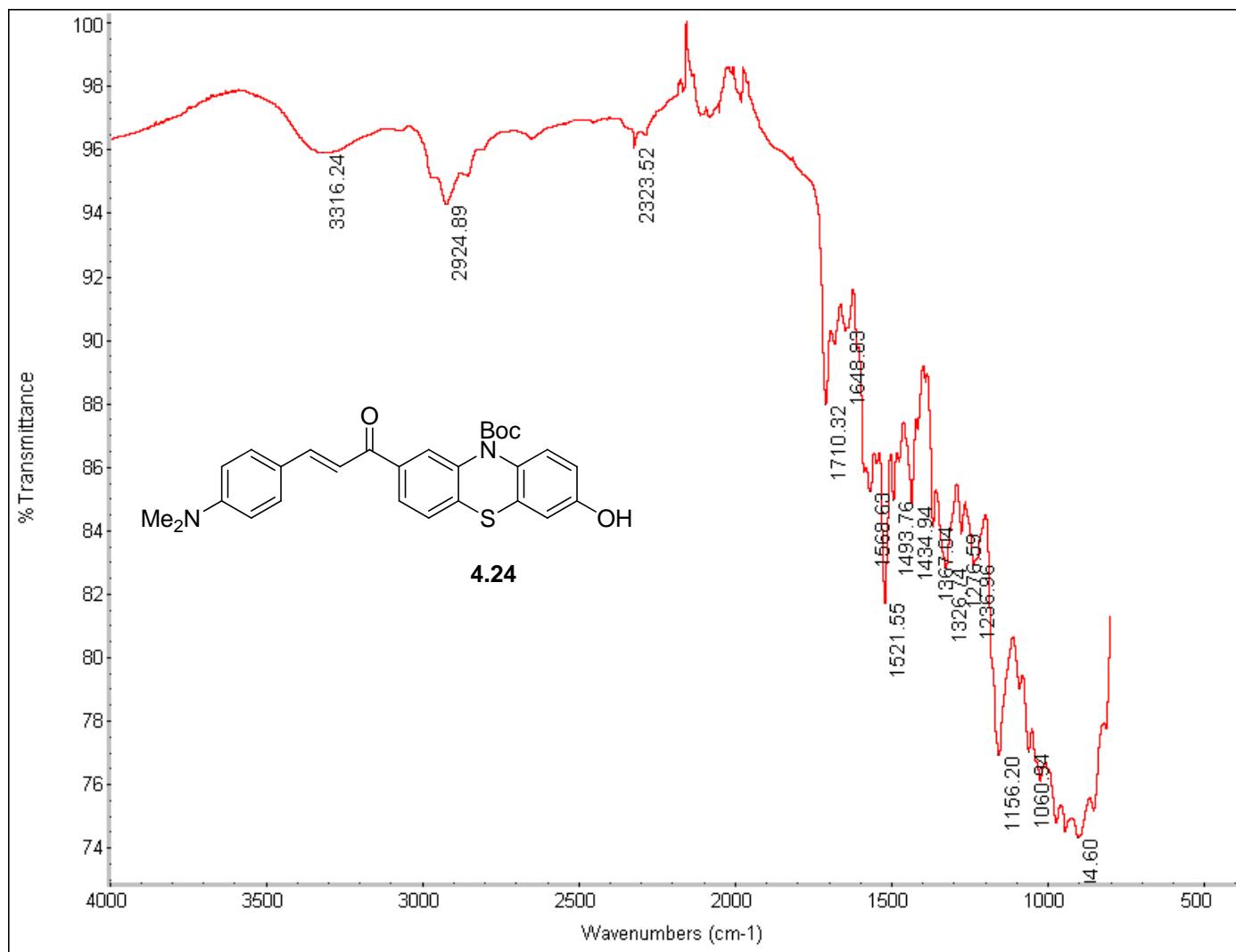


Figure B.113. FTIR of compound 4.24.

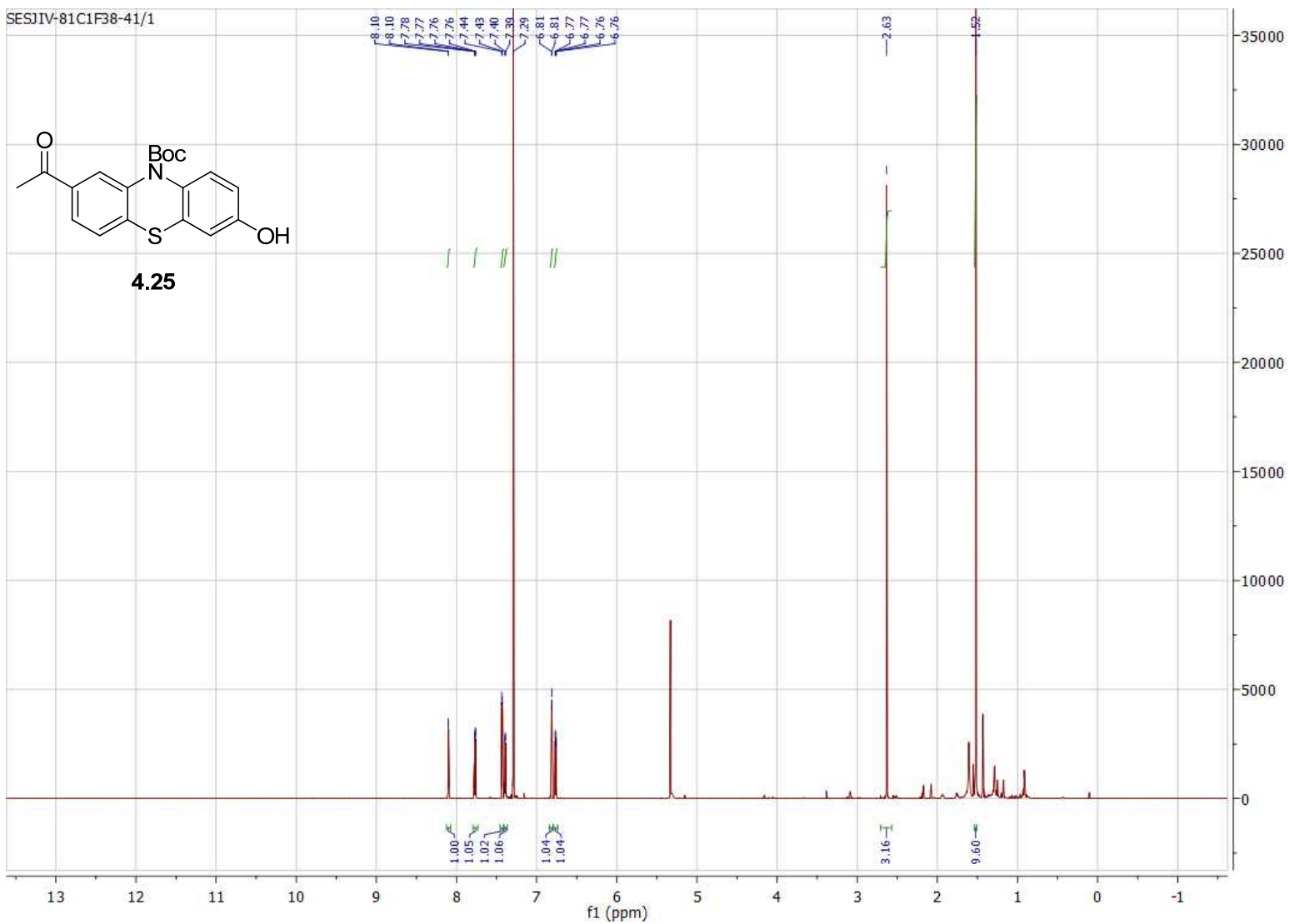


Figure B.114. 800 MHz ^1H NMR of compound **4.25** in CDCl_3 .

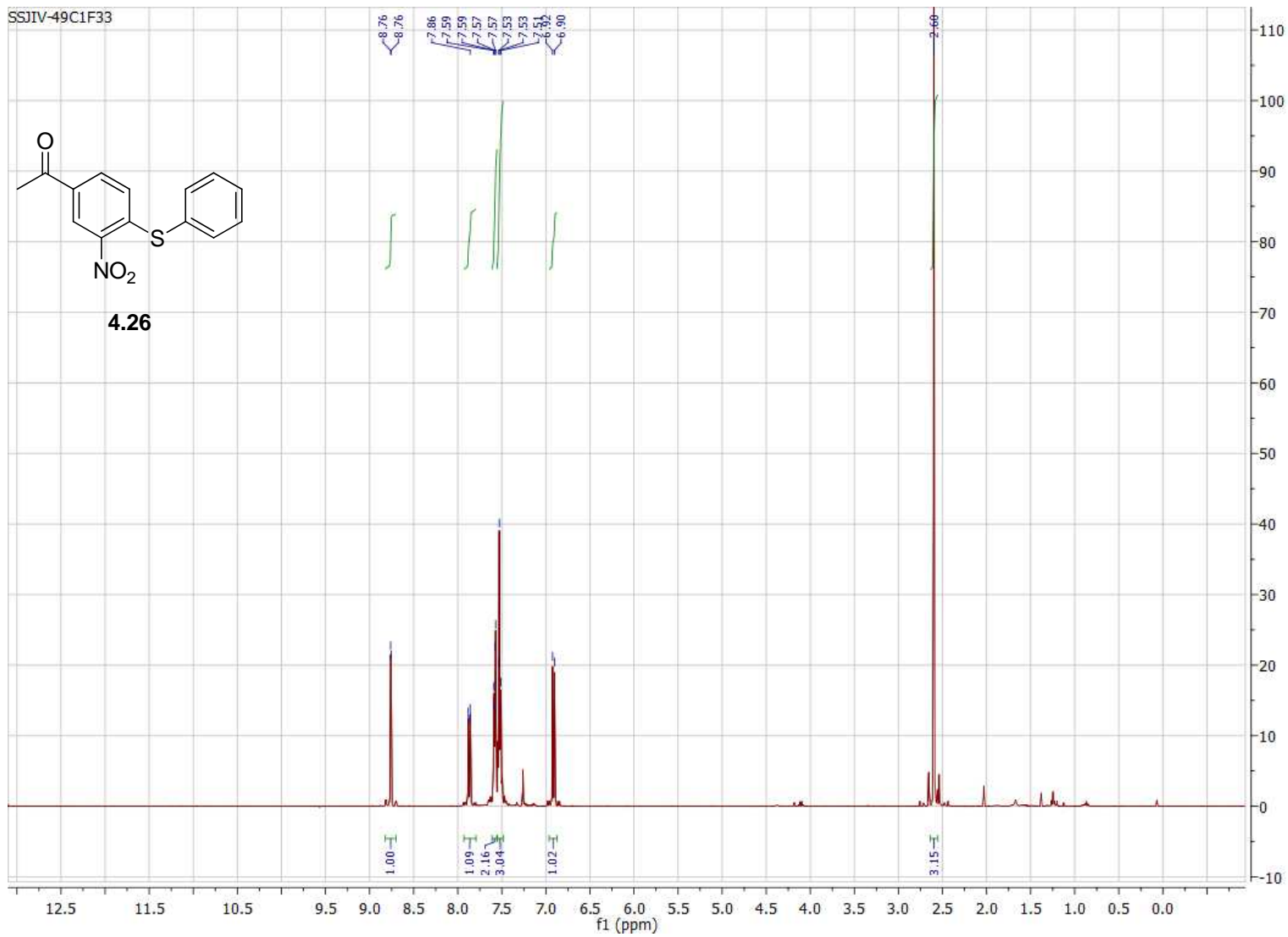


Figure B.115. 400 MHz ^1H NMR of compound **4.26** in CDCl_3 .

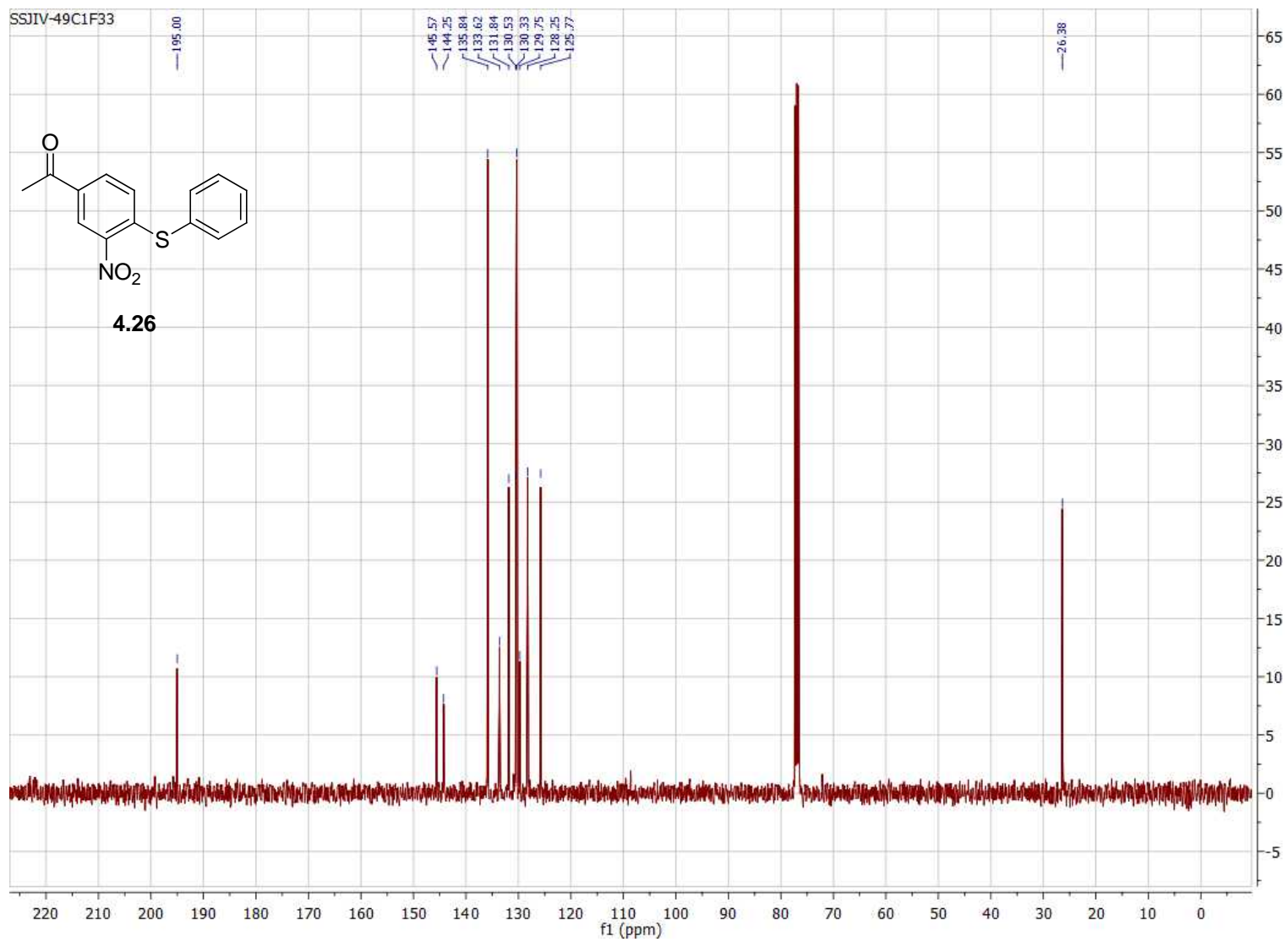


Figure B.116. 100 MHz ^{13}C NMR of compound **4.26** in CDCl_3 .

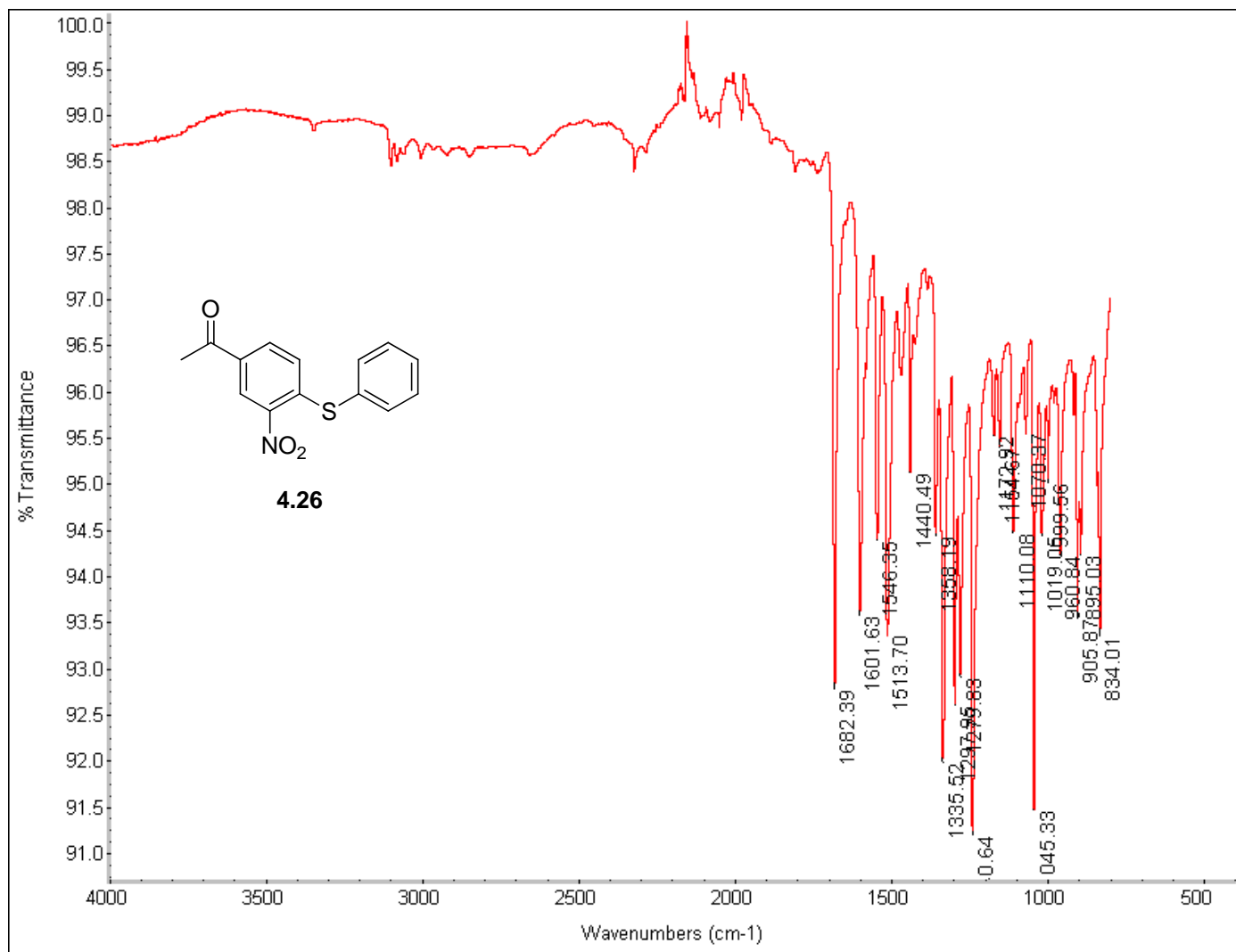


Figure B.117. FTIR of compound 4.26.

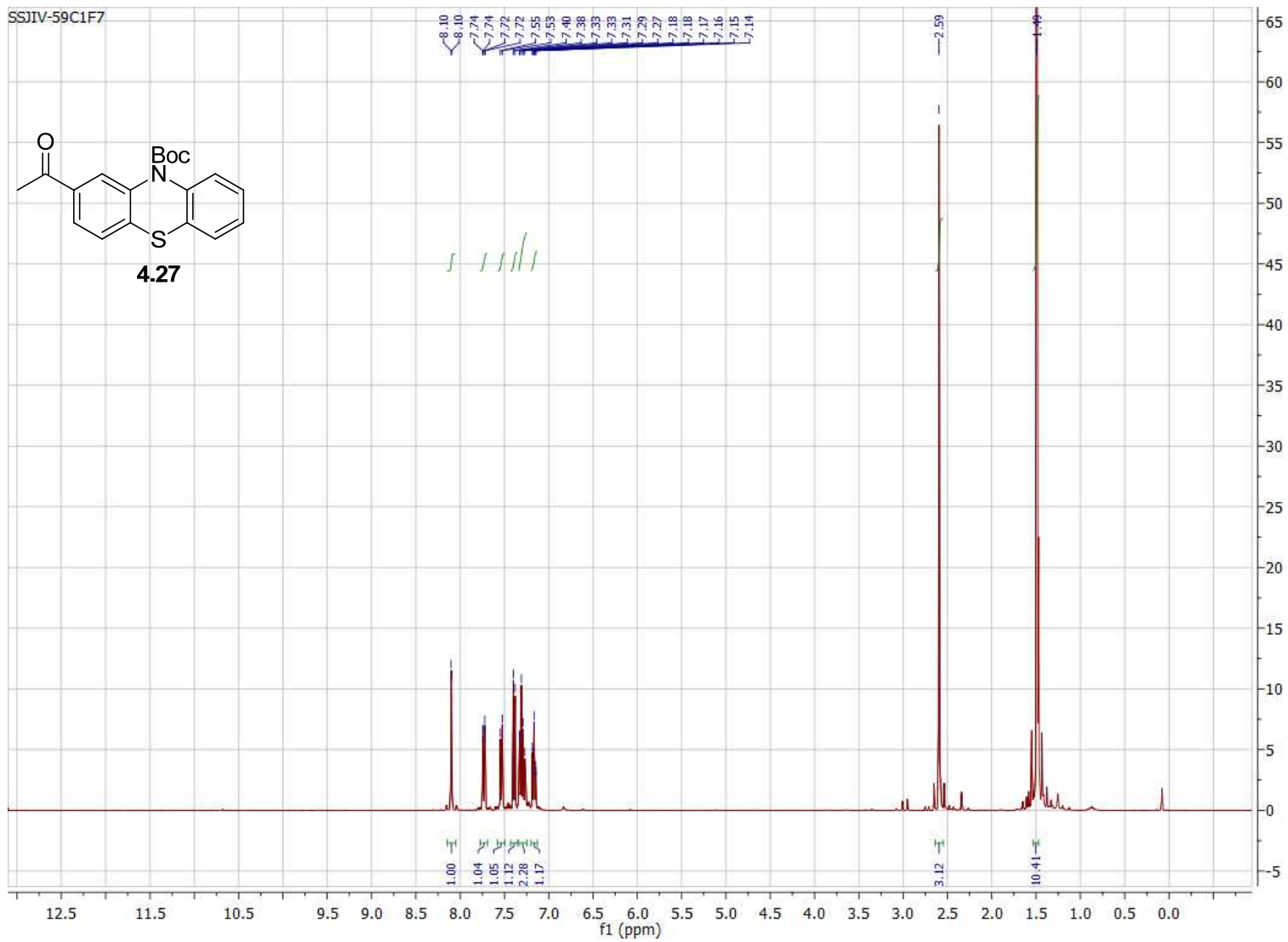


Figure B.118. 400 MHz ^1H NMR of compound **4.27** in CDCl_3 .

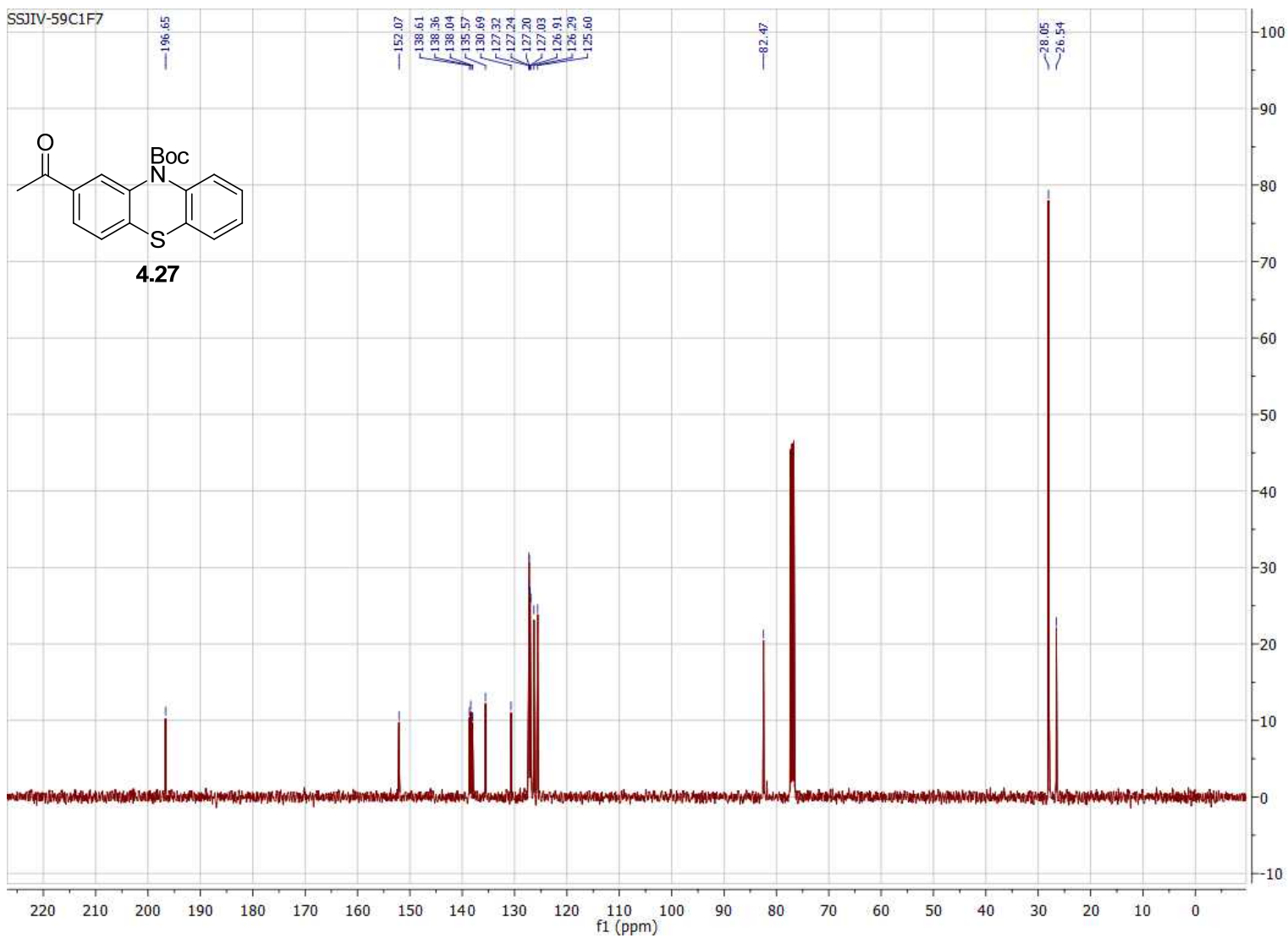


Figure B.119. 100 MHz ^{13}C NMR of compound **4.27** in CDCl_3 .

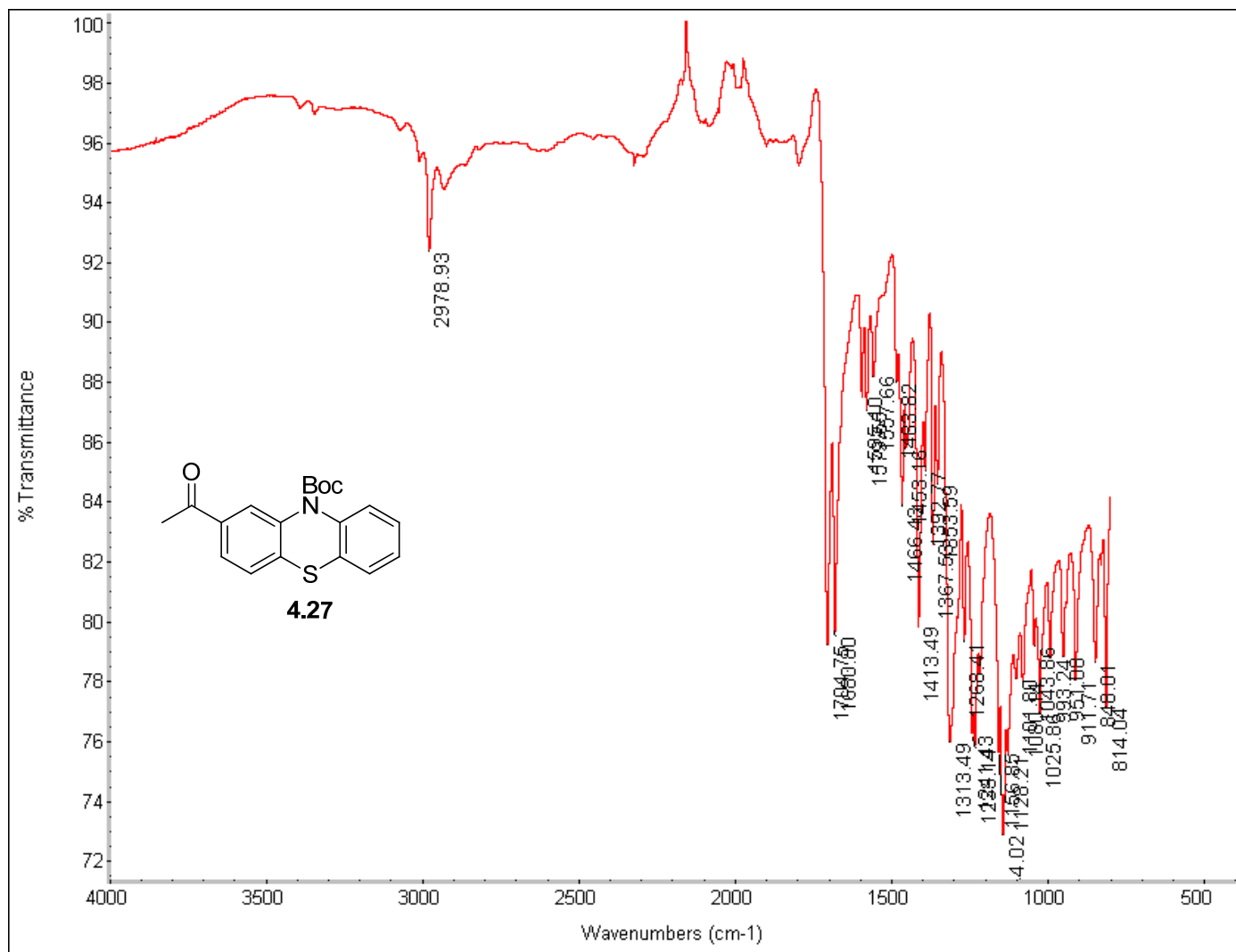


Figure B.120. FTIR of compound 4.27.

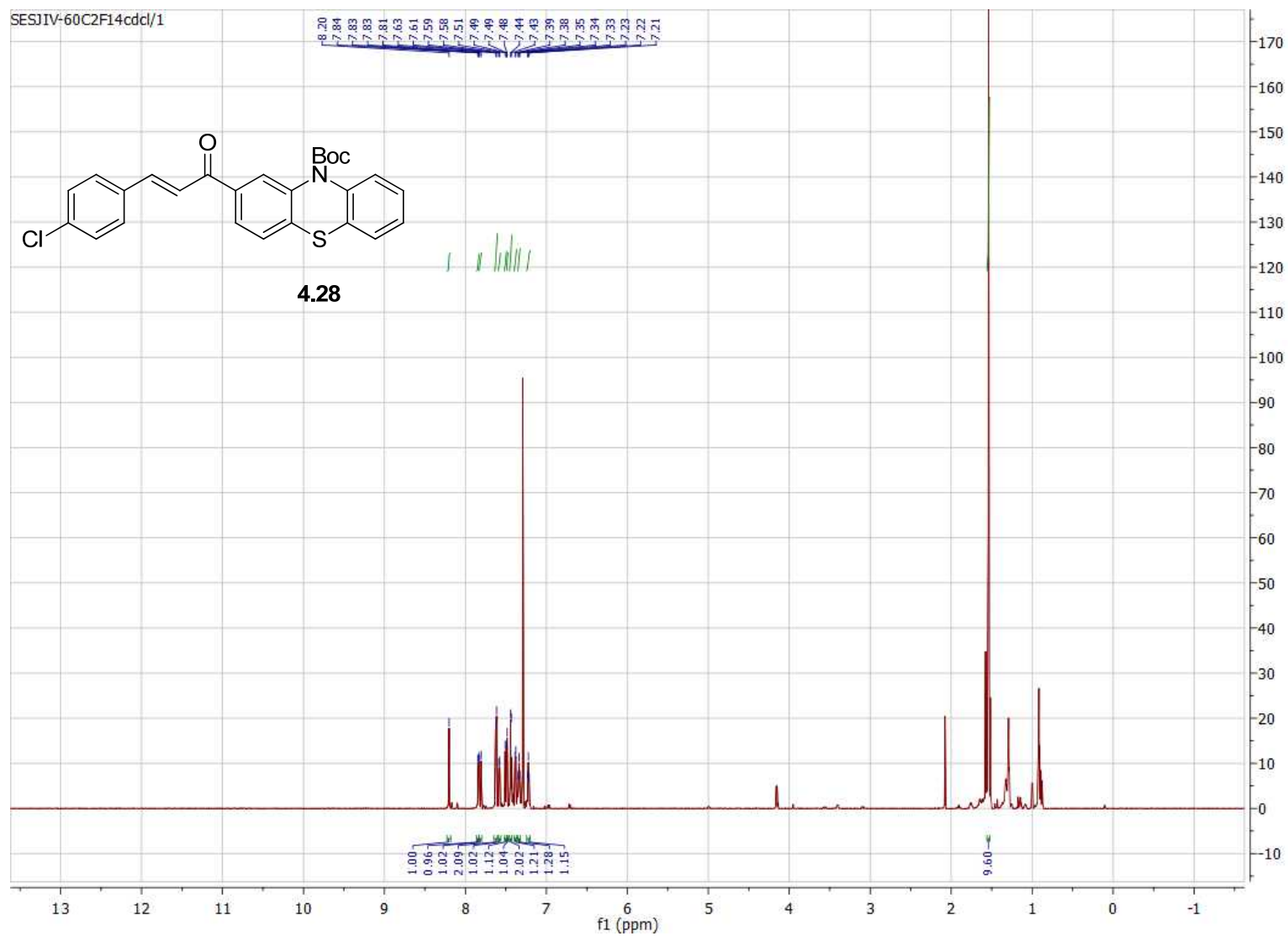


Figure B.121. 800 MHz ^1H NMR of compound **4.28** in CDCl_3 .

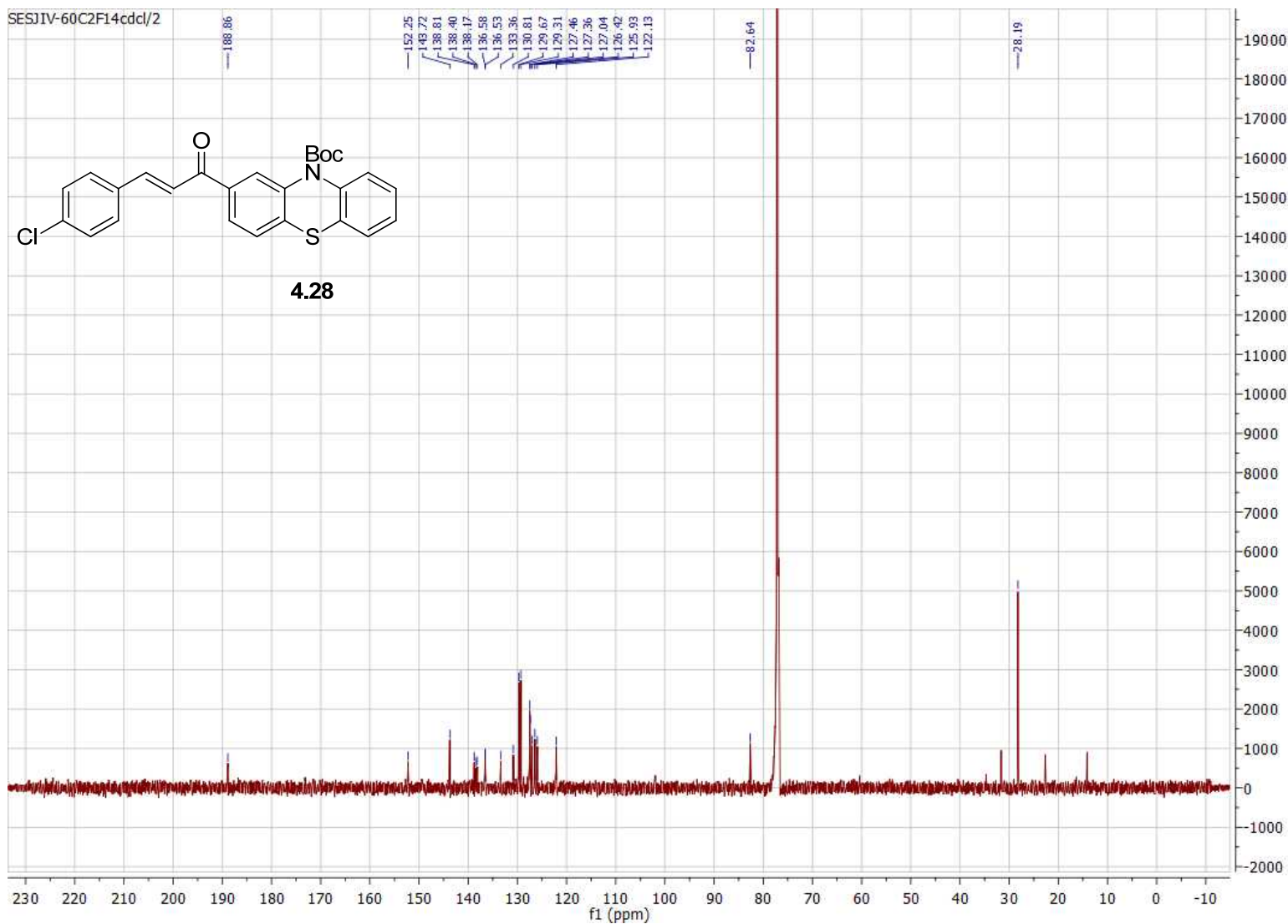


Figure B.122. 200 MHz ^{13}C NMR of compound **4.28** in CDCl_3 .

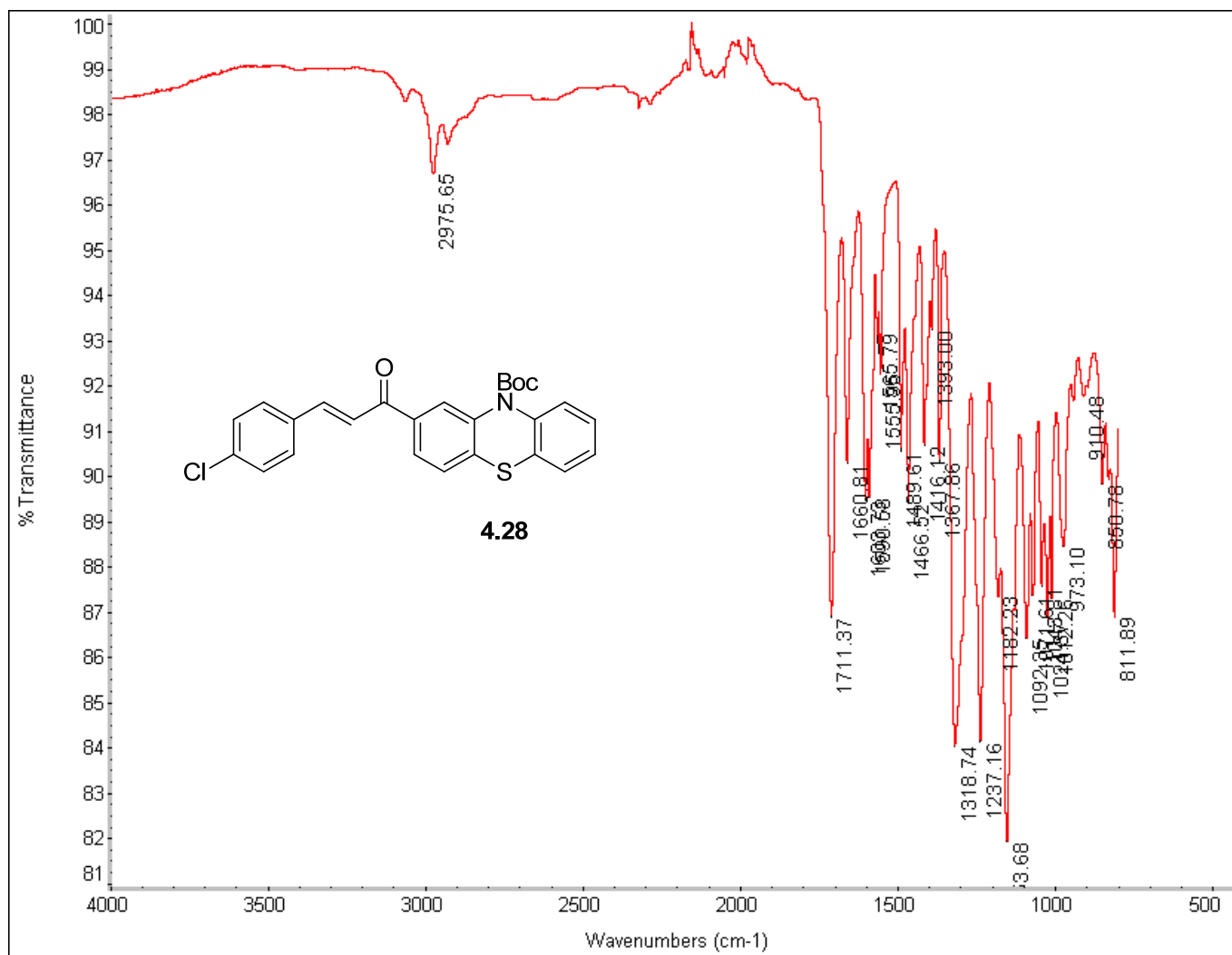


Figure B.123. FTIR of compound 4.28.

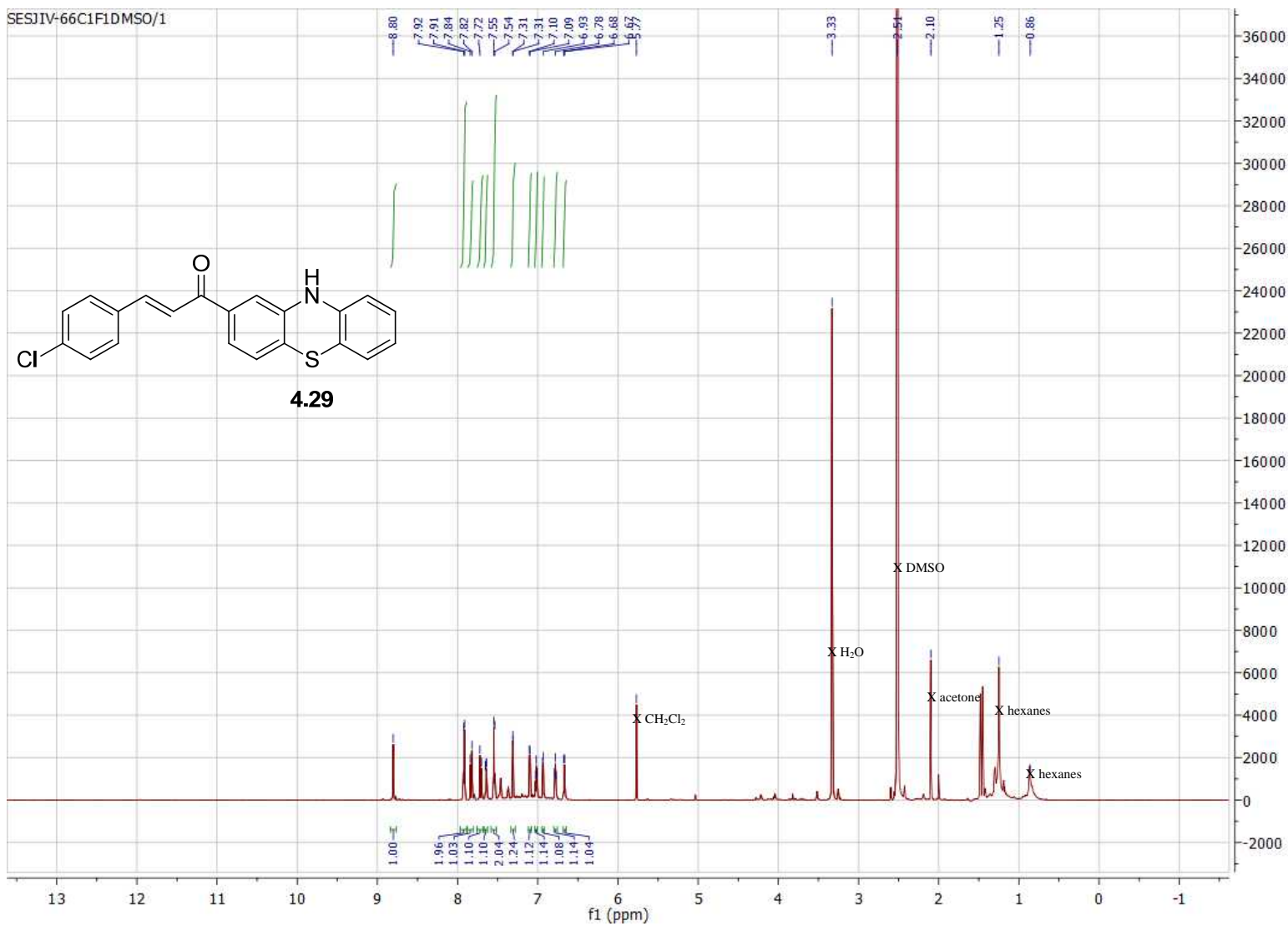


Figure B.124. 800 MHz ¹H NMR of compound **4.29** in d⁶-DMSO.

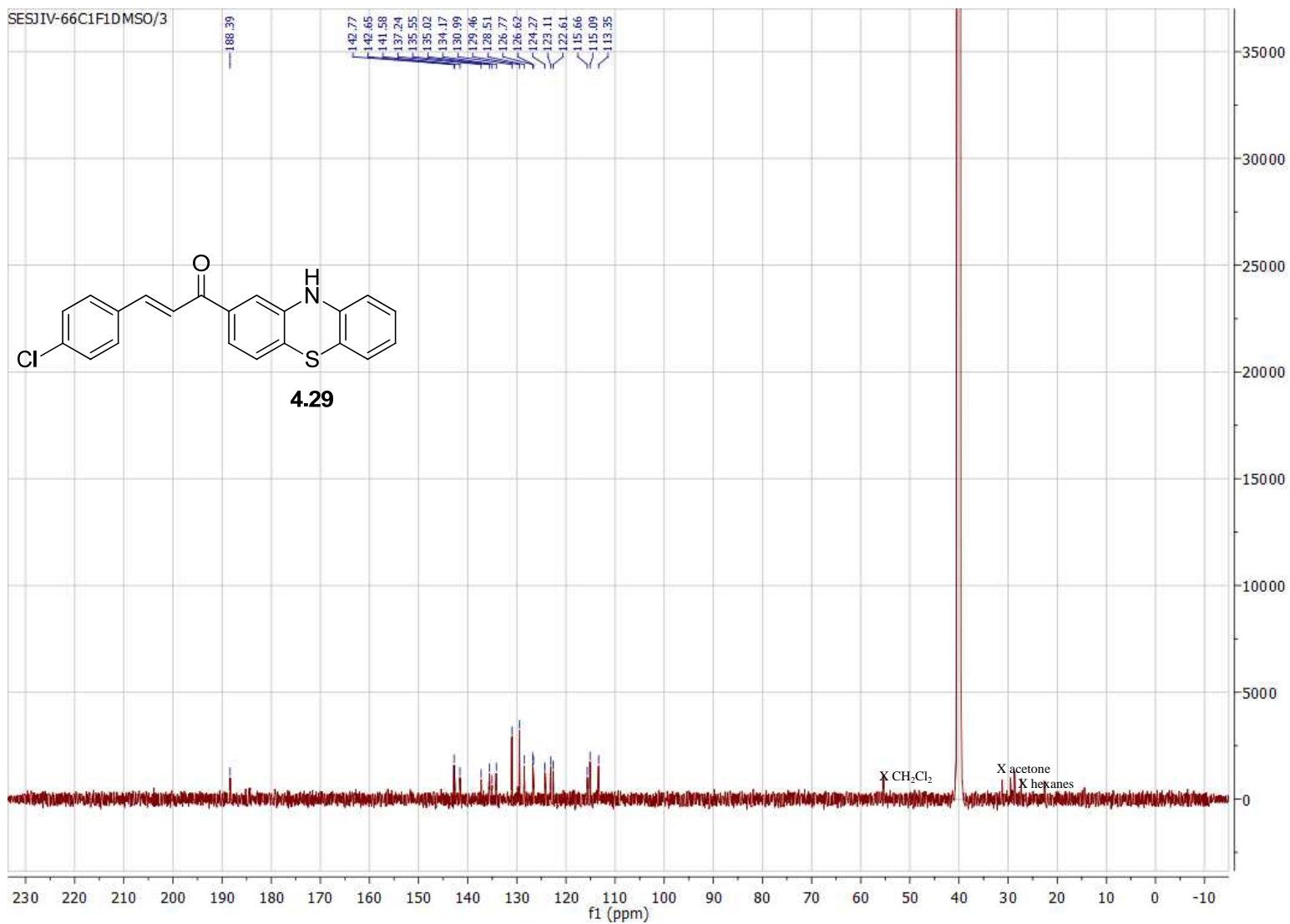


Figure B.125. 200 MHz ¹³C NMR of compound **4.29** in d⁶-DMSO.

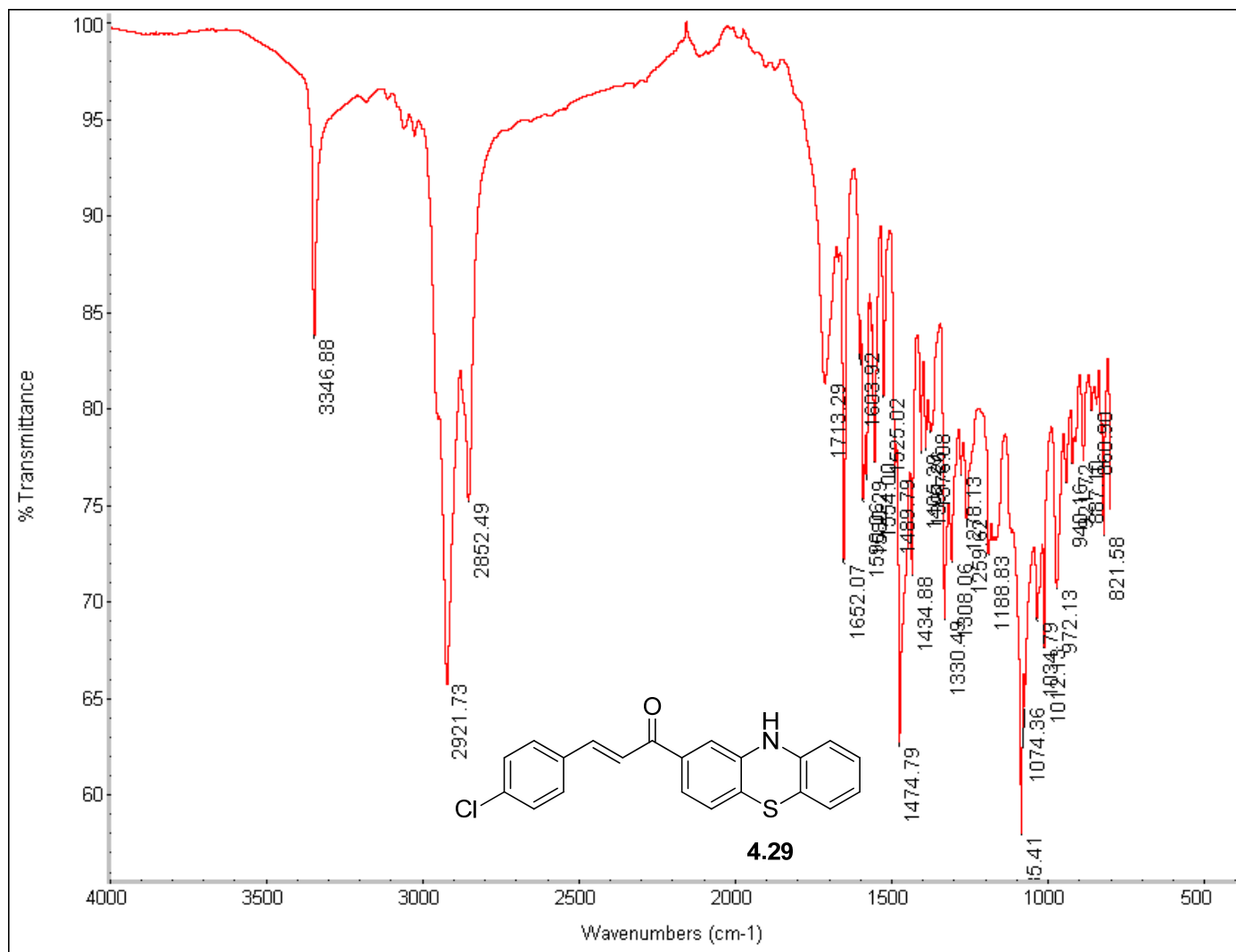


Figure B.126. FTIR of compound 4.29.

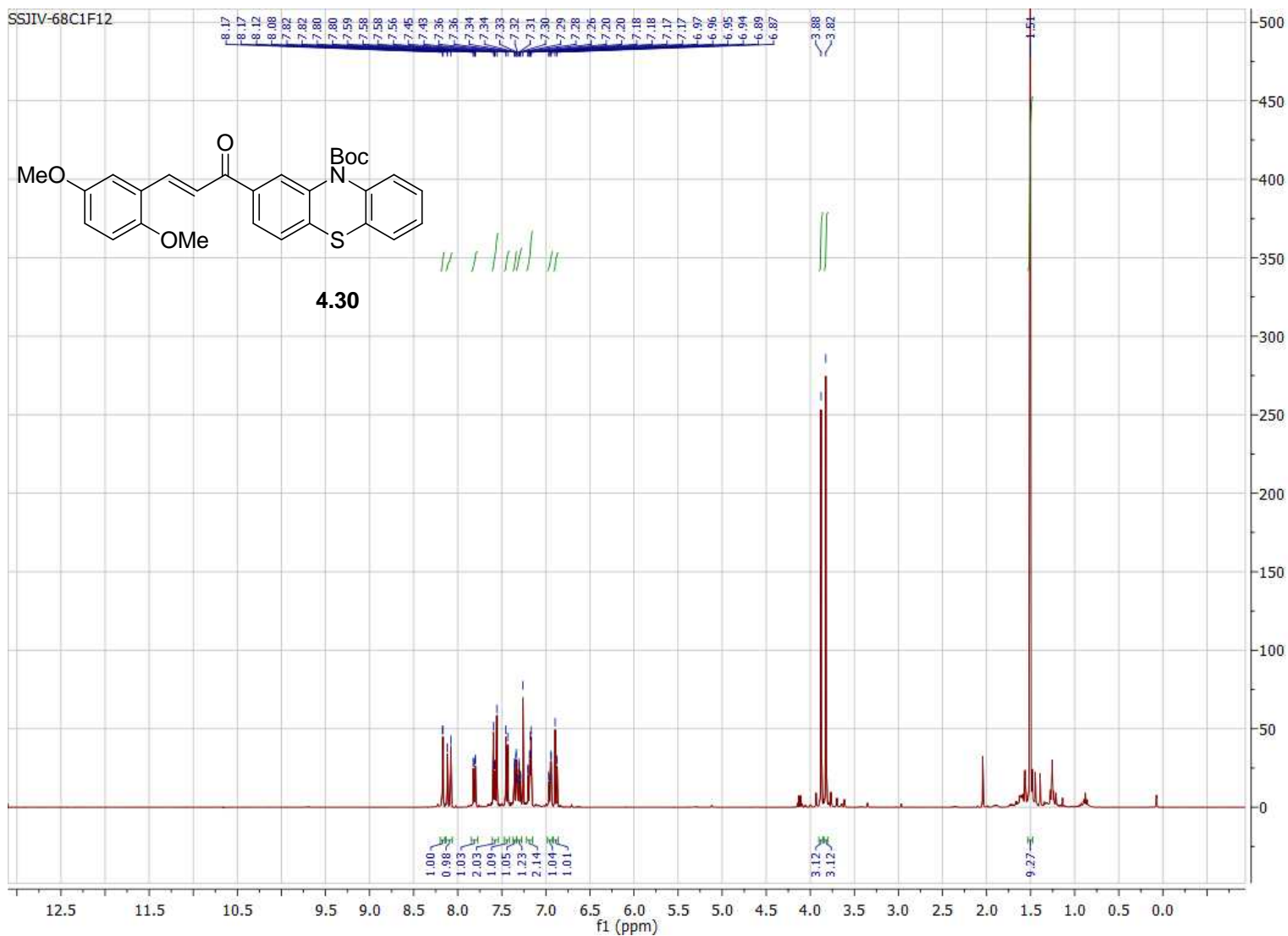


Figure B.127. 400 MHz ^1H NMR of compound **4.30** in CDCl_3 .

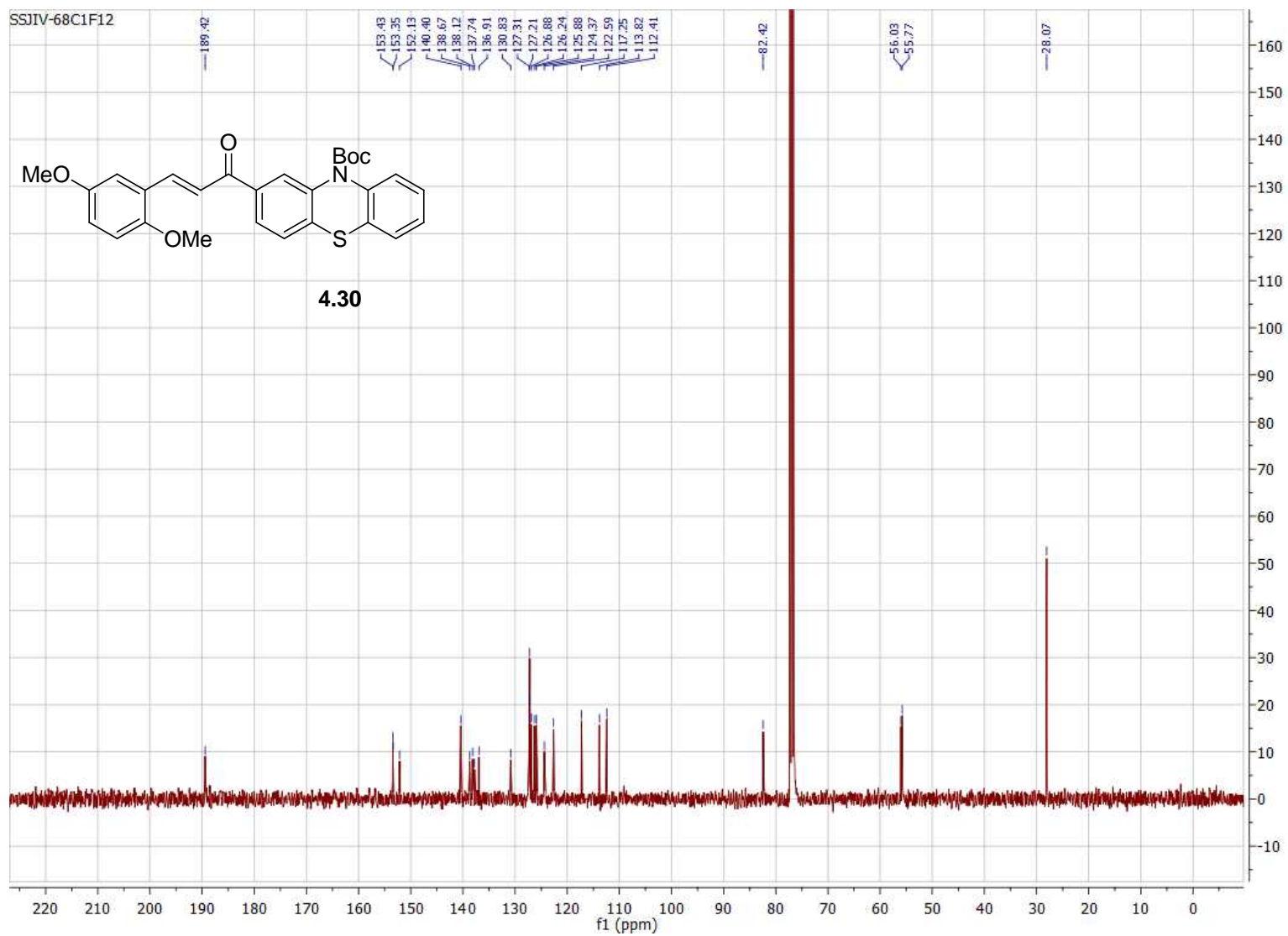


Figure B.128. 100 MHz ^{13}C NMR of compound **4.30** in CDCl_3 .

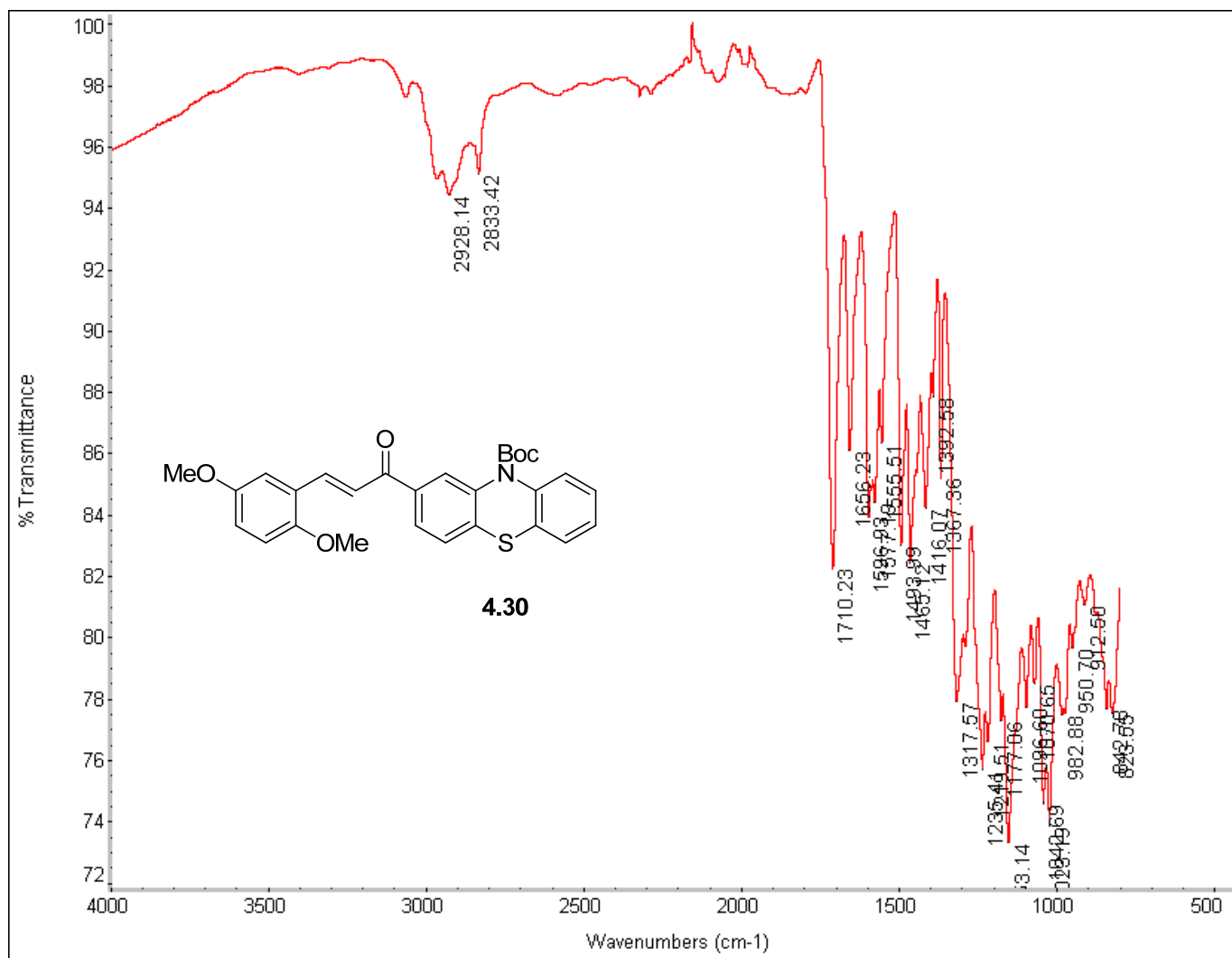


Figure B.129. FTIR of compound 4.30.

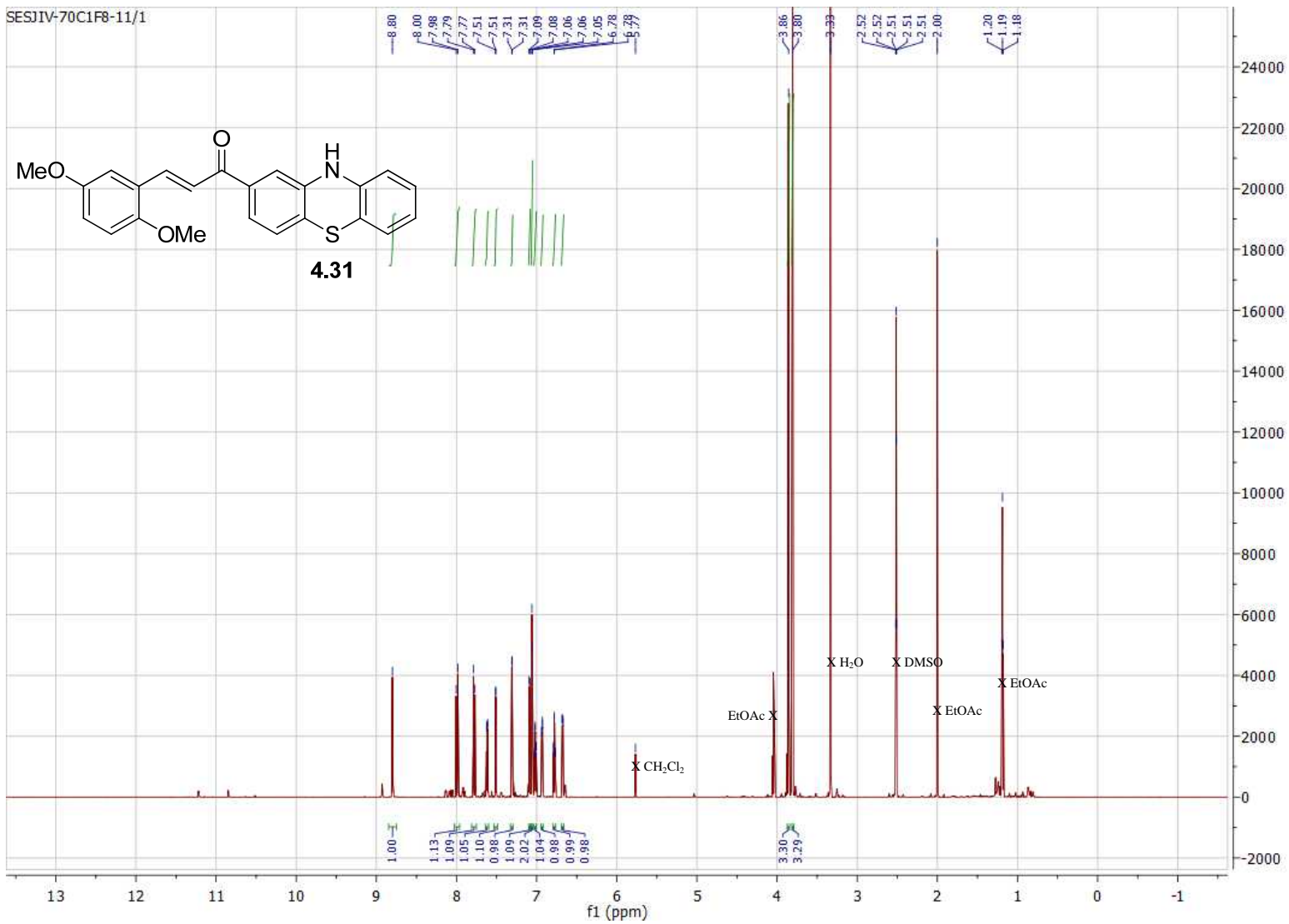


Figure B.130. 800 MHz ^1H NMR of compound **4.31** in d_6 -DMSO.

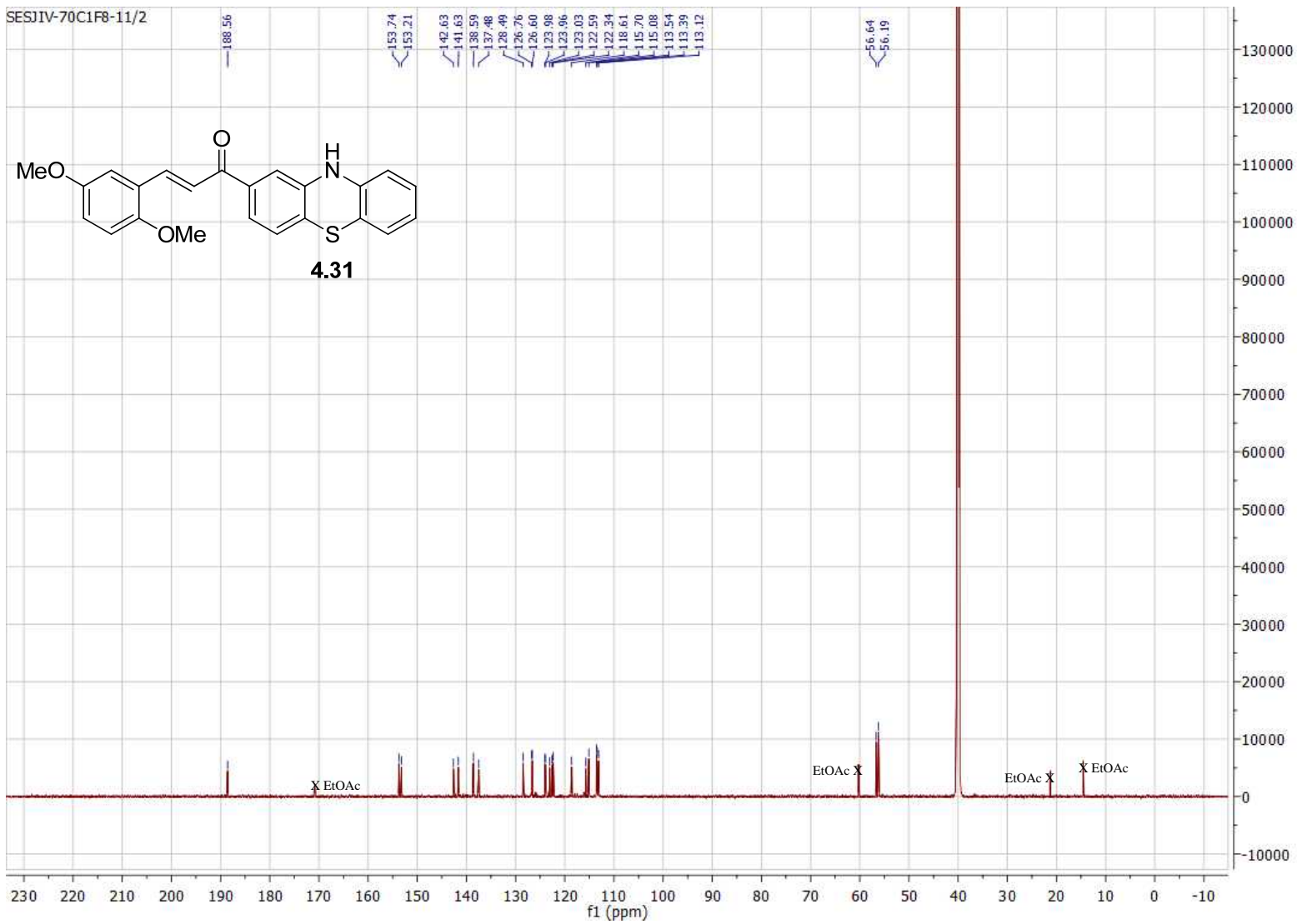


Figure B.131. 200 MHz ^{13}C NMR of compound **4.31** in $\text{d}^6\text{-DMSO}$.

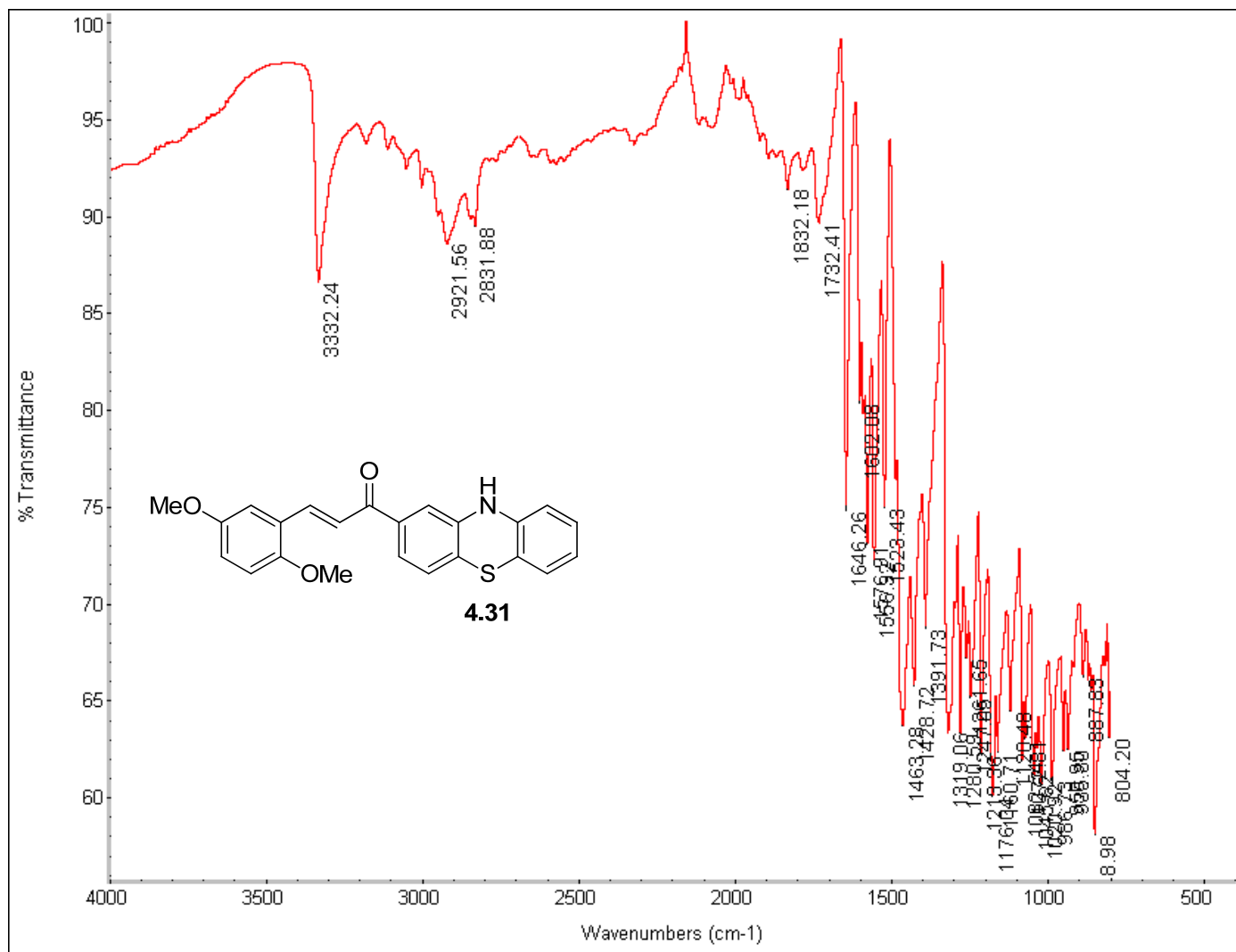


Figure B.132. FTIR of compound 4.31.

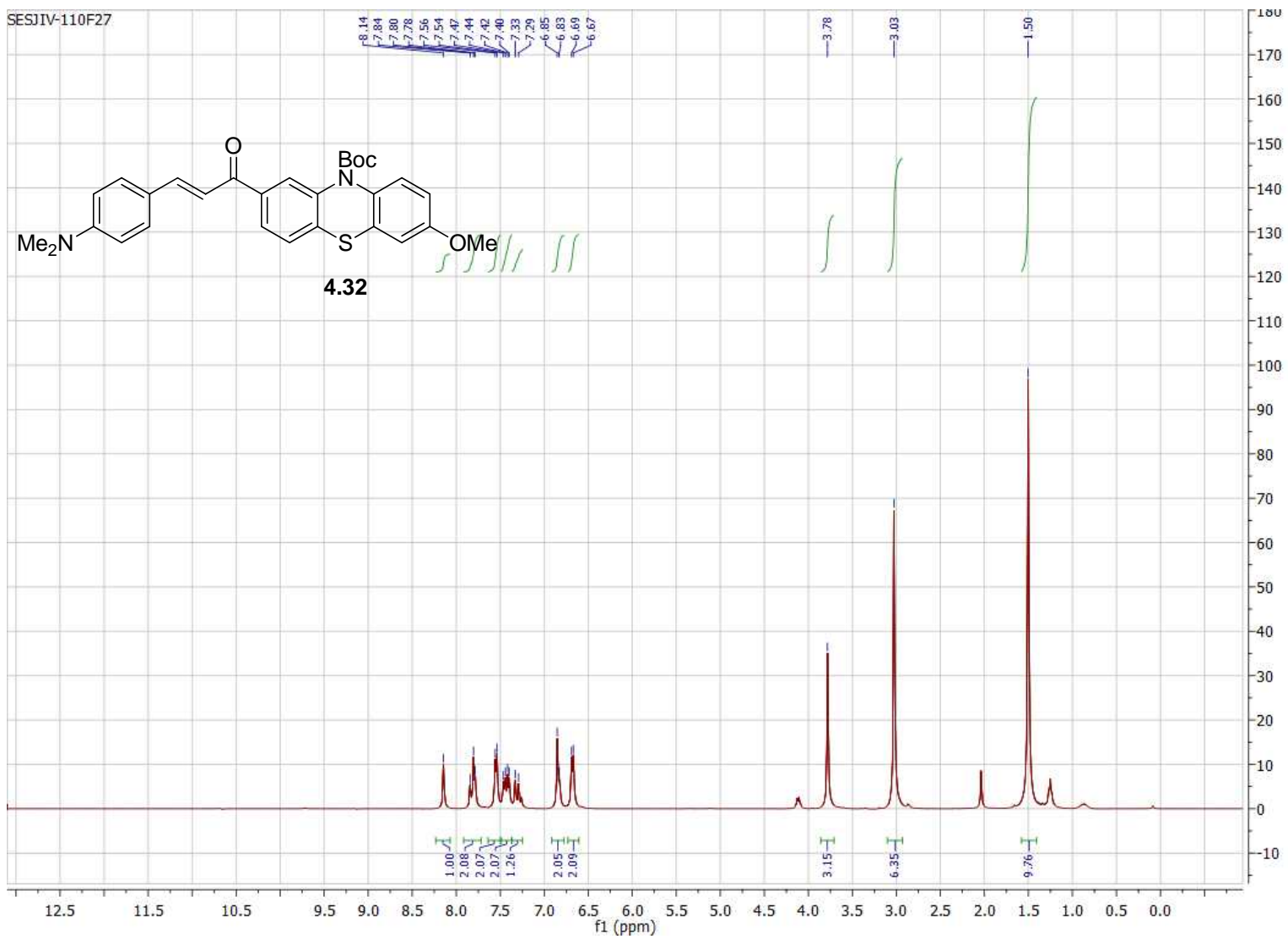


Figure B.133. 400 MHz ^1H NMR of compound **4.32** in CDCl_3 .

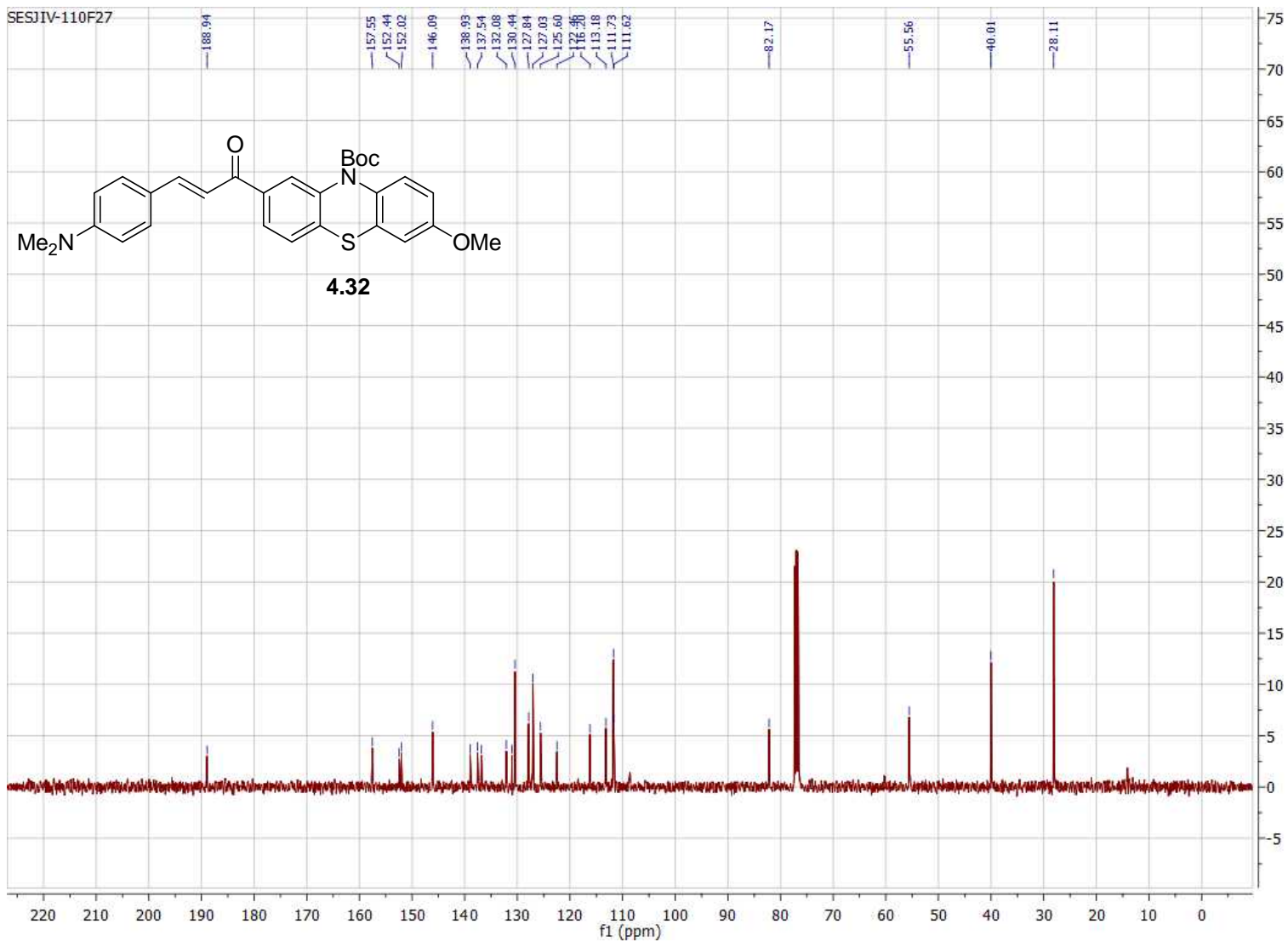


Figure B.134. 100 MHz ^{13}C NMR of compound **4.32** in CDCl_3 .

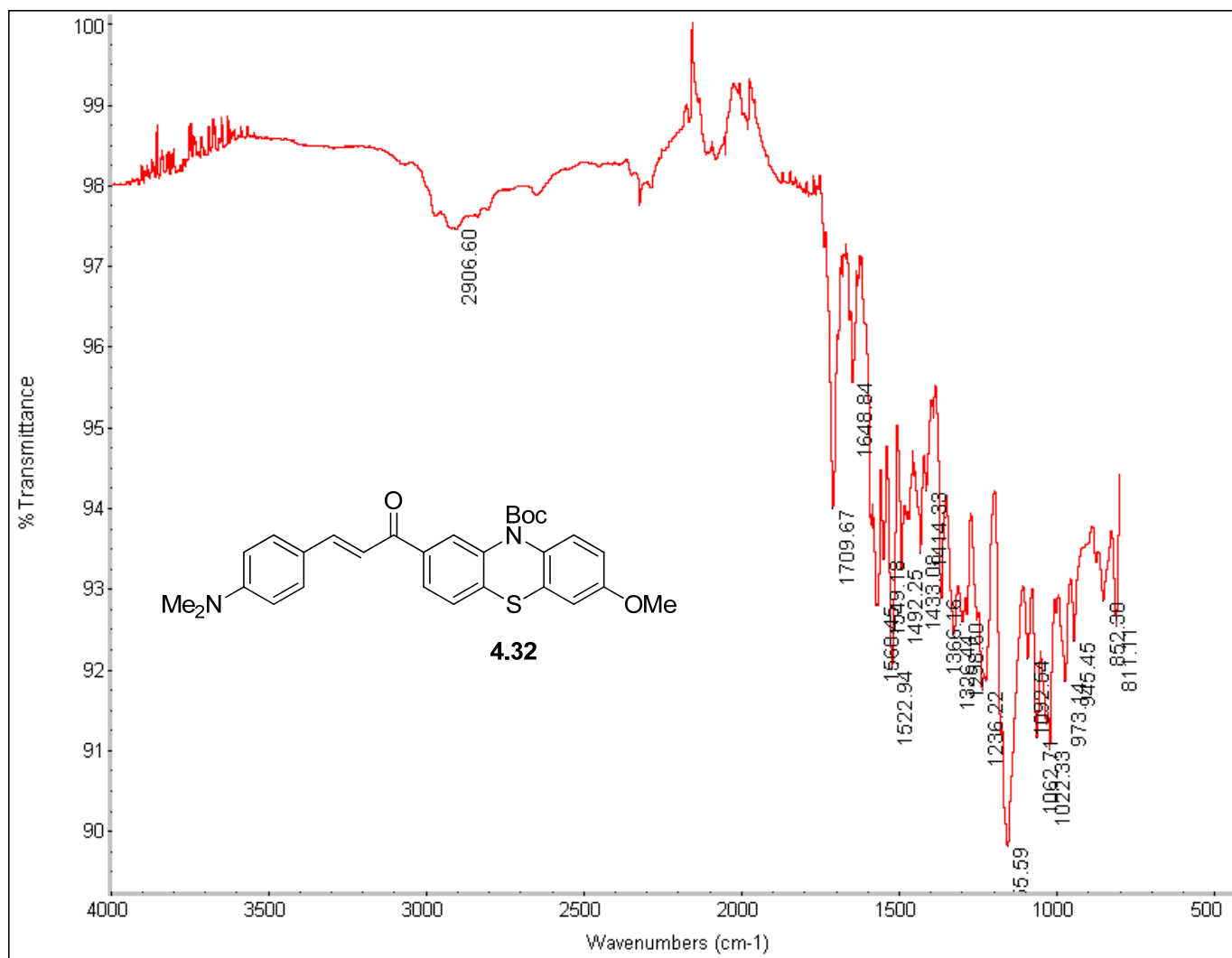


Figure B.135. FTIR of compound 4.32.

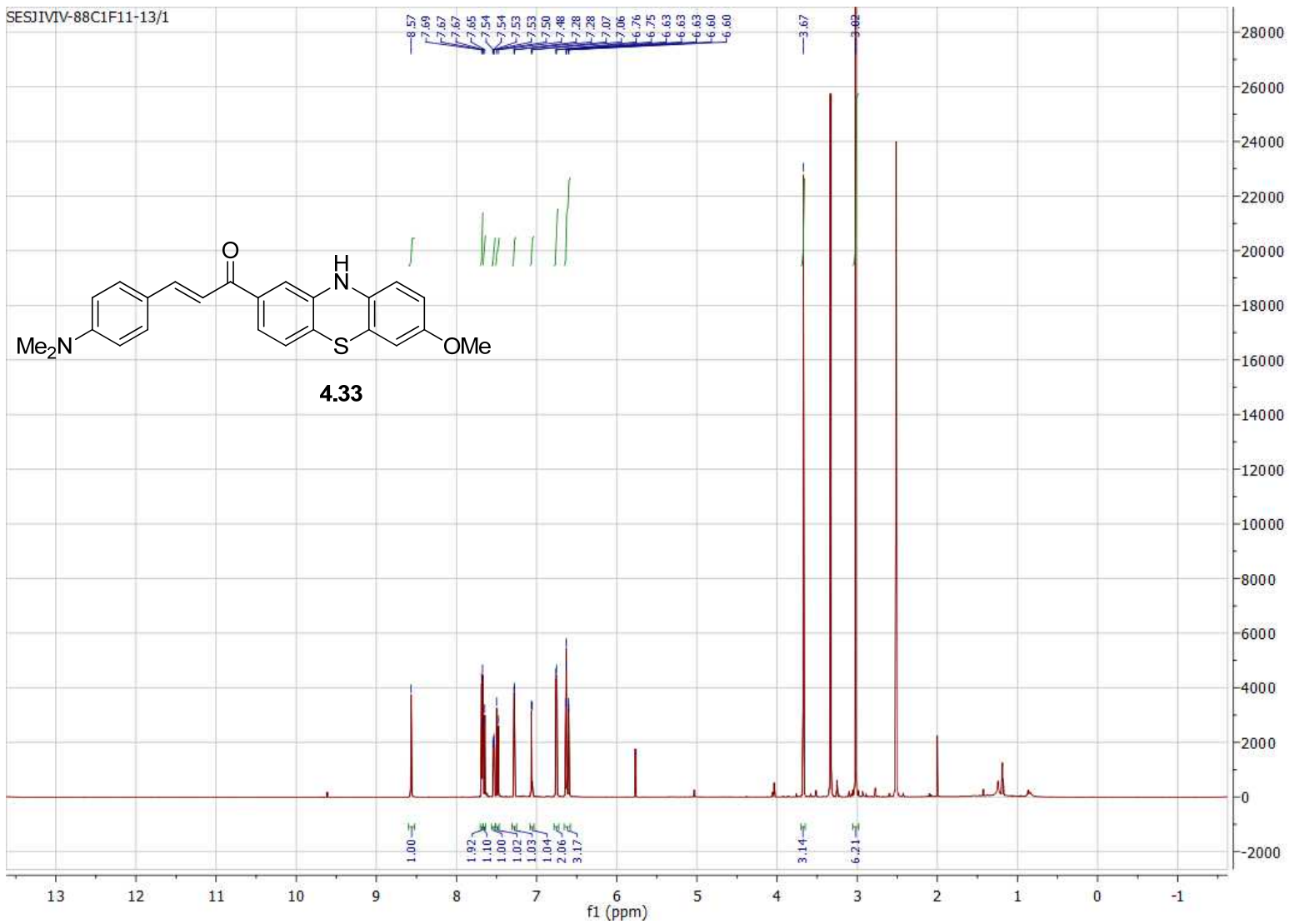


Figure B.136. 800 MHz ^1H NMR of compound **4.33** in d^6 -DMSO.

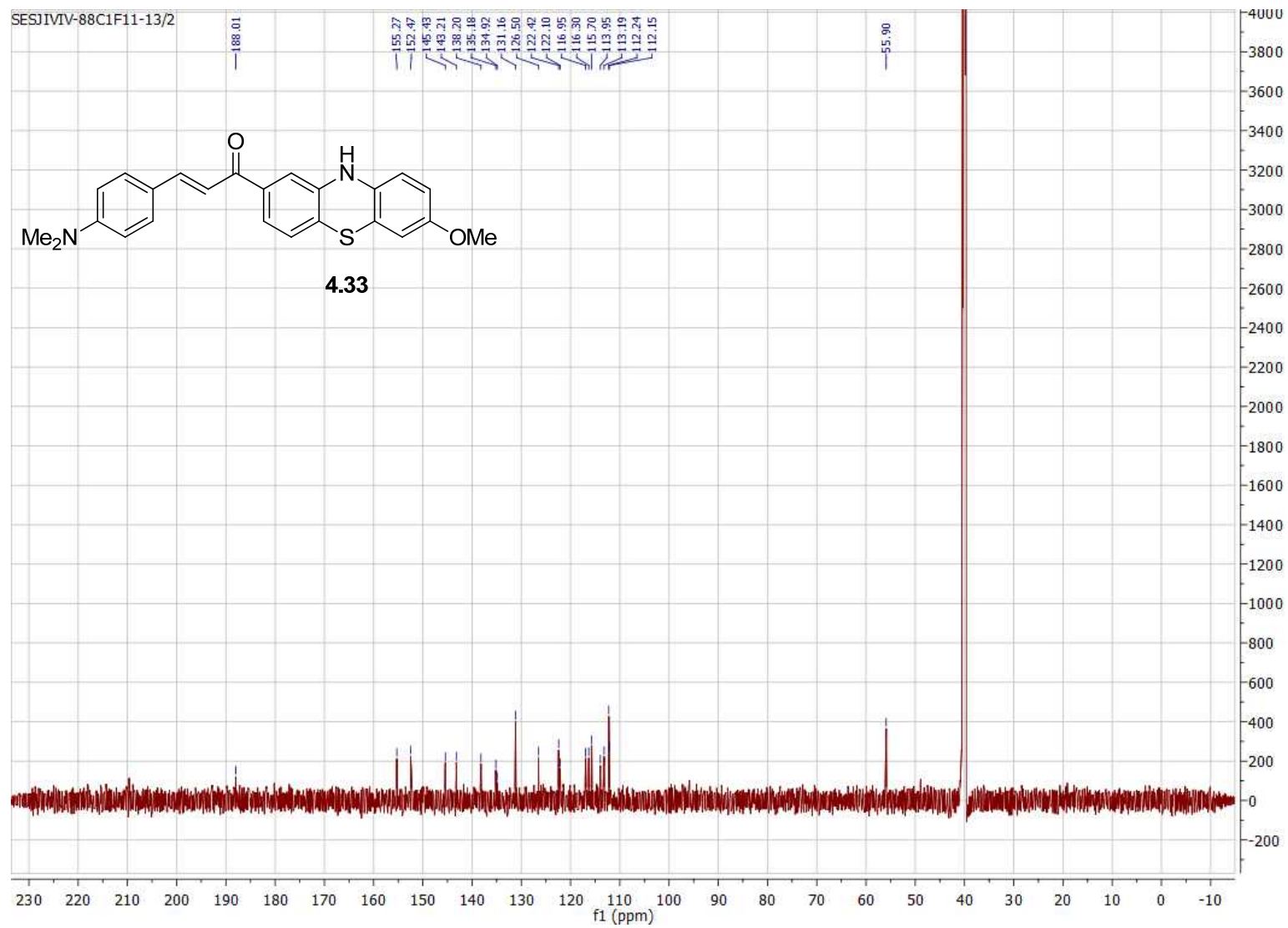


Figure B.137. 200 MHz ^{13}C NMR of compound **4.33** in $\text{d}^6\text{-DMSO}$.

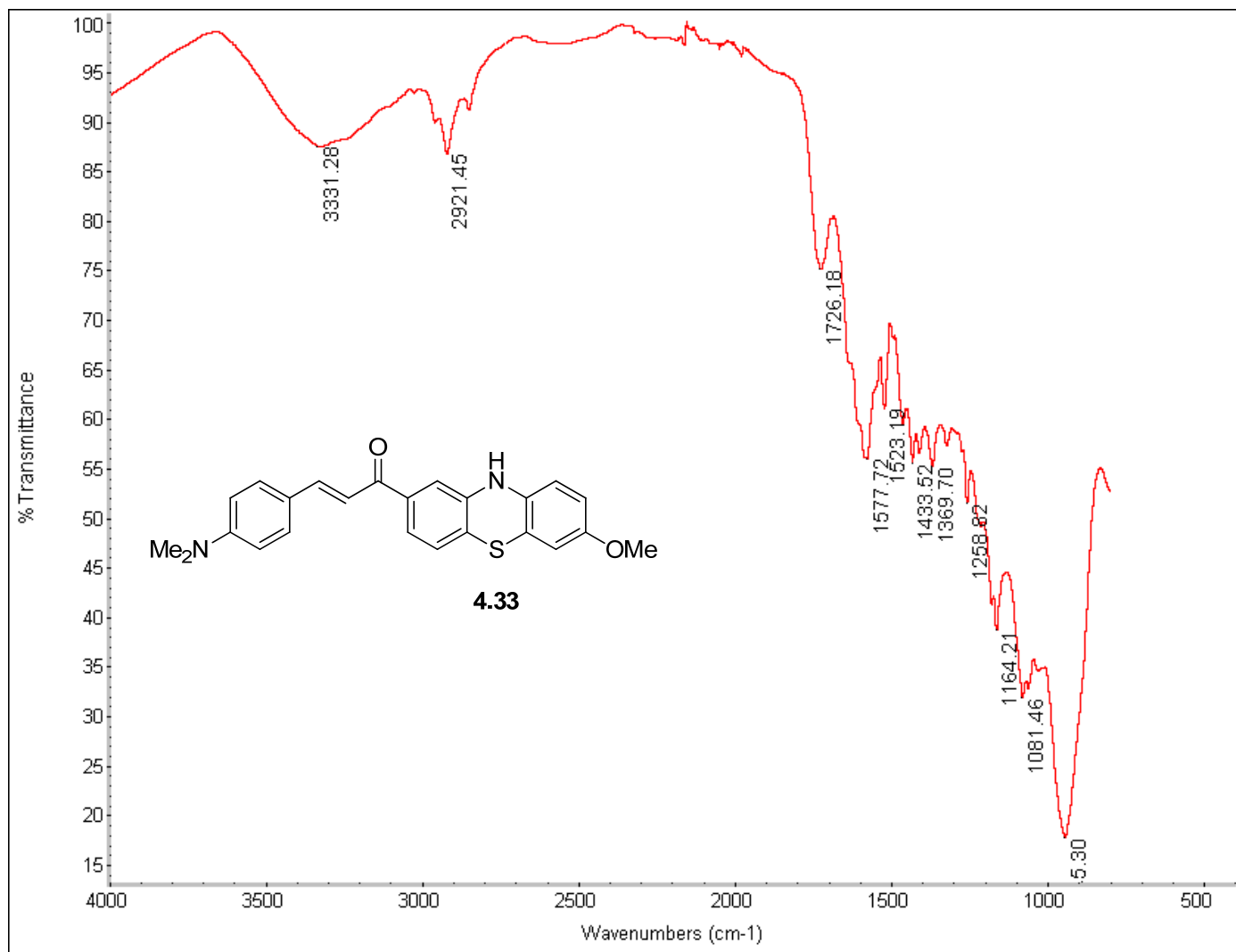


Figure B.138. FTIR of compound 4.33.

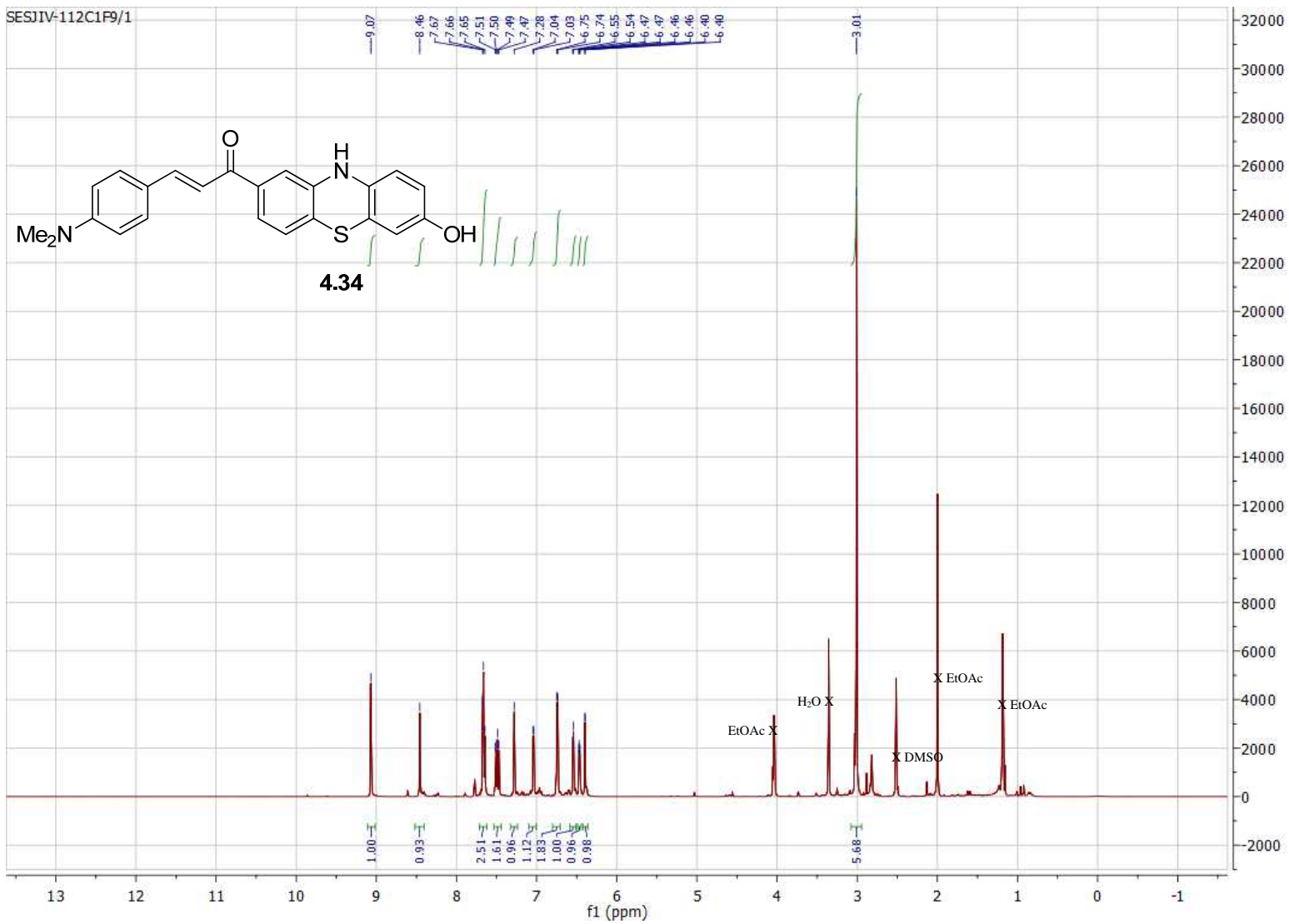


Figure B.139. 800 MHz ¹H NMR of compound **4.34** in d⁶-DMSO.

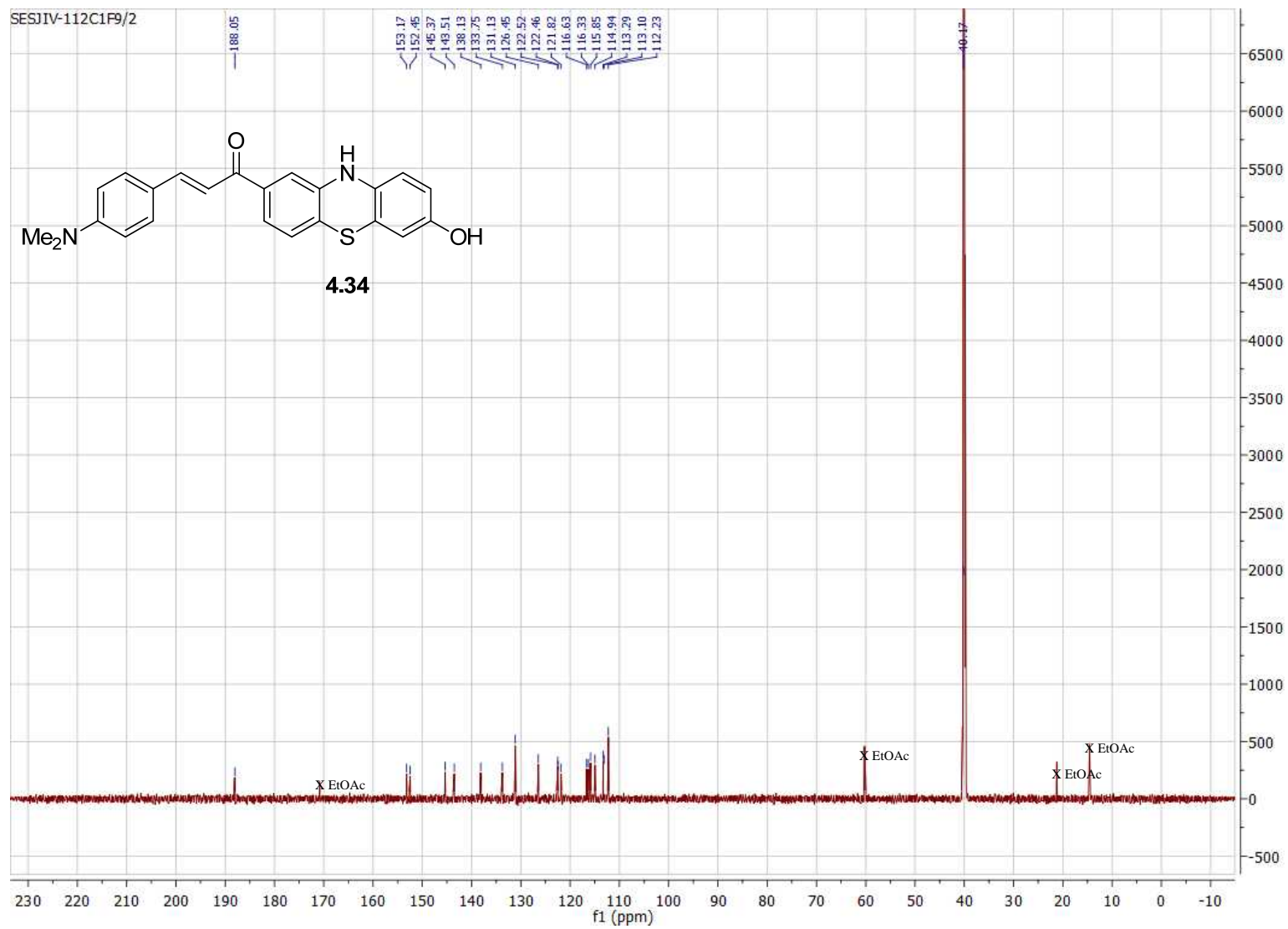


Figure B.140. 200 MHz ^{13}C NMR of compound **4.33** in $\text{d}^6\text{-DMSO}$.

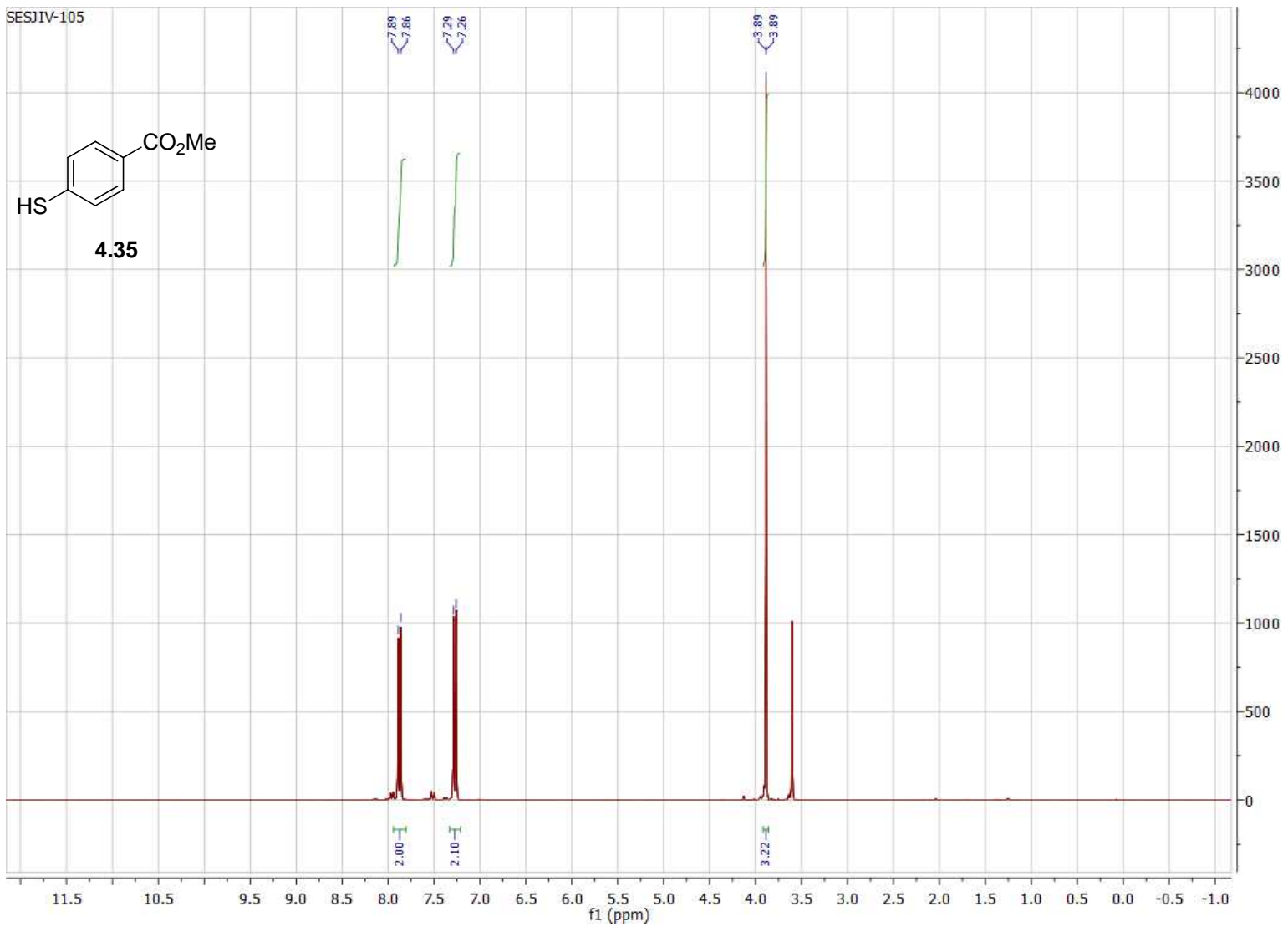


Figure B.141. 300 MHz ^1H NMR of compound **4.35** in CDCl_3 .

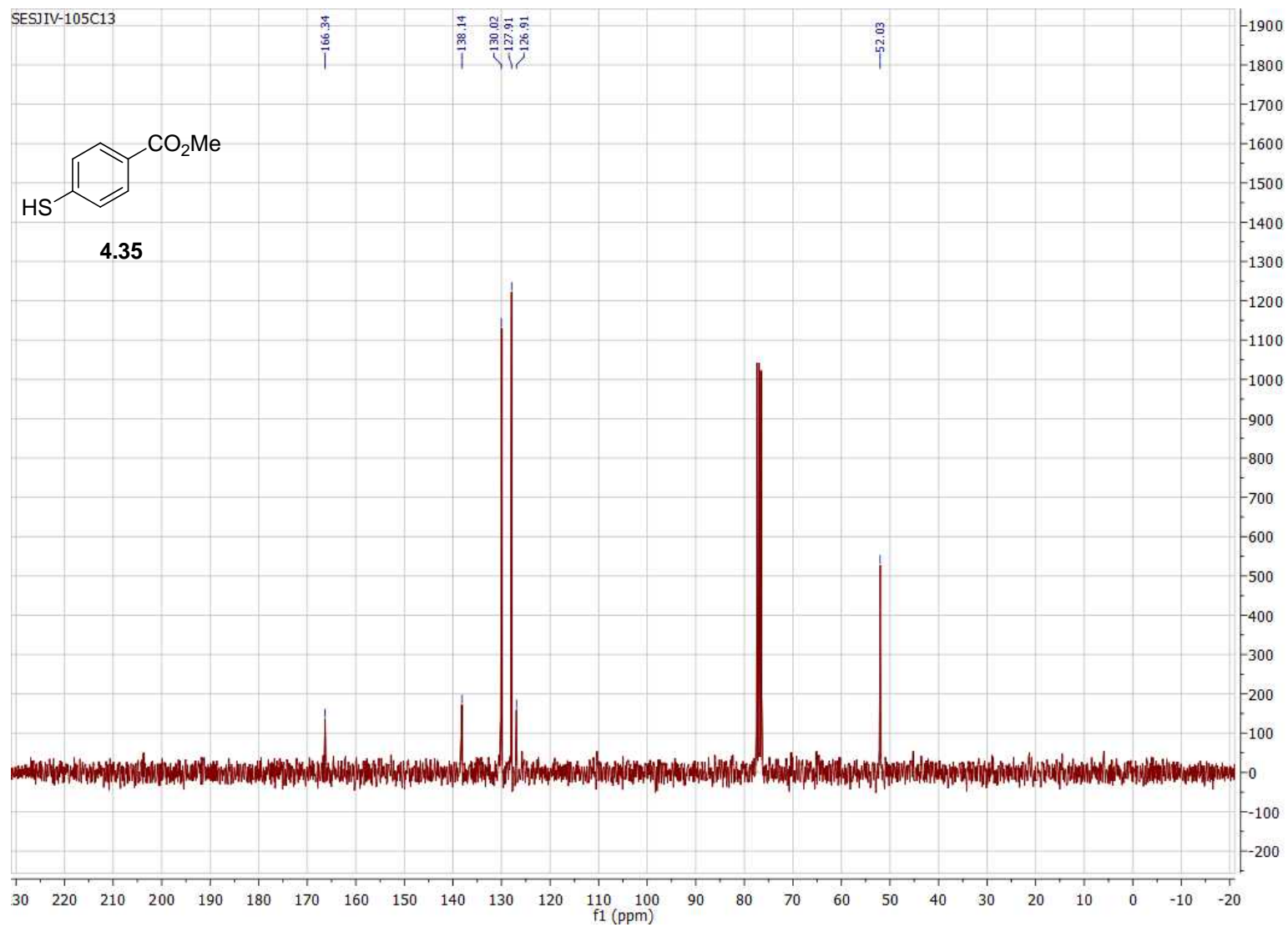


Figure B.142. 75 MHz ^{13}C NMR of compound **4.35** in CDCl_3 .

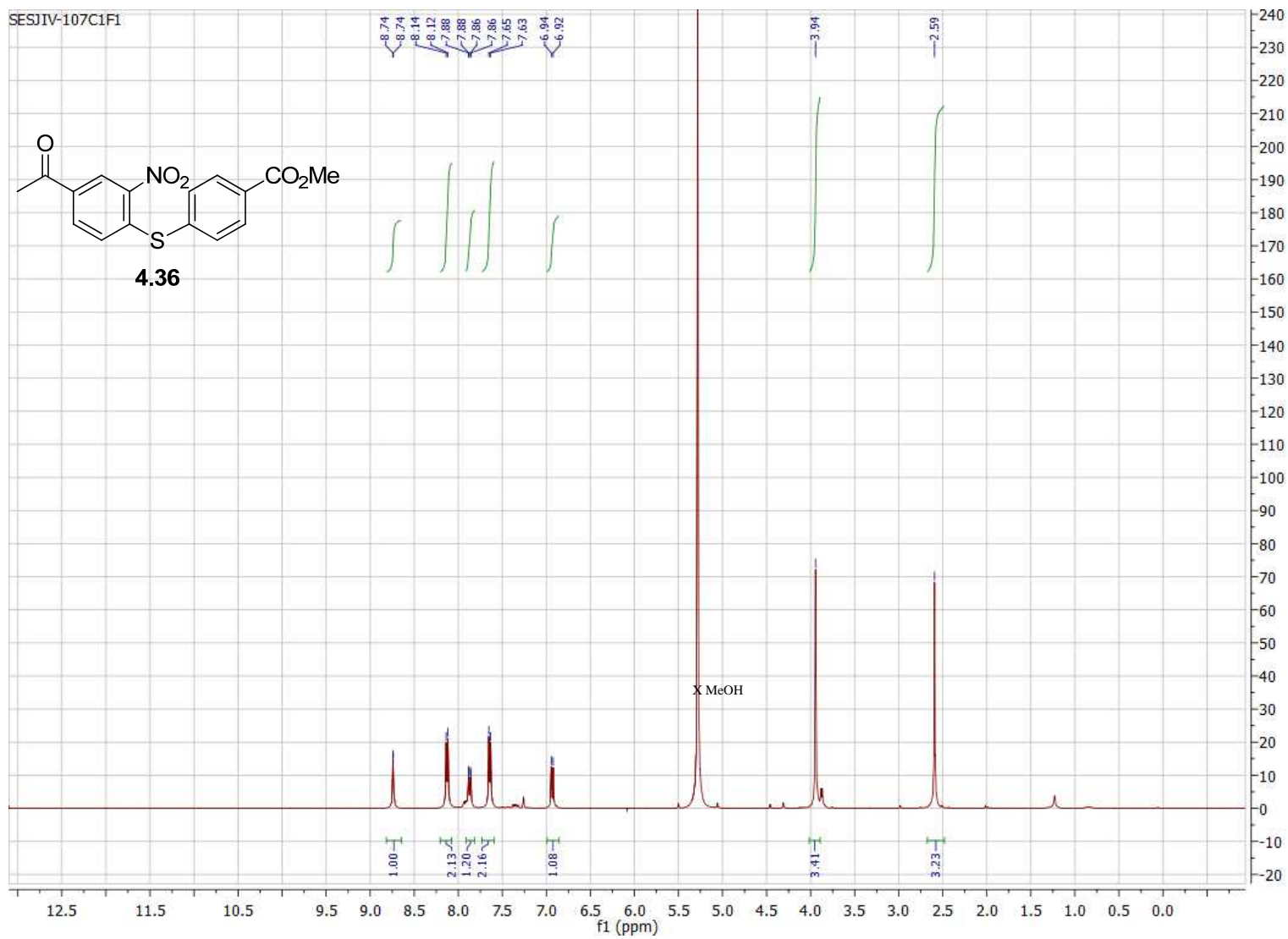


Figure B.143. 400 MHz ^1H NMR of compound **4.36** in CDCl_3 .

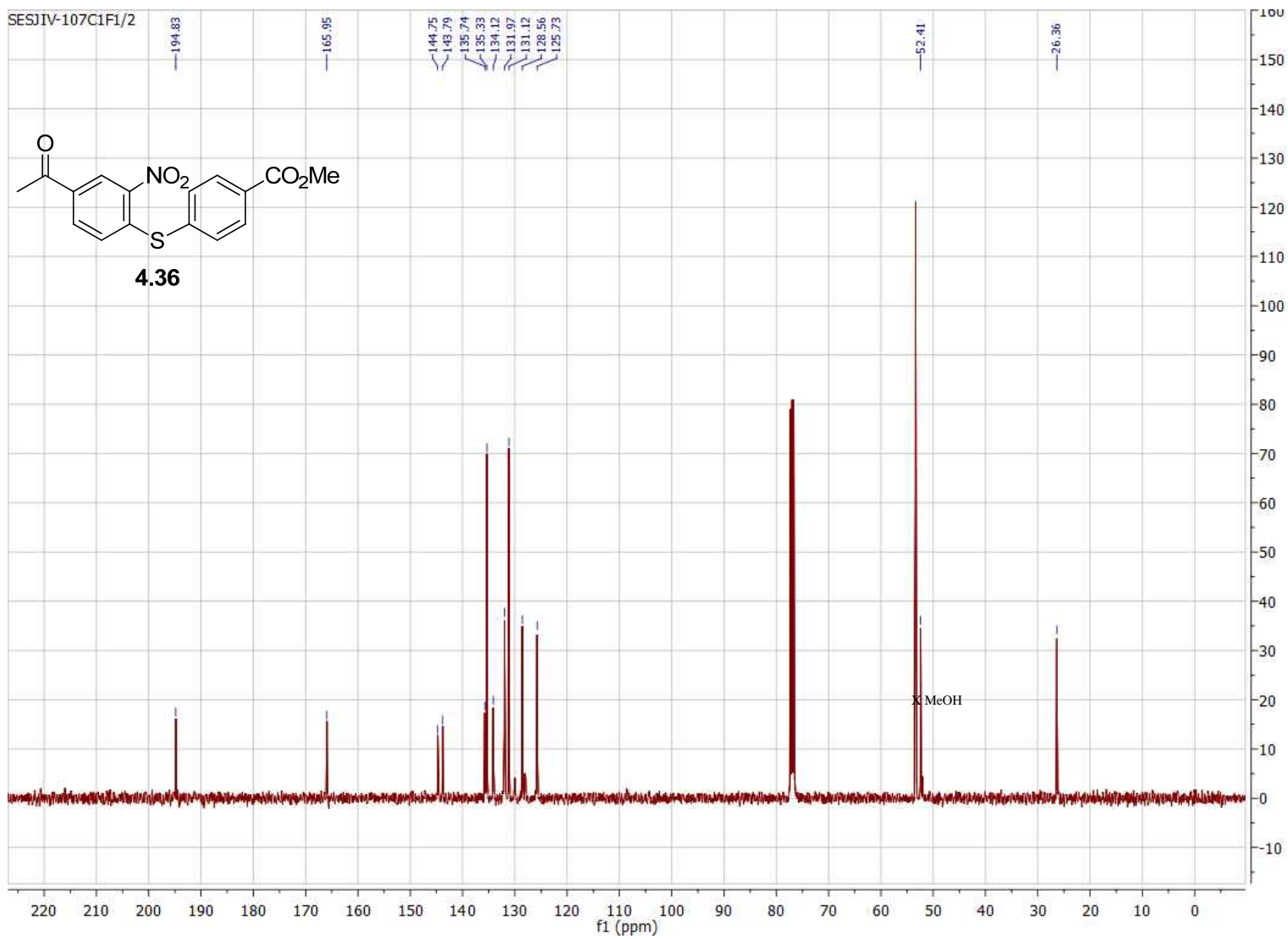


Figure B.144. 100 MHz ^{13}C NMR of compound **4.36** in CDCl_3 .

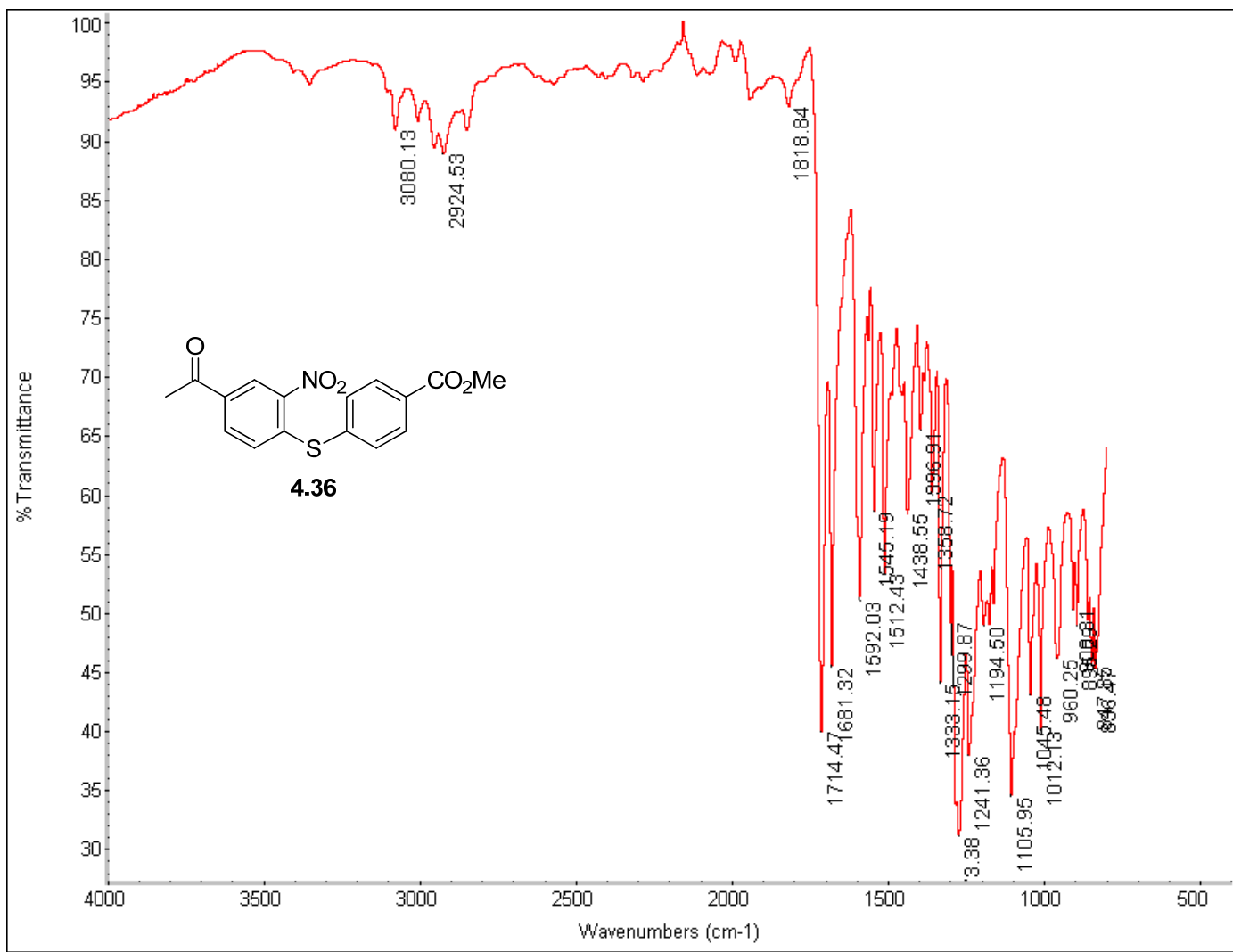


Figure B.145. FTIR of compound 4.36.

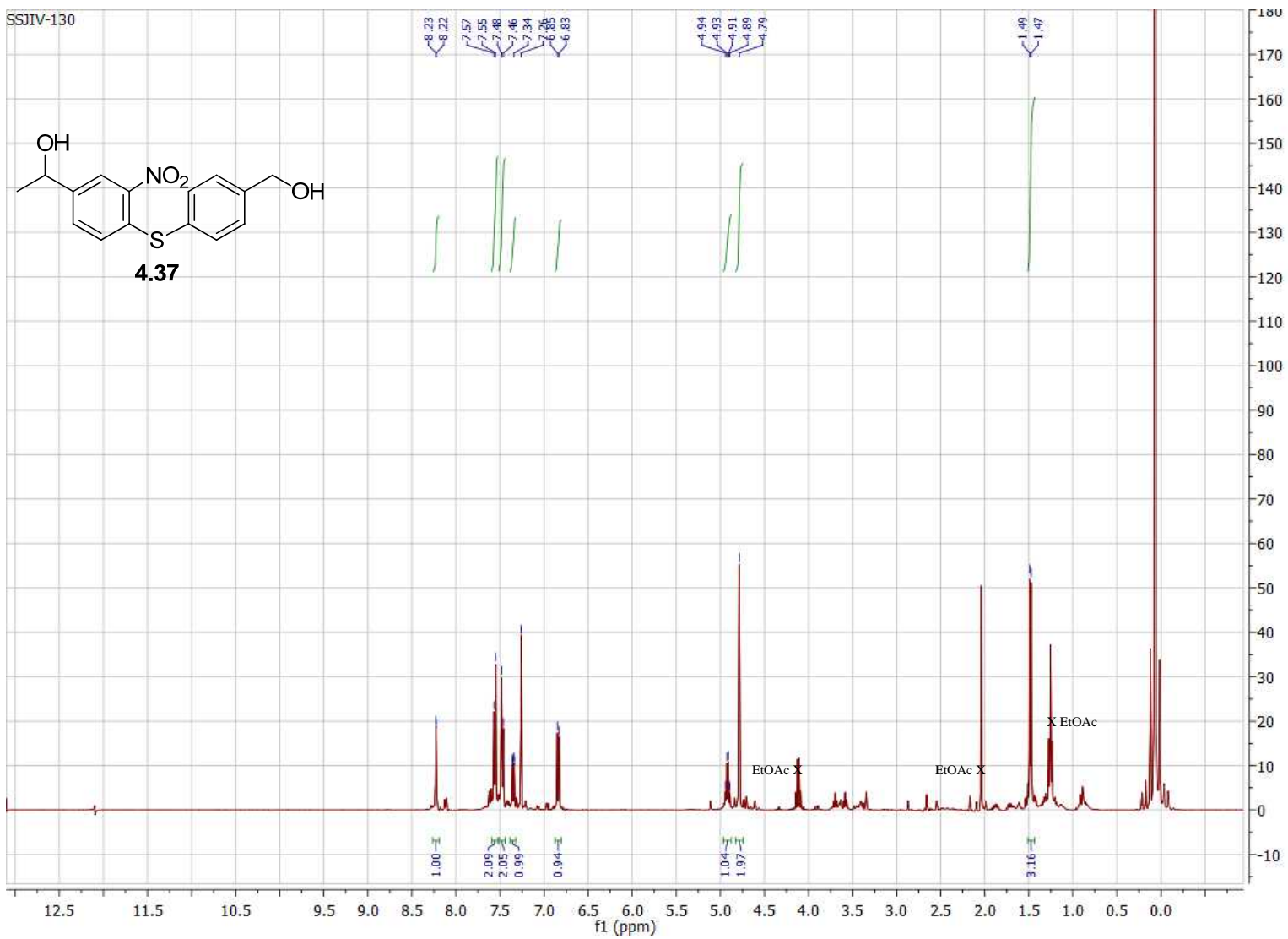


Figure B.146. 400 MHz ¹H NMR of crude compound **4.37** in CDCl₃.

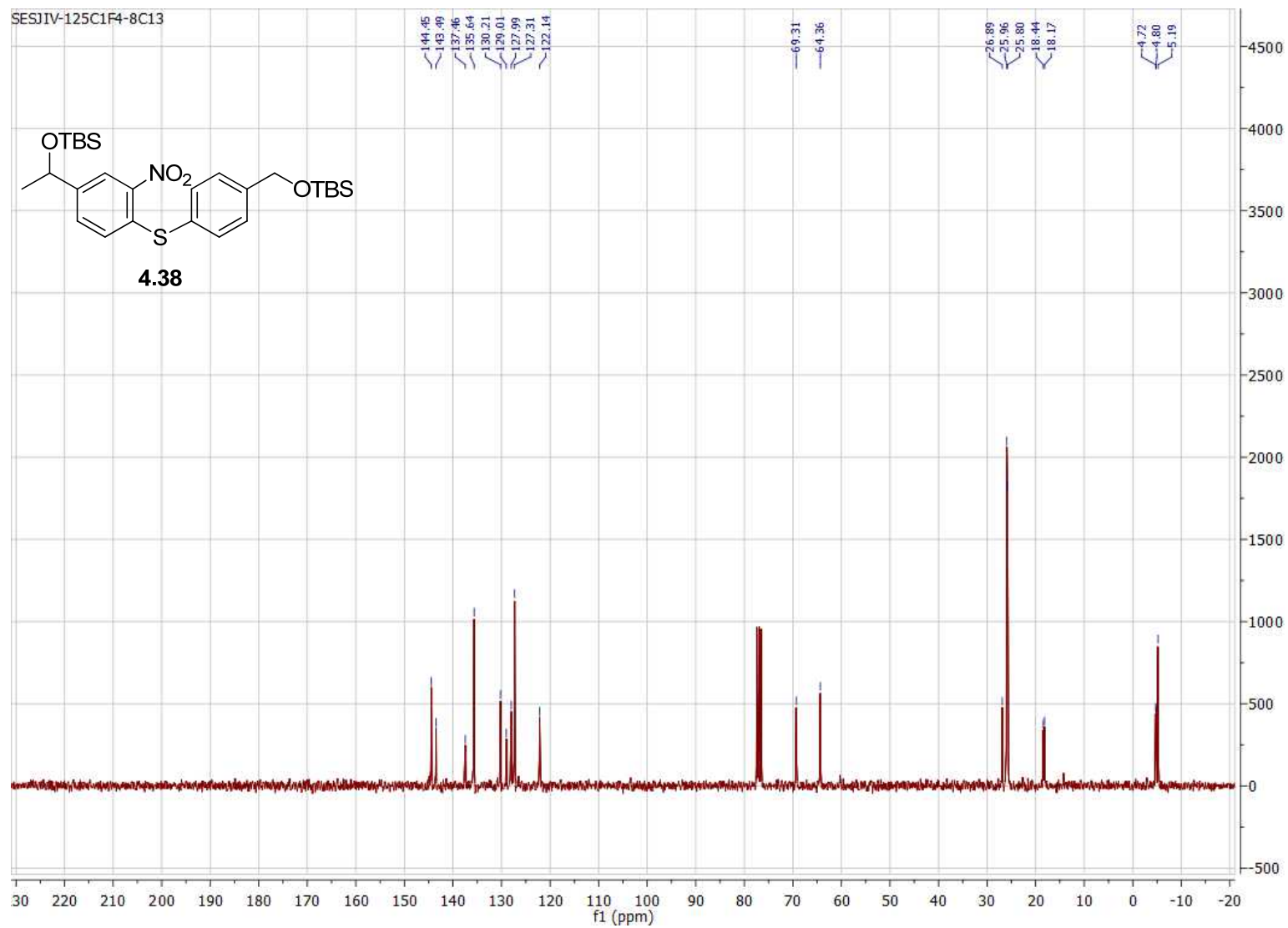


Figure B.148. 75 MHz ^{13}C -NMR of compound **4.38** in CDCl_3 .

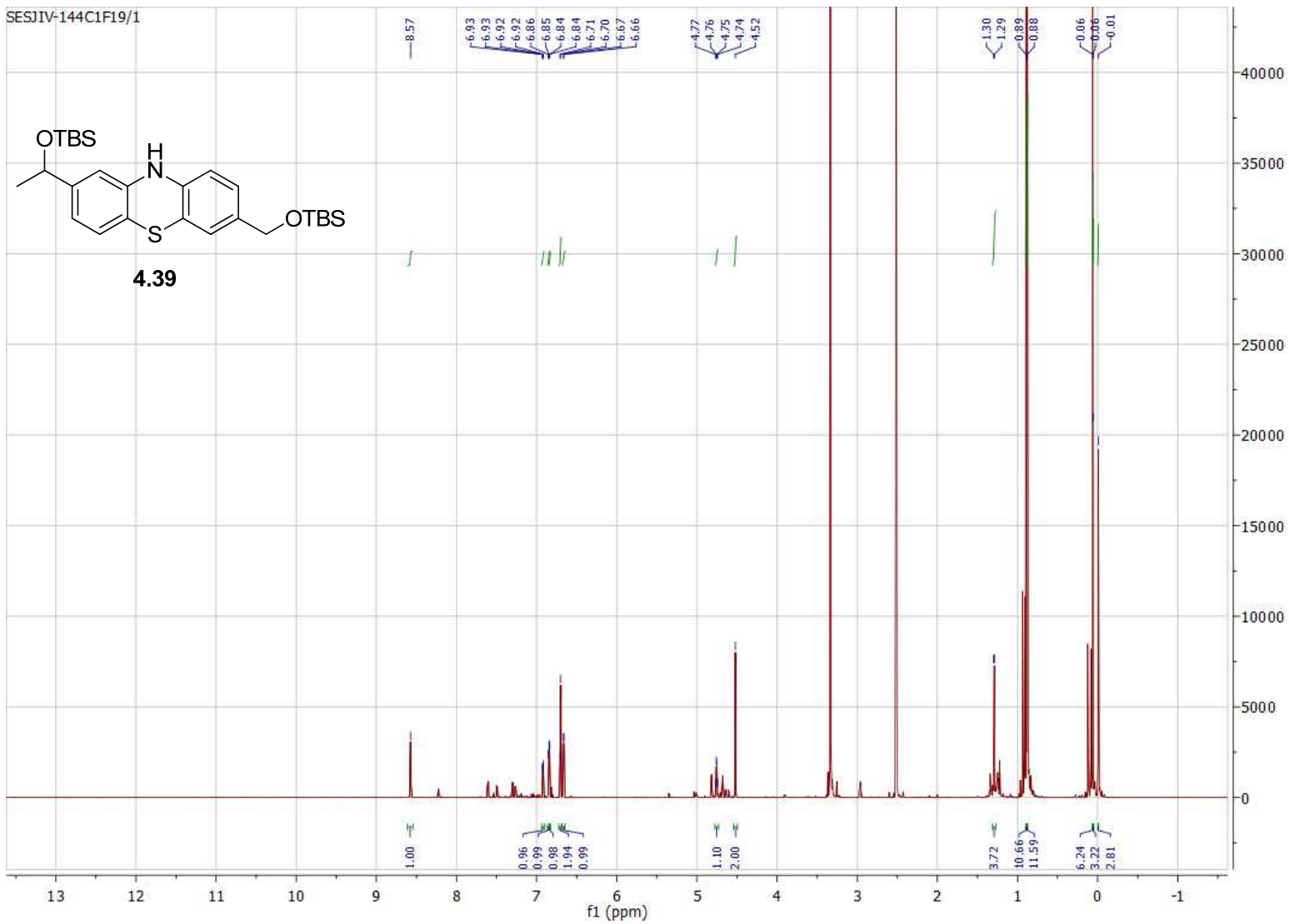


Figure B.149. 800 MHz ^1H NMR of crude compound **4.39** in $\text{d}^6\text{-DMSO}$.

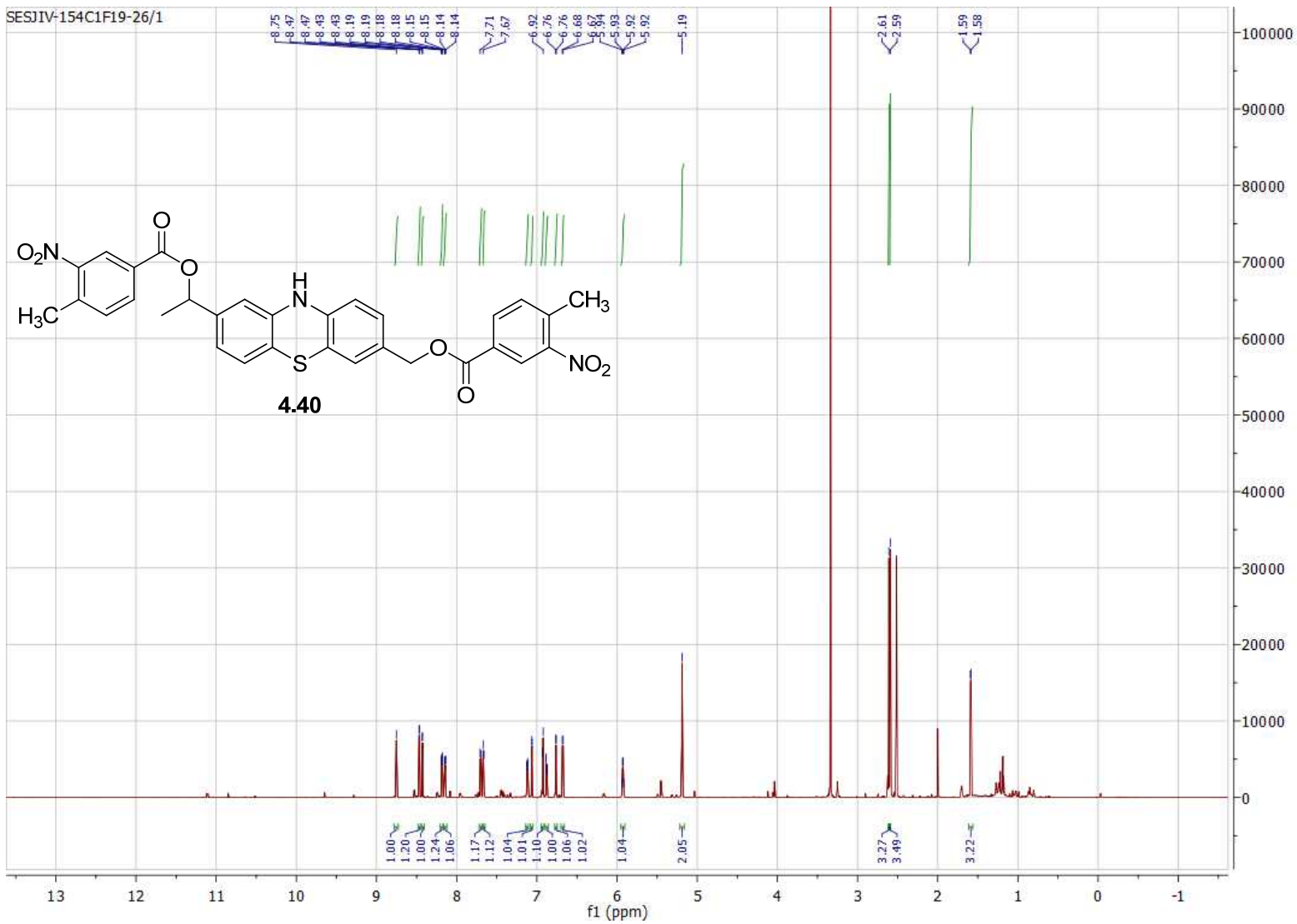


Figure B.150. 800 MHz ^1H NMR of compound **4.40** in d^6 -DMSO.

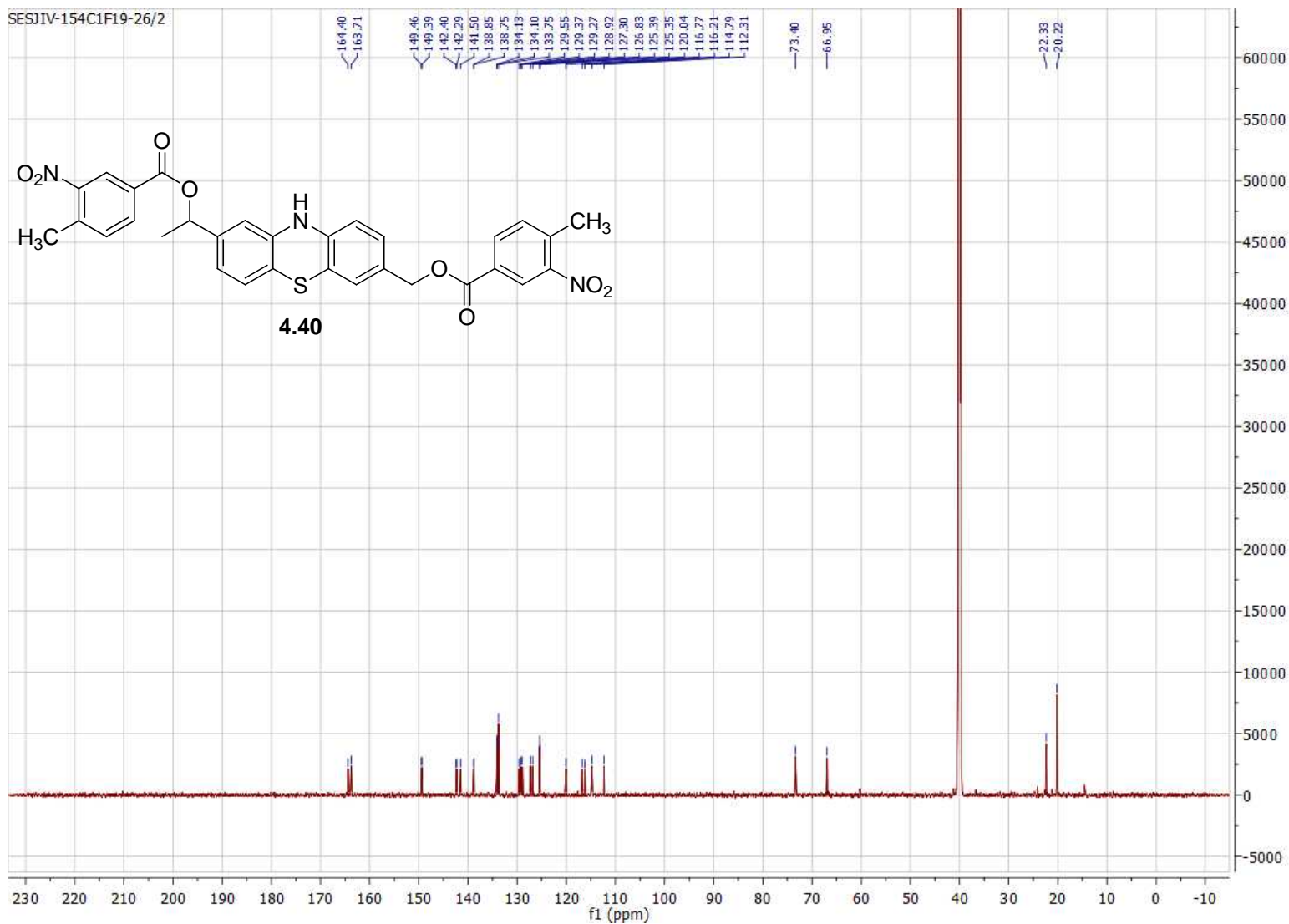


Figure B.151. 800 MHz ¹³C NMR of compound **4.40** in d⁶-DMSO.

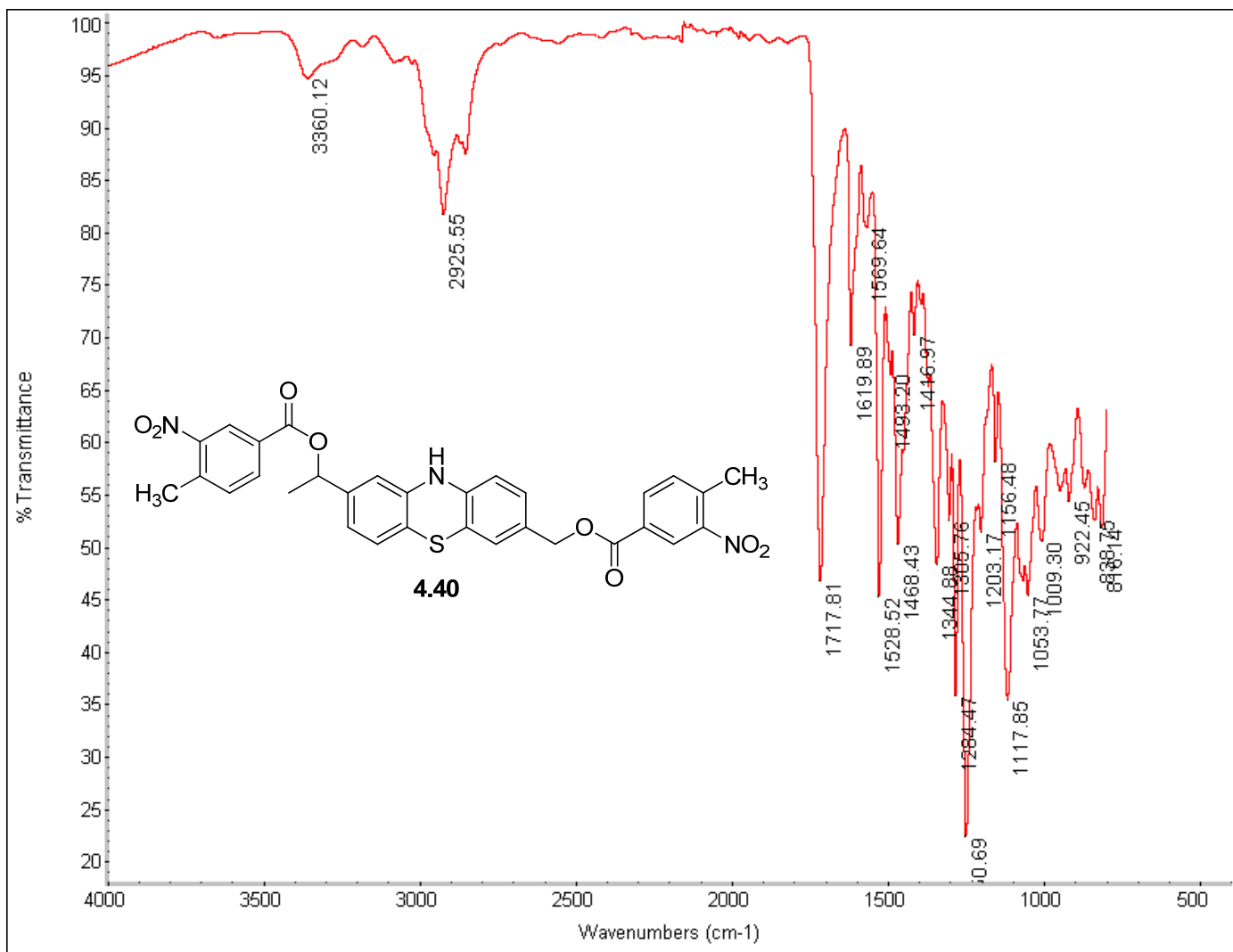


Figure B.152. FTIR of **4.40**.

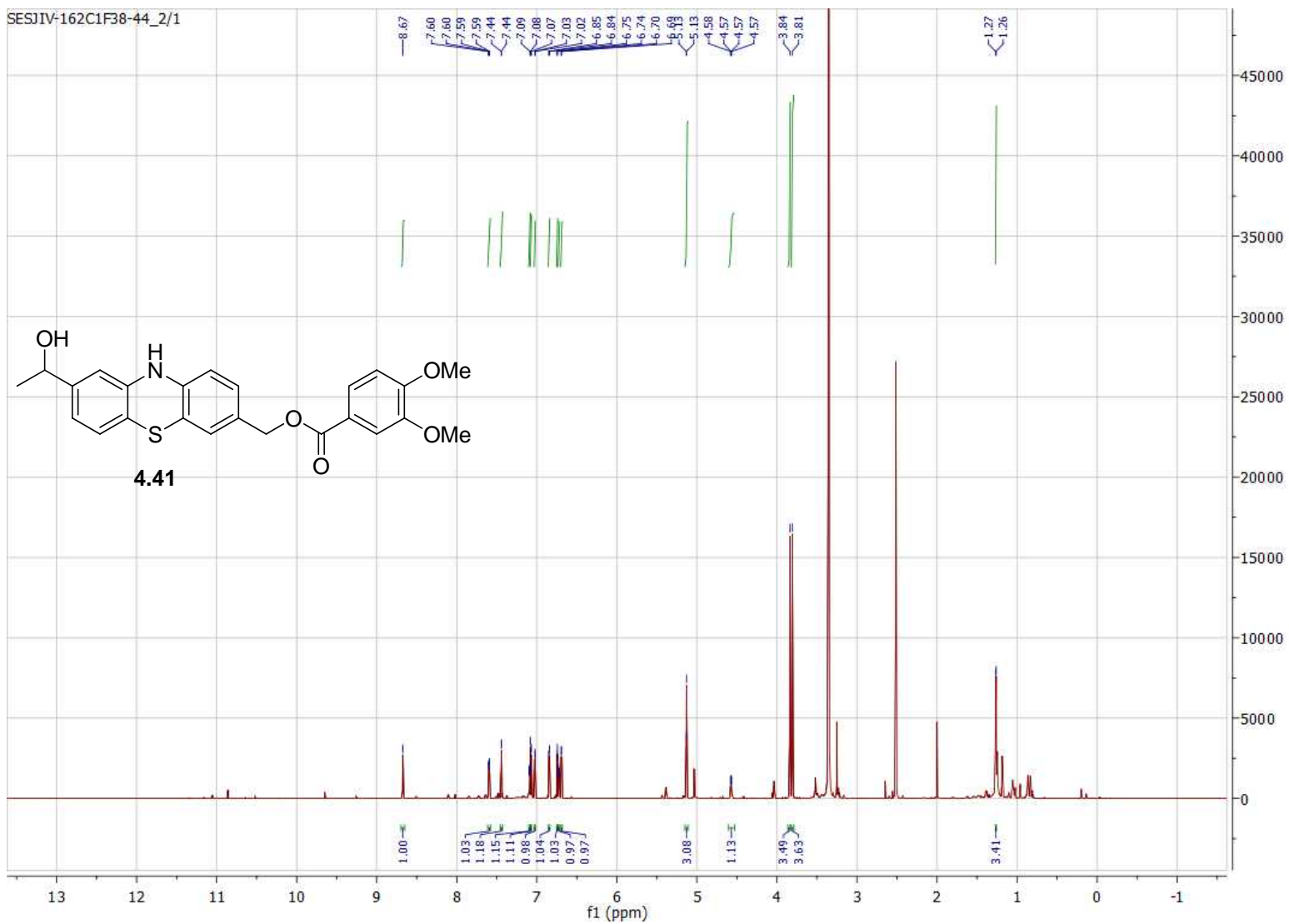


Figure B.153. 800 MHz ^1H NMR of compound **4.41** in d^6 -DMSO.

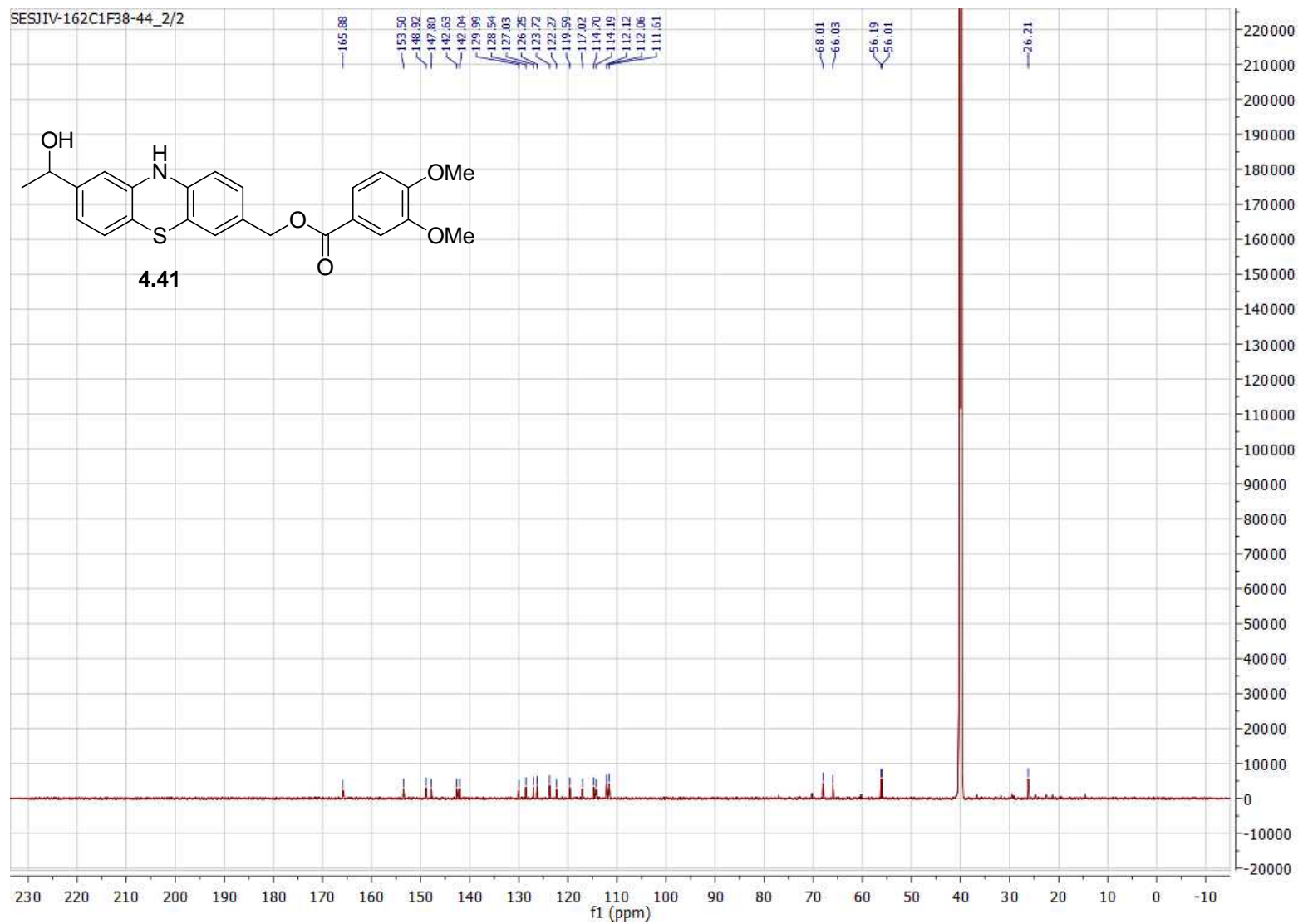


Figure B.154. 200 MHz ^{13}C NMR of compound **4.41** in $\text{d}^6\text{-DMSO}$.

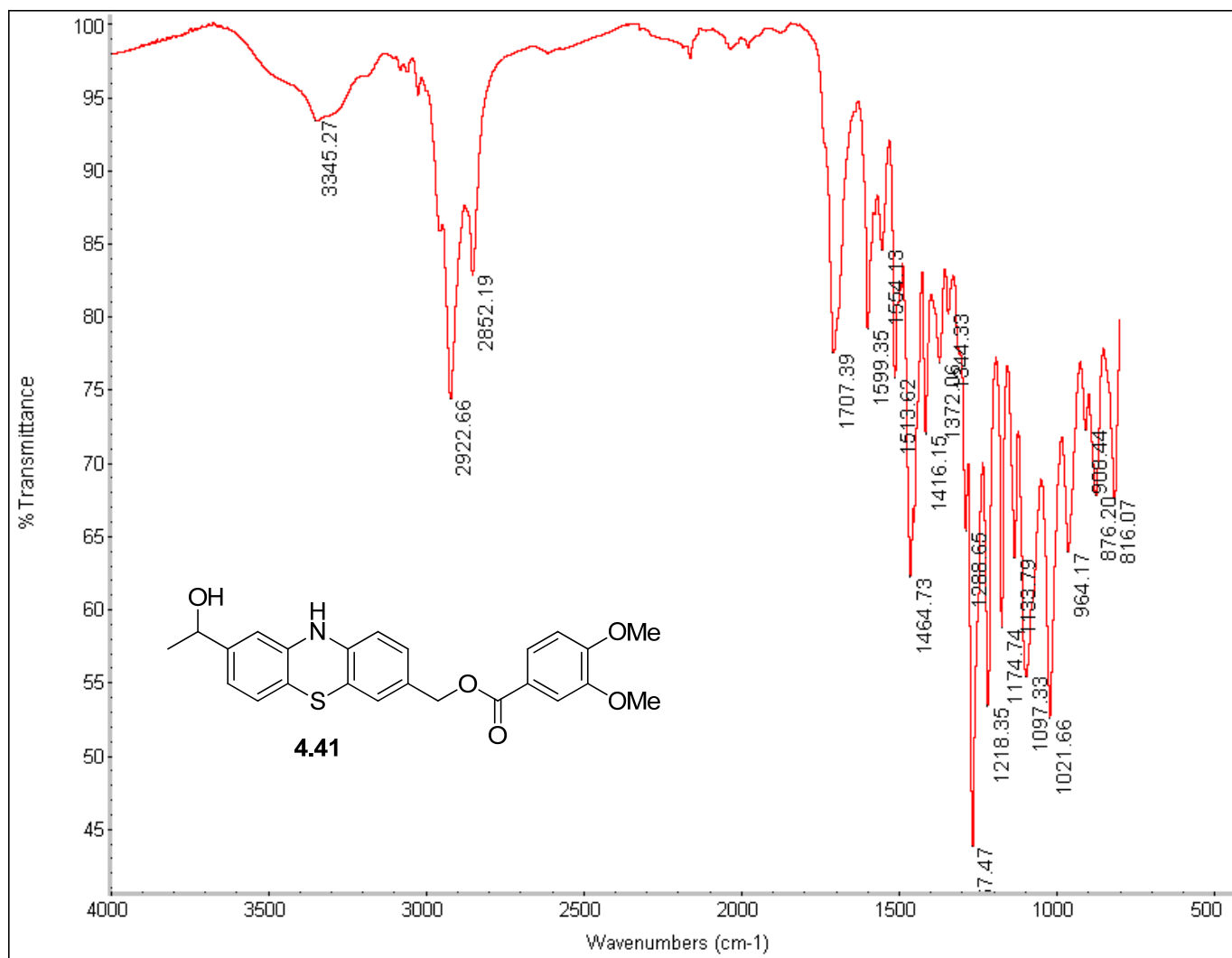


Figure B.155. FTIR of compound 4.41.

VITA

VITA

Sarah Emma St. John was born on July 15, 1985 in Arlington Heights, Illinois. She is the daughter of Kathy Vande Logt-St. John and Ronald St. John. After graduating high school at the age of sixteen, she spent the next six years attending three different colleges and making up for the studiousness of her youth. Eventually, Sarah graduated from Benedictine University in May 2008, where she earned a Bachelor of Science degree with a major in chemistry and minor in psychology. During her time at B.U. she worked in the laboratory of Professor Cheryl M. Mascarenhas, where she investigated alternative catalysts to L-Proline for the asymmetric synthesis of the Wieland-Miescher ketone through a one-pot Robinson annulation reaction. Sarah started her Ph.D. studies in the Department of Chemistry at Purdue University in August of 2008. It was there that she joined the laboratory of Professor Mark A. Lipton to study organic chemistry. During her tenure at Purdue she worked on a variety of projects involving organic synthesis, bioorganic chemistry, computational chemistry, molecular modeling, and structural elucidation through 1D- and 2D-NMR techniques. She received her Ph.D. in September of 2013 and took a position as a post-doctoral researcher in the laboratory of Professor Andrew Mesecar in the Department of Biological Sciences, Molecular Biosciences at Purdue University.

PUBLICATION



Contents lists available at ScienceDirect

Bioorganic & Medicinal Chemistry

journal homepage: www.elsevier.com/locate/bmc

Design, synthesis, biological and structural evaluation of functionalized resveratrol analogues as inhibitors of quinone reductase 2



Sarah E. St. John^a, Katherine C. Jensen^b, SooSung Kang^{a,†}, Yafang Chen^b, Barbara Calamini^{c,‡}, Andrew D. Mesecar^{a,b,d}, Mark A. Lipton^{a,d,*}

^a Department of Chemistry, Purdue University, West Lafayette, IN 47907, United States

^b Department of Biological Sciences, Purdue University, West Lafayette, IN 47907, United States

^c Center for Pharmaceutical Biotechnology and Department of Medicinal Chemistry and Pharmacognosy, College of Pharmacy, The University of Illinois at Chicago, Chicago, IL 60607, United States

^d The Purdue University Center for Cancer Research, Purdue University, West Lafayette, IN 47907, United States

ARTICLE INFO

Article history:

Received 20 May 2013

Revised 12 July 2013

Accepted 19 July 2013

Available online 27 July 2013

Keywords:

Quinone reductase 2

Resveratrol

Inhibitors

Library

X-ray crystallography

Organic synthesis

ABSTRACT

Resveratrol (3,5,4'-trihydroxystilbene) has been proposed to elicit a variety of positive health effects including protection against cancer and cardiovascular disease. The highest affinity target of resveratrol identified so far is the oxidoreductase enzyme quinone reductase 2 (QR2), which is believed to function in metabolic reduction and detoxification processes; however, evidence exists linking QR2 to the metabolic activation of quinones, which can lead to cell toxicity. Therefore, inhibition of QR2 by resveratrol may protect cells against reactive intermediates and eventually cancer. With the aim of identifying novel inhibitors of QR2, we designed, synthesized, and tested two generations of resveratrol analogue libraries for inhibition of QR2. In addition, X-ray crystal structures of six of the resveratrol analogues in the active site of QR2 were determined. Several novel inhibitors of QR2 were successfully identified as well as a compound that inhibits QR2 with a novel binding orientation.

© 2013 Elsevier Ltd. All rights reserved.

1. Introduction

Resveratrol (3,5,4'-trihydroxystilbene, Fig. 1) is a naturally occurring phytoalexin that was discovered in 1940, when it was isolated from the roots of white hellebore.^{1–3} Resveratrol occurs in nature as both the *cis*- and *trans*-isomers and it can be found in a variety of dietary sources including peanuts, pistachios, and berries.^{4,5} Of the more common dietary sources of resveratrol, the skins and seeds of grapes are the most notable with red wine being the most heavily consumed form.^{5,6}

Interest in resveratrol increased dramatically in 1992, when it was hypothesized to explain the cardioprotective effects of red wine and the 'French paradox,' the observation of reduced incidence of cardiovascular disease in regions of France where red wine and saturated fats are consumed in greater quantities than in the US.^{7,8} Since then, numerous studies have demonstrated the

ability of resveratrol to prevent or slow the progression of various disease states including cancer and cardiovascular disease.^{9,10} Resveratrol has even been shown to increase the lifespans of several organisms including yeast, worms, fruit flies and fish.^{11–13}

A number of direct targets for resveratrol have been discovered *in vitro*, including cyclooxygenase-1 (COX1), cyclooxygenase-2 (COX2), and the transcription factor NF- κ B.^{14–16} The highest affinity target of resveratrol identified to date is quinone reductase 2 (QR2), a FAD-dependent cytosolic enzyme that catalyzes the 1-, 2-, or 4-electron reduction of quinones and other compounds using *N*-alkyl- and *N*-ribosylnicotinamides.^{17,18} QR2 is an oxidoreductase thought to function in metabolic reduction and detoxification; however, the true physiological role of QR2 is currently unknown.¹⁹ Evidence exists that QR2 is capable of catalyzing the metabolic activation of quinones and anti-tumor drugs, leading to cell toxicity.^{20–22} Thus, in some cases, inhibition of QR2 by resveratrol may guard cells against these reactive species that induce DNA damage, which may subsequently lead to cancer.²³

Resveratrol has been found to bind tightly to the oxidized, FAD-form of QR2 and it acts as a competitive inhibitor against *N*-methyl-dihydroxynicotinamide (NMeH) with a K_i value of 88 ± 20 nM, determined by steady-state kinetic studies, and a K_d value of

* Corresponding author. Tel.: +1 765 494 0132.

E-mail address: lipton@purdue.edu (M.A. Lipton).

[†] Present address: Department of Chemistry, Northwestern University, Evanston, IL, United States.

[‡] Present address: Center for Drug Discovery and Department of Neurobiology, Duke University Medical Center, Durham, NC 27710, United States.

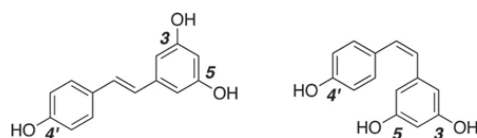


Figure 1. *Trans*- and *cis*-resveratrol.

54 ± 0.6 nM, determined by isothermal titration calorimetry^{17,24} Additionally, plasma levels of resveratrol are able to reach concentrations of 500 nM, which suggests that significant inhibition of QR2 by resveratrol *in vivo* may be achievable.²⁴ Taken together, these data suggest that the amount of resveratrol consumed from dietary sources may be sufficient for effective inhibition of QR2. However, circulating resveratrol is rapidly metabolized in the liver and gut by sulfation and glucuronation to its 3- and 4'-O-sulfate and 3-O-glucuronide conjugates.^{24–27} These primary metabolites of resveratrol have been shown to have far lower affinity for QR2.²⁴

The present work was undertaken in an attempt to identify novel analogues of resveratrol that could potentially inhibit QR2 with increased affinity and to serve as leads for the development of future QR2 inhibitors as cancer chemopreventive or anticancer drugs. To do this, we first tested a library of 78 previously synthesized resveratrol analogues designed to investigate the effects of different steric and electronic substituents on both the aryl rings and central olefin resveratrol.²⁸ Based on the inhibition of QR2 by the most active of these compounds, we set out to determine what effect functionalization of the central olefin of resveratrol with electron withdrawing substituents would have on inhibition of QR2 by creating a series of olefin-substituted and benzanilide resveratrol analogues. In addition, to circumvent inhibitory inactivation of resveratrol by its rapid metabolism, identification of effective resveratrol analogues that lacked the 3- and 4'-hydroxyl groups required for sulfation and glucuronation was of interest.

2. Results and discussion

2.1. Inhibition of QR2 by a first-generation resveratrol analogue library

The first-generation library of resveratrol analogues was designed to investigate the effects of substitution on each of the two aryl rings and central alkene of resveratrol. Therefore, to explore the electronic and steric demands of each of the aryl rings, electron-donating (OH, OMe, and NMe₂) and electron-withdrawing (F, CF₃ and NO₂) and naphthyl substituents were selected. Four substituents were chosen to determine the effect of sterics and electronics on the central olefin (H, Me, Et, CF₃). The synthesis of this first generation library of 78 resveratrol analogues has been previously reported.²⁸ Twenty-four of the seventy-eight resveratrol analogues were found to effectively inhibit QR2. These results are displayed in Table 1.

Of the 78 resveratrol analogues tested, twenty-four were found to actively inhibit QR2. Of the twenty-four active analogues, ten were more potent inhibitors of QR2 than resveratrol, five of which lacked both the 3- and 4'-hydroxyl substituents that undergo metabolic sulfation and glucuronation (**1h**, **1i**, **1j**, **1r**, and **1v**). Interestingly, two of the analogues found to be more active inhibitors of QR2 than resveratrol had a naphthyl substituted for an aryl ring (**1i** and **1l**), possibly allowing for a greater pi-stacking interaction with the oxidized isoalloxazine ring of the FAD in the active site of QR2. The most potent inhibitor of QR2 identified from the first generation library was compound **1v**, which has both a highly electron-deficient aryl ring and central olefin as a result of the

Table 1
Inhibition of QR2 by first generation resveratrol analogue library

Analogue	R ₁	R ₂	R ₃	IC ₅₀ ^a (μM)
Resveratrol	4-OH	H	3,5-(OH) ₂	11.5 ± 3.2
1a	4-OH	H	3,4-(OH) ₂	6.0 ± 1.2
1b	4-OH	H	3,5-(OMe) ₂	5.1 ± 1.2
1c	3,4-(OH) ₂	H	4-OMe	9.3 ± 3.7
1d	3,4-(OH) ₂	H	3-F	20.8 ± 8.6
1e	3,4-(OH) ₂	H	4-CF ₃	14.2 ± 4.3
1f	4-OMe	H	3,5-(OMe) ₂	14.6 ± 4.3
1g	3,5-(OMe) ₂	H	3,4-(OMe) ₂	37.1 ± 6.8
1h	3,5-(OMe) ₂	H	4-F	4.6 ± 1.0
1i	3,5-(OMe) ₂	H	2-Naphthyl	0.73 ± 0.12
1j	3,4-(OMe) ₂	H	3-OMe	6.8 ± 1.2
1k	3,4-(OMe) ₂	H	4-NMe ₂	13.0 ± 3.5
1l	3,4-(OMe) ₂	H	2-Naphthyl	5.5 ± 1.3
1m	4-OH	Me	3,5-(OH) ₂	39.0 ± 17.2
1n	4-OH	Me	4-CF ₃	2.8 ± 1.2
1o	3,5-(OH) ₂	Me	4-OH	4.8 ± 1.2
1p	4-OMe	Me	3,5-(OH) ₂	12.0 ± 8.4
1q	4-OMe	Me	3,5-(OMe) ₂	20.1 ± 0.1
1r	4-OMe	Me	3,4-(OMe) ₂	6.7 ± 3.0
1s	3,4-(OMe) ₂	Me	3,5-(OH) ₂	33.7 ± 32.4
1t	3,4-(OMe) ₂	Me	3,5-(OMe) ₂	9.9 ± 4.0
1u	3,5-(OMe) ₂	CF ₃	4-OMe	13.0 ± 3.1
1v	3-CF ₃	CF ₃	3,4-(OMe) ₂	0.18 ± 0.3
1w	3,5-(OH) ₂	Et	4-NMe ₂	10.9 ± 2.2
1x	3,4-(OMe) ₂	Et	3,5-(OMe) ₂	16.3 ± 7.0

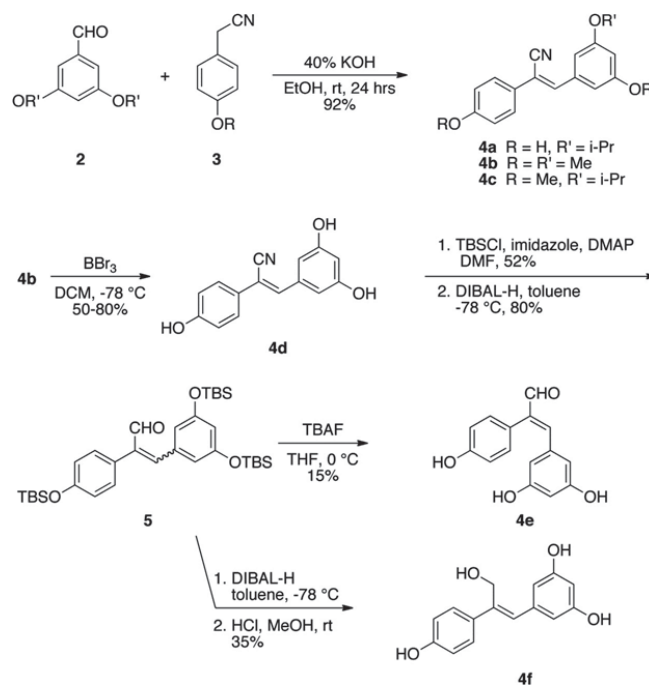
^a The lowest IC₅₀ values are highlighted in bold.

trifluoromethyl substituents. Unfortunately, attempts at obtaining an X-ray crystal structure of our most active compound **1v** in the active site of QR2 were unsuccessful; however, as a result we were determined to further investigate the effect of substitution at the central olefin. Therefore, we set out to synthesize a second-generation library comprised of analogues with electron-withdrawing substituents on the central olefin as well as a set of resveratrol analogues where the central olefin had been replaced by an amide.

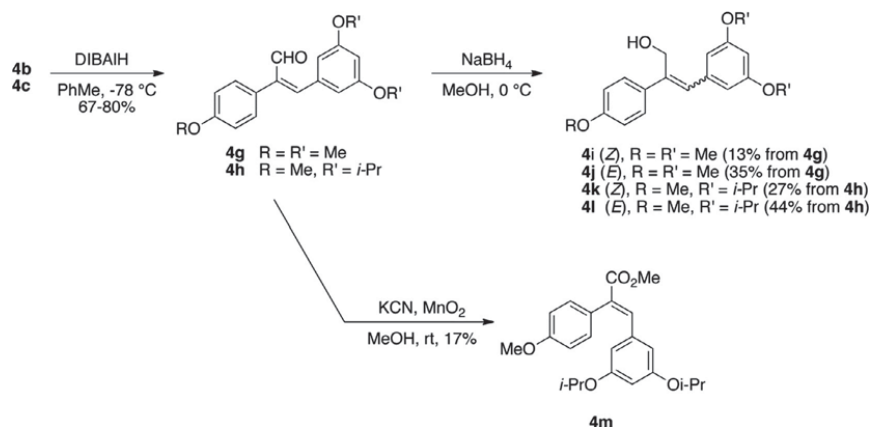
2.2. Synthesis of olefin-substituted resveratrol analogues

To investigate the effect of substitution of both the central olefin and the phenols, as well as the conformational effect of *E/Z*-isomerism of resveratrol on its inhibition of QR2, a small library of 21 olefin-substituted resveratrol analogues was synthesized. The synthesis of (*Z*)-cyano resveratrol analogues **4a**, **4b**, and **4c** was accomplished by condensation of the appropriate aldehyde **2** with the appropriate 2-phenylacetonitrile **3**, as shown in Scheme 1^{29,30} With these easily functionalized nitriles in hand, the remaining eighteen resveratrol structural analogues could be synthesized. Deprotection of **4b** with boron tribromide yielded (*Z*)-nitrile analogue **4d**. Protection of the phenols of **4d** as *tert*-butyldimethylsilyl ethers followed by the reduction of the nitrile using diisobutylaluminum hydride yielded a mixture of (*E*)- and (*Z*)-aldehydes **5**. Treatment of **5** with tetra-*n*-butylammonium fluoride resulted in the isomerically pure (*E*)-acrylaldehyde **4e**, where the (*Z*)-isomer was not detected. Further reduction of **5** with diisobutylaluminum followed by deprotection of the hydroxyls with dilute hydrochloric acid in methanol yielded the isomerically pure (*Z*)-alcohol **4f** (Scheme 1).

Reduction of (*Z*)-nitriles **4b** and **4c** using diisobutylaluminum hydride resulted in (*Z*)-aldehyde analogues **4g** and **4h** in moderate to good yields. Further reduction of the aldehydes **4g** and **4h** with sodium borohydride yielded mixtures of both (*Z*)- and (*E*)-alcohols, which could be separated by flash chromatography to give the four



Scheme 1. Synthesis of olefin-substituted resveratrol analogues.

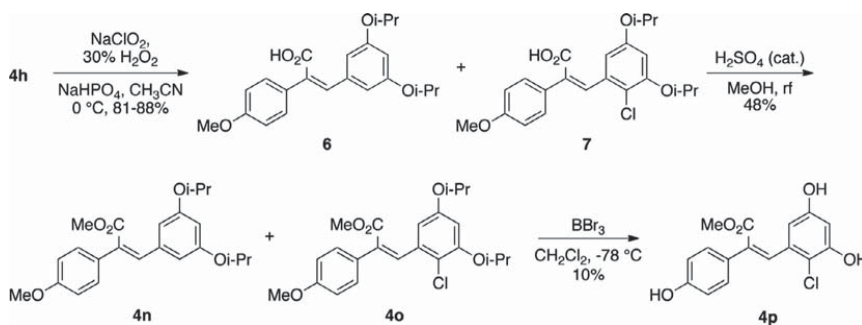
Scheme 2. Synthesis of olefin-substituted resveratrol analogues **4g**–**4m**.

analogues **4i**, **4j**, **4k**, and **4l**. The (*E*)-methyl ester **4m** was obtained by oxidation of aldehyde **4h** using manganese dioxide and potassium cyanide in methanol (Scheme 2).³¹

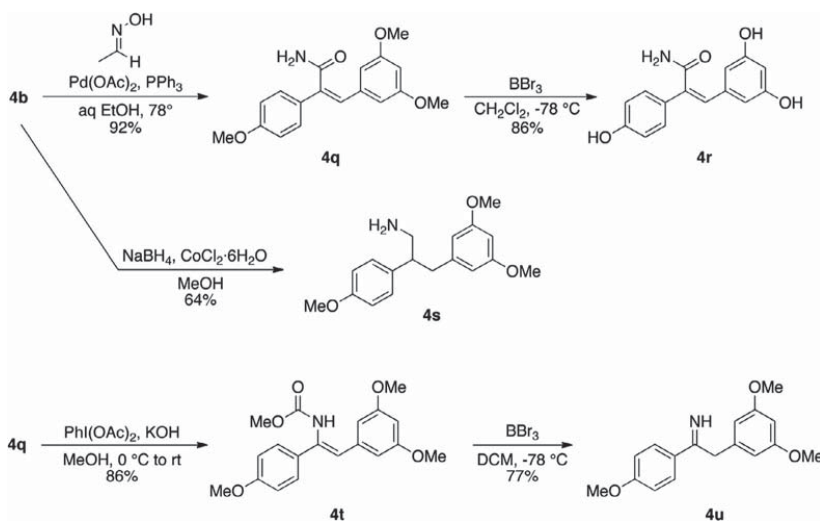
A Pinnick-type oxidation of aldehyde **4h** by sodium chlorite-hydrogen peroxide yielded an inseparable mixture of the desired (*Z*)-carboxylic acid **6** and chlorinated byproduct **7**, formed by reaction with hypochlorite generated in situ.³² Fischer esterification of the acids **6** and **7** yielded the methyl esters (*Z*)-**4n** and (*Z*)-**4o**, which could be separated by flash chromatography. Finally, depro-

tection of **4o** using boron tribromide yielded the desired (*Z*)-ester analogue **4p** (Scheme 3).

Palladium-catalyzed hydration of nitrile **4b** yielded the (*Z*)-amide **4q**, which upon treatment with boron tribromide gave (*Z*)-amide analogue **4r** in good yield, as shown in Scheme 4.³³ Concomitant reduction of the nitrile and olefin of **4b** was accomplished using sodium borohydride and cobalt chloride hexahydrate, resulting in amine analogue **4s**.³⁴ The (*Z*)-methyl carbamate **4t** was obtained in good yield by oxidative Hofmann rearrangement of **4q**



Scheme 3. Synthesis of olefin-substituted resveratrol analogues **4o**, **4n**, & **4p**.



Scheme 4. Synthesis of olefin-substituted resveratrol analogues **4q**, **4r**, **4s**, **4t**, & **4u**.

using (diacetoxyiodo)benzene. Treatment of the carbamate **4t** with boron tribromide deprotected the methyl carbamate, which upon aqueous workup afforded the imine analogue **4u** (Scheme 4).³⁵ The structures of all olefin-substituted resveratrol analogues are displayed in Figure 2.

2.3. Synthesis of benzanilides

A separate modification of the central alkene of resveratrol was accomplished by replacing the alkene with an amide bond; consequently, a small library of 26 substituted benzanilides (Fig. 2) was synthesized using standard amide bond forming reactions. Construction of the library was accomplished by reaction of the appropriately activated benzoic acid derivative with the corresponding substituted aniline. In most cases, benzoyl chlorides were suitable for the coupling reaction; however, when acid-sensitive substrates were used, EDC activation was employed instead. *N*-methyl benzanilide derivatives were made by treatment of the appropriate benzanilide with sodium hydride and methyl iodide. The imidate **8v** (Fig. 2) was obtained by treatment of TBS-protected **8r** with thionyl chloride and methanol.

The relationship between resveratrol and its benzanilide analogues' bioactivity was directly compared using analogues **8a**, **8b**,

8c, **8d**, and **8e** where the methylation of the amide and the phenols, and the position of the resorcinol ring relative to the nitrogen of the amide were varied. An additional 21 benzanilide resveratrol analogues were synthesized to probe the effect of different substitutions on bioactivity (Fig. 2, top).

2.4. Inhibition of QR2 by olefin-substituted and benzanilide resveratrol analogues

The ability of the second-generation analogues to inhibit QR2 is outlined in Table 2. Of the forty-seven second generation resveratrol analogues that were synthesized, nine were found to inhibit QR2. Two analogues, **4d** and **4f**, inhibited QR2 with IC_{50} s comparable to resveratrol, while the remaining seven were slightly weaker inhibitors of QR2 as compared to resveratrol ($6.9 \pm 0.4 \mu\text{M}$). Ten analogues showed weak inhibition of QR2 (between 20% and 50% at $100 \mu\text{M}$) and twenty-nine of the forty-seven analogues showed minimal inhibition of QR2 (<20% at $100 \mu\text{M}$). This result could be a consequence of substitution at the central olefin perturbing the binding orientation of the analogue within the active site of QR2. Each of the analogues that inhibited QR2 strongly had free hydroxyl groups, with the exception of analogues **4b**, **4g**, and **4k**, which had methyl ethers. In general, inhibitory activity decreased as

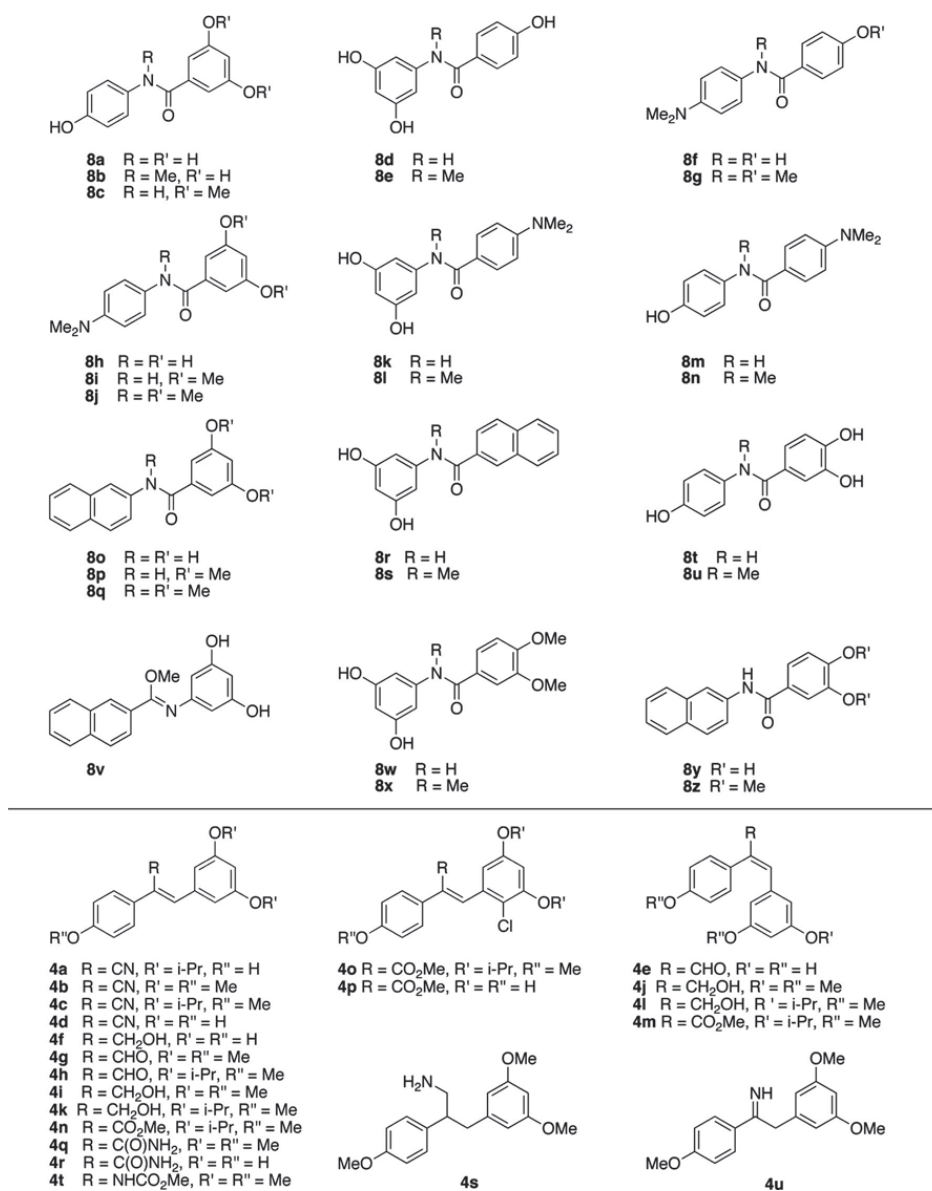


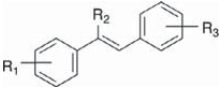
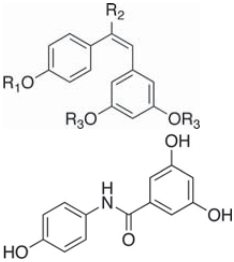
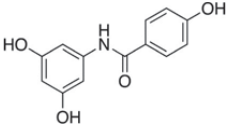
Figure 2. (Top) Benzanilide resveratrol analogue library, (bottom) olefin-substituted resveratrol analogue library.

steric bulk associated with the aryl rings increased. For example, the nitrile analogue **4d** was found to inhibit QR2 with an IC₅₀ of 5.9 ± 0.3 μM and 88.8% inhibition, while the nitrile analogue **4b**, which differs from **4d** only in that the hydroxyl groups have been replaced with methyl ethers, was found to inhibit QR2 with a six-fold increase in IC₅₀ of 31.6 ± 4.3 μM and 57.4% inhibition. Furthermore, the nitrile analogues **4a** and **4c**, where the methyl ethers of **4b** have been replaced with bulkier isopropyl ethers, did not show inhibition of resveratrol over 20% at a concentration of 100 μM. This result may be a consequence of the bulky ethers reducing the ability of the molecule to form stabilizing hydrogen bonds to ordered QR2 active site water molecules (vide infra). Previous re-

ports have demonstrated that methoxy groups and even acetates at the 2-, 3-, 4-, and 5-positions of resveratrol can be accommodated by the QR2 active site when the 4'-position is substituted with an amine.^{36,37}

Two of the olefin-substituted resveratrol analogues found to inhibit QR2, **4e** and **4k**, were of the *E* geometry, which more closely resembles *cis*-resveratrol. Interestingly, the (*E*)-alcohol **4k** was found to effectively inhibit QR2 with an IC₅₀ of 27.5 ± 4.9 μM and 57.2% inhibition at 100 μM, whereas its (*Z*)-isomer **4i** only had an average inhibition of 27.7% at 100 μM. Furthermore, the analogue **4f**, which only differs from **4i** in that the methoxy substituents have been replaced with hydroxyl groups, was found to be the

Table 2
Inhibition of QR2 by olefin-substituted and benzanilide resveratrol analogues

Structure	Analogue	R ₁	R ₂	R ₃	IC ₅₀ (μM)
	Resveratrol	4-OH	H	3,5-(OH) ₂	6.9 ± 0.4
	4b	4-OMe	CN	3,5-(OMe) ₂	31.6 ± 4.3
	4d	4-OH	CN	3,5-(OH) ₂	5.9 ± 0.3
	4f	4-OH	CH ₂ OH	3,5-(OH) ₂	5.1 ± 0.3
	4g	4-OMe	CHO	3,5-(OMe) ₂	24.2 ± 1.3
	4r	4-OH	CONH ₂	3,5-(OH) ₂	9.3 ± 1.9
	4e 4k	H Me	CHO CH ₂ OH	H Me	25.5 ± 3.5 27.5 ± 4.9
	8a	–	–	–	27.6 ± 4.6
	8d	–	–	–	16.8 ± 1.3

most potent inhibitor in our library, having an IC₅₀ of 5.1 ± 0.3 μM and 87.4% average inhibition at 100 μM of QR2. This supports our observation that substitution of sterically bulky ethers for the hydroxyl groups of resveratrol decreases inhibitory ability of a given compound; however, this data suggests that this trend may be negated when taking into consideration the effect of conformation. To the best of our knowledge, this is the first report of an isomerically pure (*E*)-resveratrol analogue inhibiting QR2 and having greater inhibition of QR2 than its corresponding (*Z*)-conformation (Fig. 3).

Two of the twenty-six benzanilide resveratrol analogues were found to inhibit QR2, **8a** and **8d**. Examination of the IC₅₀ data shows that the position of the amide nitrogen relative to the resorcinol ring has a measurable effect on the ability of the benzanilide analogue to inhibit QR2: when the nitrogen is directly bound to the resorcinol ring the IC₅₀ is decreased by roughly 40% (16.8 ± 1.3 μM vs 27.6 ± 4.6 μM). Additionally, only hydroxyl substituents on the aryl rings are tolerated for good inhibition of QR2 by the benzanilide analogues and even then, only at the same positions found in resveratrol itself. Comparison of **8a**, which has free hydroxyl groups at the 3-, 5-, and 4'-positions, to **8c**, where the 3- and 5-hydroxyls are replaced by methyl ethers, shows the average percent inhibition at 100 μM of QR2 decreases from 59.7% to 43.2%, respectively. Additionally, moving one hydroxyl substituent from the 3- to the 4-position on the resorcinol ring, as observed in the comparison of **8a** and **8t**, decreases the analogue's ability to inhibit

QR2 from 59.7% to 49.9% at 100 μM. Replacement of the 4'-hydroxyl group by a 4'-dimethylamino group eliminates inhibition of QR2, which is seen in both the comparison of **8a** to **8f** and **8d** to **8k**. This is significant since previous reports have shown that replacement of the hydroxyl group at the 4'-position of resveratrol by an amine can increase its inhibitory activity.^{36,37}

Of the eight synthesized naphthyl-substituted benzanilide analogues, only **8z** showed weak inhibition of QR2 (30.5% average inhibition at 100 μM). In contrast, the first generation analogue **1i**, which differs from **8z** only in that **8z** has an amide in place of the central alkene, was a potent inhibitor of QR2, having an IC₅₀ of 5.5 μM. Interestingly, second generation benzanilide analogue **8p** showed no inhibition of QR2 at 100 μM, while compound **1i** was the second most active analogue in the first generation library, having an IC₅₀ of 0.7 μM.

2.5. X-ray crystallographic analysis of QR2 in complex with active olefin-substituted and benzanilide resveratrol analogues

To elucidate the structural factors underlying the inhibitory trends observed in the kinetic data, and to answer questions such as why does the (*E*)-geometry **4k** analogue lead to a more potent inhibitor of QR2 than its (*Z*)-isomer **4i**, a series of X-ray crystal structures were determined for the most potent olefin-substituted and benzanilide QR2 inhibitors. Resveratrol binds in the active site of QR2 fitting into a hydrophobic cleft that is approxi-

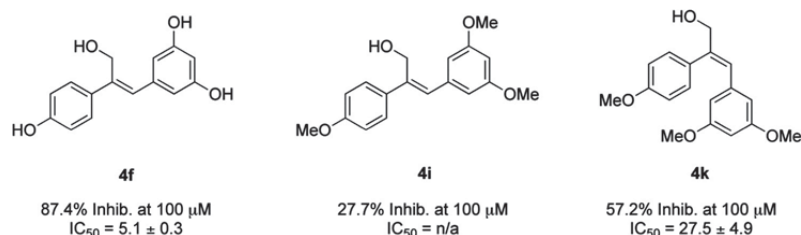


Figure 3. Effect of substitution and alkene geometry on QR2 inhibition.

mately 17 Å long and 7 Å wide (Fig. 4A and B). Three sides of the QR2 binding cavity are composed of hydrophobic amino acids, while the fourth side is solvent exposed. The ends of the cavity contain residues that are available for hydrogen bond formation. The planar structure of resveratrol allows it to fit into the QR2 binding cleft in an orientation coplanar to the isoalloxazine ring of the FAD cofactor.¹⁷ The narrow width of the QR2 binding site dictates that it can only accommodate molecules such as resveratrol that can adopt essentially planar conformations. Additionally, molecules that bind tightly to QR2 are generally planar and polyaromatic with the ability to stack with the isoalloxazine ring of FAD, possibly utilizing a pi-stacking interaction with the isoalloxazine for binding (Fig. 4A and B).^{38,39}

Complete X-ray crystallographic data sets of QR2 in complex with inhibitors **4d**, **4f**, **4k**, **4r**, **8a**, and **8d** were collected and the structures for each complex were determined. The final data collection and refinement statistics are summarized in Table 3. With the exception of **4k**, all of the olefin-substituted and benzanilide resveratrol analogues bind in the same orientation as resveratrol, coplanar to the oxidized isoalloxazine ring of the bound cofactor FAD (Fig. 5). The binding of analogs **4d**, **4f**, **4k**, **4r**, **8a**, and **8d** does not significantly alter the conformation of the active site residues compared to the resveratrol-bound structure. As with resveratrol, the (*Z*)-analogues show water mediated hydrogen bonds from the 4'-hydroxyl group of the ligand to the hydroxyl group of Thr71, a tight hydrogen bond from the 5-hydroxyl to Asn161, and a hydrogen bond from the 3-hydroxyl to the carbonyl oxygen of Gly174.¹⁷ The 5-hydroxyls of the (*Z*)-configured analogues also form a hydrogen bond to an ordered active site water molecule. In some cases, such as **8a** (Fig. 5E) and **8d** (Fig. 5F), a network of water molecules within the active site can extend to the substitution at the central olefin.

Examination of the X-ray crystal structures of the (*Z*)-configured resveratrol analogues show that they bind in identical conformations. The substitution of methyl ethers for phenols, such as in analogue **4b**, could change this preferred binding orientation. In support of this, we did not observe strong electron density of **4b** in the QR2 active site, suggesting that the ligand was only present at partial occupancy. This also supports our observations regarding the series of analogues **4f**, **4i**, and **4k** (Fig. 3). Our most active inhibitor, **4f**, has a *Z* geometry and has hydroxyl substituents that hydrogen-bond key residues and structural waters in the QR2 active site. The inhibitor **4i**, which differs from **4f** only by substitution of methyl ethers for the hydroxyl groups of **4f**, did not show potent enough inhibition of QR2 to make determination of an IC₅₀ feasible, suggesting that increasing the size of the 4'-, 3-, and 5-substituents is not readily accommodated by the QR2 active site.

Most surprisingly, the *E* isomer of **4i**, **4k**, is a potent inhibitor of QR2 and binds in a completely different orientation than the other analogues where only one aryl ring occupies the same molecular space as the other *Z* analogues (Fig. 5E). Examination of the binding orientation of **4k** shows that it does not form a direct hydrogen bond to the network of active site water molecules that hydrogen bond to the side chain of Thr71. Instead, an additional water molecule is present in the active site and is positioned where the 4'-hydroxyl group of the (*Z*)-configured resveratrol analogues usually resides, forming a water-mediated hydrogen bond to the side chain of Asn161. Taking together the structure of **4k** in the active site and the partial occupancy observed for the **4b** analogue, we hypothesize that, for the QR2 active site to accommodate resveratrol analogues with bulkier substituents, the molecules must rotate 90° from their preferred binding orientation to allow at least one aryl ring to stack on the isoalloxazine ring (Fig. 6A). Whether this rotation will be accommodated by the QR2 active site depends on the other substituents on the analogs and whether water molecules can aid in the binding process.

The two most active benzanilide analogues, **8a** and **8d** (Fig. 5E and F, respectively), orient their hydroxyl substituents in identical locations (Fig. 6B), taking advantage of the same hydrogen bond network. The carbonyl groups of the amide core of each analogue are positioned to interact with the solvent exposed region of the active site, avoiding the hydrophobic interior, again both utilizing almost identical water molecules.

3. Conclusions

In conclusion, two sets of resveratrol analogue libraries were designed, synthesized and tested for inhibition of QR2. Twenty-four of the seventy-eight first generation resveratrol analogues were found to potently inhibit QR2 and, of those twenty-four analogues, ten were more potent QR2 inhibitors than resveratrol. Our goal of identifying analogues that were both more potent than resveratrol and lacking the metabolically sensitive 3- and 4'-hydroxyl groups was achieved with the identification of five analogues—**1h**, **1i**, **1j**, **1r**, and **1v**—from the first-generation library. A second-generation library of 47 resveratrol analogues was designed to probe the effects of substitution on the central alkene. Nine of the second-generation resveratrol analogues were found to inhibit QR2. Two of the analogues, **4d** and **4f**, had comparable IC₅₀ values to that of resveratrol while the remaining seven analogues were slightly weaker inhibitors of QR2 in comparison to resveratrol. Because of the unique substitutions made at the central alkene, X-ray crystal structures of six of the nine inhibitors in complex with QR2 were determined. From the series of crystal structures obtained, we

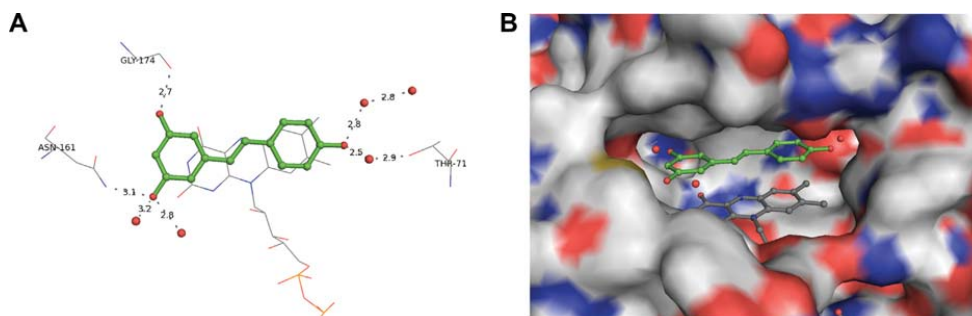


Figure 4. Resveratrol-QR2 complex (PDB: 1SG0). Resveratrol is shown in green, colored by atom type, and shown in ball and stick representation. Water molecules are shown as red spheres. Hydrogen bonds are shown as grey dashes labeled with the distance in Ångstroms (Å). (A) X-ray structure of QR2 in complex with resveratrol displaying hydrogen bond network, (B) Resveratrol in binding cavity of QR2, where QR2 is shown in grey surface representation and colored according to atom type.¹⁷

Table 3
X-ray data collection and refinement statistics

Data collection	4d	4r	4f	8a	8d	4k	4k
Detector	MarMosaic 300 mm	MarMosaic 300 mm	MarMosaic 300 mm	MarMosaic 225 mm	MarMosaic 225 mm	MarMosaic 225 mm	MarMosaic 225 mm
Space group	P2 ₁ 2 ₁ 2 ₁	P2 ₁ 2 ₁ 2 ₁	P2 ₁ 2 ₁ 2 ₁	P2 ₁ 2 ₁ 2 ₁	P2 ₁ 2 ₁ 2 ₁	P2 ₁ 2 ₁ 2 ₁	P2 ₁ 2 ₁ 2 ₁
a,b,c (Å)	56.90, 83.36, 106.53	56.94, 83.39, 106.64	56.65, 83.39, 106.57	56.69, 83.15, 106.68	57.10, 83.51, 106.47	56.33, 83.59, 106.43	56.26, 83.58, 106.34
$\alpha = \beta = \gamma$ (degrees)	90	90	90	90	90	90	90
Resolution (Å)	50–1.40	50–1.45	50–1.45	50–1.55	50–1.63	50–1.45	50–1.40
Reflections observed	436515	402271	389780	349634	287051	437831	441401
Unique reflections	85793	90632	84618	72933	62952	86788	98717
R_{merge} (%)	58.7 (5.1)	54.4 (5.6)	50.2 (5.2)	53.0 (6.6)	54.9 (7.8)	46.1 (5.7)	50.3 (5.2)
I/σ	33.1 (2.5)	28.0 (2.9)	28.3 (2.9)	27.1 (2.6)	17.4 (2.0)	31.7 (3.0)	31.4 (2.5)
% Completeness	85.9 (85.8)	99.8 (99.8)	94.0 (98.7)	98.9 (98.1)	98.4 (97.6)	96.8 (99.8)	99.4 (98.6)
Refinement							
Resolution range (Å)	(1.40–1.42)	(1.45–1.48)	(1.45–1.48)	(1.55–1.58)	(1.63–1.66)	(1.45–1.48)	(1.40–1.42)
Reflections in working set	81481	86029	80331	69206	59715	82382	93724
Reflections in test set	5532	5778	5840	3672	3968	5772	6413
R_{work} (%)	16.3	15.4	16.7	16.8	16.4	16.4	16.6
R_{free} (%)	19.0	18.0	19.2	18.9	19.3	18.7	18.8
Average B-factor (Å ²)	14.0	13.8	13.8	12.9	11.7	14.0	14.1

learned that all of the Z-configured resveratrol analogues share a common binding orientation within the active site of QR2. Additionally, the analogues all utilize the same ordered, active site water molecules to form water-mediated hydrogen bonds to the same residues within the QR2 active site, Asn161, Gly174 and Thr71. We also identified a novel binding orientation of the E-configured resveratrol analogue **4k**, which is the first example of an E-configured resveratrol analogue bound in the QR2 active site. Future investigations will focus on the identification of additional E-configured resveratrol analogues that lack the metabolically sensitive 3- and 4'-hydroxyl groups, but also have more potent inhibition of QR2.

4. Experimental

4.1. General procedures

All reagents (chemicals) were purchased from Sigma or Acros and used without further purification. Infrared spectra were obtained using a Thermo Nicolet Nexus 470 FT-IR spectrometer with OMNIC software package. Mass spectral analyses were performed using a Waters Micromass ZQ with ESI-MS injection port utilizing MassLynx V4.1 software package. Analytical thin-layer chromatography was performed on Sorbent Technologies Glass Backed Silica Gel HL TLC Plates w/UV254. Flash chromatography was performed with Sorbent Technologies 200–400 mesh silica gel. ¹H NMR spectra were obtained at 300 or 400 MHz and ¹³C NMR spectra were obtained at 75 or 100 MHz, using Varian Inova300 and Bruker ARX400 spectrometers, respectively. E/Z isomerism was determined by Nuclear Overhauser Effect experiments. All compounds were purified by flash chromatography to >90% purity by ¹H NMR (see Supplementary data).

4.2. Synthesis

4.2.1. 3,5-Diisopropoxybenzaldehyde (2)

A mixture of 3,5-dihydroxybenzoic acid (1.00 g, 6.49 mmol), potassium carbonate (4.04 g, 29.2 mmol) and isopropyl bromide (3.65 mL, 38.93 mmol) in 12 mL dimethylformamide was heated to reflux for 4 days. After cooling to room temperature, 6 mL water and 6 mL 2 M hydrochloric acid were added to dissolve the carbonate and acidify the reaction mixture. The aqueous layer was extracted with ethyl acetate (3 × 20 mL) and the combined organic

layers were dried over magnesium sulfate, filtered and concentrated to yield 3,5-diisopropoxybenzoic acid as a clear oil that was used without further purification.

A 0.54 M solution of DIBAL-H in dichloromethane (4.66 mL, 2.52 mmol) was added to a solution of 3,5-diisopropoxybenzoic acid (282 mg, 1.01 mmol) in toluene (5 mL) at –78 °C. The reaction mixture was allowed to stir for 45 min at that temperature before quenching with 5% aqueous hydrochloric acid (1 mL). After warming to room temperature, the reaction mixture was diluted with water and the aqueous layer was extracted with ethyl acetate (3 × 5 mL), the combined organic layers were dried over magnesium sulfate, filtered and concentrated to yield a mixture of 3,5-diisopropoxybenzaldehyde and (3,5-diisopropoxyphenyl)methanol in 97% combined yield. 3,5-Diisopropoxybenzaldehyde: ¹H NMR (400 MHz, CDCl₃) δ (ppm): 9.77 (1H, s), 6.86 (2H, d, $J = 2.31$), 6.57 (1H, t, $J = 2.31$), 4.48 (2H, m, $J = 6.15$), 1.24 (6H, d, $J = 6.16$). ¹³C NMR (100 MHz, CDCl₃) δ (ppm): 191.72, 159.44, 110.10, 108.33, 70.03, 21.72.

4.2.2. 2-(4-Methoxyphenyl)acetonitrile (3)

Triphenyl phosphine (1.14 g, 4.34 mmol) was added portionwise to a solution of (4-methoxyphenyl)methanol (300 mg, 2.17 mmol) and carbon tetrabromide (1.22 g, 3.69 mmol) in anhydrous dichloromethane (7.2 mL) at 0 °C. The reaction mixture was stirred at that temperature for 20 min then concentrated to yield a viscous oil which was dissolved in 10 mL of 50% hexanes 50% ethyl acetate. The precipitate was filtered off and the filtrate concentrated. The residue was taken up in dimethylformamide (7.2 mL) and potassium cyanide (0.99 g, 15.2 mmol) was added. The reaction mixture was allowed to stir for 90 min before quenching with saturated aqueous sodium bicarbonate (10 mL). The aqueous layer was extracted with ethyl acetate (3 × 10 mL) and the combined organic layers were washed with brine, dried over magnesium sulfate, filtered and concentrated. The crude product was purified by flash chromatography using 20% ethyl acetate 80% hexanes to yield the pure product **3** in 45% yield. ¹H NMR (300 MHz, CDCl₃) δ (ppm): 7.19 (2H, d, $J = 8.38$), 6.86 (2H, d, $J = 8.38$), 3.74 (3H, s), 3.61 (2H, s). ¹³C NMR (75 MHz, CDCl₃) δ (ppm): 159.15, 129.01, 121.89, 118.42, 114.35, 55.18, 22.50.

4.2.3. General procedure for Aldol condensation (4a–4c)

Aqueous 40% potassium hydroxide (0.23 mL/mmol nitrile) was diluted with absolute ethanol (0.46 mL/mmol nitrile) and added

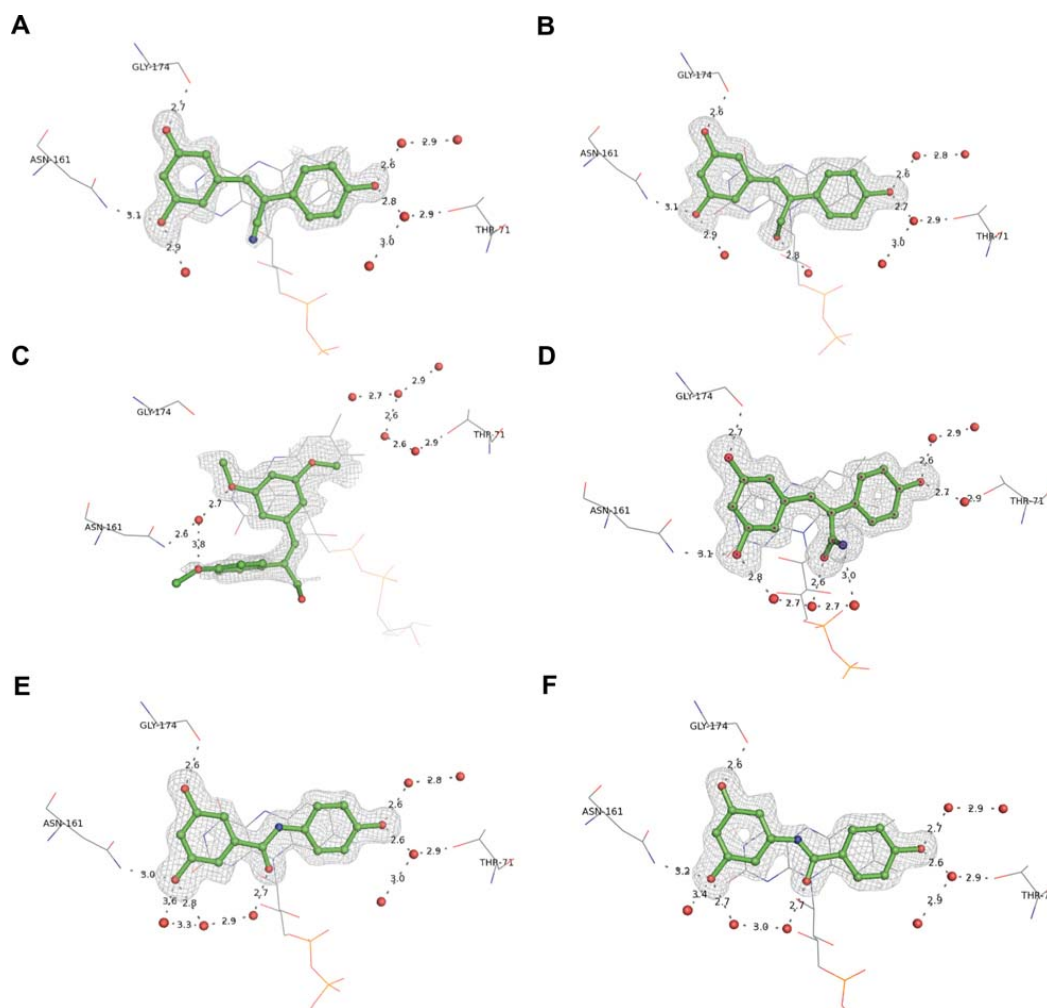


Figure 5. X-ray crystal structures of (A) **4d**, (B) **4f**, (C) **4k**, (D) **4r**, (E) **8a**, and (F) **8d** in complex with QR2. Resveratrol analogues are shown in green, colored according to atom type, and shown in ball and stick representation. Water molecules are shown as red spheres. Hydrogen bonds are shown as grey dashes with distances (Å) labeled. The FAD cofactor is shown in grey lines and colored according to atom. Electron density omit maps ($F_o - F_c$) are shown in white mesh and contoured to 3.0σ around the ligand only. The binding orientation of each resveratrol analogue was the same in both active sites of the QR2 dimer, therefore only one active site is shown for clarity.

at room temperature to a solution of the appropriate aldehyde (1.1 equiv) and nitrile (1.0 equiv) in absolute ethanol (0.35 mL/mmol nitrile). The reaction was then allowed to stir at room temperature for 12–24 h before concentrating. The resulting yellow residue was taken up in water and ethyl acetate and dilute hydrochloric acid was added to neutralize the aqueous layer. The aqueous layer was then extracted with ethyl acetate and the combined organic layers were washed with brine, dried over magnesium sulfate, filtered and concentrated to yield the crude product. Purification by flash chromatography yielded the pure nitrile products in 80–95% yield.

4.2.4. (Z)-3-(3,5-Diisopropoxyphenyl)-2-(4-hydroxyphenyl)acrylonitrile (**4a**)

General procedure for Aldol condensation was used in combination with **2** and 2-(4-((*tert*-butyldimethylsilyloxy)phenyl)

acetonitrile (28%), ^1H NMR (300 MHz, CDCl_3) δ (ppm): 7.56 (2H, d, $J = 8.71$), 7.31 (1H, s), 6.98 (2H, d, $J = 2.15$), 6.90 (2H, d, $J = 8.71$), 6.50 (1H, t, $J = 2.15$), 5.06 (1H, s), 4.58 (2H, m, $J = 6.05$), 1.36 (12H, d, $J = 2.05$). ESIMS(+) m/z 338 (M+H), 360 (M+Na), 376 (M+K).

4.2.5. (Z)-3-(3,5-Dimethoxyphenyl)-2-(4-methoxyphenyl)acrylonitrile (**4b**)

General procedure for Aldol condensation was used in combination with 3,5-dimethoxybenzaldehyde and **3** (95%). ^1H NMR (300 MHz, CDCl_3) δ (ppm): 7.61 (2H, d, $J = 8.91$), 7.34 (1H, s), 7.04 (2H, d, $J = 2.13$), 6.96 (2H, d, $J = 8.91$), 6.53 (1H, t, 2.13), 3.85 (9H, s). ^{13}C NMR (75 MHz, CDCl_3) δ (ppm): 160.73, 160.32, 139.83, 135.47, 127.16, 126.59, 118.11, 114.27, 111.14, 106.71, 102.65, 55.28. ESIMS(+) m/z 318 (M+Na).

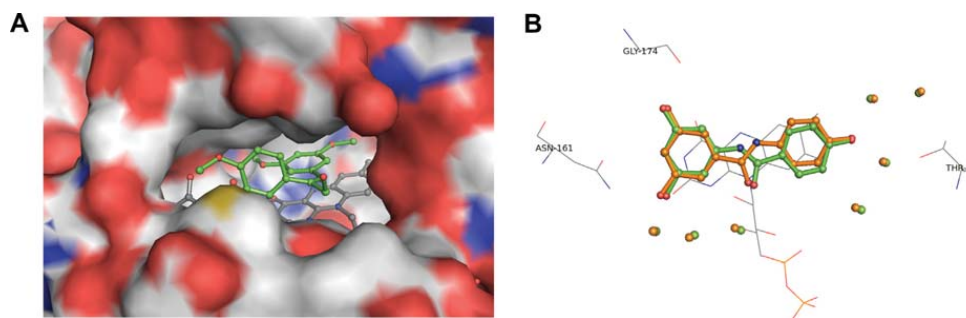


Figure 6. (A) Crystal structure of inhibitor **4k** bound in the QR2 active site. QR2 is shown in grey surface representation and colored according to atom type; **4k** is shown in green ball and stick and colored according to atom. FAD and active site residue Asn161 are shown in grey ball and stick and colored according to atom. (B) Superposition of X-ray structures of benzanilides **8a** (shown in orange ball and stick) and **8d** (shown in green ball and stick) in complex with QR2, where active site waters are shown as non-bonding spheres, are colored according to ligand and are identical between the two compounds.

4.2.6. (Z)-3-(3,5-Diisopropoxyphenyl)-2-(4-methoxyphenyl)-acrylonitrile (**4c**)

General procedure for Aldol condensation was used in combination with **2** and **3** (92%). $^1\text{H NMR}$ (300 MHz, CDCl_3) δ (ppm): 7.56 (2H, d, $J = 8.83$), 7.32 (1H, s), 7.01 (2H, d, $J = 1.86$), 6.94 (2H, d, $J = 8.83$), 6.51 (1H, t, 1.86), 4.58 (2H, m, $J = 6.04$), 3.81 (3H, s), 1.37 (12H, d, $J = 6.04$). $^{13}\text{C NMR}$ (75 MHz, CDCl_3) δ (ppm): 160.31, 159.15, 140.24, 135.45, 127.19, 126.79, 118.08, 114.30, 110.98, 108.30, 108.24, 106.13, 70.07, 70.01, 55.25, 21.96. ESIMS(+) m/z 352 (M+H), 374 (M+Na), 390 (M+K).

4.2.7. (Z)-3-(3,5-Dihydroxyphenyl)-2-(4-hydroxyphenyl)-acrylonitrile (**4d**)

A 1.0 M solution of boron tribromide in dichloromethane (2.34 mL, 2.34 mmol) was added slowly to a solution of **4b** (138 mg, 0.46 mmol) in dichloromethane (2.3 mL) at -78°C under nitrogen atmosphere. The reaction was allowed to stir at room temperature for 4 h before cooling to -78°C and quenching with an aqueous solution of saturated sodium bicarbonate (2 mL). The reaction mixture was warmed to room temperature and the aqueous layer was extracted with ethyl acetate (3×2 mL). The combined organic layers were washed with saturated sodium bicarbonate (3×5 mL), water (1×5 mL), and brine (1×5 mL) before being dried over magnesium sulfate, filtered, and concentrated. The pure product was obtained in 80% yield after purification by flash chromatography using 50% ethyl acetate 50% hexanes. $^1\text{H NMR}$ (400 MHz, CD_3OD) δ (ppm): 7.52 (2H, d, $J = 8.70$), 7.42 (1H, s), 6.85 (2H, d, $J = 8.70$), 6.82 (2H, d, $J = 2.02$), 6.33 (1H, t, $J = 2.02$). $^{13}\text{C NMR}$ (100 MHz, CD_3OD) δ (ppm): 159.85, 141.34, 137.32, 128.35, 127.07, 119.17, 116.86, 111.91, 108.56, 105.58. IR ν_{max} 3216 (OH), 2227 (CN) cm^{-1} .

4.2.8. (E)-3-(3,5-Dihydroxyphenyl)-2-(4-hydroxyphenyl)acrylaldehyde (**4e**)

A 1.0 M solution of tetrabutylammonium fluoride solution in THF (0.15 mL, 0.15 mmol) was added to a solution of **5** (29 mg, 0.05 mmol) in THF (0.25 mL) at 0°C . The reaction was allowed to stir overnight before quenching with saturated ammonium chloride. The aqueous layer was extracted with ethyl acetate (3×3 mL) and the combined organic layers were washed with brine, dried over magnesium sulfate, filtered and concentrated. The pure product **4e** was obtained in 15% yield after flash chromatography using 50% ethyl acetate 50% hexanes. $^1\text{H NMR}$ (400 MHz, $\text{CD}_3\text{OD}:\text{CDCl}_3$ 50:50) δ (ppm): 9.44 (1H, s), 7.03 (1H, s), 6.81 (2H, d, $J = 8.59$), 6.63 (2H, d, $J = 8.59$), 6.07 (2H, s). $^{13}\text{C NMR}$ (100 MHz, CD_3

OD) δ (ppm): 195.25, 157.48, 157.33, 151.12, 140.98, 135.65, 130.39, 123.78, 115.27, 109.10, 104.54. ESIMS(+) m/z 257 (M+H).

4.2.9. 3-(3,5-Bis((tert-butyl)dimethylsilyloxy)phenyl)-2-(4-((tert-butyl)dimethylsilyloxy)phenyl)-acrylaldehyde (**5**)

Tert-Butyldimethylsilyl chloride (202 mg, 1.34 mmol) and imidazole (228 mg, 3.35 mmol) were added to a stirred solution of **4d** (94 mg, 0.37 mmol) in dimethylformamide (2 mL) at 0°C . The reaction mixture was warmed to room temperature. After stirring overnight, the reaction mixture was diluted with water and extracted with ethyl acetate (3×5 mL). The combined organic layers were then washed with brine, dried over magnesium sulfate, filtered and concentrated to yield the protected nitrile in 52% yield after flash chromatography using 5% ethyl acetate 95% hexanes.

A 0.54 M solution of DIBAL-H in hexanes (0.31 mmol, 0.57 mL) was added slowly to the protected nitrile (155 mg, 0.26 mmol) in toluene (1.3 mL) at 0°C under nitrogen atmosphere. After 40 min the reaction was quenched by addition of methanol (0.32 mL) and water (0.31 mL), warmed to room temperature and stirred for an additional 3 h. The reaction mixture was diluted with water and the aqueous phase was extracted with ethyl acetate (3×5 mL). The combined organic layers were washed with brine, dried over magnesium sulfate, filtered and concentrated. Flash chromatography using 5% ethyl acetate 95% hexanes yielded the pure aldehyde product **5** in 80% yield. (Z)-**5**: $^1\text{H NMR}$ (300 MHz, CDCl_3) δ (ppm): 9.71 (1H, s), 7.20 (1H, s), 7.05 (2H, d, $J = 8.41$), 6.85 (2H, s, $J = 8.41$), 6.39 (2H, d, $J = 2.18$), 6.29 (1H, t, $J = 2.18$), 1.00 (12H, s), 0.92 (18H, s), 0.23 (6H, s), 0.08 (9H, s). (E)-**5**: $^1\text{H NMR}$ (300 MHz, CDCl_3) δ (ppm): 10.10 (1H, 1), 7.70 (1H, s), 7.39 (2H, d, $J = 8.38$), 6.94 (2H, d, $J = 8.38$), 6.50 (2H, d, $J = 2.07$), 6.41 (1H, t, $J = 2.07$), 1.00 (12H, s), 0.92 (18H, s), 0.23 (6H, s), 0.08 (9H, s). $^{13}\text{C NMR}$ (75 MHz, CDCl_3) δ (ppm): 192.46, 156.47, 145.57, 140.63, 135.76, 129.80, 128.96, 127.20, 119.85, 115.32, 113.12, 25.56, 18.13.

4.2.10. (Z)-5-(3-Hydroxy-2-(4-hydroxyphenyl)prop-1-en-1-yl)benzene-1,3-diol (**4f**)

A 0.54 M solution of DIBAL-H in hexanes (0.7 mmol, 0.12 mL) was added slowly to **5** (40 mg, 0.07 mmol) in toluene (4 mL) at -78°C under nitrogen atmosphere. The reaction was allowed to warm to room temperature and stirred for 4 h. The reaction was quenched by addition of methanol (0.12 mL) and 0.1 N HCl (0.12 mL) at -78°C . The reaction mixture was diluted with water and the aqueous phase was extracted with ethyl acetate (3×5 mL). The combined organic layers were washed with brine,

dried over magnesium sulfate, filtered and concentrated. Flash chromatography using 5% ethyl acetate 95% hexanes yielded the pure protected alcohol in 55% yield.

The protected alcohol (15 mg, 0.04 mmol) was dissolved in methanol (0.5 mL) and a catalytic amount of hydrochloric acid was added. The reaction was allowed to stir until all of the starting material had disappeared from TLC. The reaction mixture was then concentrated. The residue was taken up in ethyl acetate and water, and the aqueous phase was extracted with ethyl acetate (3×). The combined organic layers were washed with brine, dried over magnesium sulfate, filtered and concentrated. The product **4f** was obtained in 35% yield after purification by flash chromatography using 70% ethyl acetate 30% hexanes. ¹H NMR (400 MHz, CD₃OD) δ (ppm): 7.43 (2H, d, *J* = 8.64), 6.78 (2H, d, *J* = 8.64), 6.73 (1H, s), 6.37 (2H, d, *J* = 2.13), 6.19 (1H, t, *J* = 2.13), 4.59 (2H, s). ¹³C NMR (100 MHz, CD₃OD) δ (ppm): 159.33, 158.05, 141.01, 140.74, 133.78, 130.22, 128.76, 116.09, 109.11, 108.50, 102.42, 101.57, 84.02, 60.22.

4.2.11. General procedure for nitrile reduction (**4g**, **4h**)

A 0.54 M solution of DIBAL-H in hexanes (2.0 equiv) was added slowly to a solution of the appropriate nitrile (1.0 equiv) in toluene (0.2 M) at –78 °C. The reaction mixture was stirred at that temperature for 4 h before quenching with water and ethyl acetate. The organic layer was washed (3×) with dilute hydrochloric acid. The combined aqueous layers were extracted with ethyl acetate (3×) and the combined organic layers were washed with brine, dried over magnesium sulfate, filtered and concentrated. The desired aldehyde products were obtained in 67–80% yield after flash chromatography.

4.2.12. (Z)-3-(3,5-Dimethoxyphenyl)-2-(4-methoxyphenyl)acryl-aldehyde (**4g**)

General procedure for nitrile reduction was used starting from **4b** (67%). ¹H NMR (400 MHz, CDCl₃) δ (ppm): 9.75 (1H, s), 7.28 (1H, s), 7.15 (2H, d, *J* = 8.71), 6.96 (2H, d, *J* = 8.71), 6.41 (3H, s), 3.83 (3H, s), 3.59 (6H, s). ¹³C NMR (100 MHz, CDCl₃) δ (ppm): 194.16, 160.36, 159.56, 149.81, 141.68, 135.80, 130.70, 125.30, 114.23, 108.37, 102.83, 55.23, 55.06.

4.2.13. (Z)-3-(3,5-Diisopropoxyphenyl)-2-(4-methoxyphenyl)acryl-aldehyde (**4h**)

General procedure for nitrile reduction was used starting from **4c** (80%). ¹H NMR (300 MHz, CDCl₃) δ (ppm): 10.13 (1H, s), 7.73 (1H, s), 7.37 (2H, d, *J* = 8.77), 6.94 (2H, d, *J* = 8.77), 6.49 (3H, s), 4.54 (2H, m, *J* = 6.04), 3.84 (3H, s), 1.35 (12H, d, *J* = 6.04). ¹³C NMR (75 MHz, CDCl₃) δ (ppm): 192.58, 159.69, 158.88, 145.96, 140.65, 135.82, 129.89, 128.43, 113.72, 109.81, 104.68, 70.07, 55.22, 21.94.

4.2.14. General procedure for aldehyde reduction (**4i**–**4l**)

Sodium borohydride (1.2 equiv) was added portion-wise to a stirred solution of the appropriate aldehyde (1.0 equiv) in methanol (0.2 M) at 0 °C. The reaction mixture was concentrated under reduced pressure after 30 min. The residue was dissolved in CH₂Cl₂ and extracted with H₂O, and the aqueous layer was washed with CH₂Cl₂ (3×). The combined organic layers were washed with H₂O (3×) and brine, dried over MgSO₄, filtered and concentrated. Purification by flash chromatography afforded the pure alcohol products in 13–44% yield.

4.2.15. (Z)-3-(3,5-Dimethoxyphenyl)-2-(4-methoxyphenyl)prop-2-en-1-ol (**4i**)

General procedure for aldehyde reduction as used from **4g** (13%). ¹H NMR (300 MHz, CDCl₃) δ (ppm): 7.53 (2H, d, *J* = 8.82), 6.94 (2H, d, *J* = 8.82), 6.85 (1H, s), 6.57 (2H, d, *J* = 2.16), 6.42 (1H, t, *J* = 2.16), 4.70 (2H, s), 3.84 (3H, s), 3.82 (6H, s). ¹³C NMR

(100 MHz, CDCl₃) δ (ppm): 160.63, 159.32, 139.94, 139.00, 132.70, 129.62, 127.68, 114.01, 106.80, 99.44, 60.39, 55.29.

4.2.16. (Z)-3-(3,5-Diisopropoxyphenyl)-2-(4-methoxyphenyl)prop-2-en-1-ol (**4j**)

General procedure for aldehyde reduction was used from **4h** (27%). ¹H NMR (400 MHz, CDCl₃) δ (ppm): 7.52 (2H, d, *J* = 8.71), 6.93 (2H, d, *J* = 8.71), 6.82 (1H, s), 6.53 (2H, d, *J* = 2.16), 6.39 (1H, t, *J* = 2.16), 4.70 (2H, s), 4.54 (2H, m, *J* = 6.07), 3.84 (3H, s), 1.34 (12H, d, *J* = 6.07). ¹³C NMR (100 MHz, CDCl₃) δ (ppm): 159.25, 158.92, 139.60, 138.86, 132.80, 129.84, 127.66, 113.98, 108.49, 102.90, 69.87, 60.39, 55.25, 22.03.

4.2.17. (E)-3-(3,5-Dimethoxyphenyl)-2-(4-methoxyphenyl)prop-2-en-1-ol (**4k**)

General procedure for aldehyde reduction was used from **4g** (35%). ¹H NMR (300 MHz, CDCl₃) δ (ppm): 7.17 (2H, d, *J* = 8.77), 6.88 (2H, d, *J* = 8.77), 6.59 (1H, s), 6.24 (1H, t, *J* = 2.23), 6.20 (2H, d, *J* = 2.23), 4.43 (2H, s), 3.80 (3H, s), 3.56 (6H, s). ¹³C NMR (75 MHz, CDCl₃) δ (ppm): 160.05, 158.97, 141.52, 138.37, 130.47, 129.86, 126.01, 114.09, 106.98, 99.50, 68.36, 55.17, 54.88.

4.2.18. (E)-3-(3,5-Diisopropoxyphenyl)-2-(4-methoxyphenyl)prop-2-en-1-ol (**4l**)

General procedure for aldehyde reduction was used from **4h** (44%). ¹H NMR (300 MHz, CDCl₃) δ (ppm): 7.17 (2H, d, *J* = 8.63), 6.88 (2H, d, *J* = 8.63), 6.56 (1H, s), 6.21 (1H, t, *J* = 2.02), 6.16 (2H, d, *J* = 2.02), 4.41 (2H, s), 4.19 (2H, m, *J* = 6.05), 1.17 (12H, d, *J* = 6.05).

4.2.19. (E)-Methyl 3-(3,5-diisopropoxyphenyl)-2-(4-methoxyphenyl)acrylate (**4m**)

To a stirred solution of **4h** (64 mg, 0.18 mmol) in methanol (1.8 mL) was added potassium cyanide (59 mg, 0.91 mmol) and manganese dioxide (317 mg, 3.65 mmol). After six days, the reaction mixture was diluted with dichloromethane and filtered through a celite pad. The combined organic layers were washed with brine, dried over magnesium sulfate, filtered and concentrated. Flash chromatography using 10% ethyl acetate 90% hexanes afforded the pure product in 17% yield. ¹H NMR (300 MHz, CDCl₃) δ (ppm): 7.72 (1H, s), 7.16 (2H, d, *J* = 8.70), 6.92 (2H, d, *J* = 8.70), 6.29 (1H, t, *J* = 2.22), 6.20 (2H, d, *J* = 2.22), 4.16 (2H, m, *J* = 6.06), 3.81 (3H, s), 3.79 (3H, s), 1.17 (12H, d, *J* = 6.06).

4.2.20. (Z)-Methyl 3-(3,5-diisopropoxyphenyl)-2-(4-methoxyphenyl)acrylate (**4n**)

See procedure for **4o** (34%). ¹H NMR (400 MHz, CDCl₃) δ (ppm): 7.37 (2H, d, 8.86), 6.91 (2H, d, *J* = 8.86), 6.85 (1H, s), 6.49 (2H, d, *J* = 2.11), 6.38 (1H, t, *J* = 2.11), 4.50 (2H, m, *J* = 6.07), 3.83 (3H, s), 3.80 (3H, s), 1.33 (12H, d, *J* = 6.07). ¹³C NMR (100 MHz, CDCl₃) δ (ppm): 170.24, 159.71, 159.02, 137.48, 134.37, 129.44, 129.23, 127.52, 114.06, 107.71, 104.14, 69.92, 55.26, 52.17, 22.03, 21.90.

4.2.21. (Z)-Methyl 3-(2-chloro-3,5-diisopropoxyphenyl)-2-(4-methoxyphenyl)acrylate (**4o**)

Sodium chlorite (66 mg, 0.73 mmol) in water (0.73 mL) was added drop-wise to a mixture of **4h** (185 mg, 0.52 mmol) in acetonitrile (0.54 mL), monosodium phosphate (108 mg, 0.78 mmol) in water (0.25 mL) and 30% hydrogen peroxide (0.07 mL) at 0 °C. The reaction was then allowed to stir for 48 h at room temperature before addition of a saturated solution of sodium thiosulfate. The aqueous phase was then extracted with ethyl acetate (3 × 5 mL). The combined organic layers were washed with brine, dried over magnesium sulfate, filtered and concentrated to afford an inseparable mixture of (Z)-3-(3,5-diisopropoxyphenyl)-2-(4-methoxyphenyl)acrylic acid and (Z)-3-(2-chloro-3,5-diisopropoxyphenyl)-2-(4-methoxyphenyl)acrylic acid in 81–88% yield.

The above mixture of acids was dissolved in methanol (2.33 mL) and a catalytic amount of concentrated sulfuric acid was added. The reaction mixture was then refluxed for 48 h, cooled to room temperature and concentrated. The residue was taken up in ethyl acetate and water, and the aqueous layer was extracted with ethyl acetate (3 × 8 mL). The combined organic layers were washed with brine, dried over magnesium sulfate, filtered and concentrated to yield a mixture of **4o** and **4n**, which were separated by flash chromatography using 49% petroleum ether, 49% toluene, 1% *t*-butanol to yield **4o** in 34% yield and **4n** in 14% yield. ¹H NMR (400 MHz, CDCl₃) δ (ppm): 7.42 (2H, d, *J* = 8.84), 7.15 (1H, s), 6.92 (2H, d, *J* = 8.84), 6.55 (1H, d, *J* = 2.63), 6.47 (1H, d, *J* = 2.63), 4.51 (1H, m, *J* = 6.03), 4.46 (1H, m, *J* = 6.05), 3.83 (3H, s), 3.71 (3H, s), 1.39 (6H, d, *J* = 6.05), 1.33 (6H, d, *J* = 6.03). ¹³C NMR (100 MHz, CDCl₃) δ (ppm): 169.70, 159.88, 156.63, 154.38, 136.10, 135.85, 128.97, 127.97, 127.73, 115.50, 114.03, 106.95, 104.71, 71.99, 70.39, 55.27, 52.04, 21.97. ESIMS *m/z* 441 (M+Na). IR ν_{\max} 1726 (CO) cm⁻¹.

4.2.22. (Z)-Methyl 3-(2-chloro-3,5-dihydroxyphenyl)-2-(4-hydroxyphenyl)acrylate (**4p**)

A 1.0 M solution of boron tribromide in dichloromethane (0.60 mL, 0.60 mmol) was added slowly to a solution of **4o** (50 mg, 0.12 mmol) in dry dichloromethane (0.60 mL) at -78 °C. The reaction was gradually allowed to warm to room temperature. After 6 h the reaction mixture was cooled to -78 °C and quenched with saturated sodium bicarbonate. The aqueous layer was extracted with ethyl acetate (3 × 5 mL) and the combined organic layers were washed with brine, dried over magnesium sulfate, filtered and concentrated. The pure product was obtained in 10% yield after flash chromatography using 50% ethyl acetate 50% hexanes. ¹H NMR (400 MHz, CD₃OD) δ (ppm): 7.80 (1H, s), 6.94 (2H, d, *J* = 8.67), 6.69 (2H, d, *J* = 8.67), 6.26 (1H, d, *J* = 2.70), 5.84 (1H, d, *J* = 2.70). ¹³C NMR (100 MHz, CD₃OD) δ (ppm): 170.02, 158.35, 157.17, 155.04, 137.90, 136.51, 135.48, 132.47, 128.87, 115.98, 112.88, 110.09, 104.76, 52.77.

4.2.23. (Z)-3-(3,5-Dimethoxyphenyl)-2-(4-methoxyphenyl)-acrylamide (**4q**)

A mixture of **2b** (45 mg, 0.15 mmol), acetaldoxime (0.02 mL, 0.30 mmol), palladium acetate (3 mg, 0.02 mmol), and triphenylphosphine (8 mg, 0.03 mmol) in aqueous ethanol (0.5 mL, 1:4 water:ethanol) was heated to reflux for 3 h under nitrogen atmosphere. The reaction mixture was diluted with ethanol, filtered through a celite pad, washed with dichloromethane, and the combined organic layers were concentrated. The pure product was obtained in 92% yield after purification by flash chromatography using 40% ethyl acetate 60% hexanes. ¹H NMR (300 MHz, CDCl₃) δ (ppm): 7.34 (2H, d, *J* = 8.91), 6.79 (2H, d, *J* = 8.91), 6.70 (1H, s), 6.57 (2H, d, *J* = 2.06), 6.28 (1H, t, *J* = 2.06), 3.86 (2H, s), 3.71 (3H, s), 3.66 (6H, s). ¹³C NMR (100 MHz, CDCl₃) δ (ppm): 173.13, 160.51, 159.62, 137.32, 137.24, 129.21, 127.30, 126.65, 113.92, 106.17, 100.24, 55.05.

4.2.24. (Z)-3-(3,5-Dihydroxyphenyl)-2-(4-hydroxyphenyl)-acrylamide (**4r**)

A 1.0 M solution of boron tribromide in dichloromethane (0.94 mL, 0.94 mmol) was added slowly to a solution of **4q** (50 mg, 0.13 mmol) in dry dichloromethane (0.60 mL) at -78 °C. The reaction was gradually allowed to warm to room temperature. After 4 h the reaction mixture was cooled to -78 °C and quenched with saturated sodium bicarbonate. The aqueous layer was extracted with ethyl acetate (3 × 5 mL) and the combined organic layers were washed with brine, dried over magnesium sulfate, filtered and concentrated. The pure product was obtained in quantitative yield after flash chromatography using 60% ethyl acetate 40%

hexanes. ¹H NMR (400 MHz, CD₃OD) δ (ppm): 7.38(2H, d, *J* = 8.66), 6.79(2H, d, *J* = 8.66), 6.70(1H, s), 6.52(2H, s), 6.19(1H, s). ¹³C NMR (100 MHz, CD₃OD) δ (ppm): 175.86, 159.43, 158.82, 139.17, 138.47, 130.03, 128.45, 126.91, 116.43, 108.12, 103.31.

4.2.25. 3-(3,5-Dimethoxyphenyl)-2-(4-methoxyphenyl)propan-1-amine (**4s**)

To a mixture of **4b** (20 mg, 0.07 mmol) cobalt chloride hexahydrate (32 mg, 0.14 mmol) in anhydrous methanol (0.5 mL) was added sodium borohydride (26 mg, 0.68 mmol) portionwise. After stirring overnight a second portion of sodium borohydride was added. After 1 h, an aqueous solution of 3 N HCl was added to the reaction mixture until it became clear in appearance. The aqueous layer was then extracted with ether (3 ×) to remove any remaining nitrile. The aqueous layer was then made alkaline using ammonium hydroxide (pH 10) and extracted with ethyl acetate (3 × 5 mL). The combined organic layers were washed with brine, dried over magnesium sulfate, filtered and concentrated. The pure product was obtained in 64% yield after purification by flash chromatography using 5% methanol 95% dichloromethane. ¹H NMR (400 MHz, CDCl₃) δ (ppm): 7.09 (2H, d, *J* = 8.57), 6.84 (2H, d, *J* = 8.57), 6.26 (1H, t, *J* = 2.17), 6.21 (2H, d, *J* = 2.17), 3.78 (3H, s), 3.71 (6H, s), 2.96–2.81 (5H, m). ¹³C NMR (100 MHz, CDCl₃) δ (ppm): 160.42, 158.22, 142.46, 134.57, 128.82, 113.89, 107.01, 97.93, 55.11, 49.88, 46.82, 41.15.

4.2.26. (Z)-Methyl 2-(3,5-dimethoxyphenyl)-1-(4-methoxyphenyl)vinylcarbamate (**4t**)

Potassium hydroxide (14 mg, 0.26 mmol) was added to **4q** (32 mg, 0.10 mmol) in anhydrous methanol (1.25 mL) at room temperature under nitrogen atmosphere. Once a clear reaction mixture was obtained, (diacetoxyiodo)benzene (33 mg, 0.10 mmol) was added in one portion. The reaction mixture was concentrated after 3 h and the crude residue as taken up in water and dichloromethane. The aqueous phase was extracted with dichloromethane (3 × 5 mL) and the combined organic layers were washed with brine, dried over magnesium sulfate, filtered and concentrated. The pure product was obtained in 86% yield after purification by flash chromatography using 30% ethyl acetate 70% hexanes. ¹H NMR (400 MHz, CDCl₃) δ (ppm): 7.44 (2H, d, *J* = 8.80), 6.91 (2H, d, *J* = 8.80), 6.58 (2H, d, *J* = 2.20), 6.37 (1H, t, *J* = 2.20), 6.20 (1H, s), 3.83 (3H, s), 3.78 (6H, s), 3.67 (3H, s). ¹³C NMR (100 MHz, CDCl₃) δ (ppm): 160.84, 159.85, 154.67, 137.66, 135.13, 130.56, 127.38, 118.19, 113.72, 106.30, 99.55, 55.20, 52.51.

4.2.27. 2-(3,5-Dimethoxyphenyl)-1-(4-methoxyphenyl)-ethanimine (**4u**)

A 1.0 M solution of boron tribromide in dichloromethane (0.66 mL, 0.66 mmol) was added slowly to a solution of **4t** (30 mg, 0.09 mmol) in dichloromethane (0.5 mL) at -78 °C under nitrogen atmosphere. The reaction was allowed to stir at room temperature for 4 h before cooling to -78 °C and quenching with an aqueous solution of saturated sodium bicarbonate (2 mL). The reaction mixture was warmed to room temperature and the aqueous layer was extracted with ethyl acetate (3 × 2 mL). The combined organic layers were washed with saturated sodium bicarbonate (3 × 5 mL), water (1 × 5 mL), and brine (1 × 5 mL) before being dried over magnesium sulfate, filtered, and concentrated. The pure product was obtained in 77% yield after purification by flash chromatography using 30% ethyl acetate 70% hexanes. ¹H NMR (400 MHz, CDCl₃) δ (ppm): 7.99 (2H, d, *J* = 8.97), 6.92 (2H, d, *J* = 8.97), 6.43 (2H, d, *J* = 2.26), 6.34 (1H, t, *J* = 2.26), 4.15 (2H, s), 3.85 (3H, s), 3.76 (6H, s). ¹³C NMR (100 MHz, CDCl₃) δ (ppm): 195.94, 163.45, 160.83, 137.07, 130.90, 129.50, 113.70, 107.32, 98.76, 55.37, 55.20, 45.53.

4.2.28. General benzanilide synthesis, Method A

The benzoyl chloride was prepared by stirring benzoic acid (1.0 mmol) with SOCl_2 (0.363 mL, 5.0 mmol) and DMF (1 drop) in CH_2Cl_2 (5 mL) for overnight and evaporating the volatile materials under reduced pressure. To the solution of benzoyl chloride in CH_2Cl_2 (5 mL) were added an aniline (1.0 mmol) and DIEA (0.871 mL, 5.0 mmol), and the reaction was stirred until no starting material by TLC (1–24 h) at room temperature. After dilution with CH_2Cl_2 (30 mL), the organic layer was washed with brine (40 mL), dried with anhydrous MgSO_4 , and evaporated to dryness under reduced pressure. The residue was purified by flash column chromatography to obtain a benzanilide.

4.2.29. General benzanilide synthesis, Method B

To the solution of benzoic acid (1.0 mmol) in CH_2Cl_2 (5 mL) were added EDC (192 mg, 1.0 mmol) and DIEA (0.523 mL, 3.0 mmol), and stirred for 5 min at room temperature. To the solution of activated benzoic acid was added an aniline (1.0 mmol) and the reaction was stirred for overnight at room temperature. After dilution with CH_2Cl_2 (35 mL), the organic layer was washed with brine (40 mL), dried with anhydrous MgSO_4 , and evaporated to dryness under reduced pressure. The residue was purified by flash column chromatography to obtain a benzanilide.

4.2.30. General benzanilide synthesis, Method C

To the solution of secondary amide (0.5 mmol) in THF (5 mL) were added NaH (25 mg, 60% in oil, 0.6 mmol) and stirred for 30 min at 0 °C. MeI (0.062 mL, 1 mmol) was added dropwise to the solution, and the reaction was stirred for overnight at room temperature. After dilution with CH_2Cl_2 (40 mL), the organic layer was washed with brine (40 mL), dried with anhydrous MgSO_4 , and evaporated to dryness under reduced pressure. The residue was purified by flash column chromatography to obtain a benzanilide.

4.2.31. General benzanilide deprotection, Method D

If R_1 or R_2 were protected by TBS, that were deprotected before final column purification by TBAF treatment; the product was dissolved in THF (5 mL), and TBAF (1.0 mmol per protecting group) was added and stirred for 20 min. After dilution with CH_2Cl_2 (30 mL), the organic layer was washed with brine (40 mL), dried with anhydrous MgSO_4 , and evaporated to dryness under reduced pressure.

4.2.32. *N*-(3,5-Dihydroxyphenyl)-4-hydroxybenzamide (8a)

Method B and D were used in combination with 3,5-bis(*tert*-butyldimethylsilyloxy)benzoic acid and 4-(*tert*-butyldimethylsilyloxy)aniline (79%). ^1H NMR (300 MHz, $(\text{CD}_3)_2\text{CO}$) δ (ppm): 7.69 (2H, d, $J = 8.7$), 7.04 (2H, d, $J = 1.8$), 6.91 (2H, d, $J = 8.7$), 6.62 (1H, t, $J = 1.8$). ^{13}C NMR (75 MHz, $(\text{CD}_3)_2\text{CO}$) δ (ppm): 206.88, 166.03, 158.68, 154.13, 137.68, 131.11, 122.52, 115.25, 106.12. ESIMS(+) m/z 246 (M+H), 268 (M+Na), 284 (M+K).

4.2.33. 3,5-Dihydroxy-*N*-(4-hydroxyphenyl)-*N*-methylbenzamide (8b)

Method C and D were used starting from TBS protected form of **8a** (38%). ^1H NMR (300 MHz, $(\text{CD}_3)_2\text{CO}$) δ (ppm): 7.05 (2H, d, $J = 8.1$), 6.80 (2H, d, $J = 8.1$), 6.38 (2H, s), 6.32 (1H, s), 3.40 (3H, s). ^{13}C NMR (75 MHz, $(\text{CD}_3)_2\text{CO}$) δ (ppm): 205.98, 157.95, 155.98, 138.69, 136.84, 128.13, 115.67, 107.13, 103.57, 37.96. ESIMS(+) m/z 260 (M+H), 282 (M+Na).

4.2.34. *N*-(4-Hydroxyphenyl)-3,5-dimethoxybenzamide (8c)

Method A and D were used in combination with 3,5-dimethoxybenzoic acid and 4-(*tert*-butyldimethylsilyloxy)aniline (90%). ^1H NMR (300 MHz, $(\text{CD}_3)_2\text{CO}$) δ (ppm): 7.70 (2H, d, $J = 8.7$), 7.20 (2H, d, $J = 2.4$), 6.91 (2H, d, $J = 8.7$), 6.72 (1H, t, $J = 2.4$), 3.89 (6H, s).

^{13}C NMR (75 MHz, $(\text{CD}_3)_2\text{CO}$) δ (ppm): 165.05, 161.01, 154.07, 137.68, 131.25, 122.32, 115.14, 105.31, 103.23, 55.06. ESIMS(+) m/z 274 (M+H), 296 (M+Na), 312 (M+K).

4.2.35. *N*-(3,5-Dihydroxyphenyl)-4-hydroxybenzamide (8d)

Method B and D were used in combination with 4-(*tert*-butyldimethylsilyloxy)benzoic acid and 3,5-bis(*tert*-butyldimethylsilyloxy)aniline (41%). ^1H NMR (300 MHz, CD_3OD) δ (ppm): 7.86 (2H, d, $J = 9.0$), 6.93 (2H, d, $J = 9.0$), 6.78 (2H, d, $J = 1.8$), 6.16 (1H, t, $J = 1.8$). ^{13}C NMR (75 MHz, CD_3OD) δ (ppm): 167.40, 160.89, 158.28, 140.20, 129.34, 125.78, 114.77, 99.75, 98.54. ESIMS(+) m/z 246 (M+H), 268 (M+Na), 284 (M+K).

4.2.36. *N*-(3,5-Dihydroxyphenyl)-4-hydroxy-*N*-methylbenzamide (8e)

Method B and D were used in combination with 4-(*tert*-butyldimethylsilyloxy)benzoic acid and *N*-methyl 3,5-bis(*tert*-butyldimethylsilyloxy)aniline (11%). ^1H NMR (300 MHz, CD_3OD) δ (ppm): 7.31 (2H, d, $J = 9.0$), 6.69 (2H, d, $J = 9.0$), 6.19 (1H, t, $J = 1.8$), 6.12 (2H, d, $J = 1.8$), 3.45 (3H, s). ^{13}C NMR (75 MHz, CD_3OD) δ (ppm): 171.34, 159.24, 158.82, 146.61, 130.44, 126.39, 114.12, 105.48, 100.87, 37.74. ESIMS(+) m/z 260 (M+H), 282 (M+Na), 298 (M+K).

4.2.37. *N*-(4-(Dimethylamino)phenyl)-4-hydroxybenzamide (8f)

Method B and D were used in combination with 4-(*tert*-butyldimethylsilyloxy)benzoic acid and 4-(*N,N*-dimethylamino)aniline (46%). ^1H NMR (300 MHz, CD_3OD) δ (ppm): 7.87 (2H, d, $J = 9.6$), 7.53 (2H, d, $J = 9.6$), 6.92 (2H, d, $J = 8.7$), 6.87 (2H, d, $J = 8.7$), 2.98 (6H, s). ^{13}C NMR (75 MHz, CD_3OD) δ (ppm): 167.18, 161.34, 148.35, 129.17, 128.64, 125.35, 122.72, 114.94, 113.09, 40.04. ESIMS(+) m/z 257 (M+H), 279 (M+Na), 295 (M+K).

4.2.38. *N*-(4-(Dimethylamino)phenyl)-4-methoxy-*N*-methylbenzamide (8g)

Method C was used starting from **8f** (12%). ^1H NMR (300 MHz, CDCl_3) δ (ppm): 7.34 (2H, d, $J = 9$), 6.96 (2H, d, $J = 8.7$), 6.73 (2H, d, $J = 8.7$), 6.61 (2H, d, $J = 9$), 3.78 (3H, s), 3.48 (3H, s), 2.96 (6H, s). ^{13}C NMR (75 MHz, CDCl_3) δ (ppm): 170.30, 160.28, 148.85, 134.51, 130.88, 128.47, 127.60, 112.89, 112.61, 55.20, 40.57, 38.94. ESIMS(+) m/z 285 (M+H), 307 (M+Na).

4.2.39. *N*-(4-(Dimethylamino)phenyl)-3,5-dimethoxybenzamide (8h)

Method A was used in combination with 3,5-hydroxybenzoic acid and 4-(*N,N*-dimethylamino)aniline (9%). ^1H NMR (300 MHz, $(\text{CD}_3)_2\text{SO}$) δ (ppm): 9.87 (1H, s), 9.60 (2H, s), 7.62 (2H, d, $J = 8.7$), 6.82 (2H, s), 6.76 (2H, d, $J = 8.7$), 6.41 (1H, s), 2.91 (6H, s). ^{13}C NMR (75 MHz, $(\text{CD}_3)_2\text{SO}$) δ (ppm): 165.56, 158.79, 147.73, 138.02, 129.57, 122.18, 112.97, 106.18, 105.62, 40.26. ESIMS(+) m/z 273 (M+H), 295 (M+Na), 311 (M+K).

4.2.40. *N*-(4-(Bimethylamino)phenyl)-3,5-dimethoxybenzamide (8i)

Method A was used in combination with 3,5-dimethoxybenzoic acid and 4-(*N,N*-dimethylamino)aniline (83%). ^1H NMR (300 MHz, CDCl_3) δ (ppm): 8.51 (1H, s), 7.54 (2H, d, $J = 8.7$), 7.03 (2H, d, $J = 2.4$), 6.71 (2H, d, $J = 8.7$), 6.58 (1H, t, $J = 2.4$), 3.77 (6H, s), 2.95 (6H, s). ^{13}C NMR (75 MHz, CDCl_3) δ (ppm): 165.78, 160.78, 148.09, 137.51, 127.97, 122.38, 112.95, 105.03, 103.71, 55.51, 40.91. ESIMS(+) m/z 301 (M+H), 323 (M+Na), 339 (M+K).

4.2.41. *N*-(4-(Dimethylamino)phenyl)-3,5-dimethoxy-*N*-methylbenzamide (8j)

Method C was used from **8i** (67%). ^1H NMR (300 MHz, CDCl_3) δ (ppm): 6.97 (2H, d, $J = 9.0$), 6.61 (2H, d, $J = 9.0$), 6.54 (2H, d, $J = 1.8$),

6.38 (1H, t, $J = 1.8$), 3.70 (6H, s), 3.49 (3H, s), 2.96 (6H, s). ^{13}C NMR (75 MHz, CDCl_3) δ (ppm): 170.44, 159.97, 149.10, 138.21, 133.94, 127.52, 112.64, 106.71, 102.28, 55.37, 40.60, 38.66. ESIMS(+) m/z 315 (M+H), 337 (M+Na), 353 (M+K).

4.2.42. *N*-(3,5-Dihydroxyphenyl)-4-(dimethylamino)benzamide (8k)

Method A and D were used in combination with 4-(*N,N*-dimethylamino)benzoic acid and 3,5-bis(*tert*-butyldimethylsilyloxy)aniline (54%). ^1H NMR (300 MHz, $(\text{CD}_3)_2\text{SO}$) δ (ppm): 7.88 (2H, d, $J = 8.7$), 6.80 (2H, s), 6.78 (2H, d, $J = 8.7$), 5.98 (1H, s), 3.04 (6H, s). ^{13}C NMR (75 MHz, $(\text{CD}_3)_2\text{SO}$) δ (ppm): 165.56, 158.62, 152.78, 141.55, 129.62, 121.93, 111.23, 99.19, 98.29, 40.26. ESIMS(+) m/z 273 (M+H), 295 (M+Na), 311 (M+K).

4.2.43. *N*-(3,5-Dihydroxyphenyl)-4-(dimethylamino)-*N*-methylbenzamide (8l)

Method A and D were used in combination with 4-(*N,N*-dimethylamino)benzoic acid and *N*-methyl-3,5-bis(*tert*-butyldimethylsilyloxy)aniline (69%). ^1H NMR (300 MHz, CD_3OD) δ (ppm): 7.34 (2H, d, $J = 8.7$), 6.53 (2H, d, $J = 8.7$), 6.21 (1H, t, $J = 2.4$), 6.16 (2H, d, $J = 2.4$), 3.42 (3H, s), 2.91 (6H, s). ^{13}C NMR (75 MHz, CD_3OD) δ (ppm): 171.82, 158.82, 151.80, 147.14, 130.41, 121.70, 110.33, 105.53, 100.82, 38.92, 38.07. ESIMS(+) m/z 287 (M+H), 309 (M+Na), 325 (M+K).

4.2.44. 4-(Dimethylamino)-*N*-(4-hydroxyphenyl)benzamide (8m)

Method A and D were used in combination with 4-(*N,N*-dimethylamino)benzoic acid and 4-(*tert*-butyldimethylsilyloxy)aniline (81%). ^1H NMR (300 MHz, $(\text{CD}_3)_2\text{SO}$) δ (ppm): 7.91 (2H, d, $J = 8.7$), 7.59 (2H, d, $J = 8.1$), 6.80 (4H, d, $J = 8.7$), 3.05 (6H, s). ^{13}C NMR (75 MHz, $(\text{CD}_3)_2\text{SO}$) δ (ppm): 165.24, 153.79, 152.70, 131.73, 129.45, 122.60, 121.93, 115.39, 111.29, 40.26. ESIMS(+) m/z 257 (M+H), 279 (M+Na), 295 (M+K).

4.2.45. 4-(Dimethylamino)-*N*-(4-hydroxyphenyl)-*N*-methylbenzamide (8n)

Method C and D was used from TBS protected **8m** (51%). ^1H NMR (300 MHz, $(\text{CD}_3)_2\text{SO}$) δ (ppm): 7.16 (2H, d, $J = 8.7$), 6.98 (2H, d, $J = 9.0$), 6.70 (2H, d, $J = 8.7$), 6.52 (2H, d, $J = 9.0$), 3.13 (3H, s), 2.92 (6H, s). ^{13}C NMR (75 MHz, $(\text{CD}_3)_2\text{SO}$) δ (ppm): 169.85, 155.93, 151.21, 137.65, 130.86, 128.53, 122.97, 116.17, 110.76, 40.60, 40.32.

4.2.46. 3,5-Dihydroxy-*N*-(naphthalen-2-yl)benzamide (8o)

Method A and D was used in combination with 3,5-bis(*tert*-butyldimethylsilyloxy)benzoic acid and 2-naphthyl amine (43%). ^1H NMR (300 MHz, $(\text{CD}_3)_2\text{CO}$) δ (ppm): 8.57 (1H, s), 7.94–7.85 (4H, m), 7.52–7.40 (4H, m), 7.05 (2H, d, $J = 1.8$), 6.63 (1H, t, $J = 1.8$). ^{13}C NMR (75 MHz, $(\text{CD}_3)_2\text{CO}$) δ (ppm): 166.28, 158.99, 137.90, 137.28, 134.25, 130.86, 128.55, 127.80, 126.62, 125.02, 120.97, 116.88, 106.38, 105.98. ESIMS(+) m/z 280 (M+H), 302 (M+Na), 318 (M+K).

4.2.47. 3,5-Dimethoxy-*N*-(naphthalen-2-yl)benzamide (8p)

Method A was used in combination with 3,5-dimethoxybenzoic acid and 2-naphthylamine (87%). ^1H NMR (300 MHz, CDCl_3) δ (ppm): 8.31 (1H, s), 7.78–7.62 (4H, m), 7.46–7.38 (2H, m), 7.02 (2H, d, $J = 2.4$), 6.55 (1H, t, $J = 2.4$), 3.74 (6H, s). ^{13}C NMR (75 MHz, CDCl_3) δ (ppm): 137.15, 135.57, 133.86, 130.83, 128.75, 127.80, 127.63, 126.51, 125.19, 120.50, 117.44, 108.20, 107.13, 105.17, 103.91, 55.56. ESIMS(+) m/z 308 (M+H), 330 (M+Na), 346 (M+K).

4.2.48. 3,5-Dimethoxy-*N*-methyl-*N*-(naphthalen-2-yl)benzamide (8q)

Method A was used in combination with 3,5-dimethoxybenzoic acid and *N*-methyl 2-naphthylamine (91%). ^1H NMR (300 MHz, CDCl_3) δ (ppm): 7.81–7.12 (3H, m), 7.56 (1H, d, $J = 1.8$), 7.49–7.46 (2H, m), 7.26 (1H, dd, $J = 1.8, 8.7$), 6.58 (2H, d, $J = 2.4$), 6.33 (1H, t, $J = 2.4$), 3.61 (3H, s), 3.57 (6H, s). ^{13}C NMR (75 MHz, CDCl_3) δ (ppm): 170.50, 160.14, 142.34, 137.71, 133.47, 131.64, 129.20, 127.74, 126.76, 126.34, 125.21, 124.74, 106.83, 102.39, 55.25, 38.66. ESIMS(+) m/z 322 (M+H), 344 (M+Na), 360 (M+K).

4.2.49. *N*-(3,5-Dihydroxyphenyl)-2-naphthamide (8r)

Method A and D were used in combination with 2-naphthoic acid and 3,5-bis(*tert*-butyldimethylsilyloxy)aniline (61%). ^1H NMR (300 MHz, CD_3OD) δ (ppm): 8.51 (1H, s), 8.09–7.99 (4H, m), 7.66 (2H, m), 6.87 (2H, d, $J = 2.1$), 6.19 (1H, t, $J = 2.1$). ^{13}C NMR (75 MHz, CD_3OD) δ (ppm): 167.66, 158.42, 140.06, 134.96, 132.65, 132.32, 128.84, 128.11, 127.85, 127.66, 127.52, 126.59, 123.89, 99.92, 99.11. ESIMS(+) m/z 280 (M+H), 302 (M+Na), 318 (M+K).

4.2.50. *N*-(3,5-Dihydroxyphenyl)-*N*-methyl-2-naphthamide (8s)

Method A and D were used in combination with 2-naphthoic acid and *N*-methyl 3,5-bis(*tert*-butyldimethylsilyloxy)aniline (32%). ^1H NMR (300 MHz, $(\text{CD}_3)_2\text{CO}$) δ (ppm): 8.09 (1H, s), 7.91–7.87 (2H, m), 7.80 (1H, d, $J = 8.7$), 7.61–7.52 (3H, m), 6.32 (3H, s), 3.51 (3H, s). ^{13}C NMR (75 MHz, $(\text{CD}_3)_2\text{CO}$) δ (ppm): 170.13, 158.99, 146.69, 134.09, 133.75, 132.54, 128.75, 128.64, 127.71, 127.29, 127.24, 126.56, 125.49, 106.07, 101.35, 37.88. ESIMS(+) m/z 294 (M+H), 316 (M+Na), 332 (M+K).

4.2.51. 3,4-Dihydroxy-*N*-(4-hydroxyphenyl)benzamide (8t)

Method B and D were used in combination with 3,4-bis(*tert*-butyldimethylsilyloxy)benzoic acid and 4-(*tert*-butyldimethylsilyloxy)aniline (26%). ^1H NMR (300 MHz, CD_3OD) δ (ppm): 7.47 (2H, d, $J = 8.7$), 7.45 (1H, d, $J = 2.4$), 7.22 (1H, dd, $J = 2.4, 8.4$), 6.91 (1H, d, $J = 8.4$), 6.85 (2H, d, $J = 8.7$). ^{13}C NMR (75 MHz, CD_3OD) δ (ppm): 167.41, 154.21, 148.94, 145.01, 130.38, 127.38, 126.22, 123.16, 119.54, 114.85, 114.63. ESIMS(+) m/z 246 (M+H), 268 (M+Na), 284 (M+K).

4.2.52. 3,4-Dihydroxy-*N*-(4-hydroxyphenyl)-*N*-methylbenzamide (8u)

Method C and D were used starting from **8t** (58%). ^1H NMR (300 MHz, CD_3OD) δ (ppm): 6.99 (2H, d, $J = 8.7$), 6.86 (1H, d, $J = 1.8$), 6.75 (2H, d, $J = 8.7$), 6.71–6.61 (2H, m), 3.44 (3H, s). ^{13}C NMR (75 MHz, CD_3OD) δ (ppm): 171.87, 156.01, 147.00, 144.33, 136.78, 127.80, 127.01, 121.12, 115.89, 115.44, 113.98, 37.99. ESIMS(+) m/z 260 (M+H), 282 (M+Na).

4.2.53. (*Z*)-Methyl *N*-(3,5-dihydroxyphenyl)-2-naphthimidate (8v)

Compound **8v** was prepared by *O*-methylation of **8r**; **8r** (200 mg, 0.39 mmol) was stirred with SOCl_2 (5 mL) for 3 h, and volatile materials were removed by evaporation under reduced pressure. MeOH (5 mL) was added to the residue and continued the stirring for 1 h. After evaporation, method D was used to deprotect TBS group and purified by flash column chromatography (ethyl acetate only) to obtain a benzanilide (41 mg, 36%). ^1H NMR (300 MHz, $(\text{CD}_3)_2\text{SO}$) δ (ppm): 8.59 (1H, s), 8.15–8.02 (4H, m), 7.71–7.67 (2H, m), 6.87 (2H, d, $J = 2.1$), 6.05 (1H, t, $J = 2.1$), 3.42 (3H, s). ^{13}C NMR (75 MHz, $(\text{CD}_3)_2\text{SO}$) δ (ppm): 207.05, 165.98, 158.79, 141.10, 134.70, 133.10, 132.57, 129.45, 128.39, 128.16, 127.32, 125.07, 99.33, 98.91, 31.22. ESIMS(+) m/z 332 (M+K).

4.2.54. N-(3,5-Dihydroxyphenyl)-3,4-dimethoxybenzamide (8w)

Method A and D were used in combination with 3,4-dimethoxyaniline and 3,5-bis(*tert*-butyldimethylsilyloxy)benzoic acid (71%). ¹H NMR (300 MHz, (CD₃)₂CO) δ (ppm): 7.65 (1H, dd, *J* = 1.8, 8.4), 7.62 (1H, d, *J* = 1.8), 7.08 (1H, d, *J* = 8.4), 7.03 (2H, d, *J* = 2.4), 6.22 (1H, t, *J* = 2.4), 3.93 (6H, s). ¹³C NMR (75 MHz, (CD₃)₂CO) δ (ppm): 165.30, 158.62, 152.30, 149.10, 141.13, 127.77, 120.72, 111.06, 110.78, 99.02, 98.32, 55.31. ESIMS(+) *m/z* 290 (M+H), 312 (M+Na), 328 (M+K).

4.2.55. N-(3,5-Dihydroxyphenyl)-3,4-dimethoxy-N-methylbenzamide (8x)

Method A and D were used in combination with 3,4-dimethoxybenzoic acid and *N*-methyl 3,5-bis(*tert*-butyldimethylsilyloxy)aniline (64%). ¹H NMR (300 MHz, CD₃OD) δ (ppm): 7.14 (1H, d), 7.01 (1H, d), 6.86 (1H, d), 6.21 (1H, s), 6.15 (2H, s), 3.83 (3H, s), 3.70 (3H, s), 3.46 (3H, s). ¹³C NMR (75 MHz, CD₃OD) δ (ppm): 170.80, 159.04, 150.70, 147.95, 146.61, 127.71, 122.32, 112.22, 110.22, 105.51, 101.01, 54.92, 37.65. ESIMS(+) *m/z* 304 (M+H), 326 (M+Na), 342 (M+K).

4.2.56. 3,4-Dihydroxy-N-(naphthalen-2-yl)benzamide (8y)

Method B and D were used in combination with 3,4-bis(*tert*-butyldimethylsilyloxy)benzoic acid and 2-naphthyl amine (77%). ¹H NMR (300 MHz, (CD₃)₂SO) δ (ppm): 8.30 (1H, d, *J* = 1.8), 7.88–7.45 (4H, m), 7.55–7.43 (4H, m), 6.96 (1H, d, *J* = 8.1). ¹³C NMR (75 MHz, CD₃OD) δ (ppm): 167.72, 149.24, 145.12, 136.22, 133.89, 130.86, 128.08, 127.26, 126.17, 126.06, 124.74, 120.95, 119.85, 117.63, 114.83, 114.63. ESIMS(+) *m/z* 318 (M+K).

4.2.57. 3,4-Dimethoxy-N-(naphthalen-2-yl)benzamide (8z)

Method A was used in combination with 3,4-dimethoxybenzoic acid and 2-naphthyl amine (99%). ¹H NMR (300 MHz, CDCl₃) δ (ppm): 7.76 (3H, m), 7.70 (1H, m), 7.55 (2H, m), 7.45 (2H, m), 6.65 (1H, d), 3.79 (3H, s), 3.76 (3H, s). ¹³C NMR (75 MHz, CDCl₃) δ (ppm): 166.23, 151.94, 148.88, 135.94, 133.83, 130.74, 128.64, 127.71, 127.60, 127.26, 126.48, 125.13, 120.89, 120.33, 117.66, 110.70, 110.25, 55.87, 55.79.

4.3. Expression and purification of human QR2

Human QR2 was purified from 4L of *Escherichia coli* BL21(DE3) grown in Luria–Bertani medium supplemented with 100 μg/mL ampicillin as previously described.²³ The concentration of purified hQR2 was determined using BioRad Protein assay. QR2 was concentrated to 4 mg/mL for all kinetic and crystallization assays.

4.4. Steady-state kinetic assays and IC₅₀ value determination

The enzymatic activity of QR2 at steady-state was determined using two assays, where both utilized NMeH (N-methylidihydro-nicotinamide) as the co-substrate.^{23,35,36} In the first assay, menadione was used as the quinone substrate and QR2 activity was monitored by the decrease in absorbance of NMeH at 360 nm. The second assay utilized MTT ((3-(4,5-dimethylthiazol-2-yl)-2,5-diphenyltetrazolium bromide)) as a quinone substrate and QR2 activity was monitored by the increase of the formazan product at 612 nm. Both assays were performed at 25 °C on a BioTek Synergy H1 multimode microplate reader. Reactions were carried out in a 96-well plate to a final volume of 200 μL. Each assay mixture contained 12 nM QR2, NMeH (100 μM for the first assay and 17.5 μM on the second assay), either 30 μM menadione in the first assay or 200 μM MTT in the second assay, in a reaction buffer containing 100 mM NaCl, 50 mM Tris (pH 7.5) and 0.1% Triton-X-100. Substrates, inhibitor and buffer were added to the wells, and the plate was shaken for 5 s using a Thermo LabSystems WellMix

microtiter plate shaker at a setting of 9–10 to mix the assay components. With the microtiter plate still on the shaker (not shaking), the enzyme, and associated control with no enzyme, were rapidly pipetted into the appropriate wells using a multi-channel pipette, and the plate was immediately shaken for 5 s to mix the enzyme with reagents. The plate was immediately transferred to the plate reader and the change in absorbance was monitored until the reaction reached completion. Initial slopes of the reaction ($\Delta\text{Abs}/\Delta\text{time}$) were measured and were used to calculate initial rates of the reaction using a value of 7060 M⁻¹ cm⁻¹ as an extinction coefficient for NMeH and 11,300 M⁻¹ cm⁻¹ as an extinction coefficient for MTT.

Inhibitors were tested at 100 μM and compounds that showed greater than 50% inhibition at 100 μM were assayed for their IC₅₀ determination. The inhibition of QR2 activity by resveratrol analogs were determined using the same assay conditions described above except that inhibitor concentrations were varied from 0.2 to 100 μM. Assays at each inhibitor concentration were performed in triplicate and the average and standard deviations in the rates were used to determine the final IC₅₀ values by calculating the percent inhibition at each inhibitor concentration versus the negative control with zero inhibitor. The percent inhibition data were then plotted as a function of inhibitor concentration $[I]$ and the data were fit to the following equation using nonlinear regression:

$$\text{Inhibition (\%)} = \text{Inhibition}_{\text{max}} (\%) / (1 + [I] / \text{IC}_{50})$$

All data were fit to the equation using the Enzyme Kinetics Module of the program SigmaPlot from SPSS Scientific. IC₅₀ values are reported along with their standard error.

4.5. Crystallization and X-ray structure determination of human QR2 in complex with inhibitors

QR2 was crystallized using our previously described methods.^{23,35,36} Briefly, the hanging-drop, vapor-diffusion method was used by setting up drops adding 1 μL purified QR2 with 1 μL of reservoir solution that contained between 1.3 and 1.7 M ammonium sulfate, 0.1 M Bis-Tris buffer pH between 6.0 and 7.0, 0.1 M NaCl, 5 mM DTT and 12 μM FAD. Crystals were transferred from hanging-drops to a 10 μL drop of prepared with 9 μL reservoir solution and 1 μL stock solution of inhibitor (10 mM in 100% DMSO). Crystals were soaked for 24 h, retrieved with a nylon loop, which was then swiped through the same mother-liquor solution supplemented with 20% glycerol. The crystals were flash-frozen by plunging into liquid nitrogen. Crystals were stored in shipping dewars containing liquid nitrogen until X-ray data collection.

All diffraction data were collected at 100 K at the Life Sciences Collaborative Access Team (LS-CAT) at the Advanced Photon Source (APS) at Argonne National Laboratories. Crystals were transferred from shipping dewars and mounted on a goniostat under a stream of dry N₂. X-ray data sets were collected using both MarMosaic 300 and 225 mm CCD detectors. QR2-inhibitor complexes were processed and scaled using the program HKL2000. The crystals belonged to the primitive orthorhombic space group P2₁2₁2₁ with a dimer in the asymmetric unit.

The initial phases for QR2 in complex with the inhibitors were determined by molecular replacement using PHASER in the CCP4 suite.⁴⁰ The search model used was the structure of human QR2 in complex with resveratrol (PDB 1SGO).¹⁷ Molecular library files and coordinates for the inhibitors were built using SKETCHER in CCP4. The inhibitors were manually built into density using the program COOT. Fourier maps were calculated and visualized using the program COOT,⁴¹ and the structures were refined using the program REFMAC. Water molecules were added manually to 2F_o - F_c density peaks that were greater than 3.0 σ. Iterative rounds of refinement were continued until R_{work} and R_{free} values reached

their lowest values.⁴² At this point, TLS refinement was used by submitting the coordinates to the TLS server,^{43–45} and then two rounds of TLS and restrained refinement were performed in REFMAC to arrive at the final models, which were validated using Mol-Probity.⁴⁶ Electron density maps presented in the figures were calculated using CCP4 and the figures were generated using the program PyMol.

Acknowledgments

Use of the Advanced Photon Source, an Office of Science User Facility operated for the U.S. Department of Energy (DOE) Office of Science by Argonne National Laboratory, was supported by the U.S. DOE under Contract No. DE-AC02-06CH11357. Use of the LS-CAT Sector 21 was supported by the Michigan Economic Development Corporation and the Michigan Technology Tri-Corridor (Grant 085P1000817). K.C.J. acknowledges support by the National Institute of Health Biophysics Training Grant T32 GM008296 (NIH/GM). This research was supported in part by Grants from the Walter Cancer Foundation (to A.D.M.) and the NIH (NCI CA48112 to A.D.M.) We would also like to acknowledge support from the Macromolecular Crystallography Shared Research Facility via the Purdue University Center for Cancer Research.

Supplementary data

Supplementary data associated with this article can be found, in the online version, at <http://dx.doi.org/10.1016/j.bmc.2013.07.037>.

References and notes

- Takaoka, M. J. *J. Fac. Sci. Hokkaido Imperial Univ.* **1940**, 3, 1.
- Langcake, P.; Pryce, R. J. *Phytochemistry* **1977**, 16, 1193.
- Langcake, P.; Pryce, R. J. *Physiol. Plant Pathol.* **1976**, 9, 77.
- Burns, J.; Yokota, T.; Ashihara, H.; Lean, M. E. J.; Crozier, A. J. *Agric. Food Chem.* **2002**, 50, 3337.
- Baur, J. A.; Sinclair, D. A. *Nat. Rev. Drug Disc.* **2006**, 5, 493.
- Fernandez-Mar, M. I.; Mateos, R.; Garcia-Parrilla, M. C.; Puertas, B.; Cantos-Villar, E. *Food Chem.* **2012**, 130, 797.
- Siemann, E. H.; Creasy, L. L. *Am. J. Enolo. Viticulture* **1992**, 43, 49.
- Renaud, S.; Delorgeril, M. *Lancet* **1992**, 339, 1523.
- Jang, M. S. et al. *Science* **1997**, 275, 218.
- Bradamante, S.; Barenghi, L.; Villa, A. *Cardiovasc. Drug Rev.* **2004**, 22, 169.
- Howitz, K. T. et al. *Nature* **2003**, 425, 191.
- Valenzano, D. R. et al. *Curr. Biol.* **2006**, 16, 296.
- Wood, J. C. et al. *Nature* **2004**, 430, 686.
- Jang, M. et al. *Science* **1997**, 275, 218.
- Subbaramaiah, K. et al. In *Cancer Prevention: Novel Nutrient and Pharmaceutical Developments*; Bradlow, H. L., Fishman, J., Osborne, M. P., Eds.; New York Acad Sciences: New York, 1999; Vol. 889, pp 214–223.
- Holmes-McNary, M.; Baldwin, A. S. *Cancer Res.* **2000**, 60, 3477.
- Buryanovskyy, L. et al. *Biochemistry* **2004**, 43, 11417.
- Winger, J. A.; Hantschel, O.; Superti-Furga, G.; Kuriyan, J. *BMC Struct. Biol.* **2009**, 9, 7.
- Vella, F.; Gilles, F. A.; Delagrangue, P.; Boutin, J. A. *Biochem. Pharmacol.* **2005**, 71, 1.
- Celli, C. M.; Tran, N.; Knox, R.; Jaiswal, A. K. *Biochem. Pharmacol.* **2006**, 72, 366.
- Jamieson, D.; Tung, A. T. Y.; Knox, R. J.; Boddy, A. V. *Br. J. Cancer* **2006**, 95, 1229.
- Knox, R. J. et al. *Cancer Res.* **2000**, 60, 4179.
- Maiti, A. et al. *J. Med. Chem.* **1973**, 2009, 52.
- Calamini, B. et al. *Biochem. J.* **2010**, 429, 273.
- Boocock, D. J. et al. *J. Chromatogr. B* **2007**, 848, 182.
- De Santi, C.; Pietrabissa, A.; Mosca, F.; Pacifici, G. M. *Xenobiotica* **2000**, 30, 1047.
- De Santi, C.; Pietrabissa, A.; Spisni, R.; Mosca, F.; Pacifici, G. M. *Xenobiotica* **2000**, 30, 857.
- Kang, S. S. et al. *Bioorg. Med. Chem.* **2009**, 17, 1044.
- Meyers, M. J. et al. *J. Med. Chem.* **2001**, 44, 4230.
- Knoevenagel, E. *Ber. Dtsch. Chem. Ges.* **1898**, 31, 2596.
- Lai, G.; Anderson, W. K. *Synth. Commun.* **1997**, 27, 1281.
- Dalcanale, E.; Montanari, F. *J. Org. Chem.* **1986**, 51, 567.
- Kim, E. S.; Lee, H. S.; Kim, J. N. *Tetrahedron Lett.* **2009**, 50, 6286.
- Satoh, T.; Suzuki, S.; Suzuki, Y.; Miyaji, Y.; Imai, Z. *Tetrahedron Lett.* **1969**, 10, 4555.
- Butler, D. C. D.; Alper, H. *Chem. Commun.* **1998**, 2575.
- Kondratyuk, T. P. et al. *Mol. Nutr. Food Res.* **2011**, 55, 1249.
- Sun, B. et al. *Bioorg. Med. Chem.* **2012**, 18, 5352.
- Foster, C. E.; Bianchet, M. A.; Talalay, P.; Faig, M.; Amzel, L. M. *Free Radical Biol. Med.* **2000**, 29, 241.
- Zhou, Z. et al. *Biochemistry* **1985**, 2003, 42.
- C.C.P.N. CCP4, The CCP4 Suite: Programs for Protein Crystallography. *Acta Crystallogr.*, **1994**, D50, 760.
- Emsley, P.; Cowtan, K. *Acta Crystallogr. D Biol. Crystallogr.* **2004**, 60, 2126.
- Brunger, A. T. *Nature* **1992**, 355, 472.
- Painter, J.; Merritt, E. A. *Acta Crystallogr. D Biol. Crystallogr.* **2005**, 61, 465.
- Painter, J.; Merritt, E. A. *Acta Crystallogr. D Biol. Crystallogr.* **2006**, 62, 439.
- Painter, J.; Merritt, E. A. *J. Appl. Crystallogr.* **2006**, 39, 109.
- Chen, V. B. et al. *Acta Crystallogr. D Biol. Crystallogr.* **2010**, 66, 12.